

**Charles University**

**Faculty of Science**

**Study program: Inorganic chemistry (P1401)**

**Branch of study: 4XANOR (1401V000)**



Lewis acids and Frustrated Lewis pair catalysts for reduction and reductive coupling reactions of carbon dioxide.

Lewisovy kyseliny a frustrované Lewisovy párové katalyzátory pro redukční a redukční vazebné reakce oxidu uhličitého.


Doctoral thesis Supervisor: Msci. Martin Hulla, Ph.D.

Prague, 2024

**Declaration:**

I hereby declare that I have worked on and prepared this thesis independently and that I have listed all the sources and literature used. This thesis or a substantial part of it has not been submitted to obtain another or the same academic degree.

In Prague, September 2024

Signature: 



**Financial Support:**

The research project presented in this Thesis was financially supported by the Czech Science Foundation (project junior STAR 21-27431M).

## Acknowledgements

I would like to thank everyone who has been with me on this journey for the past 4 years in Prague. First, I would like to thank my supervisor Dr Martin Hulla for all the fruitful discussions and impassioned talks about catalysis. I would like to thank him for helping me become the chemist and firm believer in developing useful catalysis that I am today. Secondly, I would like to thank my lab mates, Nitin, Pritha, Andrea, Dani and Adam for teaching me so much over the years and helping me become a good mentor and chemist. Most importantly I would like to thank Marianna Gerina who began this journey with me in October 2020 and has helped me every step of the way. Lastly, I would like to thank my family, friends and my partner for being there to encourage and support me throughout the years.

## Contents

Acknowledgements.....	3
Abstract.....	6
Shrnutí.....	7
1.0 'Frustrated Lewis Pair'?	8
1.1 FLPs in catalysis.....	9
1.1.1 Activation of small molecules by FLPs.....	9
1.1.2 FLP catalysed hydrogenations.....	10
1.1.3 FLP catalysed hydrogenations of CO <sub>2</sub> .....	12
2.0 Reductive coupling reactions of CO <sub>2</sub> and amines.....	17
2.1 N-formylation of amines from CO <sub>2</sub> .....	17
2.1.1 N-Formylation of amines from CO <sub>2</sub> and H <sub>2</sub> catalysed by transition metal complexes.....	17
2.1.2 N-Formylation of amines from CO <sub>2</sub> catalysed by main group catalysts and hydrosilanes.....	19
3.0 Aims of thesis.....	24
4.0 Summary of the results.....	26
4.1 Tin catalysed reductive coupling of amines with CO <sub>2</sub> and H <sub>2</sub> .....	26
4.2 Frustrated Lewis Pairs Catalyse the Solvent-Assisted Synthesis of Azoles from ortho-Substituted Anilines, CO <sub>2</sub> and H <sub>2</sub> .....	33
4.3 Hexacoordinated tin complexes catalyse imine hydrogenation with H <sub>2</sub> .....	37
4.4 Unpublished results – Indium(III) triflate catalyses the transfer-hydrogenation of CO <sub>2</sub> to formate for the N-formylation of amines.....	42
5.0 Conclusions.....	48
References.....	49
List of abbreviations.....	62
Statement of contribution.....	64
List of appendices.....	64

Appendix 1 Tin-catalyzed reductive coupling of amines with CO <sub>2</sub> and H <sub>2</sub> .....	65
Appendix 2 Frustrated Lewis Pairs Catalyse the Solvent-Assisted Synthesis of Azoles from ortho-Substituted Anilines, CO <sub>2</sub> and H <sub>2</sub> .....	114
Appendix 3 Hexacoordinated tin complexes catalyse imine hydrogenation with H <sub>2</sub> .....	159
.....	160
Appendix 4 Unpublished results .....	250

## Abstract

Frustrated Lewis pairs (FLPs) are sterically precluded combinations of Lewis acids and Lewis bases that are unable to form a Lewis adduct. The FLPs presented in this thesis are targeted towards the development of novel hydrogenation methods for the reductive coupling of CO<sub>2</sub> to amines.

Firstly, we present FLPs based on R<sub>3</sub>SnX Lewis acids (R = alkyl and X = Cl<sup>-</sup>, OTf<sup>-</sup>, NTF<sub>2</sub><sup>-</sup> or ClO<sub>4</sub><sup>-</sup>) for the reductive coupling of CO<sub>2</sub> and amines in the presence of H<sub>2</sub> gas for the synthesis of N-formamides. R<sub>3</sub>SnX Lewis acids with larger R groups (e.g. cyclohexyl) and weakly coordinating X group (e.g. OTf<sup>-</sup>, NTF<sub>2</sub><sup>-</sup> or ClO<sub>4</sub><sup>-</sup>) presented larger activity than Lewis acids with smaller R substituents (e.g. isopropyl) and strongly coordinating X group (Cl<sup>-</sup>). Among the tested catalysts, Cy<sub>3</sub>SnOTf demonstrated the highest activity (TON > 300), stability in the presence of water and selectivity for CO<sub>2</sub> reduction. In turn, a variety of functionalised amines was selectively N-formylated without the concomitant reduction of unsaturated groups present in the substrate molecule.

Secondly, we present the solvent assisted synthesis of azoles from *ortho*-substituted anilines, CO<sub>2</sub> and H<sub>2</sub> gas. Amine based solvents are N-formylated via the R<sub>3</sub>SnX FLP catalysed N-formylation reaction with CO<sub>2</sub> and H<sub>2</sub>. Subsequent R<sub>3</sub>SnX Lewis acid catalysed transfer of the formyl group to the otherwise unreactive *ortho*-substituted aniline substrate and cyclization of N-formylated intermediate yields the desired azole product. Solvent mixtures of polyethyleneimine and N-methylmorpholine (1:1) were the most effective and allowed for a 70-times increase in catalytic activity of the system compared to simple R<sub>3</sub>SnX Lewis acid promoted N-formylations in sulfolane. The recorded activities are in line with the best transition metal catalysts for the reaction. Consequently, various functionalised *ortho*-substituted anilines were successfully transformed into the corresponding azoles at low catalyst loadings (<1 mol%).

Thirdly, we replaced the tetravalent R<sub>3</sub>SnX Lewis acids by hexa-coordinate tin (IV) salen and salophen complexes, which allows for greater variation in steric and electronic properties of the Lewis acids and their FLPs. The complexes can activate H<sub>2</sub> gas at room temperature and act as hydrogenation catalysts at temperatures >150 °C. The novel LA hydrogenated various imine substrates and acted as CO<sub>2</sub> hydrogenation catalysts in the N-formylation reaction. Lastly, the operating temperatures and pressures of the N-formylations were reduced using transfer hydrogenations with  $\gamma$ -terpinene instead of H<sub>2</sub>. The reactions are catalysed by metal triflates and proceed at 130°C and 4 bar of CO<sub>2</sub> instead of 180°C and >100 bar with H<sub>2</sub> and R<sub>3</sub>SnX based FLPs.

**Keywords:** FLPs, Lewis acids, Lewis bases, catalysis, carbon dioxide, hydrogenation, N-formylamines,

## Shrnutí

Frustrované Lewisovy páry (FLPs) jsou kombinace Lewisových kyselin a Lewisových bází, které nejsou ze sterických důvodů schopny vytvořit Lewisův adukt. FLPs představené v této práci jsou zaměřeny na vývoj nových hydrogenačních metod, zejména pro reduktivně kondenzační reakce  $\text{CO}_2$  s aminy.

Nejprve představujeme FLPs založené na Lewisových kyselinách  $\text{R}_3\text{SnX}$  ( $\text{R}$  = alkyl a  $\text{X} = \text{Cl}^-$ ,  $\text{OTf}^-$ ,  $\text{NTf}_2^-$  nebo  $\text{ClO}_4^-$ ) pro reduktivně kondenzační reakce  $\text{CO}_2$  a aminů v přítomnosti  $\text{H}_2$  plynu pro syntézu N-formamidů. Lewisovy kyseliny  $\text{R}_3\text{SnX}$  s většími R skupinami (např. cyklohexyl) a slabě koordinujícími X skupinami (např.  $\text{OTf}^-$ ,  $\text{NTf}_2^-$  nebo  $\text{ClO}_4^-$ ) vykazují vyšší aktivitu než Lewisovy kyseliny s menšími R substituenty (např. isopropyl) a silně koordinujícími X skupinami ( $\text{Cl}^-$ ). Mezi testovanými katalyzátory  $\text{Cy}_3\text{SnOTf}$  vykázal nejvyšší aktivitu ( $\text{TON} > 300$ ), stabilitu v přítomnosti vody a selektivitu pro redukci  $\text{CO}_2$ . Různé funkčně substituované aminy byly selektivně N-formylovány bez současné redukce nenasycených skupin přítomných v molekule substrátu.

Dále představujeme syntézu azolů asistovanou rozpouštědlem z *ortho*-substituovaných anilinů,  $\text{CO}_2$  a  $\text{H}_2$  plynu. Aminové rozpouštědla jsou N-formylovány reakcí katalyzovanou  $\text{R}_3\text{SnX}$  FLP  $\text{CO}_2$  a  $\text{H}_2$ . Následný přenos formylové skupiny katalyzovaný Lewisovou kyselinou  $\text{R}_3\text{SnX}$  na jinak nereaktivní *ortho*-substituovaný anilinový substrát a cyklizace N-formylovaného meziprojektu vede k požadovanému azolu. Směsi rozpouštědel polyethyleniminu a N-methylmorfolinu (1:1) byly nejučinnější a umožnily 70-násobné zvýšení katalytické aktivity systému ve srovnání s jednoduchými N-formylacemi podporovanými Lewisovými kyselinami  $\text{R}_3\text{SnX}$  v sulfolanu. Zaznamenané aktivity jsou srovnatelné s nejlepšími katalyzátory přechodných kovů pro tuto reakci. Následně byly různé funkčně substituované *ortho*-aniliny úspěšně přeměněny na odpovídající azoly při nízkém zatížení katalyzátorem (<1 mol%).

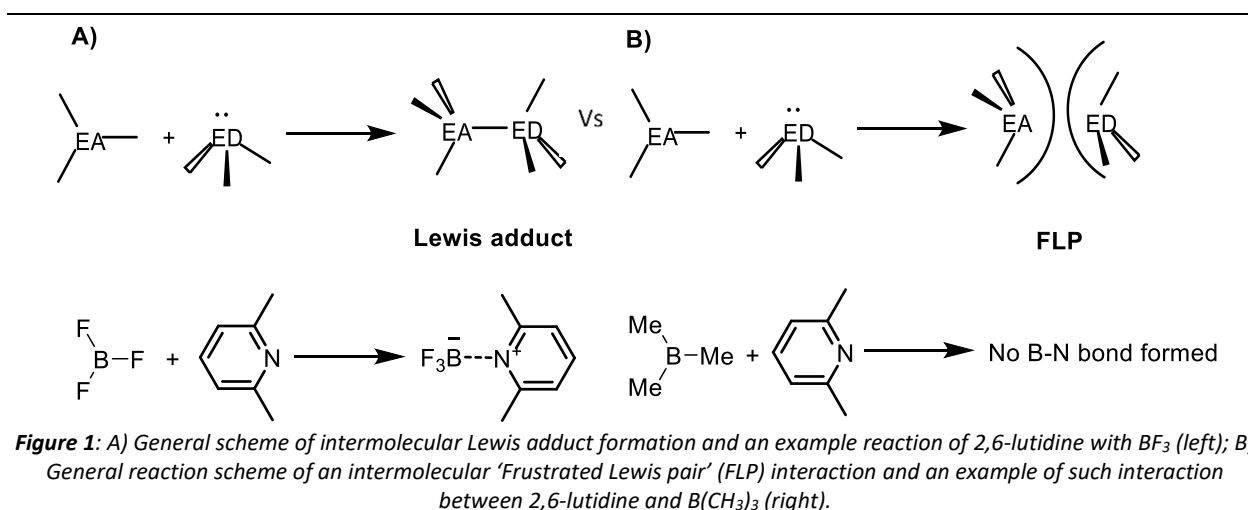
Dále jsme nahradili čtyřmocné Lewisovy kyseliny  $\text{R}_3\text{SnX}$  hexa-koordinovanými komplexy cínu se salenovými a salofenovými ligandy, což umožňuje větší variabilitu ve sterických a elektronických vlastnostech Lewisových kyselin a jejich FLPs. Komplexy mohou aktivovat  $\text{H}_2$  plyn při pokojové teplotě a působí jako katalyzátory hydrogenací při teplotách nad  $150^\circ\text{C}$ . Tyto nové Lewisovy kyseliny hydrogenovaly různé iminy a působily jako katalyzátory hydrogenace  $\text{CO}_2$  v N-formylačních reakcích. Nakonec byly provozní teploty a tlaky N-formylací sníženy použitím přenosových hydrogenací s  $\gamma$ -terpinenem místo  $\text{H}_2$ . Reakce jsou katalyzovány kovovými trifláty a probíhají při  $130^\circ\text{C}$  a 4 barů  $\text{CO}_2$  místo  $180^\circ\text{C}$  a  $>100$  barů s  $\text{H}_2$  a FLPs na bázi  $\text{R}_3\text{SnX}$ .

**Klíčová slova:** FLP, Lewisovy kyseliny, Lewisovy báze, katalýza, hydrogenace, oxid uhličitý, formamidy

# 1. Introduction

## 1.0 'Frustrated Lewis Pair'?

Gilbert N. Lewis proposed the theory of Lewis acids, Lewis bases and Lewis adducts in the early 20<sup>th</sup> century. Accordingly, Lewis adducts are composed of an electron acceptor (EA or Lewis acid (LA)) and an electron donor (ED or Lewis Base (LB)) which have formed a pairing. The pair is formed due to the donation of an electron pair from the LB to the LA forming a dative covalent bond (Figure 1A). In contrast, FLPs are combinations of LA and LB that are sterically, energetically, or electronically precluded from forming a dative covalent bond (Figure 1B). Both Lewis adducts and FLPs can either be formed inter- or intra-molecularly.<sup>1</sup>



In 1942 Brown showed that upon exposing 2,6-lutidine to  $\text{BF}_3$  a typical Lewis adduct was formed. However, upon exposure of 2,6-lutidine to the bulkier  $\text{BMe}_3$  no such adduct was formed (Figure 1 and 2).<sup>2</sup> In 1959 Wittig found that when  $\text{BPh}_3$  and  $\text{PPh}_3$  are exposed to 1-bromo-2-fluorobenzene and magnesium, which generates benzyne *in situ*, a zwitterionic product was formed by 1,2- addition as opposed to the expected classic Lewis adduct (Figure 2).<sup>3</sup> Similar reaction occurs between trityl anion and  $\text{BPh}_3$ , which undergo 1,2- and 1,4- additions when exposed to butadiene instead of forming the Lewis adduct. First catalytic reaction with an 'FLP' was completed in 1996 when Piers reported the  $\text{B}(\text{C}_6\text{F}_5)_3$  catalysed hydrosilylation of ketones. Two years later it was shown that  $\text{B}(\text{C}_6\text{F}_5)_3$  and the ylide  $\text{Ph}_3\text{PC}(\text{H})\text{P}$  undergo thermal rearrangement from a classic Lewis adduct to a zwitterionic salt (Figure 2).<sup>4</sup>

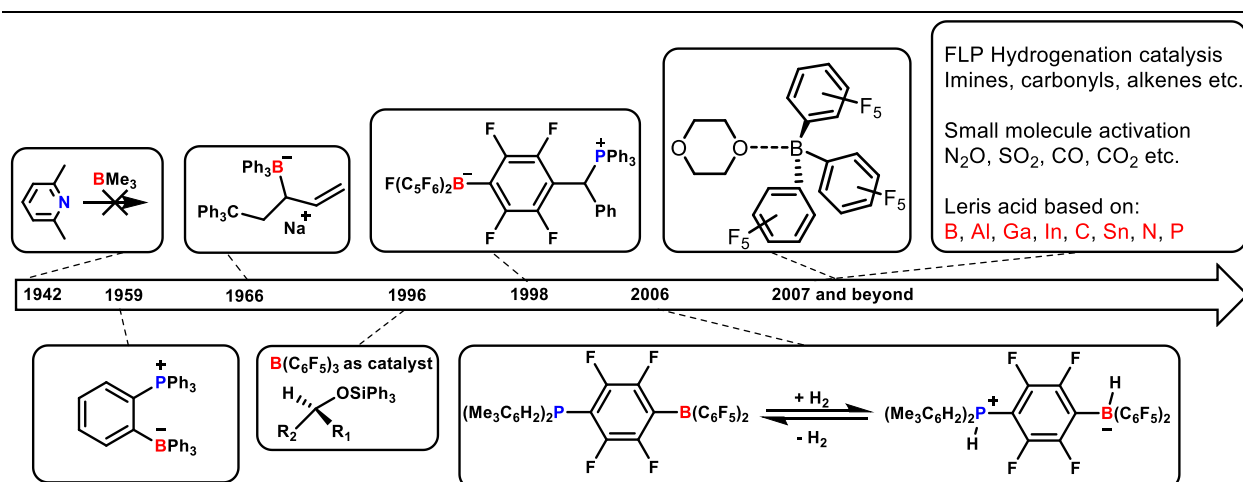


**Figure 2:** Timeline of important discoveries in the lead-up to the modern FLP. This figure was adapted from reference X.

Following on from these early examples of Lewis acid and Lewis base cooperative catalysis, in 2006 the Stephan group published the first example of reversible dihydrogen activation by a phosphaborane FLP (Figure 2). This challenged the notion that transition metals are needed for the activation of dihydrogen and hydrogenation catalysis.<sup>1</sup>

## 1.1 FLPs in catalysis.

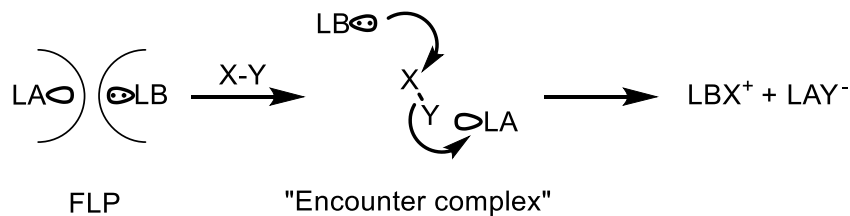
### 1.1.1 Activation of small molecules by FLPs

Hydrogenations using dihydrogen allow for atom economic reduction reactions for the synthesis of molecules important in the petrochemical, pharmaceutical and food industries.<sup>5-8</sup> Both FLPs and transition metals activate dihydrogen and other small molecules.<sup>9-11</sup> The mechanism that transition metals activate dihydrogen and the mechanism that FLPs activate dihydrogen are theorized to be similar.<sup>12,13</sup> Both can use orbitals of  $\sigma$  and  $\sigma^*$  symmetry to donate electron density into the  $\sigma^*$  orbital and accept electron density from the  $\sigma$  orbital of dihydrogen respectively.<sup>12</sup> Although, the research on the activation of dihydrogen with FLPs is still ongoing and there are different interpretations as to the exact mechanism but in many interpretations, it is believed that the orbital interactions between dihydrogen and an FLP occur via an 'encounter complex' leading to heterolytic splitting of H<sub>2</sub> (Figure 3A).<sup>14,15</sup> The main difference between FLPs and transition metals is that transition metals can act as both the Lewis base and as the Lewis acid leading to the homolytic splitting of dihydrogen.<sup>12</sup> In contrast, FLPs are multi-component systems where the Lewis basic moiety and Lewis acidic moiety are located on different atoms and thus requires the formation of an encounter complex.<sup>1,15</sup> The encounter complex is hypothesized to incorporate a 'guest' molecule which then is split by either polarization of the electric field between the



Lewis acid and Lewis base or by a donor-acceptor interaction between FLP and the substrate, which allows FLPs to split  $H_2$  and to act as hydrogenation catalysts.<sup>15,16</sup>

### A) Heterolytic cleavage of small molecules by FLP



### B) $H_2$ activation by $B(C_6F_5)_3$ : dioxane FLP

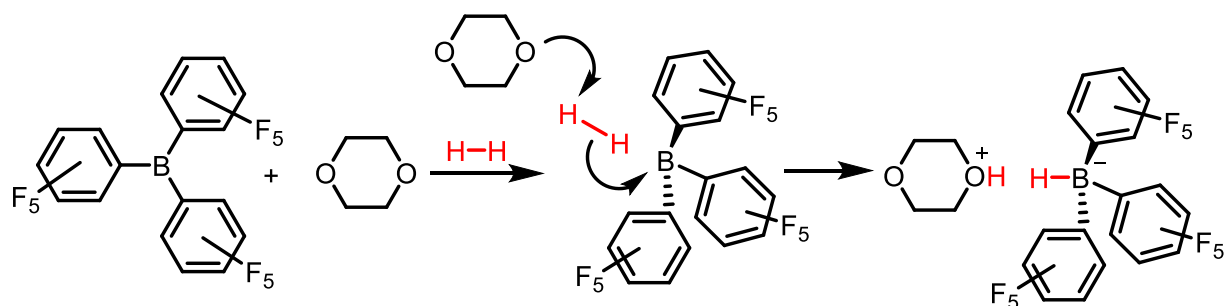


**Figure 3:** A) General mechanism of small molecule activation by FLP via an "encounter complex"; B) Example of  $H_2$  activation by an intermolecular FLP [ $B(C_6F_5)_3$ : dioxane]

## 1.1.2 FLP catalysed hydrogenations

FLPs catalyse the hydrogenation of imines, enamines, *N*-heterocyclic compounds, ketones, esters, silyl ethers, oxime ethers, alkenes, alkynes, aromatics and other unsaturated molecules (Figure 4).<sup>9,14,17</sup>

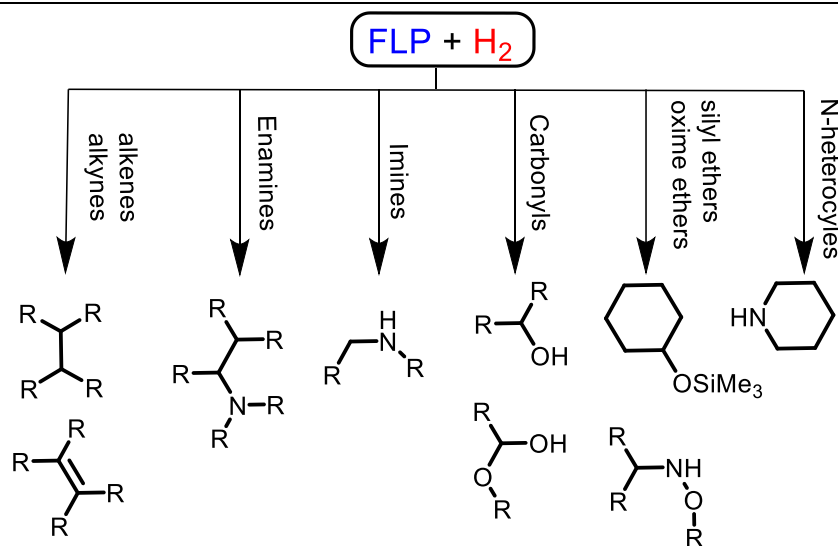


**Figure 4:** Examples of products that can be synthesized by FLP using  $H_2$  gas (names of starting materials are stated below products)

The archetypical hydrogenation of imines in the presence of dihydrogen gas proceeds without an added base for sufficiently basic imines, which may act as the Lewis basic counterpart of the FLP catalyst.<sup>18,19</sup> Encounter complex forms, which heterolytically splits hydrogen gas (Figure 5, steps I and II). This results in a LA-hydride and a conjugate acid of the Lewis base. The LA-hydride then inserts the imine (or iminium cation) reducing the imine to an amine- LA complex (Figure 5, step III). The resulting amine-LA complex then dissociates liberating the amine product (Figure 5, step IV) completing the reduction of the imine to an amine (Figure 5).<sup>18</sup>

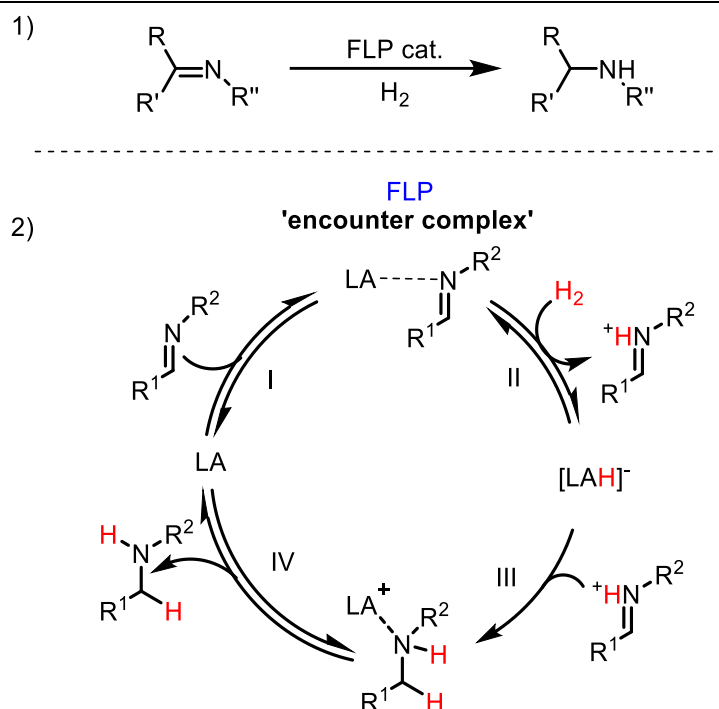


**Figure 5:** 1) Reaction scheme for the FLP catalysed hydrogenation of imines with  $\text{H}_2$  as the hydride source. 2) General mechanism for FLP catalysed imine hydrogenation with substrate as the Lewis base

The reaction is mostly catalysed by boron-based Lewis acids. However, recently it has been shown that heavier p-block based Lewis acids, including Sn, can hydrogenate imines and therefore can be compared with boranes. The motivation to switch from boron-based acids to other main group acids was driven by the need for catalysts with greater water and functional group tolerance in particular alcohols. Boranes strongly interact with  $-\text{hydroxyl}$  groups, which leads to LA-HOR adducts that are strongly acidic [cf.  $\text{H}_2\text{O}$   $\text{pK}_a = 8.4$  (MeCN);  $\text{H}_2\text{O}-\text{B}(\text{C}_6\text{F}_5)_3$   $\text{pK}_a < 1$  ( $\text{H}_2\text{O}$ , est.)] which, in turn, when deprotonated by a Lewis base leads to catalyst inactivity.<sup>18,20,21</sup>

The most notable class of heavy p-block Lewis acids used in FLP chemistry are  $\text{R}_3\text{SnOTf}$  Lewis acids.  $\text{R}_3\text{SnOTf}$  Lewis acids are surrogates for the stannylum cation " $\text{R}_3\text{Sn}^+$ " which is isolobal with  $\text{R}_3\text{B}$  Lewis acids

(Figure 6) and has been calculated to possess similar hydride ion affinities ( $\Delta G_{\text{Hydride}}$  in MeCN = 65.83 and 64.95 kcal mol<sup>-1</sup> for <sup>n</sup>Bu<sub>3</sub>Sn-H and [H-B(C<sub>6</sub>F<sub>5</sub>)<sub>3</sub>]<sup>-</sup> respectively).<sup>18,20</sup>

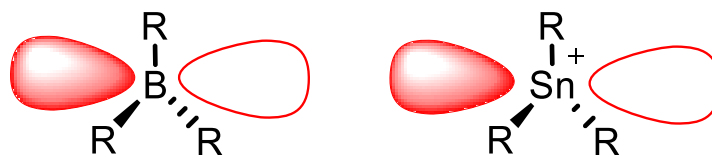


**Figure 6:** Diagram showing the isolobality between  $R_3B$  species and  $R_3Sn^+$  cations.

Notably, the adduct of <sup>n</sup>Bu<sub>3</sub>Sn<sup>+</sup> with water is weaker than the adduct of B(C<sub>6</sub>F<sub>5</sub>)<sub>3</sub> which results in higher water and alcohol tolerance of this Lewis acid. However, <sup>n</sup>Bu<sub>3</sub>SnX does not form FLPs instead tending to form a classical Lewis adduct as the <sup>n</sup>Bu groups do not provide enough steric hinderance to the tin Lewis acidic centre. This led to the replacement of the <sup>n</sup>Bu groups with <sup>i</sup>Pr with the greater steric bulk precluding adduct formation. <sup>i</sup>Pr<sub>3</sub>SnOTf and 2,4,6- collidine (**FLP1**) is hence a known Sn/N FLP.<sup>18</sup> **FLP1** has been shown to efficiently hydrogenate imines, aldehydes and ketones.<sup>18,20</sup> However, it failed in the direct reduction of CO<sub>2</sub>, which is a prominent target for FLP catalysed hydrogenations due to its promise as a renewable C1 source. Nevertheless, due to the formation of water as a byproduct upon 4e<sup>-</sup> and 6e<sup>-</sup> reductions of CO<sub>2</sub> and the products of CO<sub>2</sub> reduction forming strong adducts with LAs, FLP catalysed CO<sub>2</sub> reductions with H<sub>2</sub> remained challenging.<sup>22</sup>

### 1.1.3 FLP catalysed hydrogenations of CO<sub>2</sub>

Carbon dioxide is a promising renewable C1 source for the synthesis of fine chemicals (Figure 7), fuels, and polymers, however, most of these syntheses require the reduction of CO<sub>2</sub>.<sup>23</sup> Using CO<sub>2</sub> as a C1 feedstock would allow reduced reliance on fossil fuels as a feedstock and therefore contribute to decreasing emissions by turning the focus to CCSU (Carbon Capture Sequestration and Utilisation).<sup>23,24</sup>

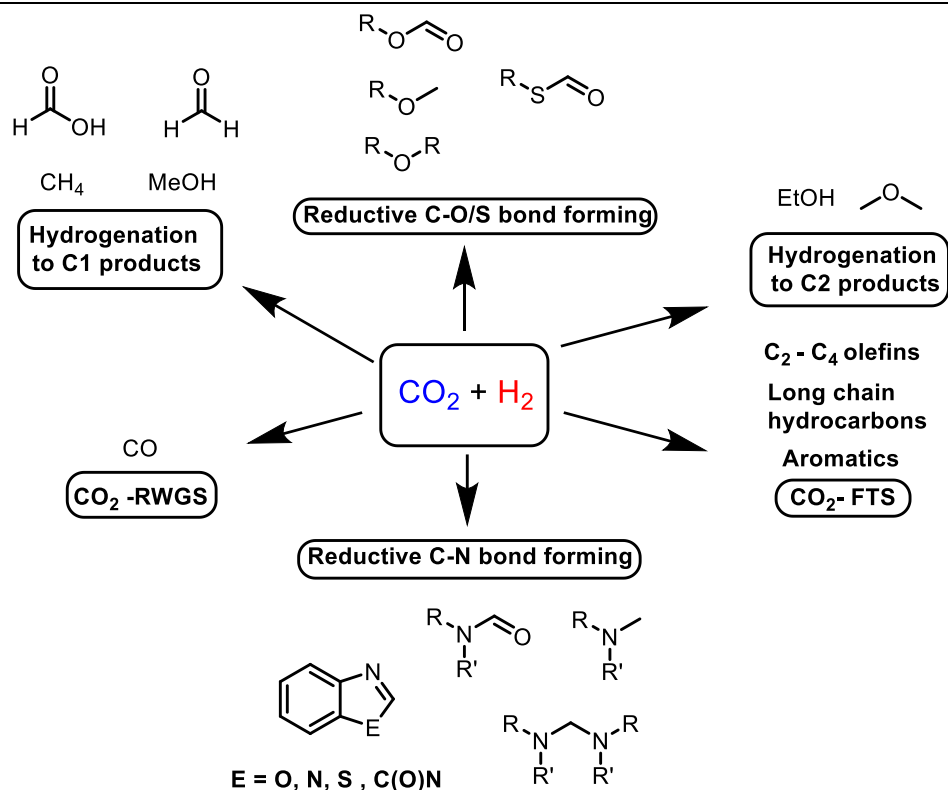


**Figure 7:** Examples of useful products produced from the hydrogenation of  $\text{CO}_2(\text{g})$  using  $\text{H}_2(\text{g})$ . RWGS = Reverse Water Gas Shift, FTS = Fischer Tropsch Synthesis.

$\text{CO}_2$  may be used to produce formic acid (Figure 7), which is used as an  $\text{H}_2$  storage medium, in rubber production and as a chemical precursor in various organic transformations.<sup>23,25–27</sup> Further hydrogenations lead to formaldehyde and methanol, which has value as a fuel source and in chemical synthesis.<sup>28–30</sup> Reverse water gas shift and Fischer Tropsch type synthesis generate carbon monoxide,  $\text{C}_2$ - $\text{C}_4$  olefins and long chain hydrocarbons.<sup>23,29,31</sup> Carbon dioxide may also be reduced and incorporated into aromatic rings, various carbocycles or coupled to nucleophiles such as amines, thiols or alcohols allowing for the synthesis of complex molecular scaffolds from  $\text{CO}_2$  via partial or complete  $\text{CO}_2$  deoxygenation (Figure 7).<sup>23,24,31</sup>

However, the valorisation of  $\text{CO}_2$  often requires a high energy and a catalyst, due to thermodynamic stability of  $\text{CO}_2$  ( $\Delta G_f = -396 \text{ kJ mol}^{-1}$ ).<sup>32</sup> The catalysts are most often based on transition metals, in particular, the platinum group metals  $\text{Ru}$ <sup>33,34</sup>,  $\text{Rh}$ <sup>35,36</sup>,  $\text{Pt}$ <sup>37,38</sup>,  $\text{Pd}$ <sup>38,39</sup>,  $\text{Ir}$ <sup>40,41</sup>. Platinum group metals are rare and expensive therefore there has been a push to develop  $\text{CO}_2$  hydrogenation with  $\text{H}_2(\text{g})$  methods using earth abundant metals and non-metals including FLPs.<sup>22</sup> Early examples of FLP catalysed  $\text{CO}_2$  reductions focused on stoichiometric reaction using boron based FLPs (Figure 8).<sup>22</sup>

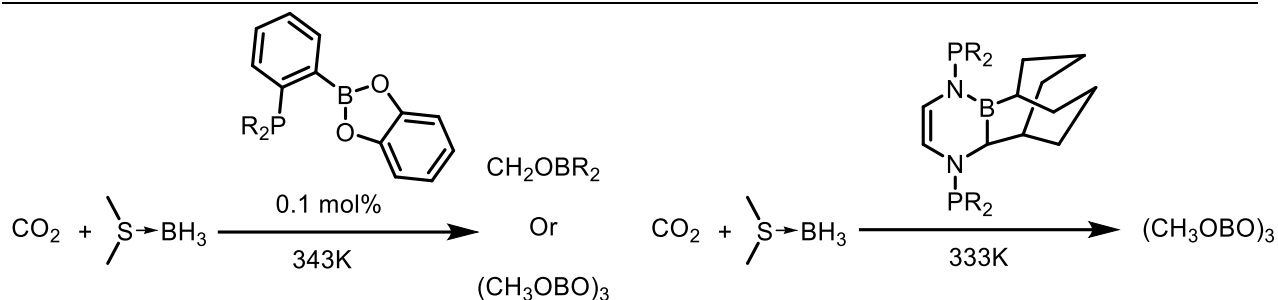


**Figure 8:** Examples of hydroborations of  $\text{CO}_2$  catalysed by FLPs comprising boron Lewis acids and P/N Lewis bases.

B/P FLPs have been shown to efficiently activate  $\text{CO}_2$  both inter- and intramolecularly (Figure 8). However, these FLPs required stoichiometric reducing agents such as  $\text{BH}_3\text{-SMe}_2$  or  $\text{NH}_3\text{-BH}_3$  instead of  $\text{H}_{2(\text{g})}$  for catalytic reductions.<sup>22</sup> Strong Lewis adduct formation with formic acid, methanol and water produced by direct hydrogenation of  $\text{CO}_2$  using  $\text{H}_2$  gas hindered or completely inhibited catalytic turnover.<sup>42</sup> Notably, this was observed by Fontaine and colleagues upon  $\text{CO}_2$  hydrogenation with  $\text{H}_2$  and 1- $\text{BR}_2$ -2- $\text{NMe}_2\text{-C}_6\text{H}_4$  ( $\text{R} = (2,4,6\text{-Me}_3\text{C}_6\text{H}_2, 1, 2,4,5\text{Me}_3\text{C}_6\text{H}_2)_2$ ) catalysts that resulted in stoichiometric hydrogenation of  $\text{CO}_2$  to a mixture of formyl, acetal and methoxy derivatives of the FLP Lewis acids (Figure 9).<sup>43</sup>

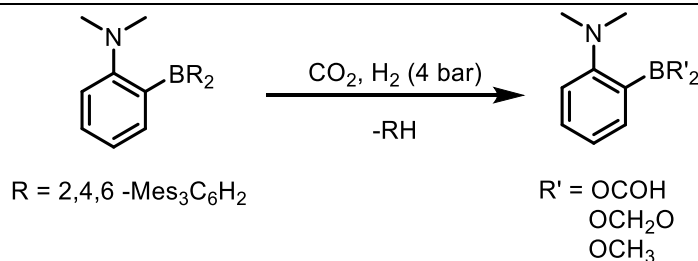


**Figure 9:** Example of stoichiometric reduction of  $\text{CO}_2$  with  $\text{H}_2$  catalysed by B/N FLP.

Elimination of methanol from  $[\text{TMP-H}][\text{MeO-B}(\text{C}_6\text{F}_5)]$  ( $\text{TMP} = 2,2,6,6\text{-tetramethylpiperidine}$ ) was demonstrated by O'Hare and colleagues together with the sequential reduction of  $\text{CO}_2$  with  $\text{H}_2$  to the methoxide level.<sup>42</sup> The reaction was promoted by  $[\text{B}(\text{C}_6\text{F}_5) : \text{TMP}]$  FLP leading to the formation of  $[\text{TMP-H}][\text{MeO-B}(\text{C}_6\text{F}_5)]$  over 6 days at  $160^\circ\text{C}$  in a yield of 25% (Figure 10).<sup>42</sup>

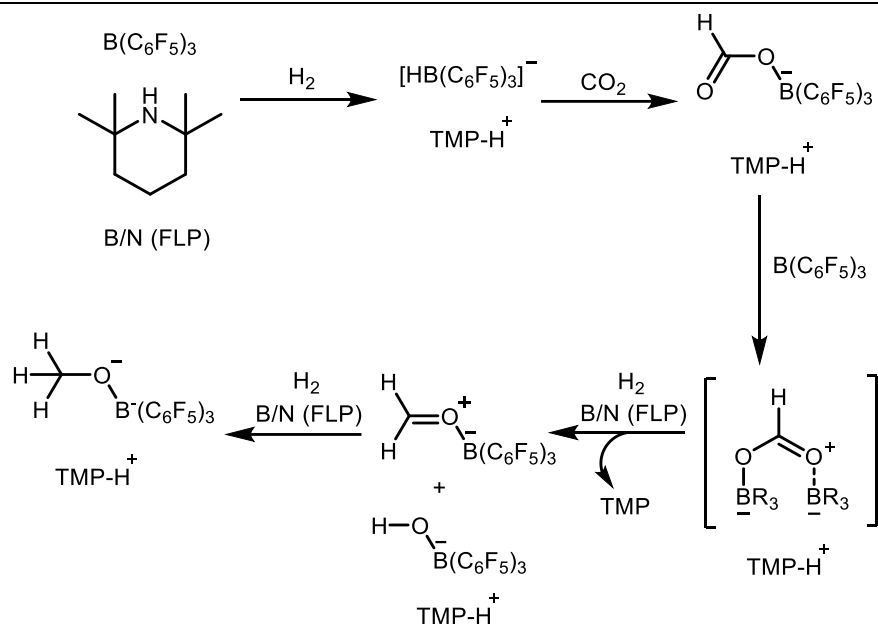


**Figure 10:** Simplified scheme for the synthesis of [TMP-H][MeO-B(C<sub>6</sub>F<sub>5</sub>)<sub>3</sub>] from CO<sub>2</sub> and H<sub>2</sub> promoted by [B(C<sub>6</sub>F<sub>5</sub>)<sub>3</sub>]:TMP FLP

In the reaction, [HB(C<sub>6</sub>F<sub>5</sub>)<sub>3</sub>]<sup>-</sup> was able to effectively hydrogenate CO<sub>2</sub> to formate at pressures as low as 1 bar and at temperatures of 110 °C. This demonstrated the relative ease of 2e<sup>-</sup> CO<sub>2</sub> reductions by main group hydrides. However, to achieve further reductions of CO<sub>2</sub> increased temperatures were required, which lead to LA decomposition by protodearylation. Water produced in the reaction binds the LA B(C<sub>6</sub>F<sub>5</sub>)<sub>3</sub>, protonates the aryl ring and eliminates it in the form ArylH. The resulting HOB(C<sub>6</sub>F<sub>5</sub>)<sub>2</sub> further decomposes into the inactive boroxin (OB(C<sub>6</sub>F<sub>5</sub>)) (Figure 11). As a result, it was not possible to liberate MeOH from [TMP-H][MeO-B(C<sub>6</sub>F<sub>5</sub>)<sub>3</sub>] without the protodearylation, which precluded catalytic turnovers.<sup>42</sup>

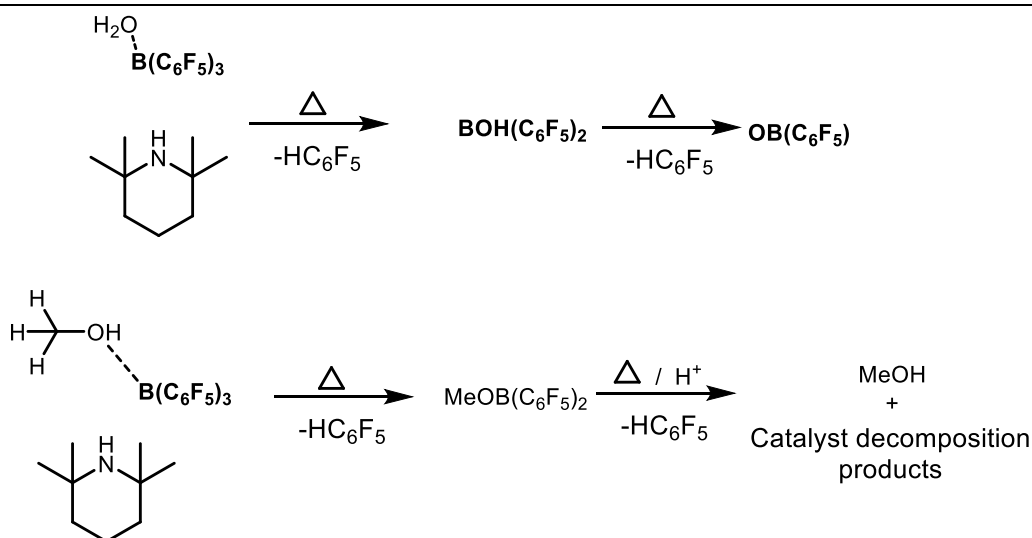


**Figure 11:** Mechanism for the decomposition of boranes during the synthesis of MeOH from H<sub>2</sub> and CO<sub>2</sub>.

To overcome the issue of cleaving the formate and methoxy from the formatoborate and methoxyborate products respectively Stephan and colleagues employed the use of silyl halides.<sup>44</sup> This was able to efficiently cleave the formate- and methoxy- groups from the boron center acting as an ‘oxygen sponge’, in the  $[B(C_6F_5)_3 : 2,6\text{-lutidine}]$  FLP, allowing for turnover (Figure 12). Moreover, the silyl halides promoted the reaction at lower temperatures (100 °C vs 160°C for O’Hare and colleagues). Therefore, mitigating the temperature induced decomposition of the borane, which was further inhibited by the silyl halide acting as a drying agent preventing water-assisted decomposition (Figure 11). The system achieved up to 8 turnovers of  $Me_3OSiMe_3$  at 2 bars of  $CO_2$  and 4 bars of  $H_2$  in 40 hours.<sup>44</sup>

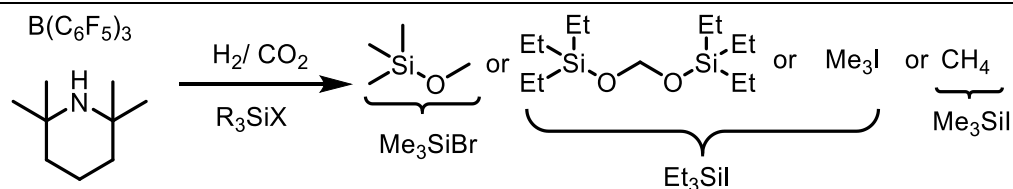


**Figure 12:** Mechanism for the synthesis of various  $C_1$  products from  $CO_2$  and  $H_2$  catalysed by an FLP and assisted by a silyl halide.

Zhang and colleagues employed a similar approach in which  $B(C_6F_5)_3$  was found to form a Lewis pair with  $M_2CO_3$  ( $M = Na, K, Cs$ ), where the group 1 metal ion assisted in cleavage of the formate from the boron center thus allowing for turnover (Figure 13).<sup>45</sup> Zhang and co-workers also found that addition of potassium metal to the reaction greatly increased the turnover of the reaction (653 (without) vs. 3941 (with)) wherein the potassium metal likely dried the reaction *in situ*, prevented LA decomposition and assisted in formate cleavage. However, both these systems share the need of an additional sacrificial Lewis acid or other additive to cleave the desired product and dry the reaction, which decreases the overall atom economy of the reaction by producing waste such as K and Si oxides.<sup>45</sup>

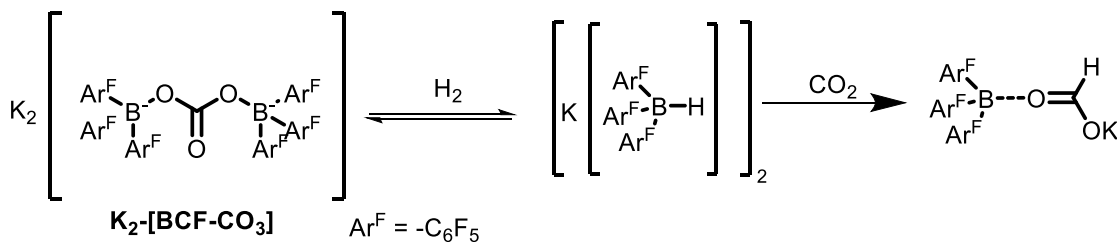


**Figure 13:** Hydrogenation of  $CO_2$  catalysed by a  $K_2CO_3$  and  $B(C_6F_5)_3$  Lewis pair

## 2.0 Reductive coupling reactions of CO<sub>2</sub> and amines.

### 2.1 N-formylation of amines from CO<sub>2</sub>.

Reductive coupling of amines and CO<sub>2</sub> represents an alternative pathway to utilize CO<sub>2</sub> in synthesis, which contrasts to the synthesis of formic acid, methanol or methane. Formic acid, methanol and methane are potentially viable ways to turn CO<sub>2</sub> into fuels, but the prices of these chemicals are set by the petrochemical industry as they are commonly produced from natural gas.<sup>46,47</sup> Therefore, prize competitive synthesis of these fuels from CO<sub>2</sub> hydrogenation remains a challenge. The reductive coupling of amines and CO<sub>2</sub> may be able to circumvent this issue by producing valuable products, which can offset some of the costs of CCU technologies used to isolate CO<sub>2</sub>.<sup>48</sup> N-formylation of amines with CO<sub>2</sub> and H<sub>2(g)</sub> is one example of a CO<sub>2</sub> reductive coupling reaction by way of CO<sub>2</sub> hydrogenation to the formate level and then condensation of the formate with an amine substrate (Figure 14).<sup>49,50</sup> The produced N-formylamines are useful as fine chemicals, solvents, pharmaceuticals and as precursors in organic synthesis.<sup>49–51</sup>

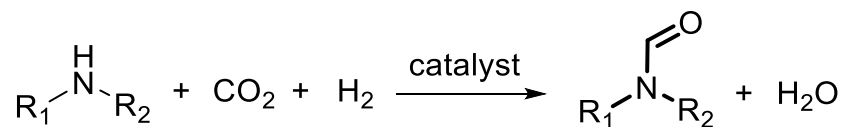


**Figure 14:** General reaction scheme of the N-formylation of amines with H<sub>2</sub> and CO<sub>2</sub>

---

#### 2.1.1 N-Formylation of amines from CO<sub>2</sub> and H<sub>2</sub> catalysed by transition metal complexes.

The N-formylation of amines with CO<sub>2</sub> and H<sub>2</sub> is catalysed by various transition metal containing species including but not limited to complexes (Figure 15) and materials<sup>49,51–54</sup>. Most notable are ruthenium complexes which, while using supercritical CO<sub>2</sub> (scCO<sub>2</sub>) as the solvent were shown to achieve up to 7.4 x 10<sup>5</sup> turnovers.<sup>55</sup> Initial studies by Jessop et al found that RuCl<sub>2</sub>(PMe<sub>3</sub>)<sub>4</sub> is able to formylate a variety of secondary amines, a variety of carbamates of secondary amines and of ammonium carbamate at 100 °C and 130 atm partial pressure (pp) of CO<sub>2</sub> and 80 atm ppH<sub>2</sub>.<sup>56</sup> The reaction has since been completed by a variety of metals including, but not limited to, Rh,<sup>57</sup> Ir,<sup>52</sup> Fe,<sup>58</sup> Co<sup>54</sup> and Pd.<sup>59</sup>

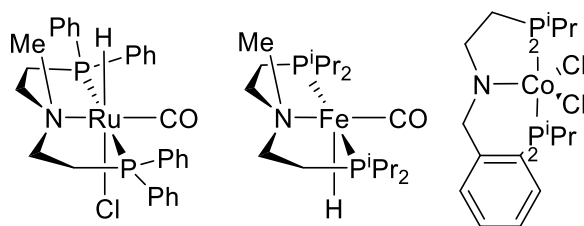


**Figure 15:** Examples of transition metal catalysts, which can complete the hydrogenation of CO<sub>2</sub> and its reductive coupling to amines.

---



The N-formylation is hypothesized to proceed *via* the production of a dialkylammonium dialkylcarbamate,<sup>56</sup> which forms a salt with the amine substrate and subsequently condenses in the presence of formic acid into the formamide product liberating water as a byproduct (Figure 16). Jessop et al. have also reported the N-formylation of aniline using  $[\text{RuCl}_2(\text{PMe}_3)_4]$  and 1,8-diazabicyclo[5.4.0]undec-7-ene (DBU).<sup>60</sup> The nature of the phosphine ligand attached to the Ru center has also been shown to have a major effect on the activity moving from  $\text{PMe}_3$  to  $\text{Ph}_2\text{PCH}_2\text{CH}_2\text{PPh}_2$  (dppe) lead to an increase of the TON from  $3.7 \times 10^5$  to  $7.4 \times 10^{55,56}$  turnovers demonstrating the facile tuning of the Ru catalysts for the reaction. The current most active catalyst for the N-formylation of amines with  $\text{CO}_2$  and  $\text{H}_2$  is  $[(^{\text{Ph}}\text{P}^{\text{Me}}\text{NP})\text{RuClH}(\text{CO})]$  which has demonstrated turnovers of up to  $1.85 \times 10^6$  at 70 bar  $\text{CO}_2/\text{H}_2$  (1:1) at  $120^\circ\text{C}$ .<sup>53</sup> However, this activity comes at the cost of chemoselectivity as the ruthenium complexes mentioned above are unable to selectively reduce  $\text{CO}_2$  over other reducible functional groups.<sup>34,53,55</sup> Functional tolerance is imperative for the synthesis of complex pharmaceutically relative formamides, possibly containing many other functional groups.<sup>49,50,58</sup>

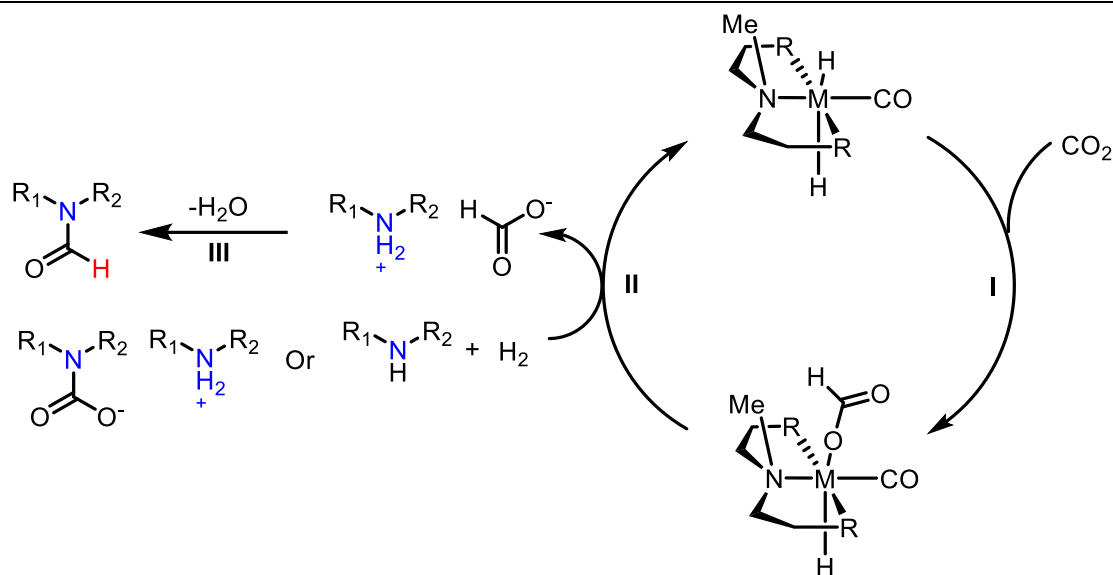


**Figure 16:** Proposed mechanism of the N-formylation of amines with  $\text{H}_2$  and  $\text{CO}_2$  catalysed by transition metal-pincer complex (the catalyst activation step is omitted for clarity). R = phosphine and M = Ru, Co, Fe.

Despite the success of noble metals and Ru in particular, there has been a notable improvement in the number of systems, which involve non-precious metals, most notably Fe,<sup>58</sup> Co<sup>54</sup> and Cu.<sup>49</sup> Nevertheless, much like the platinum group metals Fe & Co are not fully chemoselective for the reduction of  $\text{CO}_2$  in the presence of other functional groups.<sup>54,58</sup>

Uniquely, one of the only examples that is selective is  $\text{Cu}(\text{OAc})_2$ .  $\text{Cu}(\text{OAc})_2$  in combination with DMAP (4-Dimethylaminopyridine) has been shown to selectively hydrogenate  $\text{CO}_2$  over other reducible functional groups in the N-formylation reaction leading to the ability to functionalise amines containing alkenes, esters, amides, nitriles and halides (Figure 17).<sup>49</sup>

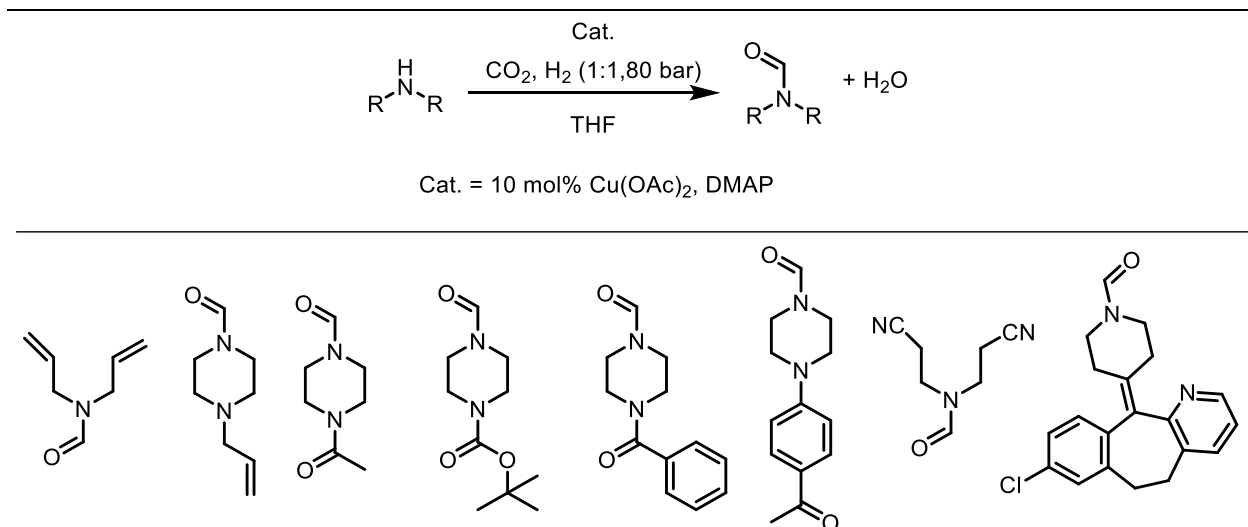


**Figure 17:** General scheme for the N-formylation of amines catalysed by  $\text{Cu}(\text{OAc})_2$  (top). Examples of substrates containing unsaturated groups which were tolerated by  $\text{Cu}(\text{OAc})_2$  in the presence of  $\text{H}_2$  gas and  $\text{CO}_2$  (bottom).

Nevertheless,  $\text{Cu}(\text{OAc})_2$  in combination with DMAP remains a rare example of chemoselectivity among transition metal catalysts utilizing  $\text{H}_2$  as the reductant.

### 2.1.2 N-Formylation of amines from $\text{CO}_2$ catalysed by main group catalysts and hydrosilanes.

In contrast to transition metals, selective N-formylation of amines with  $\text{CO}_2$  is frequently observed with main group hydrides instead of  $\text{H}_2$ .<sup>61-63</sup> More specifically hydrosilanes or boranes, and a main group catalyst (Figure 18) such as Lewis base or ionic liquid.<sup>64-69</sup> Sacrificial hydrides provide many advantages: 1) they tend to be far more selective for the hydrogenation of  $\text{CO}_2$  over other functional groups<sup>61,66,70</sup> 2) they tend to run at lower temperatures and pressures<sup>61-63,71,72</sup> and 3) they tend to be easier to store and handle than  $\text{H}_2$  gas.<sup>73</sup> For the N-formylation of amines with  $\text{CO}_2$ , hydrosilanes, like  $\text{PhSiH}_3$ , are the most ubiquitous sacrificial reductants used.

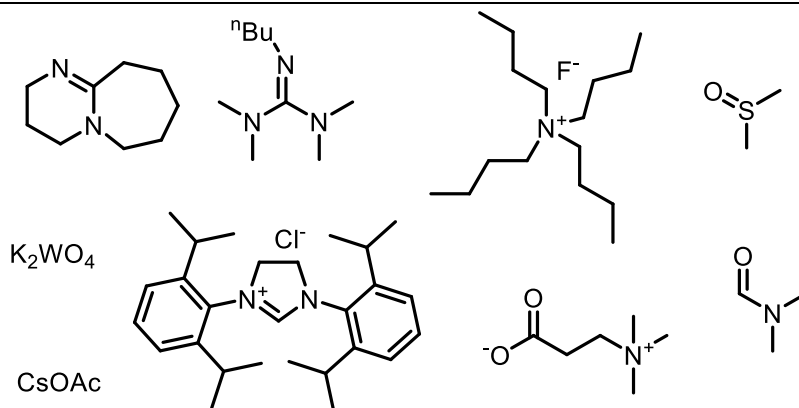


**Figure 18:** Examples of organocatalysts and inorganic salts, which catalyse the reaction of N-formylation of amines with CO<sub>2</sub> and hydrosilanes.

Organic superbases such as DBU have been shown to activate CO<sub>2</sub> to form a DBU-CO<sub>2</sub> adduct which is hypothesized to allow hydrosilane reduction.<sup>69</sup> Organic superbases have also been hypothesized to activate Si-H bonds *via* a S<sub>n</sub>2-type interaction, which increases the hydride donor ability of the hydrosilane, and promotes CO<sub>2</sub> reduction (Figure 19). Other superbases bases such as triazabicyclo[4.4.0]dec-5-ene (TBD) are known to form carbamates with CO<sub>2</sub> [TBD-COO] or in combination with the substrate amine [TBDH][RR'N-COO].<sup>70,74</sup> In such cases it has been calculated that the activation of the hydrosilane for CO<sub>2</sub> reduction occurs *via* the carbamate and not the free Lewis base.<sup>69,70,74</sup> Carbenes are another well-known class of catalysts for the N-formylation of CO<sub>2</sub> with hydrosilanes.<sup>75</sup> They are hypothesized to activate CO<sub>2</sub> much in the same way as the organic bases described above; they form a complex with the substrate amine and activate the hydrosilane *via* a carbamate S<sub>n</sub>2 type interaction.<sup>75</sup> Organic salts and ionic liquids are the third well established class of catalysts for the N-formylation of amines with CO<sub>2</sub> and hydrosilanes. Like carbenes and organic superbases they are hypothesized to act as nucleophiles to activate hydrosilanes for CO<sub>2</sub> reduction.<sup>66-68</sup> Their activity is attributed mainly to the anion, where the cation have a minor effect based on its pairing energy.<sup>69</sup> The reaction is then favoured with cations that have minimal pairing energy with the anion. To assess the effect of the anion [TBA][X] (X = F, Cl, Br and I) were tested and a trend of activity was established with [TBA]F being most active and [TBA]I being least.<sup>61,76</sup> Interestingly Lewis acids such as B(C<sub>6</sub>F<sub>5</sub>)<sub>3</sub> can also catalyse the N-formylation of amines with CO<sub>2</sub> and hydrosilanes. B(C<sub>6</sub>F<sub>5</sub>)<sub>3</sub> is hypothesized to interact with the hydrosilane by activating the hydride *via* μ<sup>1</sup>-coordination. B(C<sub>6</sub>F<sub>5</sub>)<sub>3</sub> is also hypothesized to activate CO<sub>2</sub> *via* the 'CO<sub>2</sub>-phillic fluorine atom of the aryl ring. Moreover, B(C<sub>6</sub>F<sub>5</sub>)<sub>3</sub> may also activate the amine *via* a donor acceptor interaction between the LAs boron centre and the substrate nitrogen.<sup>77</sup>

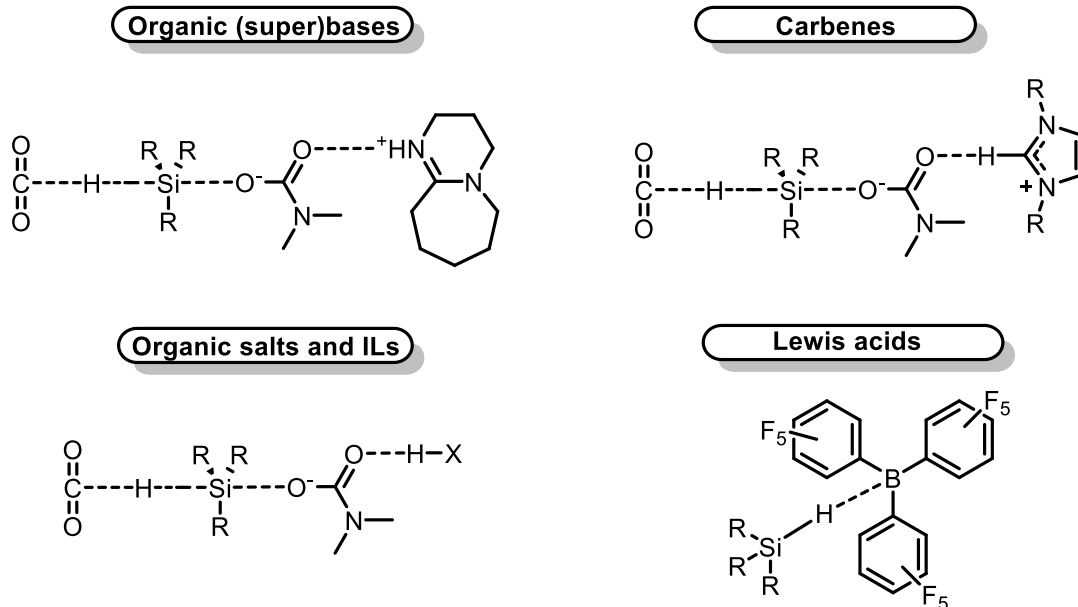


**Figure 19:** Examples of how organocatalysts activate hydrosilanes via carbamates for the reduction of CO<sub>2</sub>.

In contrast to transition metal (TM) complexes described in section 2.1.1, hydrosilanes tend to be far more selective for the reduction of CO<sub>2</sub>.<sup>52,55,61</sup> This is believed to be due to the high affinity for CO<sub>2</sub> insertion into main group hydride bonds over the reaction with other functional groups. Whilst TM complexes often require high CO<sub>2</sub> pressures to proceed, hydrosilanes and boranes often run under ambient pressure and temperature. As such, hydrosilanes and boranes have been shown to tolerate a wide range of functional groups including but not limited to ketones, ethers, esters, alkenes, halides, and imines etc (Figure 20).<sup>61,70,74,75</sup>

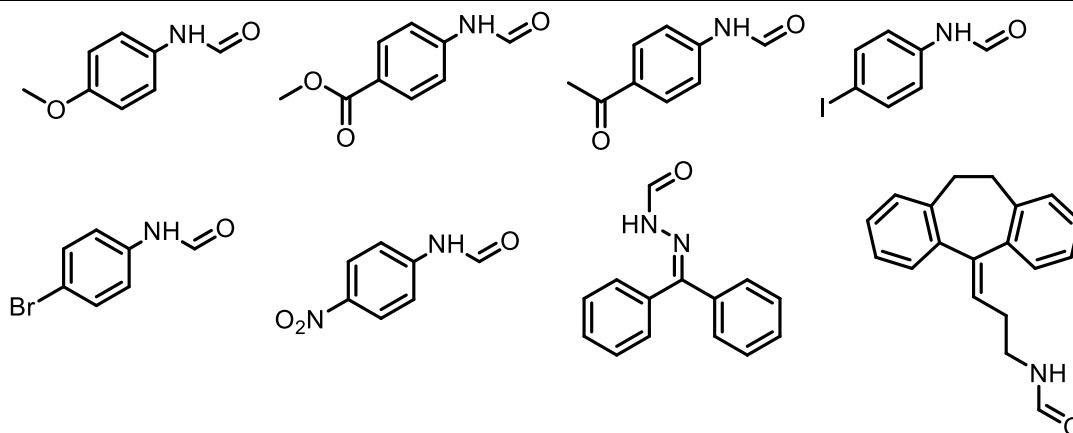


**Figure 20:** Examples of amines containing other reducible functional groups that are tolerated in the presence of hydrosilanes for the N-formylation of amines with CO<sub>2</sub>

Moreover, hydrosilanes in combination with base catalyst demonstrate increased reactivity towards aromatic amines over aliphatic ones.<sup>53,56,60,61</sup> In contrast, TM complexes react primarily with alkyl amines and examples of aromatic amine functionalization remain rare.<sup>56</sup> This difference is explained by the different reaction mechanisms. The mechanism of hydrosilylation of CO<sub>2</sub> for the N-formylation of amines differs depending on the basicity of the amine substrate.<sup>78</sup> For amines of low basicity such as aromatic amines, the substrate forms a carbamate with CO<sub>2</sub> only in the presence of a base catalyst. The resulting carbamate then activates the hydrosilane towards CO<sub>2</sub> reduction to a formoxysilane, which is then cleaved by the substrate forming the desired formamide product and liberating a silanol (R<sub>3</sub>SiOH). For amines of high basicity, the initial carbamate formation is spontaneous, and an external base is not required. Due to higher stability of carbamates formed from highly basic amines, the second step involves protonation of the hydrosilane, formation of silyl-carbamate and liberation of H<sub>2</sub>. The silyl-carbamate is then hydrogenated by another equivalent of hydrosilane leading to the formation of the formamide product (Figure 21).<sup>78</sup>

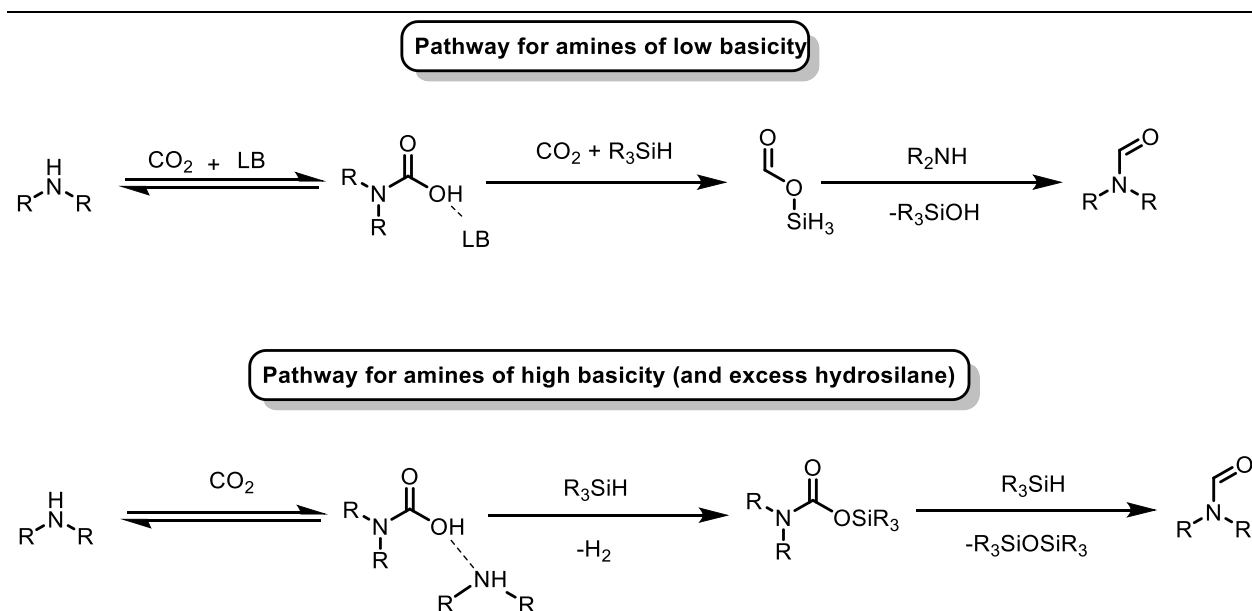


**Figure 21:** Proposed mechanisms for the reduction of CO<sub>2</sub> by hydrosilanes.

Interestingly while carbamates activate hydrosilanes for CO<sub>2</sub> hydrogenation *via* an S<sub>n</sub>2 type mechanism (Figure 22) carbamates inhibit transition metal catalysts by ligating to free coordination site(s) on the metal, which is required for H<sub>2</sub> activation, and protonation of metal hydrides leading to the reversibility of H<sub>2</sub> activation.<sup>55</sup>

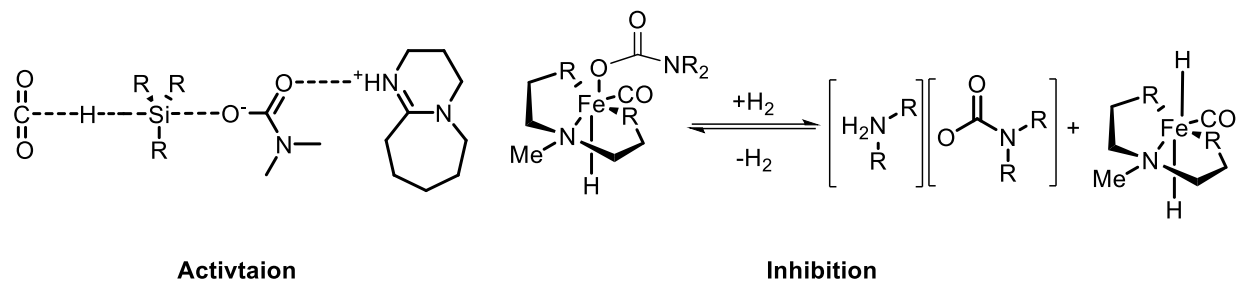


**Figure 22:** Carbamates used in the activation of hydrosilanes (left) and in the inhibition of transition metal catalyst (right)

Aromatic amines and other amines of low basicity react sluggishly with formic acid, which is the main reaction pathway for N-formylation of amines catalysed by TMs.<sup>52,53,55</sup> However, in the case of hydrosilanes the aromatic amine instead reacts with a formylsiloxane, which unlike formic acid readily reacts with amines of low basicity. This allows systems utilizing hydrosilanes to N-formylate aromatic amines with CO<sub>2</sub>.<sup>78</sup>

The ability to N-formylate aromatic amines and the high selectivity of main group hydrides towards CO<sub>2</sub> hydrogenation over other functional groups (Figure 20) makes them the reductant of choice in small laboratory scale reactions of fine chemicals, where selectivity is key. However, since hydrosilanes are sacrificial reagents, they produce a lot of unnecessary waste in the form of silanols and siloxanes, which decreases the atom efficiency of the reaction and complicates product purification.<sup>78</sup> In contrast, TMs in combination with H<sub>2</sub> produce only water as the reaction byproduct. Therefore, there is an interest in developing main group catalysts that can form selective main group hydrides *in situ* from H<sub>2</sub> thereby combining the high chemoselectivity of main group hydrides with the mitigation of waste by using H<sub>2</sub> as the hydride source.

### 3.0 Aims of thesis.

The research presented in this thesis was conducted with the goal of developing novel FLPs for catalytic hydrogenations of CO<sub>2</sub> and reductive coupling reactions of CO<sub>2</sub> with amines. This work was motivated by the lack of efficient water tolerant main group catalysts for the N-formylation of amines with CO<sub>2</sub> utilizing H<sub>2</sub> gas or other atom efficient hydride source and by the lack of selectivity for CO<sub>2</sub> reduction over other reducible functional groups presented by transition metal catalysts developed for the reactions.

The lack of water tolerant FLPs has hindered the use of FLPs in CO<sub>2</sub> reductive coupling reactions with H<sub>2</sub> as water is the main byproduct of the reaction. In general, main group catalysts rely on the use of an auxiliary hydride source such as hydrosilanes or boranes but there are no examples of main group catalysts that can conduct the N-formylation of amines with molecular hydrogen as the reductant. FLPs can generate main group hydrides *in situ* from H<sub>2</sub> gas and due to the facile insertion of CO<sub>2</sub> into main group hydride bonds. FLPs may provide a pathway towards selective N-formylation of amines utilizing CO<sub>2</sub> and H<sub>2</sub> without the concomitant reduction of other reducible functional groups. This may provide an advantage over transition metal complexes, which usually require high CO<sub>2</sub> pressures and demonstrate low chemoselectivity towards reduction of other reducible functional groups.

We aim to use tin based FLPs to generate tin hydrides, via splitting of hydrogen gas. Tin hydrides have been shown previously to insert CO<sub>2</sub> into the tin-hydride bond. Therefore, we aim to use these generated tin hydrides to reduce CO<sub>2</sub> *in situ* to generate tin formates, which like formoxysilanes can react with amines to produce N-formamides. As tin hydrides are heavier congeners of known reducing agents such as hydrosilanes, which preferentially reduce CO<sub>2</sub> over other functional groups, we believe they will behave similarly leading to the ability to synthesise variously functionalized N-formamides from CO<sub>2</sub> and H<sub>2</sub>.

A secondary goal of this thesis is to expand the scope of Lewis acids that can act as part of FLP hydrogenation catalysts. Generally, FLPs are based on simple Lewis acids such as boranes, alanes or stannanes, however there are many complexes of main group metals which exceed the standard valence of group 13 and 14 Lewis acids. Main group metal complexes may provide a way to expand the electronic and steric properties of Lewis acids used in FLPs, which is required to expand FLP hydrogenation chemistry as it has been hypothesized that commonly applied Lewis acids, particularly boranes, have reached an impasse in terms of the modulation of their steric and electronic properties. Therefore, we sought to use Schiff base complexes of tin to expand the scope of FLP Lewis acids. We aim to synthesize various

hexacoordinated tin(IV) salen and salophen complexes. We aim to modify these hexacoordinated tin(IV) complexes by varying the X ligand and the aromatic substituents and we aim to test their ability to act as hydrogenation catalysts by hydrogenating polar functional groups such as imines.

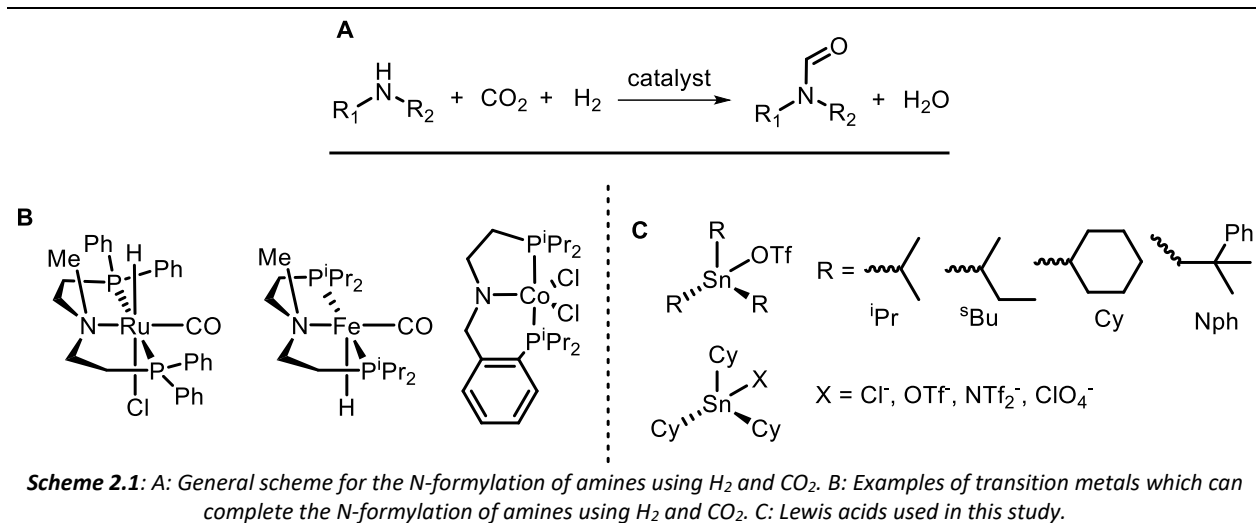
Main group Lewis acids also catalyse transfer hydrogenations using an organic molecule such as isopropanol or glycerol. Transfer hydrogenations are often run at lower temperatures and pressures than their counterparts utilizing H<sub>2</sub> gas. Therefore, we aim to develop an efficient synthetic method in which simple Lewis acids, such as commercially available metal triflates can utilize  $\gamma$ -terpinene as a H<sub>2</sub> surrogate to reduce CO<sub>2</sub> and reductively coupling it to amines. This method will allow the reactions to run at lower temperatures and pressures than known CO<sub>2</sub> coupling methodologies while simultaneously generating only value added products.



## 4.0 Summary of the results

### 4.1 Tin catalysed reductive coupling of amines with CO<sub>2</sub> and H<sub>2</sub>

Carbon dioxide has promise as a renewable C1 source to produce fuels, pharmacologically active compounds and fine chemicals.<sup>23</sup> However oftentimes this process requires the reduction of CO<sub>2</sub> and to that effect H<sub>2</sub> gas is the most atom economical reductant.<sup>23</sup> Transition metals have been known for many decades to reduce CO<sub>2</sub> using hydrogen gas. One notable reaction in the field of CO<sub>2</sub> reduction with H<sub>2</sub> gas is the N-formylation of amines in which CO<sub>2</sub> is reduced to formate and coupled to an amine (primary or secondary) liberating water as the by product. Many transition metal complexes, such as those based on Ru,<sup>53</sup> Rh,<sup>57</sup> Ir,<sup>52</sup> Pd,<sup>38</sup> Fe,<sup>58</sup> and Co<sup>54</sup> have been shown to efficiently complete this reaction (Figure 2.1). However, despite their high activity very few of these metal complexes can selectively hydrogenate CO<sub>2</sub> over other reducible functional groups, which vastly limits the scope of substrates that can undergo N-formylation.<sup>49</sup> One alternative to transition metal complexes and H<sub>2</sub> gas is to use a stoichiometric reductant such as a hydrosilane or borane along with a catalyst often comprising a basic component.<sup>69</sup> Examples include amines, metal salts, carbenes and solvents like DMSO or  $\gamma$ -valerolactone. Hydrosilanes and boranes are often able to selectively hydrogenate CO<sub>2</sub> over other functional groups which is one notable advantage of using main group hydrides over transition metal hydrides.<sup>66,69,74,75</sup> To that effect, we decided to study 'Frustrated Lewis Pairs' (FLPs), which are a Lewis acid and base pair whose reactivity is unquenched in solution.<sup>1</sup> FLPs are mostly comprised of a main group Lewis acid like a borane or stannane, which along with an N/P based Lewis base have been shown to activate small molecules including H<sub>2</sub> gas.<sup>18</sup> Most FLPs, however, do not hydrogenate CO<sub>2</sub> and the FLPs which have demonstrated efficient CO<sub>2</sub> reduction often use an additive like a silyl halide or potassium metal to achieve turnover.<sup>44,45</sup> This is the result of the Lewis acids propensity to strongly bind the resulting formate and therefore requires an exogenous acid to assist in formate cleavage. FLPs are also often intolerant to water, which as the byproduct of the N-formylation reaction, has hampered their use in this reaction thus far.<sup>20,21</sup>



One promising set of FLPs are those comprising Sn Lewis acids and N Lewis bases. Sn/N FLPs have been shown to efficiently hydrogenate imines and carbonyls as well as catalysing the reductive amination of a wide array of ketones and aldehydes in the presence of  $H_2$  gas of which water is the by-product.<sup>18,21</sup> Therefore, we used [ $^iPr_3SnOTf$ : 2,4,6-collidine] (**FLP1**) as the starting point from which to study the N-formylation reaction. To model the reaction morpholine was chosen as the substrate as morpholine is the model substrate of choice for transition metal systems.<sup>53,55</sup> Initial reactions were run at 180°C, 30 bar  $H_2$  and 4 bar  $CO_2$ . FLP catalysed hydrogenations are most often run in aromatic or ethereal solvents, however, due to the temperature constraints solvents like THF and Diethyl ether were unsuitable. Aromatic solvents were also tested such as toluene and 1,3-dichlorobenzene and whilst their boiling points were appropriate their ability to solubilize the morpholinium carbamate, which results from  $CO_2$  capture by morpholine, was limited thus creating a mass transfer problem that hindered the desired reaction.<sup>79</sup> To this effect we screened high boiling and dipolar aprotic solvents and found that among them sulfolane was the best for the reaction which is line with DMSO and DMF being efficient solvents in the case of  $CO_2$  reduction with hydrosilanes.<sup>50,62</sup>

Optimising the reaction conditions disclosed that upon increasing the temperature from 160°C to 180°C, increased the N-formylmorpholine yield from 25% to 57% but in the temperature regime of 180°C - 200°C the yield slightly decreased (Figure 2.2). This is the result of the energetic benefit of increased temperature being outweighed by the decomposition of the LA component as evidenced by GC presence of  $^iPr_4Sn$ , produced by high temperature disproportionation of  $^iPr_3SnOTf$ , after the reaction. Increase of  $H_2$  pressure had a positive effect on the reaction in the regime of 20 bar to 100 bar and plateaued between 100 bar and 120 bar. We attribute this to the hydrogen binding or activation being rate limiting in this

process as is common with FLPs.<sup>9,80</sup> Changes in the pressure of CO<sub>2</sub> from 1 bar to 4 bar increased the yield. However, at pressures above 4 bar the reactivity of the system decreased. Investigation of the system disclosed that it is due to higher partial pressures of CO<sub>2</sub> favouring carbamic acid formation, which protonates the R<sub>3</sub>Sn-H and therefore reversing hydrogen activation and decreasing the overall activity. The large disparity in partial pressures of H<sub>2</sub> and CO<sub>2</sub> (molar ratio >12.5) again suggests that hydrogen activation is slow and is possibly rate limiting.

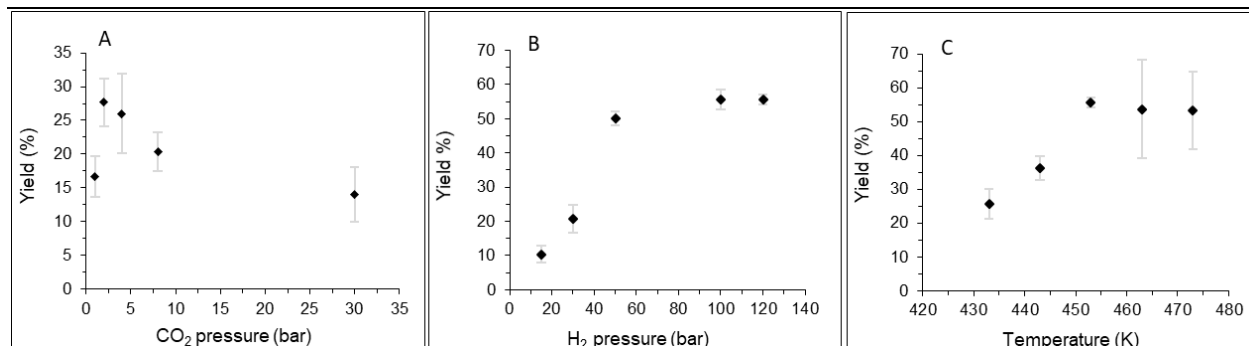
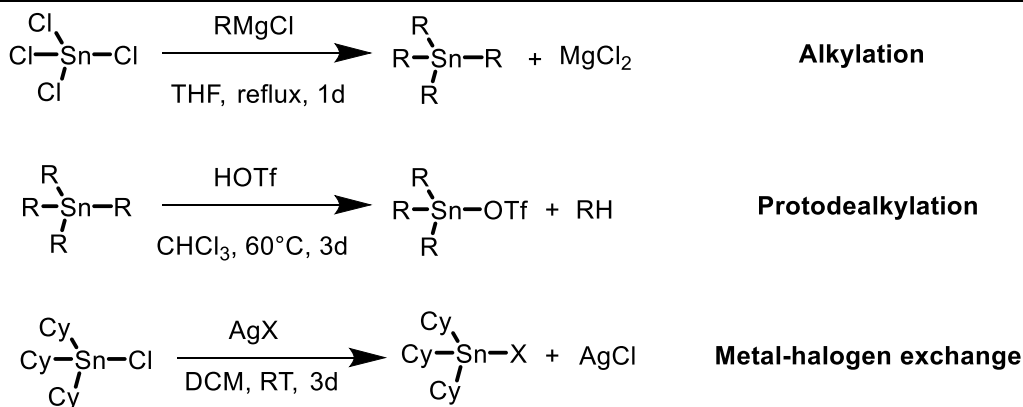


**Figure 2.2:** Optimization of reaction conditions: morpholine (0.5 mmol), FLP1 (10 mol%), sulfolane (5 mL), 24 h and unless otherwise specified H<sub>2</sub> (100 bar), CO<sub>2</sub> (4 bar), temperature (453 K); a) Effect of CO<sub>2</sub> partial pressure at a constant partial pressure of H<sub>2</sub> (30 bar); b) Effect of H<sub>2</sub> partial pressure; c) Effect of reaction temperature. All reactions were repeated in triplicate, and the reaction product was quantified by <sup>1</sup>H NMR with DCM as the internal standard. Error bars represent one standard deviation.

Under the optimized reaction conditions, FLP1 yielded N-formylmorpholine in 57% yield with a turnover frequency of 0.25 h<sup>-1</sup> (Table 2.1). The Lewis acid ability to cleave H<sub>2</sub> gas and stability is related to the nature of the R and X groups. In order to expand the scope of water-tolerant tin Lewis acids we synthesized a series of R<sub>3</sub>SnX Lewis acids (Figure 2.3), where we varied the nature of the R and X groups. Only Lewis acids with large R groups were prepared as smaller R groups could preclude FLP catalysis due to Lewis adduct formation and larger R groups may assist in hydrolytic stability (Table 2.1).



**Scheme 2.3:** General syntheses of R<sub>3</sub>SnX LAs starting via 1) alkylation of SnCl<sub>4</sub> with Grignard reagents; 2) protodealkylation using triflic acid and 3) metal-halogen exchange using an AgX salt.

By running the R<sub>3</sub>SnX Lewis acids under optimised conditions, we were able to establish Cy<sub>3</sub>SnOTf as the most efficient Lewis acid (Table 2.1). We believe this is the case due to the increased bulk of cyclohexyl compared to the isopropyl group mitigating the formation of the tetra-alkyl R<sub>4</sub>Sn species thus increasing the stability of the catalyst as demonstrated by increase in the maximum turnover number from 162 with [<sup>i</sup>Pr<sub>3</sub>SnOTf : 2,4,6-collidine] to >300 with [Cy<sub>3</sub>SnOTf : 2,4,6-collidine] FLP.

Entry	Lewis Acid	Loading (mol%)	Yield (%)	TOF [h <sup>-1</sup> ] <sup>b</sup>
1	<sup>i</sup> Pr <sub>3</sub> SnOTf	10	57	0.25
2	<sup>s</sup> Bu <sub>3</sub> SnOTf	10	43	0.17
3	Nph <sub>3</sub> SnOTf	10	39	0.17
4	Cy <sub>3</sub> SnOTf	10	95 <sup>d</sup>	-
5	Cy <sub>3</sub> SnClO <sub>4</sub>	10	83 <sup>d</sup>	-
6	Cy <sub>3</sub> SnNTf <sub>2</sub>	10	82 <sup>d</sup>	-
7	Cy <sub>3</sub> SnCl	10	70	0.29
8	Cy <sub>3</sub> SnOTf	1	28	1.16
9	Cy <sub>3</sub> SnClO <sub>4</sub>	1	17	0.71
10	Cy <sub>3</sub> SnNTf <sub>2</sub>	1	16	0.67
11	-	0	0	0
12	<sup>i</sup> Pr <sub>2</sub> Sn(OTf) <sub>2</sub>	10	28	0.13
13 <sup>a</sup>	<sup>i</sup> Pr <sub>3</sub> SnOTf	10	95	-

**Table 2.1:** Optimisation of Lewis acid component of FLP by varying alkyl and X substituents (left). Reaction conditions: morpholine (1 mmol), sulfolane (4 mL), LA: 2,4,6-collidine (1-10 mol%), CO<sub>2</sub> (4 bar), H<sub>2</sub> (100 bar), 453 K, 24 h, average yield after three runs. Yield was determined by <sup>1</sup>H NMR with an internal standard.

Triflate (OTf) was found to be the best X group for Cy<sub>3</sub>SnX Lewis acids when compared to the more coordinating Cl<sup>-</sup> as the increased acidity aids in hydrogen activation. Triflate was also found to outperform both triflimide (NTf<sub>2</sub><sup>-</sup>) and perchlorate (ClO<sub>4</sub><sup>-</sup>) despite their increased acidity, which, was confirmed by the Guttmann-Beckett method. The decreased activity is likely due to a decrease in water tolerance or stability. Varying the Lewis base component of the FLP found that [Cy<sub>3</sub>SnOTf : 2,4,6-collidine] was the most efficient Lewis acid/base pair (Table 2.2).

Entry	Lewis acid	Lewis base <sup>c</sup>	Yield (%)	TOF [h <sup>-1</sup> ] <sup>c</sup>
1	<sup>i</sup> Pr <sub>3</sub> SnOTf <sup>a</sup>	Collidine <sup>a</sup>	57	0.25
2	<sup>i</sup> Pr <sub>3</sub> SnOTf <sup>a</sup>	-	44	0.21
3	Cy <sub>3</sub> SnOTf <sup>b</sup>	Collidine <sup>b</sup>	28	1.16
4	Cy <sub>3</sub> SnOTf <sup>b</sup>	-	15	0.63
5	Cy <sub>3</sub> SnOTf <sup>b</sup>	TMP-H <sup>b</sup>	20	0.73
6	Cy <sub>3</sub> SnOTf <sup>b</sup>	TMP-Me <sup>b</sup>	17	0.71

**Table 2.2:** Optimisation of Lewis base in R<sub>3</sub>SnX: LB FLPs. Reaction conditions: morpholine (1 mmol), sulfolane (4 mL), LA: 2,4,6-collidine (1-10 mol%), CO<sub>2</sub> (4 bar), H<sub>2</sub> (100 bar), 453 K, 24 h, average yield after three runs. Yield was determined by <sup>1</sup>H NMR with an internal standard.

With an efficient system at hand, we conducted a substrate scope focusing on substrates containing other reducible functional groups (Figure 2.3).

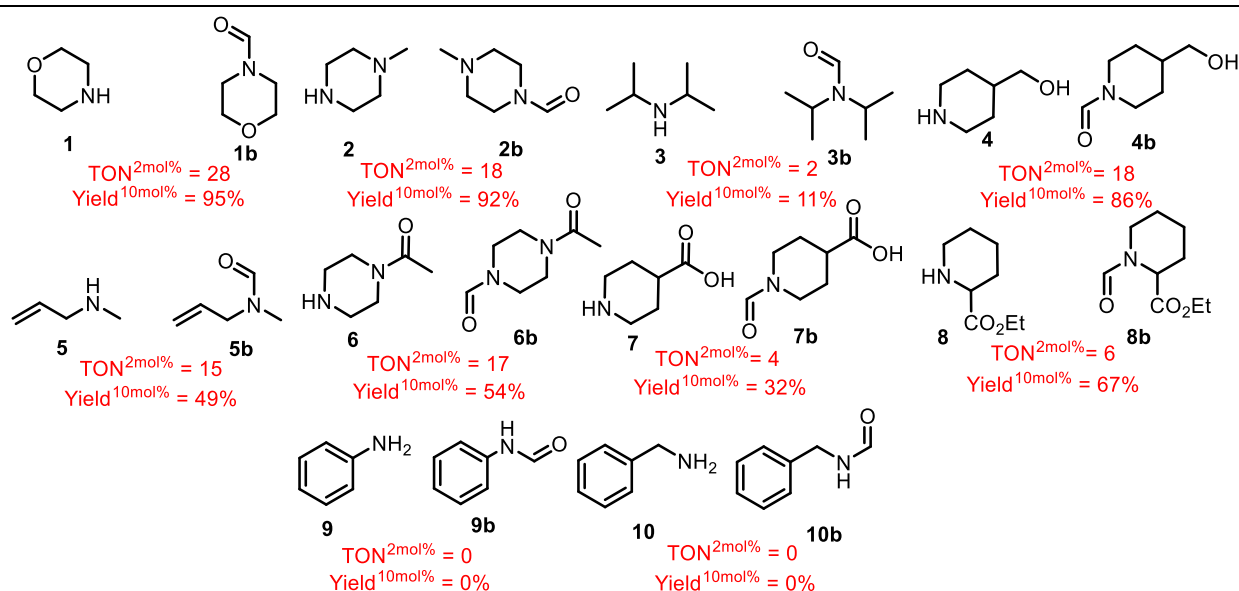


**Figure 2.3:** Substrate scope for the N-formylation reaction with CO<sub>2</sub>, H<sub>2</sub> and Cy<sub>3</sub>SnOTf catalyst. Reaction conditions: amine (1 mmol), sulfolane (4 mL), LA : 2,4,6-collidine (2 mol%), CO<sub>2</sub> (4 bars), H<sub>2</sub> (100 bars), 453 K, 24 h. Yields were determined by <sup>1</sup>H NMR with DCM as internal standards and structures confirmed by GC-MS.

In order to highlight kinetic differences and reactivity between substrates the reactions were run at 2 mol% catalyst loadings to achieve low to moderate conversions. We found that secondary amines containing no other reducible functional groups such as substrates **1-3** were efficiently formylated, however **3** proceeded at a much slower rate due to the increased steric hindrance of the isopropyl groups on the amine. Substrate **4**, which contains an alcohol functionality, was also efficiently formylated demonstrating the alcohol tolerance of catalyst. Unsaturated groups such as the alkene, amide and

carboxylic acid on substrates **5**, **6** and **7** respectively were tolerated with no concomitant hydrogenation. However, the ester functionality of substrate **8** partially decomposed to a mixture of ethyl 1-formylpiperidine-2-carboxylate and N-formylpiperidine in the ratio of 7 to 3. The ester functionality positioned one carbon atom away from the nitrogen also reduced the reaction rate compared with morpholine and this may be due to steric hindrance. Ultimately the ability to formylate amines containing other functional groups is of the utmost importance for formamides with biological applications as pharmacological structure activity relationships are very sensitive. Substrates **9** and **10**, containing aromatic rings, were found to be unreactive which may be due to aromatic amines low nucleophilicity. Benzylamine (**10**) undergoes a side reaction to form a mixture of N-benzyl-1-phenylmethanimine and dibenzylamine in the 24-h test. Most substrates were found to scale with catalyst loading (2 mol% vs 10 mol%), however, substrates **3**, **5**, and **6** did not scale directly with catalyst loading. In the case of N-allylmethylamine (**5**) showed significant over reduction of CO<sub>2</sub> to the N-methylation product as confirmed by GC-MS. Whereas in the reaction of substrate **6** there was a build-up of Cy<sub>3</sub>Sn(OCOH) suggesting slow formate transfer is concomitant with a decrease in activity.

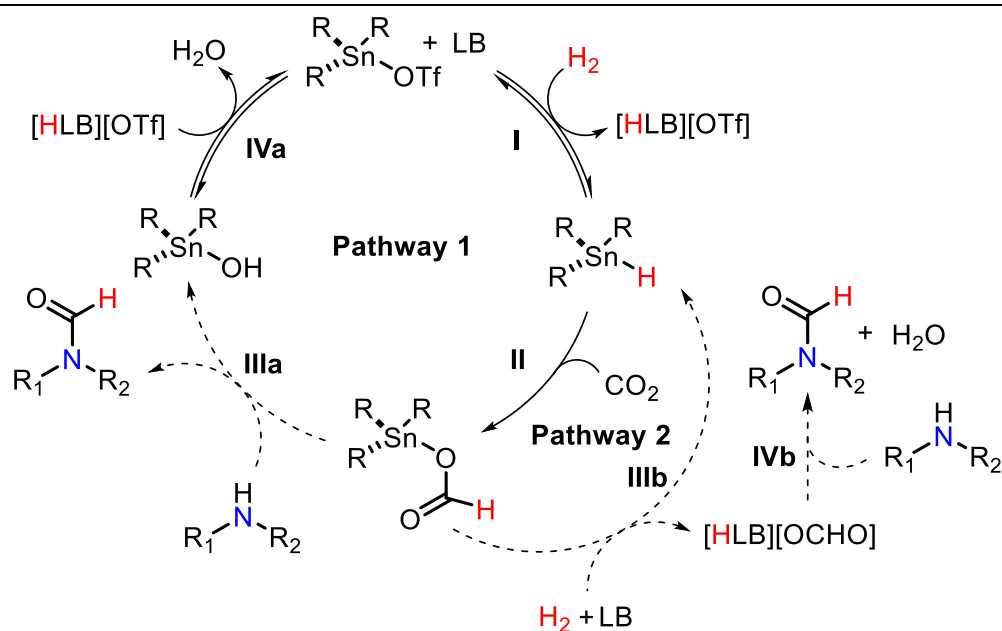


**Figure 2.4:** Proposed reaction mechanism for the N-formylation reaction with CO<sub>2</sub>, H<sub>2</sub> and Cy<sub>3</sub>SnOTf catalyst.

Based on our results, synthesis of postulated reaction intermediates and previous literature we propose the mechanism shown above (Figure 2.4). First, we posit that H<sub>2</sub> is split heterolytically into a R<sub>3</sub>Sn-H and an ammonium triflate salt (Step I) with 2,4,6-collidine as the base. Despite morpholine also being a suitable base for the activation of CO<sub>2</sub>, morpholine tends to react with CO<sub>2</sub> forming a carbamate lowering

the *in-situ* basicity of morpholine. This is supported by the addition of 2,4,6-collidine increasing the activity (see table 2.2). Secondly, CO<sub>2</sub> is reduced by insertion into the Sn-H bond forming R<sub>3</sub>Sn-OCHO as is also the case for hydrosilanes. Facile insertion of CO<sub>2</sub> into tin hydrides has been previously demonstrated.<sup>81</sup> However, attempted reduction of CO<sub>2</sub> to tin formate without the amine substrate resulted in the hydrogenation of the aromatic ring of 2,4,6-collidine indicating that the CO<sub>2</sub> reduction is base assisted as is the case for hydrosilane reductants. Synthesis and direct reaction of tin formate with morpholine was fast and efficiently produced the formamide product. Formate transfer was found to even proceed under high partial pressures of CO<sub>2</sub> and was uninhibited at 6 bar or 30 bar. This suggests that the lower partial pressures required for the overall reaction may be due to higher partial pressures of CO<sub>2</sub> affecting the hydrogen activation step. This may proceed *via* the carbamic acid, that is formed, rendering hydrogen activation reversible *via* protonation of the Sn-H bond. The formation of the formamide product may be formed in one of two ways; 1) as described above the substrate interacts with the tin formate generating the formamide and a tin hydroxide which can be protonated by the ammonium triflate eliminating water and regenerating the catalyst (Steps IIIa and IVa). To test if step IVa is possible we synthesised Cy<sub>3</sub>SnOH and morpholinium triflate (added in catalytic amounts (10 mol%)) to replicate this step. Within 24hrs the reaction did occur, however, it was 9x slower than starting the reaction from Cy<sub>3</sub>SnOTf suggesting that while this step is possible it may not be the main pathway. Alternatively, pathway 2) (steps IIIb and IVb) the formate group may be eliminated by hydrogenation from the tin centre leading to the direct reaction of morpholine and formate, which is a known pathway for transition metal catalyst (Scheme 3 steps IIIb and IVb). Starting the reaction from Cy<sub>3</sub>SnOCOH and morpholinium triflate results in the same rate as starting from Cy<sub>3</sub>SnOH and morpholinium triflate suggesting that this reaction may proceed *via* the slow R<sub>3</sub>SnOH cycle. On the other hand, starting the reaction with [Cy<sub>3</sub>SnOCOH : 2,4,6-collidine] results in twice the activity in the N-formylation of morpholine compared to when morpholinium triflate is included suggesting that very little morpholinium triflate is formed during the overall reaction.

In conclusion, we have developed an efficient system in which Sn/N FLPs can catalytically reduce CO<sub>2</sub> in the presence of amines and H<sub>2</sub> gas to form formamides. We found that R<sub>3</sub>SnX LAs and 2,4,6-collidine can efficiently catalyse the N-formylation of morpholine with a max TON > 300 and a TOF of 1.16h<sup>-1</sup>. We also found that Sn/N FLPs are selective for the reduction of CO<sub>2</sub> over other reducible functional groups leading to the synthesis of various functionalized amides. Catalyst optimization showed that upon varying the R groups from <sup>i</sup>Pr to Cy resulted in an increased in a 2-time increase in stability and a 4-time increase in activity. With these improvements in mind, we have shown that FLPs have the potential to

replace the very selective main group hydrides for the valorization of CO<sub>2</sub> to amides while maintaining functional tolerance.

#### 4.2 Frustrated Lewis Pairs Catalyse the Solvent-Assisted Synthesis of Azoles from *ortho*-Substituted Anilines, CO<sub>2</sub> and H<sub>2</sub>

While the [R<sub>3</sub>SnX : 2,4,6-collidine] FLPs catalyse the selective N-formylation of secondary aliphatic amines, the system was completely unreactive towards aromatic amines.<sup>79</sup> To address the issues, we undertook a study on the synthesis of azoles from *ortho*-substituted anilines. *Ortho*-substituted anilines, in contrast to aniline, form heterocyclic products upon N-formylation and cyclization (Figure 3.1), which acts as a thermodynamic driving force for the reaction. The N-formylation of *ortho*-substituted anilines can be achieved using CO<sub>2</sub> and H<sub>2</sub> in the presence of a transition metal complex of Pd,<sup>59</sup> Ru,<sup>59</sup> Co<sup>82</sup> and with Au<sup>83</sup> nanoparticles, however high catalyst loadings (of 5-10 mol%) are a prerequisite for high activity. Therefore, new strategies are required for the synthesis of azoles from *ortho*-substituted anilines utilizing CO<sub>2</sub> and H<sub>2</sub>.

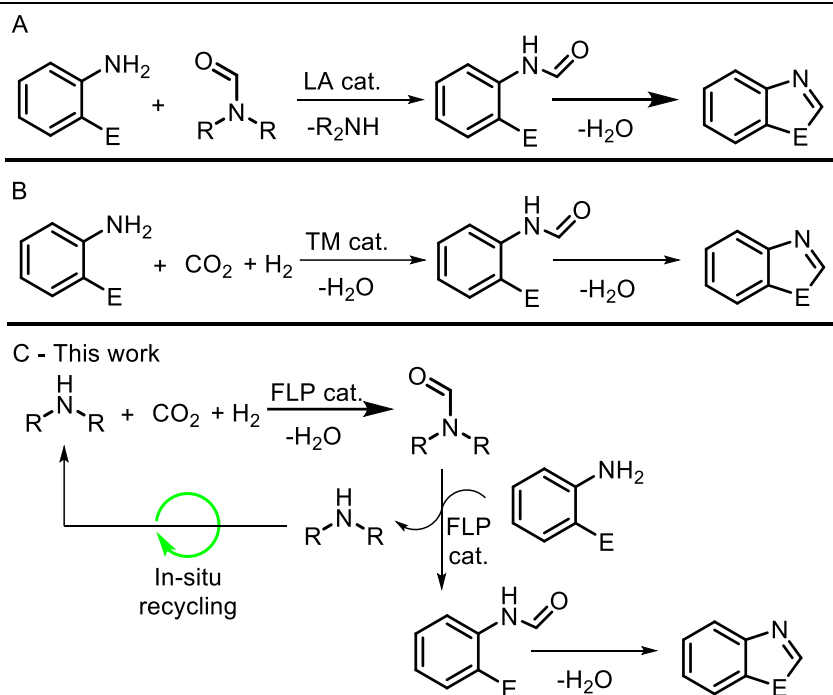


**Figure 3.1:** A) formation of azoles from *ortho*-substituted anilines using a formamide as a C1 source catalyst by a Lewis acid. B) Reductive coupling of CO<sub>2</sub> to *ortho*-substituted anilines in the presence of H<sub>2</sub> for the synthesis of azoles. C) Formylation of aliphatic amines and in situ transfer to an *ortho*-substituted aniline to form azoles catalysed by an FLP.



Frustrated Lewis pairs (FLPs) are a potential alternative to transition metal complexes for catalytic N-formylation of *ortho*-substituted anilines as they can hydrogenate CO<sub>2</sub> in the presence of H<sub>2</sub> for the reductive coupling of CO<sub>2</sub> and aliphatic amines.<sup>79</sup> Due to the ability of FLPs to complete the N-formylation reaction, we propose a method in which an aliphatic amine is N-formylated and then transfers the formyl group *in situ* to *ortho*-substituted aniline. The transfer simultaneously recycles the amine and since it is a LA catalysed reaction it would be effective with an FLP catalyst (figure 3.1C). Initially the reaction to convert *ortho*-phenylenediamine to benzimidazole was attempted using R<sub>3</sub>SnX-based FLPs in combination with N-methylmorpholine (0.05 mol%) (NMM) as a Lewis base in pure sulfolane at 180°C, H<sub>2</sub> (96 bar) and CO<sub>2</sub> (4 bar), which resulted in a TOF of only 0.22 h<sup>-1</sup>. Upon increasing the amount of NMM to promote 'encounter complex' formation the activity increased to 0.48 h<sup>-1</sup> at 1000 mol% of NMM. The increase in rate was only observed for high concentrations of NMM and not at 100 mol% which may suggest that an increase in NMM may assist the reaction in ways other than assisting H<sub>2</sub> activation. Increased concentrations of NMM may also activate *ortho*-phenylenediamine *via* deprotonation, increasing its nucleophilicity and its reactivity with Cy<sub>3</sub>Sn(OCOH), the formylation agent. Therefore, we posited the use of aliphatic amines as a surrogate, which would be preferentially formylated and transfer formylate *ortho*-phenylenediamine *in situ* as is the case with hydrosilanes and DMF.<sup>84,85</sup>

Polyethyleneimine (600 MW, PEI) was selected as the surrogate amine due to its ability to act as a LB and its ability to be N-formylated. Upon addition of 0.1 mL of PEI to the reaction the activity increased 10-fold to 2.23 h<sup>-1</sup> which further increased to 11.8 h<sup>-1</sup> in a 1:1 mixture of PEI : sulfolane. The activity increase further to 16.8 h<sup>-1</sup> upon replacement of the sulfolane for NMM (1:1 mix of NMM : PEI) likely due to amines, like NMM, being able to solubilise CO<sub>2</sub> well as well as increasing the likelihood of 'encounter complex' formation. The TOF of 16.8 h<sup>-1</sup> matches the activity of the best ruthenium catalyst for the reaction (12.1 h<sup>-1</sup>) under equivalent pressures. Morpholine was also found to act as an N-formylation surrogate and transfer formylation agent leading to similar activity as PEI.

To understand the reaction pathway, we attempted several control experiments (Figure 3.2). Firstly, we attempted to hydrogenate the product of CO<sub>2</sub> capture by *ortho*-phenylenediamine, 2-hydroxybenzimidazole, which proved unsuccessful ruling out the possibility of urea's involvement and its hydrogenation in the reaction mechanism. In the case of the reaction without PEI, to test whether [Cy<sub>3</sub>SnNTf<sub>2</sub> : NMM] was able to cyclise the formylated *ortho*-phenylenediamine, 2-aminoacetanilide was added to the reaction and was quantitatively cyclised. The synthesis of benzimidazole under the same conditions resulted in 65% yield suggesting the cyclisation is not rate determining. To test whether the

formylated PEI could act as a formate transfer agent, PEI was formylated without the presence of *ortho*-phenylene diamine, isolated *ex-situ* and then reacted directly with *ortho*-phenylenediamine, which resulted in the formation of benzimidazole at temperatures above 140°C (Figure 3.2C).

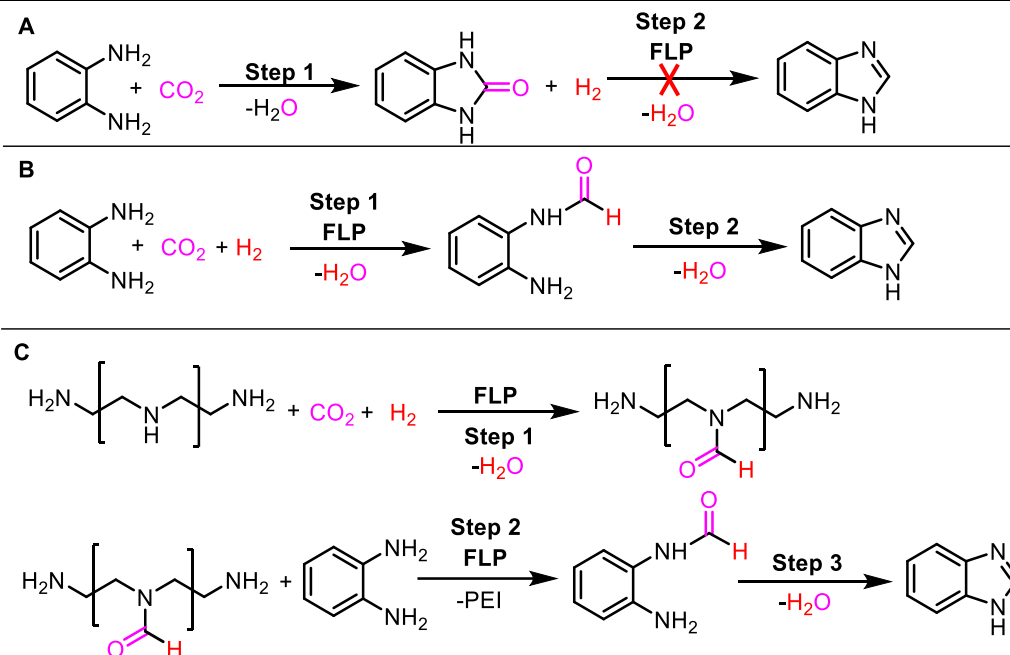


**Figure 3.2:** Possible pathways for benzimidazole synthesis from *ortho*-phenylenediamine, CO<sub>2</sub> and H<sub>2</sub> catalysed by FLPs.

With an efficient system in place, a substrate scope was conducted with various *ortho*-substituted anilines (Figure 3.3). The substrate scope was conducted at catalyst loading of 0.2 – 1.0 mol% and in mixtures of 1:1 or 4:1 NMM:PEI. Primary diamines with alkyl ring substituents, **1-3**, were efficient formylated and cyclised. Substrates containing methoxy (**4**) and halides (**5&6**) were also converted to their respective azoles. Interesting substrates **5** and **6** also resulted in some benzimidazole. This is the result of catalytic dehalogenation by the FLP and may be the reason for poor product yield. Substrate **7** containing the ester functionality was found to be unreactive. Substrates with N-substituents (**8** and **9**) were both converted to the desired azole with minimal loss in activity. Indicating increased N bulk does not hinder the reaction. Substrate **10** resulted in the selective synthesis of two different products depending on CO<sub>2</sub> partial pressure (Figure 3.4). At higher partial pressures **10b** was formed with the imine functionality intact and at lower partial pressures the imine functionality was also hydrogenated forming **10c**. Interestingly both molecules are drug precursors with **10c** being a precursor to quinethazone (antihypertensive and diuretic), fenquizone (diuretic) and methaqualone (sedative and hypnotic).<sup>86</sup>

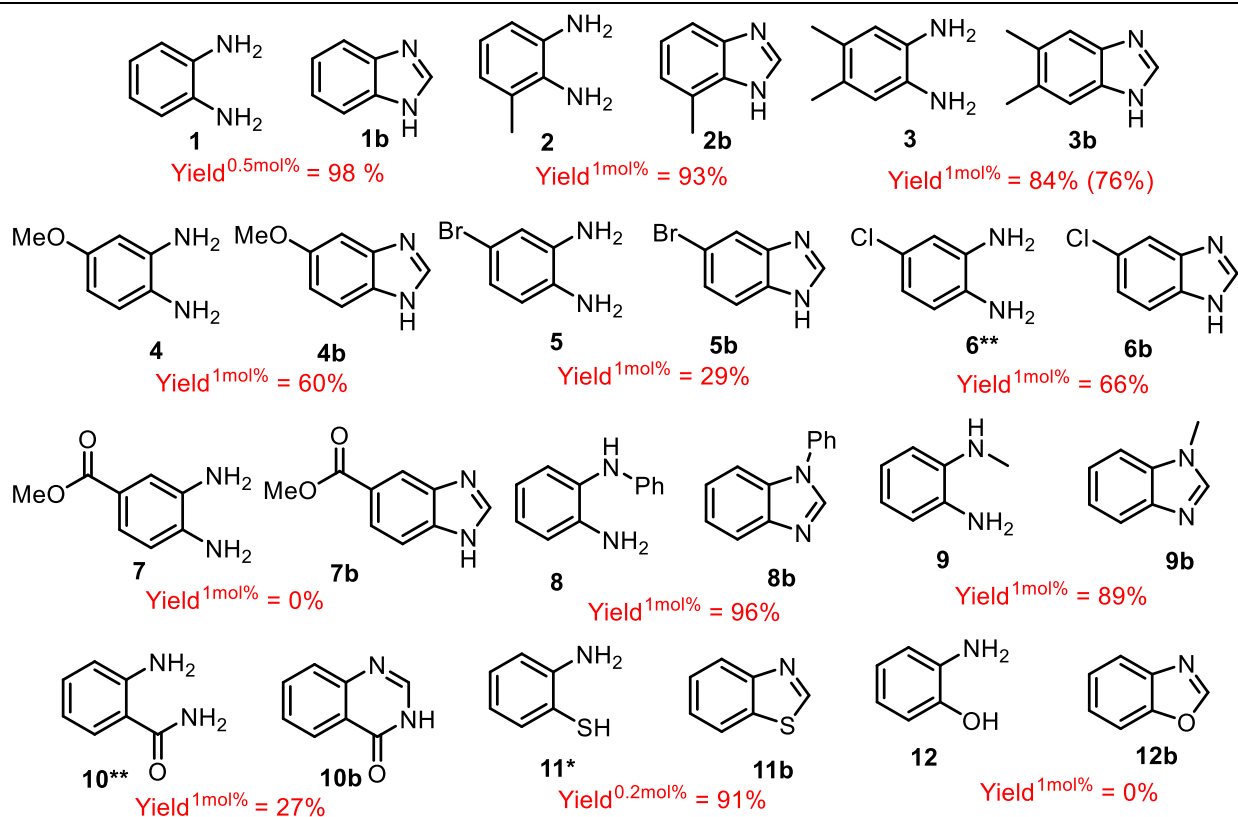


**Figure 3.3:** Substrate scope for the tandem synthesis of azoles with CO<sub>2</sub>, H<sub>2</sub> and [Cy<sub>3</sub>SnNTf<sub>2</sub>: NMM] catalyst. Reaction conditions: amine (10 mmol), NMM (4 mL), LA (0.01 mmol), 1 mL PEI, CO<sub>2</sub> (4 bars), H<sub>2</sub> (96 bars), 180 °C, 22 hrs; the yields were determined by <sup>1</sup>H NMR with an internal standard, and the structures were confirmed by GC-MS. Yield in brackets indicates isolated yield. Superscripts indicate catalyst loading. \*DBU instead of NMM. \*\*10 bars CO<sub>2</sub> instead of 4 bars CO<sub>2</sub>.

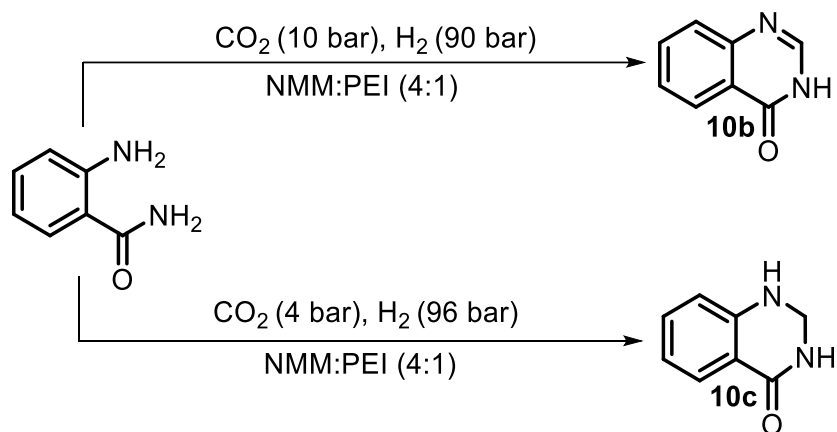


**Figure 3.4:** Pressure controlled synthesis of 10b or 10c starting from 2-aminobenzamide.

Lastly, substrates containing a non-nitrogen *ortho*-heteroatom (**11** & **12**) were tested. Whilst benzothiazole was efficiently formed in the presence of DBU (replacing NMM) benzoxazole did not form as observed with transition metal catalysts.

In conclusion, we were able to develop an efficient solvent-assisted synthesis of azoles from CO<sub>2</sub> using H<sub>2</sub> as the reductant. Secondary amines increase the reaction rate in several ways, most importantly by acting as a scaffold, which is preferentially formylated and then transfers the formate to the substrate, which then cyclises forming the desired product. For this purpose, mixtures of NMM: PEI lead to the highest increase in activity compared to pure sulfolane. As a result, the TOF of 16.8 h<sup>-1</sup> is on par with the best transition metals for this reaction. This strategy of producing a transfer formylation source *in-situ* and recycling the amine may provide a way to increase the number of efficient systems for the synthesis of azoles from CO<sub>2</sub> and H<sub>2</sub>.

### 4.3 Hexacoordinated tin complexes catalyse imine hydrogenation with H<sub>2</sub>

The use of Sn-based Lewis acids in FLP catalysed hydrogenations are so far limited to the use of R<sub>3</sub>SnX LAs,<sup>18,21,79,87</sup> which are limited in scope and hence steric and electronic properties. Equally, triaryl Lewis acid of boron, aluminium, gallium and indium have a narrow margin of maneuverability for electronic and steric tuning while maintaining stability of the LA.<sup>88,89</sup> Particularly, they lack the structural diversity of transition metal complexes, which use ligands to fine-tune the properties of the complexes.

Therefore, we sought to use coordination complexes of tin, namely Schiff base complexes, to expand upon the LAs that can achieve FLP catalysed hydrogenations of functional groups. Schiff bases were chosen as ligands as they can stabilise various oxidation states of tin and tin salen complexes are known Lewis acid catalysts.<sup>89,90</sup> Moreover, their ability to act as hydrogenation catalysts was tested on the FLP model reaction of imine hydrogenation (Figure 4.1).

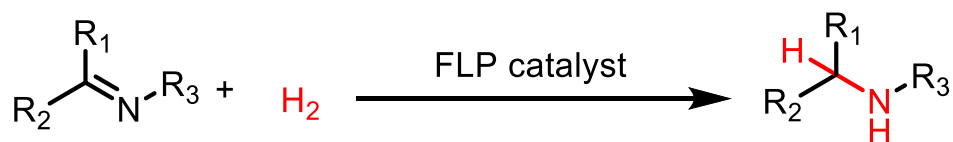
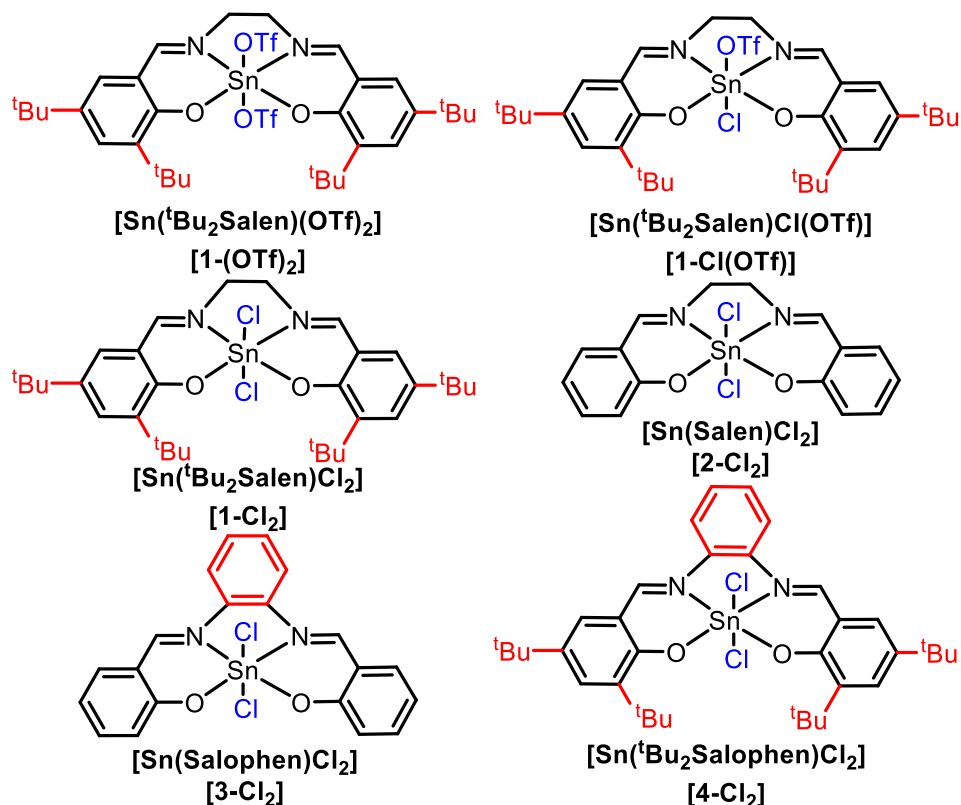
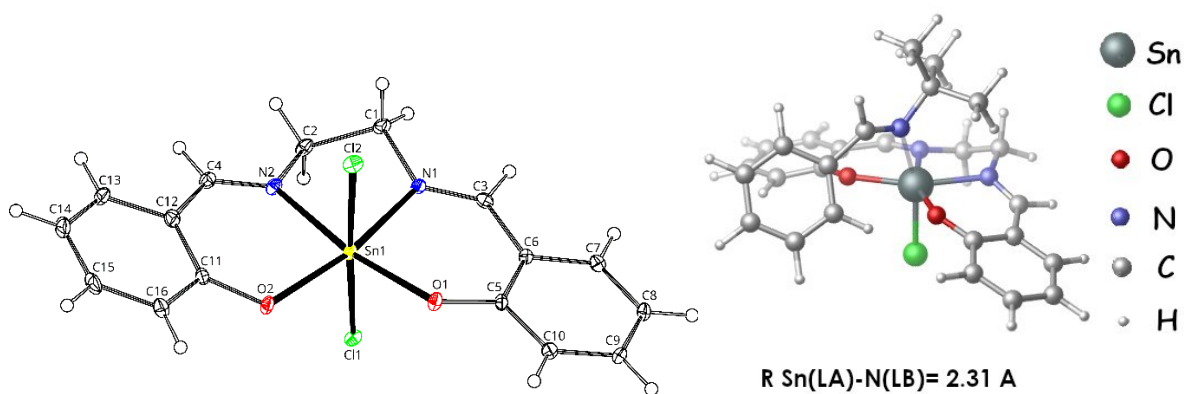


Figure 4.1: Hydrogenation of imines with H<sub>2</sub> catalysed by FLP catalysts.



**Figure 4.2:** Structures of Schiff base complexes of tin used in this study for the hydrogenation of imines.

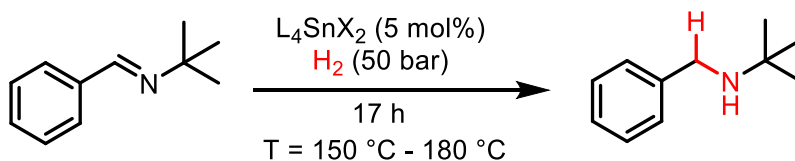
In this study we used complexes of the  $L_4SnX_2$  type where  $L = \text{salen}$ ,  $^{t\text{bu}}\text{salen}$ ,  $\text{salophen}$  and  $^{t\text{bu}}\text{salophen}$  and  $X = \text{Cl}$  or  $\text{OTf}$  for the hydrogenation of imines (Figure 4.2). A crystal structure of  $[2-\text{Cl}_2]$  is shown below (Figure 4.3) and the DFT calculated structure of its FLP with *N-tert*-butyl-1-phenylmethanimine.



**Figure 4.3:** (A) X-ray structure of  $[2-\text{Cl}_2]$  and (B) calculated FLP structure at the DSD-PBEB86-D3BJ/def2-QZVP level.

Initial studies on the hydrogenation activity of the complexes elucidated that the ability to activate hydrogen gas was directly linked to coordination strength of the  $X$  group where  $1-(\text{OTf})_2 > 1-\text{Cl}(\text{OTf}) > 1-$

Cl<sub>2</sub>. Hydrogen activation was tested *via* HD scrambling and 1-(OTf)<sub>2</sub> and 1-Cl(OTf) scrambled HD (10 bar) at 25 °C and 60 °C respectively. Whereas 1-Cl<sub>2</sub> showed no ability to scramble HD gas under the conditions tested. This trend was further affirmed by the acceptor numbers (AN) of the complexes as calculated by the Guttmann-Beckett method where 1-(OTf)<sub>2</sub> > 1-Cl(OTf) > 1-Cl<sub>2</sub>. Incidentally 1-Cl<sub>2</sub> had an AN = 0 due to the lack of a free binding site due to the strong coordination of the Cl<sup>-</sup>. Indicating a free binding site via a labile ligand is required as a prerequisite of H<sub>2</sub> activation. Interestingly neither complex 1-(OTf)<sub>2</sub> or 1-Cl(OTf) displayed any ability to hydrogenate N-*tert*-butyl-1-phenylmethanimine at the temperatures required for hydrogen activation. This is in line with the high hydrogen ion affinity (HIA) of the complexes, 1-(OTf)<sub>2</sub> or 1-Cl(OTf), being high at 1170 and 660 kJ mol<sup>-1</sup> respectively and associated low hydride donor ability. Hydrogenation of imine, N-*tert*-butyl-1-phenylmethanimine, proceeded at 180 °C and at 50 bars of H<sub>2</sub>. Under these conditions, 1-Cl<sub>2</sub> was also an efficient catalyst suggesting that chloride becomes a sufficient leaving group under these reaction conditions (Table 4.1). Removing the bulk by replacing the *tert*-butyl groups (complex 2-Cl<sub>2</sub>) lead to an increase in yield from 23% to 53%.



ENTRY	CATALYST	SOLVENT	TEMPERATURE (°C)	YIELD (%)
1	1-(OTf) <sub>2</sub>	sulfolane	180	10
2	1-Cl(OTf)	sulfolane	180	49
3	1-Cl <sub>2</sub>	sulfolane	180	29
4	2-Cl <sub>2</sub>	sulfolane	180	53
5	3-Cl <sub>2</sub>	sulfolane	180	42
6	4-Cl <sub>2</sub>	sulfolane	180	28
7	1-(OTf) <sub>2</sub>	toluene	180	30
8	1-Cl(OTf)	toluene	180	86
9	1-Cl <sub>2</sub>	toluene	180	84
10	2-Cl <sub>2</sub>	toluene	180	98
11	1-Cl <sub>2</sub>	toluene	150	NR
12	2-Cl <sub>2</sub>	toluene	150	27
13	2-Cl <sub>2</sub>	collidine	180	85

**Table 4.1:** Optimisation of the hydrogenation of N-*tert*-butyl-1-phenylmethanimine by tin Schiff base complexes by varying the temperature, solvent and H<sub>2</sub> pressure of the reaction.

This suggests that the *tert*-butyl groups hinder the reaction and that increased steric hinderance decreases hydrogenation performance. Moving from salen to salophen there was a decrease in yield to 42% and 28% from 3-Cl<sub>2</sub> and 4-Cl<sub>2</sub> respectively.

With 2-Cl<sub>2</sub> we varied the solvent and found that toluene gave a quantitative yield of the desired amine and that it is a more suitable solvent for the reaction than sulfolane or collidine, which can also act as a Lewis base. Toluene also increased the performance of 1-(OTf)<sub>2</sub> and 1-Cl(OTf) likely as a result of the increased solubility of H<sub>2</sub> compared to sulfolane. Temperature also had a large effect on the reaction where a decrease in temperature lead to a decrease in yield with 2-Cl<sub>2</sub> from 98% to 28% at 180 °C and 150 °C respectively.

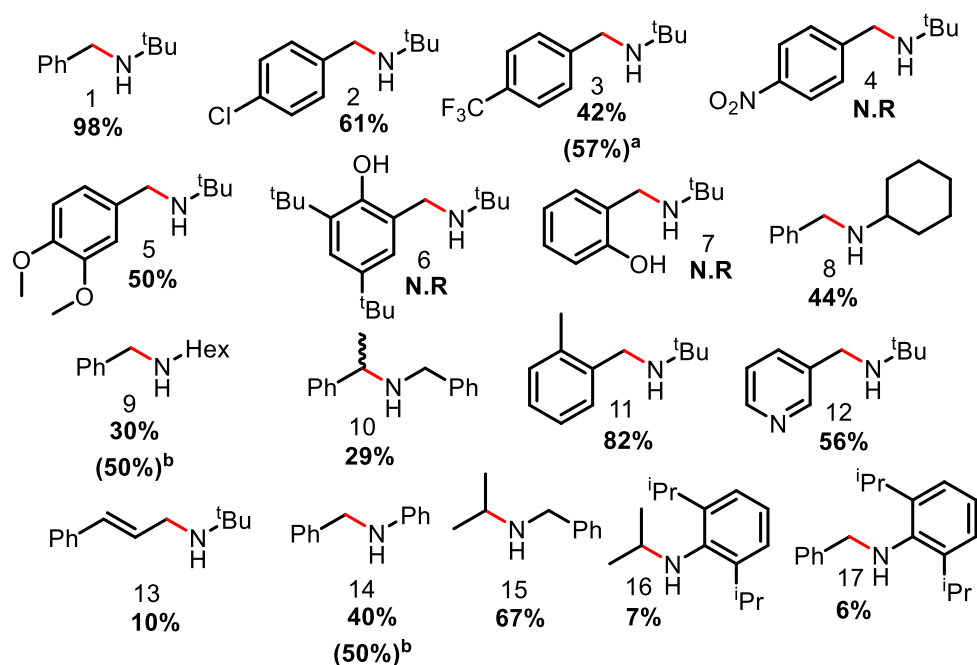


**Figure 4.4:** Substrate scope for the hydrogenation of imines by 2-Cl<sub>2</sub>. Reaction conditions: imine (1 mmol), toluene (4 mL) and LA (5 mol%), H<sub>2</sub> (50 bars), 180 °C, 17 h. All yields were determined by <sup>1</sup>H NMR with CH<sub>2</sub>Br<sub>2</sub> as the internal standard, and all structures were confirmed by ESI-MS. a) 70 bar b) Extended reaction time to 48 h.

With an efficient system at hand a series of imines were tested in the hydrogenation reaction catalysed by 2-Cl<sub>2</sub> at 180 °C, 50 bar of H<sub>2</sub> and in toluene (Figure 4.4). Substrate 1 was quantitatively hydrogenated under the reaction conditions. Substrates containing electron-withdrawing groups, **2-4**, decreased the activity of the system, and in the case of the nitro group, completely pacified the reactivity. This can be attributed to the Lewis base of the reaction, which is also the substrate, being less basic and therefore less likely to activate H<sub>2</sub> with 2-Cl<sub>2</sub>. Substrates containing methoxy groups (**5**) also lead to a

decrease in activity. Substrates containing hydroxy groups (**6** & **7**) ortho to the imine functionality completely stopped the reaction. This hydroxy substituent is Brønsted acidic and therefore the inhibition may be attributed to reversible hydrogen activation by protonation of the tin hydride. Varying the alkyl substituents (**8** to **17**) from *tert*-butyl to -Hex, -Cy, -Ph, -Bn resulted in the formation of the target amine, with the notable tolerance of the *ortho*-methyl substituent (**11**).

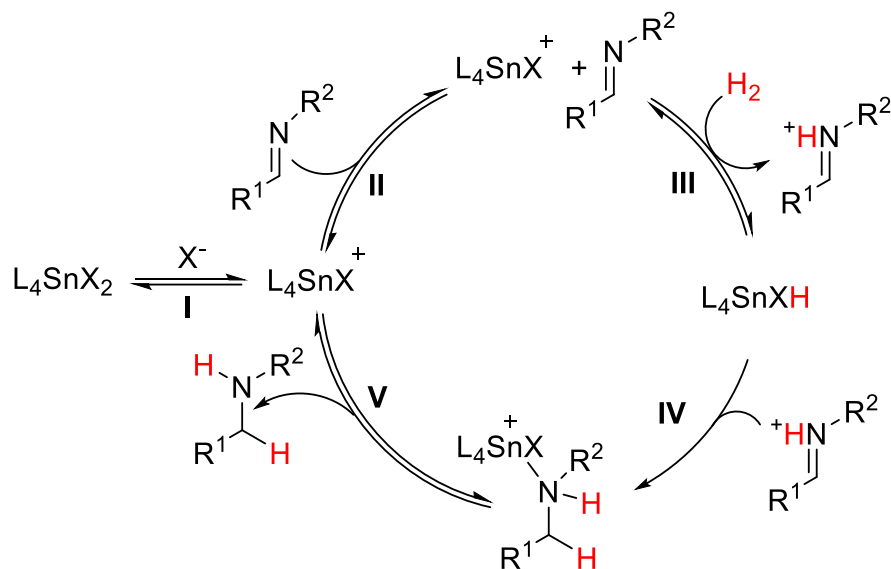


**Figure 4.4:** Proposed catalytic cycle for the hydrogenation of imines catalysed by tin (IV) salen complexes.

The substrate acts as the LB in both sulfolane and toluene as the tin(IV) salen complexes and the solvent lack the ability to do so by themselves. As mentioned, previously a free binding site must be available to activate H<sub>2</sub> gas and in accordance with previous literature the following catalytic cycle was proposed (Figure 4.4). Initially the X ligand dissociates from the tin centre (step I) after which an ‘encounter’ complex is formed by the newly generated L<sub>4</sub>SnX<sup>+</sup> species and the substrate. This then activates H<sub>2</sub> gas generating a tin hydride and an iminium salt (steps II & III). The tin hydride species inserts the iminium cation generating an amine L<sub>4</sub>SnX complex, which dissociates regenerating the active catalyst L<sub>4</sub>SnX<sup>+</sup>.

In conclusion, we have developed a series of tin(IV) Schiff base complexes that expands the current library of Lewis acids used in FLP that can scramble HD gas and be used in catalytic hydrogenations. The hexacoordinated tin(IV) salen and salophen complexes are easily sterically and electronically modified for further fine tuning of reactivity. Optimization of reaction conditions for imine hydrogenation revealed optimal reaction conditions of 180 °C and 50 bar H<sub>2</sub> gas in toluene. Interestingly the catalyst, which displayed the lowest ability to activate hydrogen gas, was the most efficient catalyst for imine



hydrogenation suggesting that hydrogen activation is not rate limiting, which is rare for FLP mediated hydrogenations. We believe that the use of main group metal complexes will allow access to new chemoselectivity and reactivity accessible with FLP hydrogenation catalysts.

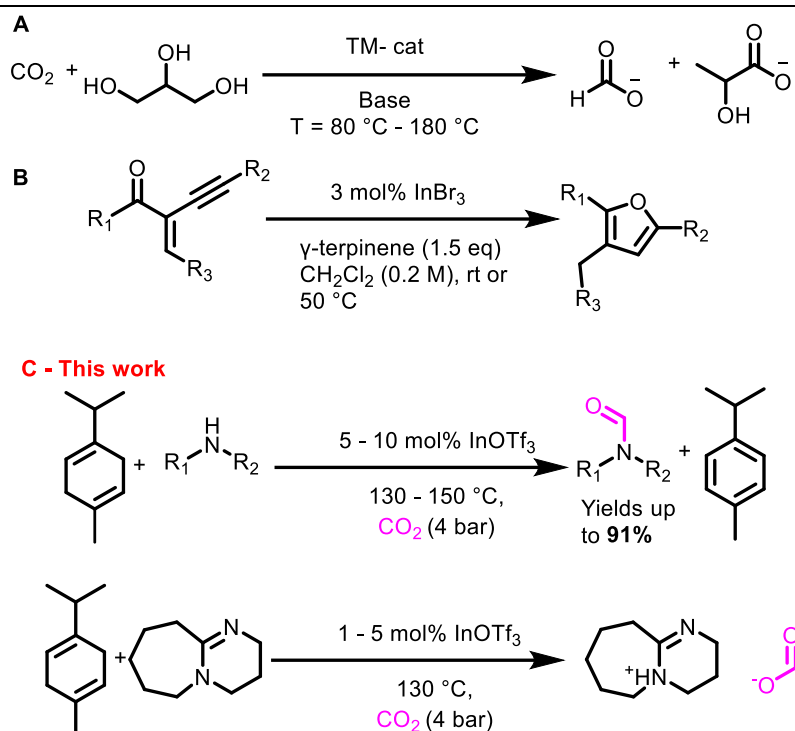
#### 4.4 Unpublished results – Indium(III) triflate catalyses the transfer-hydrogenation of CO<sub>2</sub> to formate for the N-formylation of amines.

Transition metals catalyse the N-formylation of amines with CO<sub>2</sub> and H<sub>2</sub> but are oftentimes not chemoselective for CO<sub>2</sub> reduction over other reducible functional groups.<sup>49,52,60</sup> Similarly, FLPs also catalyse the N-formylation of amines with CO<sub>2</sub> and H<sub>2</sub> but, unlike the TM catalysts, are chemoselective for CO<sub>2</sub> hydrogenation.<sup>79,87</sup> However, the operating pressures required reach 100 bar of total pressure of which 96 bar is hydrogen gas and only 4 bars is CO<sub>2</sub>. Whilst H<sub>2</sub> is the most atom economic hydride source there are issues with its generation, high storage and compression costs.<sup>91,92</sup> Moreover, high-pressure plants and specialized equipment are needed for its practical and safe utilization. One alternative to using hydrogen gas is auxiliary hydride sources or H<sub>2</sub> surrogates such as hydrosilanes. However, there are also disadvantages to using hydrosilanes or boranes. One notable disadvantage is that hydrosilanes or boranes generate undesirable reaction waste in the form of silanols, boronic acids and oxides of both boron and silicon.<sup>63,78</sup>

Potential alternatives are so called ‘transfer hydrogenation sources’, which are organic molecules that can have a hydride abstracted by a Lewis acid and transferred to the desired substrate such as CO<sub>2</sub>. A major advantage of transfer hydrogenation sources is that useful byproducts are produced as part of these reactions, for example, p-cymene (from oxidation of  $\gamma$ -terpinene) is an important flavouring agent, it also has medicinal uses, and it is a common ligand in transition metal chemistry.<sup>93,94</sup> Other common byproducts from transfer hydrogenation are acetone (from oxidation of isopropanol), which is a common laboratory solvent and lactic acid (from glycerol oxidation) is a common preservative and flavouring agent in food production.<sup>95–98</sup>

Transfer hydrogenation sources have been used in conjunction with a wide variety of metals such as Ru<sup>99</sup>, Ir,<sup>100</sup> Co,<sup>101</sup> Mn,<sup>102</sup> Fe,<sup>103</sup> Al,<sup>104</sup> Ga<sup>105</sup> and In<sup>106</sup> to hydrogenate nitriles,<sup>107,108</sup> ketones<sup>109</sup> and alkenes<sup>105</sup> amongst other functional groups.<sup>102,103,106</sup> Ru<sup>99</sup> and Ir,<sup>100</sup> are also known to transfer hydrogenate CO<sub>2</sub> to both formic acid and methanol with the aid of a sacrificial base and an alcohol hydride source (Scheme 5.1A). The requirement of sacrificial base decreases the overall atom economy and, along with

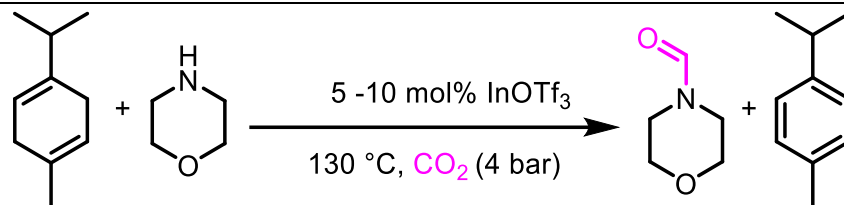
the use of high pressures, represents an area for improvement within CO<sub>2</sub> transfer hydrogenation reactions (CO<sub>2</sub>TH).



**Scheme 5.1:** A) General scheme of transfer hydrogenation of CO<sub>2</sub> to formate catalysed by transition metal complexes (cations are omitted for clarity) B) Indium catalysed Transfer hydrogenation of 2-Alkynyl Enones for the reductive cyclisation towards trisubstituted furans C) Indium catalysed transfer hydrogenation of CO<sub>2</sub> and reductive coupling to amines and Indium catalysed hydrogenation of CO<sub>2</sub> to formate.

Successful CO<sub>2</sub>TH reductive coupling reactions could open an avenue to upcycle CO<sub>2</sub> and simultaneously form useful by-products, which would increase the economic efficiency of the process. InX<sub>3</sub> Lewis acids have been shown to effectively catalyse transfer hydrogenations using  $\gamma$ -terpinene<sup>106</sup> (Scheme 5.1B) suggesting that they are a compatible hydride/LA combination hence they were selected as the starting point for main group LA catalysed CO<sub>2</sub>TH towards reductive coupling of CO<sub>2</sub> to amines in this study.

In this study we demonstrate that commercially available Indium triflate catalyses CO<sub>2</sub>TH with  $\gamma$ -terpinene to [DBUH][formate] and *p*-cymene as the co-product, when DBU is employed as a base (Scheme 5.1C), and reductive coupling of CO<sub>2</sub> to amines to yield N-formyl amines and *p*-cymene as the co-product (Scheme 5.1C and 5.2).



**Scheme 5.2:** Transfer hydrogenation reactions of CO<sub>2</sub> and reductive coupling to morpholine catalysed by indium triflate. Solvent: DMSO (2 mL), N-methylmorpholine (1 mL) and  $\gamma$ -terpinene (1 mL).

To study the reaction, morpholine was selected as the model substrate. Initial optimization disclosed that Indium triflate is the most efficient and suitable catalyst when compared to other metal triflates due to its high acidity, hydrolytic stability and low toxicity (Table 5.1).<sup>110,111</sup>

Entry	LA	LB	Temp (°C)	CO <sub>2</sub> Pressure (bar)	Time (hours)	Yield (%)
1	GaOTf <sub>3</sub>	NMM	130	4	48	56
2	InOTf <sub>3</sub>	NMM	130	4	48	65
3	YbOTf <sub>3</sub>	NMM	130	4	48	30
4	AlOTf <sub>3</sub>	NMM	130	4	48	32
5	InCl <sub>3</sub>	NMM	130	4	48	31
6	InOTf <sub>3</sub>	DBU	130	4	48	26*
7	InOTf <sub>3</sub>	2,4,6 -col	130	4	48	31
8	InOTf <sub>3</sub>	NMM	130	4	48	26**

**Table 5.1:** Optimisation of Lewis acid for the CO<sub>2</sub>TH reaction and subsequent reductive coupling to morpholine. DMSO (2 mL), N-methylmorpholine (1 mL),  $\gamma$ -terpinene (1 mL), catalyst (10 mol%) \* Formation of 0.6 mmol formic acid (equivalent to 13 turnovers) \*\* Run with 0.5 mol% of InOTf<sub>3</sub> which achieved 52 turnovers

The initial reaction pressure, solvent, catalyst loading, and Lewis bases were selected based on the results of our previously reported N-formylation reactions.<sup>79,87</sup> Temperature and quantity of transfer hydride source were selected based on other main group Lewis acid catalysed transfer hydrogenation reactions. The optimization of the solvent revealed that a large excess of  $\gamma$ -terpinene is required for the reaction to proceed efficiently but above 1 mL (ca. 6-time excess) there was no perceived increase in activity (Table 5.2). This is in line with other transfer hydrogenation reactions, where the hydride source is usually used in excess.<sup>103,106,108,112,113</sup> The removal of either DMSO or N-methylmorpholine (NMM) decreased the activity likely due to N-methylmorpholine's role as the Lewis base required for deprotonation of a

Wheland intermediate, which is the proposed intermediate after hydride abstraction from  $\gamma$ -terpinene. Other bases such as DBU and 2,4,6-collidine were tested and the N-formylation reaction did not proceed efficiently (see appendix 4 table S1). DMSO is necessary to solubilise all reactants in particularly carbamate salts formed from the reaction of morpholine with CO<sub>2</sub>. The reaction was found to be temperature dependent with increasing yields from 90 °C to 150 °C (19% to 49% over 22 hrs). Full conversion was achieved upon running the reaction for 48 hrs at 150 °C and 4 bars of CO<sub>2</sub>.

Entry	DMSO / NMM / $\gamma$ -terp (mL)	Temperature (°C)	InOTf <sub>3</sub> (mol%)	Yield (%)
1	2.0 / 1.0/ 0.5	90	10	15
2	2.0 / 1.0 / 1.0	90	10	19
3	2.0 / 1.0 / 1.5	90	10	17
4	2.5/ 0.5 / 1.0	90	10	12
5	1.5/ 1.5 / 1.0	90	10	11
6	2.0 / 1.0 / 1.0	110	10	29
7	2.0 / 1.0 / 1.0	130	10	35
8	2.0 / 1.0 / 1.0	150	10	49
9 <sup>a</sup>	2.0 / 1.0 / 1.0	130	5	65
10 <sup>a</sup>	2.0 / 1.0 / 1.0	150	10	91
11	2.0 / 1.0 / 1.0	130	0	0

**Table 5.2:** Effect of solvent and of temperature on the InOTf<sub>3</sub> catalysed transfer hydrogenation of CO<sub>2</sub> and its reductive coupling to amines. Reaction conditions: Morpholine (1 mmol), LA = InOTf<sub>3</sub>, CO<sub>2</sub> (4 bar), 22 hrs, average yield after three runs. Yields were determined by <sup>1</sup>H NMR with an internal standard. a) 48 hrs. NMM,  $\gamma$ -terpinene and DMSO were both used as received without further drying or purification.

With an efficient system at hand, we investigated the substrate scope (Figure 5.1) of the reaction. The substrate scope was initially investigated with 10 mol% catalyst loading and reaction times of 48hrs to achieve high conversions. However, at 150 °C and at 10 mol% catalyst loading some substrates did not proceed efficiently, likely due to the elevated temperatures and the catalyst promoting the decomposition of the product and/or formate, which is known to occur at these temperatures. To test whether or not In(OTf)<sub>3</sub> catalyses the decomposition of formic acid we added formic acid and In(OTf)<sub>3</sub> to an NMR tube containing DMSO and NMM and heated it to 130 °C. At 130 °C the formic acid decomposed into hydrogen gas overnight. Therefore, the remainder of the scope was run at 130 °C and with 5 mol% catalyst loading.

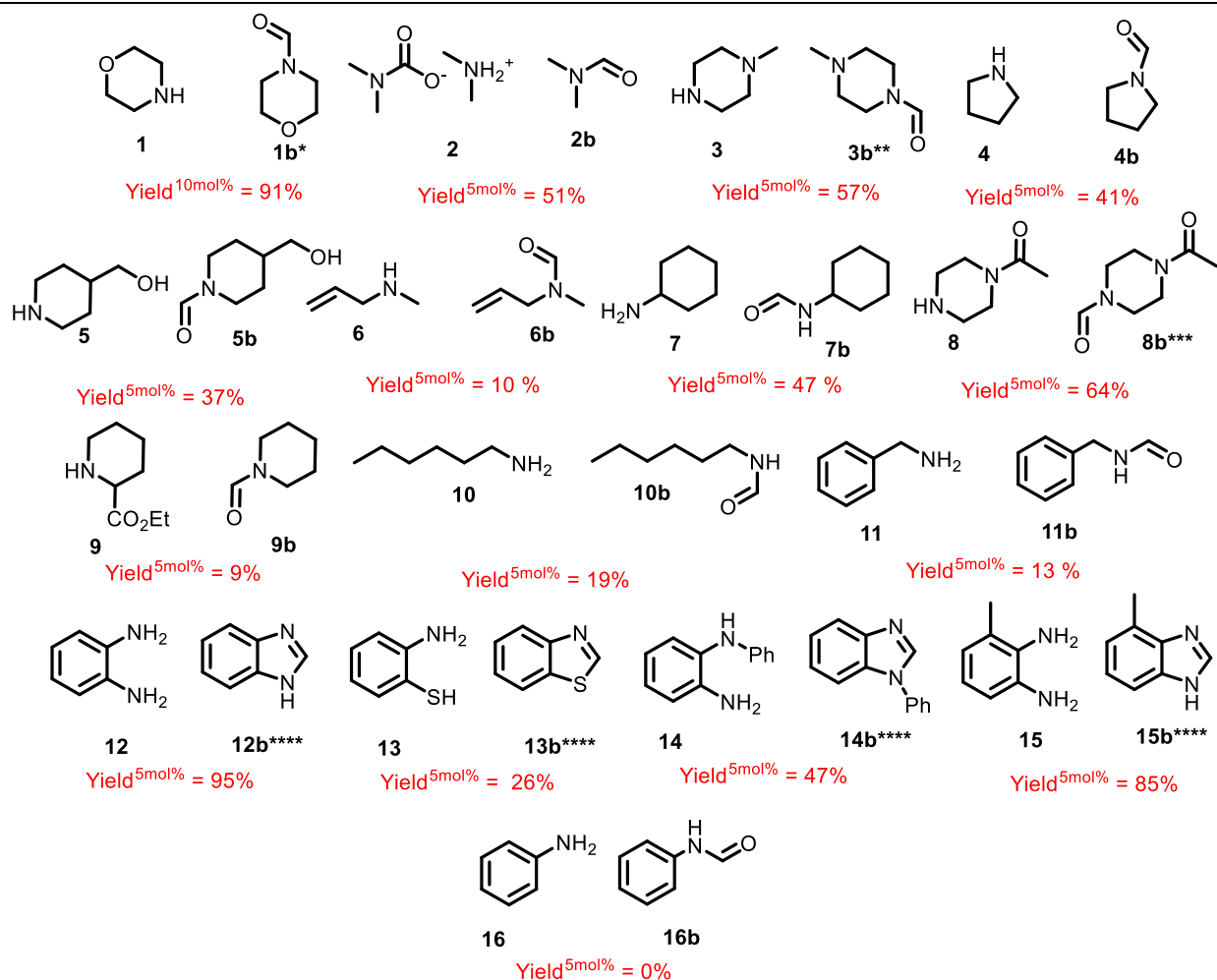
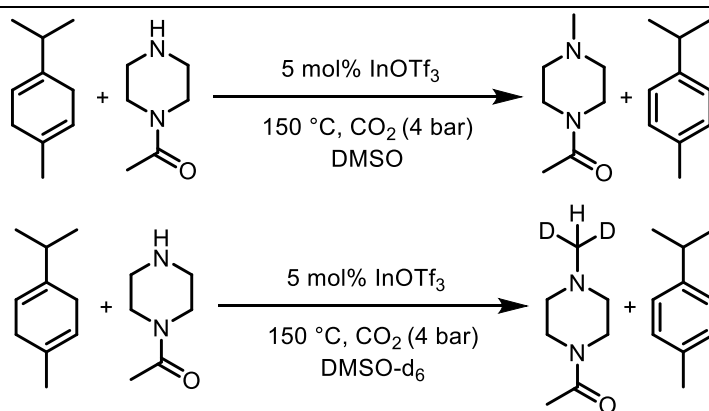


**Figure 5.1:** Substrate scope for the N-formylation reaction with CO<sub>2</sub>,  $\gamma$ -terpinene and InOTf<sub>3</sub> catalyst. Reaction conditions: amine (1 mmol), DMSO (2 mL), NMM (1 mL),  $\gamma$ -terpinene (1 mL), LA (5 mol%), CO<sub>2</sub> (4 bars), 130 °C, 48 h. Yields were determined by <sup>1</sup>H NMR and structures confirmed by GC-MS. \* Reaction run at 150 °C \*\* reaction run for 24 h at 130 °C and with 6 bars CO<sub>2</sub>. \*\*\* reaction run with 6 bars CO<sub>2</sub>. \*\*\*\* 0.1 mL of polyethyleneimine (MW = 1200) added.

Alkyl amines such as morpholine (**1**), dimethylammonium dimethyl carbamate (**2**) N-methylpiperazine (**3**) and pyrrolidine (**4**) were all successfully formylated. The system was found to be functionally tolerant towards the presence of alcohols (**5**) and alkenes (**6**) with no evidence of concomitant reduction of the unsaturated bond. InOTf<sub>3</sub> was able to formylate primary amines like **7**. **7** showed evidence of N-cyclohexyl-N-methylformamide as well in 10% yield. Interestingly there was no evidence of N-formylation of acetyl-piperazine (**8**), instead the reaction furnished only the N-methylated product. DMSO is also a known C1 synthon for the N-methylation of amines. The reaction is catalysed by formic acid, which is formed by CO<sub>2</sub>TH *in situ* prior to the N-formylation. To test whether the carbon source in the N-methylation reaction was CO<sub>2</sub> or DMSO the reaction was run with DMSO-d<sub>6</sub> as a solvent, which showed that the carbon source

was DMSO, as evidenced by the GC-MS giving a spectrum in which each of the species' mass increased by 2 mass units (see appendix 4 section 8.2). Substrate **3** demonstrated some N-methylated products as well which were detected by GC-MS. To achieve N-formylation of **3** and **8** the reactions were performed at a lower temperature and at an increased CO<sub>2</sub> pressure to disfavour the DMSO decomposition pathway and favour CO<sub>2</sub> hydrogenation. This resulted in a yield of 57% and 64% for **3b** and **8b** respectively. The ester functionality of substrate **9** was partially removed during the reaction resulting in only 10% yield of **9b**. This is likely due to the high acidity of In(OTf)<sub>3</sub>. **10** was found to be selectively mono-formylated unlike **11** which under the standard conditions resulted in a mixture of products including mono-formylated product and trace amounts of the bis-formylated product and dimethylated product as detected by GC-MS. This system can also successfully formylate and cyclise *ortho*-substituted anilines and convert them to azoles as evidenced by substrates **12** and **13** with **12** being particularly active. This reactivity was achieved by utilising polyethyleneimine as a scaffold which is preferentially N-formylated and after transfer of the formate to an *ortho*-substituted aniline yields the desired products **12b**, **13b**, **14b** and **13b** after cyclisation. This procedure was adapted from our previous work on solvent assisted FLP catalysed CO<sub>2</sub> hydrogenations. Aniline (**16**) was found to be unreactive to N-formylation or N-methylation.



**Scheme 5.3:** Control experiments for the N-methylation of **8** catalysed by InOTf<sub>3</sub>

In conclusion we have developed a mild and chemoselective approach for the synthesis of N-formamides from CO<sub>2</sub> and  $\gamma$ -terpinene catalysed by metal triflates producing p-cymene as a co-product. In contrast to our previous work this synthesis proceeds at 50 °C lower temperature and at 25x lower starting pressure. Indium(III) triflate is the most efficient catalyst for the reaction over other group 13 triflates. This is believed to be a result of the increased water tolerance of In(OTf)<sub>3</sub> over Ga(OTf)<sub>3</sub> and Al(OTf)<sub>3</sub>. DFT calculations are ongoing to elucidate the mechanism of the reaction.

## 5.0 Conclusions

In conclusion we developed 7 new  $R_3SnX$  LAs that in combination with nitrogenous LBs were able to selectively hydrogenate  $CO_2$  and reductively couple the resulting formate to amines, containing various other reducible functional groups, to selectively form formamides and water as the only byproduct. This marks a major advance in water tolerant FLP hydrogenations of  $CO_2$  as previous FLP catalysed  $CO_2$  hydrogenations involved a sacrificial component to both dry the reaction *in situ* and cleave the resulting C1 products.

We then expanded the catalytic activity of  $R_3SnX$ -based FLPs to the synthesis of azoles from  $CO_2$ ,  $H_2$  and *ortho*-substituted anilines. In this study we found that  $R_3SnX$  were able to reductively couple  $CO_2$  to *ortho*-substituted anilines, which are both aromatic and primary, yielding the desired azole products after spontaneous cyclisation. To increase the activity of our  $R_3SnX$  catalysed system we employed the use of polyethyleneimine as a co-catalyst. Polyethyleneimine, in the presence of the FLP catalyst and  $CO_2$ , is preferentially formylated and then transfers the formate to the *ortho*-substituted anilines, which then cyclized yielding the desired products. By this method catalytic activity on par with the best TM catalysts for this synthesis of azoles were achieved.

Thirdly, to expand the scope of LAs that can be used in FLPs we developed various Schiff base complexes of tin. The activity of the complexes was probed using imine hydrogenation as a target reaction. We found that tin(IV) salen and salophen complexes were easily sterically and electronically tuned by varying the nature of the ligand's aromatic substituents, the nature of the moiety which bridged the two halves of the ligand and of the X groups attached to the metal center. Interestingly the catalyst with the lowest activity in hydrogen activation had the highest activity for the imine hydrogenation. This challenges the well accepted notion that  $H_2$  activation is the rate limiting step in FLP hydrogenation catalysis.

Lastly, we sought to develop a catalytic system for the N-formylation reaction, which operated at lower pressures and temperatures. Employing transfer hydrogenation of  $CO_2$  with  $\gamma$ -terpinene as the hydride source as opposed to  $H_2$  in combination with  $In(OTf)_3$  allowed the reductive coupling of  $CO_2$  to amines to form formamides. The temperature and pressure of this reaction was  $50^\circ C$  and 94 bar lower respectively than our previous reductive coupling reactions with  $CO_2$ .  $In(OTf)_3$  and  $\gamma$ -terpinene also promoted the formation of azoles using the solvent assisted method from *ortho*-substituted anilines and  $CO_2$  demonstrating the generality of the method. Ultimately this work will assist in the development of

main group systems which can reductively valorize CO<sub>2</sub> and allow for an alternative to the widespread use of transition metal catalysts.

## References

- (1) Welch, G. C.; San Juan, R. R.; Masuda, J. D.; Stephan, D. W. Reversible, Metal-Free Hydrogen Activation. *Science* (1979) **2006**, 314 (5802), 1124–1126. <https://doi.org/10.1126/science.1134230>.
- (2) Brown, H. C.; Schlesinger, H. I.; Cardon, S. Z. Studies in Stereochemistry. I. Steric Strains as a Factor in the Relative Stability of Some Coördination Compounds of Boron. *J Am Chem Soc* **1942**, 64 (2), 325–329. <https://doi.org/10.1021/ja01254a031>.
- (3) Wittig, G.; Benz, E. Über Das Verhalten von Dehydrobenzol Gegenüber Nucleophilen Und Elektrophilen Reagenzien. *Chem Ber* **1959**, 92 (9), 1999–2013. <https://doi.org/10.1002/cber.19590920904>.
- (4) Tochtermann, W. Structures and Reactions of Organic Ate-Complexes. *Angewandte Chemie International Edition in English* **1966**, 5 (4), 351–371. <https://doi.org/10.1002/anie.196603511>.
- (5) Serrano-Maldonado, A.; Bendounan, A.; Silly, M. G.; Pla, D.; Gómez, M. Selective Catalytic Hydrogenation of Fatty Acids with Cobalt-Halloysite Nanocomposites for Waste Valorization. *ACS Appl Nano Mater* **2023**, 6 (13), 11317–11326. <https://doi.org/10.1021/acsanm.3c01361>.
- (6) Liu, W.; Cheng, S.; Malhi, H. S.; Gao, X.; Zhang, Z.; Tu, W. Hydrogenation of CO<sub>2</sub> to Olefins over Iron-Based Catalysts: A Review. *Catalysts*. 2022, p 1432. <https://doi.org/10.3390/catal12111432>.
- (7) Zhang, L.; Zhou, M.; Wang, A.; Zhang, T. Selective Hydrogenation over Supported Metal Catalysts: From Nanoparticles to Single Atoms. *Chemical Reviews*. 2020, pp 683–733. <https://doi.org/10.1021/acs.chemrev.9b00230>.



- (8) Behera, P.; Ramakrishna, D. S.; Chandrasekhar, M. M.; Kothakapu, S. R. A Concise Review on Recent Advances in Catalytic Asymmetric Hydrogenation. *Chirality*. 2023, pp 477–497. <https://doi.org/10.1002/chir.23559>.
- (9) Lam, J.; Szkop, K. M.; Mosaferi, E.; Stephan, D. W. FLP Catalysis: Main Group Hydrogenations of Organic Unsaturated Substrates. *Chemical Society Reviews*. 2019, pp 3592–3612. <https://doi.org/10.1039/c8cs00277k>.
- (10) Kagan, H. B.; Dang, T. P. Asymmetric Catalytic Reduction with Transition Metal Complexes. I. A Catalytic System of Rhodium(I) with (–)-2,3-O-Isopropylidene-2,3-Dihydroxy-1,4-Bis(Diphenyl-Phosphino)Butane, a New Chiral Diphosphine. *J Am Chem Soc* **1972**, *94* (18), 6429–6433. <https://doi.org/10.1021/ja00773a028>.
- (11) Trost, B. M. Atom Economy—A Challenge for Organic Synthesis: Homogeneous Catalysis Leads the Way. *Angewandte Chemie International Edition in English*. 1995, pp 259–281. <https://doi.org/10.1002/anie.199502591>.
- (12) Power, P. P. Main-Group Elements as Transition Metals. *Nature*. 2010, pp 171–177. <https://doi.org/10.1038/nature08634>.
- (13) Weetman, C.; Inoue, S. The Road Travelled: After Main-Group Elements as Transition Metals. *ChemCatChem* **2018**, *10* (19), 4213–4228. <https://doi.org/10.1002/cctc.201800963>.
- (14) Stephan, D. W. Frustrated Lewis Pairs: From Concept to Catalysis. *Acc Chem Res* **2015**, *48* (2), 306–316. <https://doi.org/10.1021/ar500375j>.
- (15) Grimme, S.; Kruse, H.; Goerigk, L.; Erker, G. The Mechanism of Dihydrogen Activation by Frustrated Lewis Pairs Revisited. *Angewandte Chemie - International Edition* **2010**, *49* (8), 1402–1405. <https://doi.org/10.1002/anie.200905484>.
- (16) Brown, L. C.; Hogg, J. M.; Gilmore, M.; Moura, L.; Imberti, S.; Gärtner, S.; Gunaratne, H. Q. N.; O'Donnell, R. J.; Artioli, N.; Holbrey, J. D.; Swadźba-Kwaśny, M. Frustrated Lewis Pairs in Ionic Liquids and Molecular Solvents—a Neutron Scattering and NMR Study of Encounter Complexes. *Chemical Communications* **2018**, *54* (63), 8689–8692. <https://doi.org/10.1039/c8cc03794a>.
- (17) Stephan, D. W.; Greenberg, S.; Graham, T. W.; Chase, P.; Hastie, J. J.; Geier, S. J.; Farrell, J. M.; Brown, C. C.; Heiden, Z. M.; Welch, G. C.; Ullrich, M. Metal-Free Catalytic Hydrogenation of Polar

- Substrates by Frustrated Lewis Pairs. *Inorg Chem* **2011**, *50* (24), 12238–12348. <https://doi.org/10.1021/ic200663v>.
- (18) Scott, D. J.; Phillips, N. A.; Sapsford, J. S.; Deacy, A. C.; Fuchter, M. J.; Ashley, A. E. Versatile Catalytic Hydrogenation Using A Simple Tin(IV) Lewis Acid. *Angewandte Chemie - International Edition* **2016**, *55* (47), 14738–14742. <https://doi.org/10.1002/anie.201606639>.
- (19) Tussing, S.; Kaupmees, K.; Paradies, J. Structure-Reactivity Relationship in the Frustrated Lewis Pair (FLP)-Catalyzed Hydrogenation of Imines. *Chemistry - A European Journal* **2016**, *22* (22), 7422–7426. <https://doi.org/10.1002/chem.201600716>.
- (20) Scott, D. J.; Simmons, T. R.; Lawrence, E. J.; Wildgoose, G. G.; Fuchter, M. J.; Ashley, A. E. Facile Protocol for Water-Tolerant “Frustrated Lewis Pair”-Catalyzed Hydrogenation. *ACS Catal* **2015**, *5* (9), 5540–5544. <https://doi.org/10.1021/acscatal.5b01417>.
- (21) Sapsford, J. S.; Scott, D. J.; Allcock, N. J.; Fuchter, M. J.; Tighe, C. J.; Ashley, A. E. Direct Reductive Amination of Carbonyl Compounds Catalyzed by a Moisture Tolerant Tin(IV) Lewis Acid. *Adv Synth Catal* **2018**, *360* (6), 1066–1071. <https://doi.org/10.1002/adsc.201701418>.
- (22) Khan, M. N.; van Ingen, Y.; Boruah, T.; McLauchlan, A.; Wirth, T.; Melen, R. L. Advances in CO<sub>2</sub> Activation by Frustrated Lewis Pairs: From Stoichiometric to Catalytic Reactions. *Chemical Science*. 2023, pp 13661–13695. <https://doi.org/10.1039/d3sc03907b>.
- (23) Liu, Q.; Wu, L.; Jackstell, R.; Beller, M. Using Carbon Dioxide as a Building Block in Organic Synthesis. *Nature Communications*. 2015, pp 1–15. <https://doi.org/10.1038/ncomms6933>.
- (24) Dabral, S.; Schaub, T. The Use of Carbon Dioxide (CO<sub>2</sub>) as a Building Block in Organic Synthesis from an Industrial Perspective. *Advanced Synthesis and Catalysis*. 2019, pp 223–246. <https://doi.org/10.1002/adsc.201801215>.
- (25) Thijs, B.; Rongé, J.; Martens, J. A. Matching Emerging Formic Acid Synthesis Processes with Application Requirements†. *Green Chemistry* **2022**, *24* (6), 2287–2295. <https://doi.org/10.1039/d1gc04791d>.
- (26) Mardini, N.; Bicer, Y. Direct Synthesis of Formic Acid as Hydrogen Carrier from CO<sub>2</sub> for Cleaner Power Generation through Direct Formic Acid Fuel Cell. *Int J Hydrogen Energy* **2021**, *46* (24), 13050–13060. <https://doi.org/10.1016/j.ijhydene.2021.01.124>.

- (27) Majhi, J.; Molander, G. A. Recent Discovery, Development, and Synthetic Applications of Formic Acid Salts in Photochemistry. *Angewandte Chemie - International Edition*. 2024, p e202311853. <https://doi.org/10.1002/anie.202311853>.
- (28) Nie, X.; Li, W.; Jiang, X.; Guo, X.; Song, C. Recent Advances in Catalytic CO<sub>2</sub> Hydrogenation to Alcohols and Hydrocarbons. In *Advances in Catalysis*; 2019; Vol. 65, pp 121–233. <https://doi.org/10.1016/bs.acat.2019.10.002>.
- (29) Zhou, Z.; Gao, P. Direct Carbon Dioxide Hydrogenation to Produce Bulk Chemicals and Liquid Fuels via Heterogeneous Catalysis. *Chinese Journal of Catalysis* **2022**, *43* (8), 2045–2056. [https://doi.org/10.1016/S1872-2067\(22\)64107-X](https://doi.org/10.1016/S1872-2067(22)64107-X).
- (30) Jiang, X.; Nie, X.; Guo, X.; Song, C.; Chen, J. G. Recent Advances in Carbon Dioxide Hydrogenation to Methanol via Heterogeneous Catalysis. *Chemical Reviews*. 2020, pp 7984–8034. <https://doi.org/10.1021/acs.chemrev.9b00723>.
- (31) Asare Bediako, B. B.; Qian, Q.; Han, B. Synthesis of C<sub>2</sub>+Chemicals from CO<sub>2</sub> and H<sub>2</sub> via C-C Bond Formation. *Acc Chem Res* **2021**, *54* (10), 2467–2476. <https://doi.org/10.1021/acs.accounts.1c00091>.
- (32) Sun, Z.; Talreja, N.; Tao, H.; Texter, J.; Muhler, M.; Strunk, J.; Chen, J. Katalyse Der Kohlenstoffdioxid-Photoreduktion an Nanoschichten: Grundlagen Und Herausforderungen. *Angewandte Chemie* **2018**, *130* (26), 7734–7752. <https://doi.org/10.1002/ange.201710509>.
- (33) Kann, A.; Hartmann, H.; Besmehn, A.; Hausoul, P. J. C.; Palkovits, R. Hydrogenation of CO<sub>2</sub> to Formate over Ruthenium Immobilized on Solid Molecular Phosphines. *ChemSusChem* **2018**, *11* (11), 1857–1865. <https://doi.org/10.1002/cssc.201800413>.
- (34) Hao, C.; Wang, S.; Li, M.; Kang, L.; Ma, X. Hydrogenation of CO<sub>2</sub> to Formic Acid on Supported Ruthenium Catalysts. *Catal Today* **2011**, *160* (1), 184–190. <https://doi.org/10.1016/j.cattod.2010.05.034>.
- (35) Wang, C.; Guan, E.; Wang, L.; Chu, X.; Wu, Z.; Zhang, J.; Yang, Z.; Jiang, Y.; Zhang, L.; Meng, X.; Gates, B. C.; Xiao, F. S. Product Selectivity Controlled by Nanoporous Environments in Zeolite Crystals Enveloping Rhodium Nanoparticle Catalysts for CO<sub>2</sub> Hydrogenation. *J Am Chem Soc* **2019**, *141* (21), 8482–8488. <https://doi.org/10.1021/jacs.9b01555>.

- (36) Zhu, S.; Chen, Y.; Somayaji, V.; Novello, P.; Chacko, D.; Li, F.; Liu, J. One-Step Synthesis of a High Entropy Oxide-Supported Rhodium Catalyst for Highly Selective CO Production in CO<sub>2</sub> Hydrogenation. *ACS Appl Mater Interfaces* **2023**, *15* (26), 31384–31392. <https://doi.org/10.1021/acsami.3c02829>.
- (37) Li, H.; Wang, L.; Dai, Y.; Pu, Z.; Lao, Z.; Chen, Y.; Wang, M.; Zheng, X.; Zhu, J.; Zhang, W.; Si, R.; Ma, C.; Zeng, J. Synergetic Interaction between Neighbouring Platinum Monomers in CO<sub>2</sub> Hydrogenation. *Nat Nanotechnol* **2018**, *13* (5), 411–417. <https://doi.org/10.1038/s41565-018-0089-z>.
- (38) Mabena, K. G.; Ocansey, E.; Kinfe, H. H.; Makhubela, B. C. E. Palladium(II) and Platinum(II) Based S<sup>N</sup>AS and Se<sup>N</sup>Se Pincer Complexes as Catalysts for CO<sub>2</sub> Hydrogenation and N-Formylation of Diethylamine to Diethylformamide. *Journal of CO<sub>2</sub> Utilization* **2021**, *50*, 101606. <https://doi.org/10.1016/j.jcou.2021.101606>.
- (39) Tian, G.; Wu, Y.; Wu, S.; Huang, S.; Gao, J. CO<sub>2</sub> Hydrogenation to Methanol over Pd/MnO/In<sub>2</sub>O<sub>3</sub> Catalyst. *J Environ Chem Eng* **2022**, *10* (1), 106965. <https://doi.org/10.1016/j.jece.2021.106965>.
- (40) Lo, H. K.; Thiel, I.; Copéret, C. Efficient CO<sub>2</sub> Hydrogenation to Formate with Immobilized Ir-Catalysts Based on Mesoporous Silica Beads. *Chemistry - A European Journal* **2019**, *25* (40), 9443–9446. <https://doi.org/10.1002/chem.201901663>.
- (41) Mo, X. F.; Ge, S.; Yi, P. P.; Chen, G.; Liu, J. H.; Liu, C.; Yi, X. Y.; He, P. Precisely Controlling Ancillary Ligands to Improve Catalysis of Cp\*Ir Complexes for CO<sub>2</sub> Hydrogenation. *Inorg Chem* **2023**, *62* (28), 11225–11232. <https://doi.org/10.1021/acs.inorgchem.3c01466>.
- (42) Ashley, A. E.; Thompson, A. L.; O'Hare, D. Non-Metal-Mediated Homogeneous Hydrogénation of CO<sub>2</sub> to CH<sub>3</sub>OH. *Angewandte Chemie - International Edition* **2009**, *48* (52), 9839–9843. <https://doi.org/10.1002/anie.200905466>.
- (43) Courtemanche, M. A.; Pulis, A. P.; Rochette, É.; Légaré, M. A.; Stephan, D. W.; Fontaine, F. G. Intramolecular B/N Frustrated Lewis Pairs and the Hydrogenation of Carbon Dioxide. *Chemical Communications* **2015**, *51* (48), 9797–9800. <https://doi.org/10.1039/c5cc03072b>.
- (44) Wang, T.; Xu, M.; Jupp, A. R.; Qu, Z. W.; Grimme, S.; Stephan, D. W. Selective Catalytic Frustrated Lewis Pair Hydrogenation of CO<sub>2</sub> in the Presence of Silylhalides. *Angewandte Chemie - International Edition* **2021**, *60* (49), 25771–25775. <https://doi.org/10.1002/anie.202112233>.

- (45) Zhao, T.; Hu, X.; Wu, Y.; Zhang, Z. Hydrogenation of CO<sub>2</sub> to Formate with H<sub>2</sub>: Transition Metal Free Catalyst Based on a Lewis Pair. *Angewandte Chemie - International Edition* **2019**, *58* (3), 722–726. <https://doi.org/10.1002/anie.201809634>.
- (46) Olah, G. A. Beyond Oil and Gas: The Methanol Economy. *Angewandte Chemie - International Edition* **2005**, *44* (18), 2636–2639. <https://doi.org/10.1002/anie.200462121>.
- (47) Yang, C. J.; Jackson, R. B. China's Growing Methanol Economy and Its Implications for Energy and the Environment. *Energy Policy* **2012**, *41*, 878–884. <https://doi.org/10.1016/j.enpol.2011.11.037>.
- (48) Lin, S.; Liu, J.; Ma, L. A Review on Recent Developments in N-Methylation Using CO<sub>2</sub>. *Journal of CO<sub>2</sub> Utilization*. 2021, p 101759. <https://doi.org/10.1016/j.jcou.2021.101759>.
- (49) Liu, H.; Mei, Q.; Xu, Q.; Song, J.; Liu, H.; Han, B. Synthesis of Formamides Containing Unsaturated Groups by: N-Formylation of Amines Using CO<sub>2</sub> with H<sub>2</sub>. *Green Chemistry* **2017**, *19* (1), 196–201. <https://doi.org/10.1039/c6gc02243j>.
- (50) Zou, Q.; Long, G.; Zhao, T.; Hu, X. Catalyst-Free Selective: N-Formylation and N-Methylation of Amines Using CO<sub>2</sub> as a Sustainable C<sub>1</sub> Source. *Green Chemistry* **2020**, *22* (4), 1134–1138. <https://doi.org/10.1039/c9gc03637g>.
- (51) Newar, R.; Kalita, R.; Akhtar, N.; Antil, N.; Chauhan, M.; Manna, K. N-Formylation of Amines Utilizing CO<sub>2</sub> by a Heterogeneous Metal-Organic Framework Supported Single-Site Cobalt Catalyst. *Catal Sci Technol* **2022**, *12* (22), 6795–6804. <https://doi.org/10.1039/d2cy01231f>.
- (52) Shen, Y.; Zheng, Q.; Chen, Z. N.; Wen, D.; Clark, J. H.; Xu, X.; Tu, T. Highly Efficient and Selective N-Formylation of Amines with CO<sub>2</sub> and H<sub>2</sub> Catalyzed by Porous Organometallic Polymers. *Angewandte Chemie - International Edition* **2021**, *60* (8), 4125–4132. <https://doi.org/10.1002/anie.202011260>.
- (53) Zhang, L.; Han, Z.; Zhao, X.; Wang, Z.; Ding, K. Highly Efficient Ruthenium-Catalyzed N-Formylation of Amines with H<sub>2</sub> and CO<sub>2</sub>. *Angewandte Chemie - International Edition* **2015**, *54* (21), 6186–6189. <https://doi.org/10.1002/anie.201500939>.
- (54) Daw, P.; Chakraborty, S.; Leitun, G.; Diskin-Posner, Y.; Ben-David, Y.; Milstein, D. Selective N-Formylation of Amines with H<sub>2</sub> and CO<sub>2</sub> Catalyzed by Cobalt Pincer Complexes. *ACS Catal* **2017**, *7* (4), 2500–2504. <https://doi.org/10.1021/acscatal.7b00116>.

- (55) Schmid, L.; Schneider, M. S.; Engel, D.; Baiker, A. Formylation with “Supercritical” CO<sub>2</sub>: Efficient Ruthenium-Catalyzed Synthesis of N-Formylmorpholine. *Catal Letters* **2003**, *88* (3–4), 105–113. <https://doi.org/10.1023/A:1024009722078>.
- (56) Jessop, P. G.; Hsiao, Y.; Ikariya, T.; Noyori, R. Homogeneous Catalysis in Supercritical Fluids: Hydrogenation of Supercritical Carbon Dioxide to Formic Acid, Alkyl Formates, and Formamides. *J Am Chem Soc* **1996**, *118* (2), 344–355. <https://doi.org/10.1021/ja953097b>.
- (57) Lam, R. H.; McQueen, C. M. A.; Pernik, I.; McBurney, R. T.; Hill, A. F.; Messerle, B. A. Selective Formylation or Methylation of Amines Using Carbon Dioxide Catalysed by a Rhodium Perimidine-Based NHC Complex. *Green Chemistry* **2019**, *21* (3), 538–549. <https://doi.org/10.1039/c8gc03094d>.
- (58) Jayarathne, U.; Hazari, N.; Bernskoetter, W. H. Selective Iron-Catalyzed N-Formylation of Amines Using Dihydrogen and Carbon Dioxide. *ACS Catal* **2018**, *8* (2), 1338–1345. <https://doi.org/10.1021/acscatal.7b03834>.
- (59) Yu, B.; Zhang, H.; Zhao, Y.; Chen, S.; Xu, J.; Huang, C.; Liu, Z. Cyclization of O-Phenylenediamines by CO<sub>2</sub> in the Presence of H<sub>2</sub> for the Synthesis of Benzimidazoles. *Green Chemistry* **2013**, *15* (1), 95–99. <https://doi.org/10.1039/c2gc36517k>.
- (60) Munshi, P.; Heldebrant, D. J.; McKoon, E. P.; Kelly, P. A.; Tai, C. C.; Jessop, P. G. Formanilide and Carbanilide from Aniline and Carbon Dioxide. *Tetrahedron Lett* **2003**, *44* (13), 2725–2727. [https://doi.org/10.1016/S0040-4039\(03\)00384-8](https://doi.org/10.1016/S0040-4039(03)00384-8).
- (61) Hulla, M.; Bobbink, F. D.; Das, S.; Dyson, P. J. Carbon Dioxide Based N-Formylation of Amines Catalyzed by Fluoride and Hydroxide Anions. *ChemCatChem* **2016**, *8* (21), 3338–3342. <https://doi.org/10.1002/cctc.201601027>.
- (62) Lv, H.; Xing, Q.; Yue, C.; Lei, Z.; Li, F. Solvent-Promoted Catalyst-Free: N -Formylation of Amines Using Carbon Dioxide under Ambient Conditions. *Chemical Communications* **2016**, *52* (39), 6545–6548. <https://doi.org/10.1039/c6cc01234e>.
- (63) Riduan, S. N.; Ying, J. Y.; Zhang, Y. Solid Poly-N-Heterocyclic Carbene Catalyzed CO<sub>2</sub> Reduction with Hydrosilanes. *J Catal* **2016**, *343*, 46–51. <https://doi.org/10.1016/j.jcat.2015.09.009>.

- (64) Luo, R.; Lin, X.; Chen, Y.; Zhang, W.; Zhou, X.; Ji, H. Cooperative Catalytic Activation of Si–H Bonds: CO<sub>2</sub>-Based Synthesis of Formamides from Amines and Hydrosilanes under Mild Conditions. *ChemSusChem* **2017**, *10* (6), 1224–1232. <https://doi.org/10.1002/cssc.201601490>.
- (65) Li, X. Y.; Fu, H. C.; Liu, X. F.; Yang, S. H.; Chen, K. H.; He, L. N. Design of Lewis Base Functionalized Ionic Liquids for the N-Formylation of Amines with CO<sub>2</sub> and Hydrosilane: The Cation Effects. *Catal Today* **2020**, *356*, 563–569. <https://doi.org/10.1016/j.cattod.2020.01.030>.
- (66) Pąchalska, P.; Skarżyńska, A.; Matias, I. A. S.; Trzeciak, A. M. Borohydride Ionic Liquids as Reductants of CO<sub>2</sub> in the Selective N-Formylation of Amines. *ChemSusChem* **2024**, *17* (7), e202301120. <https://doi.org/10.1002/cssc.202301120>.
- (67) Gopakumar, A.; Lombardo, L.; Fei, Z.; Shyshkanov, S.; Vasilyev, D.; Chidambaram, A.; Stylianou, K.; Züttel, A.; Dyson, P. J. A Polymeric Ionic Liquid Catalyst for the N-Formylation and N-Methylation of Amines Using CO<sub>2</sub>/PhSiH<sub>3</sub>. *Journal of CO<sub>2</sub> Utilization* **2020**, *41*, 101240. <https://doi.org/10.1016/j.jcou.2020.101240>.
- (68) Li, C.; Wang, M.; Lu, X.; Zhang, L.; Jiang, J.; Zhang, L. Reusable Brønsted Acidic Ionic Liquid Efficiently Catalyzed N-Formylation and N-Acylation of Amines. *ACS Sustain Chem Eng* **2020**, *8* (11), 4353–4361. <https://doi.org/10.1021/acssuschemeng.9b06591>.
- (69) Hulla, M.; Dyson, P. J. Pivotal Role of the Basic Character of Organic and Salt Catalysts in C–N Bond Forming Reactions of Amines with CO<sub>2</sub>. *Angewandte Chemie - International Edition*. 2020, pp 1002–1017. <https://doi.org/10.1002/anie.201906942>.
- (70) Baghbanian, S. M.; Farhang, M. Protic [TBD][TFA] Ionic Liquid as a Reusable and Highly Efficient Catalyst for N-Formylation of Amines Using Formic Acid under Solvent-Free Condition. *J Mol Liq* **2013**, *183*, 45–49. <https://doi.org/10.1016/j.molliq.2013.04.001>.
- (71) Song, Z.; Liu, J.; Xing, S.; Shao, X.; Li, J.; Peng, J.; Bai, Y. PNP-Type Ligands Enabled Copper-Catalyzed N-Formylation of Amines with CO<sub>2</sub> in the Presence of Silanes. *Org Biomol Chem* **2022**, *21* (4), 832–837. <https://doi.org/10.1039/d2ob01986h>.
- (72) Wen, Q.; Yuan, X.; Zhou, Q.; Yang, H. J.; Jiang, Q.; Hu, J.; Guo, C. Y. Efficient N-Formylation of Carbon Dioxide and Amines with Alkanolamine as Eco-Friendly Catalyst under Mild Conditions. *Journal of CO<sub>2</sub> Utilization* **2023**, *69*, 102398. <https://doi.org/10.1016/j.jcou.2023.102398>.

- (73) Yang, M.; Hunger, R.; Berrettoni, S.; Sprecher, B.; Wang, B. A Review of Hydrogen Storage and Transport Technologies. *Clean Energy* **2023**, *7* (1), 190–216. <https://doi.org/10.1093/ce/zkad021>.
- (74) Li, G.; Chen, J.; Zhu, D. Y.; Chen, Y.; Xia, J. B. DBU-Catalyzed Selective N-Methylation and N-Formylation of Amines with CO<sub>2</sub> and Polymethylhydrosiloxane. *Adv Synth Catal* **2018**, *360* (12), 2364–2369. <https://doi.org/10.1002/adsc.201800140>.
- (75) Das, S.; Bobbink, F. D.; Bulut, S.; Soudani, M.; Dyson, P. J. Thiazolium Carbene Catalysts for the Fixation of CO<sub>2</sub> onto Amines. *Chemical Communications* **2016**, *52* (12), 2497–2500. <https://doi.org/10.1039/c5cc08741d>.
- (76) Hulla, M.; Ortiz, D.; Katsyuba, S.; Vasilyev, D.; Dyson, P. J. Delineation of the Critical Parameters of Salt Catalysts in the N-Formylation of Amines with CO<sub>2</sub>. *Chemistry - A European Journal* **2019**, *25* (47), 11074–11079. <https://doi.org/10.1002/chem.201901686>.
- (77) Saptal, V. B.; Juneja, G.; Bhanage, B. M. B(C<sub>6</sub>F<sub>5</sub>)<sub>3</sub>: A Robust Catalyst for the Activation of CO<sub>2</sub> and Dimethylamine Borane for the N-Formylation Reactions. *New Journal of Chemistry* **2018**, *42* (19), 15847–15851. <https://doi.org/10.1039/c8nj02816h>.
- (78) Hulla, M.; Laurenczy, G.; Dyson, P. J. Mechanistic Study of the N-Formylation of Amines with Carbon Dioxide and Hydrosilanes. *ACS Catal* **2018**, *8* (11), 10619–10630. <https://doi.org/10.1021/acscatal.8b03274>.
- (79) Paparakis, A.; Turnell-Ritson, R. C.; Sapsford, J. S.; Ashley, A. E.; Hulla, M. Tin-Catalyzed Reductive Coupling of Amines with CO<sub>2</sub> and H<sub>2</sub>. *Catal Sci Technol* **2022**, *13* (3), 637–644. <https://doi.org/10.1039/d2cy01659a>.
- (80) Stephan, D. W. Frustrated Lewis Pairs. *Journal of the American Chemical Society*. 2015, pp 10018–10032. <https://doi.org/10.1021/jacs.5b06794>.
- (81) Hadida, S.; Super, M. S.; Beckman, E. J.; Curran, D. P. Radical Reactions with Alkyl and Fluoroalkyl ((Fluorous) Tin Hydride Reagents in Supercritical CO<sub>2</sub>. *J Am Chem Soc* **1997**, *119* (31), 7406–7407. <https://doi.org/10.1021/ja971120i>.
- (82) Ke, Z.; Yu, B.; Wang, H.; Xiang, J.; Han, J.; Wu, Y.; Liu, Z.; Yang, P.; Liu, Z. Cobalt-Catalyzed Synthesis of N-Containing Heterocycles: Via Cyclization of Ortho -Substituted Anilines with CO<sub>2</sub>/H<sub>2</sub>. *Green Chemistry* **2019**, *21* (7), 1695–1701. <https://doi.org/10.1039/c9gc00095j>.



- (83) Mitsudome, T.; Urayama, T.; Fujita, S.; Maeno, Z.; Mizugaki, T.; Jitsukawa, K.; Kaneda, K. A Titanium Dioxide Supported Gold Nanoparticle Catalyst for the Selective N-Formylation of Functionalized Amines with Carbon Dioxide and Hydrogen. *ChemCatChem* **2017**, *9* (19), 3632–3636. <https://doi.org/10.1002/cctc.201700726>.
- (84) Mostafavi, H.; Islami, M. R.; Ghonchepour, E.; Tikdari, A. M. Synthesis of 1H-1,3-Benzimidazoles, Benzothiazoles and 3H-Imidazo[4,5-c]Pyridine Using DMF in the Presence of HMDS as a Reagent under the Transition-Metal-Free Condition. *Chemical Papers* **2018**, *72* (12), 2973–2978. <https://doi.org/10.1007/s11696-018-0540-5>.
- (85) Nale, D. B.; Bhanage, B. M. N-Substituted Formamides as C1-Sources for the Synthesis of Benzimidazole and Benzothiazole Derivatives by Using Zinc Catalysts. *Synlett* **2015**, *26* (20), 2835–2842. <https://doi.org/10.1055/s-0035-1560319>.
- (86) Badolato, M.; Aiello, F.; Neamati, N. 2,3-Dihydroquinazolin-4(1H)-One as a Privileged Scaffold in Drug Design. *RSC Advances*. 2018, pp 20894–20921. <https://doi.org/10.1039/c8ra02827c>.
- (87) Paparakis, A.; Hulla, M. Frustrated Lewis Pairs Catalyse the Solvent-Assisted Synthesis of Azoles from Ortho-Substituted Anilines, CO<sub>2</sub> and H<sub>2</sub>. *ChemCatChem* **2023**, *15* (12), e202300510. <https://doi.org/10.1002/cctc.202300510>.
- (88) Dorkó, É.; Szabó, M.; Kótai, B.; Pápai, I.; Domján, A.; Soós, T. Expanding the Boundaries of Water-Tolerant Frustrated Lewis Pair Hydrogenation: Enhanced Back Strain in the Lewis Acid Enables the Reductive Amination of Carbonyls. *Angewandte Chemie - International Edition* **2017**, *56* (32), 9512–9516. <https://doi.org/10.1002/anie.201703591>.
- (89) Abu-Dief, A. M.; Mohamed, I. M. A. A Review on Versatile Applications of Transition Metal Complexes Incorporating Schiff Bases. *Beni Suef Univ J Basic Appl Sci* **2015**, *4* (2), 119–133. <https://doi.org/10.1016/j.bjbas.2015.05.004>.
- (90) Jing, H.; Edulji, S. K.; Gibbs, J. M.; Stern, C. L.; Zhou, H.; Nguyen, S. B. T. (Salen)Tin Complexes: Syntheses, Characterization, Crystal Structures, and Catalytic Activity in the Formation of Propylene Carbonate from CO<sub>2</sub> and Propylene Oxide. *Inorg Chem* **2004**, *43* (14), 4315–4327. <https://doi.org/10.1021/ic034855z>.
- (91) Ouyang, L.; Chen, K.; Jiang, J.; Yang, X. S.; Zhu, M. Hydrogen Storage in Light-Metal Based Systems: A Review. *J Alloys Compd* **2020**, *829*, 154597. <https://doi.org/10.1016/j.jallcom.2020.154597>.

- (92) He, T.; Cao, H.; Chen, P. Complex Hydrides for Energy Storage, Conversion, and Utilization. *Advanced Materials* **2019**, *31* (50), 1902757. <https://doi.org/10.1002/adma.201902757>.
- (93) Balahbib, A.; El Omari, N.; Hachlafi, N. EL; Lakhdar, F.; El Menyiy, N.; Salhi, N.; Mrabti, H. N.; Bakrim, S.; Zengin, G.; Bouyahya, A. Health Beneficial and Pharmacological Properties of P-Cymene. *Food and Chemical Toxicology* **2021**, *153*, 112259. <https://doi.org/10.1016/j.fct.2021.112259>.
- (94) Tian, F.; Woo, S. Y.; Lee, S. Y.; Chun, H. S. P-Cymene and Its Derivatives Exhibit Antiaflatoxicogenic Activities against *Aspergillus Flavus* through Multiple Modes of Action. *Appl Biol Chem* **2018**, *61* (5), 489–497. <https://doi.org/10.1007/s13765-018-0382-4>.
- (95) Yu, J.; Xu, S.; Liu, B.; Wang, H.; Qiao, F.; Ren, X.; Wei, Q. PLA Bioplastic Production: From Monomer to the Polymer. *European Polymer Journal*. 2023, p 112076. <https://doi.org/10.1016/j.eurpolymj.2023.112076>.
- (96) Komesu, A.; de Oliveira, J. A. R.; da Silva Martins, L. H.; Maciel, M. R. W.; Filho, R. M. Lactic Acid Production to Purification: A Review. *Bioresources* **2017**, *12* (2), 688. <https://doi.org/10.15376/BIORES.12.2.KOMESU>.
- (97) Cunha, B. L. C.; Bahú, J. O.; Xavier, L. F.; Crivellin, S.; de Souza, S. D. A.; Lodi, L.; Jardini, A. L.; Maciel Filho, R.; Schiavon, M. I. R. B.; Cárdenas Concha, V. O.; Severino, P.; Souto, E. B. Lactide: Production Routes, Properties, and Applications. *Bioengineering*. 2022, p 164. <https://doi.org/10.3390/bioengineering9040164>.
- (98) Castillo Martinez, F. A.; Balciunas, E. M.; Salgado, J. M.; Domínguez González, J. M.; Converti, A.; Oliveira, R. P. de S. Lactic Acid Properties, Applications and Production: A Review. *Trends in Food Science and Technology*. 2013, pp 70–83. <https://doi.org/10.1016/j.tifs.2012.11.007>.
- (99) Kumar, A.; Bhardwaj, R.; Choudhury, J. Integrated CO<sub>2</sub> Capture and Conversion to Methanol Leveraged by the Transfer Hydrogenation Approach. *ACS Catal* **2023**, *13* (2), 927–933. <https://doi.org/10.1021/acscatal.2c05302>.
- (100) Cheong, Y. J.; Sung, K.; Kim, J. A.; Kim, Y. K.; Yoon, W.; Yun, H.; Jang, H. Y. Iridium(Nhc)-Catalyzed Sustainable Transfer Hydrogenation of Co<sub>2</sub> and Inorganic Carbonates. *Catalysts* **2021**, *11* (6), 695. <https://doi.org/10.3390/catal11060695>.

- (101) Pang, M.; Chen, J. Y.; Zhang, S.; Liao, R. Z.; Tung, C. H.; Wang, W. Controlled Partial Transfer Hydrogenation of Quinolines by Cobalt-Amido Cooperative Catalysis. *Nat Commun* **2020**, *11* (1), 1249. <https://doi.org/10.1038/s41467-020-15118-x>.
- (102) Wei, D.; Bruneau-Voisine, A.; Dubois, M.; Bastin, S.; Sortais, J. B. Manganese-Catalyzed Transfer Hydrogenation of Aldimines. *ChemCatChem* **2019**, *11* (21), 5256–5259. <https://doi.org/10.1002/cctc.201900314>.
- (103) Wienhöfer, G.; Westerhaus, F. A.; Jagadeesh, R. V.; Junge, K.; Junge, H.; Beller, M. Selective Iron-Catalyzed Transfer Hydrogenation of Terminal Alkynes. *Chemical Communications* **2012**, *48* (40), 4827–4829. <https://doi.org/10.1039/c2cc31091k>.
- (104) Nikonov, G. I. New Tricks for an Old Dog: Aluminum Compounds as Catalysts in Reduction Chemistry. *ACS Catalysis*. 2017, pp 7257–7266. <https://doi.org/10.1021/acscatal.7b02460>.
- (105) Michelet, B.; Bour, C.; Gandon, V. Gallium-Assisted Transfer Hydrogenation of Alkenes. *Chemistry - A European Journal* **2014**, *20* (44), 14488–14492. <https://doi.org/10.1002/chem.201404139>.
- (106) Li, L.; Kail, S.; Weber, S. M.; Hilt, G. Indium-Catalysed Transfer Hydrogenation for the Reductive Cyclisation of 2-Alkynyl Enones towards Trisubstituted Furans. *Angewandte Chemie - International Edition* **2021**, *60* (44), 23661–23666. <https://doi.org/10.1002/anie.202109266>.
- (107) Shao, Z.; Fu, S.; Wei, M.; Zhou, S.; Liu, Q. Mild and Selective Cobalt-Catalyzed Chemodivergent Transfer Hydrogenation of Nitriles. *Angewandte Chemie - International Edition* **2016**, *55* (47), 14653–14657. <https://doi.org/10.1002/anie.201608345>.
- (108) Martínez-Ferraté, O.; Werlé, C.; Franciò, G.; Leitner, W. Aminotriazole Mn(I) Complexes as Effective Catalysts for Transfer Hydrogenation of Ketones. *ChemCatChem* **2018**, *10* (20), 4514–4518. <https://doi.org/10.1002/cctc.201800953>.
- (109) Schneekönig, J.; Junge, K.; Beller, M. Manganese Catalyzed Asymmetric Transfer Hydrogenation of Ketones Using Chiral Oxamide Ligands. *Synlett* **2019**, *30* (4), 503–507. <https://doi.org/10.1055/s-0037-1611669>.
- (110) Rebacz, N. A.; Savage, P. E. Hydration of 1-Phenyl-1-Propyne in High-Temperature Water with Catalysis by Water-Tolerant Lewis Acids. *Ind Eng Chem Res* **2010**, *49* (2), 535–540. <https://doi.org/10.1021/ie9017513>.

- (111) Yin, W. P.; Shi, M. Indium Triflate as a Recyclable Catalyst for the Nitration of Aromatic Compounds without a Halogenated Solvent. *J Chem Res* **2006**, No. 9, 549–551. <https://doi.org/10.3184/030823406778521374>.
- (112) Khan, I.; Reed-Berendt, B. G.; Melen, R. L.; Morrill, L. C. FLP-Catalyzed Transfer Hydrogenation of Silyl Enol Ethers. *Angewandte Chemie - International Edition* **2018**, 57 (38), 12356–12369. <https://doi.org/10.1002/anie.201808800>.
- (113) Kumar, A.; Bhardwaj, R.; Mandal, S. K.; Choudhury, J. Transfer Hydrogenation of CO<sub>2</sub> and CO<sub>2</sub> Derivatives Using Alcohols as Hydride Sources: Boosting an H<sub>2</sub>-Free Alternative Strategy. *ACS Catalysis*. 2022, pp 8886–8903. <https://doi.org/10.1021/acscatal.2c01982>.

## List of abbreviations

FLP	Frustrated Lewis Pair
LA	Lewis acid
LB	Lewis base
EA	Electron acceptor
ED	Electron donor
Cy	Cyclohexyl
<sup>i</sup> Pr	iso-propyl
NPh	neophyl
Me	Methyl
Et	Ethyl
EtO	Ethoxy
<sup>s</sup> Bu	sec-butyl
<sup>n</sup> Bu	n-butyl
<sup>t</sup> Bu	tertiary-butyl
Ph	phenyl
Hex	n-hexyl
Bn	Benzyl
dppe	1,2-Bis(diphenylphosphino)ethane
R	alkyl
MeCN	acetonitrile
OTf	Trifluoromethanesulfonate
NTf <sub>2</sub>	bis(trifluoromethane)sulfonimide

OAc	acetate
X	halide or heteroatom containing substituent
Salen	N,N'-Ethylenebis(salicylimine)
Salophen	6,6'-dimethyl-2,2'-[1,2-phenylenebis(nitrilomethylidyne)]diphenol
TON	Turnover number
TOF	Turnover frequency
NMM	N-methyl morpholine
DBU	1,8-Diazabicyclo[5.4.0]undec-7-ene
RWGS	reverse water gas shift
FTS	Fischer tropesch synthesis
TMP	tetramethylpiperidine
MeOH	Methanol
CCU	carbon capture and utilization
sc	supercritical
DMAP	4-(dimethylamino)pyridine
IL	ionic liquid
PEI	polyethylene imine
TH	transfer hydrogenation
TBD	triazabicyclo[4.4.0]dec-5-ene
TBA	tertbutylammonium
GC	gas chromatography
MS	Mass spectrometry

## Statement of contribution

The candidate (Alexandros Paparakis) designed and optimized the synthetic procedures of appendices 1, 2 and 4. He also recorded all NMR spectra associated with appendices 1, 2 and 4. The candidate performed and designed catalytic experiments of appendices 1, 2 and 4 and interpreted the results afterwards. Additionally, he synthesized the catalysts for appendix 3, conducted and designed catalytic experiments, recorded NMR and interpreted the IR data. The contributions of other authors are as follows. Martin Hulla collected the high-pressure NMR data for appendices 1 and 3. Roland Turnell-Ritson and Joshua Sapsford synthesized  ${}^5\text{Bu}_3\text{SnOTf}$  and  $\text{NPh}_3\text{SnOTf}$ . Andrew Ashley worked as an advisor on appendix 1. Andrea Žáková and Pritha Saha conducted catalytic experiments, interpreted NMR data and synthesized catalysts for appendix 3. Martin Zábranský collected the X-ray structural data for all the compounds in appendix 3. Jaroslav Kukla conducted the elemental analysis for all compounds in appendix 3. Gabriela Gastelu and Jorge G. Uranga completed all the calculations associated with appendix 3.

## List of appendices

### Appendix 1

Tin-catalyzed reductive coupling of amines with  $\text{CO}_2$  and  $\text{H}_2$

Alexandros Paparakis,<sup>a</sup> Roland C. Turnell-Ritson,<sup>b</sup> Joshua S. Sapsford,<sup>b</sup> Andrew E. Ashley<sup>b</sup> and Martin Hulla

\*<sup>a</sup>

### Appendix 2

Frustrated Lewis Pairs Catalyse the Solvent-Assisted Synthesis of Azoles from ortho-Substituted Anilines,  $\text{CO}_2$  and  $\text{H}_2$

Alexandros Paparakis<sup>a</sup> and Martin Hulla\*<sup>a</sup>

### Appendix 3

Hexacoordinated tin complexes catalyse imine hydrogenation with  $\text{H}_2$

Andrea Žáková,<sup>a</sup> Pritha Saha,<sup>a</sup> Alexandros Paparakis,<sup>a</sup> Martin Zábranský,<sup>a</sup> Gabriela Gastelu,<sup>b</sup> Jaroslav Kukla,<sup>c</sup> Jorge G. Uranga<sup>b</sup> and Martin Hulla \*<sup>a</sup>

#### **Appendix 4**

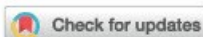
Unpublished results – Indium(III) triflate catalyses the transfer-hydrogenation of CO<sub>2</sub> to formate for the N-formylation of amines.

Alexandros Paparakis<sup>a</sup>, Daniel Shirwani<sup>a</sup> and Martin Hulla<sup>\*a</sup>



## Appendix 1 Tin-catalyzed reductive coupling of amines with CO<sub>2</sub> and H<sub>2</sub>

Alexandros Paparakis,<sup>a</sup> Roland C. Turnell-Ritson,<sup>b</sup> Joshua S. Sapsford,<sup>b</sup> Andrew E. Ashley<sup>b</sup> and Martin Hulla<sup>\*a</sup> **Catal. Sci. Technol.**, 2023,**13**, 637-644

Cite this: *Catal. Sci. Technol.*, 2023,  
13, 637Tin-catalyzed reductive coupling of amines with  
CO<sub>2</sub> and H<sub>2</sub>†Alexandros Paparakis,<sup>a</sup> Roland C. Turnell-Ritson,<sup>b</sup> Joshua S. Sapsford,<sup>b</sup>  
Andrew E. Ashley<sup>b</sup> and Martin Hulla<sup>b</sup> \*<sup>a</sup>

Reductive coupling of amines with CO<sub>2</sub> and H<sub>2</sub> can be catalyzed by transition metals. However, functional group (FG) tolerance is improved when using auxiliary main group hydrides (instead of H<sub>2</sub>), which makes them more suitable for the synthesis of functionalized molecules. Replacing auxiliary main group hydrides with frustrated Lewis pairs (FLPs) can, in theory, generate comparably selective hydrides *in situ* from H<sub>2</sub> activation. Herein, we report the selective *N*-formylation of amines via CO<sub>2</sub> hydrogenation catalyzed by a series of R<sub>3</sub>SnX (R = alkyl, X = Cl, OTf, NTf<sub>2</sub>, ClO<sub>4</sub>) Lewis acids, which form an FLP with the amine substrate and/or 2,4,6-collidine. FLP dihydrogen activation leads to the *in situ* formation of an R<sub>3</sub>Sn-H species with excellent selectivity toward CO<sub>2</sub> hydrogenation over other reducible FGs. Consequently, amines containing alkenes, amides, esters, and carboxylic acids can be *N*-formylated with CO<sub>2</sub> and H<sub>2</sub>. Increasing the steric bulk of the alkyl substituents prevents the redistribution of the R<sub>3</sub>SnX Lewis acid to R<sub>4</sub>Sn and R<sub>2</sub>SnX<sub>2</sub>, which is the primary cause of catalyst decomposition. Cy<sub>3</sub>SnOTf reached turnovers of >300 and amine conversions of up to 100%. In addition to synthesis, isolation, and testing of key intermediates for their reactivity, we identified an off-cycle intermediate by *in operando* <sup>1</sup>H NMR spectroscopy and therefore propose a mechanistic cycle. By avoiding the use of any transition metals or auxiliary main group hydrides, our procedure opens a pathway for developing transition-metal-free CO<sub>2</sub> hydrogenation methods utilising hydrogen gas.

Received 22nd September 2022  
Accepted 7th December 2022

DOI: 10.1039/d2cy01659a

rsc.li/catalysis

## Introduction

Carbon dioxide may be used as a renewable C1 source to produce fine chemicals, pharmaceuticals and fuels.<sup>1–4</sup> However, many applications require CO<sub>2</sub> reduction. For this purpose, H<sub>2</sub> is the most atom-economical reductant. Since reversible dihydrogen activation by phosphoranes<sup>5</sup> first highlighted the potential of small-molecule activation by main-group frustrated Lewis pairs (FLPs), FLPs have been shown to activate other small molecules, including CO,<sup>6</sup> N<sub>2</sub>O<sup>7</sup> and SO<sub>2</sub>,<sup>8,9</sup> amongst others.<sup>10</sup> In addition, FLPs can also promote the catalytic reduction of various organic

substrates.<sup>11–16</sup> Direct CO<sub>2</sub> hydrogenation by FLPs and H<sub>2</sub> has, nevertheless, proved more difficult.<sup>11,12,17</sup>

Using FLPs, CO<sub>2</sub> is stoichiometrically reduced to methanol with H<sub>2</sub> by B(C<sub>6</sub>F<sub>5</sub>)<sub>3</sub> and 2,2,6,6-tetramethylpiperidine (TMP).<sup>18</sup> However, at the high temperatures of this reaction, Lewis acid (LA) decomposition by the by-product H<sub>2</sub>O precludes catalysis.<sup>18,19</sup> A similar catalytic hydrogenation with B(C<sub>6</sub>F<sub>5</sub>)<sub>3</sub> and 2,6-lutidine requires a silyl halide, which captures the products *in situ* and assists LA-oxygen bond splitting, promoting turnover.<sup>20</sup> In turn, CO<sub>2</sub> reduction to formate by H<sub>2</sub> with B(C<sub>6</sub>F<sub>5</sub>)<sub>3</sub> and excess M<sub>2</sub>CO<sub>3</sub> (M = Li, Na, Cs) only results in high turnover numbers (TONs) in the presence of potassium metal, which acts as a hydroxyl scavenger.<sup>21</sup> In the absence of additives, FLPs promote CO<sub>2</sub> reduction when using auxiliary reductants such as hydrosilanes or hydroboranes.<sup>19,22–24</sup>

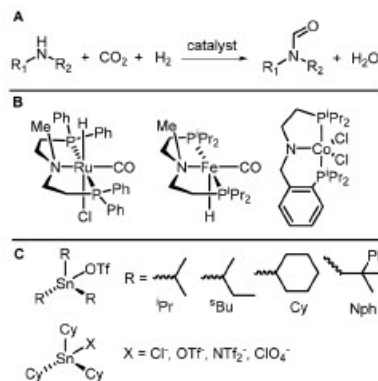
An alternative approach to catalytic CO<sub>2</sub> reduction with H<sub>2</sub> consists of reductive coupling of CO<sub>2</sub> and amines. For example, *N*-formylation (Scheme 1A) simultaneously yields valuable products, including solvents,<sup>25–27</sup> pharmacologically relevant compounds,<sup>28–30</sup> and synthetic building blocks.<sup>31,32</sup>

FLP-catalyzed reductive coupling of amines with CO<sub>2</sub> and H<sub>2</sub>, however, remains unprecedented. Although transition-metals (TMs) such as Ru,<sup>33</sup> Rh,<sup>34</sup> Fe,<sup>35,36</sup> and Co<sup>2</sup> complexes

<sup>a</sup> Department of Inorganic Chemistry, Faculty of Science, Charles University, Prague 128 00, Czech Republic. E-mail: Martin.hulla@natur.cuni.cz

<sup>b</sup> Department of Chemistry, White City Campus, Imperial College London, London W12 0BZ, UK

† Electronic supplementary information (ESI) available: General procedures, detailed experimental data, optimization of reaction conditions, effect of reaction solvent, kinetic tests of isolated intermediates, heterocycle reduction, analysis of catalysts, Gutman-Beckett analysis, catalyst stability tests and benzylamine reactivity, *in situ* NMR measurements, and substrate scope analysis. See DOI: <https://doi.org/10.1039/d2cy01659a>



**Scheme 1** A) *N*-formylation of amines with CO<sub>2</sub> and H<sub>2</sub>; B) examples of transition metal catalysts; C) Lewis acid components of FLP catalysts reported in this study.

and/or salts (Scheme 1B) catalyze *N*-formylation reactions with CO<sub>2</sub> and H<sub>2</sub> at 10<sup>2</sup>–10<sup>4</sup> TONs, only a few of these reactions are selective for CO<sub>2</sub> reduction over other reducible FGs.<sup>34</sup> Given their lack of selectivity and the search for inexpensive, greener catalysts, TM-free catalysts have emerged, including carbenes,<sup>37,38</sup> ionic liquids<sup>39,40</sup> and inorganic salts.<sup>14,41</sup> These TM-free catalysts tend to be selective to CO<sub>2</sub> reduction over other reducible FGs and more active toward *N*-formylation of aromatic amines than TM catalysts.<sup>42</sup> However, they require auxiliary, main-group hydride sources such as hydrosilanes or hydroboranes. As a result, the atom economy of these reactions is low.

In theory, FLPs and H<sub>2</sub> may replace these auxiliary main-group hydrides by *in situ* generation of comparable reducing agents with potentially high selectivity to CO<sub>2</sub> hydrogenation. Catalytic turnovers would then be achieved by formate transfer to an amine and elimination of water from the FLPs. Nevertheless, other than a few exceptions, FLPs tend to be water sensitive.<sup>15,43–48</sup> This property of FLPs might have hindered the development of FLP catalysts for reductive *N*-functionalization of amines with CO<sub>2</sub> and H<sub>2</sub>.

In this study, we developed several novel water-tolerant FLPs comprising R<sub>3</sub>SnX LAs (where R = alkyl group and X = Cl, OTf, NTf<sub>2</sub> or ClO<sub>4</sub>) in combination with the amine substrate or 2,4,6-collidine as the Lewis base (LB). These FLPs efficiently catalyzed *N*-formylation of various amines with CO<sub>2</sub> and H<sub>2</sub> at 453 K, under 100 bar H<sub>2</sub> and 4 bar CO<sub>2</sub> pressure, in sulfolane ((CH<sub>2</sub>)<sub>4</sub>SO<sub>2</sub>) solvent. Low partial pressures of CO<sub>2</sub> were beneficial for this reaction catalyzed by our water tolerant FLPs, in contrast to TM catalysts, thus demonstrating the comparative ease of CO<sub>2</sub> reduction by main group hydrides. Consequently, amines can be selectively *N*-formylated with CO<sub>2</sub> and H<sub>2</sub> in the presence of other FGs (alkenes, amides, esters, and carboxylic acids) without concomitant reduction.

## Results and discussion

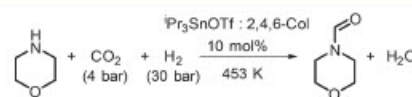
Considering the success of hydrosilanes as selective CO<sub>2</sub> reducing agents<sup>42,49</sup> in previous *N*-formylation reactions, we studied group 14-based FLPs as H<sub>2</sub> activation catalysts for *in situ* generation of group 14 hydrides. Our initial study was performed using [Pr<sub>3</sub>SnOTf: 2,4,6-collidine] (FLP1), as it is a water tolerant FLP.<sup>15</sup> To model the reaction with FLP1 morpholine was chosen as the model substrate at 453 K,<sup>14</sup> 30 bar of H<sub>2</sub> (ref. 2) and 4 bar of CO<sub>2</sub> (Scheme 2). Morpholine was selected because it is often the model substrate of choice for TM catalysts for this reaction and the product (*N*-formylmorpholine) can be used as a solvent and as an anticorrosive agent in the petrochemical industry.<sup>25–27</sup>

Although FLP reactions have been almost exclusively performed in aromatic or ethereal solvents,<sup>43,46,50</sup> the low solubility of carbamate salts (formed from amines and CO<sub>2</sub>) in these media render them unsuitable for the target application. After screening high-boiling-point solvents, we identified dipolar aprotic solvents, such as *N*-methylpyrrolidone (NMP) and sulfolane, compatible with these R<sub>3</sub>SnX/base FLPs as the most suitable reaction media (see ESI†). In line with these results, the related dimethylformamide (DMF) and dimethylsulfoxide (DMSO) have been previously shown to be the most efficient solvent systems for *N*-functionalization of amines with CO<sub>2</sub> using main group hydrides.<sup>49,51,52</sup> Considering its lower toxicity, sulfolane was selected for further reactions.

Increasing the CO<sub>2</sub> partial pressure from 1 bar to 4 bar improved the formation of formamide from 16% to 26% (Fig. 1A) most likely due to the increase in the rate of CO<sub>2</sub> insertion into the Sn–H bond. By contrast, partial pressures above 4 bar lowered the reactivity of the system (Fig. 1A).

This reaction slowed down at higher partial pressures of CO<sub>2</sub>, but reactions catalyzed by TMs, such as Co<sup>2</sup> and Ru<sup>3+</sup> complexes, use partial pressures of 30–35 bar CO<sub>2</sub> and a typical equimolar ratio of H<sub>2</sub> to CO<sub>2</sub>. Equivalent experiments using partial pressures of H<sub>2</sub> and CO<sub>2</sub> of 30 bar with FLP1, however, resulted in only 14% conversion, in contrast to 26% at 4 bar of CO<sub>2</sub>. This difference implies that in the *N*-formylation reaction CO<sub>2</sub> insertion into the Sn–H bond is easier with FLP1 than with previously reported TM *N*-formylation catalysts and that high selectivity to CO<sub>2</sub> reduction may be reached.

Increasing the H<sub>2</sub> partial pressure increased morpholine conversion (Fig. 1B) rapidly up to 50 bar, and more gradually up to 100 bar. The disparity between H<sub>2</sub> and CO<sub>2</sub> partial pressure, and a H<sub>2</sub>-to-CO<sub>2</sub> molar ratio >12.5 suggest that



**Scheme 2** *N*-formylation of morpholine with CO<sub>2</sub> and H<sub>2</sub> catalyzed by [Pr<sub>3</sub>SnOTf: 2,4,6-collidine].



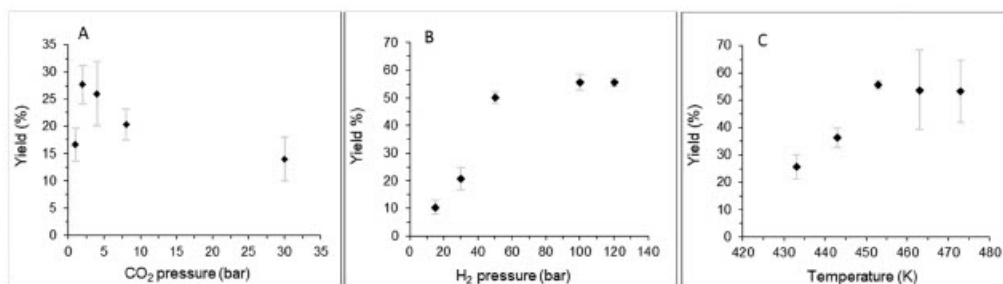


Fig. 1 Optimization of reaction conditions: morpholine (0.5 mmol), FLP1 (10 mol%), sulfolane (5 mL), 24 h and unless otherwise specified H<sub>2</sub> (100 bar), CO<sub>2</sub> (4 bar), temperature (453 K); A) effect of CO<sub>2</sub> partial pressure at a constant partial pressure of H<sub>2</sub> (30 bar); B) effect of H<sub>2</sub> partial pressure; C) effect of reaction temperature. All reactions were repeated in triplicate, and the reaction product was quantified by <sup>1</sup>H NMR with DCM as the internal standard. Error bars represent one standard deviation.

hydrogen activation by FLP1 is slow and possibly the rate determining step, as observed in numerous examples for FLP hydrogenation systems.<sup>53</sup>

Increasing the reaction temperature also increased morpholine conversion up to 453 K (Fig. 1C). At higher temperatures, <sup>1</sup>H NMR and GC-MS measurements indicated that the LA component of FLP1 redistributes to <sup>1</sup>Pr<sub>4</sub>Sn, which is clearly identified by mass spectrometry measurement (291 *m/z*) with a characteristic tin isotopic pattern, and presumably to <sup>1</sup>Pr<sub>2</sub>Sn(OTf)<sub>2</sub>, which is the expected thermodynamic product of the redistribution.<sup>54,55</sup> After synthesizing and testing authentic <sup>1</sup>Pr<sub>2</sub>Sn(OTf)<sub>2</sub>: 2,4,6-collidine (FLP1b), we found that this product is also an active catalyst in the presence of a suitable base, albeit with a lower activity (Table 1, compare entries 1 and 12).

At temperatures above 453 K, the favourable temperature effect is, at least in part, balanced out by the decrease in the amount of the more active <sup>1</sup>Pr<sub>2</sub>SnOTf LA and its conversion

to <sup>1</sup>Pr<sub>2</sub>Sn(OTf)<sub>2</sub> (and inactive <sup>1</sup>Pr<sub>4</sub>Sn). This conversion to <sup>1</sup>Pr<sub>2</sub>Sn(OTf)<sub>2</sub> may partly account for the plateau observed at higher temperatures (Fig. 1C; *vide infra*). Further testing of FLP1 stability at 453 K in a 2-week long reaction revealed that the maximum TON of the system in the *N*-formylation of morpholine with CO<sub>2</sub> and H<sub>2</sub> is 162 (see ESI†).

The stability and ability of LA to split H<sub>2</sub> is closely related to the identity of the R<sup>43,56</sup> and X groups<sup>57</sup> attached to the tin center. However, only FLP1 and [<sup>1</sup>Pr<sub>2</sub>SnNTf<sub>2</sub>: 2,4,6-collidine] were demonstrated to be both water tolerant and active FLP hydrogenation catalysts. Hence, to improve the activity and stability of the system and to expand the scope of water-tolerant, tin-based FLPs, we tested various R<sub>3</sub>SnX species (Table 1) under optimized *N*-formylation reaction conditions: morpholine (1 mmol), sulfolane (4 mL), [LA: 2,4,6-collidine] (10 mol%), CO<sub>2</sub> (4 bar), H<sub>2</sub> (100 bar), 453 K, 24 h. Only R groups larger than isopropyl (R = Nph, <sup>t</sup>Bu & Cy; Fig. 2) were considered because excessively small groups could preclude FLP-type chemistry due to adduct formation,<sup>58</sup> whereas larger steric profiles should promote water stability of FLPs,<sup>47</sup> and should hinder the undesirable redistribution reaction for FLP1, which likely involves two R<sub>3</sub>SnX molecules in a bimolecular mechanism<sup>57</sup> and thus be inhibited by increased steric hindrance.<sup>46,47,51</sup>

The increase in Lewis acid steric hindrance from FLP1 to <sup>t</sup>Bu<sub>3</sub>SnOTf: 2,4,6-collidine (FLP2) or to Nph<sub>3</sub>SnOTf: 2,4,6-collidine (FLP3) decreased the *N*-formylmorpholine yield to

Table 1 Effect of R and X groups of R<sub>3</sub>SnX and R<sub>2</sub>SnX<sub>2</sub> on *N*-formylation of morpholine in the presence of 2,4,6-collidine

Entry	Lewis acid	Loading (mol%)	Yield (%)	TOF <sup>b</sup> [h <sup>-1</sup> ]
1	<sup>1</sup> Pr <sub>2</sub> SnOTf	10	57	0.25
2	<sup>t</sup> Bu <sub>3</sub> SnOTf	10	43	0.17
3	Nph <sub>3</sub> SnOTf	10	39	0.17
4	Cy <sub>3</sub> SnOTf	10	95 <sup>c</sup>	—
5	Cy <sub>3</sub> SnClO <sub>4</sub>	10	83 <sup>c</sup>	—
6	Cy <sub>3</sub> SnNTf <sub>2</sub>	10	82 <sup>c</sup>	—
7	Cy <sub>3</sub> SnCl	10	70	0.29
8	Cy <sub>3</sub> SnOTf	1	28	1.16
9	Cy <sub>3</sub> SnClO <sub>4</sub>	1	17	0.71
10	Cy <sub>3</sub> SnNTf <sub>2</sub>	1	16	0.67
11	—	0	0	0
12	<sup>1</sup> Pr <sub>2</sub> Sn(OTf) <sub>2</sub>	10	28	0.13
13 <sup>a</sup>	<sup>1</sup> Pr <sub>2</sub> SnOTf	10	95	—

Reaction conditions: morpholine (1 mmol), sulfolane (4 mL), LA: 2,4,6-collidine (1–10 mol%), CO<sub>2</sub> (4 bar), H<sub>2</sub> (100 bar), 453 K, 24 h, average yield after three runs. Yield was determined by <sup>1</sup>H NMR with an internal standard. <sup>a</sup> 48 h reaction. <sup>b</sup> TOF was only calculated for reactions that did not approach thermodynamic conversions. <sup>c</sup> Morpholine was completely consumed *i.e.* 100% conversion.

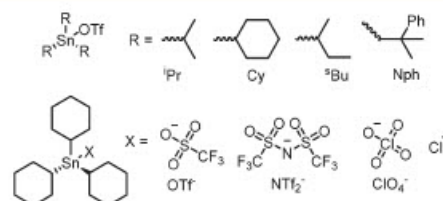


Fig. 2 Structures of R<sub>3</sub>SnX Lewis acid tested as components of FLP catalysts for the *N*-formylation of morpholine.

43 and 39%, respectively (Table 1, entries 1–3). In addition, the build-up of tin formate and hydride as confirmed by diagnostic resonances in the  $^1\text{H}$  NMR spectrum (at 8.58 and 5.67 ppm respectively) suggests that too large an increase in steric bulk can either slow  $\text{CO}_2$  insertion into the tin-hydride bond and/or hinder formate transfer to the amine substrate. Nevertheless,  $\text{Cy}_3\text{SnOTf}$ : 2,4,6-collidine (**FLP4**) showed 100% morpholine conversion and 95% *N*-formylmorpholine yield (Table 1, entry 4) without  $\text{Cy}_3\text{SnOTf}$  redistribution or other decomposition. The maximum TON for **FLP4** exceeded 300 (see ESI $^\dagger$ ), thus confirming that **FLP4** is more stable than **FLP1**.

For the  $\text{Cy}_3\text{SnX}$ : 2,4,6-collidine system, the X moiety was subsequently investigated using the conjugate bases of three other strong Brønsted acids: perchlorate ( $\text{ClO}_4^-$ ) (**FLP5**), trifluoromethanesulfonimide ( $\text{NTf}_2^-$ ) (**FLP6**), and chloride (**FLP7**). All but chloride gave full conversion in 24 h at 10 mol% loading (Table 1, entries 5–7) and so were tested at a loading of 1 mol% (Table 1, entries 8–10) for accurate comparison. Although  $\text{Cy}_3\text{SnNTf}_2$  and  $\text{Cy}_3\text{SnClO}_4$  are more Lewis acidic than  $\text{Cy}_3\text{SnOTf}$ , as determined using the Gutmann–Beckett method (see ESI $^\dagger$ ) and hence **FLP5** and **FLP6** should be better able to activate  $\text{H}_2$ , however, their catalytic activity in the *N*-formylation reaction was lower than that of **FLP4**, indicating a decrease in water tolerance or stability. Nevertheless, **FLP4**–**FLP7** demonstrated higher activity than **FLP1** (Table 1, entries 1 and 4–7), confirming the superiority of  $\text{Cy}_3\text{SnX}$  over  $^i\text{Pr}_3\text{SnX}$  in tin-based FLP-catalyzed hydrogenation reactions.

Both 2,4,6-collidine and morpholine can act as the Lewis base in FLP catalysis. While morpholine is the stronger Lewis base, and is hence expected to better promote  $\text{H}_2$  activation, its reactivity with  $\text{CO}_2$  decreases its basicity under the reaction conditions (*vide infra*) resulting in higher FLP activity of **FLP1** than that of  $^i\text{Pr}_3\text{SnOTf}$ : morpholine (**FLP1c**) (Table 2 entries 1 and 2). Similar results were obtained for **FLP4** and  $\text{Cy}_3\text{SnOTf}$ : morpholine (**FLP4b**), where *N*-formylmorpholine was obtained in 28% and 15% yield respectively (Table 2, entries 3 and 4).

Table 2 Effect of an added Lewis base on *N*-formylation of morpholine with  $^i\text{Pr}_3\text{SnOTf}$  and  $\text{Cy}_3\text{SnOTf}$  LAs

Entry	Lewis acid	Lewis base <sup>c</sup>	Yield (%)	TOF <sup>c</sup> [h <sup>-1</sup> ]
1	$^i\text{Pr}_3\text{SnOTf}^a$	Collidine <sup>a</sup>	57	0.25
2	$^i\text{Pr}_3\text{SnOTf}^a$	—	44	0.21
3	$\text{Cy}_3\text{SnOTf}^b$	Collidine <sup>b</sup>	28	1.16
4	$\text{Cy}_3\text{SnOTf}^b$	—	15	0.63
5	$\text{Cy}_3\text{SnOTf}^b$	TMP-H <sup>b</sup>	20	0.73
6	$\text{Cy}_3\text{SnOTf}^b$	TMP-Me <sup>b</sup>	17	0.71

Reaction conditions: morpholine (1 mmol), sulfolane (4 mL),  $\text{CO}_2$  (4 bar),  $\text{H}_2$  (100 bar), 453 K, 24 h, average yield after three runs. Yield was determined by  $^1\text{H}$  NMR with an internal standard. <sup>a</sup> 10 mol% of FLP. <sup>b</sup> 1 mol% of FLP. <sup>c</sup> Added Lewis base and where no base is indicated morpholine acts as the Lewis base. TMP-H is 2,2,6,6-tetramethylpiperidine and TMP-Me is 1,2,2,6,6-pentamethylpiperidine.

In combination with  $\text{Cy}_3\text{SnOTf}$  the use of 2,2,6,6-tetramethylpiperidine (TMP-H) (**FLP4c**) and 1,2,2,6,6-pentamethylpiperidine (TMP-Me) (**FLP4d**) instead of 2,4,6-collidine resulted in 20 and 18% yield respectively (Table 2, entries 5 and 6), which are both lower than obtained with **FLP4** (Table 2 entry 3) under equivalent reaction conditions. Moreover, TMP-Me showed signs of instability in the presence of  $\text{Cy}_3\text{SnOTf}$  and when **FLP4d** was used in the reaction in the absence of  $\text{H}_2$ , the system still achieved 3% yield of *N*-formylmorpholine indicating a possible hydride abstraction from TMP-Me by  $\text{Cy}_3\text{SnOTf}$  and subsequent  $\text{CO}_2$  reduction *via* transfer hydrogenation rather than  $\text{H}_2$  activation. *N*-formylation of TMP-H has not been observed presumably due to its large steric profile.

Due to its highest activity, substrate scope was explored with **FLP4** as the catalyst at low-to-moderate conversions, which were achieved with 2 mol% of the catalyst for both highly and poorly reactive substrates, to highlight kinetic differences in reactivity between various amines (Fig. 3). Secondary amines such as morpholine (**1**), *N*-methylpiperazine (**2**) and diisopropylamine (**3**) were all successfully *N*-formylated. However, (**3**) proceeded at a much slower rate, most likely due to the increased steric profile of the amine. The tertiary amine (**2**), alcohol (**4**) alkene (**5**) and amide (**6**) functional groups were well tolerated. These results

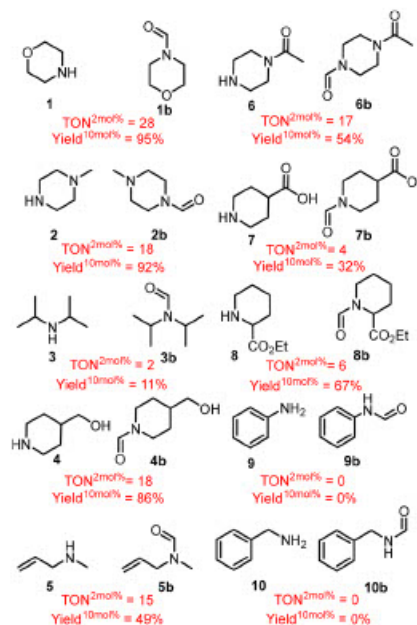


Fig. 3 Substrate scope for the *N*-formylation reaction with  $\text{CO}_2$ ,  $\text{H}_2$  and  $\text{Cy}_3\text{SnOTf}$  catalyst. Reaction conditions: amine (1 mmol), sulfolane (4 mL), LA: 2,4,6-collidine (2 mol%),  $\text{CO}_2$  (4 bars),  $\text{H}_2$  (100 bars), 453 K, 24 h. Yields were determined by  $^1\text{H}$  NMR and structures confirmed by GC-MS.



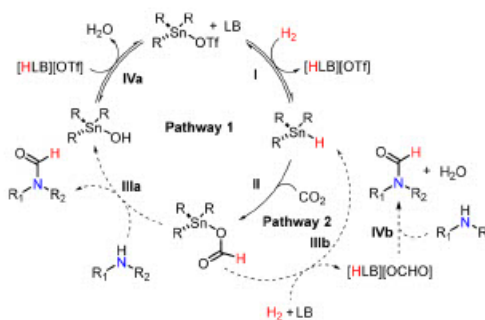
demonstrate the high tolerance of the system to alcohol functionalities, which usually inhibit FLP reactivity. Moreover, concomitant reduction of the alkene (5) or the amide (6) double bonds was not observed. Carboxylic acid FG (7) was also tolerated although the reaction was 7 times slower than with morpholine presumably due to the reversibility of H<sub>2</sub> activation *via* protonation of the tin-hydride. Partial elimination of the ester FG (8) resulted in a mixture of ethyl 1-formylpiperidine-2-carboxylate and *N*-formylpiperidine in the ratio of 7 to 3. The reaction rate also decreased when positioning the ester group next to the reactive amine. Accordingly, steric hindrance might have played a key role in this deceleration. Moreover, such functional group tolerance is the key to the synthesis of *N*-formamides with biological applications because pharmacological structure activity relationships are extremely sensitive and *N*-formylated compounds are known to modulate physiological processes related to sepsis, Alzheimer's disease, and respiratory failure.<sup>28–30</sup>

Aromatic (9) and benzylic (10) amines were unreactive towards *N*-formylation. The poor reactivity of aromatic amines, which may be attributed to their low nucleophilicity, matches that of TM-catalyzed reactions.<sup>2</sup> Benzylamine undergoes a side reaction to form a mixture of *N*-benzyl-1-phenylmethanimine and dibenzylamine in the 24 h test (see ESI†).

To demonstrate the synthetic utility of the protocol the substrate scope was performed at higher conversion rates (using 10 mol% catalyst loading). The conversions of morpholine (1), *N*-methylpiperazine (2), *N*-formyl-4-piperidinemethanol (4), isonipecotic acid (7) and ethyl-pipecolate (8) all scaled directly with catalyst loading. The conversions of diisopropylamine (3), *N*-allylmethylamine (5) and 1-acetylpiperazine (6), however, did not scale directly with catalyst loading. The reaction of *N*-allylmethylamine (5) showed significant CO<sub>2</sub> over reduction to *N*-methylation product, as confirmed by GC-MS, of the substrate which likely contributed to the decreased presence of the *N*-formyl product. Analysis of the reaction of 1-acetylpiperazine (6) by <sup>1</sup>H NMR showed a buildup of Cy<sub>3</sub>Sn(OCOH) suggesting slow formate transfer and concurrent decrease in yield. Analysis of the reaction of diisopropylamine (6) by <sup>1</sup>H NMR showed build of Sn–H suggesting this amine slowed down insertion into the tin hydride bond which is likely due to the steric bulk of the amine being less suited to activate the Lewis acid hydride bond.

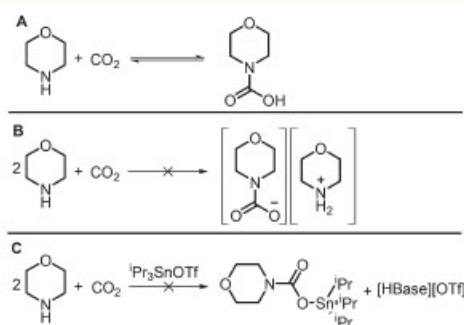
Based on our results and on previous literature, we proposed the following catalytic cycle (Scheme 3):

In the first step, H<sub>2</sub> is split heterolytically into tin hydride and ammonium triflate (Scheme 3, step I),<sup>15,16,43,56,57</sup> where the amine substrate or 2,4,6-collidine acts as the FLP base (Table 1, entry 1 (FLP1) and 13 (FLP1c)). Although the amine would be usually the stronger base, strong bases react with CO<sub>2</sub> (Scheme 4A), which results in lower *in situ* basicity of the amines and a beneficial effect of the much weaker base 2,4,6-collidine. As shown in Table 2, the reaction with 2,4,6-



Scheme 3 Catalytic cycle proposed for the *N*-formylation of amines with CO<sub>2</sub> and H<sub>2</sub> catalyzed by tin-based FLPs.

collidine (FLP1) achieves higher conversion than the reaction without (FLP1c) where morpholine acts as the Lewis base. This is also the case for Cy<sub>3</sub>SnOTf, when collidine is removed from the reaction (FLP4b) the rate is reduced by half. As often occurs with FLPs,<sup>53</sup> H<sub>2</sub> splitting is likely the rate-determining step, judging by the required H<sub>2</sub> pressure and by the disparity between H<sub>2</sub> and CO<sub>2</sub> partial pressures suitable for the productive reaction. In addition, H<sub>2</sub> activation is partly inhibited by reversible water<sup>15</sup> binding to FLP, but CO<sub>2</sub> binding to FLP was not observed in this system. *In situ* <sup>1</sup>H NMR experiments at 4 bar CO<sub>2</sub> and 100 bar H<sub>2</sub> between 298 K and 393 K revealed that morpholine captures CO<sub>2</sub> to form a carbamic acid (Scheme 4A), as shown by peaks at  $\delta = 3.19, 3.66$  and  $8.37$  ppm in a 4:4:1 ratio (see ESI†), rather than the expected carbamate salt (Scheme 4B), which precipitates from low polarity solvents. CO<sub>2</sub> capture by FLP1 or FLP1c or subsequent inhibition of FLP reactivity were not observed either (Scheme 4C).<sup>19</sup> Based on these results, above 4 bar CO<sub>2</sub>, the morpholine–carbamic acid equilibrium may hinder *N*-formylation<sup>26</sup> by inhibiting formate transfer or by protonating the tin hydride, leading to reversible hydrogen activation from FLP1. Further mechanistic insights are needed to confirm these hypotheses.



Scheme 4 A) Reaction of morpholine with CO<sub>2</sub> to carbamic acid in sulfolane; B) reaction of morpholine with CO<sub>2</sub> to carbamate salt in low-polarity media; C) hypothetical trapping of CO<sub>2</sub> by FLP1.

In the second step, CO<sub>2</sub> is reduced by the tin hydride to tin formate (Scheme 3, step II); facile CO<sub>2</sub> insertion into tin hydride bonds has been repeatedly demonstrated,<sup>59,60</sup> and is even reversible for some tin hydrides, such as tri-*n*-butyltin hydride.<sup>61</sup> Attempted CO<sub>2</sub> reduction to tin formate by **FLP4** without morpholine resulted only in the reduction of 2,4,6-collidine (indicated by the absence of the aromatic peak and the presence of two new methyl group signals in <sup>1</sup>H NMR, see ESI†). No tin formate was formed, suggesting that the presence of an amine may assist CO<sub>2</sub> insertion into the Cy<sub>3</sub>-Sn-H tin hydride bond, as observed for hydrosilane reductants.<sup>39</sup> Alternatively the reversibility of CO<sub>2</sub> insertion into the Cy<sub>3</sub>-Sn-H tin hydride bond may be ruled out as has been shown previously that CO<sub>2</sub> elimination from Cy<sub>3</sub>-Sn(OCOH) is not reversible, with neither CO nor CO<sub>2</sub> being formed at temperatures of up to 463 K.<sup>62</sup> Instead, Cy<sub>3</sub>-Sn(OCOH) decomposes into an insoluble orange solid.<sup>62</sup> The decomposition of Cy<sub>3</sub>-Sn(OCOH) at elevated temperatures may also explain the conversion plateau observed at temperatures above 463 K.

Synthesis of Cy<sub>3</sub>-Sn(OCOH) and its direct reaction with morpholine shows that formate transfer between the tin formate and amine substrate is fast, and subsequently forms the formamide product (Scheme 3, step IIIa see ESI† for details). The formate transfer is uninhibited, even at high partial pressures of CO<sub>2</sub>, as evidenced by the same conversion in the direct reaction of Cy<sub>3</sub>-Sn(OCOH) with morpholine at 6 bar CO<sub>2</sub> and 30 bar CO<sub>2</sub> (determined by <sup>1</sup>H NMR). Considering that the formate transfer reaction yield is the same at higher partial pressures of CO<sub>2</sub>, the off-cycle equilibrium between carbamic acid and amine may instead negatively affect hydrogen activation because protonation of the hydride may render H<sub>2</sub> activation reversible as opposed to hindering formate transfer.

The formamide product may be formed *via* two possible pathways, either by (1) direct formate transfer from the LA to the amine (Scheme 3 step IIIa) or (2) formate elimination from the LA and subsequent formylation of the amine (Scheme 3 step IIIb). Pathway 1 would result in the formation of Cy<sub>3</sub>-SnOH, and water would be eliminated (Scheme 3, steps IIIa and IVa) by its protonation, as previously shown for reversible binding of water by **FLP1**.<sup>15</sup> We synthesized Cy<sub>3</sub>-SnOH and morpholinium triflate to replicate the last step of the cycle. After 24 hours, the reaction of Cy<sub>3</sub>-SnOH, 2,4,6-collidine and morpholinium triflate (all present in catalytic amounts (10 mol%)) was 9 times slower for the *N*-formylation of morpholine than for **FLP4** under the same partial pressures of H<sub>2</sub> and CO<sub>2</sub> and at the same reaction temperature. This may mean that the reaction does not proceed exclusively *via* the hydroxide.

Instead, an alternate reduction pathway, like pathway 2, may be responsible such as the elimination of formate from Cy<sub>3</sub>-Sn(OCOH), leading to the direct reaction of morpholine and formate, which is a known pathway for transition metal catalyst (Scheme 3 steps IIIb and IVb).<sup>2</sup> Starting the *N*-formylation of morpholine at Cy<sub>3</sub>-Sn(OCOH), 2,4,6-collidine

and morpholinium triflate (all present in catalytic amounts (10 mol%)), which can both form the hydroxide and eliminate the formate, resulted in the same rate as starting from Cy<sub>3</sub>-SnOH and morpholinium triflate, *i.e.* 9 times slower than the reaction of **FLP4** with morpholine under the same conditions thus suggesting that this reaction proceeds *via* the hydroxide. However, running the standard reaction with Cy<sub>3</sub>-Sn(OCOH): 2,4,6-collidine as the catalyst (10 mol%) resulted in twice as much conversion as with Cy<sub>3</sub>-Sn(OCOH): 2,4,6-collidine and morpholinium triflate in 24 h, showing that very little morpholinium triflate is likely formed during the reaction and that the reaction may proceed *via* formate elimination (Scheme 3 steps IIIb and IVb).

## Conclusions

In conclusion, tin-based FLPs catalytically reduce CO<sub>2</sub> to formate with H<sub>2</sub>. Once CO<sub>2</sub> is reduced by the tin hydride to tin formate, the subsequent formate transfer to the amine substrate forms the formamide product. The *N*-formylation reaction is catalyzed by R<sub>3</sub>SnX LAs, which, together with the amine substrate or an additional LB such as 2,4,6-collidine, form the active FLP catalyst. Lewis bases that do not react with CO<sub>2</sub> seem to form more active FLP catalysts for the *N*-formylation reaction than stronger bases that react with CO<sub>2</sub>. The R and X groups of the LA have a strong effect on both catalyst activity and stability. With a TOF of 1.16 h<sup>-1</sup> and TON >300, **FLP4** is 4 times more active and at least 2 times more stable than our initial **FLP1** catalyst. These improvements in the stability and activity of the LA catalyst and its selectivity to CO<sub>2</sub> reduction show promise for further developments of FLP-catalyzed reductions of CO<sub>2</sub> and for the replacement of sacrificial main group hydrides in reductive coupling reactions of amines with CO<sub>2</sub>. FLPs have the potential to replace the now very selective auxiliary main group hydrides with H<sub>2</sub>, while maintaining comparable FG tolerance.

## Conflicts of interest

There are no conflicts to declare.

## Acknowledgements

We would like to thank Czech Science Foundation (GAČR 21-27431M) for funding this study. We would also like to thank Marianna Gerina for PXRD measurements and Carlos V. Melo for editing the manuscript.

## Notes and references

- G. A. Olah, A. Goepfert and G. K. S. Prakash, *J. Org. Chem.*, 2009, 74, 487–498.
- P. Daw, S. Chakraborty, G. Leitus, Y. Diskin-Posner, Y. Ben-David and D. Milstein, *ACS Catal.*, 2017, 7, 2500–2504.
- A. Modak, P. Bhanja, S. Dutta, B. Chowdhury and A. Bhaumik, *Green Chem.*, 2020, 22, 2500–2504.



- 4 Q. Liu, L. Wu, R. Jackstell and M. Beller, *Nat. Commun.*, 2015, **6**, 5933.
- 5 G. C. Welch, R. R. San Juan, J. D. Masuda and D. W. Stephan, *Science*, 2006, **314**, 1124–1126.
- 6 M. Sajid, L. M. Elmer, C. Rosorius, C. G. Daniliuc, S. Grimme, G. Kehr and G. Erker, *Angew. Chem., Int. Ed.*, 2013, **52**, 2243–2246.
- 7 E. Otten, R. C. Neu and D. W. Stephan, *J. Am. Chem. Soc.*, 2009, **131**, 9918–9919.
- 8 M. Sajid, A. Klose, B. Birkmann, L. Liang, B. Schirmer, T. Wiegand, H. Eckert, A. J. Lough, R. Fröhlich, C. G. Daniliuc, S. Grimme, D. W. Stephan, G. Kehr and G. Erker, *Chem. Sci.*, 2013, **4**, 213–219.
- 9 K. Y. Ye, M. Bursch, Z. W. Qu, C. G. Daniliuc, S. Grimme, G. Kehr and G. Erker, *Chem. Commun.*, 2017, **53**, 633–635.
- 10 F. Fontaine and É. Rochette, *Acc. Chem. Res.*, 2018, **51**, 454–464.
- 11 A. Jupp and D. Stephan, *Trends Chem.*, 2019, **1**, 35–48.
- 12 N. Li and W. X. Zhang, *Chin. J. Chem.*, 2020, **38**, 1360–1370.
- 13 A. Yanagisawa, Y. Yamashita, C. Uchiyama, R. Nakano, M. Horiguchi and K. Ida, *Synlett*, 2019, **30**, 738–742.
- 14 X. Jiang, Z. Huang, M. Makha, C. X. Du, D. Zhao, F. Wang and Y. Li, *Green Chem.*, 2020, **22**, 5317–5324.
- 15 J. Sapsford, D. Scott, N. Allcock, M. Fuchter, A. Ashley and C. Tighe, *Adv. Synth. Catal.*, 2018, **360**, 1066–1071.
- 16 J. S. Sapsford, D. Csókás, R. C. Turnell-Ritson, L. A. Parkin, A. D. Crawford, I. Pápai and A. E. Ashley, *ACS Catal.*, 2021, **11**, 9143–9150.
- 17 F. G. Fontaine, M. A. Courtemanche, M. A. Légaré and É. Rochette, *Coord. Chem. Rev.*, 2017, **334**, 124–135.
- 18 A. E. Ashley, A. L. Thompson and D. O'Hare, *Angew. Chem., Int. Ed.*, 2009, **48**, 9839–9843.
- 19 A. E. Ashley and D. O'Hare, *Top. Curr. Chem.*, 2012, 191–217.
- 20 T. Wang, M. Xu, A. R. Jupp, Z. W. Qu, S. Grimme and D. W. Stephan, *Angew. Chem., Int. Ed.*, 2021, **60**, 25771–25775.
- 21 T. Zhao, X. Hu, Y. Wu and Z. Zhang, *Angew. Chem., Int. Ed.*, 2019, **58**, 722–726.
- 22 S. N. Riduan, Y. Zhang and J. Y. Ying, *Angew. Chem., Int. Ed.*, 2009, **48**, 3322–3325.
- 23 E. R. Clark and M. J. Ingleson, *Angew. Chem., Int. Ed.*, 2014, **53**, 11306–11309.
- 24 M. A. Courtemanche, M. A. Légaré, L. Maron and F. G. Fontaine, *J. Am. Chem. Soc.*, 2013, **135**, 9326–9329.
- 25 J. Klankermayer, S. Wesselbaum, K. Beydoun and W. Leitner, *Angew. Chem., Int. Ed.*, 2016, **55**, 7296–7343.
- 26 L. Schmid, M. S. Schneider, D. Engel and A. Baiker, *Catal. Lett.*, 2003, **88**, 105–113.
- 27 S. Kar, A. Goepfert, J. Kothandaraman and G. K. S. Prakash, *ACS Catal.*, 2017, **7**, 6347–6351.
- 28 D. A. Dorward, C. D. Lucas, M. K. Doherty, G. B. Chapman, E. J. Scholefield, A. C. Morris, J. M. Felton, T. Kipari, D. C. Humphries, C. T. Robb, A. J. Simpson, P. D. Whitfield, C. Haslett, K. Dhaliwal and A. G. Rossi, *Thorax*, 2017, **72**, 928–936.
- 29 P. J. G. Cussell, M. G. Escalada, N. G. N. Milton and A. W. J. Paterson, *Neural Regen. Res.*, 2020, **15**, 1191.
- 30 C. F. Wenceslau, C. G. McCarthy, S. Gouloupoulou, T. Szasz, E. G. NeSmith and R. C. Webb, *Med. Hypotheses*, 2013, **81**, 532–535.
- 31 D. B. Nale and B. M. Bhanage, *Synlett*, 2015, **26**, 2835–2842.
- 32 P. D. Williams, M. G. Bock, B. E. Evans, R. M. Freidinger, S. N. Gallicchio, M. T. Guidotti, M. A. Jacobson, M. S. Kuo, M. R. Levy, E. V. Lis, S. R. Michelson, J. M. Pawluczyk, D. S. Perlow, D. J. Pettibone, A. G. Quigley, D. R. Reiss, C. Salvatore, K. J. Stauffer and C. J. Woyden, *Bioorg. Med. Chem. Lett.*, 1999, **9**, 1311–1316.
- 33 L. Zhang, Z. Han, X. Zhao, Z. Wang and K. Ding, *Angew. Chem., Int. Ed.*, 2015, **54**, 6186–6189.
- 34 T. V. Q. Nguyen, W.-J. Yoo and S. Kobayashi, *Angew. Chem.*, 2015, **127**, 9341–9344.
- 35 U. Jayarathne, N. Hazari and W. H. Bernskoetter, *ACS Catal.*, 2017, **8**, 1338–1345.
- 36 W. D. Li, D. Y. Zhu, G. Li, J. Chen and J. B. Xia, *Adv. Synth. Catal.*, 2019, **361**, 5098–5104.
- 37 S. N. Riduan, J. Y. Ying and Y. Zhang, *J. Catal.*, 2016, **343**, 46–51.
- 38 S. Das, F. D. Bobbink, S. Bulut, M. Soudani and P. J. Dyson, *Chem. Commun.*, 2016, **52**, 2497–2500.
- 39 M. Hulla, G. Laurenczy and P. J. Dyson, *ACS Catal.*, 2018, **8**, 10619–10630.
- 40 S. Majumdar, J. De, J. Hossain and A. Basak, *Tetrahedron Lett.*, 2013, **54**, 262–266.
- 41 M. Hulla, D. Ortiz, S. Katsyuba, D. Vasilyev and P. J. Dyson, *Chem. – Eur. J.*, 2019, **25**, 11074–11079.
- 42 M. Hulla, F. D. Bobbink, S. Das and P. J. Dyson, *ChemCatChem*, 2016, **8**, 3338–3342.
- 43 D. J. Scott, N. A. Phillips, J. S. Sapsford, A. C. Deacy, M. J. Fuchter and A. E. Ashley, *Angew. Chem., Int. Ed.*, 2016, **55**, 14738–14742.
- 44 D. J. Scott, T. R. Simmons, E. J. Lawrence, G. G. Wildgoose, M. J. Fuchter and A. E. Ashley, *ACS Catal.*, 2015, **5**, 5540–5544.
- 45 D. J. Scott, M. J. Fuchter and A. E. Ashley, *Chem. Soc. Rev.*, 2017, **46**, 5689–5700.
- 46 D. J. Scott, M. J. Fuchter and A. E. Ashley, *Angew. Chem., Int. Ed.*, 2014, **53**, 10218–10222.
- 47 Á. Gyömöre, M. Bakos, T. Földes, I. Pápai, A. Domján and T. Soós, *ACS Catal.*, 2015, **5**, 5366–5372.
- 48 É. Dorkó, M. Szabó, B. Kótai, I. Pápai, A. Domján and T. Soós, *Angew. Chem., Int. Ed.*, 2017, **56**, 9512–9516.
- 49 X. F. Liu, C. Qiao, X. Y. Li and L. N. He, *Pure Appl. Chem.*, 2018, **90**, 1099–1107.
- 50 S. Mummadi, A. Brar, G. Wang, D. Kenefake, R. Diaz, D. K. Unruh, S. Li and C. Krempner, *Chem. – Eur. J.*, 2018, **24**, 16526–16531.
- 51 Q. Zou, G. Long, T. Zhao and X. Hu, *Green Chem.*, 2020, **22**, 1134–1138.
- 52 M. Hulla and P. J. Dyson, *Angew. Chem., Int. Ed.*, 2020, **59**, 1002–1017.
- 53 D. W. Stephan, *J. Am. Chem. Soc.*, 2015, **137**, 10018–10032.
- 54 W. Caseri, *J. Organomet. Chem.*, 2014, **751**, 20–24.
- 55 K. Moedritzer, *Adv. Organomet. Chem.*, 1968, **6**, 171–271.



- 56 R. T. Cooper, J. S. Sapsford, R. C. Turnell-Ritson, D. H. Hyon, A. J. P. White and A. E. Ashley, *Philos. Trans. R. Soc., A*, 2017, **375**, 8.
- 57 J. S. Sapsford, D. Csókás, D. J. Scott, R. C. Turnell-Ritson, A. D. Piascik, I. Pápai and A. E. Ashley, *ACS Catal.*, 2020, **10**, 7573–7583.
- 58 G. R. Whittell, E. I. Balmond, A. P. M. Robertson, S. K. Patra, M. F. Haddow and I. Manners, *Eur. J. Inorg. Chem.*, 2010, **2010**, 3967–3975.
- 59 L. Plasseraud, *Inorganics*, 2021, **9**, 18.
- 60 S. Hadida, M. S. Super, E. J. Beckman and D. P. Curran, *J. Am. Chem. Soc.*, 1997, **119**, 7406–7407.
- 61 R. J. Klingler, I. Bloom and J. W. Rathke, *Organometallics*, 1985, **4**, 1893–1894.
- 62 B. D. Ellis, T. M. Atkins, Y. Peng, A. D. Sutton, J. C. Gordon and P. P. Power, *Dalton Trans.*, 2010, **39**, 10659–10663.

## Tin-catalyzed reductive coupling of amines with CO<sub>2</sub> and H<sub>2</sub>

Alexandros Paparakis,<sup>[a]</sup> Roland C. Turnell-Ritson,<sup>[b]</sup> Joshua S. Sapsford,<sup>[b]</sup> Andrew E. Ashley,<sup>[b]</sup> and Martin Hulla\*<sup>[a]</sup>

---

[a] Alexandros Paparakis, Martin Hulla  
Department of Inorganic Chemistry, Faculty of Science  
Charles University  
Prague 128 00  
Czech Republic  
E-mail: martin.hulla@natur.cuni.cz

---

[b] Roland C. Turnell-Ritson, Joshua S. Sapsford, Andrew E. Ashley  
Department of Chemistry  
Imperial College London  
White City Campus  
London W12 0BZ  
United Kingdom

### Supporting information

#### Contents

1. General procedures .....	3
2. Catalytic tests .....	3
2.1 General Procedure: .....	3
2.2 Typical result(s) of N-formylation of morpholine with CO <sub>2</sub> and H <sub>2</sub> : .....	4
2.3 Optimization of reaction solvent: .....	5
2.4 Optimization of CO <sub>2</sub> pressure: .....	6
2.5 Optimization of H <sub>2</sub> pressure: .....	6
2.6 Optimization of temperature: .....	7
3. Synthesis of catalysts .....	7
3.1 <sup>1</sup> Pr <sub>3</sub> SnOTf synthesis: This procedure was adapted from reference <sup>1</sup> .....	7
3.2 <sup>1</sup> Pr <sub>2</sub> Sn(OTf) <sub>2</sub> synthesis: .....	7
3.3 Cy <sub>3</sub> SnX synthesis: .....	9
3.4 Synthesis of <sup>t</sup> Bu <sub>4</sub> Sn .....	16
3.5 Synthesis of <sup>t</sup> Bu <sub>3</sub> SnOTf .....	16
3.6 Synthesis of (Nph) <sub>4</sub> Sn .....	18
3.7 (Nph) <sub>3</sub> SnOTf .....	18
4. Catalyst stability testing .....	21
4.1 General procedure for catalyst stability testing .....	21
5. Gutman-Beckett acidity measurements .....	21
5.1 General procedure for Gutman-Beckett acidity measurements .....	21
5.2 Results of Gutman-Beckett acidity measurements .....	21

6. Substrate scope.....	22
6.1 N-formylmorpholine .....	22
6.2 1-Formyl-4-methylpiperazine .....	22
6.3 N-Formylpiperidine-4-carboxylic acid.....	23
6.4 4-Acetylpiperazine-1-carbaldehyde.....	23
6.5 Ethyl 1-formylpiperidine-2-carboxylate.....	24
6.6 N-allyl-N-methylformamide .....	25
6.7 N,N-diisopropylformamide .....	25
6.8 N-Formyl-4-piperidinemethanol .....	26
6.9 Attempted N-formylation of benzylamine.....	26
7. Synthesis of 4-hydroxymethylpiperidine. ....	27
8. Heterocycle hydrogenation .....	29
9. Mechanism investigation: Formate transfer .....	30
9.1 $Cy_3SnOCOH$ synthesis: The procedure was adapted from reference <sup>9</sup> .....	30
9.2 Standard procedure for direct reaction of $Cy_3SnOCOH$ with morpholine:.....	32
9.3 Formate transfer experiments:.....	32
10. Mechanism investigation: $Cy_3SnOH$ reaction with morpholinium triflate .....	33
10.1 Standard procedure for direct reaction of $Cy_3SnOH$ with morpholinium triflate: .....	33
10.2 $Cy_3SnOH$ synthesis: .....	33
11. Mechanism investigation: In-situ $^1H$ NMR of the reaction mixture.....	36
12. References: .....	38

## 1. General procedures

All reagents and solvents were purchased from commercial suppliers (Sigma-Aldrich, Merck, Alpha-Aesar, TCI, Across, abcr, Thermo scientific, Linde gas a.s. and Lach:ner). Specifically, tricyclohexyltin chloride was purchased from Thermo scientific, silver triflate was purchased from Sigma-Aldrich, silver triflimide was purchased from TCI and silver perchlorate was purchased from Thermo scientific. Synthetic reagents were used as received and without further purification including hydrogen gas (99.90%) and carbon dioxide for food industry (99.90%) purchased from Linde gas a.s. Solvents used were reagent grade or better. THF, hexane and DCM were dried on PureSolv MD 5 automated solvent drying system from Inert®. All other solvents were dried and stored over 3Å molecular sieves (20%w/v) and degassed by sparging with dry N<sub>2</sub> for a minimum of 20 minutes before use. All synthetic experiments were carried out using standard Schlenk techniques. Unless otherwise specified <sup>1</sup>H, <sup>13</sup>C and <sup>119</sup>Sn NMRs were taken on a Bruker AVANCE-III (400 MHz) at 298K spectrometer and reported in ppm (δ). Deuterated solvents were purchased from abcr and used as received except for Gutmann-Beckett measurements, where CDCl<sub>3</sub> was dried and stored over 3Å molecular sieves (20%w/v). NMR spectroscopy abbreviations: s, singlet; d, doublet; t, triplet; m, multiplet. All the products of catalytic tests were identified by <sup>1</sup>H NMR data in comparison with literature, by GC coupled to mass spectrometry on a Shimadzu QP-2010 GC-MS with a Supelcowax 10 column and where necessary by comparison with genuine samples of the targeted compounds.

## 2. Catalytic tests

### 2.1 General Procedure:

In air R<sub>3</sub>SnX (0.1 mmol), 2,4,6-collidine (0.1 mmol) and morpholine (1 mmol) were dissolved in sulfolane (5 mL) in a steel autoclave. The autoclave was then sealed and purged 5 times with the desired pressure of CO<sub>2</sub>. The reaction was then topped up with the desired H<sub>2</sub> reaction pressure. The temperature and stirring rate were set using the Specview program on Parr 5000 series multi reactor system. T = 0 was defined as the time the heating starts. The heating was turned off 2 hours before the end of the stated reaction time and allowed to cool down under pressure over the course of the remaining 2 hours of the test i.e., for a reaction time of 24 hours the heating was turned off after 22 hours and the reaction was depressurized after the 24-hour mark. DCM (1 mmol) was added to the reactor, stirred and an aliquot was taken for <sup>1</sup>H NMR analysis in CDCl<sub>3</sub>. The conversion of morpholine and the yield of N-formylmorpholine were quantified by <sup>1</sup>H NMR analysis with the added DCM as the internal standard. Other reaction products were quantified by their respective N-formate signal in <sup>1</sup>H NMR and structures confirmed by GC-MS on a Shimadzu QP-2010 GC-MS with a Supelcowax 10 column.

## 2.2 Typical result(s) of N-formylation of morpholine with CO<sub>2</sub> and H<sub>2</sub>:

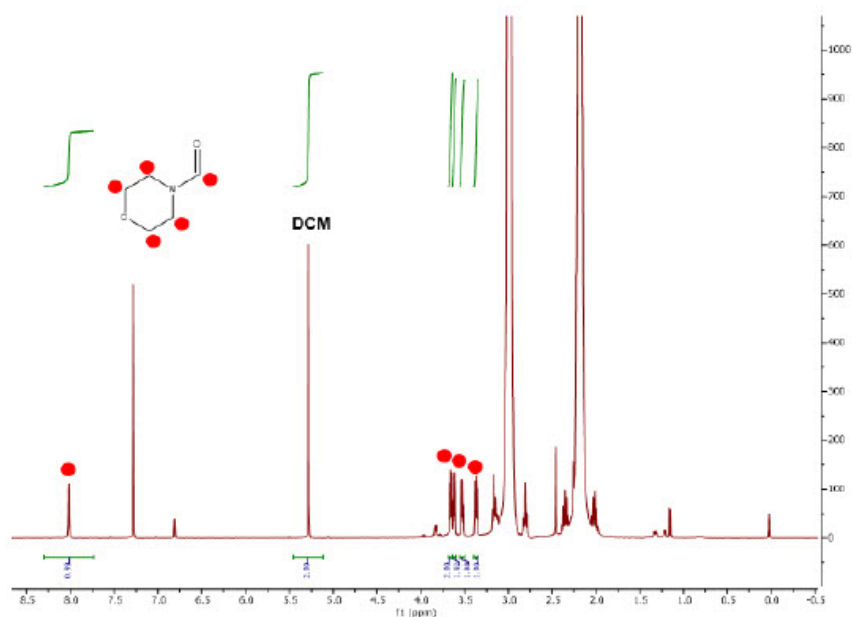
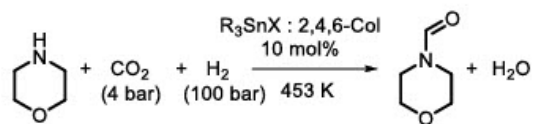
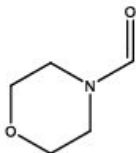


**Figure S1:** <sup>1</sup>H NMR of a reaction mixture at the end of a catalytic test of N-formylation of morpholine, where N-formylmorpholine peaks are marked by red spots. All unmarked peaks can be assigned to the reaction catalyst and sulfolane i.e R<sub>3</sub>SnX, 2,4,6-collidine and the reaction solvent.

### N-formylmorpholine:



$^1\text{H}$  NMR (400 MHz,  $\text{CDCl}_3$ )  $\delta$ : 3.36 (2H), 3.53 (m, 2H), 3.60-3.67 (m, 4H), 8.02 (1H); GC retention time 9.5 to 9.6 minutes; EI-MS ( $m/z$ ) calculated: 115.1, found 115.1 with a 92-98% agreement of EI-MS molecular fragmentation with NIST EI-MS library.

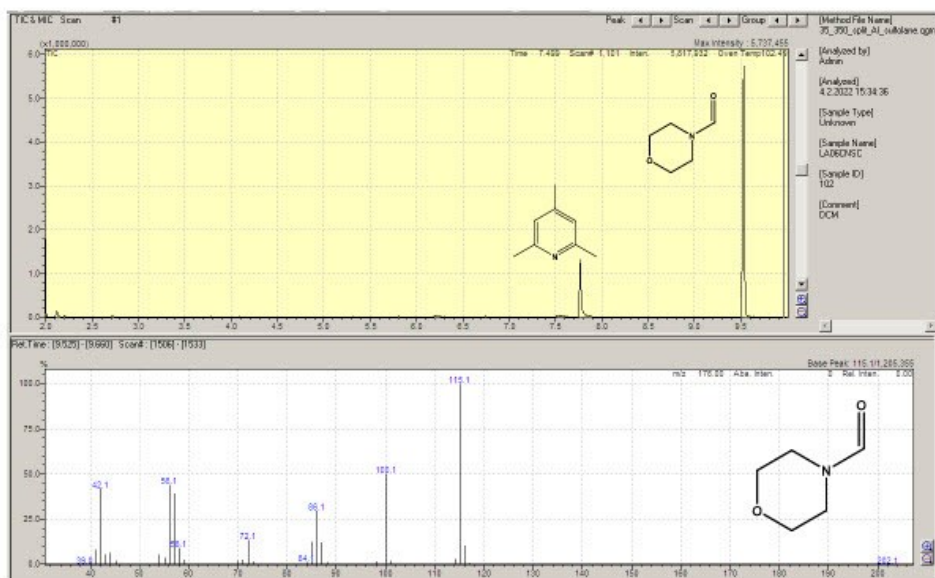


**Figure S2:** GC-MS analysis of a reaction mixture at the end of a catalytic test of N-formylation of morpholine with  $\text{R}_3\text{SnX}$  : 2,4,6-collidine as the reaction catalyst.

### 2.3 Optimization of reaction solvent:

$^i\text{Pr}_3\text{SnOTf}$  : 2,4,6-collidine (FLP1) have been reported to hydrogenate imines and aldehydes<sup>1,2</sup> in 1,2-dichlorobenzene (DCB) as the solvent. All other reported FLPs also used aromatic or ether solvents such as toluene, fluorobenzene, THF, dioxane or diethylether<sup>2-5</sup>. Nevertheless, initial attempts to N-formylate morpholine with  $\text{CO}_2$  and  $\text{H}_2$  as the reductant and FLP1 catalyst in DCB were limited by mass transfer due to poor solubility of morpholinium carbamate salt, which precipitated out of the reaction medium upon addition of  $\text{CO}_2$ . Thus, we turned to dipolar aprotic solvents namely sulfolane, N-methylpyrrolidone (NMP), ethylene carbonate, dimethylformamide



(DMF) and benzonitrile. It was found that NMP gave the highest conversion, however, it has been shown that it may decompose to a formylated product<sup>6</sup> so would be unreliable in the quantification of further reactions. DMF acted as a formylating reagent as well as the reaction solvent when it was tested so it was also disregarded. Considering this, sulfolane was selected as the reaction solvent as it gave comparable yields to NMP, and it is comparably less toxic.

**Table S1:** Effect of reaction solvent on the N-formylation of morpholine with FLP1 (10 mol%), H<sub>2</sub> (30 bar) and CO<sub>2</sub> (4 bar).

Catalyst (LA)	Solvent	Temperature (K)	Time (hr)	Yield (%)
<sup>i</sup> Pr <sub>3</sub> SnOTf	DCB	453	24	8
<sup>i</sup> Pr <sub>3</sub> SnOTf	Benzonitrile	453	24	15
<sup>i</sup> Pr <sub>3</sub> SnOTf	Sulfolane	453	24	22
<sup>i</sup> Pr <sub>3</sub> SnOTf	NMP	453	24	25
<sup>i</sup> Pr <sub>3</sub> SnOTf	Ethylene carbonate	453	24	5

#### 2.4 Optimization of CO<sub>2</sub> pressure:

**Table S2:** Effect of CO<sub>2</sub> partial pressure on the N-formylation of morpholine with FLP1 (10 mol%) and 5 mL sulfolane.

Catalyst (LA)	H <sub>2</sub> Pressure (bar)	CO <sub>2</sub> Pressure (bar)	Temperature (K)	Time (hr)	Yield (%)
<sup>i</sup> Pr <sub>3</sub> SnOTf	30	1	453	24	17
<sup>i</sup> Pr <sub>3</sub> SnOTf	30	2	453	24	27
<sup>i</sup> Pr <sub>3</sub> SnOTf	30	4	453	24	26
<sup>i</sup> Pr <sub>3</sub> SnOTf	30	8	453	24	20
<sup>i</sup> Pr <sub>3</sub> SnOTf	60	30	453	24	14

#### 2.5 Optimization of H<sub>2</sub> pressure:

**Table S3:** Effect of H<sub>2</sub> partial pressure on the N-formylation of morpholine with FLP1 (10 mol%) and 5 mL sulfolane.

Catalyst (LA)	H <sub>2</sub> Pressure (bar)	CO <sub>2</sub> Pressure (bar)	Temperature (K)	Time (hr)	Yield (%)
<sup>i</sup> Pr <sub>3</sub> SnOTf	15	4	453	24	10
<sup>i</sup> Pr <sub>3</sub> SnOTf	30	4	453	24	21
<sup>i</sup> Pr <sub>3</sub> SnOTf	50	4	453	24	50
<sup>i</sup> Pr <sub>3</sub> SnOTf	100	4	453	24	56
<sup>i</sup> Pr <sub>3</sub> SnOTf	120	4	453	24	56

## 2.6 Optimization of temperature:

**Table S4:** Effect of temperature on the N-formylation of morpholine with FLP1 (10 mol%) and 5 mL sulfolane.

Catalyst (LA)	H <sub>2</sub> Pressure (bar)	CO <sub>2</sub> Pressure (bar)	Temperature (K)	Time (hr)	Yield (%)
<sup>i</sup> Pr <sub>3</sub> SnOTf	100	4	433	24	26
<sup>i</sup> Pr <sub>3</sub> SnOTf	100	4	443	24	36
<sup>i</sup> Pr <sub>3</sub> SnOTf	100	4	453	24	56
<sup>i</sup> Pr <sub>3</sub> SnOTf	100	4	463	24	54
<sup>i</sup> Pr <sub>3</sub> SnOTf	100	4	473	24	53

## 3. Synthesis of catalysts

### 3.1 <sup>i</sup>Pr<sub>3</sub>SnOTf synthesis: This procedure was adapted from reference<sup>1</sup>

<sup>i</sup>Pr<sub>4</sub>Sn (5.0 g, 17.2 mmol) and HOTf (3.3 g, 14.6 mmol) were added to CHCl<sub>3</sub> (80 mL) and stirred at RT for 5 days. After which the solution was filtered and evaporated under reduced pressure. The resulting solid was washed with heptane (3 x 10 mL) affording <sup>i</sup>Pr<sub>3</sub>SnOTf as a white solid (4.8 g, 83%).

<sup>1</sup>H NMR (400 MHz, CDCl<sub>3</sub>) δ: 1.48 [6H, d, J<sub>(1H-1H)</sub> = 7.6 Hz, J<sub>(117Sn-1H)</sub> = 86 Hz, J<sub>(119Sn-1H)</sub> = 90 Hz, CH<sub>3</sub>], 2.18 [1H, sept, J<sub>(1H-1H)</sub> = 7.6 Hz, J<sub>(119Sn-1H)</sub> = 39 Hz, CH].

### 3.2 <sup>i</sup>Pr<sub>2</sub>Sn(OTf)<sub>2</sub> synthesis:

<sup>i</sup>Pr<sub>4</sub>Sn (2.0g, 6.9mmol) and HOTf (3.2 g, 14 mmol) were added to CHCl<sub>3</sub> (80 mL) and stirred at RT for 5 days. After which the solid was separated, washed with hexane (3 x 10mL) and dried. <sup>i</sup>Pr<sub>2</sub>Sn(OTf)<sub>2</sub> was afforded as a white solid in 85% yield.

<sup>1</sup>H NMR (400 MHz, acetone-d<sub>6</sub>) δ: 1.53 (6H), 2.52 (1H); <sup>13</sup>C and <sup>119</sup>Sn were measured at 600 MHz Bruker NMR instrument. <sup>13</sup>C NMR (150 MHz, acetone-d<sub>6</sub>) δ: 120.1(q, CF<sub>3</sub>) 20.49 (s, CH), 19.4 (s, CH<sub>3</sub>); <sup>119</sup>Sn NMR (224 MHz, acetone-d<sub>6</sub>) δ: -381.4 (s)



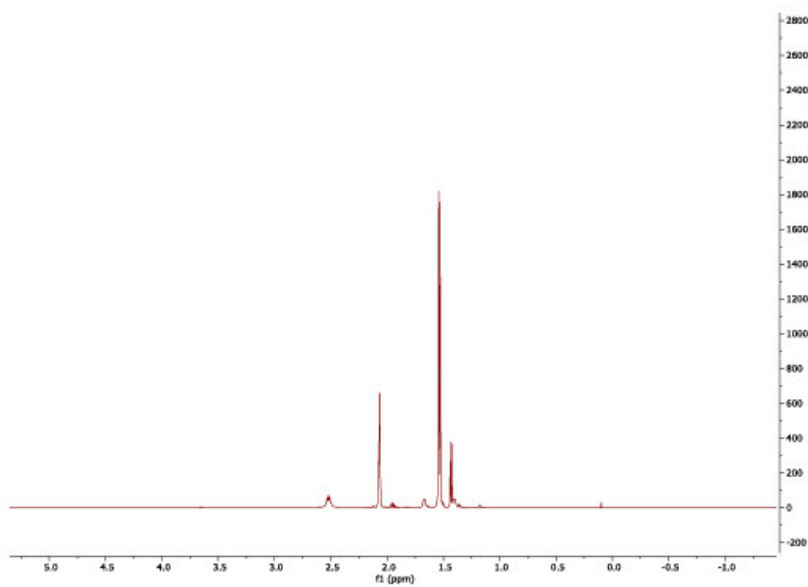


Figure S3:  $^1\text{H}$  NMR spectrum of  $i\text{Pr}_2\text{SnOTf}_2$

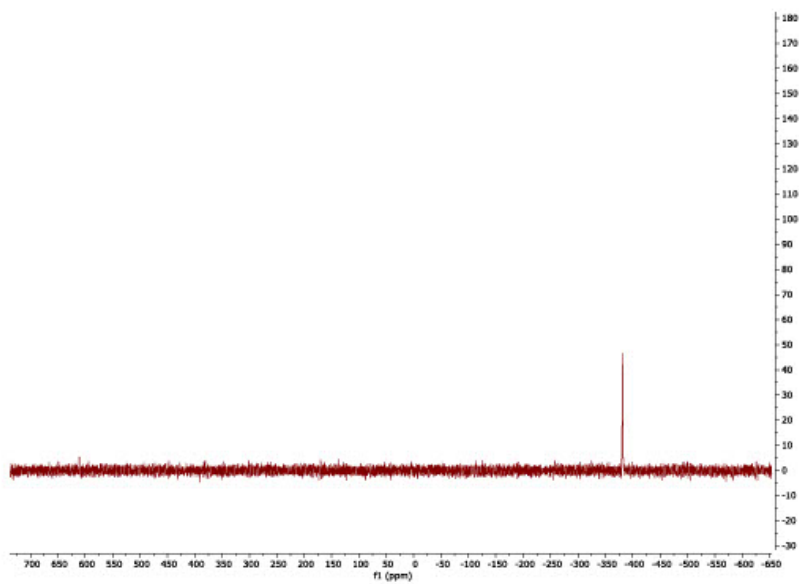


Figure S4:  $^{119}\text{Sn}$  NMR spectrum of  $i\text{Pr}_2\text{SnOTf}_2$

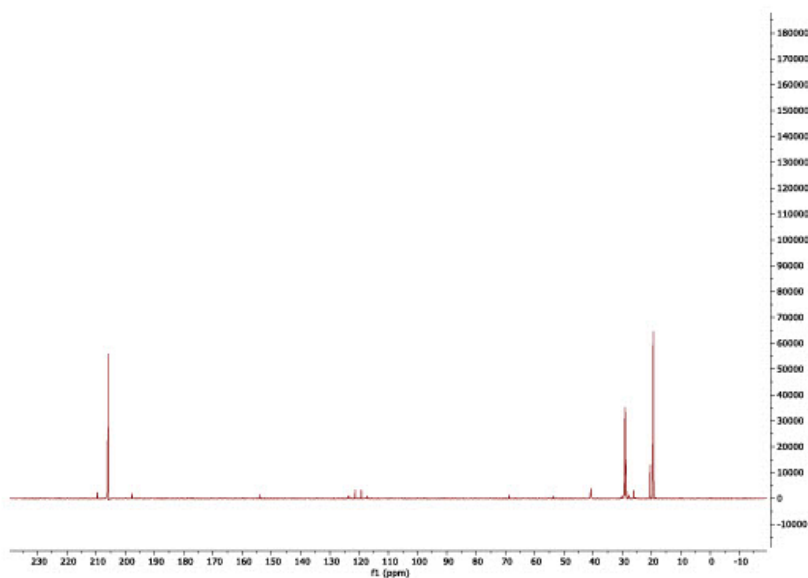


Figure S5:  $^{13}\text{C}$  NMR spectrum of  $^i\text{Pr}_2\text{SnOTf}_2$

### 3.3 $\text{Cy}_3\text{SnX}$ synthesis:

To a solution of  $\text{Cy}_3\text{SnCl}$  (500 mg, 1.24 mmol) in  $\text{CH}_2\text{Cl}_2$  (50 mL) was added  $\text{AgX}$  (1.24 mmol,  $\text{X} = \text{OTf}, \text{NTf}_2, \text{ClO}_4$ ). The reaction was stirred at RT for 3 days. The solution was then filtered and evaporated under reduced pressure affording a white solid.

#### $\text{Cy}_3\text{SnOTf}$ :

$^1\text{H}$  NMR (400 MHz,  $\text{CDCl}_3$ )  $\delta$ : 2.29 – 1.21 ppm (m, 33H);  $^{13}\text{C}$ ,  $^{19}\text{F}$  and  $^{119}\text{Sn}$  were measured at 600 MHz Bruker NMR instrument.  $^{13}\text{C}$  NMR (150 MHz,  $\text{CDCl}_3$ )  $\delta$ : 38.72 ppm (s), 30.64 ppm (s), 28.76 ppm (s), 26.57 ppm (s);  $^{119}\text{Sn}$  NMR (224 MHz,  $\text{CDCl}_3$ )  $\delta$ : 73.9 ppm;  $^{19}\text{F}$  NMR (376 MHz,  $\text{CDCl}_3$ )  $\delta$ : -77.20 ppm (s); HRMS+ for  $\text{C}_{19}\text{H}_{33}\text{F}_3\text{O}_3\text{SSn}$   $m/z$ : 517.2972 (calculated: 517.2352); HRMS- for  $\text{CF}_3\text{O}_3\text{S}^-$   $m/z$ : 148.9580 (calculated: 148.9520)

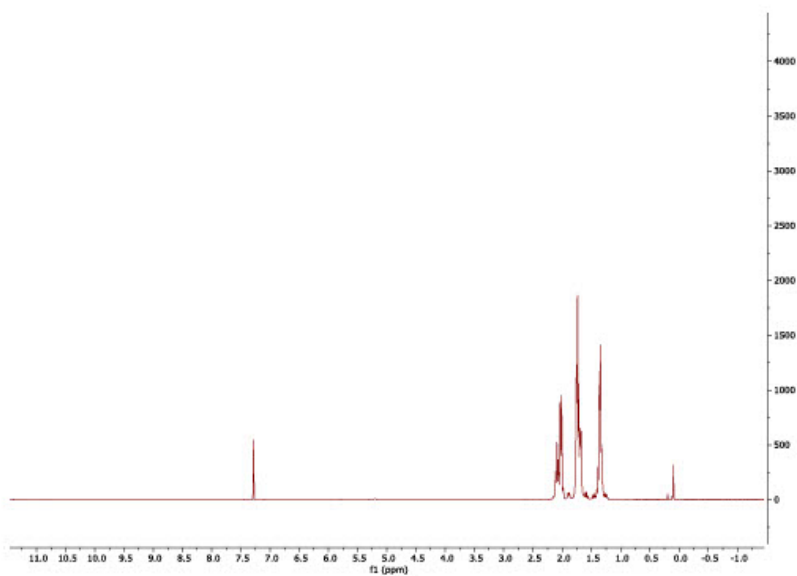


Figure S6: <sup>1</sup>H NMR spectrum of Cy<sub>3</sub>SnOTf

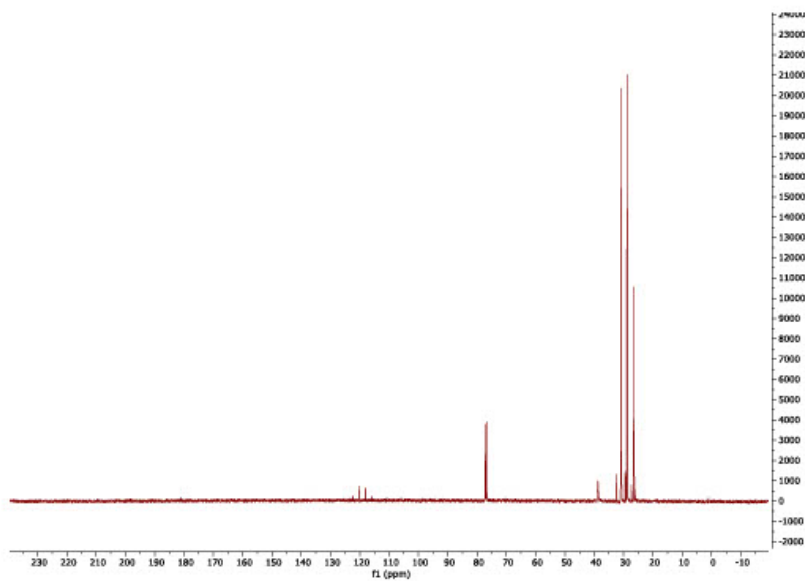


Figure S7: <sup>13</sup>C NMR spectrum of Cy<sub>3</sub>SnOTf

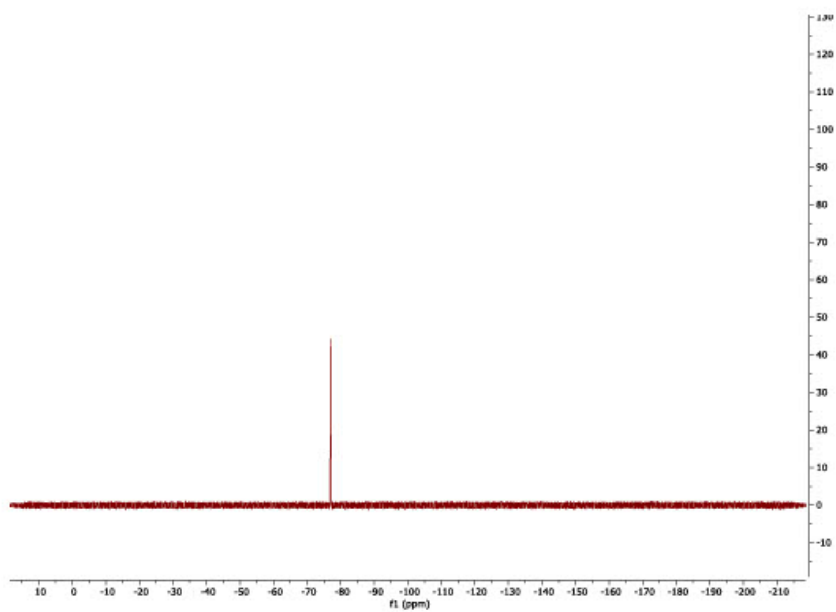


Figure S8:  $^{19}\text{F}$  NMR spectrum of  $\text{Cy}_3\text{SnOTf}$

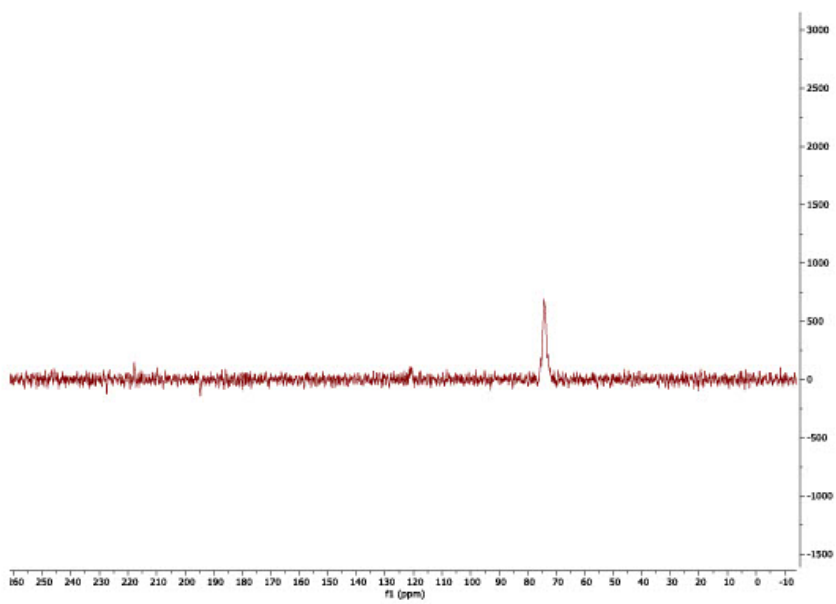
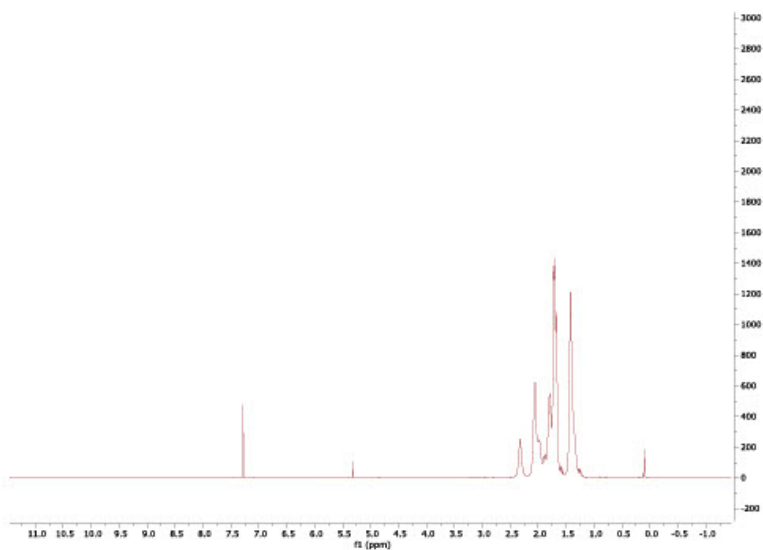


Figure S9:  $^{119}\text{Sn}$  NMR spectrum of  $\text{Cy}_3\text{SnOTf}$

**Cy<sub>3</sub>SnClO<sub>4</sub>:**

<sup>1</sup>H NMR (400 MHz, CDCl<sub>3</sub>) δ: 2.40 – 1.23ppm (m, 33H); <sup>13</sup>C, <sup>19</sup>F and <sup>119</sup>Sn were measured at 600 MHz Bruker NMR instrument. <sup>13</sup>C NMR (150 MHz, CDCl<sub>3</sub>) δ: 38.66ppm (s), 30.66ppm (s), 28.83ppm (s), 26.56ppm (s); <sup>119</sup>Sn NMR (224 MHz, CDCl<sub>3</sub>) δ: 74.3ppm (s); HRMS+ for C<sub>18</sub>H<sub>33</sub>Sn<sup>+</sup> m/z: 369.1661 (calculated: 369.1604); HRMS- for ClO<sub>4</sub><sup>-</sup> m/z: 98.9501 (calculated: 98.9489)



**Figure S10:** <sup>1</sup>H NMR spectrum of Cy<sub>3</sub>SnClO<sub>4</sub>

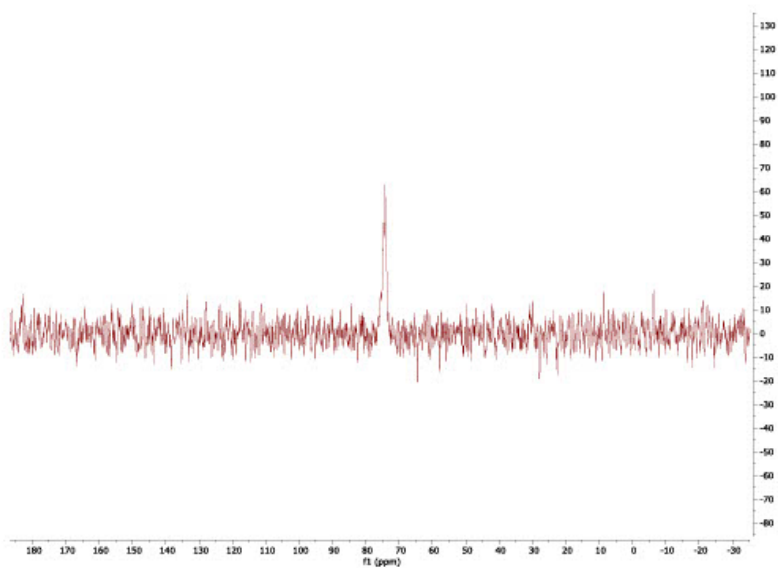


Figure S11:  $^{119}\text{Sn}$  NMR spectrum of  $\text{Cy}_3\text{SnClO}_4$

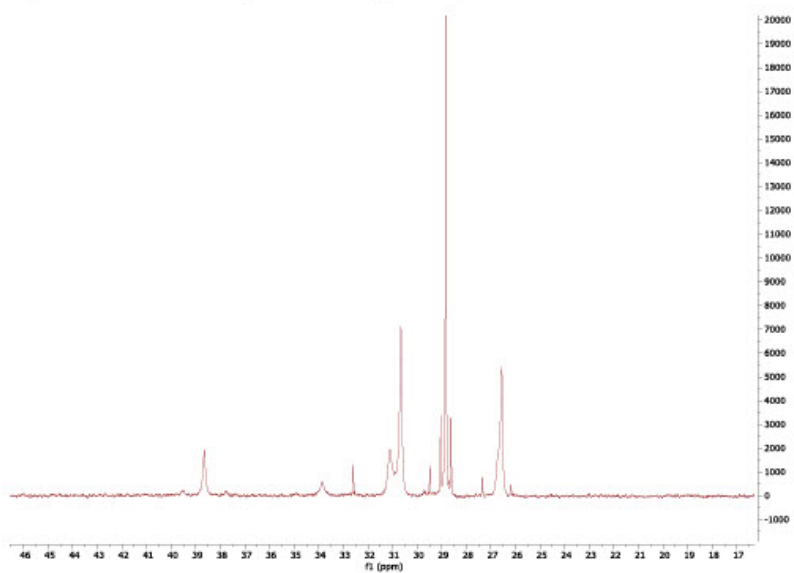
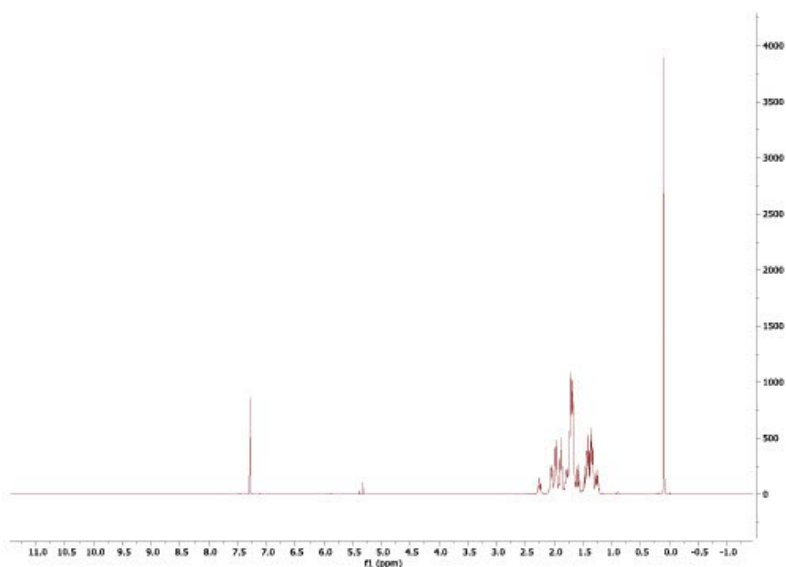


Figure S12:  $^{13}\text{C}$  spectrum of  $\text{Cy}_3\text{SnClO}_4$

**Cy<sub>3</sub>SnNTf<sub>2</sub>:**

<sup>1</sup>H NMR (400 MHz, CDCl<sub>3</sub>) δ: 2.15 – 1.21ppm (m, 33H); <sup>13</sup>C, <sup>19</sup>F and <sup>119</sup>Sn were measured at 600 MHz Bruker NMR instrument. <sup>13</sup>C NMR (150 MHz, CDCl<sub>3</sub>) δ: 118.95 ppm (q) (two peaks of the quartet are obscured by the baseline), 38.78ppm (s), 31.0ppm (s), 28.90ppm (s), 26.50ppm (s); <sup>19</sup>F NMR (376 MHz, CDCl<sub>3</sub>) δ: -78.2ppm (s); HRMS+ for C<sub>18</sub>H<sub>33</sub>Sn<sup>+</sup> m/z: 369.1661 (calculated: 369.1614); HRMS- for C<sub>2</sub>F<sub>6</sub>NO<sub>4</sub>S<sub>2</sub><sup>-</sup> m/z: 279.9304 (calculated: 279.9173)



**Figure S13:** <sup>1</sup>H NMR spectrum of Cy<sub>3</sub>SnNTf<sub>2</sub>

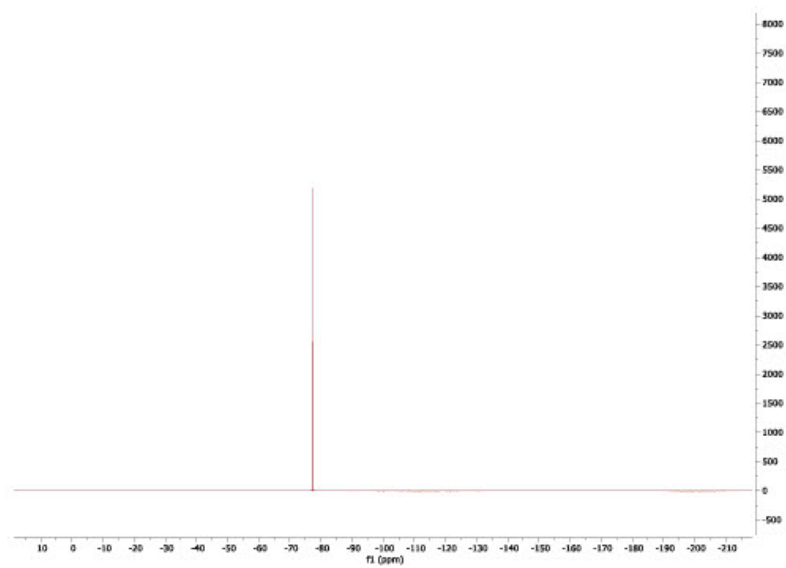


Figure S14:  $^{19}\text{F}$  NMR spectrum of  $\text{Cy}_3\text{SnNTf}_2$

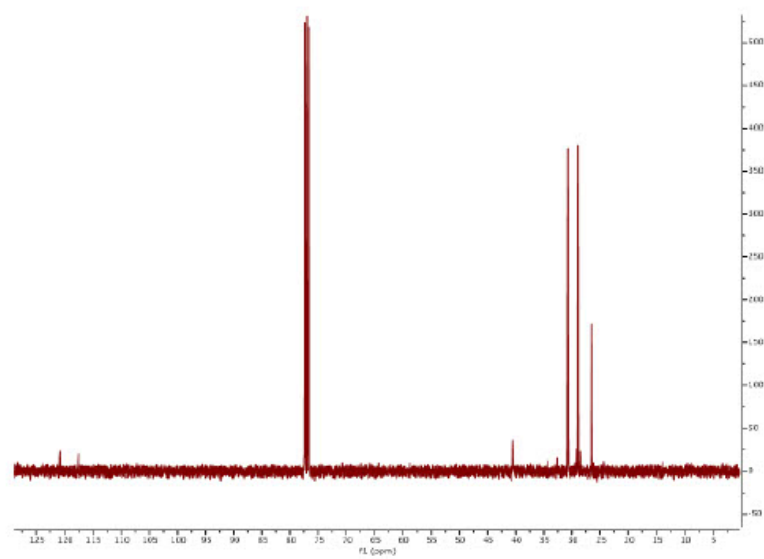


Figure S15:  $^{13}\text{C}$  NMR spectrum of  $\text{Cy}_3\text{SnNTf}_2$



### 3.4 Synthesis of <sup>4</sup>Bu<sub>4</sub>Sn

To a suspension of Mg turnings (3.65 g, 150 mmol) and iodine (50.0 mg) in THF (40 mL) was added 2-chlorobutane (14.4 mL, 135 mmol) at 0 °C with vigorous stirring. After the addition, the solution was warmed to RT and left stirring for 10 h. The suspension was filtered through a frit and washed with THF (2 x 40 mL). The <sup>4</sup>BuMgCl solution was added dropwise to a stirred solution of SnCl<sub>4</sub> (7.50 g, 28.8 mmol) in THF (50 mL) cooled to 0 °C. After complete addition, the solution was heated to 80 °C for 3 d. After the solution was cooled to RT, H<sub>2</sub>O (20 mL) was added carefully.

This synthesis gave a mixture of all six possible diastereomers in a statistical ratio. No attempt was made to separate them. The characterisation data presented are for this mixture.

<sup>1</sup>H NMR (400 MHz, C<sub>6</sub>D<sub>6</sub>) δ 0.95 (t, <sup>3</sup>J<sub>1H-1H</sub> = 7.3 Hz, 12H, SnCHCH<sub>2</sub>CH<sub>3</sub>), 2.25 (d, <sup>3</sup>J<sub>1H-1H</sub> = 7.1 Hz, <sup>3</sup>J<sub>1H-117/119Sn</sub> = 60.2 Hz, 12H, SnCHCH<sub>3</sub>), 1.29-1.44 (m), 1.46-1.64 (m), 1.67-1.87 (m); <sup>119</sup>Sn{<sup>1</sup>H} NMR (149 MHz, C<sub>6</sub>D<sub>6</sub>) δ -45.5, -45.1, -45.0

### 3.5 Synthesis of <sup>4</sup>Bu<sub>3</sub>SnOTf

To a solution of <sup>4</sup>Bu<sub>4</sub>Sn (2.50 g, 7.20 mmol) in CHCl<sub>3</sub> (40 mL) was added HOTf (1.03 g, 6.84 mmol), which was stirred for 19 h at 50 °C. The solvent was removed in vacuo to yield a white gum, which would not dry further. Pentane (10 mL) was added and the solution was cooled to -40 °C and left for 12 h, whereupon a white solid precipitated. The solid was filtered, washed with cold pentane (2 x 10 mL) and dried in vacuo to furnish <sup>4</sup>Bu<sub>3</sub>SnOTf as a free-flowing white powder (2.87 g, 6.53 mmol, 95%).

This synthesis gave a mixture of all four possible diastereomers in statistical ratio. No attempt was made to separate these. The characterisation data presented are for this mixture.

<sup>1</sup>H NMR (400 MHz, C<sub>6</sub>D<sub>6</sub>) δ 1.04 (t, <sup>3</sup>J<sub>1H-1H</sub> = 7.3 Hz, 9H, SnCHCH<sub>2</sub>CH<sub>3</sub>), 1.46 (d, <sup>3</sup>J<sub>1H-1H</sub> = 7.4 Hz, <sup>3</sup>J<sub>1H-117/119Sn</sub> = 85.1 Hz, 9H, SnCHCH<sub>3</sub>), 1.77-1.96 (m), 2.06-2.23 (m, 3H, SnCH); <sup>119</sup>Sn{<sup>1</sup>H} NMR (149 MHz, C<sub>6</sub>D<sub>6</sub>) δ 214.7, 215.7; MS (APCI) m/z = 369 (<sup>4</sup>Bu<sub>3</sub>SnOSO<sub>2</sub><sup>+</sup>), 219 (<sup>4</sup>Bu<sub>3</sub>Sn<sup>+</sup>)

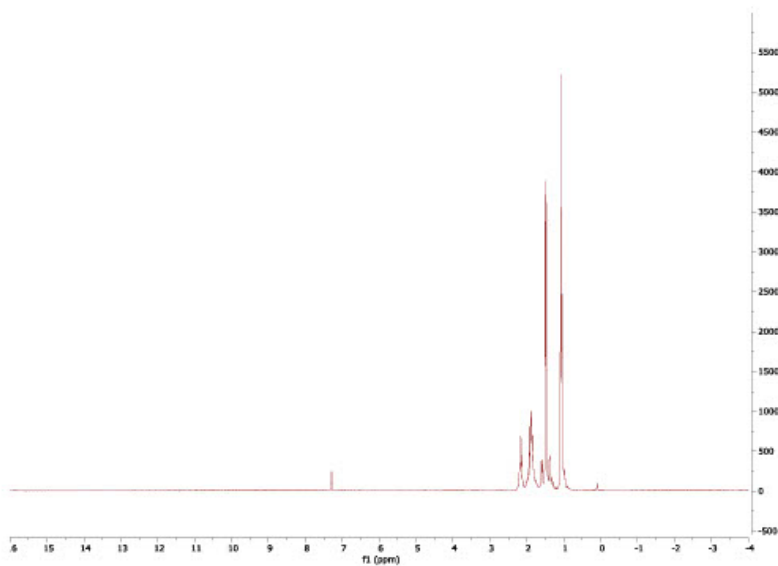


Figure S16:  $^1\text{H}$  NMR spectrum of  $^5\text{Bu}_3\text{SnOTf}$

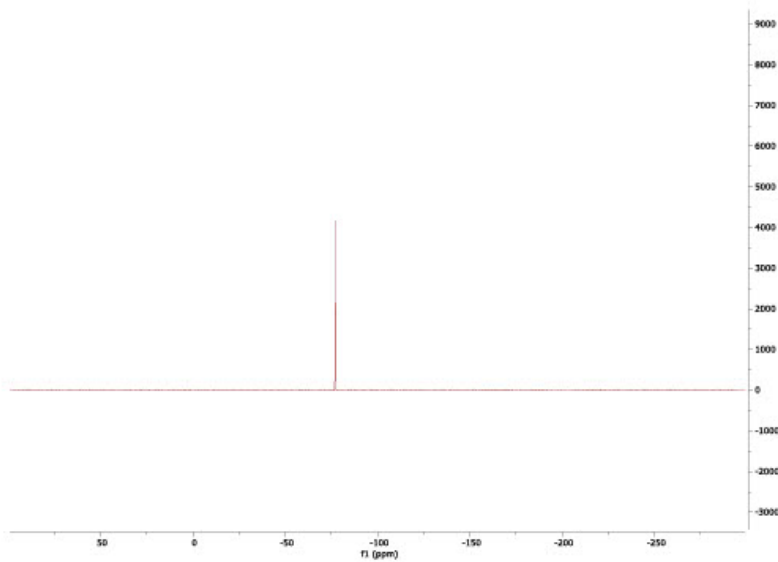
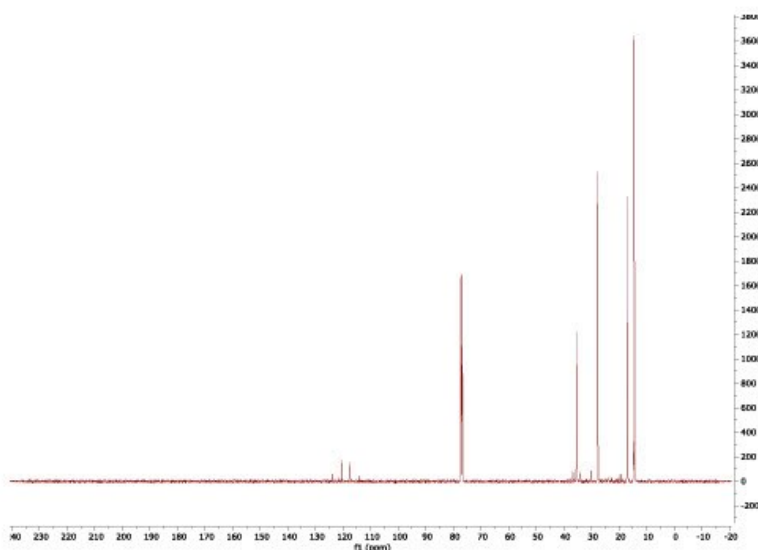


Figure S17:  $^{19}\text{F}$  NMR spectrum of  $^5\text{Bu}_3\text{SnOTf}$



**Figure S18:**  $^{13}\text{C}$  NMR spectrum of  $^5\text{Bu}_3\text{SnOTf}$

### 3.6 Synthesis of $(\text{Nph})_4\text{Sn}$

Neophylmagnesium chloride was prepared by heating magnesium turnings (7.50 g, 309 mmol) and neophylchloride (49.0 mL, 51.3 g, 304 mmol) in  $\text{Et}_2\text{O}$  (100 mL) at reflux for 24 hrs. The Grignard solution was then filtered and stirred over an ice bath.  $\text{SnCl}_4$  (5.85 mL, 13.0 g, 50.0 mmol) in benzene (40 mL) was added dropwise, and the suspension stirred at room temperature for 60 hrs. The excess Grignard was quenched carefully with water (250 mL) before the product was extracted with  $\text{Et}_2\text{O}$  (3x150 mL), washed with water (400 mL), dried ( $\text{Na}_2\text{SO}_4$ ), and the solvent removed in vacuo. Addition of an ethanol/benzene solution (3:1) resulted in the precipitation of the product, which was filtered, washed with cold ethanol (3x15 mL) and cold pentane (3x15 mL), then dried in vacuo. The product was subsequently recrystallised from pentane at  $-45^\circ\text{C}$ , yielding  $(\text{Nph})_4\text{Sn}$  as white crystals (26.4 g, 39.5 mmol, 79 %).

$^1\text{H}$  NMR (400 MHz,  $\text{CDCl}_3$ ):  $\delta$  7.25 [t,  $^3J_{\text{H-H}} = 7.5$  Hz, 8H, *m*-CH], 7.16 [t,  $^3J_{\text{H-H}} = 7.2$  Hz, 4H, *p*-CH], 7.11 [d,  $^3J_{\text{H-H}} = 7.5$  Hz, 8H, *o*-CH], 1.14 [s, 24H,  $\text{CH}_3$ ], 0.79 [s,  $^2J_{\text{H-H}} = 47.7$  Hz, 8H,  $\text{CH}_2$ ];  $^{13}\text{C}\{^1\text{H}\}$  NMR (101 MHz,  $\text{CDCl}_3$ ):  $\delta$  151.6 [*i*-C], 128.2 [*m*-CH], 125.7 [*o*-CH], 125.5 [*p*-CH], 38.5 [ $\text{C}(\text{CH}_3)_2$ ], 33.5 [ $\text{CH}_3$ ], 31.2 [ $^1J_{\text{H-Sn}} = 302$  Hz,  $^1J_{\text{H-C}} = 289$  Hz,  $\text{CH}_2$ ];  $^{119}\text{Sn}\{^1\text{H}\}$  NMR (149 MHz,  $\text{CDCl}_3$ ):  $\delta$  -52.6 (s)

### 3.7 $(\text{Nph})_3\text{SnOTf}$

Trifluoromethanesulfonic acid (0.68 mL, 1.15 g, 7.67 mmol) suspended in  $\text{CHCl}_3$  (5 mL) was added dropwise to a solution of  $(\text{Nph})_4\text{Sn}$  (5.00g, 7.67 mmol) in  $\text{CHCl}_3$  (40 mL) with rapid stirring. The

mixture was heated to 60°C for 48 hours, the solution was filtered, the solvent removed in vacuo, and the solid thoroughly washed with pentane (3x30 mL). The product was subsequently recrystallised from Et<sub>2</sub>O at -45°C, yielding (Nph)<sub>3</sub>SnOTf as colourless needles (4.06 g, 6.08 mmol, 79 %).

<sup>1</sup>H NMR (400 MHz, CDCl<sub>3</sub>): δ 7.35-7.25 [m, 9H, *m* - CH, *p* - CH], 6.91 [m, 6H, *o* - CH], 1.35 [s, <sup>2</sup>J<sub>119|117Sn-1H</sub> = 45.6 Hz, 6H, CH<sub>2</sub>], 1.21 [s, 18H, CH<sub>3</sub>]; <sup>13</sup>C{<sup>1</sup>H} NMR (101 MHz, CDCl<sub>3</sub>): δ 150.4 [*i* - C], 129.0 [*m* - CH], 126.6 [*p* - CH], 125.1 [*o* - CH], 41.1 [<sup>1</sup>J<sub>119|117Sn-13C</sub> = 307 Hz, CH<sub>2</sub>], 37.6 [C(CH<sub>3</sub>)<sub>2</sub>], 32.9 [CH<sub>3</sub>]; <sup>19</sup>F{<sup>1</sup>H} NMR (376 MHz, CDCl<sub>3</sub>): δ -77.7 (s); <sup>119</sup>Sn{<sup>1</sup>H} NMR (149 MHz, CDCl<sub>3</sub>): δ 250 (s); HRMS (EI) found (calculated) for C<sub>31</sub>H<sub>39</sub>F<sub>3</sub>O<sub>3</sub>SSn *m/z*: 668.1589 (668.1594)

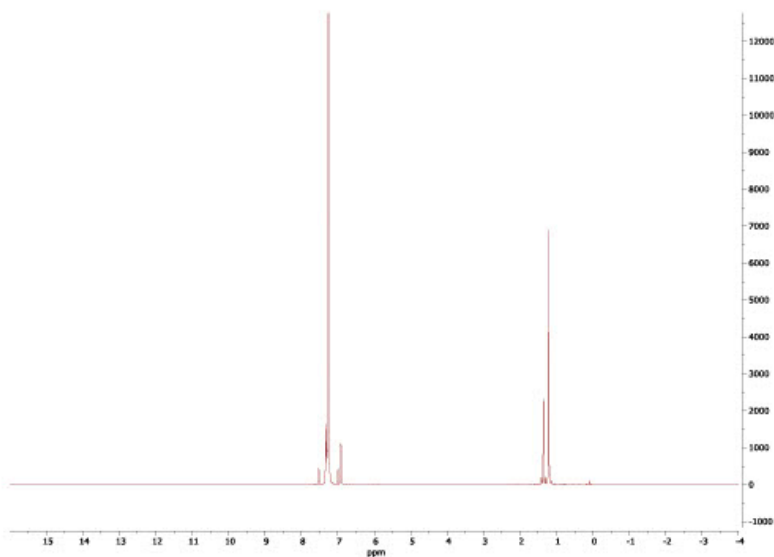


Figure S19: <sup>1</sup>H NMR spectrum of NPh<sub>3</sub>SnOTf

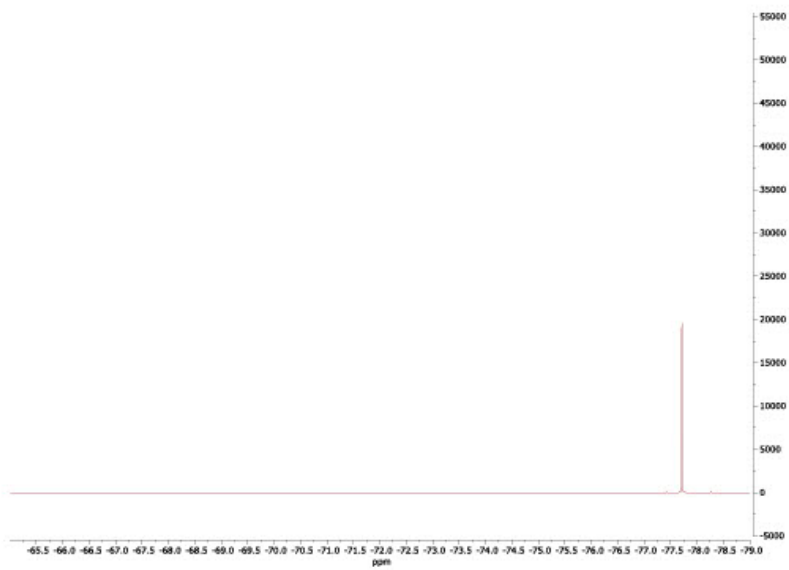


Figure S20:  $^{19}\text{F}$  NMR spectrum of  $\text{NPh}_3\text{SnOTf}$

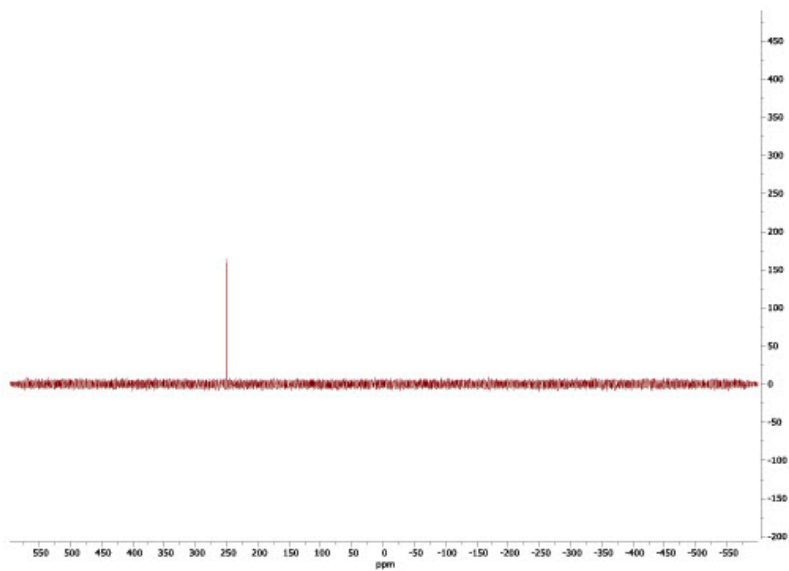


Figure S21:  $^{119}\text{Sn}$  NMR spectrum of  $\text{NPh}_3\text{SnOTf}$

## 4. Catalyst stability testing

### 4.1 General procedure for catalyst stability testing

Morpholine (1mmol), and 1 mol% of catalyst were dissolved in sulfolane under standard reaction conditions (100 bar H<sub>2</sub>, 4 bar CO<sub>2</sub> and at 453 K). The reaction was run for a week at which point the autoclave was degassed, an aliquot was taken and if no morpholine remained in the sample another 1 mmol of morpholine was added and the autoclave was repressurized. This process was repeated until the catalyst stopped fully converting starting material. The Cy<sub>3</sub>SnOTf was stopped at 300 turnovers (3 week long reaction) as this was enough to conclude it was more stable than <sup>i</sup>Pr<sub>3</sub>SnOTf which only reached 162 (2 week long reaction) turnovers.

## 5. Gutman-Beckett acidity measurements

### 5.1 General procedure for Gutman-Beckett acidity measurements

0.02 mL of a stock solution of Triethylphosphine oxide (30 mg, 0.22 mmol,) in 2 mL of dry CDCl<sub>3</sub> was added to a solution of Lewis acid (0.1 mmol) in 0.5mL of CDCl<sub>3</sub>. <sup>31</sup>P (<sup>1</sup>H) NMRs wertr then measured, after which more Lewis acid was added, the sample was then remeasured, and this process was repeated until the peak positions remained constant.

The acceptor numbers were calculated using the formula from reference<sup>7</sup>

$$\text{Acceptor number} = [\delta^{31\text{P}} [^1\text{H}]/\text{ppm} (\text{sample}) - 41.0] \times 2.22$$

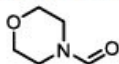
### 5.2 Results of Gutman-Beckett acidity measurements

**Table S5:** Summary of the acceptor numbers for Cy<sub>3</sub>SnX Lewis acids.

Catalyst (LA)	$\delta^{31\text{P}} [^1\text{H}]/\text{ppm}$	Acceptor number
Cy <sub>3</sub> SnOTf	68.1	60.2
Cy <sub>3</sub> SnNTf <sub>2</sub>	76.9	79.7
Cy <sub>3</sub> SnClO <sub>4</sub>	71.6	67.9

## 6. Substrate scope

### 6.1 N-formylmorpholine



$^1\text{H}$  NMR (400 MHz,  $\text{CDCl}_3$ )  $\delta$ : 3.36 (2H), 3.53 (m, 2H), 3.60-3.67 (m, 4H), 8.02 (1H); GC retention time 9.5 to 9.6 minutes; EI-MS ( $m/z$ ) calculated: 115.1, found 115.1 with a 92-98% agreement of EI-MS molecular fragmentation with NIST EI-MS library.

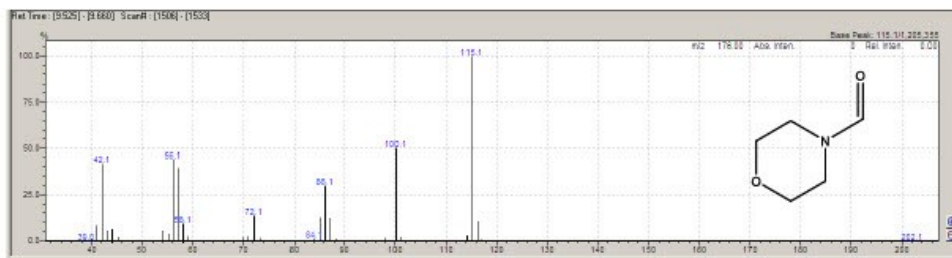
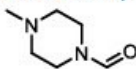


**Figure S22:** EI-MS analysis of the reaction product of N-formylation of morpholine with  $\text{CO}_2$  and  $\text{H}_2$ .

### 6.2 1-Formyl-4-methylpiperazine



$^1\text{H}$  NMR (400 MHz,  $\text{CDCl}_3$ )  $\delta$ : 8.03 (1H) 3.60-3.67 (m, 4H), 3.62 (m, 2H), 3.55 (2H); GC retention time 13.3 to 13.5 minutes; EI-MS ( $m/z$ ) calculated: 128.1, found 128.1

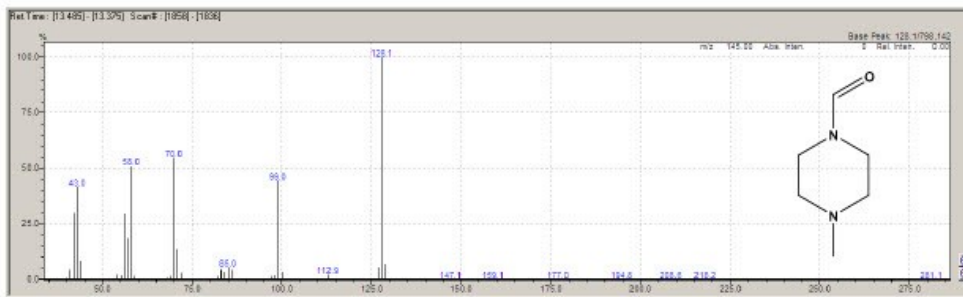
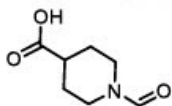


**Figure S23:** EI-MS analysis of the reaction product of N-formylation of 1-methylpiperazine with  $\text{CO}_2$  and  $\text{H}_2$ .



### 6.3 N-Formylpiperidine-4-carboxylic acid



$^1\text{H}$  NMR (400 MHz,  $\text{CDCl}_3$ )  $\delta$ : 7.98 (s 1H), all other peaks were obscured by the reaction solvent;  
GC retention time 16.7 to 17.3 minutes; EI-MS ( $m/z$ ) calculated: 157.1, found 157.1

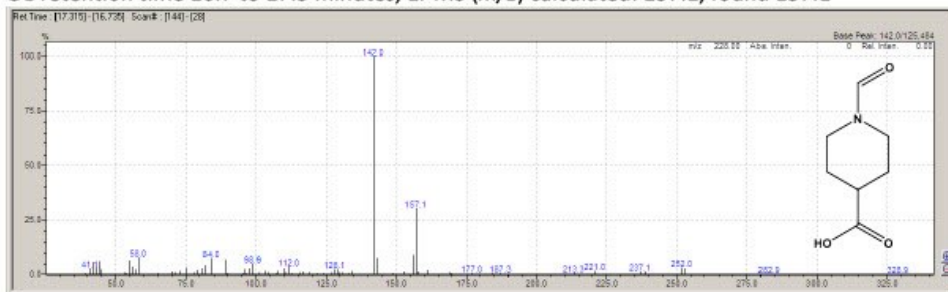
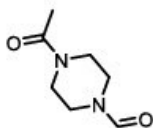


**Figure S24:** EI-MS analysis of the reaction product of N-formylation of piperidine-4-carboxylic acid with  $\text{CO}_2$  and  $\text{H}_2$ .

### 6.4 4-Acetyl-piperazine-1-carbaldehyde



$^1\text{H}$  NMR (400 MHz,  $\text{CDCl}_3$ )  $\delta$ : 8.09 (s, 1H), all other peaks were obscured by the reaction solvent;  
GC retention time 25.7 to 25.8 minutes; EI-MS ( $m/z$ ) calculated: 156.1, found 156.1

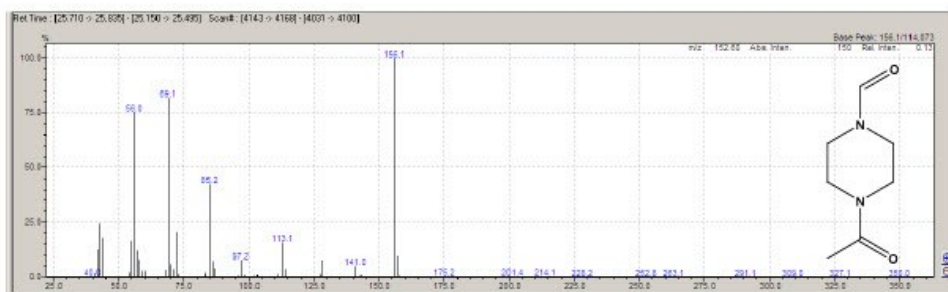
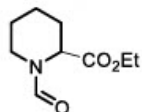


**Figure S25:** EI-MS analysis of the reaction product of N-formylation of 1-Acetyl-piperazine with  $\text{CO}_2$  and  $\text{H}_2$ .



## 6.5 Ethyl 1-formylpiperidine-2-carboxylate



$^1\text{H}$  NMR (400 MHz,  $\text{CDCl}_3$ ) mixture of rotamers  $\delta$ : 8.03 (s, 1H (rotamer 1)) 7.99 (s, 1H (rotamer 2)) 7.93 (s, 1H (rotamer 3)), 5.63 (s, 1H (rotamer 2)), 5.06 (d, 1H (rotamer 3)), 4.23 (s, 1H (rotamer 1)), all other peaks were obscured by the reaction solvent; GC retention time 16.3 to 16.4 minutes; EI-MS ( $m/z$ ) calculated: 185.2, found 185.1. The reaction product was also compared to a genuine sample of ethyl 1-formylpiperidine-2-carboxylate GC retention time 16.3 to 16.4 minutes; EI-MS ( $m/z$ ) calculated: 185.2, found 185.1

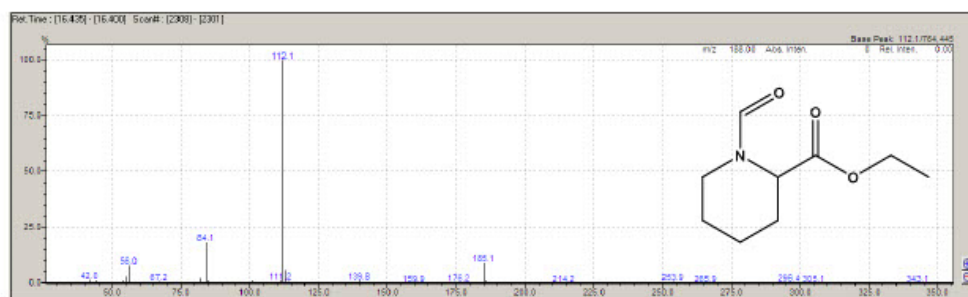


**Figure S26:** EI-MS analysis of the reaction product of N-formylation of 1-(piperidin-2-yl)butan-1-one with  $\text{CO}_2$  and  $\text{H}_2$ .

The reaction results in a mixture of products of ethyl 1-formylpiperidine-2-carboxylate and N-formylpiperidine (70:30) with the N-formylpiperidine  $^1\text{H}$  NMR peaks at 8.02 (s, 1H) 8.00 (s, 1H) 7.97 (s, 1H), all other peaks were obscured by the reaction solvent; GC retention time 12.38 to 12.29 minutes; EI-MS ( $m/z$ ) calculated: 113.1, found 113.1

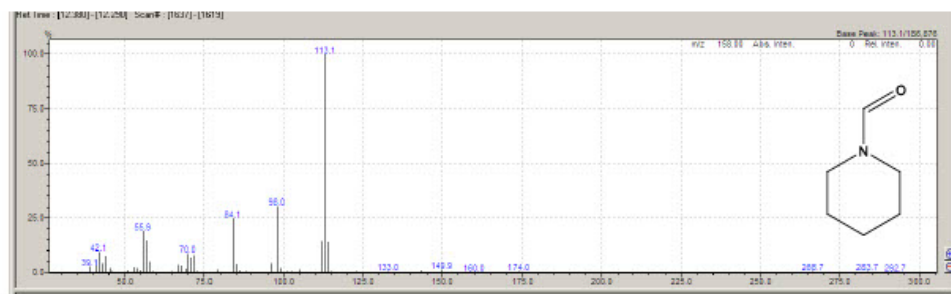
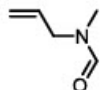


**Figure S27:** EI-MS analysis of the reaction side product of N-formylation of 1-(piperidin-2-yl)butan-1-one with  $\text{CO}_2$  and  $\text{H}_2$ .

## 6.6 N-allyl-N-methylformamide



$^1\text{H}$  NMR (400 MHz,  $\text{CDCl}_3$ )  $\delta$  (mixture of rotamers): 8.08 (1H), 5.67-5.81 (m, 1H), 5.16-5.29 (m, 2H); 3.95 (d,  $J_{1\text{H}-1\text{H}} = 5.81$  Hz, 1H), 3.83 (d,  $J_{1\text{H}-1\text{H}} = 6.15$  Hz, 1H), 2.91 (s, 3H), 2.84 (s, 3H); GC retention time 9.4 to 9.7 minutes; EI-MS ( $m/z$ ) calculated: 99.1, found 99.0

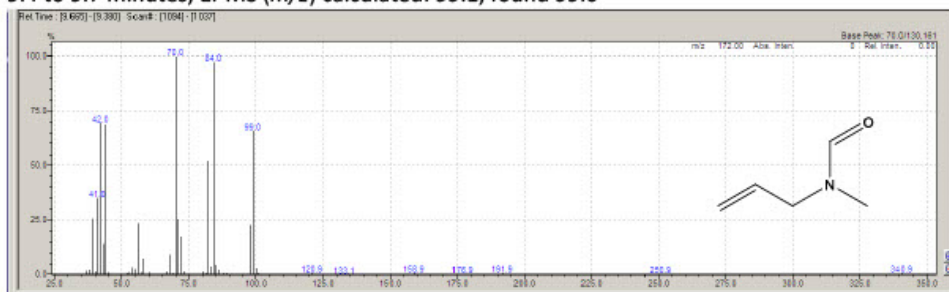
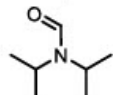


**Figure S28:** EI-MS analysis of the reaction product of N-formylation of N-methylprop-2-en-1-amine with  $\text{CO}_2$  and  $\text{H}_2$ .

## 6.7 N,N-diisopropylformamide



$^1\text{H}$  NMR (400 MHz,  $\text{CDCl}_3$ )  $\delta$ : 8.10 (1H), 3.62 (m, 2H), 1.21(d, 6H); GC retention time 9.5 to 9.7 minutes; EI-MS ( $m/z$ ) calculated: 129.2, found 129.1

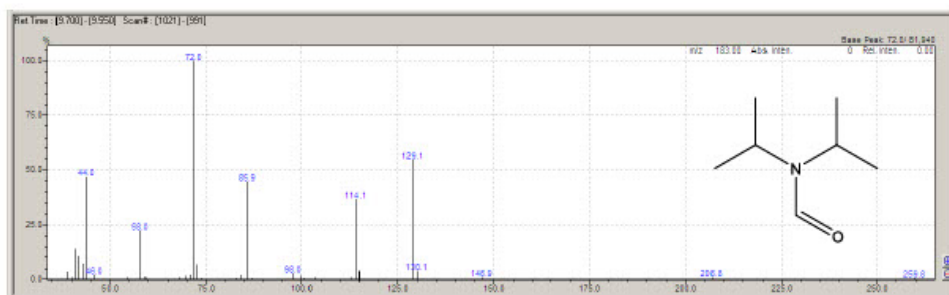
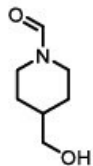


**Figure S29:** EI-MS analysis of the reaction product of N-formylation of diisopropylamine with  $\text{CO}_2$  and  $\text{H}_2$ .

### 6.8 N-Formyl-4-piperidinemethanol



$^1\text{H}$  NMR (400 MHz,  $\text{CDCl}_3$ )  $\delta$ : 8.00 (s,1H), 4.41(dt, 1H), 3.63 (dp,1H), 3.50 (m, 2H), 2.62 (td, 1H), 1.14 (m, 2H) All other peaks were obscured by the reaction solvent.; GC retention time 21.7 to 21.9 minutes; EI-MS ( $m/z$ ) calculated: 143.2, found 143.1

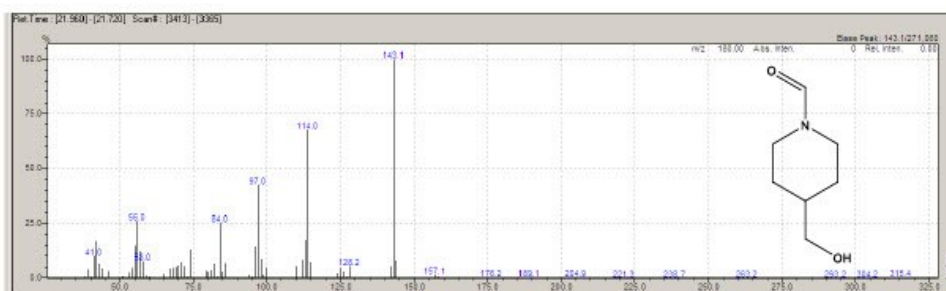
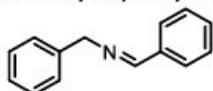


Figure S30: EI-MS analysis of the reaction product of N-formylation of 4-hydroxymethylpiperidine with  $\text{CO}_2$  and  $\text{H}_2$ .

### 6.9 Attempted N-formylation of benzylamine

Attempted N-formylation of benzylamine with  $\text{CO}_2$ ,  $\text{H}_2$  and  $\text{C}_3\text{SnOTf}$  as the reaction catalyst did not yield the expected product N-formylbenzylamine but rather the homocoupled product N-benzyl-1-phenylmethanimine and its hydrogenated analogue dibenzylamine.

#### N-benzyl-1-phenylmethanimine



$^1\text{H}$  NMR (400 MHz,  $\text{CDCl}_3$ )  $\delta$ : 8.05 (s, 1H); GC retention time 18.6 to 18.8 minutes; EI-MS ( $m/z$ ) calculated: 195.3, found 195.1

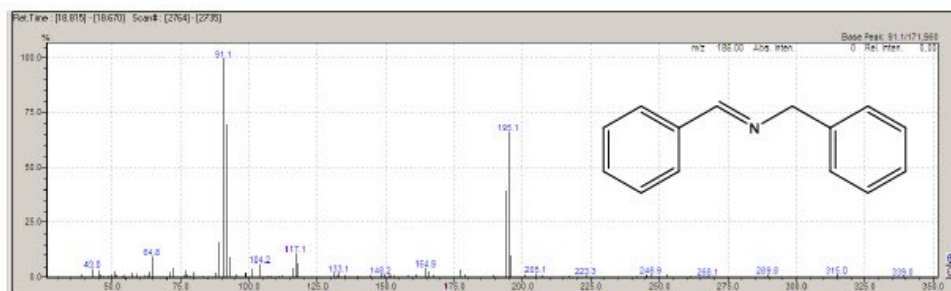
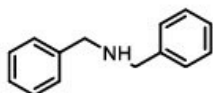


**Figure S31:** EI-MS analysis of the reaction product 1 of attempted N-formylation of benzylamine with CO<sub>2</sub> and H<sub>2</sub>.

### Dibenzylamine



GC retention time 18.6 to 18.8 minutes; EI-MS (*m/z*) calculated: 197.3, found 197.1

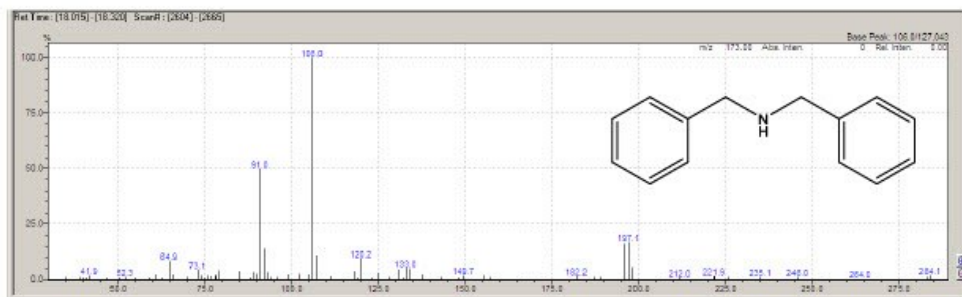


**Figure S31:** EI-MS analysis of the reaction product 2 of attempted N-formylation of benzylamine with CO<sub>2</sub> and H<sub>2</sub>.

## 7. Synthesis of 4-hydroxymethylpiperidine.

The procedure was adapted from reference.<sup>8</sup>

In a Schlenk flask, to a stirred suspension of LiAlH<sub>4</sub> (6.64 g, 175 mmol) in THF (200 mL) was added isonipecotic acid (7.54 g, 58.3 mmol). The reaction was stirred at room temperature for 24h after which 10 mL of H<sub>2</sub>O, 10 mL 15% w/w NaOH in H<sub>2</sub>O and 10 mL of H<sub>2</sub>O were carefully added in sequence. A colourless precipitate gradually formed. After which diethyl ether (200mL) was added, the solid was then

filtered. The solids were washed with ethyl acetate and the filtrate was collected and evacuated under reduced pressure. This afforded a colourless solid in a yield of 5.20 g (72% yield).

$^1\text{H}$  NMR (400 MHz,  $\text{CDCl}_3$ ): 3.43ppm (d, 2H), 3.07ppm (dt, 2H), 2.58ppm (td, 2H), 2.48ppm (br s, 2H), 1.71ppm (d, 2H), 1.58ppm (m, 1H), 1.11 (qd, 2H)

## 8. Heterocycle hydrogenation

In air, to the autoclave,  $\text{C}_3\text{SnOTf}$  (0.1 mmol), 2,4,6-collidine (0.1 mmol) were dissolved in sulfolane (5 mL). The autoclave was then sealed and purged 5 times with the desired pressure of  $\text{CO}_2$ . The reaction is then topped up with the desired  $\text{H}_2$  reaction pressure. The temperature and stirring rate were set using the Specview program on Parr 5000 series multi reactor system. The reaction was allowed to warm to 453K and was held there for 30 mins after which the heating was turned off and the reactor was allowed to cool to room temperature. DCM (1 mmol) was added to the reactor, stirred and an aliquot was taken for  $^1\text{H}$  NMR in  $\text{CDCl}_3$ . The conversion was quantified by comparing the integral of the formate peak and the integral of DCM.

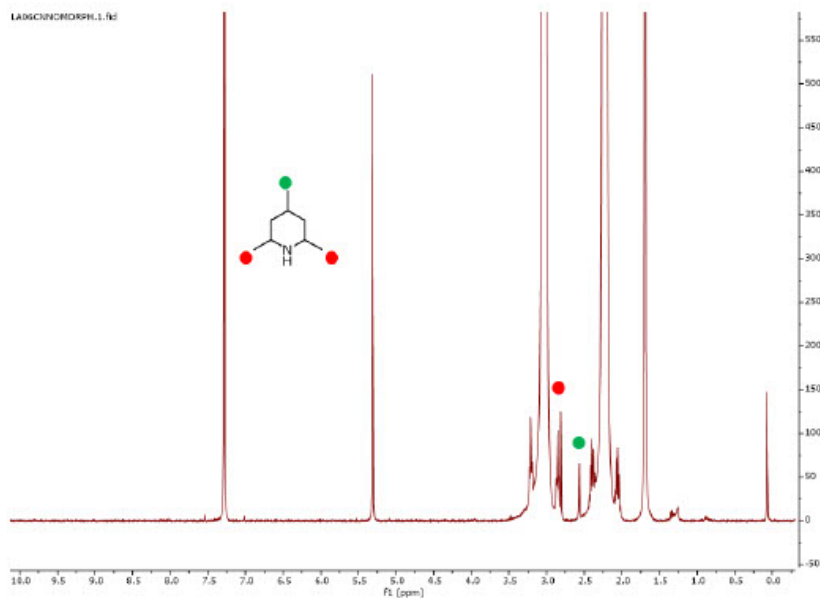


**Figure S32:**  $^1\text{H}$  NMR spectrum of the reaction of 10mol% of  $\text{C}_3\text{SnOTf}$  and of 2,4,6-collidine at 100 bar  $\text{H}_2$ , 4 bar  $\text{CO}_2$  and 453 K in the absence of morpholine.

Normally the aromatic hydrogen peak occurs at 6.9ppm however no such peak can be seen here but the alkyl groups are still present suggesting the base didn't precipitate out as a salt.

## 9. Mechanism investigation: Formate transfer

### 9.1 $Cy_3SnOCOH$ synthesis: The procedure was adapted from reference<sup>9</sup>

$Cy_3SnOH$  (0.620 g, 1.61 mmol) was added to toluene (25 mL) and heated until the solids dissolved (ca. 328K). Under rapid stirring formic acid (0.6 mL, 15.9 mmol, 98%) was added dropwise to the solution. The solution was then stirred overnight, and the volatiles were removed under reduced pressure, which afforded a white solid in a yield of 84%. This solid was used without further purification.

$^1H$  NMR (400 MHz,  $CDCl_3$ )  $\delta$ : 8.34ppm (s,1H), 2.06 – 1.85 ppm(m,), 1.76-1.63ppm(m,), 1.45-1.27ppm(m,);  $^{13}C$  and  $^{119}Sn$  were measured at 600 MHz Bruker NMR instrument.  $^{13}C$  NMR  $\{^1H\}$  (150 MHz,  $CDCl_3$ )  $\delta$ : 166.3ppm (s,  $HO\overline{C}OSn$ ), 33.9 (s,  $H\overline{C}Sn$ ), 31.0 (s,  $CH_2$ ) 28.9 (s,  $CH_2$ ), 26.8 (s,  $CH_2$ );  $^{119}Sn$  NMR  $\{^1H\}$  (224 MHz,  $CDCl_3$ )  $\delta$ : 32.3 (s)

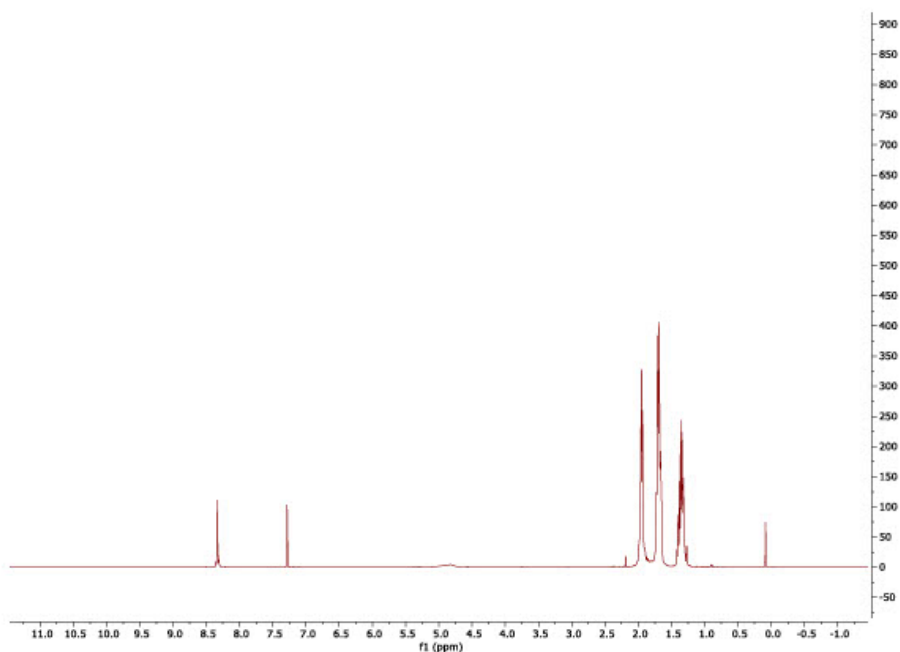


Figure S33:  $^1H$  NMR spectrum of  $Cy_3SnOCOH$

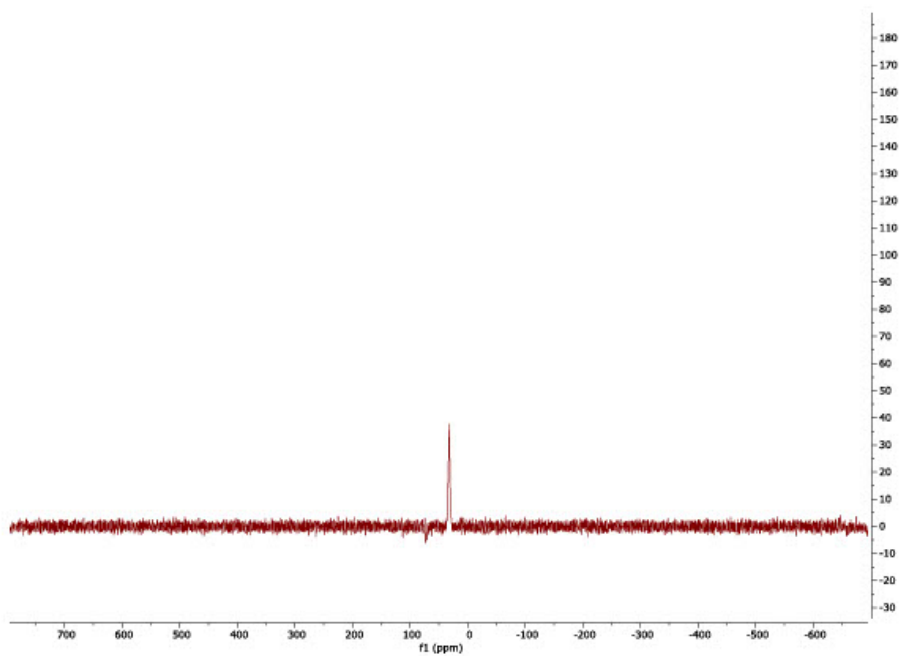
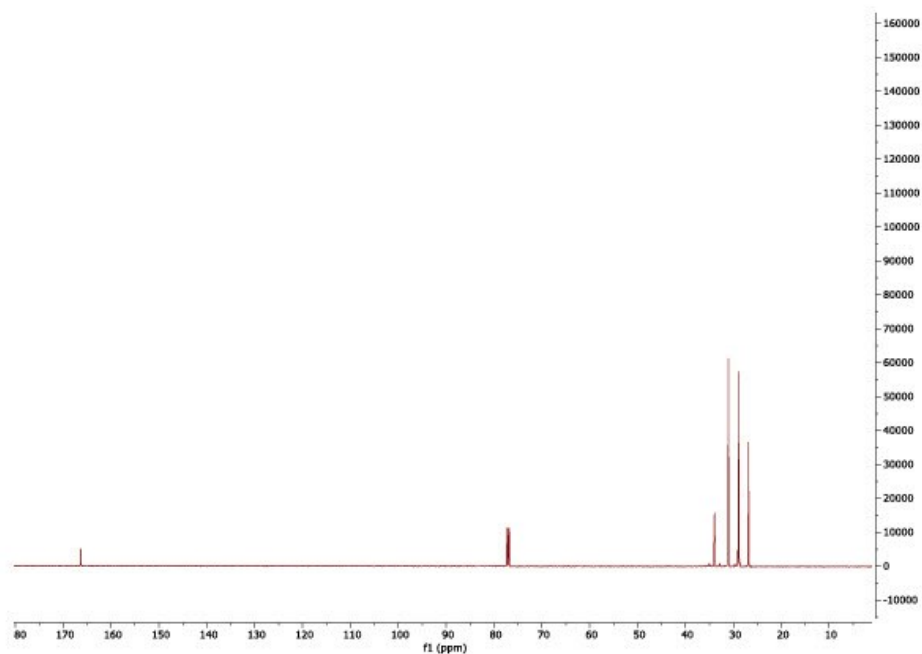


Figure S34.  $^{119}\text{Sn}$  NMR spectrum of  $\text{Cy}_3\text{SnOCOH}$





**Figure S35:**  $^{13}\text{C}$  NMR spectrum of  $\text{C}_3\text{SnOCOH}$

### 9.2 Standard procedure for direct reaction of $\text{C}_3\text{SnOCOH}$ with morpholine:

In air, to the autoclave,  $\text{C}_3\text{SnOCOH}$  (0.1 mmol), 2,4,6-collidine (0.1 mmol) and morpholine (1 mmol) were dissolved in sulfolane (5 mL). The autoclave was then sealed and purged 5 times with the desired pressure of  $\text{CO}_2$ . The reaction is then topped up with the desired  $\text{H}_2$  reaction pressure. The temperature and stirring rate were set using the Specview program on Parr 5000 series multi reactor system. The reaction was allowed to warm to 453K and was held there for 30 mins after which the heating was turned off and the reactor was allowed to cool to room temperature. DCM (1 mmol) was added to the reactor, stirred and an aliquot was taken for  $^1\text{H}$  NMR in  $\text{CDCl}_3$ . The conversion was quantified by comparing the integral of the formate peak and the integral of DCM.

### 9.3 Formate transfer experiments:

**Table S6:** Effect of  $\text{H}_2$  and  $\text{CO}_2$  on the formate transfer of  $\text{C}_3\text{SnOCOH}$  (10 mol%) to morpholine in the presence of 2,4,6-collidine (10 mol%) in 5 mL sulfolane.

Catalyst (LA)	H <sub>2</sub> Pressure (bar)	CO <sub>2</sub> Pressure (bar)	Temperature (K)	Time (min)	Yield (%)
Cy <sub>3</sub> SnOCOH	0	6	453	30	6
Cy <sub>3</sub> SnOCOH	0	30	453	30	6
Cy <sub>3</sub> SnOCOH	100	6	453	30	10
Cy <sub>3</sub> SnOCOH	100	30	453	30	10
Cy <sub>3</sub> SnOCOH	0	0	453	30	4

## 10. Mechanism investigation: Cy<sub>3</sub>SnOH reaction with morpholinium triflate

### 10.1 Standard procedure for direct reaction of Cy<sub>3</sub>SnOH with morpholinium triflate:

In air, to the autoclave, Cy<sub>3</sub>SnOH (0.1mmol), 2,4,6-collidine (0.1mmol), morpholinium triflate (0.1mmol) and morpholine (0.9mmol) were dissolved in sulfolane (5ml). The autoclave was then sealed and purged 5 times with the desired pressure of CO<sub>2</sub>. The reaction is then topped up with the desired H<sub>2</sub> reaction pressure. The temperature and stirring rate were set using **Specview program connected to the Parr 5000 series multi reactor system**. T = 0 was defined as the time the heating starts. The heating was turned off 2 hours before the end of the end of the stated reaction time i.e., for a reaction time of 24hours the heating was turned off 22 hours in and the reaction was degassed at the 24-hour mark. DCM (1mmol) was added to the reactor, stirred and an aliquot was taken for NMR in CDCl<sub>3</sub>. The conversion was quantified by comparing the integral of the formate peak and the integral of DCM. Other reaction products were determined by GC-MS.

### 10.2 Cy<sub>3</sub>SnOH synthesis:

The procedure was adapted from reference<sup>10</sup>

A 5% solution of NaOH in water (15mL) was slowly added to a solution of Cy<sub>3</sub>SnCl (807mg, 2mmol) in Et<sub>2</sub>O (15mL). The mixture was stirred for 1h and subsequently filtered. The ether layer was separated from the aqueous layer and the aqueous was washed with Et<sub>2</sub>O (3x10mL). The combined ether layers were evaporated under reduced pressure and the solids were combined with the original solids. The combined solids were recrystallized from EtOH. After which EtOH was filtered, and the solids were dried. The white solid was collected in an 87% yield.

$^1\text{H}$  NMR (400 MHz,  $\text{CDCl}_3$ )  $\delta$ : 1.98 – 1.86 ppm(m), 1.79-1.60ppm(m), 1.45-1.24ppm(m), -0.33ppm (s,1H);  $^{13}\text{C}$ ,  $^{19}\text{F}$  and  $^{119}\text{Sn}$  were measured at 600 MHz Bruker NMR instrument.  $^{13}\text{C}$  NMR (150 MHz,  $\text{CDCl}_3$ )  $\delta$ : 32.0 (s), 31.10 (s), 28.80 (s), 27.0 (s);  $^{119}\text{Sn}$  (224 MHz,  $\text{CDCl}_3$ )  $\delta$ : 10.48 ppm

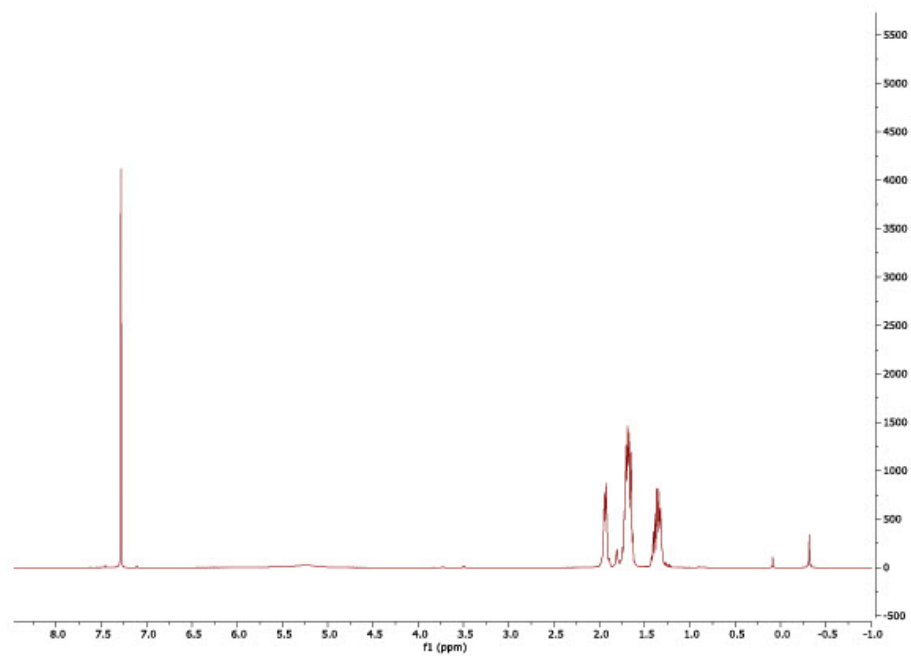


Figure S36.  $^1\text{H}$  NMR spectrum of  $\text{Cy}_3\text{SnOH}$

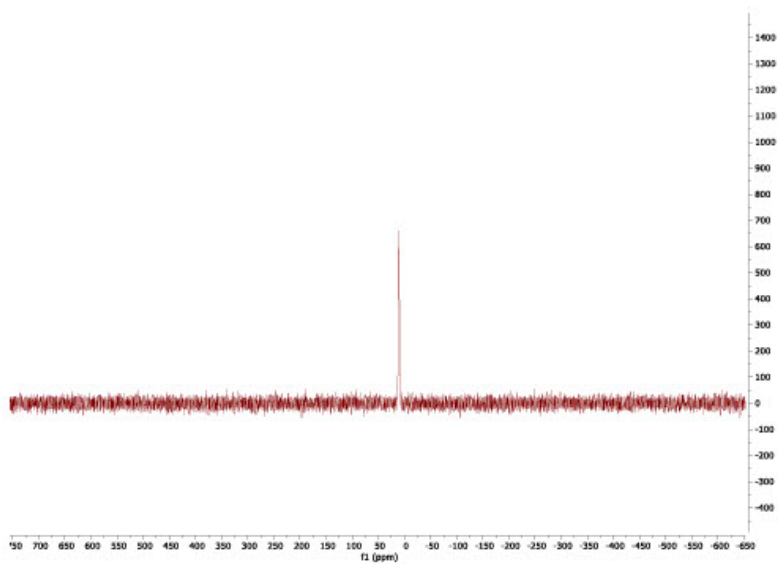


Figure S37:  $^{119}\text{Sn}$  NMR spectrum of  $\text{Cy}_3\text{SnOH}$

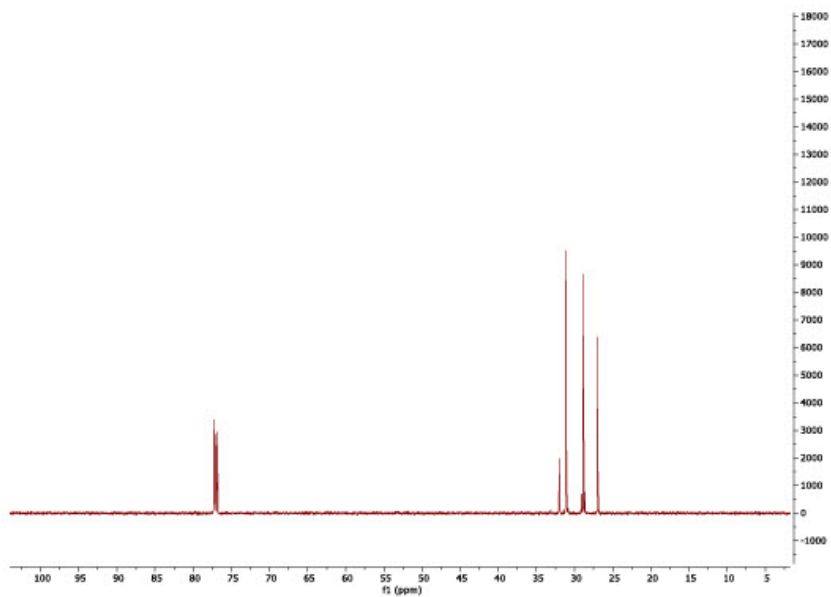
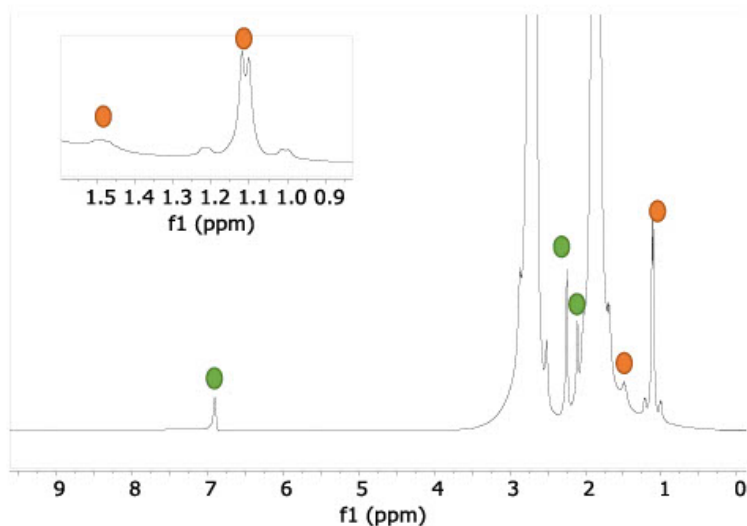


Figure S38:  $^{13}\text{C}$  NMR spectrum of  $\text{Cy}_3\text{SnOH}$

## 11. Mechanism investigation: In-situ $^1\text{H}$ NMR of the reaction mixture

$^1\text{H}$  NMR spectra of the reaction mixture were measured on a Bruker AVANCE-III (400 MHz) spectrometer in 10 mm sapphire tubes from Wilmad with custom-made stainless-steel caps. The measurements were performed in the absence of a deuterated solvent and hence without a signal lock. Position of  $^1\text{H}$  NMR signals of sulfolane was then aligned with sulfolane peaks recorded in  $\text{CDCl}_3$ .



**Figure S39:** Reference  $^1\text{H}$  NMR spectrum of FLP1 in sulfolane at 303 K; orange =  $^i\text{Pr}_3\text{SnOTf}$ , green = 2,4,6-collidine

Interaction of  $^i\text{Pr}_3\text{SnOTf}$  and 2,4,6-collidine was not observed (Figure S 13), which confirms that a FLP forms between the LA and the LB rather than a classical LA-LB adduct. However, addition of morpholine to the NMR tube resulted in splitting of  $^i\text{Pr}_3\text{SnOTf}$  signals into two set of peaks, which indicates that morpholine binds, at least in part, to the LA (Figure S S 14). This observation is in line with the lower steric profile of morpholine in comparison to 2,4,6-collidine and might also partially explain the requirement for the high reaction temperature, which is not required in the hydrogenation of bulky imines with FLP1<sup>1</sup>. Nevertheless, presence of  $\text{CO}_2$  diminishes the interaction as observed by the reformation of the original  $^i\text{Pr}_3\text{SnOTf}$  signals upon addition of  $\text{CO}_2$  and the formation of new signals that can be attributed to morpholine-4-carboxylic acid (carbamic acid) (Figure S S 15).

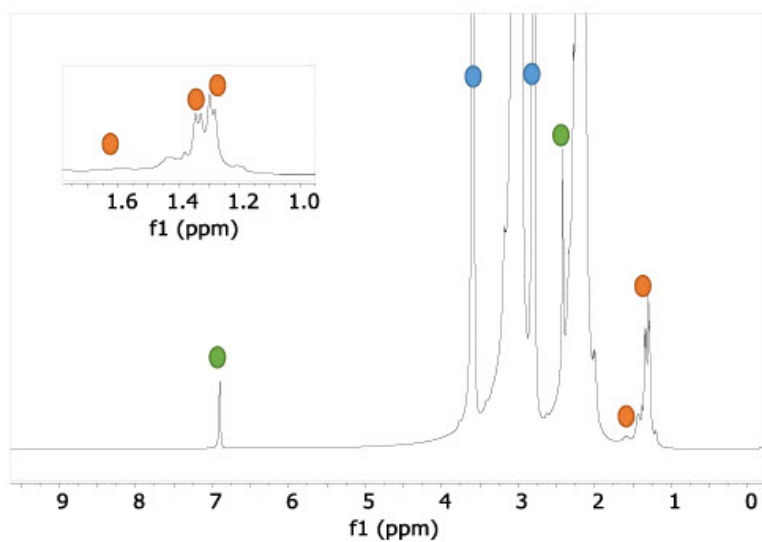


**Figure S40:**  $^1\text{H}$  NMR spectrum of FLP1 (0.02 mmol) and morpholine (0.2 mmol) in sulfolane at 303 K; orange =  $^i\text{Pr}_3\text{SnOTf}$ , green = 2,4,6-collidine, blue = morpholine

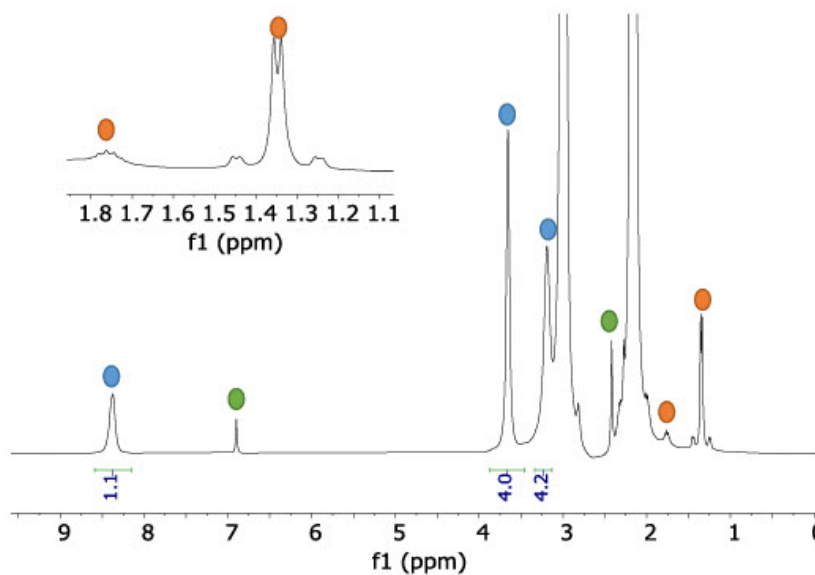


**Figure S41:**  $^1\text{H}$  NMR spectrum of FLP1 (0.02 mmol) and morpholine (0.2 mmol) in sulfolane at 303 K in the presence of  $\text{CO}_2$  (4 bar) and  $\text{H}_2$  (96 bar); orange =  $^i\text{Pr}_3\text{SnOTf}$ , green = 2,4,6-collidine, blue = morpholine carbamic acid

Heating of the reaction mixture in-situ to 393 K results in gradual collapse of the carbamic acid peaks at 3.2, 3.6 and 8.4 ppm and the formation of new peaks at 3.6 and 4.6 ppm, which cannot be attributed to morpholine nor its carbamic acid. Interaction with the reaction catalyst, however, does not take place as  $^1\text{Pr}_3\text{SnOTf}$  remains the same even after heating of the reaction mixture at 393 K in-situ for 21 h and further heating at 453 K ex-situ prior to further measurements. No intermediates were observed during the reaction only the slow and gradual formation of the desired reaction product N-formylmorpholine, which indicates that hydrogen activation is the rate-determining step.

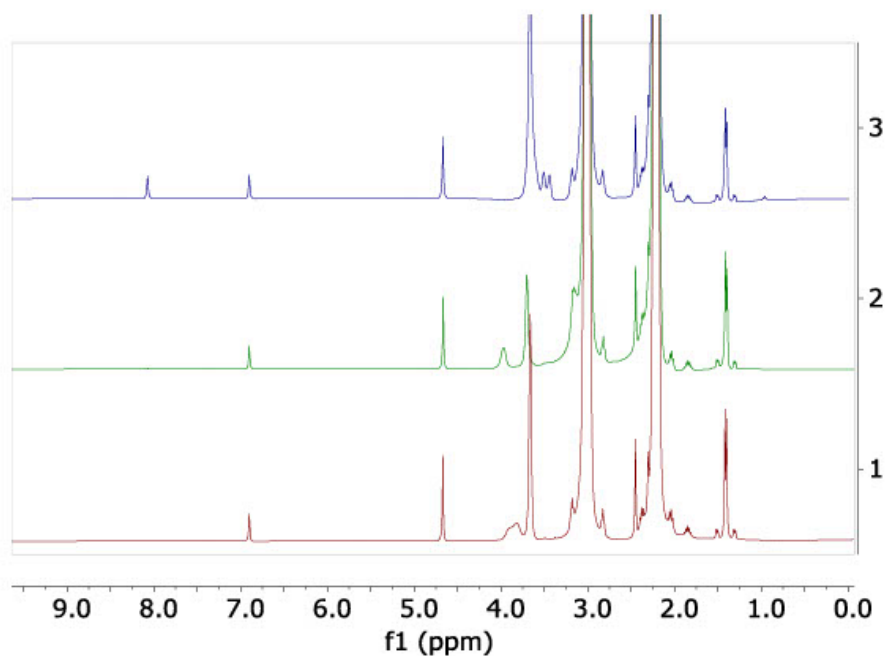


**Figure S42:**  $^1\text{H}$  NMR spectrum of FLP1 (0.02 mmol) and morpholine (0.2 mmol) in sulfolane at 393 K in the presence of  $\text{CO}_2$  (4 bar) and  $\text{H}_2$  (96 bar); red spectrum = t(0 h), green spectrum = t(6 h) @ 393 K and blue spectrum = t(21 h) @ 393 K + t(5 h) @ 453 K

## 12. References:

- (1) Scott, D. J.; Phillips, N. A.; Sapsford, J. S.; Deacy, A. C.; Fuchter, M. J.; Ashley, A. E. Versatile Catalytic Hydrogenation Using A Simple Tin(IV) Lewis Acid. *Angew. Chem. - Int. Ed.* **2016**, *55* (47). <https://doi.org/10.1002/anie.201606639>.
- (2) Sapsford, J.; Scott, D.; Allcock, N.; Fuchter, M.; Ashley, A.; Tighe, C. Direct Reductive Amination of Carbonyl Compounds Catalyzed by a Moisture Tolerant Tin(IV) Lewis Acid. *Adv. Synth. Catal.* **2018**,

360 (6). <https://doi.org/10.1002/adsc.201701418>.

- (3) Gyömöre, Á.; Bakos, M.; Földes, T.; Pápai, I.; Domján, A.; Soós, T. Moisture-Tolerant Frustrated Lewis Pair Catalyst for Hydrogenation of Aldehydes and Ketones. *ACS Catal.* **2015**, *5* (9). <https://doi.org/10.1021/acscatal.5b01299>.
- (4) Hamza, A.; Sorochkina, K.; Kótai, B.; Chernichenko, K.; Berta, D.; Bolte, M.; Nieger, M.; Repo, T.; Pápai, I. Origin of Stereoselectivity in FLP-Catalyzed Asymmetric Hydrogenation of Imines. *ACS Catal.* **2020**, *10* (23). <https://doi.org/10.1021/acscatal.0c04263>.
- (5) Sapsford, J. S.; Csókás, D.; Turnell-Ritson, R. C.; Parkin, L. A.; Crawford, A. D.; Pápai, I.; Ashley, A. E. Transition Metal-Free Direct Hydrogenation of Esters via a Frustrated Lewis Pair. *ACS Catal.* **2021**, *11* (15). <https://doi.org/10.1021/acscatal.1c01940>.
- (6) Lennon, G.; Willox, S.; Ramdas, R.; Funston, S. J.; Klun, M.; Pieh, R.; Fairlie, S.; Dobbin, S.; Cobice, D. F. Assessing the Oxidative Degradation of N-Methylpyrrolidone (Nmp) in Microelectronic Fabrication Processes by Using a Multiplatform Analytical Approach. *J. Anal. Methods Chem.* **2020**, *2020*. <https://doi.org/10.1155/2020/8265054>.
- (7) Erdmann, P.; Greb, L. What Distinguishes the Strength and the Effect of a Lewis Acid: Analysis of the Gutmann–Beckett Method. *Angew. Chem. - Int. Ed.* **2022**, *61* (4). <https://doi.org/10.1002/anie.202114550>.
- (8) Arlegui, A.; Torres, P.; Cuesta, V.; Crusats, J.; Moyano, A. A PH-Switchable Aqueous Organocatalysis with Amphiphilic Secondary Amine–Porphyrin Hybrids. *European J. Org. Chem.* **2020**, *2020* (28), 4399–4407. <https://doi.org/10.1002/EJOC.202000648>.
- (9) Ellis, B. D.; Atkins, T. M.; Peng, Y.; Sutton, A. D.; Gordon, J. C.; Power, P. P. Synthesis and Thermolytic Behavior of Tin(IV) Formates: In Search of Recyclable Metal-Hydride Systems. **2010**. <https://doi.org/10.1039/c0dt00812e>.
- (10) Howie, R. A.; Moura, M. V. H.; Wardell, J. L.; Wardell, S. M. S. V. Further Study of Tris(Cyclohexyl)Stannane Compounds, Cy<sub>3</sub>SnX. Syntheses of the Compounds with X = Br, I, N<sub>3</sub> and NCS and Redetermination of the Crystal Structures of Cy<sub>3</sub>SnX (X = Br and I). *Polyhedron* **2004**, *23* (14), 2331–2336. <https://doi.org/10.1016/J.POLY.2004.08.001>.



## Appendix 2 Frustrated Lewis Pairs Catalyse the Solvent-Assisted Synthesis of Azoles from ortho-Substituted Anilines, CO<sub>2</sub> and H<sub>2</sub>

A. Paparakis, Dr. M. Hulla ChemCatChem 2023, 15, e202300510

# Frustrated Lewis Pairs Catalyse the Solvent-Assisted Synthesis of Azoles from *ortho*-Substituted Anilines, CO<sub>2</sub> and H<sub>2</sub>

Alexandros Paparakis<sup>[a]</sup> and Martin Hulla<sup>\*[a]</sup>

Synthesizing azoles from *ortho*-substituted anilines, CO<sub>2</sub> and H<sub>2</sub> has proved difficult due to the low nucleophilicity of anilines, which hinders their N-formylation, i.e., the first step of the reaction. This study demonstrates that R<sub>3</sub>SnX Lewis acids (LA), N-methylmorpholine (NMM) or DBU and polyethyleneimine (PEI) or N-formylmorpholine efficiently catalyse the synthesis of benzimidazole and other azoles from *ortho*-substituted anilines,

CO<sub>2</sub> and H<sub>2</sub> by reductive coupling of CO<sub>2</sub> to nucleophilic amine-based solvents, PEI or morpholine, followed by in-situ transfer of the formyl group to the appropriate *ortho*-substituted aniline. Under these reaction conditions, spontaneous cyclization of the N-formylated intermediate yields the corresponding azole in up to 98% yield.

## Introduction

CO<sub>2</sub> is a promising, non-toxic, abundant and renewable C1 building block for fuels, polymers, fine chemicals and pharmaceuticals.<sup>[1–4]</sup> In particular, CO<sub>2</sub> reduction and subsequent coupling to nucleophilic substrates containing N,<sup>[5,6]</sup> S<sup>[7,8]</sup> and O<sup>[9–11]</sup> donor atoms leads to products with added complexity and value, such as N-formylamines,<sup>[2,6,12]</sup> N-methylamines,<sup>[13–16]</sup> and azoles.<sup>[7,8,17–22]</sup> These products are essential in the pharmaceutical industry, where for example azoles form the backbone of bioactive molecules such as antimicrobial and anticancer drugs (Figure 1).<sup>[23–26]</sup>

Azoles can be produced by formate transfer from formamides, such as DMF or N-formylmorpholine, in the presence of a Lewis acid (LA), to suitably *ortho*-substituted aniline followed by cyclization of the N-formylated intermediate (Scheme 1A).<sup>[8,22,27]</sup> Azoles can also be produced by N-formylation of *ortho*-substituted anilines with CO<sub>2</sub> and H<sub>2</sub>, which reduces the reaction waste to water only (Scheme 1B).<sup>[28–30]</sup> Yet, despite considerable research efforts to study the N-formylation reaction with CO<sub>2</sub> and H<sub>2</sub> and to develop high-activity catalysts for N-formylation of aliphatic amines,<sup>[12,31–38]</sup> only four systems are known to catalyse the two-step tandem synthesis of azoles from *ortho*-substituted anilines using CO<sub>2</sub> and H<sub>2</sub>.<sup>[28–30]</sup> This lack of catalysts may be due to difficulties with the N-formylation of

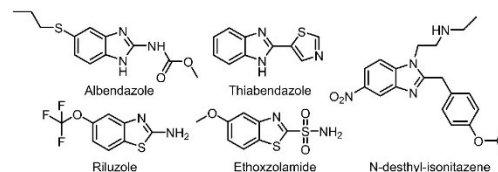
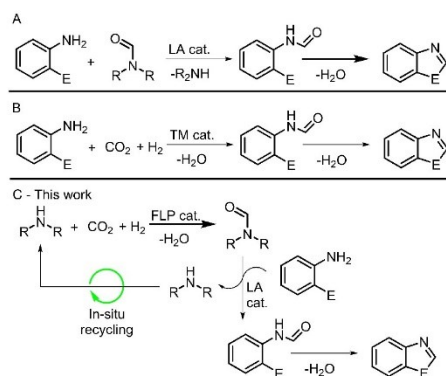


Figure 1. Examples of important azole derived drug molecules.



Scheme 1. A) N-formylation of *ortho*-substituted anilines with transfer formylation reagent and LA catalyst, B) Direct N-formylation of *ortho*-substituted anilines with CO<sub>2</sub>, H<sub>2</sub> and transition metal (TM) catalyst, C) N-formylation of nucleophilic amines with CO<sub>2</sub> and H<sub>2</sub> followed by in-situ transfer of the formyl group to *ortho*-substituted anilines with Frustrated Lewis pair (FLP) catalyst.

[a] A. Paparakis, Dr. M. Hulla  
Department of Inorganic Chemistry, Faculty of Science,  
Charles University,  
128 00 Prague (Czech Republic)  
E-mail: martin.hulla@natur.cuni.cz

Supporting information for this article is available on the WWW under <https://doi.org/10.1002/cctc.202300510>

© 2023 The Authors. ChemCatChem published by Wiley-VCH GmbH. This is an open access article under the terms of the Creative Commons Attribution Non-Commercial License, which permits use, distribution and reproduction in any medium, provided the original work is properly cited and is not used for commercial purposes.

anilines with CO<sub>2</sub> and H<sub>2</sub><sup>[31,39]</sup> because anilines are less nucleophilic than aliphatic or benzylic amines.

These difficulties can be overcome by using auxiliary reducing agents such as hydrosilanes<sup>[5,6,40,41]</sup> or boranes<sup>[5,19,42]</sup>

instead of H<sub>2</sub>, but this approach generates large amounts of undesirable waste.<sup>[6]</sup> Using CO<sub>2</sub> and H<sub>2</sub> the N-formylation of *ortho*-substituted anilines can be performed with Pd-,<sup>[28]</sup> Ru-,<sup>[28]</sup> Co-<sup>[30]</sup> and Au-based catalysts.<sup>[29]</sup> However, high activity requires high catalyst loadings ranging from 5 to 10 mol% in the case of Co<sup>[28]</sup> and Au<sup>[29]</sup> systems and pressures of > 100 bar in the case of Pd<sup>[28]</sup> and Ru.<sup>[28]</sup> RuCl<sub>2</sub>(dppf)<sub>2</sub> is the best catalyst reported, with a turnover frequency (TOF) of 12 h<sup>-1</sup> at 100 bar.<sup>[28]</sup> Therefore, new hydrogenation strategies should be developed to synthesize azoles from *ortho*-substituted anilines, CO<sub>2</sub> and H<sub>2</sub>.

Recently, Frustrated Lewis pairs (FLPs) demonstrated the ability to N-formylate secondary aliphatic amines.<sup>[39]</sup> Since FLPs are composed of LAs, suitable for transfer formylation reactions, we hypothesized that a combined strategy of N-formylation of nucleophilic amine(s) with CO<sub>2</sub> and H<sub>2</sub> followed by in-situ formate transfer and simultaneous recycling of the amine (Scheme 1C) may prove effective with FLP catalysts.

Herein, we demonstrate that R<sub>3</sub>SnX-based FLPs, where R = alkyl and X = triflate (OTf<sup>-</sup>) or triflimide (NTf<sub>2</sub><sup>-</sup>), catalyse the tandem synthesis of azoles from *ortho*-substituted anilines, CO<sub>2</sub> and H<sub>2</sub>. Reactive solvents, N-methylmorpholine (NMM) mixed with polyethyleneimine (PEI) or morpholine, act as the primary N-formylation targets and subsequently as transfer formylation agents, which increases the catalytic activity of the system in the synthesis of benzimidazole over 60-fold in comparison to inert solvents and results in TOF = 16.8 h<sup>-1</sup> at 100 bar, thus matching the performance of the best Ru-based catalyst reported in the literature thus far.

## Results and Discussion

The initial reaction conditions [o-phenylenediamine (1 mmol), sulfolane (5 mL), 180 °C, CO<sub>2</sub> (4 bar) and H<sub>2</sub> (96 bar)] were selected based on published results for N-formylation of aliphatic amines with R<sub>3</sub>SnX-based FLPs.<sup>[39]</sup> In the absence of nucleophilic amines, which could act as primary N-formylation target(s) and subsequently as transfer formylation reagents, the catalytic activity of R<sub>3</sub>SnX-based FLPs for the synthesis of benzimidazole from o-phenylenediamine was low (Table 1, entries 1–3 and Table S1, S1) in line with previous findings because R<sub>3</sub>SnX-based FLPs do not N-formylate aniline.<sup>[39]</sup>

The best FLP tested (Table S1, S1), Cy<sub>3</sub>SnNTf<sub>2</sub>:NMM, resulted in 24% benzimidazole yield in 22 hrs, which corresponds to TOF of only 0.22 h<sup>-1</sup> (Table 1, entry 1). Adding increasing quantities of NMM to promote 'encounter complex' formation and H<sub>2</sub> activation<sup>[22]</sup> did not result in an equivalent increase in the reaction rate at low NMM concentrations. When the quantity of NMM was increased from 0.05 equivalents (0.005 mL, 5 mol%) to 1.0 equivalent (0.1 mL, 100 mol%), the benzimidazole yield remained 24% after 22 hrs (Table 1, entries 1 and 2). Only when increasing NMM to 10 equivalents (1.1 mL, 1000 mol%) did the benzimidazole yield increase to 53% and TOF to 0.48 h<sup>-1</sup> (Table 1, entry 3). Since large concentrations of NMM further promoted the reaction, whereas low concentrations did not, it is possible that NMM in large

**Table 1.** Effect of transfer formylation reagents, NMM and PEI on the synthesis of benzimidazole from o-phenylenediamine, CO<sub>2</sub> and H<sub>2</sub>.

Entry	Sulfolane/NMM/PEI [mL]	Cy <sub>3</sub> SnNTf <sub>2</sub> [mol %]	Yield [%]	TON	TOF [h <sup>-1</sup> ]
1	5.0/0.005/none	5.0	24	4.8	0.22
2	4.9/0.1/none	5.0	24	4.8	0.22
3	3.9/1.1/none	5.0	53	10.6	0.48
4	4.9/none/0.1	1.0	49	49	2.23
5	4.8/none/0.2	1.0	65	65	2.95
6 <sup>[a]</sup>	4.25/none/0.75	0.5	87	174	7.91
7 <sup>[a]</sup>	3.5/none/1.5	0.5	98	196	> 8.91
8 <sup>[b]</sup>	2.5/none/2.5	0.1	26	260	11.8
9 <sup>[b]</sup>	2.0/0.5/2.5	0.1	28	280	12.7
10 <sup>[b]</sup>	1.3/1.25/2.5	0.1	30	300	13.6
11 <sup>[b]</sup>	none/2.5/2.5	0.1	37	370	16.8

Reaction conditions: o-phenylenediamine (1 mmol), total volume = 5 mL, LA = Cy<sub>3</sub>SnNTf<sub>2</sub>, CO<sub>2</sub> (4 bar), H<sub>2</sub> (96 bar), 22 hrs, 180 °C, average yield after three runs. Yields were determined by <sup>1</sup>H NMR with an internal standard. [a] 5 mmol of o-phenylenediamine. [b] 10 mmol of o-phenylenediamine. TOF values were calculated as the number of moles of product divided by the number of moles of Lewis acid divided by time. NMM and PEI were both used as received without further drying or purification.

quantities promotes the reaction in other ways apart from being involved in H<sub>2</sub> activation.

An additional base may also accelerate the N-formylation of o-phenylenediamine by its partial deprotonation, increasing the nucleophilicity and its associated reactivity with the formylation source, presumably R<sub>3</sub>SnOC(H)O.<sup>[39]</sup> Thus we hypothesized that including nucleophilic amines, acting as primary N-formylation target(s) and subsequently as transfer formylation reagents, could accelerate the reaction (Scheme 1C). Moreover, transfer formylations are catalysed by LAs<sup>[8,22]</sup> and hence should be compatible with and promoted by the FLP used here for CO<sub>2</sub> reduction to formate.

Adding 0.1 mL of branched polyethyleneimine (PEI, 600 MW), which can act as the reaction base, primary N-formylation target and formate transfer reagent, accelerated the reaction 10-fold (Table 1, entries 2 and 4). The TOF further increased from 2.23 h<sup>-1</sup> to 11.8 h<sup>-1</sup> at 1:1 mixtures of sulfolane and PEI when the reaction solvent (sulfolane) was gradually substituted for PEI (Table 1, entries 4–8). Further solvent substitution for PEI was, however, impractical due to the high density of PEI and to difficulties in analysing the reaction mixture. Instead, the remainder of sulfolane was gradually substituted for NMM, which further increased the TON to 370 and the TOF to 16.8 h<sup>-1</sup> with 1:1 mixtures of NMM and PEI (Table 1, entries 9–11) most likely because NMM facilitated H<sub>2</sub> activation and/or improved the solubility of the reactants such as CO<sub>2</sub>, which is known to dissolve well in amine-based solvents.<sup>[43]</sup> The recorded activity matched that of the best Ru-based catalyst with a TOF of 12.1 h<sup>-1</sup> at 100 bar in the same reaction.<sup>[28]</sup> Increasing the reaction time from 22 hours to 65 hours at 0.1 mol% loading of Cy<sub>3</sub>SnNTf<sub>2</sub> increased the TON from 370 to 407, which indicates decomposition of the LA overtime and also indicates the maximum TON of the system under the given conditions.

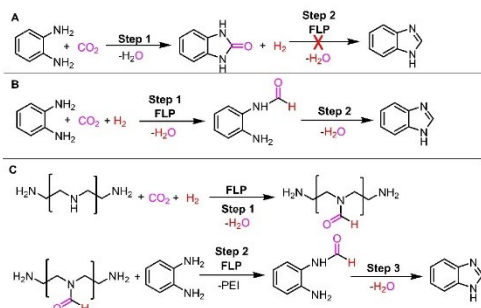
Due to large viscosity and boiling point of PEI, other secondary amines may be more suitable as primary N-



formylation targets and transfer formylation agents. Moreover, secondary amines are known to facilitate  $H_2$  activation with LA and may hence further promote the reaction.<sup>[44–46]</sup> Using morpholine:NMM (1:1) mixture as the reaction solvent resulted in similar results to PEI:NMM (1:1) mixture (SI), which confirms that other secondary amines may be used. Nevertheless, using pure morpholine as solvent was also found impractical as secondary amines react with  $CO_2$  to form carbamate salts, which resulted in crystallization of the reaction mixture in the absence of a co-solvent such as NMM.

To further support the proposed reaction pathway, via N-formylation of nucleophilic amine with  $CO_2$  and  $H_2$  followed by in-situ formate transfer reaction (Scheme 1C), we performed a number of control experiments (Scheme 2). First, hydrogenation of 2-hydroxybenzimidazole, potentially formed in the reaction of *o*-phenylenediamine with  $CO_2$ , was dismissed as the reaction did not yield benzimidazole under such reaction conditions (Pathway A). Direct N-formylation of *o*-phenylenediamine (Pathway B), which is known to be accelerated by transition metal catalysts,<sup>[28,30]</sup> likely occurs in the absence of formate transfer agent because  $R_3SnX$ -based FLPs demonstrated low catalytic activity for benzimidazole synthesis even without of a nucleophilic amine (Table 1, entry 1 and Table S1). Furthermore, 2-aminoformanilide and acetamide underwent self-cyclization at high temperatures (pathway B, step 2).<sup>[28]</sup> 2-Aminoacetanilide also quantitatively cyclised in the presence of  $Cy_3SnNTf_2$ :NMM FLP (SI), and the cyclisation was much faster than N-formylation given the 65% yield of benzimidazole synthesis (Table 1, entry 5) performed under equivalent conditions.

$R_3SnX$ -based FLPs are known to N-formylate secondary aliphatic amines.<sup>[39]</sup> Formamides such as DMF and N-formylmorpholine are also known to act as a C1 source for the synthesis of azoles from *ortho*-substituted anilines, wherein the formamides decompose in the presence of LAs.<sup>[8,22,27]</sup> To assess whether formylated PEI could act as a C1 source, the reaction was run without *o*-phenylenediamine, after which the polymer was isolated *post-situ* and added to *o*-phenylenediamine (1 mmol). Benzimidazole formation was then observed at reaction temperatures above 140 °C (SI). These results confirm



**Scheme 2.** Possible pathways for benzimidazole synthesis from *o*-phenylenediamine,  $CO_2$  and  $H_2$  catalyzed by FLPs.

that PEI can act as a primary N-formylation source and subsequent transfer formylation agent (Scheme 2, pathway C).

With an efficient system at hand, we decided to investigate the substrate scope of the reaction (Figure 2). The scope was investigated using 0.2–1 mol% of  $Cy_3SnNTf_2$  primarily in (1:1 or 4:1) NMM:PEI mixtures, adjusting the solvent composition based on the reactivity of the substrate and requirements for product detection (SI). *o*-Phenylenediamine was converted into benzimidazole in up to 98% yield (1) even at lower catalyst loadings. Primary diamines were converted into the respective azoles with both electron-donating (2 to 4) and -withdrawing groups (5&6), where functionalized substrates reacted slower than alkyl substituted diamines. Reaction with 3 showed simultaneous cyclization and potential N-methylation, detected via GC-MS, so we isolated the sample which showed that the N-methylated product was only a minor product as the desired product 3b was isolated in 76% yield. The substrates containing an ester (7) were unreactive. 4-Bromobenzene-1,2-diamine (5) was converted into the desired 4-bromobenzimidazole (5b) in only 29% yield. The remainder of the substrate was catalytically dehalogenated to benzimidazole (1b). Stoichiometric dehalogenation of aromatics with tin hydrides is well established and presumably proceeds via a radical mechanism.<sup>[47–49]</sup>

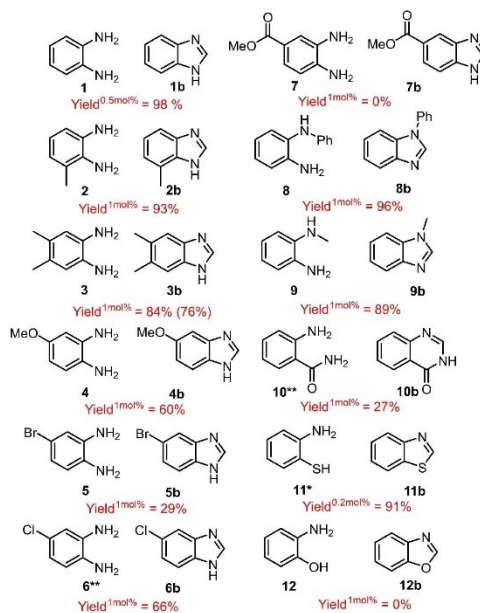
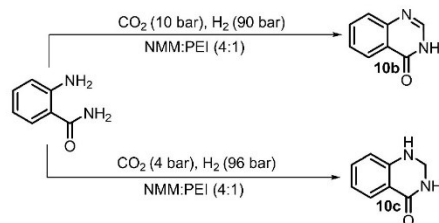


**Figure 2.** Substrate scope for the tandem synthesis of azoles with  $CO_2$ ,  $H_2$  and  $[Cy_3SnNTf_2]$ :NMM catalyst. Reaction conditions: amine (3 to 20 mmol), NMM (4 mL), LA (0.01 mmol), 1 mL PEI,  $CO_2$  (4 bars),  $H_2$  (96 bars), 180 °C, 22 hrs; the yields were determined by  $^1H$  NMR with an internal standard, and the structures were confirmed by GC-MS and comparison with reported  $^1H$  NMR shifts.<sup>[50–53]</sup> Yield in brackets indicates isolated yield. Superscripts indicate catalyst loading. \* DBU instead of NMM. \*\* 10 bars  $CO_2$  instead of 4 bars  $CO_2$ .



**Scheme 3.** Pressure controlled synthesis of **10b** and **10c** from 2-amino-benzamide.

In other words, hydride radicals are formed in the reaction to some extent. 4-Chloro-1,2-diamine (**6**) was converted into the desired product (**6b**) in 66% yield without concomitant benzimidazole formation when the partial pressure of CO<sub>2</sub> was increased from 4 to 10 bar. Substrates containing secondary amines with aryl (**8**) or alkyl (**9**) substituents also reached full conversion, indicating that the increased steric hindrance did not impair the reaction. 2-Aminobenzamide (**10**) resulted in the selective formation of 4-hydroxyquinazolin-4(1H)-one (**10b**) or 2,3-dihydroquinazolin-4(1H)-one (**10c**) depending on the reaction conditions (Scheme 3). **10b** reduction to **10c** was efficiently inhibited by increasing the partial pressure of CO<sub>2</sub> from 4 to 10 bar, which presumably removed all available hydrides from the system and prevented imine reduction.

Both molecules are important drug precursors, with 2,3-dihydroquinazolin-4(1H)-one (**10c**) serving as a scaffold for quinethazone (antihypertensive and diuretic), fenquizone (diuretic) and methaqualone (sedative and hypnotic).<sup>[26]</sup> Benzothiazole (**11b**) synthesis required using DBU instead of NMM presumably due to the acidic thiol. This thiol is deprotonated by DBU, allowing the reaction to proceed. Aminophenol (**12**) was unreactive, as previously observed with transitional metal catalysts.<sup>[28,30]</sup>

## Conclusion

In conclusion, tin-based FLPs in the form [R<sub>3</sub>SnX:N-base] catalyse the formation of azoles *via* complete deoxygenation of CO<sub>2</sub> in the presence of H<sub>2</sub> gas. Adding secondary amines as primary N-formylation targets and in-situ formed and recycled transfer formylating agents increases the activity of the system over 60-fold. As a result, activity of the tin-based FLPs in amine-based solvents match the activity of the best Ru-based catalysts for the synthesis of benzimidazole from *o*-phenylenediamine, CO<sub>2</sub> and H<sub>2</sub>. This strategy, where a transfer formylation agent is produced and recycled in-situ, may lead to the development of more efficient systems for the synthesis of azoles from *ortho*-substituted anilines, CO<sub>2</sub> and H<sub>2</sub> in the future.

## Experimental

**General procedures:** Lewis acids, R<sub>3</sub>SnX, were prepared according to literature procedures and stored in inert atmosphere.<sup>[39]</sup> Catalytic tests were performed in air and with 'wet' solvents as received from the supplier. Benzimidazole (1 to 10 mmol), R<sub>3</sub>SnX (0.1 to 5.0 mol%), Lewis base (0.1 to 10 mol%) were dissolved in the solvent mixture (5 mL) in a stainless-steel autoclave. The autoclave was then sealed and purged 5 times with the desired pressure of CO<sub>2</sub>. The reaction was then topped up with the desired H<sub>2</sub> reaction pressure. The temperature and stirring rate were set using Specview program on Parr 5000 series multi reactor system. T = 0 was defined as the time the heating starts. The heating was turned off at T = end of the stated reaction time and immediately cooled down. After which, DCM (1 mmol) was added to the reactor, stirred and an aliquot was taken for <sup>1</sup>H NMR analysis in CDCl<sub>3</sub> or DMSO-*d*<sub>6</sub>. The conversion of *o*-phenylenediamine and the yield of benzimidazole were quantified by <sup>1</sup>H NMR analysis with the added DCM as the internal standard. Other reaction products were quantified by their respective C1 hydrogen signal in <sup>1</sup>H NMR and structures confirmed by GC-MS on a Shimadzu QP-2010 GC-MS with a Supelcowax 10 column. Benzimidazole: <sup>1</sup>H NMR (400 MHz, CDCl<sub>3</sub>) δ: 8.05 (s, 1H), 7.67–7.62 (m, 2H), 7.28–7.23 (m, 2H); GC retention time 27.4 to 27.6 minutes; EI-MS (m/z) calculated: 118, found 118 with agreement of EI-MS molecular fragmentation with NIST EI-MS library.

**Isolation of 5,6-dimethylbenzimidazole:** The cyclization reaction was performed according to the general procedure using Cy<sub>3</sub>SnNTf<sub>2</sub> (0.01 mmol), 4,5-dimethyl-1,2-phenylenediamine (1 mmol), the solvent mixture NMM:PEI (4:1), CO<sub>2</sub> (4 bar) and H<sub>2</sub> (94 bar) at 180 °C for 22 hours. After the end of the reaction, the reactor was allowed to cool and was depressurised. After which the reaction liquor was decanted and filtered. The reactor was then washed with DCM (3 × 10 mL), the washings were collected, filtered and then added to the reaction liquor which was then evaporated under reduced pressure affording a brown solid (112 mg, 76% yield). <sup>1</sup>H NMR (400 MHz, CDCl<sub>3</sub>) δ: 7.90 (s, 1H), 7.51–7.30 (br s, 2H), 2.38 (s, 6H); <sup>13</sup>C NMR (400 MHz, CDCl<sub>3</sub>) δ: 140, 136, 132, 115, 21; ESI+ (m/z) calculated: 147.1, found 147.1

## Supporting Information

Additional references cited within the Supporting Information.<sup>[54–56]</sup>

## Acknowledgements

The authors thank the Czech Science foundation (GAČR 21-27431M) for financing the study and Carlos V. Melo for editing the manuscript.

## Conflict of Interests

The authors declare no conflict of interest.

## Data Availability Statement

The data that support the findings of this study are available in the supplementary material of this article.

**Keywords:** carbon dioxide · hydrogenation · FLP · solvent-assisted · transfer formylation

- [1] A. Modak, P. Bhanja, S. Dutta, B. Chowdhury, A. Bhaumik, *Green Chem.* **2020**, *22*, 4002–4033.
- [2] J. Klankermayer, S. Wesselbaum, K. Beydoun, W. Leitner, *Angew. Chem. Int. Ed.* **2016**, *55*, 7296–7343.
- [3] K. M. K. Yu, I. Curcic, J. Gabriel, S. C. E. Tsang, *ChemSusChem* **2008**, *1*, 893–899.
- [4] Q. Liu, L. Wu, R. Jackstell, M. Beller, *Nat. Commun.* **2015**, *6*, 5933.
- [5] M. Hulla, P. J. Dyson, *Angew. Chem. Int. Ed.* **2020**, *59*, 1002–1017.
- [6] A. Tlili, E. Blondiaux, X. Frogneux, T. Cantat, *Green Chem.* **2015**, *17*, 157–168.
- [7] S. Chun, S. Yang, Y. K. Chung, *Tetrahedron* **2017**, *73*, 3438–3442.
- [8] D. B. Nale, B. M. Bhanage, *Synlett* **2015**, *26*, 2835–2842.
- [9] Y. Li, B. Yang, L. Yan, W. Gao, K. M. Omer, L. K. Foong, *Synth. Commun.* **2020**, *50*, 2132–2155.
- [10] O. Kröcher, R. A. Köppel, A. Baiker, *Chem. Commun.* **1997**, *5*, 453–454.
- [11] G. Gastelu, D. Savary, M. Hulla, D. Ortiz, J. G. Uranga, P. J. Dyson, *ACS Catal.* **2023**, *13*, 2403–2409.
- [12] Y. Shen, Q. Zheng, Z. Chen, D. Wen, J. H. Clark, X. Xu, T. Tu, *Angew. Chem. Int. Ed.* **2021**, *60*, 4125–4132.
- [13] H. Niu, L. Lu, R. Shi, C.-W. W. Chiang, A. Lei, *Chem. Commun.* **2017**, *53*, 1148–1151.
- [14] K. Beydoun, G. Ghattas, K. Thener, J. Klankermayer, W. Leitner, *Angew. Chem. Int. Ed.* **2014**, *53*, 11010–11014.
- [15] S. Lin, J. Liu, L. Ma, *J. CO<sub>2</sub> Util.* **2021**, *54*, 101759.
- [16] J. R. Cabrero-Antonino, R. Adam, M. Beller, *Angew. Chem. Int. Ed.* **2019**, *58*, 12820–12838.
- [17] O. Jacquet, D. N. C. Gomes, M. Ephritikhine, T. Cantat, *ChemCatChem* **2013**, *5*, 117–120.
- [18] B. Yu, H. Zhang, Y. Zhao, S. Chen, J. Xu, C. Huang, Z. Liu, *Green Chem.* **2013**, *15*, 95–99.
- [19] V. B. Saptal, G. Juneja, B. M. Bhanage, *New J. Chem.* **2018**, *42*, 15847–15851.
- [20] V. V. Phatake, B. M. Bhanage, *Tetrahedron Lett.* **2021**, *68*, 152940.
- [21] I. H. Biswas, S. Biswas, M. S. Islam, S. Riyajuddin, P. Sarkar, K. Ghosh, S. M. Islam, *New J. Chem.* **2019**, *43*, 14643–14652.
- [22] H. Mostafavi, M. R. Islami, E. Ghoncheppour, A. M. Tikdari, *Chem. Pap.* **2018**, *72*, 2973–2978.
- [23] M. Gaba, C. Mohan, *Med. Chem. Res.* **2016**, *25*, 173–210.
- [24] C. Liu, C. Shi, F. Mao, Y. Xu, J. Liu, B. Wei, J. Zhu, M. Xiang, J. Li, *Molecules* **2014**, *19*, 15653.
- [25] I. Ali, M. N. Lone, H. Y. Aboul-Enein, *MedChemComm* **2017**, *8*, 1742.
- [26] M. Badolato, F. Aiello, N. Neamati, *RSC Adv.* **2018**, *8*, 20894–20921.
- [27] J. Zhu, Z. Zhang, C. Miao, W. Liu, W. Sun, *Tetrahedron* **2017**, *73*, 3458–3462.
- [28] B. Yu, H. Zhang, Y. Zhao, S. Chen, J. Xu, C. Huang, Z. Liu, *Green Chem.* **2012**, *15*, 95–99.
- [29] T. Mitsudome, T. Urayama, S. Fujita, Z. Maeno, T. Mizugaki, K. Jitsukawa, K. Kaneda, *ChemCatChem* **2017**, *9*, 3632–3636.
- [30] Z. Ke, B. Yu, H. Wang, J. Xiang, J. Han, Y. Wu, Z. Liu, P. Yang, Z. Liu, *Green Chem.* **2019**, *21*, 1695–1701.
- [31] P. Daw, S. Chakraborty, G. Leitus, Y. Diskin-Posner, Y. Ben-David, D. Milstein, *ACS Catal.* **2017**, *7*, 2500–2504.
- [32] L. Schmid, M. S. Schneider, D. Engel, A. Baiker, *Catal. Lett.* **2003**, *88*, 105–113.
- [33] O. Kröcher, R. A. Köppel, A. Baiker, *Chem. Commun.* **1997**, *5*, 453–454.
- [34] K. Zhang, L. Zong, X. Jia, *Adv. Synth. Catal.* **2021**, *363*, 1335–13.
- [35] L. Zhang, Z. Han, X. Zhao, Z. Wang, K. Ding, *Angew. Chem. Int. Ed.* **2015**, *54*, 6186–6189.
- [36] Y. Zhang, J. Wang, H. Zhu, T. Tu, *Chem. – An Asian J.* **2018**, *13*, 3018–3021.
- [37] M. A. Affan, P. G. Jessop, *Inorg. Chem.* **2017**, *56*, 7301–7305.
- [38] U. Jayarathne, N. Hazari, W. H. Bernskoetter, *ACS Catal.* **2018**, *8*, 1338–1345.
- [39] A. Paparakis, R. C. Turnell-Ritson, J. S. Sapsford, A. E. Ashley, M. Hulla, *Catal. Sci. Technol.* **2023**, *13*, 637–644.
- [40] F. J. Fernández-Alvarez, L. A. Oro, *ChemCatChem* **2018**, *10*, 4783–4796.
- [41] M. Hulla, S. Nussbaum, A. R. Bonnin, P. J. Dyson, *Chem. Commun.* **2019**, *55*, 13089–13092.
- [42] V. V. Phatake, A. A. Mishra, B. M. Bhanage, *Inorg. Chim. Acta* **2020**, *501*, 119274.
- [43] B. Dutcher, M. Fan, A. G. Russell, *ACS Appl. Mater. Interfaces* **2015**, *7*, 2137–2148.
- [44] V. Sumerin, F. Schulz, M. Nieger, M. Leskelä, T. Repo, B. Rieger, *Angew. Chem. Int. Ed.* **2008**, *47*, 6001–6003.
- [45] F. Schulz, V. Sumerin, M. Leskelä, T. Repo, B. Rieger, *Dalton Trans.* **2010**, *39*, 1920–1922.
- [46] P. A. Chase, T. Jurca, D. W. Stephan, *Chem. Commun.* **2008**, *14*, 1701–1703.
- [47] J. T. Groves, S. Kittisopikul, *Tetrahedron Lett.* **1977**, *18*, 4291–4294.
- [48] R. García-Loma, A. C. Albéniz, *Eur. J. Org. Chem.* **2017**, *2017*, 4247–4254.
- [49] A. H. McNeill, S. V. Mortlock, R. M. Pratt, E. J. Thomas, *J. Chem. Soc. Perkin Trans. 1* **1998**, 709–715.
- [50] X. Chen, T. Chen, Y. Zhou, D. Han, L. B. Han, S. F. Yin, *Org. Biomol. Chem.* **2014**, *12*, 3802–3807.
- [51] X. Zhu, F. Zhang, D. Kuang, G. Deng, Y. Yang, J. Yu, Y. Liang, *Org. Lett.* **2020**, *22*, 3789–3793.
- [52] Z. Sun, G. Bottari, K. Barta, *Green Chem.* **2015**, *17*, 5172–5181.
- [53] S. Livesley, A. J. Sterling, C. M. Robertson, W. R. F. Goundry, J. A. Morris, F. Duarte, C. Aissa, *Angew. Chem. Int. Ed.* **2022**, *61*, e202111291.
- [54] B. D. Ellis, T. M. Atkins, Y. Peng, A. D. Sutton, J. C. Gordon, P. P. Power, *Dalton Trans.* **2010**, *39*, 10659–10663.
- [55] D. J. Scott, N. A. Phillips, J. S. Sapsford, A. C. Deacy, M. J. Fuchter, A. E. Ashley, *Angew. Chem. Int. Ed.* **2016**, *55*, 14738–14742.
- [56] P. Erdmann, L. Greb, *Angew. Chem. Int. Ed.* **2022**, *61*, e202114550.

Manuscript received: April 5, 2023  
Revised manuscript received: April 29, 2023  
Accepted manuscript online: May 3, 2023  
Version of record online: May 16, 2023



# ChemCatChem

Supporting Information

**Frustrated Lewis Pairs Catalyse the Solvent-Assisted  
Synthesis of Azoles from *ortho*-Substituted Anilines, CO<sub>2</sub>  
and H<sub>2</sub>**

Alexandros Paparakis and Martin Hulla\*

## Contents

1. General procedures .....	2
2. Catalytic tests .....	2
2.1 General Procedure:.....	2
2.2. Initial FLP screening.....	3
2.3 Typical result(s) of synthesis of benzimidazole with CO <sub>2</sub> and H <sub>2</sub> :.....	4
2.4 Example of reproducibility between runs: .....	6
2.5 Optimization of CO <sub>2</sub> pressure: .....	8
2.6 Optimization of H <sub>2</sub> pressure:.....	9
2.7 Optimization of temperature: .....	9
3. Synthesis of catalysts .....	10
3.1 <sup>1</sup> Pr <sub>3</sub> SnOTf synthesis: .....	10
3.2 <sup>1</sup> Pr <sub>2</sub> Sn(OTf) <sub>2</sub> synthesis: .....	10
3.3 Cy <sub>3</sub> SnX synthesis:.....	12
5. Gutman-Beckett acidity measurements .....	18
5.1 General procedure for Gutman-Beckett acidity measurements .....	18
5.2 Results of Gutman-Beckett acidity measurements .....	18
6. Substrate scope.....	18
6.1 Benzimidazole.....	18
6.2 4-methylbenzimidazole.....	19
6.3 5,6-dimethylbenzimidazole.....	20
6.3.1 Isolation of 5,6-dimethylbenzimidazole .....	22
6.4 4-methoxybenzimidazole .....	23
6.5 4-bromobenzimidazole .....	24
6.6 4-chlorobenzimidazole.....	25
6.7 N-phenylbenzimidazole .....	26
6.8 N-methylbenzimidazole .....	28
6.9 4-Hydroxyquinazoline .....	29
6.10 2,3-dihydroquinazolin-4(1H)-one .....	30
6.11 Benzothiazole.....	31
7. Mechanism investigation: Formate transfer agent .....	33
7.1 Benzimidazole synthesis via formate transfer from PEI.....	33
7.2 Standard procedure for direct reaction of formylated PEI and o-phenylenediamine:.....	33
8. Mechanism investigation: Cyclisation of N-(2-aminophenyl) acetamide to 2-methyl-1H-benzimidazole .....	33
8.1 Standard procedure for cyclisation of N-(2-aminophenyl) acetamide to 2-methyl-1H-benzimidazole: .....	33



Testing of $Cy_3SnNTf_2$ stability to water .....	35
Reaction in the presence of molecular sieves .....	38
9. References:.....	38

## 1. General procedures

All reagents and solvents were purchased from commercial suppliers (Sigma-Aldrich, Merck, Alpha-Aesar, TCI, Across, abcr, Thermo scientific, Linde gas a.s. and Lach:ner). Specifically, tricyclohexyltin chloride was purchased from Thermo scientific, silver triflate was purchased from Sigma-Aldrich and silver triflimide was purchased from Thermo scientific. Synthetic reagents were used as received and without further purification including hydrogen gas (99.90%) and carbon dioxide for food industry (99.90%) purchased from Linde gas a.s. Solvents used were reagent grade or better. THF, hexane and DCM were dried on PureSolv MD 5 automated solvent drying system from Inert@. Sulfolane was dried and stored over 3Å molecular sieves (20%w/v) and degassed by sparging with dry  $N_2$  for a minimum of 20 minutes before use. All other solvents were used as received. All synthetic experiments were carried out using standard Schlenk techniques. Unless otherwise specified  $^1H$ ,  $^{13}C$  and  $^{119}Sn$  NMRs were taken on a Bruker AVANCE-III (400 MHz) at 298 K spectrometer and reported in ppm ( $\delta$ ). Deuterated solvents were purchased from abcr and used as received except for Gutmann-Beckett measurements, where  $CDCl_3$  was dried and stored over 3Å molecular sieves (20%w/v). NMR spectroscopy abbreviations: s, singlet; d, doublet; t, triplet; m, multiplet. All the products of catalytic tests were identified by  $^1H$  NMR data in comparison with literature, by GC coupled to mass spectrometry on a Shimadzu QP-2010 GC-MS with a Supelcowax 10 column and where necessary by comparison with genuine samples of the targeted compounds.

## 2. Catalytic tests

### 2.1 General Procedure:

In air  $R_3SnX$  (0.05 mmol), Lewis base (0.1 mmol) and benzimidazole (1 mmol) were dissolved in the solvent mixture (5 mL) in a stainless-steel autoclave. The autoclave was then sealed and purged 5 times with the desired pressure of  $CO_2$ . The reaction was then topped up with the desired  $H_2$  reaction pressure. The temperature and stirring rate were set using the Specview program on Parr 5000 series multi reactor system.  $T = 0$  was defined as the time the heating starts. The heating was turned off at  $T =$  end of the stated reaction time and immediately cooled down i.e., for a reaction time of 22 hours the heating was turned off after 22 hours, removed from the heating mantel and cooled immediately. After which, DCM (1 mmol) was added to the reactor, stirred and an aliquot was taken for  $^1H$  NMR analysis in  $CDCl_3$  or  $DMSO-d_6$ . The conversion of o-phenylenediamine and the yield of benzimidazole were quantified by  $^1H$  NMR analysis with the added DCM as the internal standard. Other reaction products were quantified by their respective C1 hydrogen signal in  $^1H$  NMR and structures confirmed by GC-MS on a Shimadzu QP-2010 GC-MS with a Supelcowax 10 column.

## 2.2. Initial FLP screening

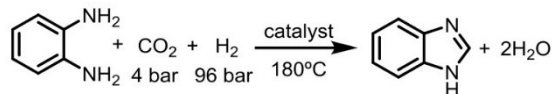


**Table S1:** Effect of R and X groups of  $R_3SnX$  and  $R_2SnX_2$  and Lewis base effect on the synthesis of benzimidazole

ENTRY	CATALYST	YIELD-RUN 1 (%)	YIELD-RUN 2 (%)	YIELD-RUN 3 (%)	TON (AVG.)	TOF ( $h^{-1}$ ) (AVG.)
1	$^iPr_3SnOTf$ : 2,4,6-COL	8	-	-	1.6	0.07
2	$^iPr_2Sn(OTf)_2$ : 2,4,6-COL	11	-	-	2.2	0.10
3	$Cy_3SnOTf$ : 2,4,6-COL	20	21	18	4.0	0.18
4	$Cy_3SnNTf_2$ : 2,4,6-COL	21	18	23	4.2	0.19
5 <sup>a</sup>	$Cy_3SnOTf$ : 2,4,6-COL	32	-	-	6.4	0.18 <sup>a</sup>
6 <sup>a</sup>	$Cy_3SnNTf_2$ : 2,4,6-COL	40	-	-	8.0	0.22 <sup>a</sup>
7	$Cy_3SnNTf_2$ : NMM	24	22	25	4.8	0.22
8	$Cy_3SnNTf_2$ : DBU	23	23	24	4.6	0.21
9	$Cy_3SnNTf_2$ : 2,6-LUT	16	15	17	3.2	0.15

Reaction conditions: o-phenylenediamine (1 mmol), sulfolane (5 mL), LA (5 mol%) and LB (10 mol%),  $CO_2$  (4 bar),  $H_2$  (96 bar), 22 hrs, 180 °C; conversion was determined by  $^1H$  NMR with an internal standard. a) 36 hrs instead of 22 hrs; DBU stands for 1,8-diazabicycloundec-7-ene and NMM for N-methylmorpholine. TOF values were calculated as the number of moles of product divided by the number of moles of Lewis acid divided by time.

FLPs with  $Cy_3SnX$  LAs outperformed FLPs with  $R_3SnX$  and  $R_2SnX_2$  ( $R = iPr$ ) LAs (Table S1, entries 1, 2 and 3).  $Cy_3SnOTf$ :2,4,6-collidine (FLP1) and  $Cy_3SnNTf_2$ :2,4,6-collidine (FLP2) showed similar activity in benzimidazole synthesis with 20 and 21% yields after 22 hrs, respectively (Table S1, entries 3 and 4). Lengthening the reaction to 36 hrs increased the benzimidazole yield to 32% with FLP1 and to 40% with FLP2, thus indicating that FLP2 is better catalyst than FLP1 (Table S1, entries 5 and 6). Notably, this is the reverse of N-formylation of secondary aliphatic amines and was presumably enabled by the more acidic  $Cy_3SnNTf_2$  (Gutmann-Beckett measurements), which better activates formate formed by  $CO_2$  reduction, for the reaction with the weakly nucleophilic o-phenylenediamine. Using  $Cy_3SnNTf_2$  and the alternative bases N-methylmorpholine (NMM) (FLP3), 1,8-diazabicycloundec-7-ene (DBU) (FLP4) or 2,6-lutidine (FLP5) improved the catalytic performance of the resulting FLPs in line with the base strength until NMM, i.e., 2,6-lutidine < 2,4,6-collidine < NMM ~ DBU (Table 1, entries 4 and 7 – 8). FLP3 provided the highest activity in an inert solvent, with a 24% benzimidazole yield in 22 hrs and a TOF of 0.22  $h^{-1}$ . All further experiments were performed with  $Cy_3SnNTf_2$  as the LA.

### 2.3 Typical result(s) of synthesis of benzimidazole with CO<sub>2</sub> and H<sub>2</sub>:

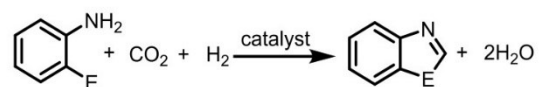
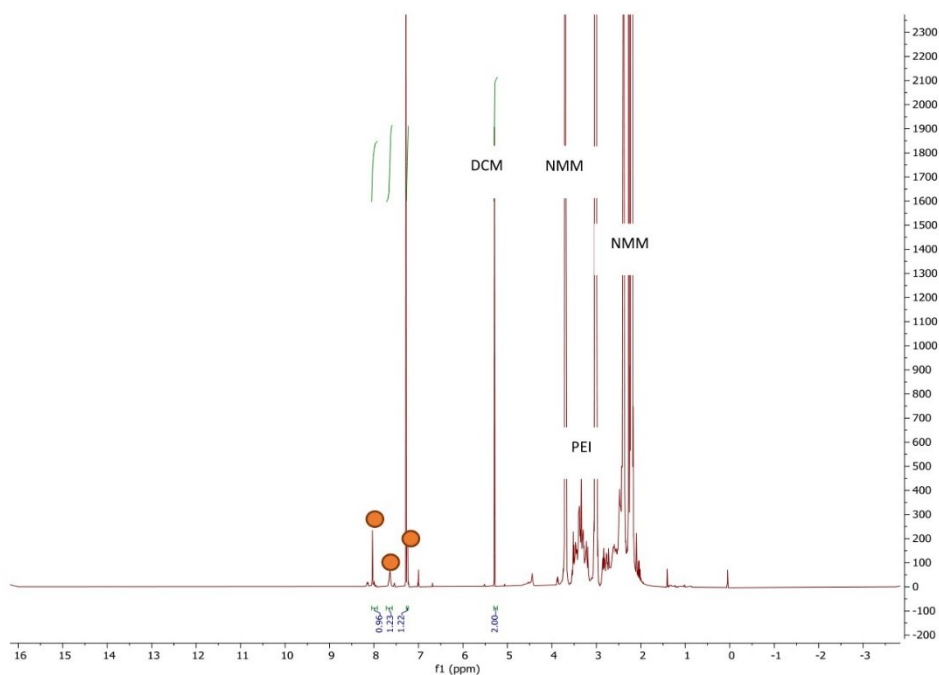
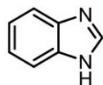


**Figure S1:** <sup>1</sup>H NMR of a reaction mixture at the end of a catalytic test of synthesis of benzimidazole, where product peaks are marked by coloured spots. All unmarked peaks can be assigned to the reaction catalyst and solvent i.e R<sub>3</sub>SnX, N-methylmorpholine, Polyethyleneimine (PEI) and the reaction solvent.



#### Benzimidazole:



<sup>1</sup>H NMR (400 MHz, CDCl<sub>3</sub>) δ: 8.05 (s, 1H), 7.67- 7.62 (m, 2H), 7.28- 7.23 (m, 2H); GC retention time 27.4 to 27.6 minutes; EI-MS (*m/z*) calculated: 118, found 118 with agreement of EI-MS molecular fragmentation with NIST EI-MS library.

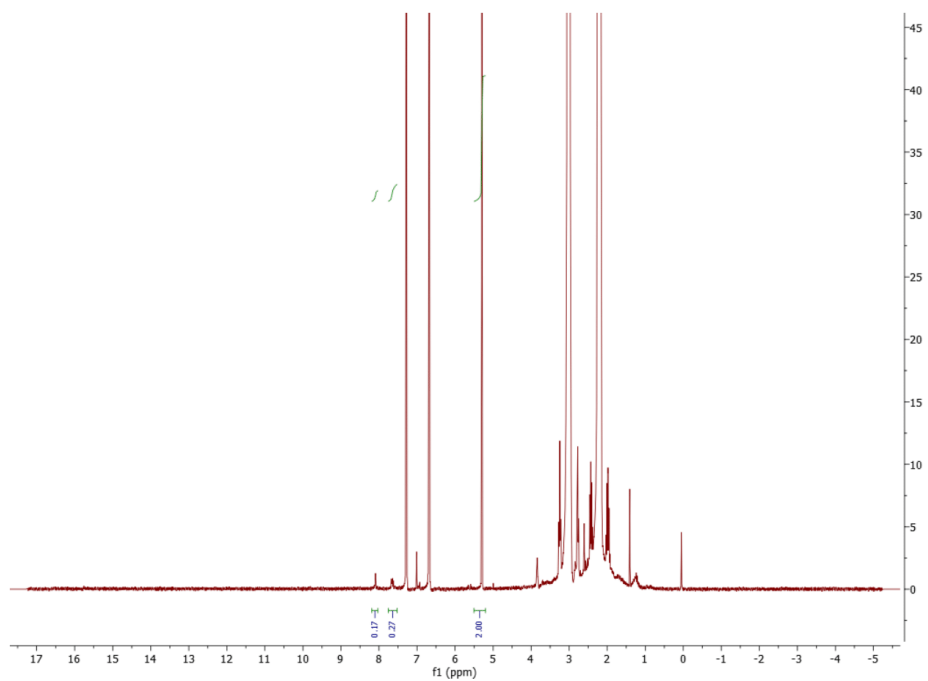


**Figure S3b:**  $^1\text{H}$  NMR analysis of a reaction mixture at the end of a second run of a catalytic test of synthesis of benzimidazole with  $\text{Cy}_3\text{SnNTf}_2\text{:NMM}$  as the reaction catalyst run under the conditions of table S4 row 3.

#### 2.4 Example of reproducibility between runs:

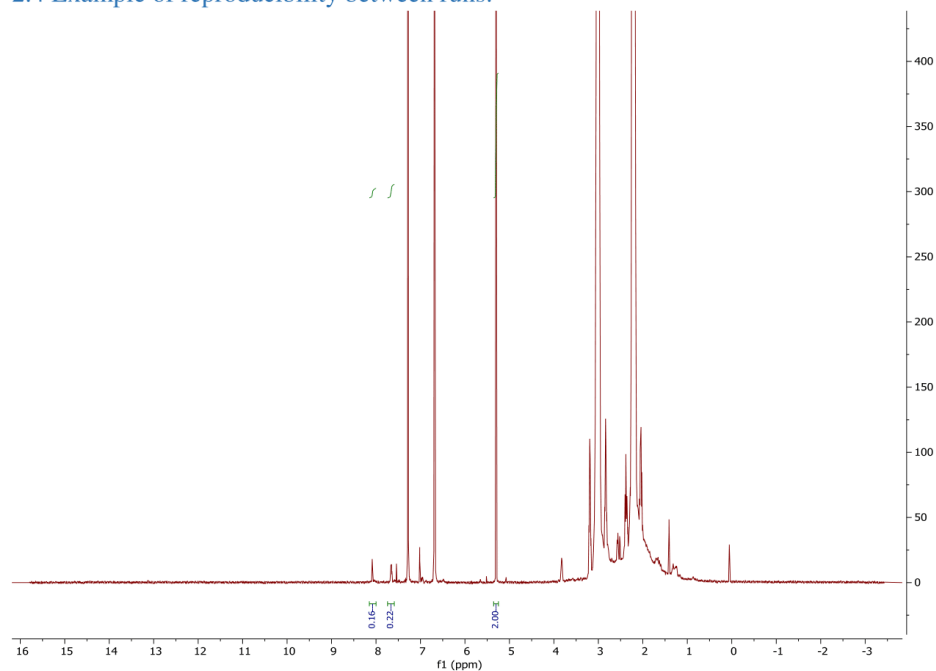


**Figure S3a:** <sup>1</sup>H NMR analysis of a reaction mixture at the end of a first run catalytic test of synthesis of benzimidazole with  $\text{Cy}_3\text{SnNTf}_2$ :NMM as the reaction catalyst run under the conditions of table S4 row 3.

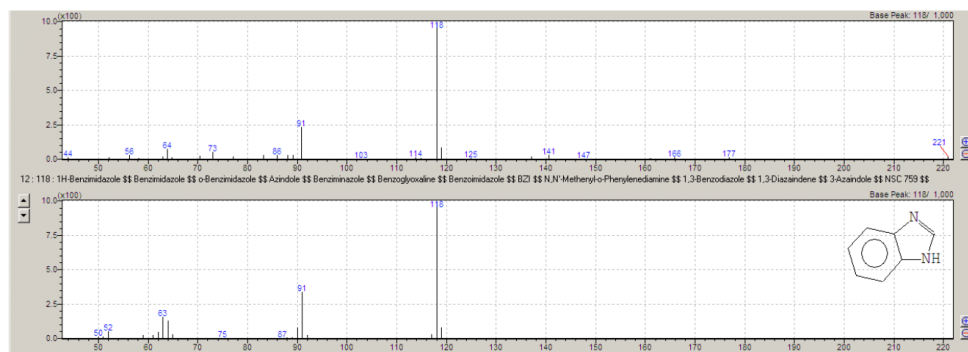


**Figure S2:** GC-MS analysis of a reaction mixture at the end of a catalytic test of synthesis of benzimidazole with  $\text{Cy}_3\text{SnNTf}_2\text{:NMM}$  as the reaction catalyst and comparison with EI-MS molecular fragmentation with NIST EI-MS library.

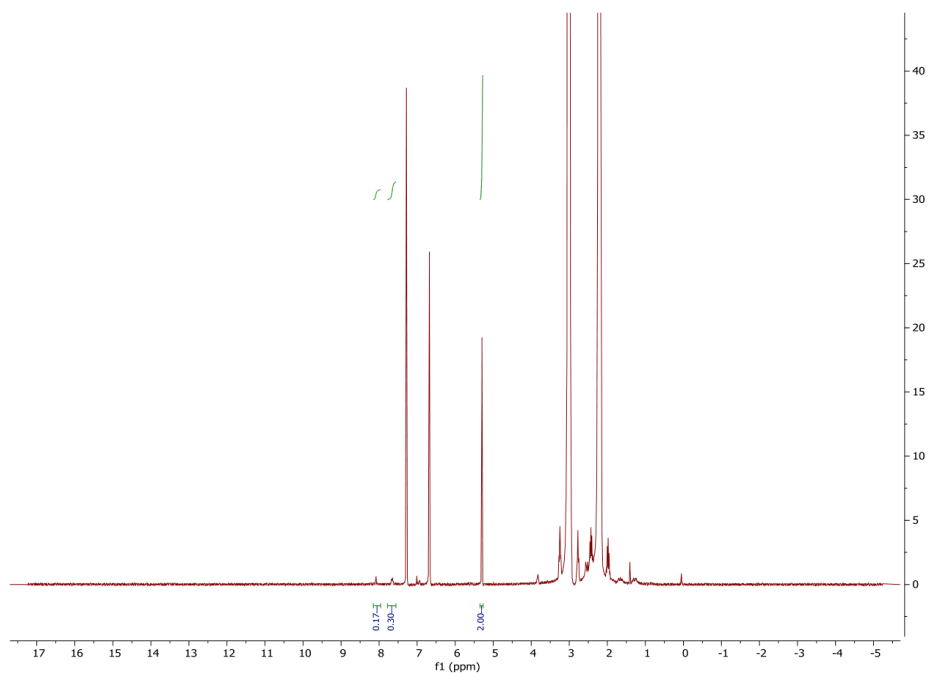


**Figure S3c:**  $^1\text{H}$  NMR analysis of a reaction mixture at the end of a third run of a catalytic test of synthesis of benzimidazole with  $\text{Cy}_3\text{SnNTf}_2$ :NMM as the reaction catalyst run under the conditions of table S4 row 3.

### 2.5 Optimization of $\text{CO}_2$ pressure:

**Table S2:** Effect of  $\text{CO}_2$  partial pressure on the synthesis of benzimidazole with **FLP3** (5 mol%) and 5 mL sulfolane.

Catalyst (LA)	$\text{H}_2$ Pressure (bar)	$\text{CO}_2$ Pressure (bar)	Temperature ( $^\circ\text{C}$ )	Time (hr)	Yield Run 1 (%)	Yield Run 2 (%)	Yield Run 3 (%)
$\text{Cy}_3\text{SnNTf}_2$	100	2	180	22	20	16	18
$\text{Cy}_3\text{SnNTf}_2$	100	5	180	22	24	22	26
$\text{Cy}_3\text{SnNTf}_2$	100	10	180	22	25	24	24
$\text{Cy}_3\text{SnNTf}_2$	100	20	180	22	25	23	21
$\text{Cy}_3\text{SnNTf}_2$	100	50	180	22	0	0	0

Increasing CO<sub>2</sub> pressure from 2 bar to 20 bar had no effect on the conversion and from 20 bars to 50 bars the yield plummeted possibly due to the substrate forming a carbamate salt/ carbamic acid which is known to slow down this reaction.<sup>1</sup> This is a marked difference from the previous study on N-formylation of amines, which found a sensitive dependence on CO<sub>2</sub> for the reaction with morpholine. The difference can be rationalised by the propensity of morpholine to form a carbamic acid vs o-phenylene diamine.

## 2.6 Optimization of H<sub>2</sub> pressure:

**Table S3** Effect of H<sub>2</sub> partial pressure on the synthesis of benzimidazole with **FLP3** (5 mol%) and 5 mL sulfolane.

Catalyst (LA)	H <sub>2</sub> Pressure (bar)	CO <sub>2</sub> Pressure (bar)	Temperature (°C)	Time (hr)	Yield Run 1 (%)	Yield Run 2 (%)	Yield Run 3 (%)
Cy <sub>3</sub> SnNTf <sub>2</sub>	20	4	180	22	6	7	6
Cy <sub>3</sub> SnNTf <sub>2</sub>	40	4	180	22	11	10	12
Cy <sub>3</sub> SnNTf <sub>2</sub>	60	4	180	22	17	13	15
Cy <sub>3</sub> SnNTf <sub>2</sub>	80	4	180	22	19	18	20
Cy <sub>3</sub> SnNTf <sub>2</sub>	100	4	180	22	24	22	26

In the absence of a nucleophilic amine, increasing the hydrogen pressure from 20 bars to 100 bars resulted in a steady increase in yield, albeit much slower than observed with N-formylation of aliphatic amines.<sup>1</sup> The increase can potentially be associated with formation of larger quantities of formate, which is then available for the presumed rate determining step of the reaction i.e. N-formylation of *ortho*-substituted aniline.

## 2.7 Optimization of temperature:

**Table S4:** Effect of temperature on the synthesis of benzimidazole with FLP3 (5 mol%) and 5 mL sulfolane.

Catalyst (LA)	H <sub>2</sub> Pressure (bar)	CO <sub>2</sub> Pressure (bar)	Temperature (°C)	Time (hr)	Yield Run 1 (%)	Yield Run 2 (%)	Yield Run 3 (%)
Cy <sub>3</sub> SnNTf <sub>2</sub>	100	4	150	22	6	6	7
Cy <sub>3</sub> SnNTf <sub>2</sub>	100	4	160	22	10	10	9
Cy <sub>3</sub> SnNTf <sub>2</sub>	100	4	170	22	17	16	17
Cy <sub>3</sub> SnNTf <sub>2</sub>	100	4	180	22	24	22	26
Cy <sub>3</sub> SnNTf <sub>2</sub>	100	4	190	22	13	12	14

Notably, the yield dropped off above 180 °C likely due to the decomposition of Cy<sub>3</sub>SnNTf<sub>2</sub>. For the N-formylation of amines, the less acidic Cy<sub>3</sub>SnOTf has been shown to be stable at reaction temperatures of up to 200 °C, therefore Cy<sub>3</sub>SnNTf<sub>2</sub> is less stable thermolytically. In addition, Cy<sub>3</sub>SnOCOH tends to decompose at similar temperatures<sup>2</sup>, so formate instability may also contribute to the large decrease in yield.



### 3. Synthesis of catalysts

#### 3.1 $^1\text{Pr}_3\text{SnOTf}$ synthesis:

This procedure was adapted from reference<sup>3</sup>

$^1\text{Pr}_4\text{Sn}$  (5.0 g, 17.2 mmol) and HOTf (3.3 g, 14.6 mmol) were added to  $\text{CHCl}_3$  (80 mL) and stirred at RT for 5 days. After which the solution was filtered and evaporated under reduced pressure. The resulting solid was washed with heptane (3 x 10 mL) affording  $^1\text{Pr}_3\text{SnOTf}$  as a white solid (4.8 g, 83%).

$^1\text{H}$  NMR (400 MHz,  $\text{CDCl}_3$ )  $\delta$ : 1.48 [6H, d,  $J_{(1\text{H}-1\text{H})} = 7.6$  Hz,  $J_{(117\text{Sn}-1\text{H})} = 86$  Hz,  $J_{(119\text{Sn}-1\text{H})} = 90$  Hz,  $\text{CH}_3$ ], 2.18 [1H, sept,  $J_{(1\text{H}-1\text{H})} = 7.6$  Hz,  $J_{(119\text{Sn}-1\text{H})} = 39$  Hz, CH].

#### 3.2 $^1\text{Pr}_2\text{Sn}(\text{OTf})_2$ synthesis:

$^1\text{Pr}_4\text{Sn}$  (2.0g, 6.9mmol) and HOTf (3.2 g, 14 mmol) were added to  $\text{CHCl}_3$  (80 mL) and stirred at RT for 5 days. After which the solid was separated, washed with hexane (3 x 10mL) and dried.  $^1\text{Pr}_2\text{Sn}(\text{OTf})_2$  was afforded as a white solid in 85% yield.

$^1\text{H}$  NMR (400 MHz,  $\text{D}_2\text{O}$ )  $\delta$ : 2.02 (h,  $J = 7.3$  Hz, 2H), 1.29 (d,  $J = 7.3$  Hz, 12H).;  $^{13}\text{C}\{^1\text{H}\}$  NMR (150 MHz,  $\text{D}_2\text{O}$ )  $\delta$ : 120 (q,  $\text{CF}_3$ ) 36 (s, CH), 20 (s,  $\text{CH}_3$ );  $^{119}\text{Sn}$  NMR (224 MHz,  $\text{D}_2\text{O}$ )  $\delta$ : -381 (s);

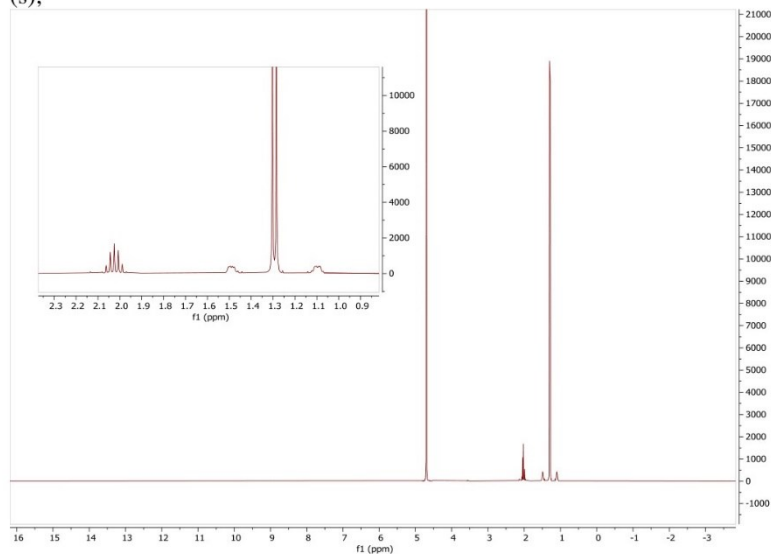


**Figure S4:**  $^1\text{H}$  NMR spectrum of  $^1\text{Pr}_2\text{Sn}(\text{OTf})_2$

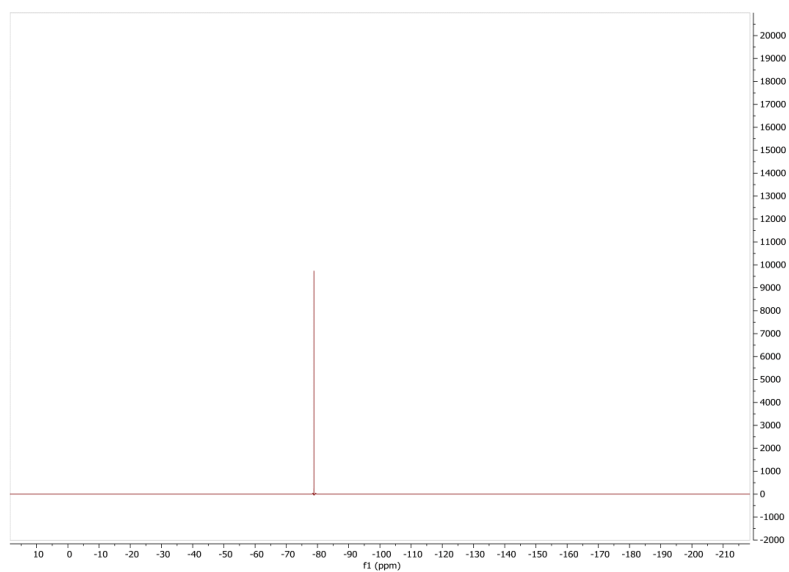


**Figure S5:**  $^{19}\text{F}$  NMR spectrum of  $i\text{Pr}_2\text{SnOTf}_2$

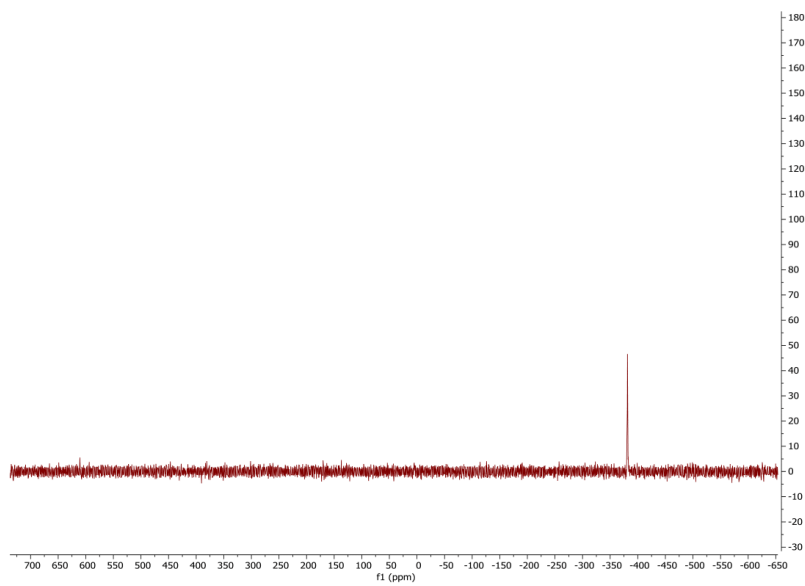


**Figure S6:**  $^{119}\text{Sn}$  NMR spectrum of  $i\text{Pr}_2\text{SnOTf}_2$

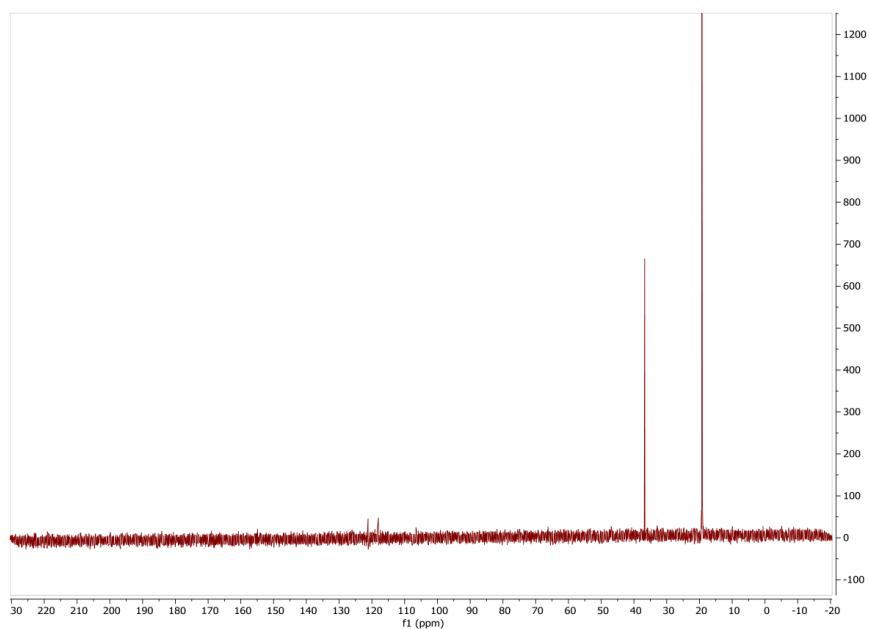


**Figure S7:**  $^{13}\text{C}\{^1\text{H}\}$  NMR spectrum of  $^1\text{Pr}_2\text{SnOTf}_2$

### 3.3 $\text{Cy}_3\text{SnX}$ synthesis:

To a solution of  $\text{Cy}_3\text{SnCl}$  (500 mg, 1.24 mmol) in  $\text{CH}_2\text{Cl}_2$  (50 mL) was added  $\text{AgX}$  (1.24 mmol,  $\text{X} = \text{OTf}, \text{NTf}_2, \text{ClO}_4$ ). The reaction was stirred at RT for 3 days. The solution was then filtered and evaporated under reduced pressure affording a white solid.

#### $\text{Cy}_3\text{SnOTf}$ :

$^1\text{H}$  NMR (400 MHz,  $\text{CDCl}_3$ )  $\delta$ : 2.29 – 1.21 ppm (m, 33H);  $^{13}\text{C}$ ,  $^{19}\text{F}$  and  $^{119}\text{Sn}$  were measured at 600 MHz Bruker NMR instrument.  $^{13}\text{C}\{^1\text{H}\}$  NMR (150 MHz,  $\text{CDCl}_3$ )  $\delta$ : 120 ppm (q), 38.72 ppm (s), 30.64 ppm (s), 28.76 ppm (s), 26.57 ppm (s);  $^{119}\text{Sn}$  NMR (224 MHz,  $\text{CDCl}_3$ )  $\delta$ : 73.9 ppm;  $^{19}\text{F}$  NMR (376 MHz,  $\text{CDCl}_3$ )  $\delta$ : -77.20 ppm (s); HRMS+ for  $\text{C}_{19}\text{H}_{33}\text{F}_3\text{O}_3\text{SSn}$  m/z: 517.2972 (calculated: 517.2352); HRMS- for  $\text{CF}_3\text{O}_3\text{S}^-$  m/z: 148.9580 (calculated: 148.9520)

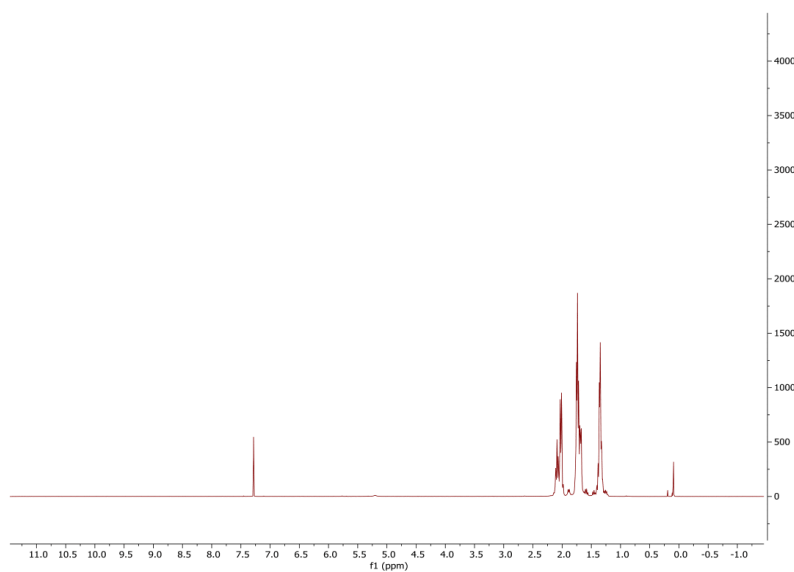


**Figure S8:**  $^1\text{H}$  NMR spectrum of  $\text{Cy}_3\text{SnOTf}$

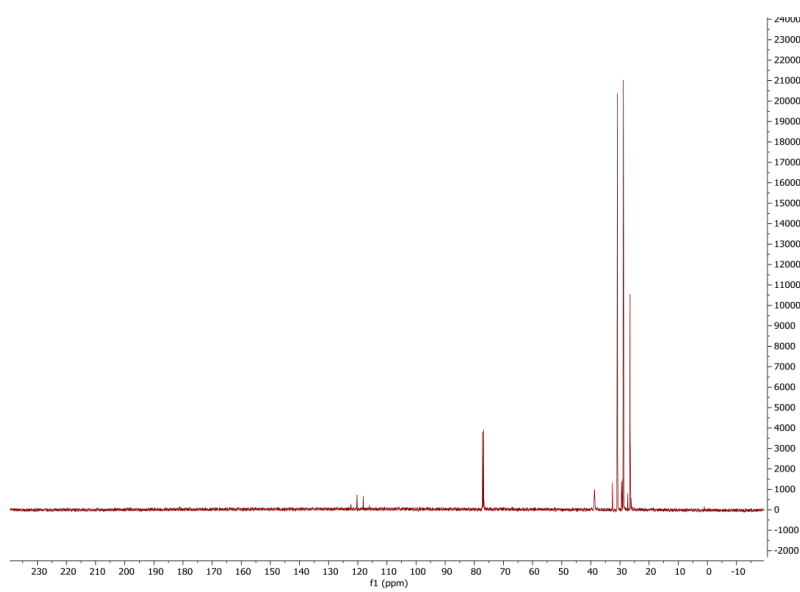


**Figure S9:**  $^{13}\text{C}\{^1\text{H}\}$  NMR spectrum of  $\text{Cy}_3\text{SnOTf}$

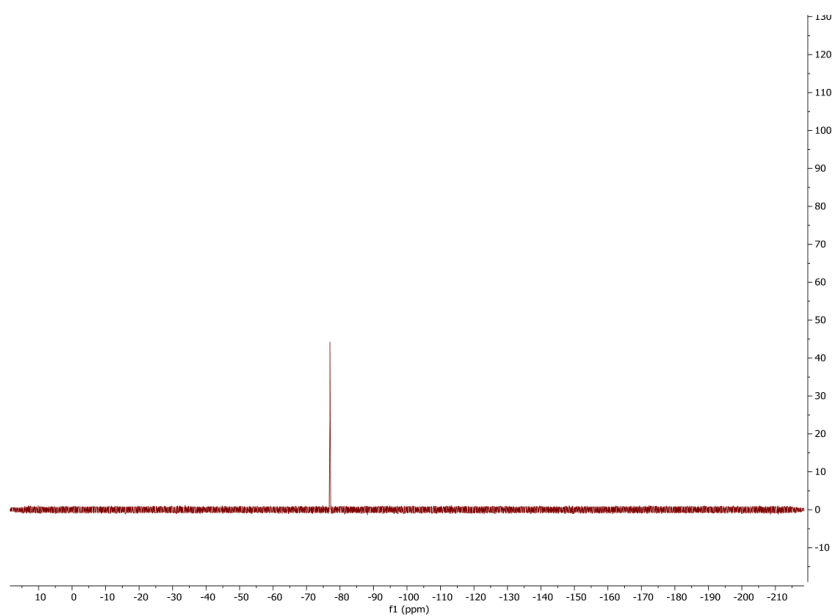


**Figure S10:**  $^{19}\text{F}$  NMR spectrum of  $\text{Cy}_3\text{SnOTf}$

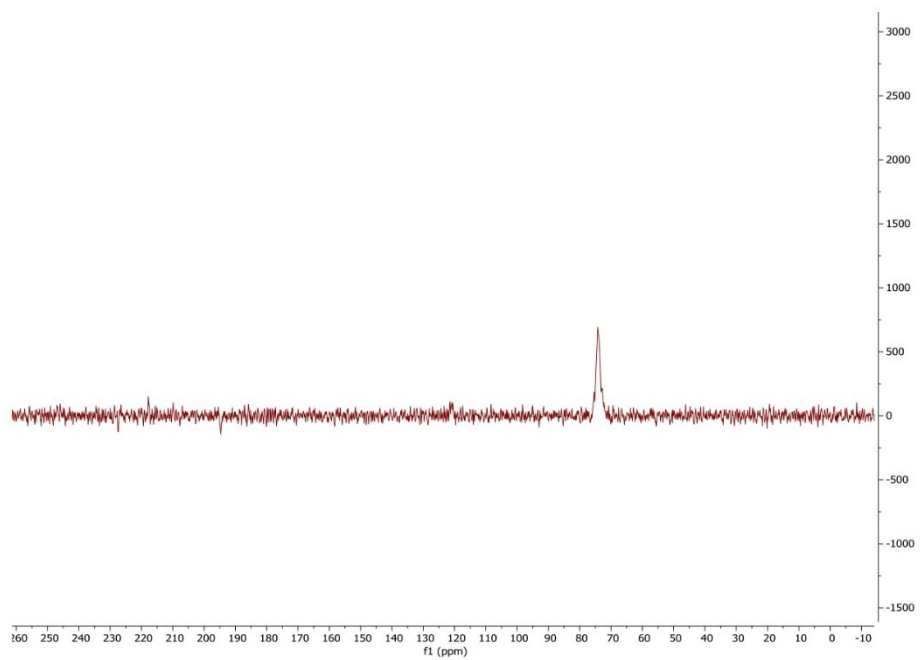


**Figure S11:**  $^{119}\text{Sn}$  spectrum of  $\text{Cy}_3\text{SnOTf}$

**Cy<sub>3</sub>SnNTf<sub>2</sub>:**

<sup>1</sup>H NMR (400 MHz, CDCl<sub>3</sub>) δ: 2.15 – 1.21ppm (m, 33H); <sup>13</sup>C, <sup>19</sup>F and <sup>119</sup>Sn were measured at 600 MHz Bruker NMR instrument. <sup>13</sup>C{<sup>1</sup>H} NMR (150 MHz, CDCl<sub>3</sub>) δ: 118.95 ppm (q) (two peaks of the quartet are obscured by the baseline), 38.78ppm (s), 31.0ppm (s), 28.90ppm (s), 26.50ppm (s); <sup>19</sup>F NMR (376 MHz, CDCl<sub>3</sub>) δ: -78.2ppm (s); HRMS+ for C<sub>18</sub>H<sub>33</sub>Sn<sup>+</sup> m/z: 369.1661 (calculated: 369.1614); HRMS- for C<sub>2</sub>F<sub>6</sub>NO<sub>4</sub>S<sub>2</sub><sup>-</sup> m/z: 279.9304 (calculated: 279.9173)

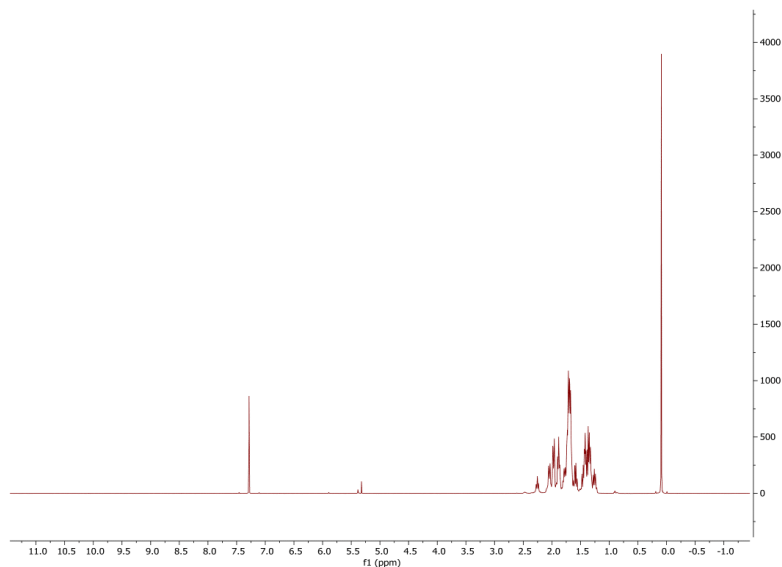


**Figure S12:** <sup>1</sup>H NMR spectrum of Cy<sub>3</sub>SnNTf<sub>2</sub>

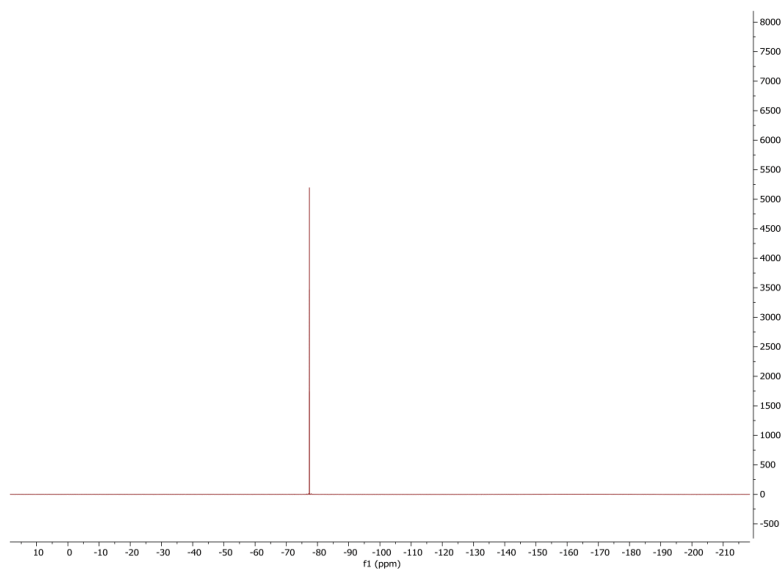


**Figure S13:**  $^{19}\text{F}$  NMR spectrum of  $\text{Cy}_3\text{SnNTf}_2$

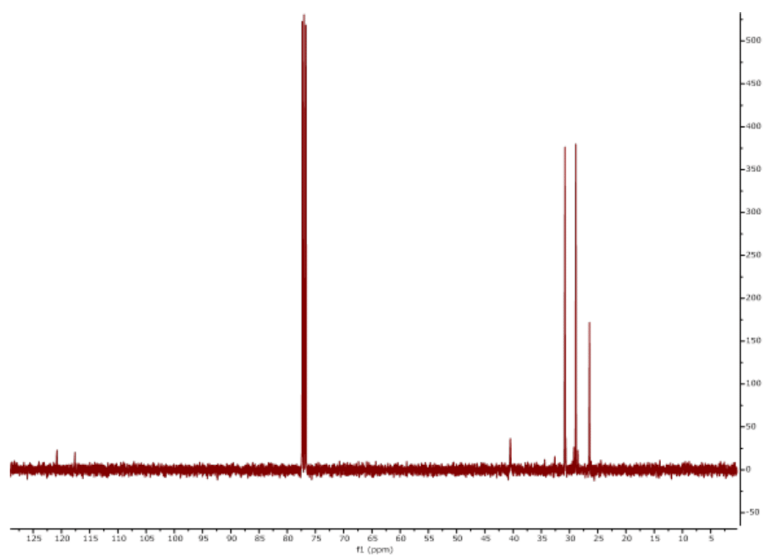


**Figure S14:**  $^{13}\text{C}\{^1\text{H}\}$  NMR spectrum of  $\text{Cy}_3\text{SnNTf}_2$



## 5. Gutman-Beckett acidity measurements

### 5.1 General procedure for Gutman-Beckett acidity measurements

0.02 mL of a stock solution of Triethylphosphine oxide (30 mg, 0.22 mmol,) in 2 mL of dry CDCl<sub>3</sub> was added to a solution of Lewis acid (0.1 mmol) in 0.5mL of CDCl<sub>3</sub>. <sup>31</sup>P {<sup>1</sup>H} NMRs were then measured, after which more Lewis acid was added, the sample was then remeasured, and this process was repeated until the peak positions remained constant.

The acceptor numbers were calculated using the formula from reference<sup>4</sup>

$$\text{Acceptor number} = [\delta^{31}\text{P} \{^1\text{H}\}/\text{ppm} (\text{sample}) - 41.0] \times 2.22$$

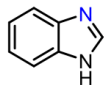
### 5.2 Results of Gutman-Beckett acidity measurements

**Table S4:** Summary of the acceptor numbers for Cy<sub>3</sub>SnX Lewis acids.

Catalyst (LA)	$\delta^{31}\text{P} \{^1\text{H}\}/\text{ppm}$	Acceptor number
Cy <sub>3</sub> SnOTf	68.1	60.2
Cy <sub>3</sub> SnNTf <sub>2</sub>	76.9	79.7

## 6. Substrate scope

### 6.1 Benzimidazole



<sup>1</sup>H NMR (400 MHz, CDCl<sub>3</sub>)  $\delta$ : 8.04 (s, 1H), 7.68-7.60 (m, 2H), 7.27-7.23 (m, 2H); GC retention time to 29.0-29.5 minutes; EI-MS (*m/z*) calculated: 118, found 118.

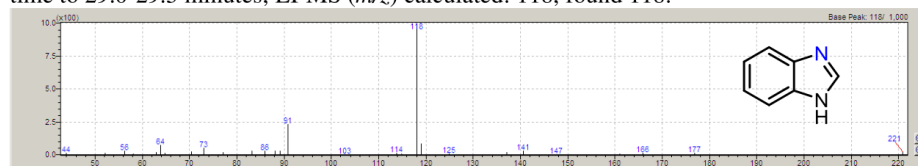
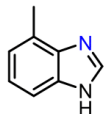


**Figure S15:** EI-MS analysis of the reaction product of o-phenylenediamine reaction with CO<sub>2</sub> and H<sub>2</sub>.

## 6.2 4-methylbenzimidazole



$^1\text{H}$  NMR (400 MHz,  $\text{DMSO-}d_6$ )  $\delta$ : 8.15 (s, 1H), 7.38 (d, 2H), 7.07 (m, 1H), 6.99 (d, 1H); all other peaks are obscured by reaction solvent. GC retention time 28.5-28.8 minutes; EI-MS ( $m/z$ ) calculated: 132, found: 132

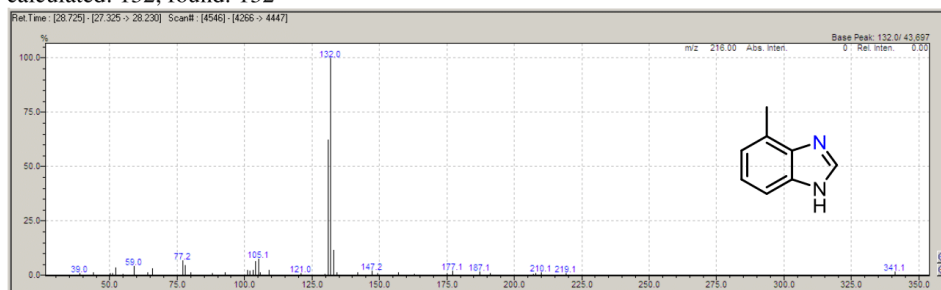


**Figure S16:** EI-MS analysis of the reaction product of 3-methylbenzene-1,2-diamine reaction with  $\text{CO}_2$  and  $\text{H}_2$ .

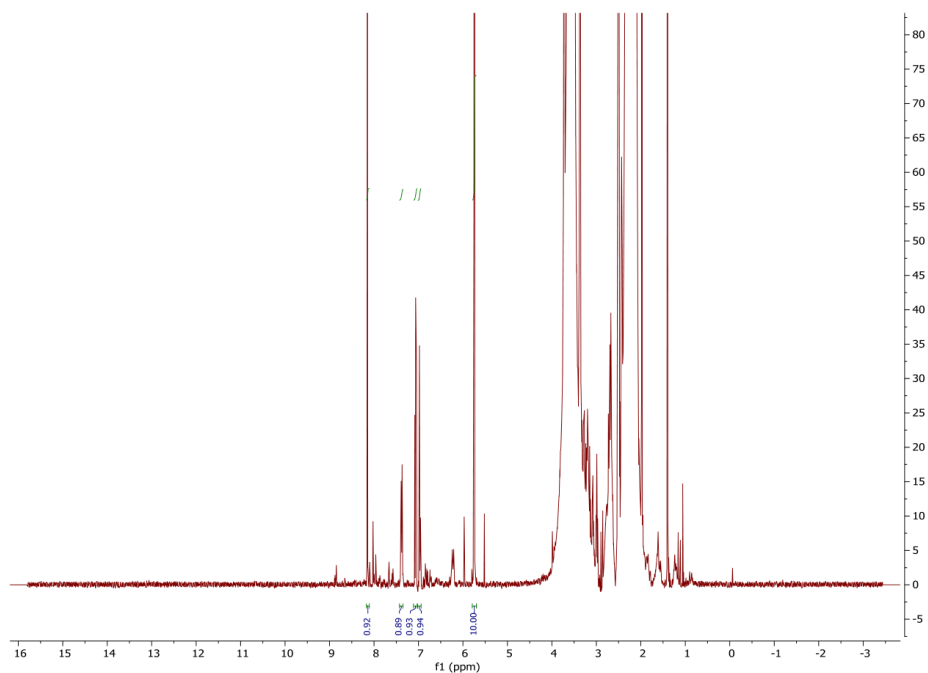
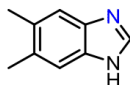


**Figure S16b:**  $^1\text{H}$  NMR analysis of the reaction product of 3-methylbenzene-1,2-diamine reaction with  $\text{CO}_2$  and  $\text{H}_2$ . NB 50 mmol of DCM was used as the internal standard.

### 6.3 5,6-dimethylbenzimidazole



$^1\text{H}$  NMR (400 MHz,  $\text{CDCl}_3$ )  $\delta$ : 7.90 (s, 1H), 7.51- 7.30 (br s, 2H), 3.43 (br s, 1H), 2.38 (s, 6H);  
 $\{^1\text{H}\}$  NMR (400 MHz,  $\text{CDCl}_3$ )  $\delta$ : 139.8, 136.1, 132.1, 115.4, 20.7; ESI ( $m/z$ ) calculated: 147.1,  
 found 147.1

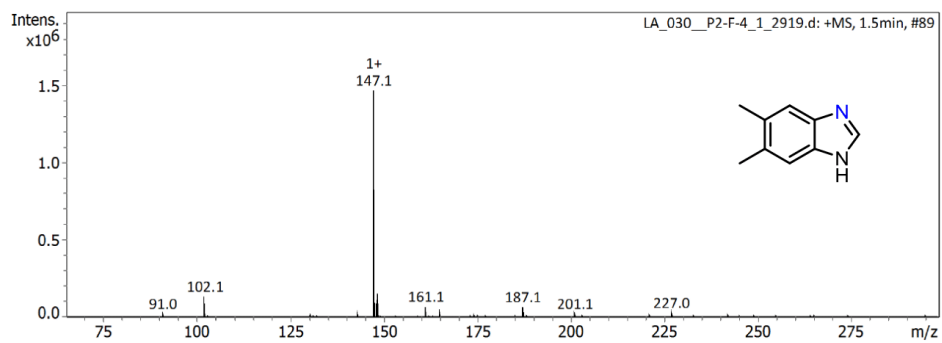


**Figure S17:** ESI-MS analysis of the reaction product of 4,5-dimethylbenzene-1,2-diamine with CO<sub>2</sub> and H<sub>2</sub>.

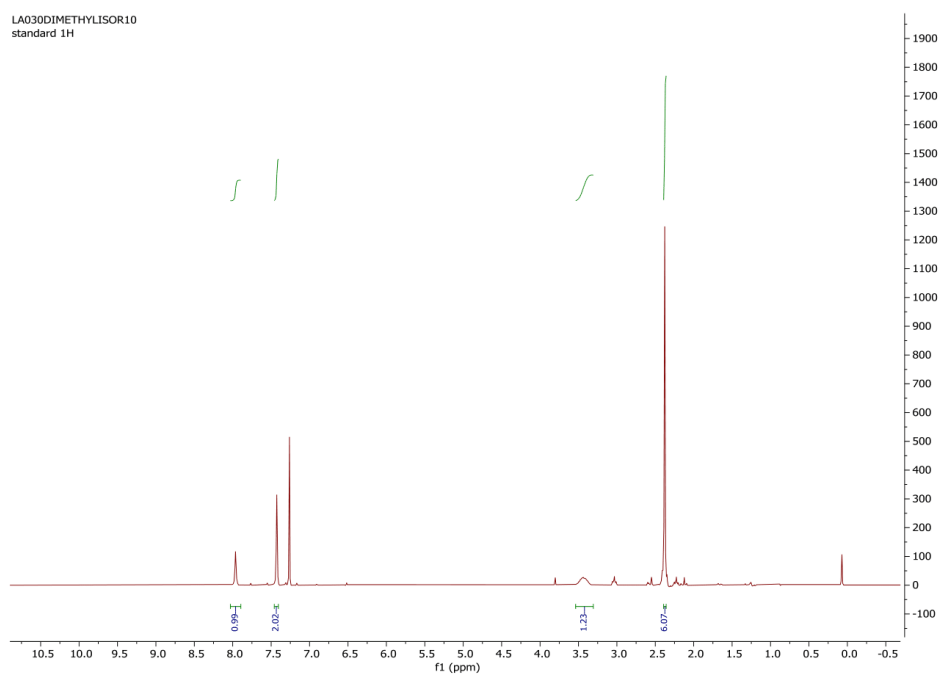


**Figure S18b:** <sup>1</sup>H NMR analysis of the isolated reaction product of 4,5-dimethylbenzene-1,2-diamine with CO<sub>2</sub> and H<sub>2</sub>.

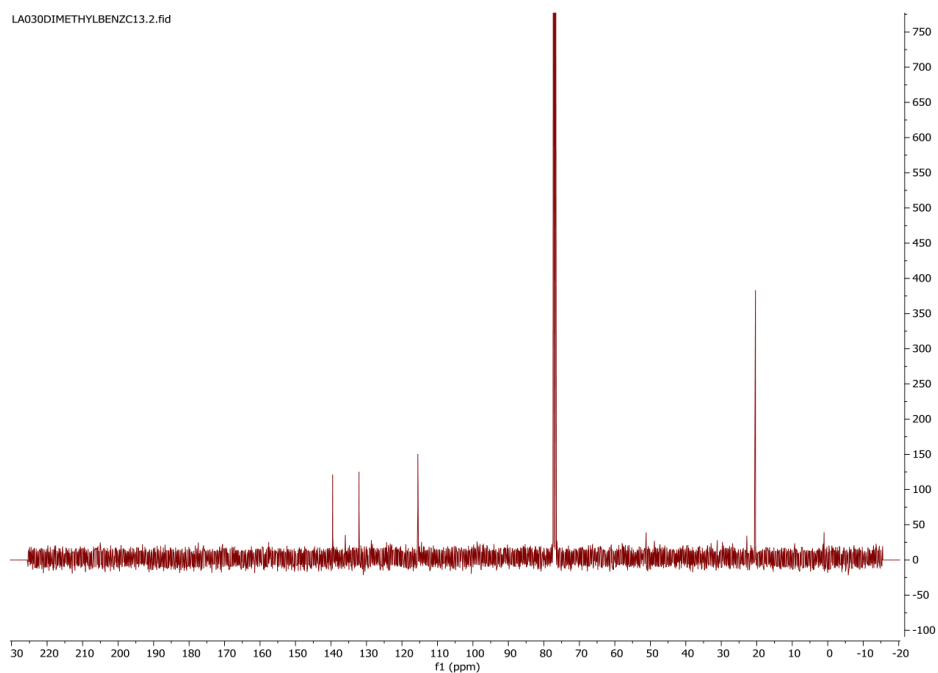
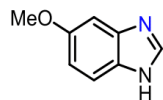


**Figure S18c:**  $^{13}\text{C}\{^1\text{H}\}$  NMR analysis of the isolated reaction product of 4,5-dimethylbenzene-1,2-diamine with  $\text{CO}_2$  and  $\text{H}_2$ .

### 6.3.1 Isolation of 5,6-dimethylbenzimidazole

In air  $\text{Cy}_3\text{SnNTf}_2$  (0.01 mmol) and 4,5-Dimethyl-1,2-phenylenediamine (1 mmol) were dissolved in the solvent mixture (4 mL *N*-methylmorpholine and 1 mL PEI) in a stainless-steel autoclave. The autoclave was then sealed and purged 5 times with the desired pressure of  $\text{CO}_2$ . The reaction was then topped up with the desired  $\text{H}_2$  reaction pressure. The reactor was then heated to 180 °C for 22hrs. The reactor was allowed to cool and was depressurised. After which the reaction liquor was decanted and filtered. The reactor was then washed with DCM (3 x 10 mL), the washings were collected, filtered and then added to the reaction liquor which was then evaporated under reduced pressure affording a brown solid (112 mg, 76 % yield).

#### 6.4 4-methoxybenzimidazole



$^1\text{H}$  NMR (400 MHz,  $\text{CDCl}_3$ )  $\delta$ : 7.91 (s, 1H), 7.57- 7.42 ppm (br s, 1H), 7.13- 7.01 ppm (br s, 1H), 6.89 ppm (dd, 1H), 3.83 ppm (s, 3H); EI-MS ( $m/z$ ) calculated: 148.1, found 147.9. All other peaks are obscured by the reaction solvent.

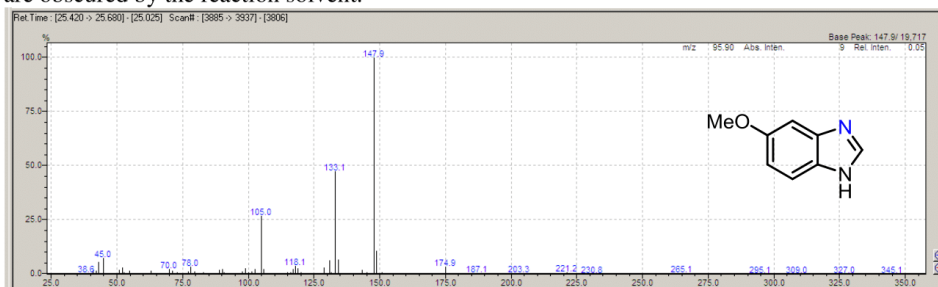


**Figure S19:** EI-MS analysis of the reaction product of synthesis of 4-methoxybenzimidazole with  $\text{CO}_2$  and  $\text{H}_2$ .

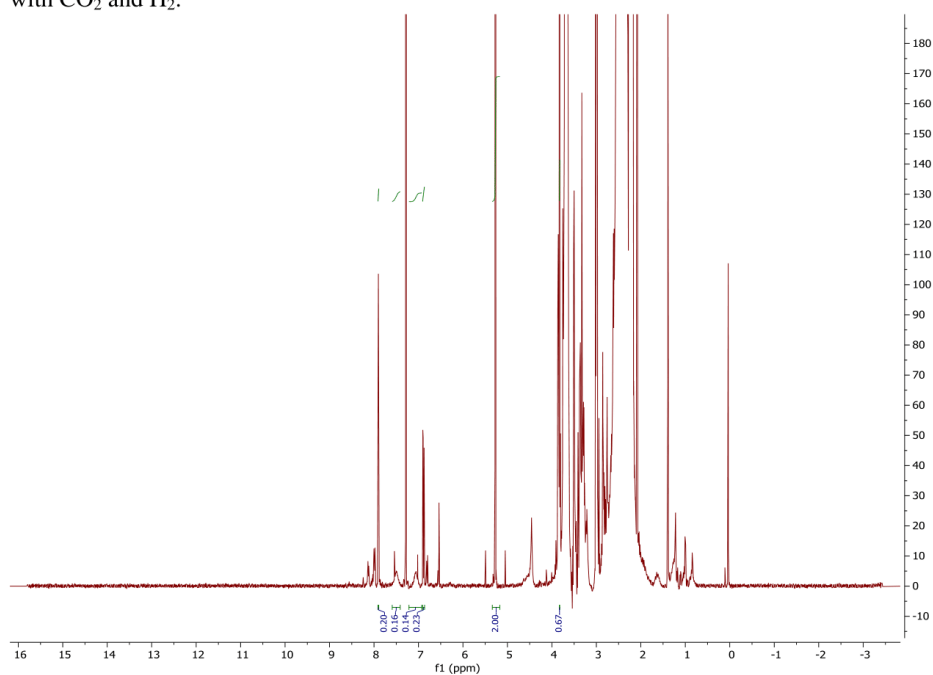
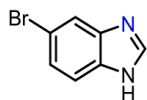


**Figure S19b:**  $^1\text{H}$  NMR analysis of the reaction product of synthesis of 4-methoxybenzimidazole with  $\text{CO}_2$  and  $\text{H}_2$ . NB the amount of substrate used in this reaction was 3 mmol and DCM internal standard 10 mmol. The yield was calculated from all aromatic signals and averaged.

#### 6.5 4-bromobenzimidazole



$^1\text{H}$  NMR (400 MHz,  $\text{DMSO-d}_6$ ) mixture of rotamers  $\delta$ : 8.25 (s, 1H) 7.79 (s, 1H) 7.56 (d, (peak partially obscured)), 7.32 (dd, 2H), EI-MS ( $m/z$ ) calculated: 198.0 found 197.8. The peaks are partially obscured by the side product benzimidazole.

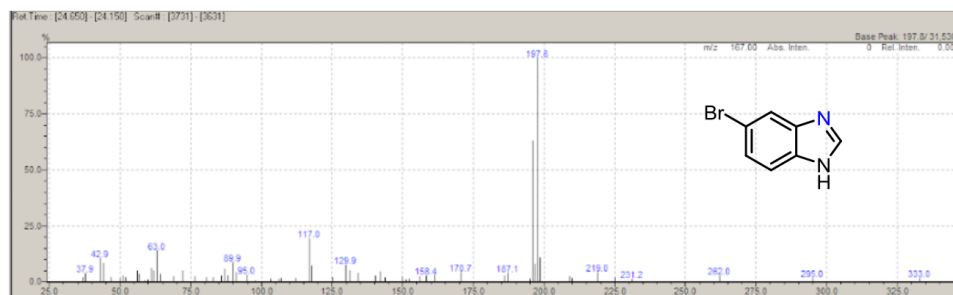


**Figure S20:** EI-MS analysis of the reaction product of synthesis of 4-bromobenzimidazole with CO<sub>2</sub> and H<sub>2</sub>.

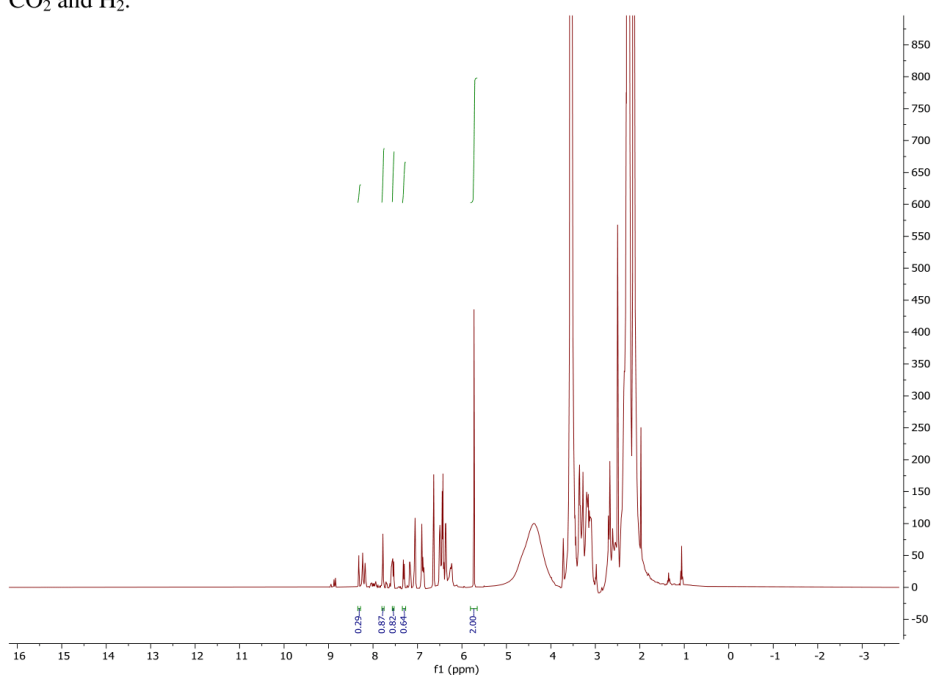
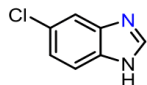


**Figure S20b:** <sup>1</sup>H NMR analysis of the reaction product of synthesis of 4-bromobenzimidazole with CO<sub>2</sub> and H<sub>2</sub>.

#### 6.6 4-chlorobenzimidazole



<sup>1</sup>H NMR (400 MHz, CDCl<sub>3</sub>) δ: 8.06 (1H), 7.62 (s, 1H), 7.55(s, 1H); 7.20 (d, 1H); EI-MS (*m/z*) calculated: 152.6, found: 151.9



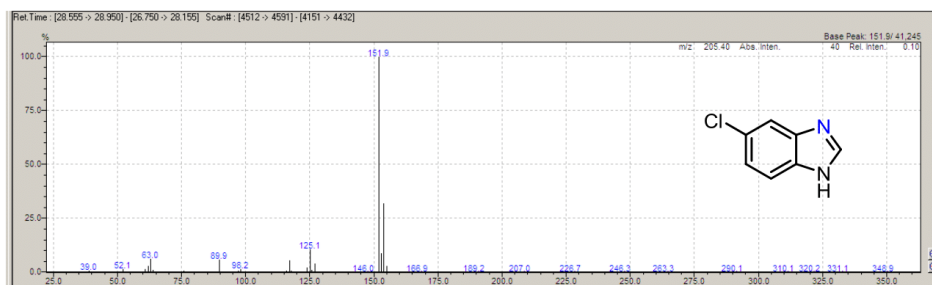


**Figure S21:** EI-MS analysis of the reaction product of synthesis of 4-chlorobenzimidazole with CO<sub>2</sub> and H<sub>2</sub>.

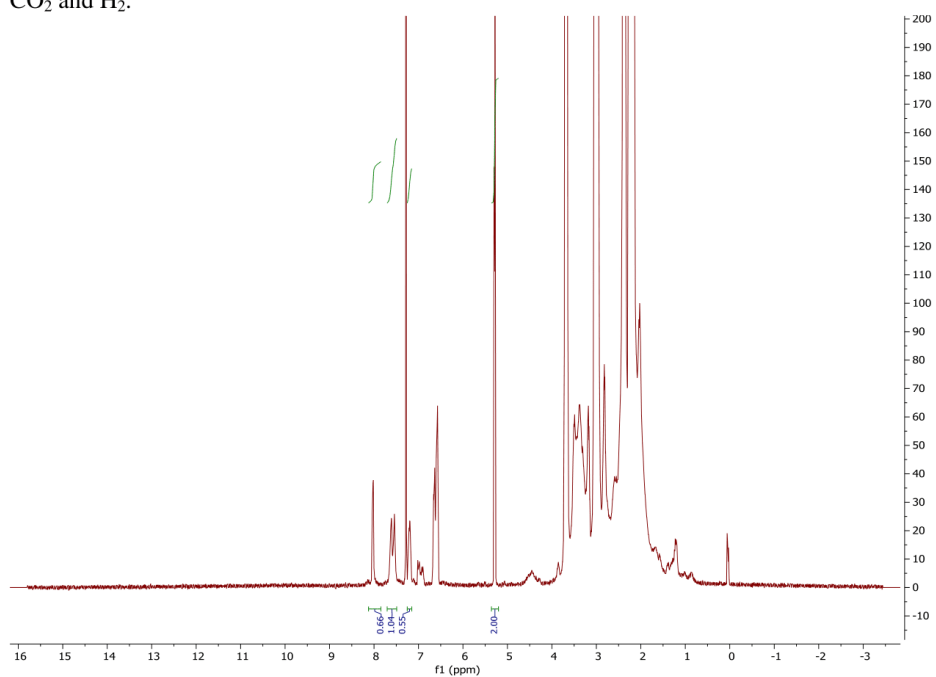
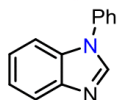


**Figure S21b:** <sup>1</sup>H NMR analysis of the reaction product of synthesis of 4-chlorobenzimidazole with CO<sub>2</sub> and H<sub>2</sub>.

### 6.7 N-phenylbenzimidazole



$^1\text{H}$  NMR (400 MHz,  $\text{CDCl}_3$ )  $\delta$ : 8.10 (s, 1H), 7.99- 7.93 (m, 1H), 7.56 – 7.40(m, 6H), 7.35- 7.28 (m, 2H); GC retention time 27.7 minutes to 28.1 minutes; EI-MS ( $m/z$ ) calculated: 194.1, found 193.9 all other peaks were obscured due to NMR solvent

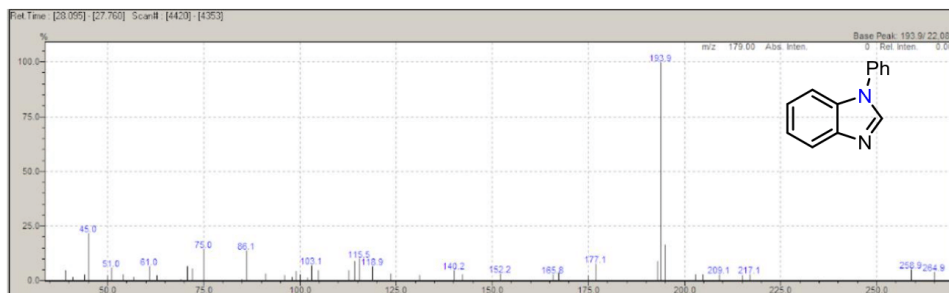


**Figure S22:** EI-MS analysis of the reaction product of synthesis of N-phenylbenzimidazole with  $\text{CO}_2$  and  $\text{H}_2$ .

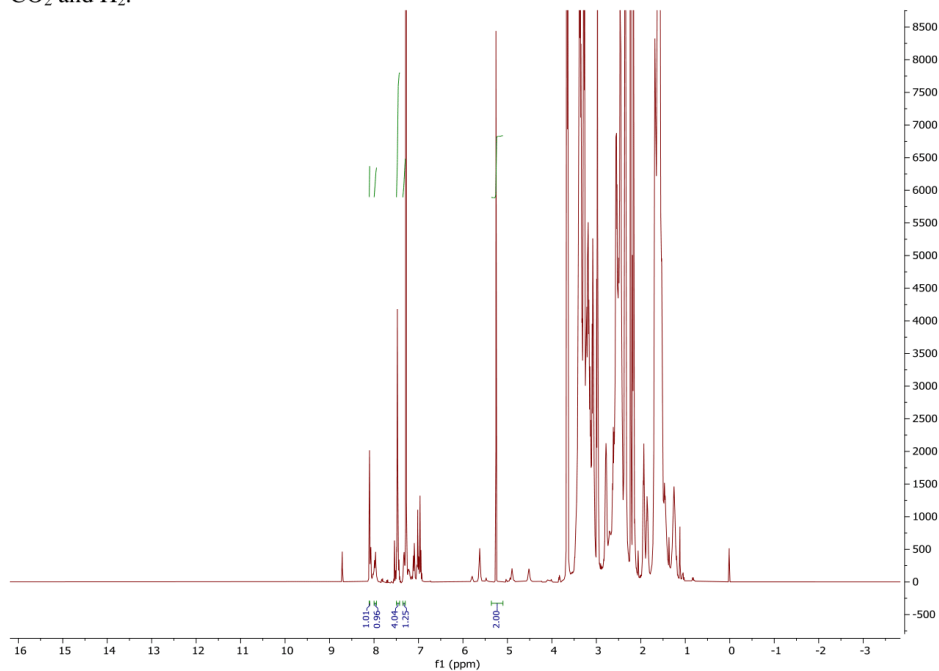
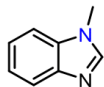


**Figure S22b:**  $^1\text{H}$  NMR analysis of the reaction product of synthesis of N-phenylbenzimidazole with  $\text{CO}_2$  and  $\text{H}_2$ .

## 6.8 N-methylbenzimidazole



$^1\text{H NMR}$  (400 MHz,  $\text{CDCl}_3$ )  $\delta$ : 7.85 (s, 1H), 7.79- 7.75 (m, 1H), 7.42-7.35 (m, 1H), 7.33- 7.22 (m, 2H) 3.81(s, 3H); GC retention time 17.6 to 17.7 minutes; EI-MS ( $m/z$ ) calculated: 132.1, found 132.0

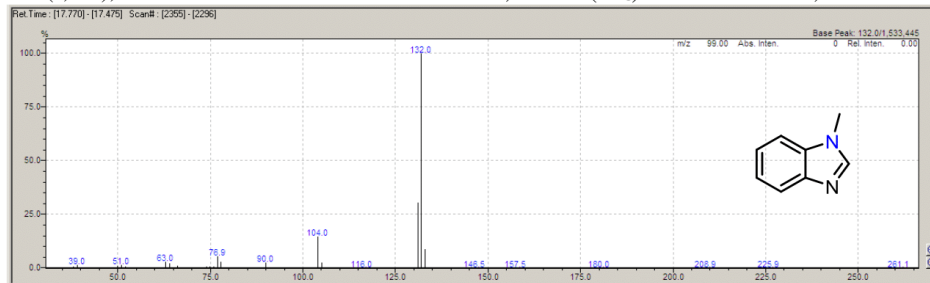


**Figure S23:** EI-MS analysis of the reaction product of synthesis of N-methylbenzimidazole with  $\text{CO}_2$  and  $\text{H}_2$ .

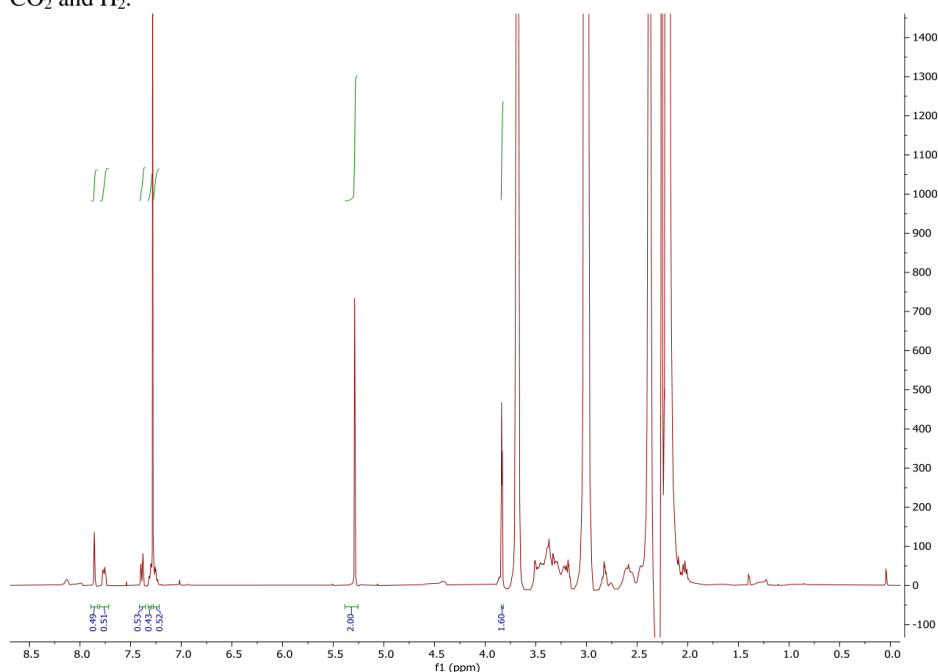
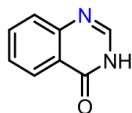


**Figure S23b:**  $^1\text{H NMR}$  analysis of the reaction product of synthesis of N-methylbenzimidazole with  $\text{CO}_2$  and  $\text{H}_2$ . NB 20 mmol of DCM was used. The reaction yield was calculated from all aromatic peaks and averaged.

## 6.9 4-Hydroxyquinazoline



$^1\text{H NMR}$  (400 MHz,  $\text{CDCl}_3$ )  $\delta$ : 8.29 (d, 1H), 8.01 (s, 1H), 7.80-7.70 (m, 2H), 7.54-7.47 (m, 1H);  
EI-MS ( $m/z$ ) calculated: 146.0, found 146.0. All other peaks were obscured by solvent.

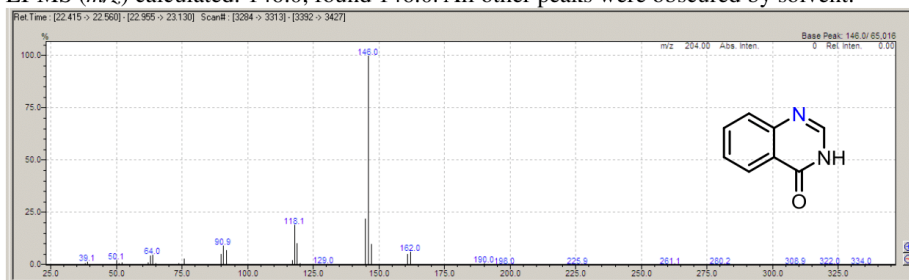


**Figure S24:** EI-MS analysis of the reaction product of synthesis of 4-Hydroxyquinazoline with  $\text{CO}_2$  and  $\text{H}_2$ .

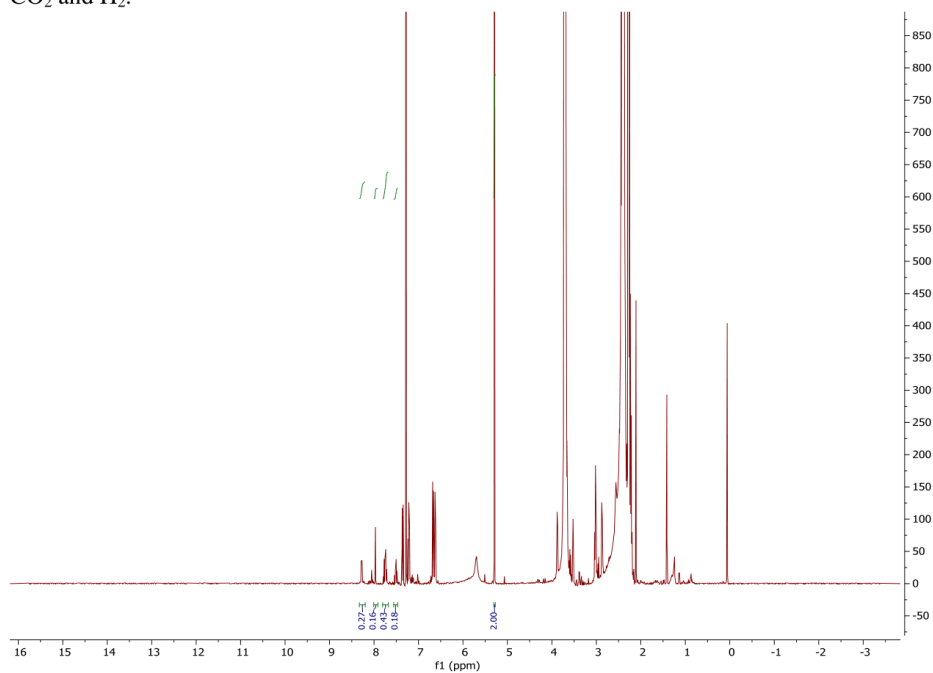
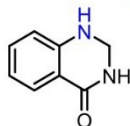


**Figure S24b:**  $^1\text{H}$  NMR analysis of the reaction product of synthesis of 4-Hydroxyquinazoline with  $\text{CO}_2$  and  $\text{H}_2$ .

6.10 2,3-dihydroquinazolin-4(1H)-one



$^1\text{H}$  NMR (400 MHz,  $\text{CDCl}_3$ )  $\delta$ : 8.08-7.83 (m, 1H), 7.35-7.28 (m, 1H), 6.88 (t, 1H), 6.43 (d, 1H);  
EI-MS ( $m/z$ ) calculated: 148.1, found 148.0.



**Figure S25:** EI-MS analysis of the reaction product of synthesis of 2,3-dihydroquinazolin-4(1H)-one with  $\text{CO}_2$  and  $\text{H}_2$ .

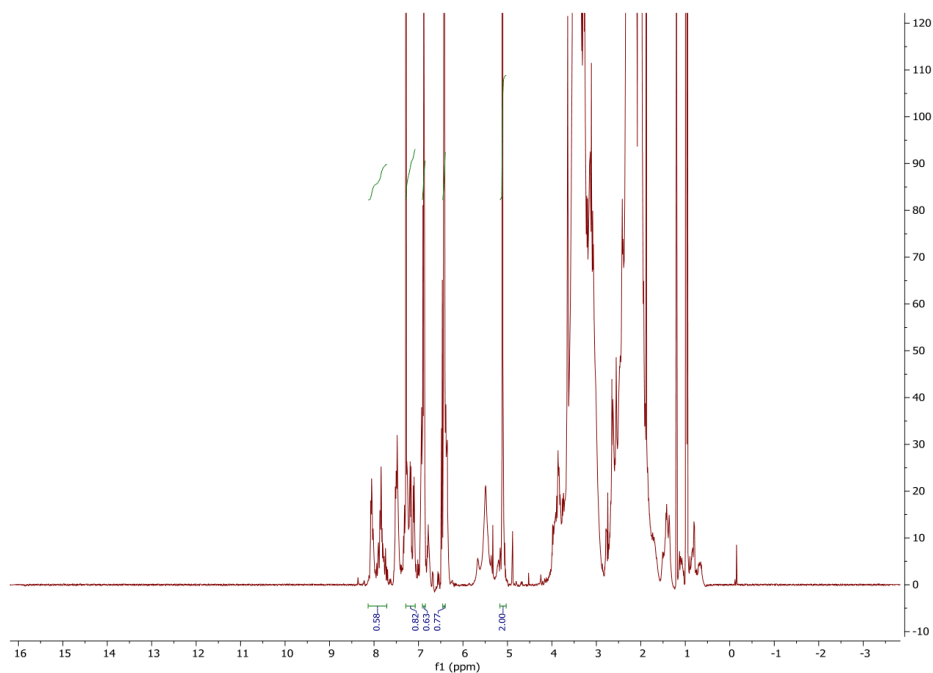
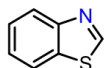


**Figure S25b:**  $^1\text{H}$  NMR analysis of the reaction product of synthesis of 2,3-dihydroquinazolin-4(1H)-one with  $\text{CO}_2$  and  $\text{H}_2$ .

### 6.11 Benzothiazole



$^1\text{H}$  NMR (400 MHz,  $\text{CDCl}_3$ )  $\delta$ : 7.95 (d, 1H), 7.83 (d, 1H), 7.45- 7.41 (m, 1H), 7.36- 7.31(m, 1H)  
 EI-MS ( $m/z$ ) calculated: 135.0 found 134.9. The C1 hydrogen peak for benzothiazole is mostly deprotonated by DBU.

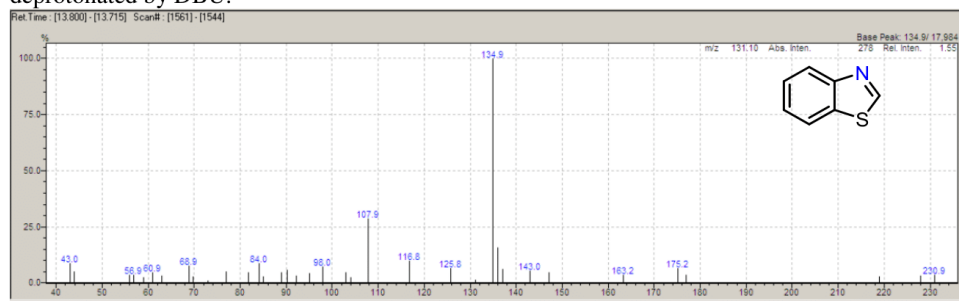


**Figure S26:** EI-MS analysis of the reaction product of synthesis of Benzothiazole with CO<sub>2</sub> and H<sub>2</sub>.

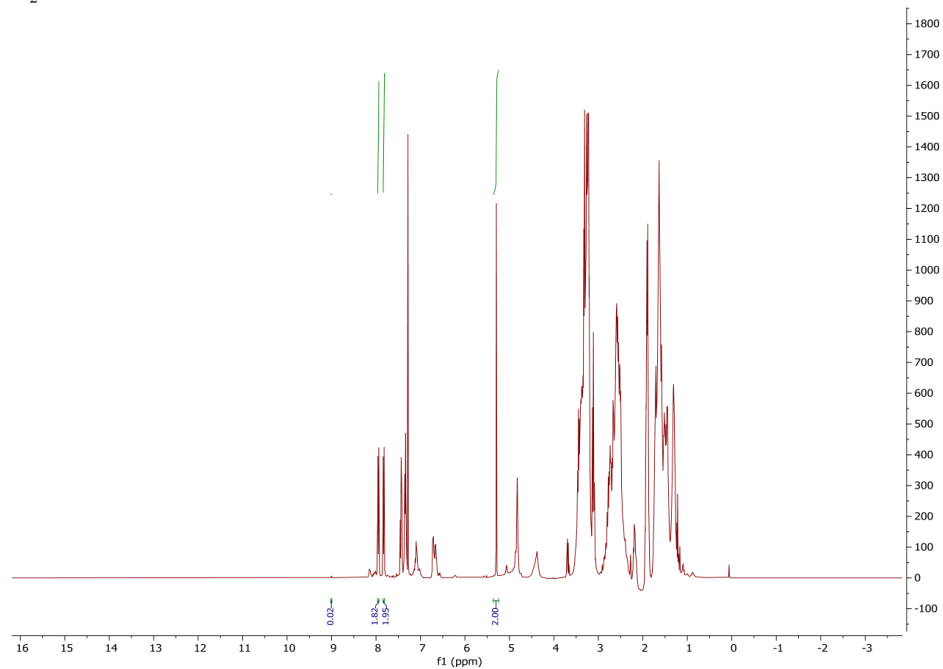


**Figure S26b:** <sup>1</sup>H NMR analysis of the reaction product of synthesis of Benzothiazole with CO<sub>2</sub> and H<sub>2</sub>.

## 7. Mechanism investigation: Formate transfer agent

### 7.1 Benzimidazole synthesis via formate transfer from PEI

Cy<sub>3</sub>SnNTf<sub>2</sub> (6.48 mg, 0.01mmol) was added to a 50:50 mixture of PEI:NMM (5 mL). The reaction was pressurized with H<sub>2</sub> (100 bar) and CO<sub>2</sub> (4 bar) and heated to 180 °C for 22hrs. After which the reaction was degassed, and an aliquot was taken for NMR analysis. The PEI solid was isolated by decanting the reaction liquor. To the PEI solid o-phenylene diamine (108mg, 1mmol) was added. The reaction was heated to 180 °C for 22hrs after which an aliquot was taken for NMR analysis. After the reaction, the first aliquot of the reaction sample displayed no signal corresponding to Cy<sub>3</sub>SnOCOH and in the second aliquot it was found that o-phenylene diamine was converted to benzimidazole after heating o- phenylene diamine in the remaining PEI for 24hrs at 453K.

### 7.2 Standard procedure for direct reaction of formylated PEI and o-phenylenediamine:

Cy<sub>3</sub>SnNTf<sub>2</sub> (6.48 mg, 0.01mmol) was added to a 50:50 mixture of PEI:NMM (5 mL). The reaction was pressurized with H<sub>2</sub> (100 bar) and CO<sub>2</sub> (4 bar) and heated to 180 °C for 22hrs. After which the reaction was degassed, and an aliquot was taken for NMR analysis. The PEI solid was isolated by decanting the reaction liquor. To the PEI solid o-phenylene diamine (108mg, 1mmol) was added. The reaction was heated to 180 °C for 24hrs after which an aliquot was taken for NMR analysis.

<sup>1</sup>H NMR (400 MHz, CDCl<sub>3</sub>) δ: 8.05 (s,1H), 7.67- 7.62 (m, 2H), 7.28- 7.23 (m, 2H); GC retention time 29.0-29.5 minutes; EI-MS (*m/z*) calculated: 118 found 118

## 8. Mechanism investigation: Cyclisation of N-(2-aminophenyl) acetamide to 2-methyl-1H-benzimidazole

### 8.1 Standard procedure for cyclisation of N-(2-aminophenyl) acetamide to 2-methyl-1H-benzimidazole:

In air, to the autoclave, Cy<sub>3</sub>SnNTf<sub>2</sub> (0.05mmol), PEI (0.2mL) and N-(2-aminophenyl)acetamide (1mmol) were added to sulfolane (4.8 mL) The autoclave was then sealed and purged 5 times with the desired pressure of CO<sub>2</sub>. The reaction is then topped up with the desired H<sub>2</sub> reaction pressure. The temperature and stirring rate were set using Specview program connected to the Parr 5000 series multi reactor system. T = 0 was defined as the time the heating starts. The



heating was turned off at the end of the 22hr reaction time. DCM (1mmol) was added to the reactor, stirred and an aliquot was taken for NMR in DMSO-*d*<sub>6</sub>. The conversion was quantified by comparing the integral of the methyl peak and the integral of DCM. Other reaction products were determined by GC-MS.

<sup>1</sup>H NMR (400 MHz, DMSO-*d*<sub>6</sub>): 12.32-11.98ppm (br s, 1H), 7.46-7.44ppm (br s, 2H), 7.14-7.06ppm (m, 2H), 2.48 ppm (s, 3H), EI-MS (m/z) calculated: 132, found 131.9

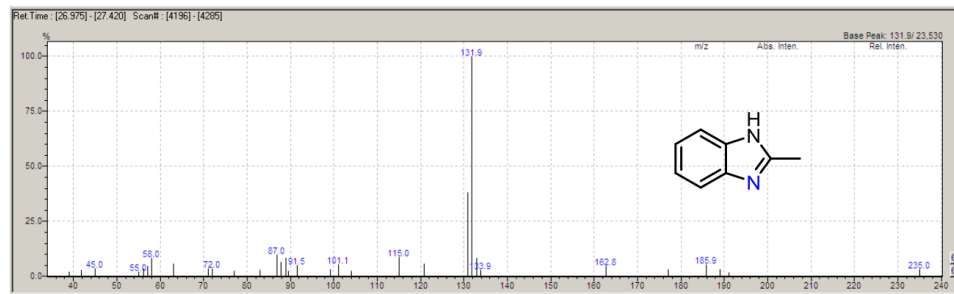


**Figure S27:** EI-MS analysis of the reaction product of synthesis of N-methyl-1,2-phenylenediamine with CO<sub>2</sub> and H<sub>2</sub>.

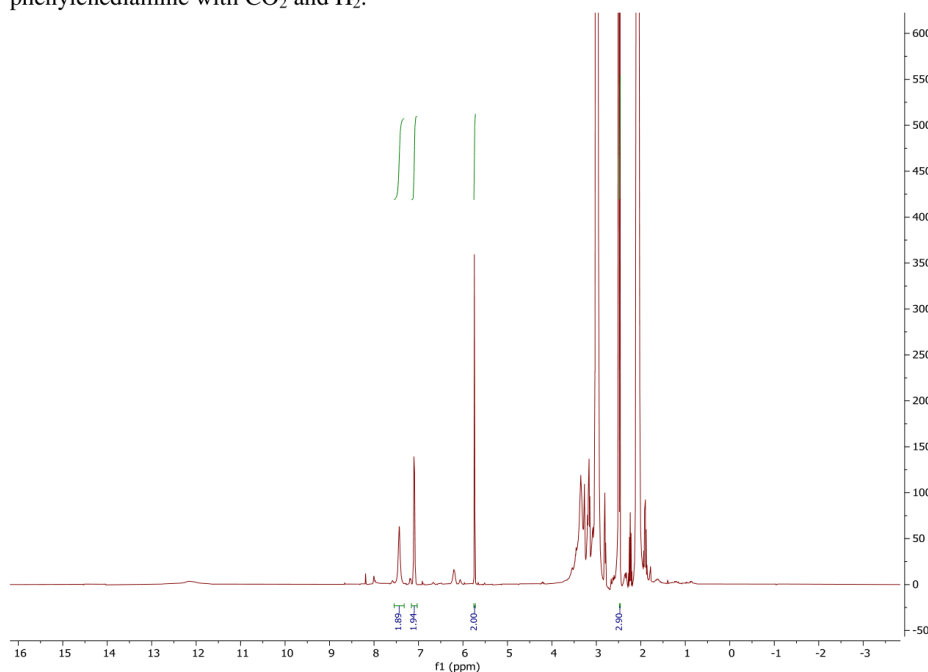


**Figure S27b:** <sup>1</sup>H NMR analysis of the reaction product of synthesis of N-methyl-1,2-phenylenediamine with CO<sub>2</sub> and H<sub>2</sub>.

### Testing of $\text{C}_3\text{SnNTf}_2$ stability to water

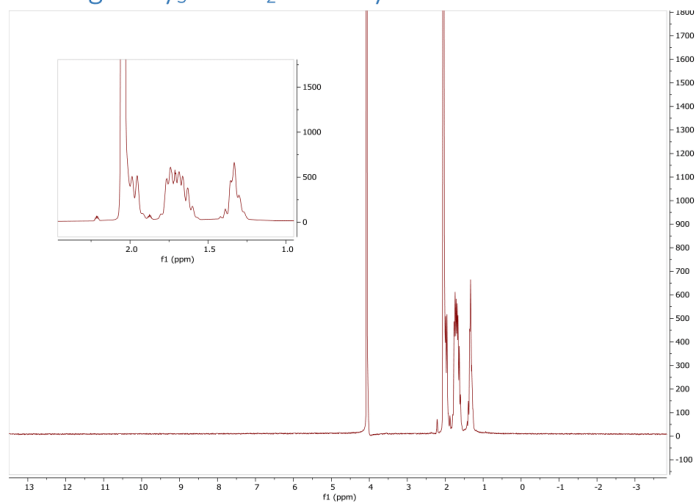


**Figure S28:**  $^1\text{H}$  NMR analysis of  $\text{C}_3\text{SnNTf}_2$  in  $\text{D}_2\text{O} : \text{MeCN-d}_3$  (1 : 1) at  $t = 0\text{h}$

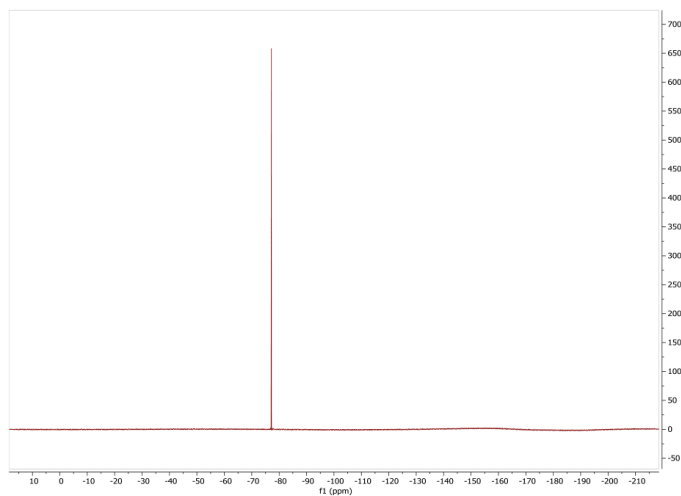


**Figure S29:**  $^{19}\text{F}$  NMR analysis of  $\text{C}_3\text{SnNTf}_2$  in  $\text{D}_2\text{O} : \text{MeCN-d}_3$  (1 : 1) at  $t = 0\text{h}$

$\text{C}_3\text{SnNTf}_2$  was dissolved in a NMR tube in a 1:1 mixture of  $\text{MeCN-d}_3$  and  $\text{D}_2\text{O}$  and  $^1\text{H}$  and  $^{19}\text{F}$  NMR sample was recorded. The sample was then left standing at room temperature for 22 hours and the same spectra were measured. No visible change occurred.

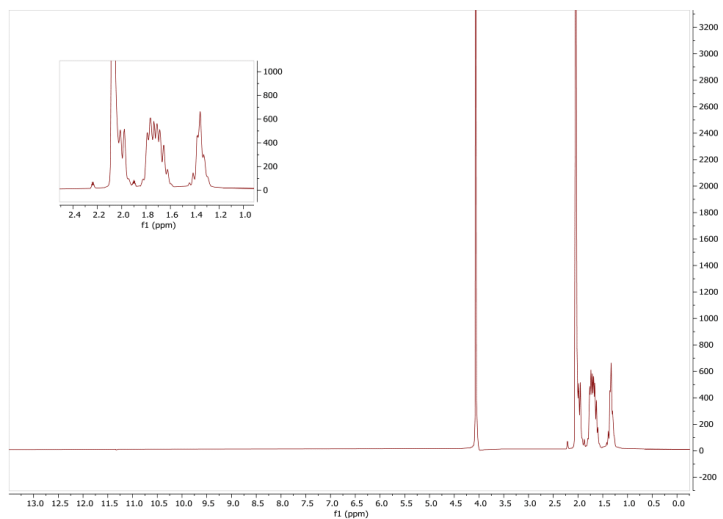


**Figure S30:**  $^1\text{H}$  NMR analysis of  $\text{C}_3\text{SnNTf}_2$  in  $\text{D}_2\text{O} : \text{MeCN-d}_3$  (1 : 1) at  $t = 22\text{h}$  at room temperature

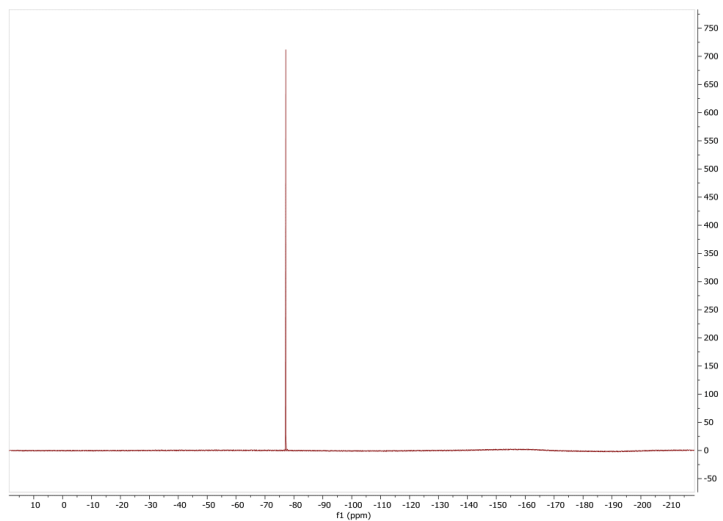


**Figure S31:**  $^{19}\text{F}$  NMR analysis of  $\text{Cy}_3\text{SnNTf}_2$  in  $\text{D}_2\text{O} : \text{MeCN-d}_3$  (1 : 1) at  $t = 22\text{h}$  at room temperature

$\text{Cy}_3\text{SnNTf}_2$  was dissolved in a NMR tube in a 1:1 mixture of  $\text{MeCN-d}_3$  and  $\text{D}_2\text{O}$  and  $^1\text{H}$  and  $^{19}\text{F}$  NMR sample was recorded. The sample was then heated to for 22 hours and the same spectra were measured. No visible change occurred.

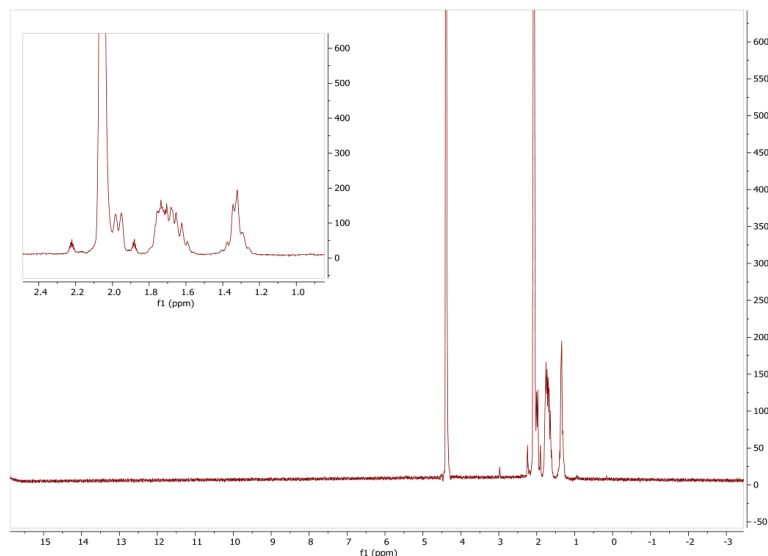


**Figure S32:**  $^1\text{H}$  NMR analysis of  $\text{Cy}_3\text{SnNTf}_2$  in  $\text{D}_2\text{O} : \text{MeCN-d}_3$  (1 : 1) at  $t = 22\text{h}$  at  $60^\circ\text{C}$

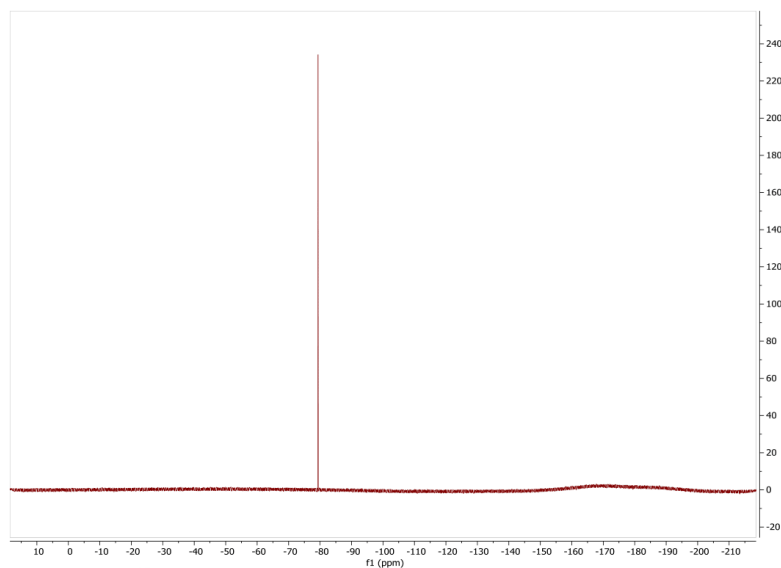


**Figure S33:**  $^{19}\text{F}$  NMR analysis of  $\text{Cy}_3\text{SnNTf}_2$  in  $\text{D}_2\text{O} : \text{MeCN-d}_3$  (1 : 1) at  $t = 22\text{h}$  at  $60^\circ\text{C}$

### Reaction in the presence of molecular sieves

A catalytic test was carried out as described in the general procedures. In addition 5 pieces of activated molecular sieves ( $300^\circ\text{C}$  overnight) were added to the reaction. The reaction was completely inhibited as no benzimidazole formed presumably due to the LA binding to the surface of the molecular sieves.

### 9. References:

- 1 A. Paparakis, R. C. Turnell-Ritson, J. S. Sapsford, A. E. Ashley and M. Hulla, *Catal. Sci. Technol.*, 2023, **13**, 637–644.
- 2 B. D. Ellis, T. M. Atkins, Y. Peng, A. D. Sutton, J. C. Gordon and P. P. Power, *Dalt. Trans.*, 2010, **39**, 10659–10663.
- 3 D. J. Scott, N. A. Phillips, J. S. Sapsford, A. C. Deacy, M. J. Fuchter and A. E. Ashley, *Angew. Chemie Int. Ed.*, 2016, **55**, 14738–14742.
- 4 P. Erdmann and L. Greb, *Angew. Chemie Int. Ed.*, 2022, **61**, e202114550.

## Appendix 3 Hexacoordinated tin complexes catalyse imine hydrogenation with H<sub>2</sub>

*Andrea Žáková,<sup>a</sup> Pritha Saha,<sup>a</sup> Alexandros Paparakis,<sup>a</sup> Martin Zábranský,<sup>a</sup> Gabriela Gastelu,<sup>b</sup> Jaroslav Kukla,<sup>c</sup> Jorge G. Uranga<sup>b</sup> and Martin Hulla<sup>\*a</sup>* **Chem. Commun.**, 2024,**60**, 3287-3290



## Hexacoordinated tin complexes catalyse imine hydrogenation with H<sub>2</sub>†

 Andrea Žáková,<sup>a</sup> Pritha Saha,<sup>a</sup> Alexandros Paparakis,<sup>a</sup> Martin Zábbransky,<sup>b</sup> Gabriela Gastelu,<sup>b</sup> Jaroslav Kukla,<sup>b</sup> Jorge G. Uranga<sup>b</sup> and Martin Hulla<sup>c\*</sup>
Cite this: *Chem. Commun.*, 2024, 60, 3287Received 1st December 2023,  
Accepted 13th February 2024

DOI: 10.1039/d3cc05878f

rsc.li/chemcomm

Frustrated Lewis pair (FLP) hydrogenation catalysts predominantly use alkyl- and aryl-substituted Lewis acids (LA) that offer a limited number of combinations of substituents, limiting our ability to tune their properties and, ultimately, their reactivity. Nevertheless, main-group complexes have numerous ligands available for such purposes, which could enable us to broaden the range of FLP catalysis. Supporting this hypothesis, we demonstrate here that hexacoordinated tin complexes with Schiff base ligands catalyse imine hydrogenation via activation of H<sub>2</sub>(g). As shown by hydrogen–deuterium scrambling, [Sn(<sup>t</sup>Bu<sub>2</sub>Salen)(OTf)<sub>2</sub>] activated H<sub>2</sub>(g) at 25 °C and 10 bar of H<sub>2</sub>. After tuning the ligands, we found that [Sn(Salen)Cl<sub>2</sub>] was the most efficient imine hydrogenation catalyst despite having the lowest activity in H<sub>2</sub>(g) activation. Moreover, various imines were hydrogenated in yields up to 98% thereby opening up opportunities for developing novel FLP hydrogenation catalysts based on hexacoordinated LA of main-group elements.

Frustrated Lewis pairs (FLPs)<sup>1</sup> combining bulky Lewis acids (LAs) with Lewis bases (LBs) catalyse imine hydrogenation via H<sub>2</sub> activation (Fig. 1A).<sup>2–4</sup> Tuning their electronic and steric properties improves the FLP hydrogenation activity, expands the substrate scope<sup>5,6</sup> and, in some cases, imparts water tolerance.<sup>7–10</sup> Notwithstanding these outcomes, tuning predominantly involves triaryl-substituted Lewis acids<sup>8,11,12</sup> of boron, aluminium, gallium and indium<sup>13</sup> with a narrow margin of manoeuvre, preventing us from further enhancing their reactivity. As a case in point, some authors argue that we cannot electronically tune the BAR<sub>3</sub> LAs any further.<sup>7</sup>

FLP reactivity has nevertheless been further modified by using group 15 and 14 LAs.<sup>14–21</sup> In particular, R<sub>3</sub>SnX (R = alkyl or aryl, X = halogen, <sup>−</sup>OTf, <sup>−</sup>NTf<sub>2</sub>, and <sup>−</sup>ClO<sub>4</sub>) Lewis acids (Fig. 1B) in their cationic form are isolobal to group 13-based LAs,<sup>15</sup> so they can act as their direct substitutes. In fact, tin-based FLPs effectively hydrogenate many functional groups and small molecules,<sup>14–16,22–25</sup> but lack the diversity of metal complexes.

In addition to simple tetravalent alkyl- and aryl-substituted LAs, tin(IV) also forms hexacoordinated complexes with various ligands, including bipyridine,<sup>26</sup> benzoylpyridine<sup>27</sup> and Schiff bases.<sup>28</sup> In particular, Schiff base ligands can stabilize various tin oxidation states, and their complexes are known LA catalysts.<sup>28,29</sup> Moreover, they have been used in asymmetric

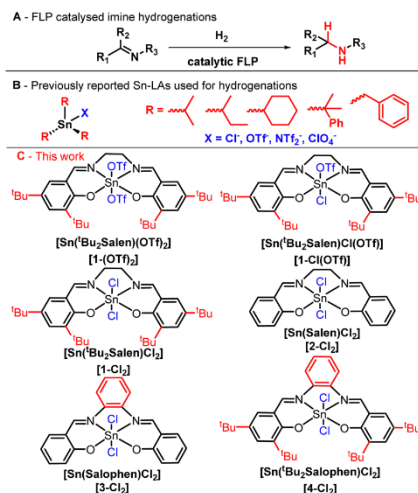


Fig. 1 (A) Reaction scheme of FLP-catalysed imine hydrogenation, (B) previously reported Sn-based LAs used in FLP-catalysed hydrogenations, and (C) L<sub>4</sub>SnX<sub>2</sub> catalysts developed for H<sub>2</sub> activation and imine hydrogenations in this study.

<sup>a</sup> Department of Inorganic Chemistry, Faculty of Science Charles, University Prague, 128 00, Czech Republic. E-mail: martin.hulla@natur.cuni.cz

<sup>b</sup> Instituto de Investigaciones en Físico-Química Córdoba Universidad Nacional de Córdoba (INFIQC-CONICET), Córdoba, 5000, Argentina

<sup>c</sup> Institute of Environmental Studies, Faculty of Science Charles, University Prague, 128 00, Czech Republic

† Electronic supplementary information (ESI) available: Catalyst synthesis and analysis; NMRs, MS, IRs, sXRD, and Lewis acidity measurements. CCDC 2330171 and 2333521. For ESI and crystallographic data in CIF or other electronic format see DOI: <https://doi.org/10.1039/d3cc05878f>



## Communication

catalysis,<sup>30,31</sup> which is currently a prominent target of FLP chemistry.<sup>32,33</sup> Despite the fact that a few main group complexes act as hydrogenation catalysts,<sup>34–36</sup> we hypothesized that hexacoordinated tin complexes with Schiff base ligands may be applied as LAs in FLPs to catalyse imine hydrogenation.

In this study, we report that hexacoordinated complexes of tin with Schiff base ligands in the form  $L_4SnX_2$ , containing N and O donor atoms (Fig. 1C), activate  $H_2$  gas and act as hydrogenation catalysts for imine reduction. The presence of labile or hemi-labile axial ligands  $X^-$ , such as triflate ( $OTf^-$ ) and chloride, promotes the formation of a vacant site on the LA metal centre, which is necessary for efficient catalysis.

Given the large positive polarization of tin(IV) and their labile triflate ligand(s),  $[Sn^{\text{tBu}_2\text{Salen}}(OTf)_2]$  (**1-OTf**) and  $[Sn^{\text{tBu}_2\text{Salen}}Cl(OTf)]$  (**1-Cl(OTf)**) showed high Lewis acidity, assessed using the Guttmann–Beckett (GB) method (AN = 83.6 and AN = 71.8, respectively), where **1-OTf** presumably dissociates both triflate ligands and **1-Cl(OTf)** dissociates the triflate but retains the chloride to form the Lewis acidic ions  $[Sn^{\text{tBu}_2\text{Salen}}]_2^+$  and  $[Sn^{\text{tBu}_2\text{Salen}}Cl]^+$ , respectively. Their Lewis acidity is similar to that of  $B(C_6F_5)_3$  (AN = 78.1).  $B(C_6F_5)_3$  is frequently used in FLP hydrogenations and is known to activate  $H_2$  with bases as weak as THF or dioxane.<sup>9,10,37,38</sup> Calculation of hydride affinities (HIA) (Table 1, entries 1 and 2), following a protocol described by Greb *et al.*, also indicates that HIA is much higher than  $B(C_6F_5)_3$  (HIA =  $481 \text{ kJ mol}^{-1}$ ).<sup>39</sup> Accordingly, **1-OTf** and **1-Cl(OTf)** may activate  $H_2$  together with Lewis bases (LBs) comparable to FLPs based on  $B(C_6F_5)_3$  if a favourably oriented encounter complex forms.

As expected, **1-OTf** and **1-Cl(OTf)** activated  $H_2$  gas in the presence of THF, as shown by hydrogen–deuterium scrambling to  $H_2$  and  $D_2$  at 10 bar and at 25 and 60 °C, respectively (Fig. 2). Conversely, the dichloride complex  $[Sn^{\text{tBu}_2\text{Salen}}Cl_2]$  (**1-Cl**) does not possess a free binding site, at least at 25 °C, and in effect has the measured AN = 0 and the hydride affinity of  $660 \text{ kJ mol}^{-1}$  (Table 1, entry 3) remains masked by the  $Cl^-$  ligands that must dissociate to reveal the cationic LA site. In line with  $Cl^-$  coordination and the lack of binding site at low temperatures, **1-Cl** failed to activate  $H_2$ , even with additional base, 2,4,6-collidine, or DABCO, at temperatures between 25 and 60 °C. These results indicate that  $H_2$  activation requires a free binding site *via* a labile ligand.

Under the reaction conditions used for  $H_2$  activation, however, neither of the complexes **1-OTf** and **1-Cl(OTf)** displayed

Table 1 Guttmann–Beckett Lewis acidity measurement and hydride affinities of the tested complexes and their ions

Entry	Lewis acid	AN <sup>a</sup>	Ionic form <sup>b</sup>	HIA ( $\text{kJ mol}^{-1}$ ) <sup>c</sup>
1	<b>1-OTf</b>	83.6	$[Sn^{\text{tBu}_2\text{Salen}}]_2^{2+}$	1170
2	<b>1-Cl(OTf)</b>	71.8	$[Sn^{\text{tBu}_2\text{Salen}}Cl]^+$	660
3	<b>1-Cl</b>	0	$[Sn^{\text{tBu}_2\text{Salen}}Cl]^+$	660
4	<b>2-Cl</b>	0	$[Sn^{\text{tBu}_2\text{Salen}}Cl]^+$	688
5	<b>3-Cl</b>	0	$[Sn^{\text{tBu}_2\text{Salen}}Cl]^+$	701
6	<b>4-Cl</b>	0	$[Sn^{\text{tBu}_2\text{Salen}}Cl]^+$	682

<sup>a</sup> Acceptor number. <sup>b</sup> Probable ionic fragments used for the calculation of hydride affinities assume dissociation of at least one ligand and all weakly coordinating anionic ligands. <sup>c</sup> Hydride ion affinities (HIA) were calculated at the DSD-PBEB86-D3BJ/def2-QZVP level.

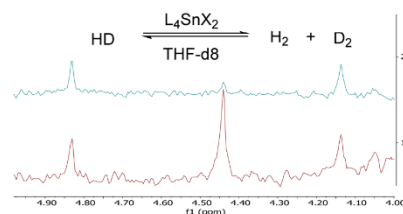


Fig. 2  $^2D$  NMR spectra of HD scrambling by **1-OTf**<sub>2</sub> in THF-*d*<sub>8</sub> at 25 °C and 10 bar of HD. The blue trace is  $T = 0$  h, and the red trace is  $T = 19$  h. The peak at 4.45 ppm corresponds to  $D_2$  gas, suggesting HD scrambling. Comparable spectra are obtained with **1-Cl(OTf)** (ESI†).

any hydrogenation activity, suggesting that hydride transfer could be hindering the desired catalytic reactivity in line with the high HIA of  $1170$  and  $660 \text{ kJ mol}^{-1}$  respectively and associated poor hydride donor ability. Catalytic hydrogenation of the FLP model substrate, *N-tert*-butyl-1-phenylmethanimine, was observed only at 180 °C and 50 bar of  $H_2$  in sulfolane with **1-OTf**, **1-Cl(OTf)** and even **1-Cl**, in 10, 49 and 29% yield, respectively (Table 2, entries 1–3). These findings suggest that chloride becomes a sufficient leaving group for  $H_2$  activation at high temperatures, albeit less so than triflate.

Replacing the bulky  $^t\text{Bu}$  groups with  $^-H$  on **1-Cl** to form  $[Sn(\text{Salen})Cl_2]$  (**2-Cl**) improved the product yield from 29 to 53% (Table 2, entries 3 and 4), implicating steric hindrance in the low hydrogenation activity of the complexes. This hypothesis was tested with  $[Sn(\text{Salophen})Cl_2]$  (**3-Cl**) and  $[Sn^{\text{tBu}_2\text{Salophen}}Cl_2]$  (**4-Cl**), which yielded the desired product in 42 and 28% yield, respectively (Table 2, entries 5 and 6), thus confirming that  $^-t\text{Bu}$  groups on complexes **1-Cl**, and **4-Cl** hinder substrate access to the metal centre. Moreover, the  $^-t\text{Bu}$ -substituted complexes **1-Cl**

Table 2 Optimization table for *N-tert*-butyl-1-phenylmethanimine reduction by  $L_4SnX_2$  complexes with Schiff base ligands

Entry	Catalyst	Solvent	Temperature (°C)	Yield (%)
1	<b>1-OTf</b>	Sulfolane	180	10
2	<b>1-Cl(OTf)</b>	Sulfolane	180	49
3	<b>1-Cl</b>	Sulfolane	180	29
4	<b>2-Cl</b>	Sulfolane	180	53
5	<b>3-Cl</b>	Sulfolane	180	42
6	<b>4-Cl</b>	Sulfolane	180	28
7	<b>1-OTf</b>	Toluene	180	30
8	<b>1-Cl(OTf)</b>	Toluene	180	86
9	<b>1-Cl</b>	Toluene	180	84
10	<b>2-Cl</b>	Toluene	180	98
11	<b>1-Cl</b>	Toluene	150	NR
12	<b>2-Cl</b>	Toluene	150	27
13	<b>2-Cl</b>	Collidine	180	85

Reaction conditions: *N-tert*-butyl-1-phenylmethanimine (1 mmol), reaction solvent (4 mL), catalyst (0.05 mmol),  $H_2$  (50 bar), 17 h. All reactions were performed in triplicate, quantifying the reaction product by  $^1H$  NMR with  $CH_2Br_2$  as the internal standard and confirming the structure by ESI-MS.





and **4-Cl<sub>2</sub>** had similar yields of the target product, at 29 and 28%, respectively (Table 2, entries 3 and 6) and the HIA of the best catalyst **2-Cl<sub>2</sub>** without the *t*-Bu groups and the worst **4-Cl<sub>2</sub>** with *t*-Bu groups are almost identical (Table 1, entries 4 and 6), further demonstrating that steric hindrance of *t*-Bu groups is the limiting factor of the activity of chloride complexes. Attempts to calculate an optimized FLP structure were only successful for **2-Cl<sub>2</sub>** (Fig. 4B) as the *t*-Bu groups on **1-Cl<sub>2</sub>** and **4-Cl<sub>2</sub>** prevented FLP formation.

Substituting sulfolane for toluene improved the catalytic performance of **1-OTf<sub>2</sub>**, **1-Cl(OTf)** and **1-Cl<sub>2</sub>** reaching 30, 86 and 84% yields of the desired amine, respectively (Table 2, entries 7–9), thus approximately doubling and trebling those obtained in sulfolane (Table 2, entries 1, 2 and 3). Among other solvent effects, this can be attributed to the enhanced solubility of H<sub>2</sub> gas in toluene<sup>40</sup> that can promote tin hydride formation *via* the Le Chatelier principle. As a result, **1-Cl(OTf)** and **1-Cl<sub>2</sub>** showed similar activities. The failure to further improve the yield of **1-(OTf)<sub>2</sub>** was attributed to the instability of this catalyst under these reaction conditions. **2-Cl<sub>2</sub>** also demonstrated improved activity in toluene and the desired product was obtained in 98% yield (Table 2, entry 10). The use of 2,4,6-collidine as the solvent, which can also act as an FLP base and enhance H<sub>2</sub> activation, decreased the yield from 98 to 85% (Table 2, entries 10 and 13). Lowering the temperature to 150 °C, in toluene, also decreased the yield and confirmed **2-Cl<sub>2</sub>** as the best catalyst (Table 2, entries 11 and 12). Based on these results, we established the optimal reaction conditions, which were 180 °C, toluene, 50 bar of H<sub>2</sub> and 17 hours over the catalyst **2-Cl<sub>2</sub>** (5 mol%).

Under optimal reaction conditions, **2-Cl<sub>2</sub>** was used as the catalyst to assess the substrate scope of the reaction (Fig. 3). The model substrate *N*-*tert*-butyl-1-phenylmethanimine was converted into the corresponding amine (**1**) in 98% yield. Introduction of functional group(s) onto the benzene ring such as 4-chloride-, 4-trifluoromethyl- or 4,5-dimethoxy- decreased the reaction yields to 61 (**2**), 42 (**3**) and 50% (**5**) respectively or

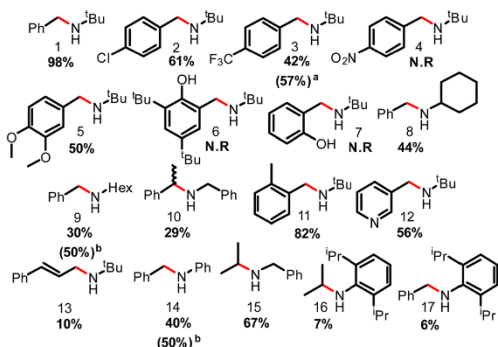


**Fig. 3** Substrate scope of the imine hydrogenation reaction with H<sub>2</sub> over **2-Cl<sub>2</sub>**. Reaction conditions: imine (1 mmol), toluene (4 mL) and LA (5 mol%), H<sub>2</sub> (50 bars), 180 °C, 17 h. All yields were determined by <sup>1</sup>H NMR with CH<sub>2</sub>Br<sub>2</sub> as the internal standard, and all structures were confirmed by ESI-MS. (a) 70 bar (b) Extended reaction time to 48 h.

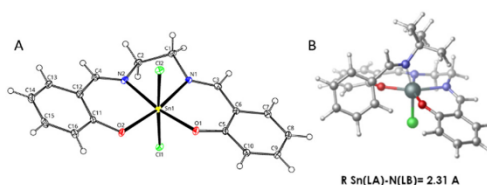


**Fig. 4** (A) X-ray structure of **2-Cl<sub>2</sub>** and (B) calculated FLP structure at the DSD-PBEB86-D3BJ/def2-QZVP level.

halted the reaction in the case of 4-nitro- (**4**), and 2-hydroxy- (**6** and **7**). As shown by mass spectrometry, nitro- and hydroxy-substitution completely inhibited imine reduction possibly due to the slow but preferential –NO<sub>2</sub> group reduction to –NH<sub>2</sub> and to the relative Bronsted acidity of phenol(s), respectively. Phenols can protonate the hydride formed in the reaction and hence reverse H<sub>2</sub> activation. Simultaneous reduction of an alkene was also observed and *N*-(*tert*-butyl)-*N*-cinnamylamine (**13**) was obtained in only 10% yield, while the rest was further hydrogenated to remove the alkene moiety.

Substitution of the *t*-Bu group for –Hex, Cy, –Ph, –Bn or other unfunctionalized aliphatic or aromatic hydrocarbon substituents resulted in the corresponding amine formation in 6 to 82% yield (**8** to **17**). Noteworthy is the tolerance of *ortho*-methyl substitution, which yielded the corresponding amine **11** in 82% yield, whereas *ortho*-diisopropyl inhibited the reactivity and the corresponding amine **17** was obtained in 6% yield.

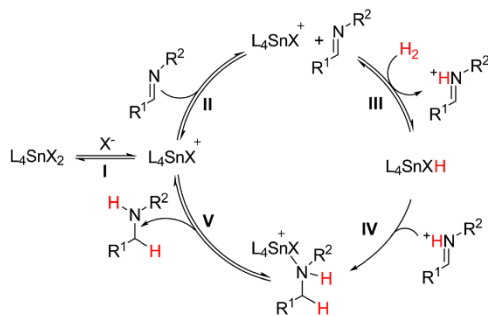
Nevertheless, further reaction trends are difficult to establish and analysis of side reactions, reaction mass balance and catalyst stability indicate that the desired reaction yield is a balance between the rate of substrate hydrogenation, its decomposition and catalyst deactivation, which decomposes to an inactive mixture of metallic tin, tin oxides and ligand fragments under the reaction conditions.

In toluene, the reaction substrate also acts as the Lewis base to activate H<sub>2</sub> because the tin(IV) complexes lack this ability on their own. Furthermore, a ligand must also dissociate from the coordinatively saturated complexes (Fig. 4A) to generate a Lewis acidic site, and generate an active FLP catalyst (Fig. 4B) as shown in our H<sub>2</sub> activation studies (Fig. 2). Based on these observations and on previous literature,<sup>4,41–44</sup> we propose a catalytic cycle for hydrogenation over hexacoordinate tin(IV) complexes (Scheme 1).

In the initial phase (Scheme 1, I), a ligand X<sup>–</sup> (Cl<sup>–</sup> or OTf<sup>–</sup>) dissociates from the complex to reveal an LA site. Interaction with the imine then forms the active FLP catalyst (II) and splits H<sub>2</sub> yielding L<sub>4</sub>SnHX and [imineH][X] (III). The protonation activates the imine towards hydride transfer from the metal centre to the iminium double bond (IV).<sup>43</sup> The produced amine reversibly binds the tin(IV) complex, which slows down the reaction as demonstrated by the addition of the product (1 mmol) to the reaction, which decreased the conversion of the starting imine from 85% to 30% in a 6-hour reaction. Eventual dissociation of the produced amine then regenerates the active LA with a free binding site (V).



## Communication



**Scheme 1** Catalytic cycle proposed for imine hydrogenation with  $H_2$  catalysed by tin(IV)-Schiff base complexes.

In conclusion, hexacoordinated tin(IV) complexes with Schiff base and labile or hemi-labile axial ligands can be used as LA components of FLPS for  $H_2$  activation and imine hydrogenation.  $H_2$  activation takes place with bases as weak as THF at 25 °C and can be reversible, as shown by HD scrambling. Nevertheless, imine reduction only occurs at temperatures  $\geq 150$  °C and optimally at 180 °C, suggesting that hydride transfer hinders the reaction. The best catalyst is  $[Sn(Salen)Cl_2]$  ( $2-Cl_2$ ) even though dichloride complexes have the lowest ability to activate  $H_2$  among all complexes tested in this study. In effect, various imines are hydrogenated in yields ranging from 6 to 98% in toluene depending on substrate substitution and functionalization. The high variability of these complexes opens up opportunities for developing hydrogenation catalysts based on hexacoordinated compounds of main-group elements.

The authors thank the Czech Science Foundation (GAČR 21-27431M) and Charles University Research Centre program No. UNCE/24/SCI/010 for funding the study. We also thank Carlos V. Melo for editing the manuscript. The research used computational resources of the Centro de Computación de Alto Desempeño – CCAD of Universidad Nacional de Córdoba – UNC (<https://ccad.unc.edu.ar/>), part of Sistema Nacional de Computación de Alto Desempeño – SNCAD of the Ministry of Science, Technology and Innovation, Argentina.

## Conflicts of interest

There are no conflicts to declare.

## Notes and references

- G. C. Welch, R. R. San Juan, J. D. Masuda and D. W. Stephan, *Science*, 2006, **314**, 1124–1126.
- D. W. Stephan and G. Erker, *Angew. Chem., Int. Ed.*, 2010, **49**, 46–76.
- D. W. Stephan, *Acc. Chem. Res.*, 2015, **48**, 306–316.
- D. J. Scott, M. J. Fuchter and A. E. Ashley, *Chem. Soc. Rev.*, 2017, **46**, 5689–5700.
- D. W. Stephan, *Science*, 2016, **354**, aaf7229–aaf7229.

- J. Lam, K. M. Szkop, E. Mosaferi and D. W. Stephan, *Chem. Soc. Rev.*, 2019, **48**, 3592–3612.
- É. Dorkó, B. Kótai, I. Pápai, T. Soós, M. Szabó and A. Domján, *Angew. Chem., Int. Ed.*, 2017, **56**, 9512–9516.
- D. J. Scott, T. R. Simmons, E. J. Lawrence, G. G. Wildgoose, M. J. Fuchter and A. E. Ashley, *ACS Catal.*, 2015, **5**, 5540–5544.
- T. Mahdi and D. W. Stephan, *J. Am. Chem. Soc.*, 2014, **136**, 15809–15812.
- D. J. Scott, M. J. Fuchter and A. E. Ashley, *J. Am. Chem. Soc.*, 2014, **136**, 15813–15816.
- V. B. Saptal, G. Juneja and B. M. Bhanage, *New J. Chem.*, 2018, **42**, 15847–15851.
- V. Fasano and M. J. Ingleson, *Chem. – Eur. J.*, 2017, **23**, 2217–2224.
- M. Xu, J. Possart, A. E. Waked, J. Roy, W. Uhl and D. W. Stephan, *Philos. Trans. Royal Soc. A*, 2017, **375**, 20170014.
- A. Paparakis, R. C. Turnell-Ritson, J. S. Sapsford, A. E. Ashley and M. Hulla, *Catal. Sci. Technol.*, 2023, **13**, 637–644.
- D. J. Scott, N. A. Phillips, J. S. Sapsford, A. C. Deacy, M. J. Fuchter and A. E. Ashley, *Angew. Chem., Int. Ed.*, 2016, **55**, 14738–14742.
- J. Sapsford, D. Scott, N. Alcock, M. Fuchter, A. Ashley and C. Tighe, *Adv. Synth. Catal.*, 2018, **360**, 1066–1071.
- P. Sarkar, S. Das and S. K. Pati, *Chem. – Asian J.*, 2022, **17**, e202200148.
- T. Thorwart, D. Hartmann and L. Greb, *Chem. – Eur. J.*, 2022, **28**, e202202273.
- T. A. Kinder, R. Pior, S. Blomeyer, B. Neumann, H. G. Stammler and N. W. Mitzel, *Chem. – Eur. J.*, 2019, **25**, 5899–5903.
- P. Holtkamp, F. Friedrich, E. Stratmann, A. Mix, B. Neumann, H. G. Stammler and N. W. Mitzel, *Angew. Chem., Int. Ed.*, 2019, **58**, 5114–5118.
- J. M. Bayne and D. W. Stephan, *Chem. Soc. Rev.*, 2016, **45**, 765–774.
- R. T. Cooper, J. S. Sapsford, R. C. Turnell-Ritson, D. H. Hyon, A. J. P. White and A. E. Ashley, *Philos. Trans. Royal Soc. A*, 2017, **375**, 20170008.
- G. R. Whittell, E. I. Balmond, A. P. M. Robertson, S. K. Patra, M. F. Haddow and I. Manners, *Eur. J. Inorg. Chem.*, 2010, 3967–3975.
- J. S. Sapsford, D. Csókás, R. C. Turnell-Ritson, L. A. Parkin, A. D. Crawford, I. Pápai and A. E. Ashley, *ACS Catal.*, 2021, **11**, 9143–9150.
- A. Paparakis and M. Hulla, *ChemCatChem*, 2023, **15**, e202300510.
- Y. M. Ahmed and G. G. Mohamed, *Inorg. Chem. Commun.*, 2022, **144**, 109864.
- A. Pérez-Rebolledo, G. M. de Lima, N. L. Speziali, O. E. Piro, E. E. Castellano, J. D. Ardisson and H. Beraldo, *J. Organomet. Chem.*, 2006, **691**, 3919–3930.
- H. Jing, S. K. Edulji, J. M. Gibbs, C. L. Stern, H. Zhou and S. B. T. Nguyen, *Inorg. Chem.*, 2004, **43**, 4315–4327.
- A. M. Abu-Dief and I. M. A. Mohamed, *J. Basic Appl. Sci.*, 2015, **4**, 119–133.
- M. Palucki, P. J. Pospisil, W. Zhang and E. N. Jacobsen, *J. Am. Chem. Soc.*, 1994, **116**, 9333–9334.
- S. De, A. Jain and P. Barman, *ChemistrySelect*, 2022, **7**, e202104334.
- W. Meng, X. Feng and H. Du, *Acc. Chem. Res.*, 2018, **51**, 191–201.
- W. Meng, X. Feng and H. Du, *Chin. J. Chem.*, 2020, **38**, 625–634.
- Y. Liang, J. Luo, Y. Diskin-Posner and D. Milstein, *J. Am. Chem. Soc.*, 2023, **145**, 9164–9175.
- H. Elsen, C. Färber, G. Ballmann and S. Harder, *Angew. Chem., Int. Ed.*, 2018, **57**, 7156–7160.
- A. Friedrich, J. Eysel, H. Elsen, J. Langer, J. Pahl, M. Wiesinger and S. Harder, *Chem. – Eur. J.*, 2021, **27**, 7756–7763.
- D. J. Scott, M. J. Fuchter and A. E. Ashley, *Angew. Chem., Int. Ed.*, 2014, **53**, 10218–10222.
- L. J. Hounjet, C. Bannwarth, C. N. Garon, C. B. Caputo, S. Grimme and D. W. Stephan, *Angew. Chem., Int. Ed.*, 2013, **52**, 7492–7495.
- E. Philipp and L. Greb, *ChemPhysChem*, 2021, **22**, 935–943.
- J. J. Simnick, H. M. Sebastian, H.-M. Lin and K.-C. Chao, *J. Chem. Eng. Data*, 1978, **23**, 339.
- P. Pérez, D. Yepes, P. Jaque, E. Chamorro, L. R. Domingo, R. S. Rojas and A. Toro-Labbé, *Phys. Chem. Chem.*, 2015, **17**, 10715–10725.
- S. Grimme, H. Kruse, L. Goerigk, G. Erker, S. Grimme, H. Kruse, L. Goerigk and G. Erker, *Angew. Chem., Int. Ed.*, 2010, **49**, 1402–1405.
- J. Paradies, *Eur. J. Org. Chem.*, 2019, 283–294.
- P. A. Chase, T. Jurca and D. W. Stephan, *Chem. Commun.*, 2008, 1701–1703.



## Supporting Information

### Contents

General procedures .....	3
General synthesis procedure of Schiff base ligands .....	3
Salen .....	3
3,5-di-tert-butyl-salen .....	6
3,5-di-tert-butyl-salophen .....	8
General synthesis procedure of dichloro-complexes .....	10
[Sn(Salen)Cl <sub>2</sub> ] .....	10
[Sn( <sup>t</sup> Bu <sub>2</sub> Salen)Cl <sub>2</sub> ] .....	12
[Sn( <sup>t</sup> Bu <sub>2</sub> Salophen)Cl <sub>2</sub> ] .....	16
[Sn(Salophen)Cl <sub>2</sub> ] .....	18
General synthesis procedure of triflate containing complexes .....	20
[Sn( <sup>t</sup> Bu <sub>2</sub> Salen)(OTf) <sub>2</sub> ] .....	21
[Sn( <sup>t</sup> Bu <sub>2</sub> Salen)Cl(OTf)] .....	23
Gutmann-Beckett acidity measurements .....	27
Activation of HD gas .....	28
Catalyst screening .....	30
Example of Reproducibility results using [Sn(Salen)Cl <sub>2</sub> ] .....	31
Solvent screening .....	33
Reproducibility test of [Sn(Salen)Cl <sub>2</sub> ] in toluene .....	33
Temperature screening .....	35
Screening of the catalyst 2-Cl <sub>2</sub> with /without the added product(N-benzyl-2-methylpropan-2-amine) .....	36
Substrate scope .....	37
N-benzyl-2-methylpropan-2-amine .....	37
2. N-(4-chlorobenzyl)-2-methylpropan-2-amine .....	38
3. 2-methyl-N-(4-(trifluoromethyl)benzyl)propan-2-amine .....	39
4. 2-methyl-N-(4-nitrobenzyl)propan-2-amine .....	41
5. N-(3,4-dimethoxybenzyl)-2-methylpropan-2-amine .....	41
6. 2-methyl-N-(2-methylbenzyl)propan-2-amine .....	43
7. N-benzyl-1-phenylethan-1-amine .....	44
8. N-benzylcyclohexanamine .....	46
9. N-benzylhexan-1-amine .....	47
10.(E)-N-(tert-butyl)-3-phenylprop-2-en-1-amine .....	51

11. 2-methyl-N-(pyridin-3-ylmethyl)propan-2-amine.....	53
12. N-benzylpropan-2-amine.....	54
13 N-benzylaniline .....	55
14 2 N-benzyl-2,6-diisopropylaniline.....	59
15 N,2,6-triisopropylaniline .....	61
Crystal structure of [Sn(Salen)Cl <sub>2</sub> ] and [Sn( <sup>t</sup> Bu <sub>2</sub> Salophen)Cl <sub>2</sub> ] complexes.....	62
Computational Details.....	70
References .....	87

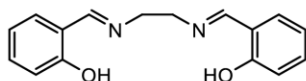
## General procedures

Solvents and chemicals were purchased from commercial suppliers (Aber, Merck, TCI, Lachner, Acros). Unless otherwise specified, solvents were dried using automatic drying system PureSolv MD5, or by storing upon activated molecular sieves and degassed by freeze-pump-thaw before use. Glassware was dried and stored in an oven heated up to 180 °C overnight. NMR spectra were measured on Bruker AVANCE-III (400 MHz) at 25 °C. Chemical shifts for  $^1\text{H}$  are given in  $\delta$  relative to tetramethylsilane (TMS) and are referenced to residual protium in the NMR solvent ( $\text{CDCl}_3$ :  $\delta = 7.26$  ppm,  $\text{DMSO-d}_6$ :  $\delta = 2.50$ ). Chemical shifts for  $^{13}\text{C}$  are given in  $\delta$  relative to TMS and are referenced to the carbon resonances in the solvent ( $\text{CDCl}_3$ :  $\delta = 77.0$  ppm,  $\text{DMSO-d}_6$ :  $\delta = 39.5$ ). Peaks of  $^{119}\text{Sn}$  NMR spectra are referenced to the external standard peak of tetramethyl-Sn (0 ppm). Peaks of  $^{19}\text{F}$  NMR spectra are referenced to the external standard peak of trifluoacetic acid (0 ppm). Mass spectrometry measurements were provided by Service centrum of Mass spectrometry at the Department of Chemistry, Charles University. Ionization method used was ESI positive and the spectra were measured in MeOH. Optimization of catalysts was performed at least in duplicate but generally in triplicate and analyzed by NMR with dibromomethane as the internal standard and structures confirmed by ESI-MS. For determination of total carbon, total nitrogen and total hydrogen were samples weighed into tin capsules (Elemental Microanalysis,  $8 \times 5$  mm) and analysed on elementar analyser with thermal conductivity detector (Flash Smart, Thermo Fisher Scientific, Bremen, Germany).

## General synthesis procedure of Schiff base ligands

The general procedure followed synthesis of the ligands according to literature<sup>1</sup>. One equivalent (eq) of the relevant diamine and 2 eq of the relevant salicylaldehyde were dissolved in EtOH. The reaction mixture was refluxed and followed by TLC (hexane : ethyl acetate, 7 : 3). After consumption of the starting materials, the reaction was left to cool down and was placed in a fridge. Solid product was filtrated, washed with ice-cold EtOH and dried in air.

Salen



50 mmol (3.34 mL) of ethylenediamine were used together with 100 mmol (10.52 mL) salicylaldehyde and 210 mL of EtOH. The mixture was refluxed for 90 min. The product was obtained in the form of yellow crystals in 95 % (12.78 g) yield.  $^1\text{H}$  NMR (400 MHz,  $\text{CDCl}_3$ )  $\delta$  13.20 (s, 2H), 8.36 (s, 2H), 7.29 (ddd,  $J = 8.3$ , 7.3, 1.7 Hz, 2H), 7.23 (dd,  $J = 7.7$ , 1.7 Hz, 2H), 6.94 (dd,  $J = 8.4$ , 1.1 Hz, 2H), 6.86 (td,  $J = 7.5$ , 1.1 Hz, 2H), 3.95 (s, 4H).  $^{13}\text{C}$  NMR (101 MHz,  $\text{CDCl}_3$ )  $\delta$  167, 161, 132, 131, 119, 119, 117, 60. ESI + ( $m/z$ ) for  $\text{C}_{16}\text{H}_{16}\text{N}_2\text{O}_2^+$  269.1, calculated 269.3.

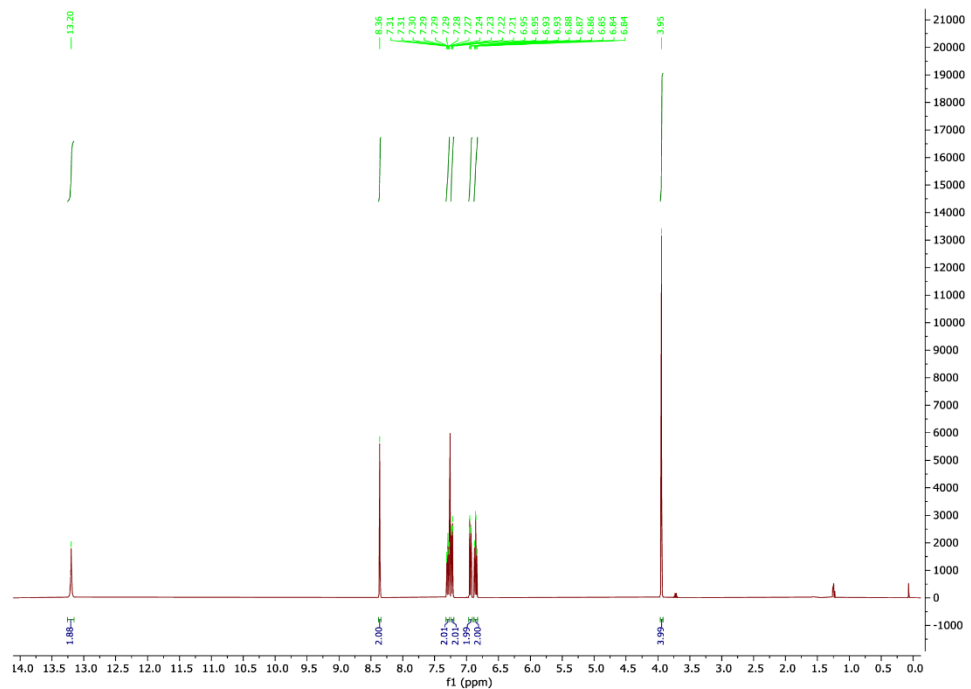


Figure 1:  $^1\text{H}$  NMR of salen in  $\text{CDCl}_3$

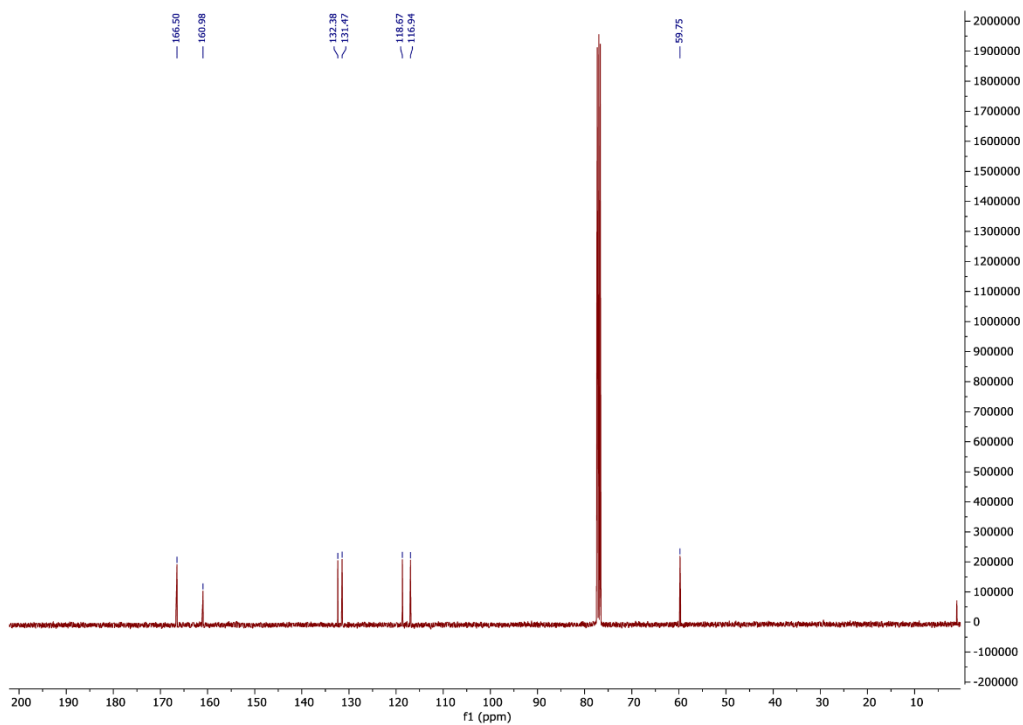


Figure 2:  $^{13}\text{C}$  NMR of salen in  $\text{CDCl}_3$

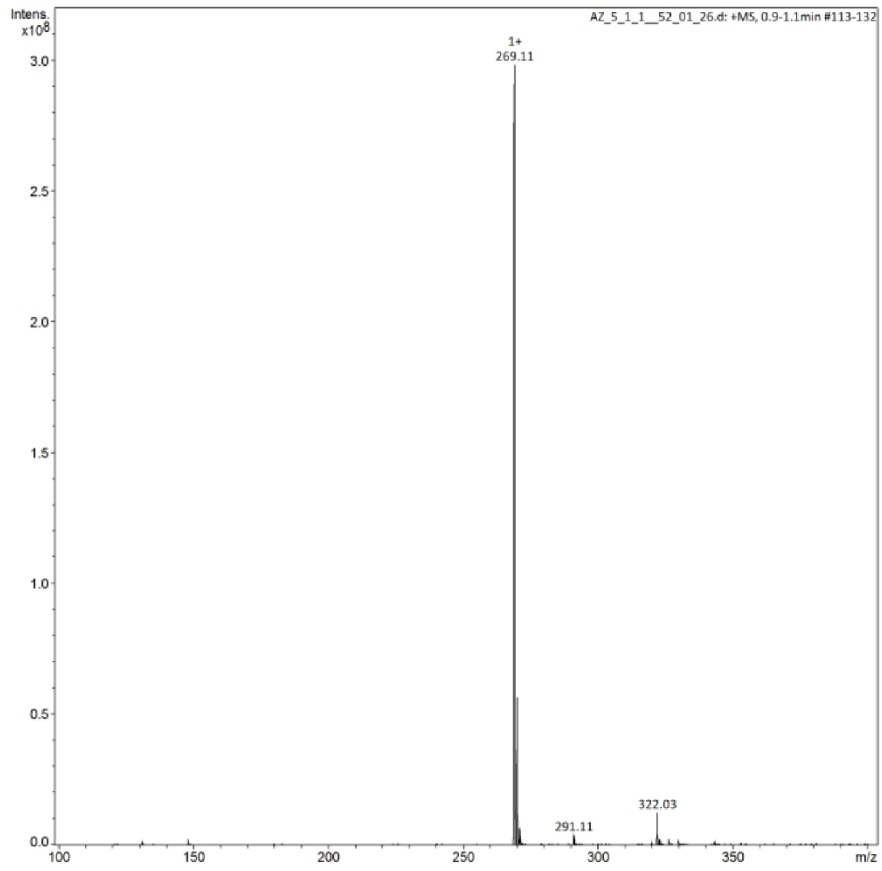


Figure 3: ESI-MS of salen



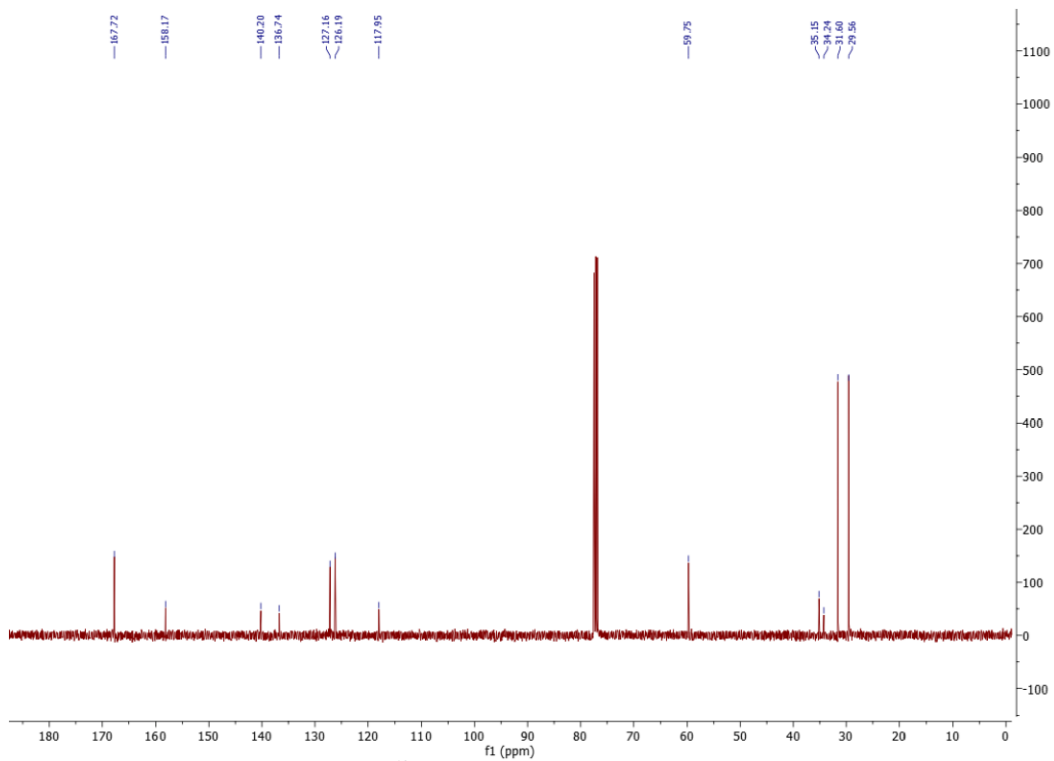


Figure 5:  $^{13}\text{C}$  NMR of 3,5-di-tert-butyl-salen in  $\text{CDCl}_3$

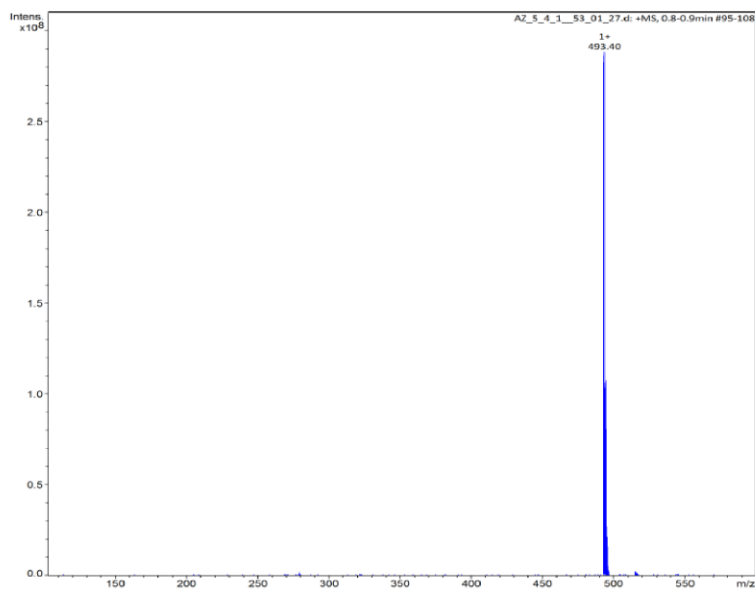
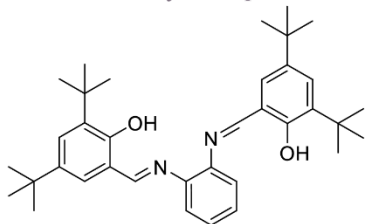


Figure 6: ESI-MS of  $^1\text{H}$  NMR of 3,5-di-tert-butyl-salen



### 3,5-di-tert-butyl-salophen



12.5 mmol (1.35 g) of phenylenediamine was used together with 25 mmol (5.86 g) 3,5-di-tert-butyl-salicylaldehyde and 105 mL of EtOH. The mixture was refluxed overnight. The product was obtained in the form of orange powder in 52 % (3.51 g) yield.  $^1\text{H NMR}$  (400 MHz,  $\text{CDCl}_3$ )  $\delta$  13.53 (s, 2H), 8.66 (s, 2H), 7.44 (d,  $J = 2.5$  Hz, 2H), 7.31 (dd,  $J = 5.9, 3.4$  Hz, 2H), 7.23 (dd,  $J = 5.9, 3.4$  Hz, 2H), 7.21 (d,  $J = 2.4$  Hz, 2H), 1.43 (s, 18H), 1.32 (s, 18H).  $^{13}\text{C NMR}$  (101 MHz,  $\text{CDCl}_3$ )  $\delta$  165, 159, 143, 140, 137, 128, 127, 127, 120, 119, 35, 34, 32, 30. ESI + ( $m/z$ ) 563.5 for  $\text{C}_{36}\text{H}_{48}\text{N}_2\text{O}_2\text{Na}^+$  and 541.5 for  $\text{C}_{36}\text{H}_{49}\text{N}_2\text{O}_2^+$ , calculated 563.4 for  $\text{C}_{36}\text{H}_{48}\text{N}_2\text{O}_2\text{Na}^+$  and 541.4 for  $\text{C}_{36}\text{H}_{49}\text{N}_2\text{O}_2^+$ .

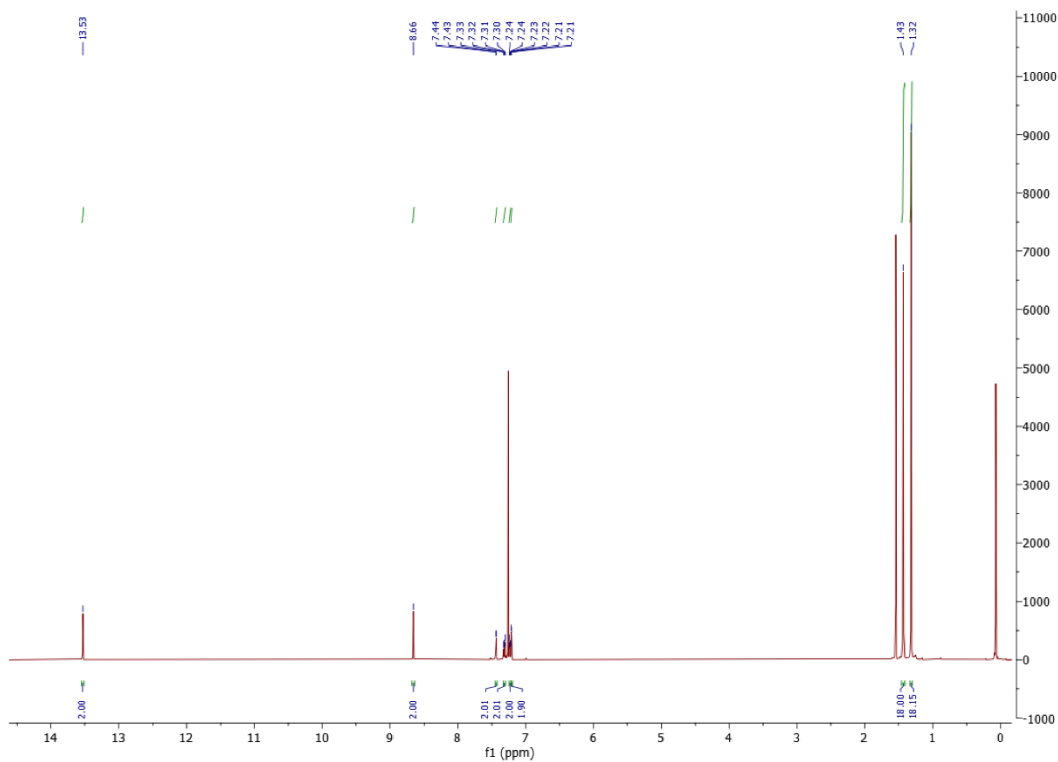


Figure 7:  $^1\text{H NMR}$  of 3,5-di-tert-butyl-salophen in  $\text{CDCl}_3$

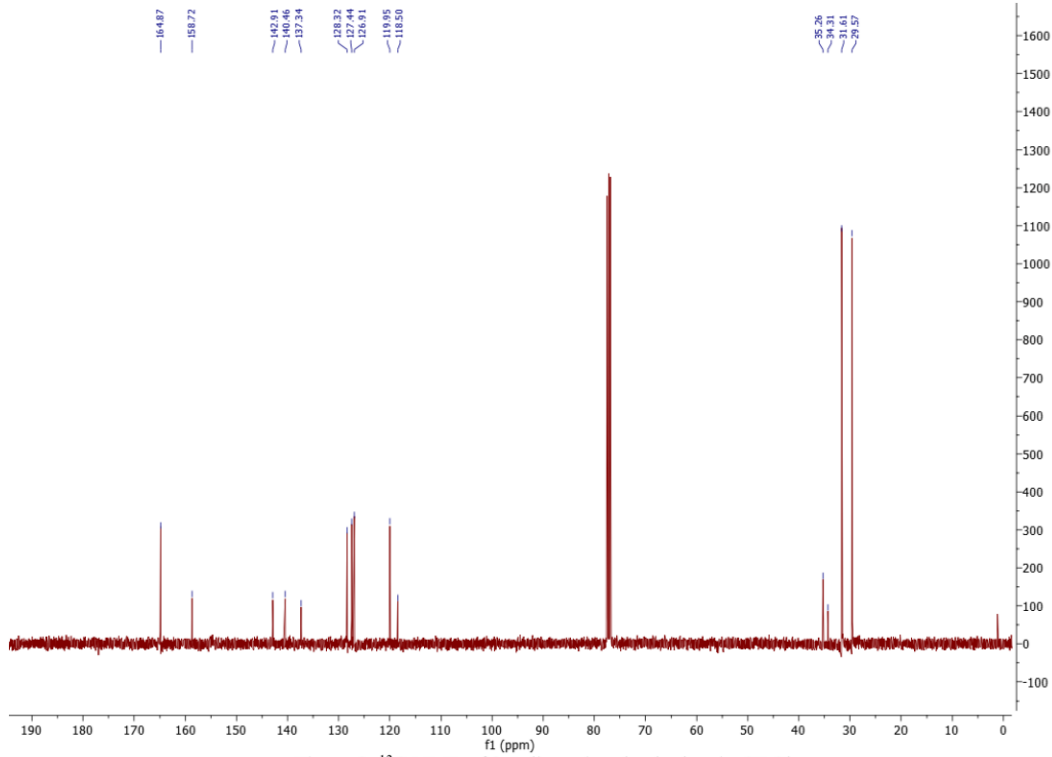


Figure 8:  $^{13}\text{C}$  NMR of 3,5-di-tert-butyl-salophen in  $\text{CDCl}_3$

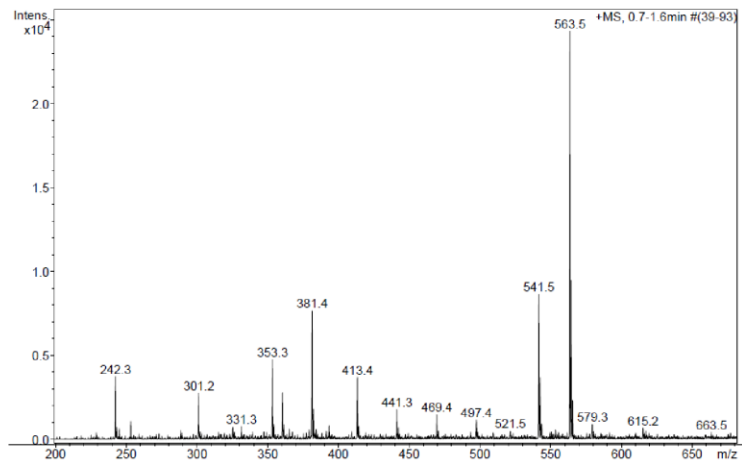


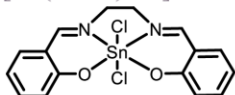
Figure 9: ESI-MS of 3,5-di-tert-butyl-salophen

## General synthesis procedure of dichloro-complexes

Complexes [Sn(Salen)Cl<sub>2</sub>] and [Sn(<sup>t</sup>Bu<sub>2</sub>Salen)Cl<sub>2</sub>] were prepared according to procedures reported in the literature<sup>2</sup>. Complexes [Sn(<sup>t</sup>Bu<sub>2</sub>Salophen)Cl<sub>2</sub>] and [Sn(Salophen)Cl<sub>2</sub>] were prepared according to a modified protocol reported for [Sn(Salen)Cl<sub>2</sub>].

Reactions were performed in an inert atmosphere of N<sub>2</sub> using Schlenk line apparatus and techniques. Solvents and glassware were dried according to the general procedures. One eq of initial ligand was dissolved in DCM. One eq of SnCl<sub>4</sub> was added to the stirring mixture followed by 2 eq of triethylamine. Reactions were followed by NMR and the reaction mixture was left to react at RT until full conversion of the starting materials occurred. Reaction work-up was performed in air and is described separately for each complex.

[Sn(Salen)Cl<sub>2</sub>]



6 mmol, (1.61 g) of salen ligand was used together with 6 mmol (0.70 mL) of SnCl<sub>4</sub>, 12 mmol (1.67 mL) of Et<sub>3</sub>N and 50 mL of DCM. The reaction was stirring for 1h. Product precipitated out of the reaction mixture and was filtrated of. The solid was washed with cold DCM and dried in vacuo. The filtrate was placed in the freezer to crash out the Et<sub>3</sub>N salt, which was filtered off. The filtrate was overlaid with pentane. Crystallised solid was washed with H<sub>2</sub>O, DCM and dried in vacuo. The solid fractions were combined to provide product as a pale-yellow powder in 54 % (1.48 g) yield. (1.12 g) yield. <sup>1</sup>H NMR (400 MHz, DMSO-d<sub>6</sub>) δ 8.79 (s, 2H, *J*(H-Sn) = 88.9), 7.53 (dd, *J* = 8.5, 6.5 Hz, 4H), 7.01 – 6.88 (m, 4H), 4.19 (s, 4H, *J*(H-Sn) = 35.9). <sup>13</sup>C NMR (101 MHz, DMSO-d<sub>6</sub>) δ 172, 165, 137, 136, 122, 119, 118, 51. <sup>119</sup>Sn NMR (149 MHz, DMSO-d<sub>6</sub>) δ -603. ESI + (*m/z*) for C<sub>16</sub>H<sub>14</sub>ClN<sub>2</sub>O<sub>2</sub>Sn<sup>+</sup> 421.0, calculated 420.9 for C<sub>16</sub>H<sub>14</sub>ClN<sub>2</sub>O<sub>2</sub>Sn<sup>+</sup>. IR 1625 cm<sup>-1</sup> ν(C=N), 1598, 1544, 1436 cm<sup>-1</sup> ν(C=C)<sub>arom</sub>, 1270 cm<sup>-1</sup> ν(C-O), 670 cm<sup>-1</sup> ν(Sn-O), 447 cm<sup>-1</sup> ν(Sn-N). Elemental. analysis: measured C 41.98%, N 6.16%, H 3.19%; calculated C 42.15%, N 6.14%, H 3.10%

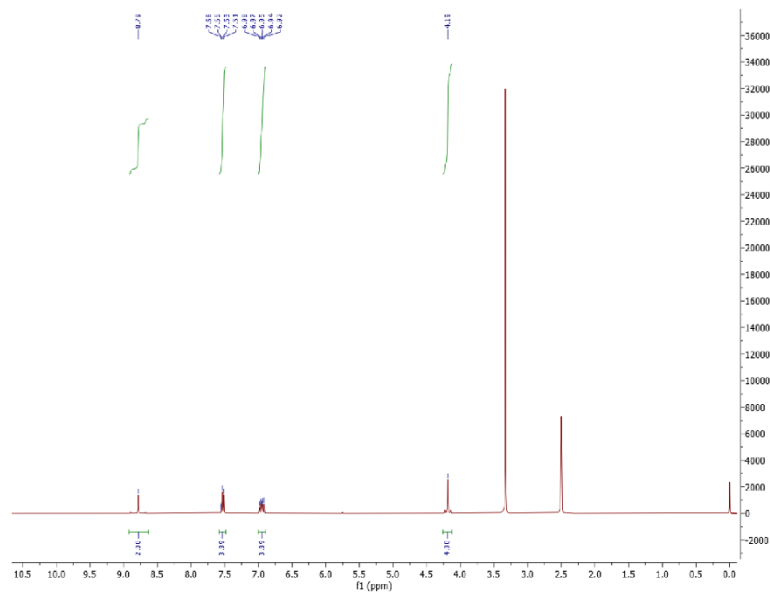


Figure 10:  $^1\text{H}$  NMR of  $[\text{Sn}(\text{Salen})\text{Cl}_2]$  in  $\text{DMSO-d}_6$

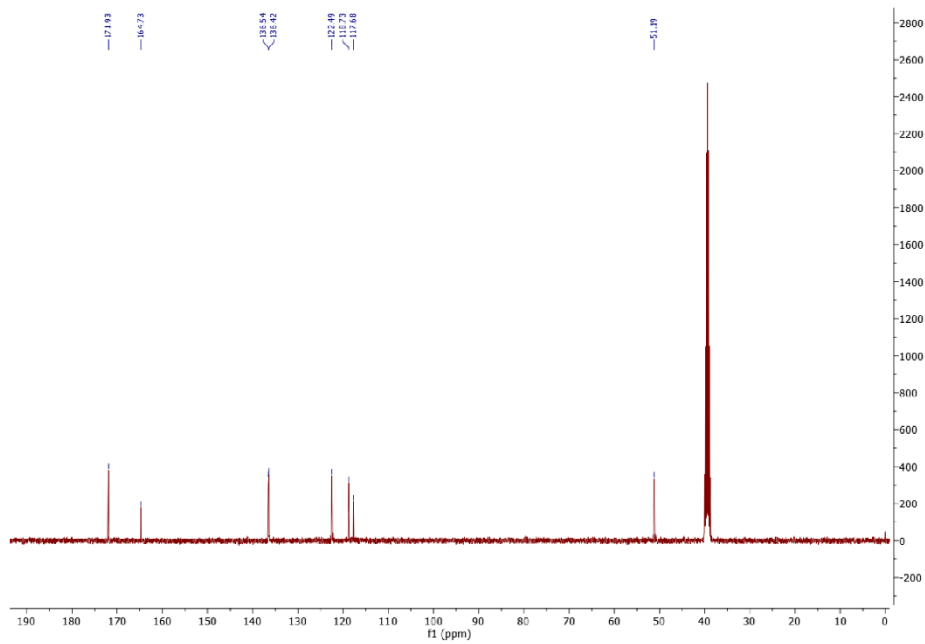


Figure 11:  $^{13}\text{C}$  NMR of  $[\text{Sn}(\text{Salen})\text{Cl}_2]$

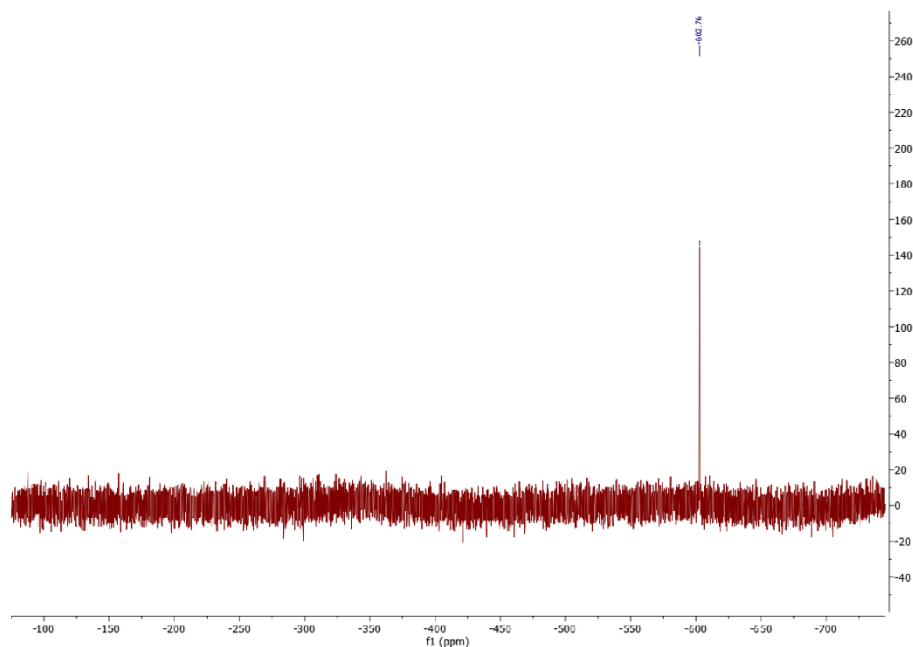


Figure 12:  $^{119}\text{Sn}$  NMR of  $[\text{Sn}(\text{Salen})\text{Cl}_2]$

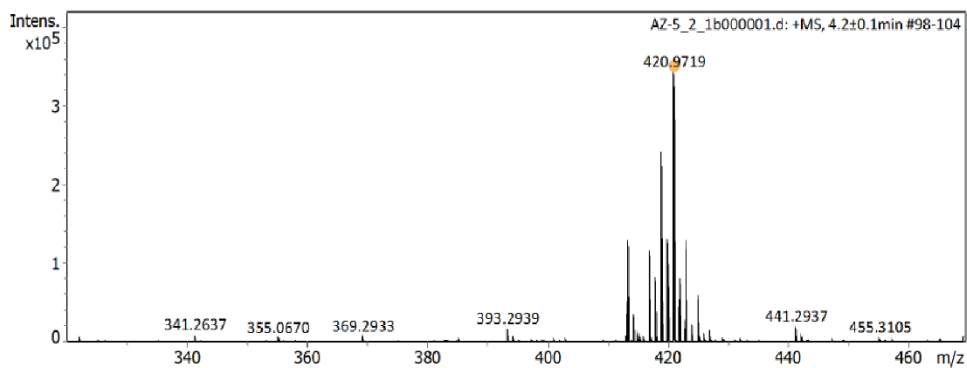
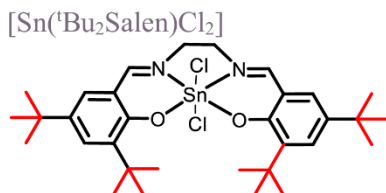


Figure 13: ESI-MS of  $[\text{Sn}(\text{Salen})\text{Cl}_2]$  after loss of chloride during ionization



7 mmol (3.45 g) of 3,5-di-tert-butyl-salen was used together with 7 mmol (0.78 mL) of  $\text{SnCl}_4$ , 14 mmol (1.95 mL) of  $\text{Et}_3\text{N}$  and 40 mL of DCM. The reaction was stirring for 3 hours. The reaction mixture was washed three times with 50 mL of water. The aqueous phase was further washed three times extracted with 15 mL of DCM. Organic phases were combined, dried over  $\text{MgSO}_4$ , filtrated and evaporated. Obtained solid was

washed with cold heptane, redissolved in  $\text{CDCl}_3$  and dried in vacuo. The product was obtained in the form of yellow powder in 90 % (4.27 g) yield.  $^1\text{H}$  NMR (400 MHz,  $\text{CDCl}_3$ )  $\delta$  8.24 (s, 2H,  $J(\text{H-Sn}) = 90.0$ ), 7.61 (d,  $J = 2.6$  Hz, 2H), 7.03 (d,  $J = 2.5$  Hz, 2H), 4.19 (s, 4H,  $J(\text{H-Sn}) = 35.6$ ), 1.51 (s, 17H), 1.30 (s, 18H).  $^{13}\text{C}$  NMR (101 MHz,  $\text{DMSO-d}_6$ )  $\delta$  172, 162, 141, 140, 131, 118, 51, 35, 34, 31, 29.  $^{119}\text{Sn}$  NMR (149 MHz,  $\text{DMSO-d}_6$ )  $\delta$  -594. ESI + ( $m/z$ ) for  $\text{C}_{33}\text{H}_{49}\text{N}_2\text{O}_3\text{Sn}^+$  641.2 and for  $\text{C}_{32}\text{H}_{47}\text{N}_2\text{O}_3\text{Sn}^+$  627.4, calculated 641.3 for  $\text{C}_{33}\text{H}_{49}\text{N}_2\text{O}_3\text{Sn}^+$  after loss of chlorides and attachment of methoxide from MeOH in the measurement and 627.3 for  $\text{C}_{32}\text{H}_{47}\text{N}_2\text{O}_3\text{Sn}^+$  after loss of chlorides and attachment of hydroxide from water in the measurement. IR  $1625\text{ cm}^{-1}$   $\nu(\text{C}=\text{N})$ ,  $1556$ ,  $1540$ ,  $1436\text{ cm}^{-1}$   $\nu(\text{C}=\text{C})_{\text{arom}}$ ,  $1247\text{ cm}^{-1}$   $\nu(\text{C}-\text{O})$ ,  $545\text{ cm}^{-1}$   $\nu(\text{Sn}-\text{O})$ ,  $468\text{ cm}^{-1}$   $\nu(\text{Sn}-\text{N})$ .

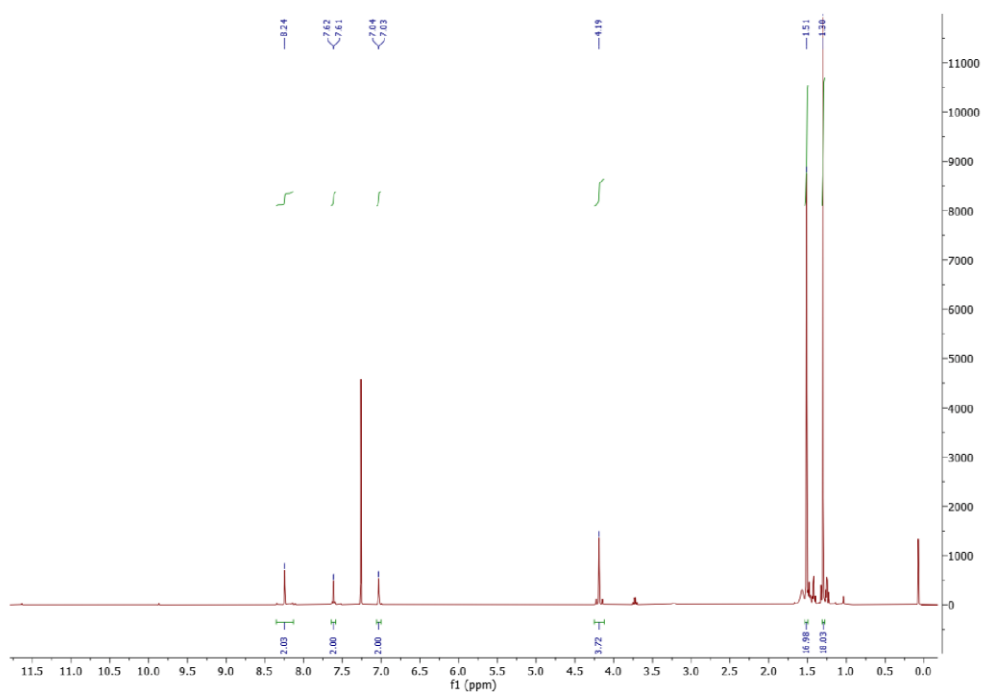


Figure 14:  $^1\text{H}$  NMR of  $[\text{Sn}(\text{}^4\text{Bu}_2\text{Salen})\text{Cl}_2]$  in  $\text{CDCl}_3$

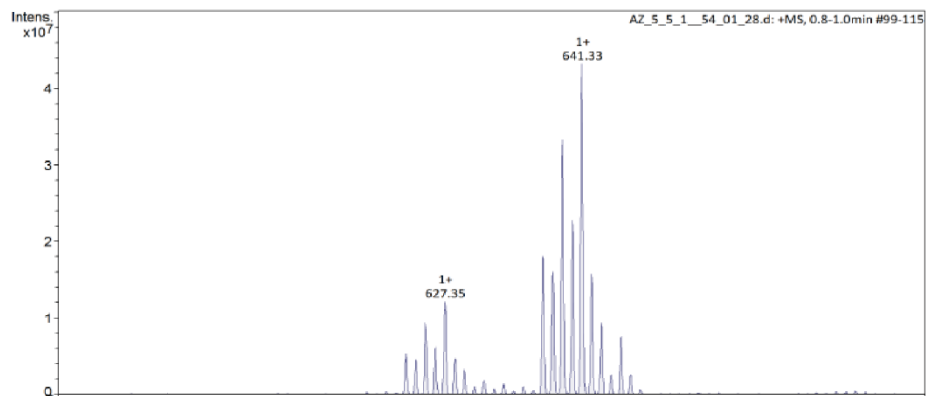


Figure 17: ESI-MS of NMR of [Sn(Bu<sub>2</sub>Salen)Cl<sub>2</sub>]

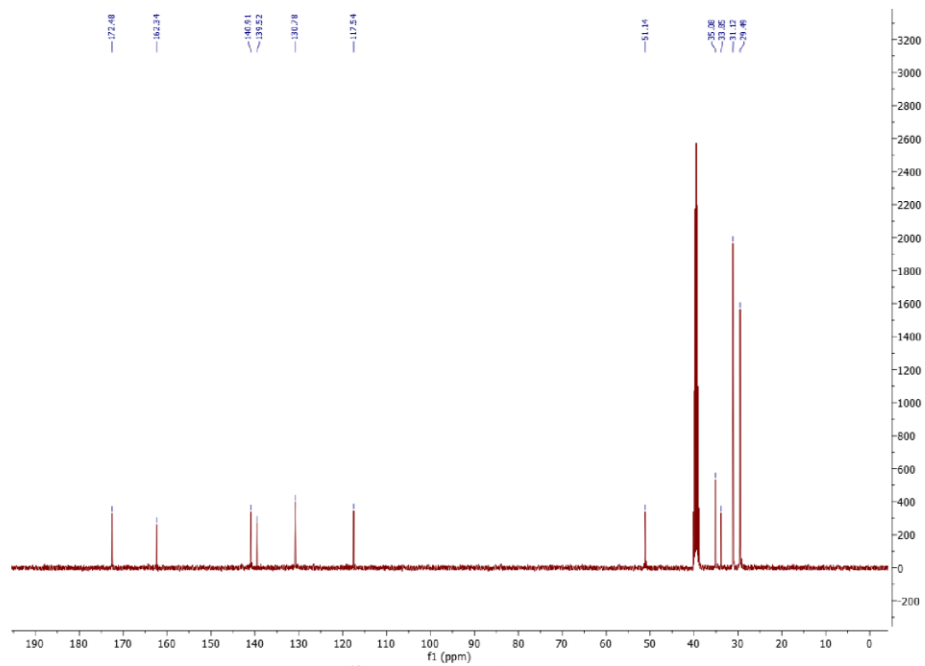


Figure 15:  $^{13}\text{C}$  NMR of  $[\text{Sn}(\text{Bu}_2\text{Salen})\text{Cl}_2]$  in  $\text{CDCl}_3$

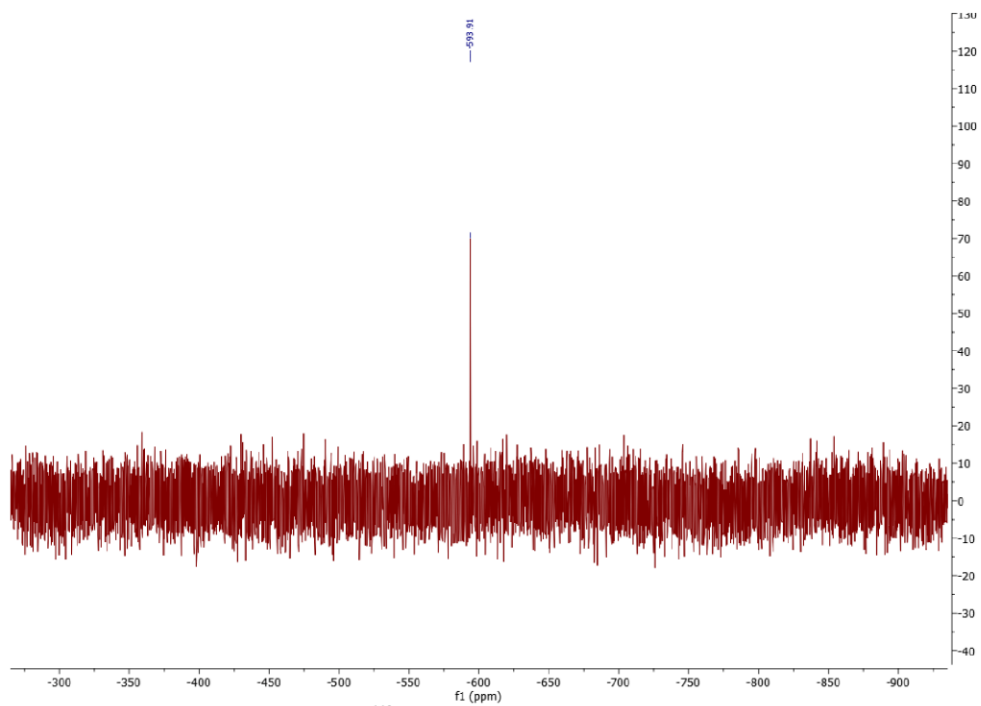
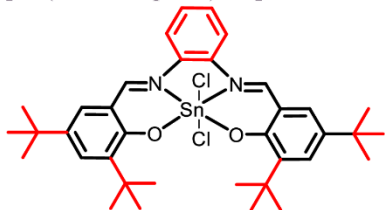


Figure 16:  $^{119}\text{Sn}$  NMR of  $[\text{Sn}(\text{Bu}_2\text{Salen})\text{Cl}_2]$  in  $\text{CDCl}_3$





1 mmol (0.54 g) of 3,5-di-tert-butyl-salophen ligand was used together with 1 mmol of SnCl<sub>4</sub> (0.11 mL), 2 mmol (0.28 mL) of Et<sub>3</sub>N and 10 mL of DCM. The reaction was stirring for 90 min. The reaction mixture was washed three times with 15 mL of water. The aqueous phase was further washed three times extracted with 30 mL of DCM. Organic phase was dried over MgSO<sub>4</sub>, filtrated and evaporated. Obtained solid was washed with cold heptane, redissolved in CDCl<sub>3</sub> and dried in vacuo. The product was obtained in the form of orange powder in 78 % (0.56 g) yield. <sup>1</sup>H NMR (400 MHz, CDCl<sub>3</sub>) δ 8.76 (s, 2H, *J*(H-Sn) = 80.0), 7.78 (dd, *J* = 6.2, 3.4 Hz, 2H), 7.74 – 7.68 (m, 2H), 7.52 (dd, *J* = 6.2, 3.4 Hz, 2H), 7.19 (d, *J* = 2.5 Hz, 2H), 1.55 (s, 18H), 1.33 (s, 19H). <sup>13</sup>C NMR (101 MHz, DMSO-d<sub>6</sub>) δ 166, 164, 142, 141, 134, 133, 133, 130, 118, 118, 36, 34, 31, 30. <sup>119</sup>Sn NMR (149 MHz, DMSO-d<sub>6</sub>) δ -589. ESI + (*m/z*) for C<sub>37</sub>H<sub>49</sub>N<sub>2</sub>O<sub>3</sub>Sn<sup>+</sup> 689.3, calculated 689.3 for C<sub>37</sub>H<sub>49</sub>N<sub>2</sub>O<sub>3</sub>Sn<sup>+</sup> after loss of chlorides and attachment of methoxide from methanol in the measurement. IR 1602 cm<sup>-1</sup> ν(C=N), 1581, 1538, 1461 cm<sup>-1</sup> ν(C=C)<sub>arom</sub>, 1180 cm<sup>-1</sup> ν(C-O), 543 cm<sup>-1</sup> ν(Sn-O), 493 cm<sup>-1</sup> ν(Sn-N).

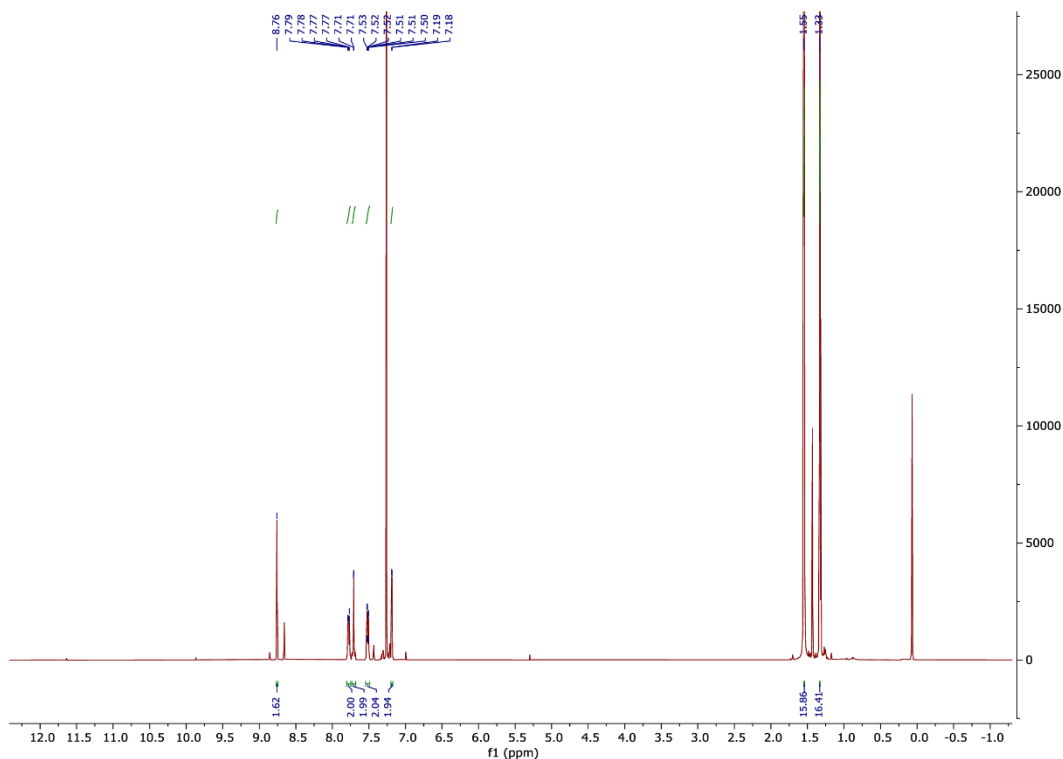


Figure 18: <sup>1</sup>H NMR of [Sn(<sup>t</sup>Bu<sub>2</sub>Salophen)Cl<sub>2</sub>] in CDCl<sub>3</sub>

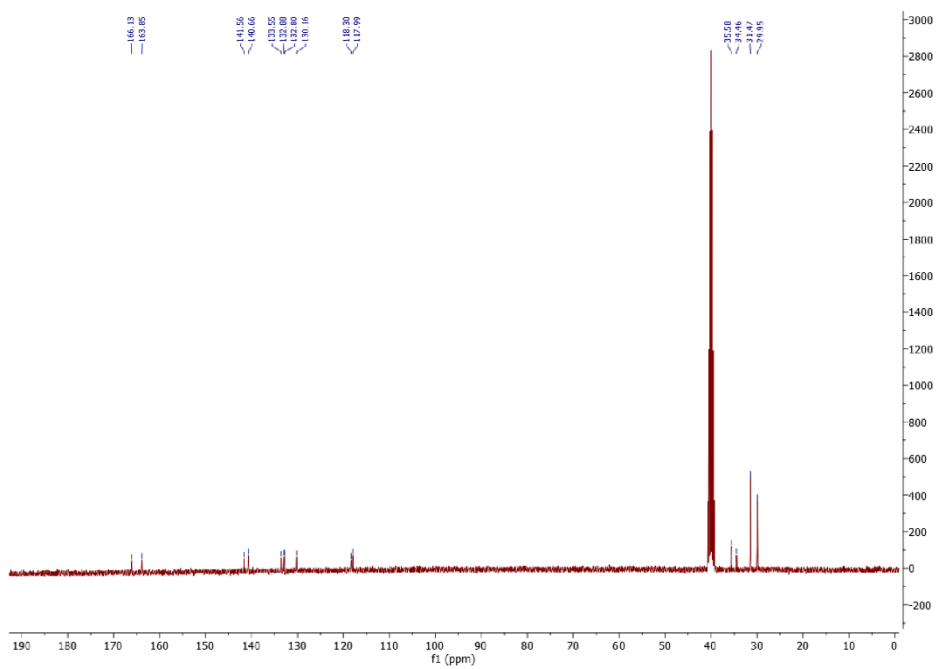


Figure 19:  $^{13}\text{C}$  NMR of  $[\text{Sn}(\text{tBu}_2\text{Salophen})\text{Cl}_2]$  in  $\text{CDCl}_3$

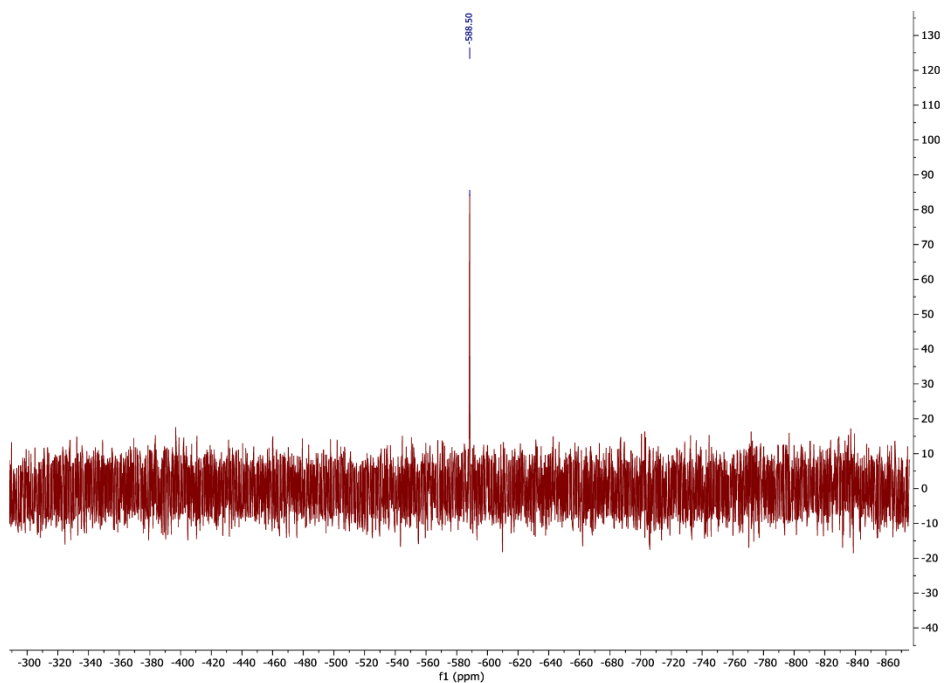


Figure 20:  $^{119}\text{Sn}$  NMR of  $[\text{Sn}(\text{tBu}_2\text{Salophen})\text{Cl}_2]$  in  $\text{CDCl}_3$

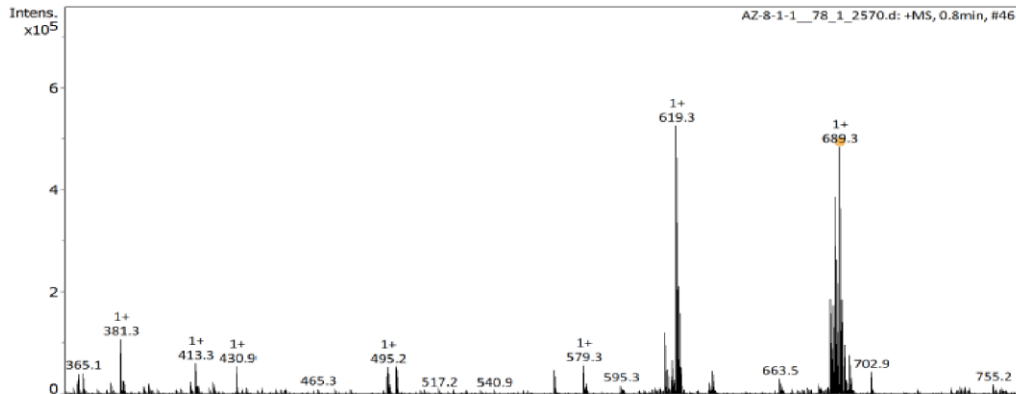
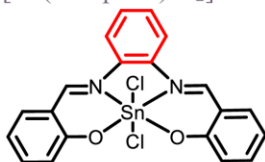


Figure 21: ESI-MS of  $[\text{Sn}(\text{Bu}_2\text{Salophen})\text{Cl}_2]$

$[\text{Sn}(\text{Salophen})\text{Cl}_2]$



1 mmol (0.32 g) of salophen ligand was used together with 1 mmol of  $\text{SnCl}_4$  (0.11 mL), 2 mmol (0.28 mL) of  $\text{Et}_3\text{N}$  and 10 mL of DCM. The reaction was stirring for 2 hours. Product precipitated out of the reaction mixture and was filtrated off. The filtrate was washed with DCM and dried in vacuo. The product was obtained in the form of orange powder in 93 % (0.47 g) yield.  $^1\text{H}$  NMR (400 MHz,  $\text{DMSO-d}_6$ )  $\delta$  9.50 (s, 2H,  $J(\text{H-Sn}) = 85.5$ ), 8.31 – 8.23 (m, 2H), 7.80 (dd,  $J = 7.9, 1.8$  Hz, 2H), 7.73 – 7.62 (m, 4H), 7.12 – 7.00 (m, 4H).  $^{13}\text{C}$  NMR (101 MHz,  $\text{DMSO-d}_6$ )  $\delta$  166, 166, 139, 139, 133, 131, 123, 120, 119, 118.  $^{119}\text{Sn}$  NMR (149 MHz,  $\text{DMSO-d}_6$ )  $\delta$  –592. ESI + ( $m/z$ ) for  $\text{C}_{21}\text{H}_{17}\text{N}_2\text{O}_3\text{Sn}^+$  465.0, calculated 465.0 for  $\text{C}_{21}\text{H}_{17}\text{N}_2\text{O}_3\text{Sn}^+$  after loss of chlorides and attachment of methoxide from methanol in the measurement. IR  $1598\text{ cm}^{-1}$   $\nu(\text{C}=\text{N})$ ,  $1573, 1535, 1461, \nu(\text{C}=\text{C})_{\text{arom}}$ ,  $1186\text{ cm}^{-1}$   $\nu(\text{C}-\text{O})$ ,  $538\text{ cm}^{-1}$   $\nu(\text{Sn}-\text{O})$ ,  $485\text{ cm}^{-1}$   $\nu(\text{Sn}-\text{N})$ .

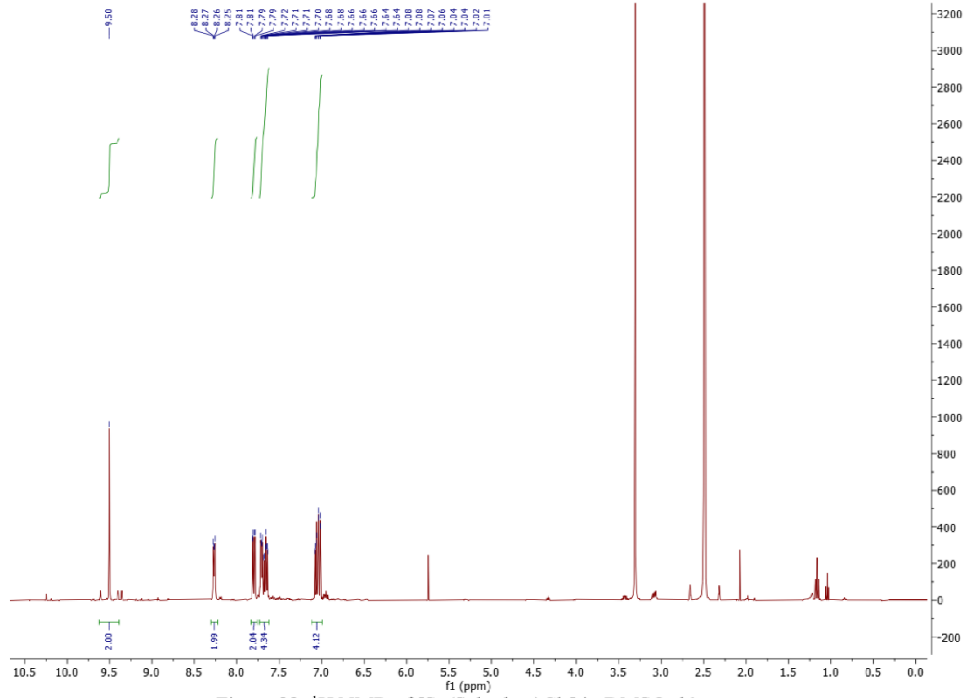


Figure 22:  $^1\text{H}$  NMR of  $[\text{Sn}(\text{Salophen})\text{Cl}_2]$  in  $\text{DMSO-d}_6$

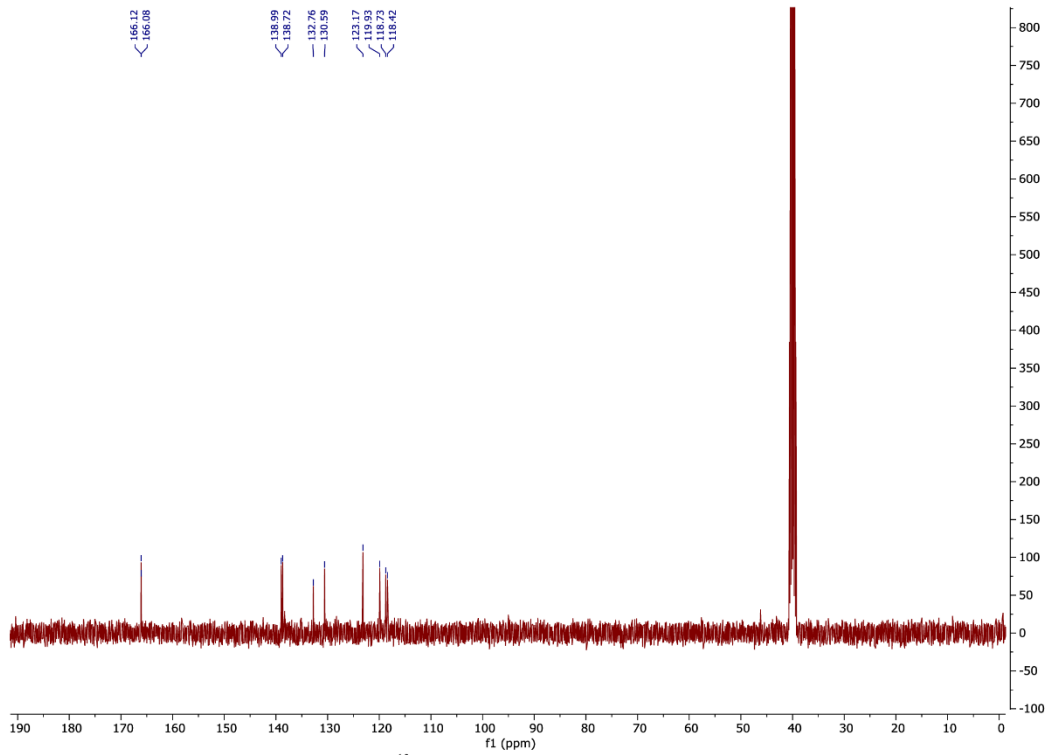


Figure 23:  $^{13}\text{C}$  NMR of  $[\text{Sn}(\text{Salophen})\text{Cl}_2]$  in  $\text{DMSO-d}_6$

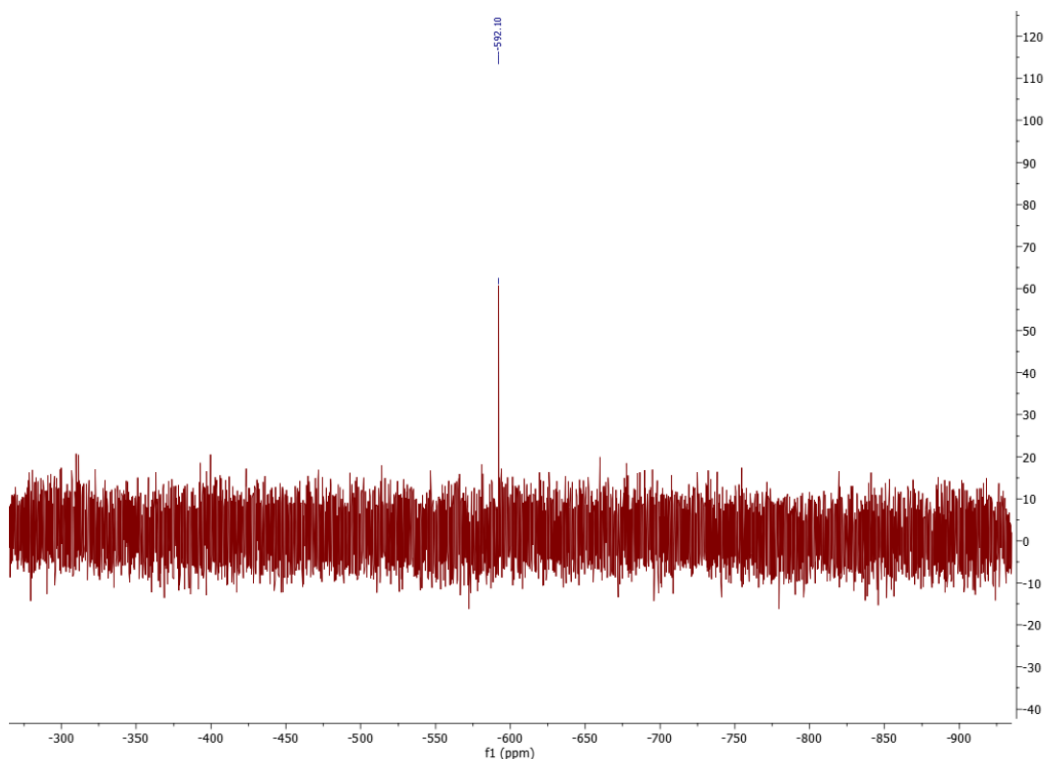


Figure 24:  $^{119}\text{Sn}$  NMR of  $[\text{Sn}(\text{Salophen})\text{Cl}_2]$  in  $\text{DMSO-d}_6$

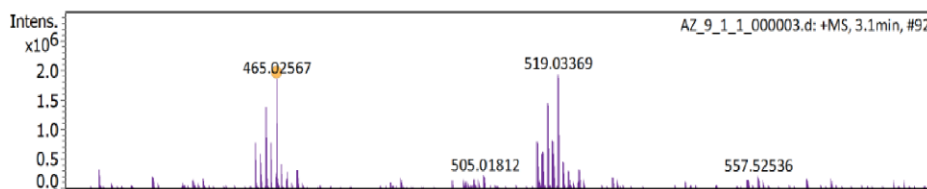


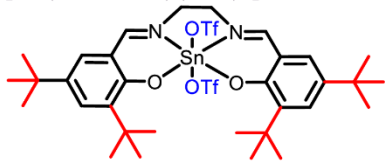
Figure 25: ESI-MS of  $[\text{Sn}(\text{Salophen})\text{Cl}_2]$ , additional peak at 519.0 represents loss of both chlorides, attachment of two methoxides and ionization via additional sodium ion.

## General synthesis procedure of triflate containing complexes

$[\text{Sn}(\text{tBu}_2\text{Salen})(\text{OTf})_2]$  was prepared according to procedures reported in the literature<sup>3</sup>.  $[\text{Sn}(\text{tBu}_2\text{Salen})\text{Cl}(\text{OTf})]$  complex was prepared by adjustment of the stoichiometry in the preparative procedure of  $[\text{Sn}(\text{tBu}_2\text{Salen})(\text{OTf})_2]$  complex.

Reactions were performed in an inert atmosphere of  $\text{N}_2$  using Schlenk line apparatus and techniques. Solvents and glassware were dried according to the general procedure mentioned above. The starting complex was dried in vacuo before use,  $\text{AgOTf}$  was heated up by heat gun under vacuum for 5 min before use. 1 eq of  $[\text{Sn}(\text{tBu}_2\text{Salen})\text{Cl}_2]$  was dissolved in DCM. For the synthesis of  $[\text{Sn}(\text{tBu}_2\text{Salen})\text{Cl}(\text{OTf})]$  and  $[\text{Sn}(\text{tBu}_2\text{Salen})(\text{OTf})_2]$  1 eq and 2 eq of  $\text{AgOTf}$  were added respectively against flow of nitrogen gas to the stirring solution. Reaction flasks were wrapped in aluminum foil. Reactions were followed by NMR and the reaction mixture was left to react at RT until full conversion of starting material. Reaction mixtures were separated from formatted solid waste by filtration via canula. The solid fractions were washed with DCM. The

solvent was evaporated, and the solid products were dried in vacuo. Products were stored and manipulated under an inert atmosphere.



1 mmol (0.68 g) of [Sn(<sup>t</sup>Bu<sub>2</sub>Salen)Cl<sub>2</sub>] was used together with 2 mmol (0.51 g) AgOTf and 125 mL of DCM. The reaction was stirred overnight. The reaction mixture was filtered via cannula and the precipitated waste was washed two times with 8 mL of DCM. After evaporation of the solvent the product was obtained in the form of yellow powder in 76 % (0.69 g) yield. <sup>1</sup>H NMR (400 MHz, CDCl<sub>3</sub>) δ 8.53 (s, 2H, *J*(H-Sn) = 110.5), 7.73 (d, *J* = 2.6 Hz, 2H), 7.13 (d, *J* = 2.6 Hz, 2H), 4.35 (s, 4H, *J*(H-Sn) = 40.4), 1.48 (s, 18H), 1.33 (s, 18H). <sup>13</sup>C NMR (101 MHz, DMSO-d<sub>6</sub>) δ 177, 162, 142, 141, 132, 132, 117, 51, 35, 34, 31, 30. <sup>119</sup>Sn NMR (149 MHz, DMSO-d<sub>6</sub>) δ -622. <sup>19</sup>F NMR (376 MHz, DMSO-d<sub>6</sub>) δ -77.75. ESI + (*m/z*) for C<sub>33</sub>H<sub>49</sub>N<sub>2</sub>O<sub>3</sub>Sn<sup>+</sup> 641.3, calculated 641.3 for C<sub>33</sub>H<sub>49</sub>N<sub>2</sub>O<sub>3</sub>Sn<sup>+</sup> after loss of triflate ligands and attachment of methoxide from the measurement. IR 1608 cm<sup>-1</sup> ν(C=N), 1542, 1438, 1346, ν(C=C)<sub>arom</sub>, 1176 cm<sup>-1</sup> ν(C-O), 630 cm<sup>-1</sup> ν(Sn-O), 512 cm<sup>-1</sup> ν(Sn-N).

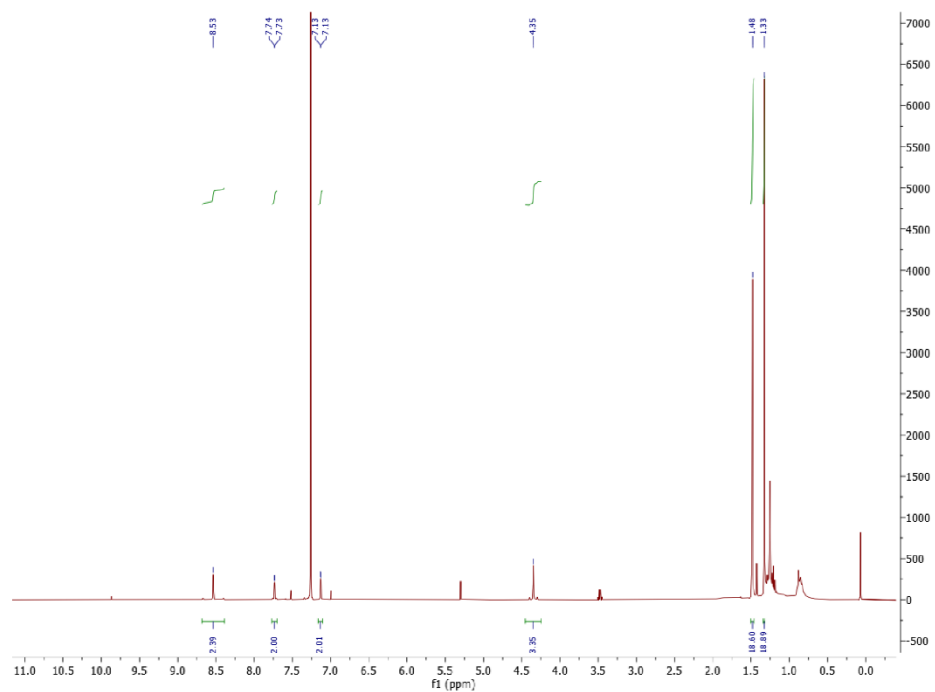


Figure 26: <sup>1</sup>H NMR of [Sn(<sup>t</sup>Bu<sub>2</sub>Salen)(OTf)<sub>2</sub>] in CDCl<sub>3</sub>.

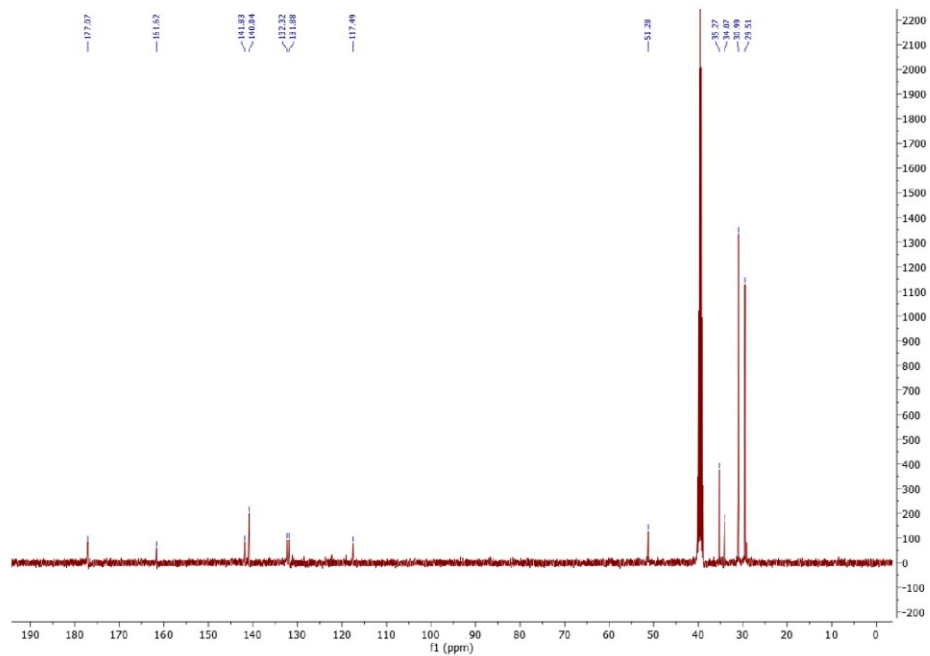


Figure 27:  $^{13}\text{C}$  NMR of  $[\text{Sn}(\text{tBu}_2\text{Salen})(\text{OTf})_2]$  in  $\text{CDCl}_3$ .

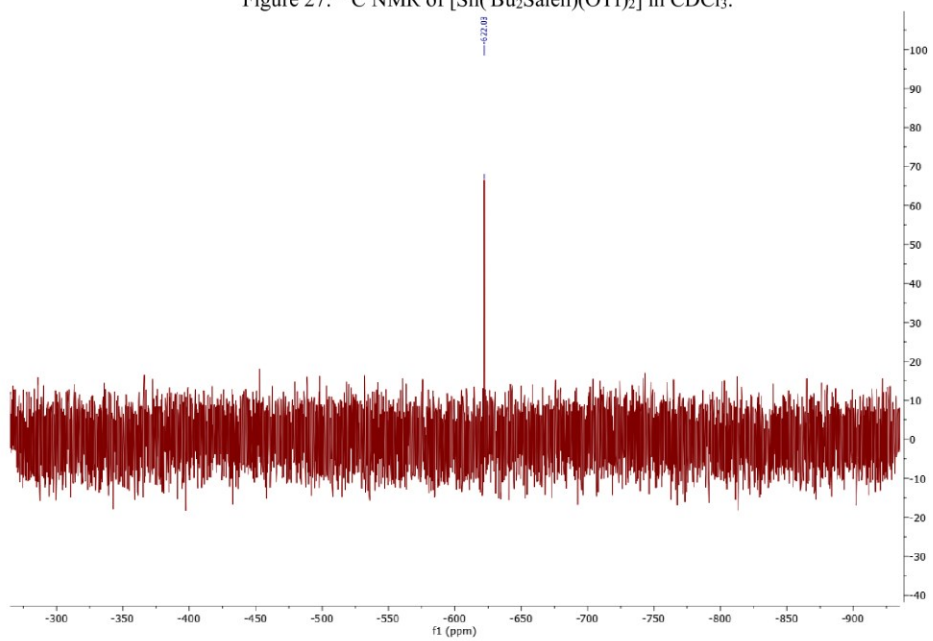


Figure 28:  $^{119}\text{Sn}$  NMR of  $[\text{Sn}(\text{tBu}_2\text{Salen})(\text{OTf})_2]$  in  $\text{CDCl}_3$ .

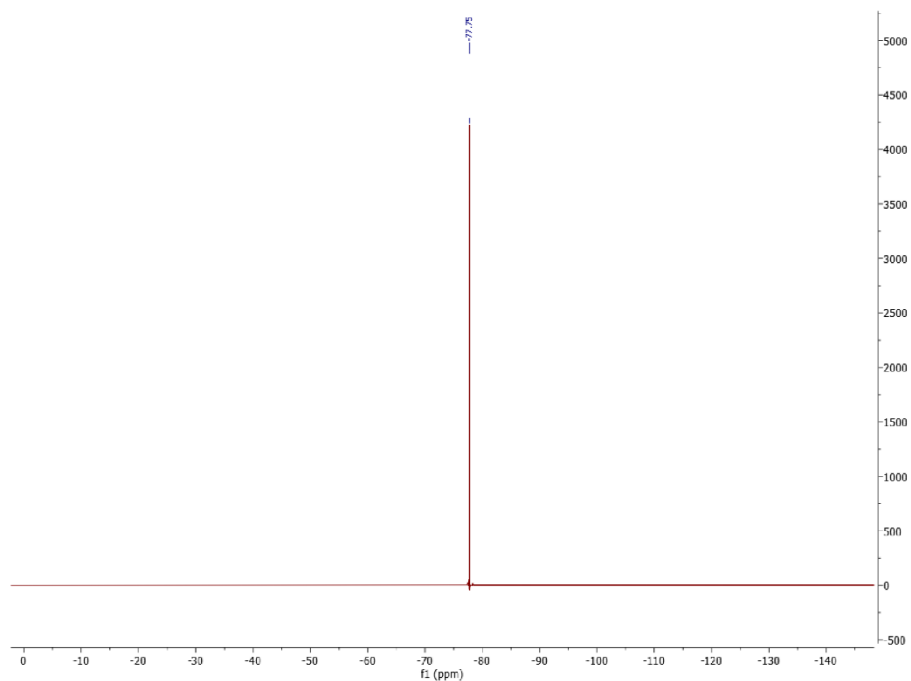


Figure 29:  $^{19}\text{F}$  NMR of  $[\text{Sn}(^4\text{Bu}_2\text{Salen})(\text{OTf})_2]$  in  $\text{CDCl}_3$ .

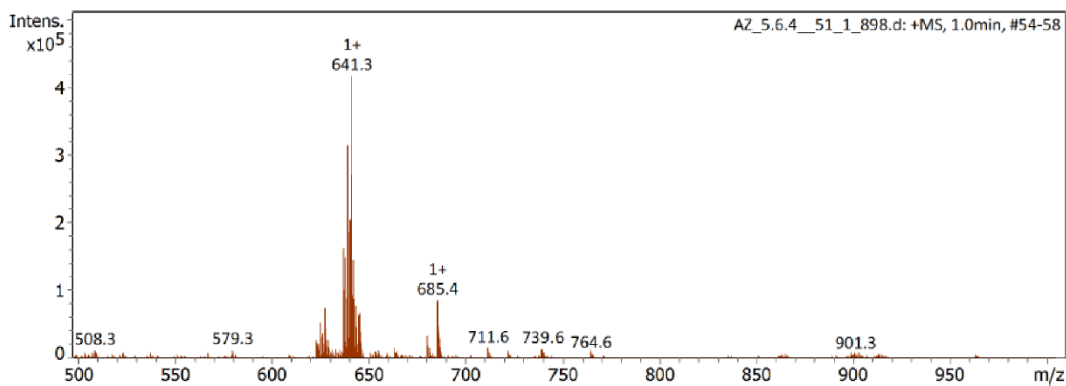
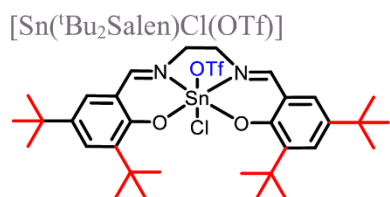


Figure 30: ESI-MS of  $[\text{Sn}(^4\text{Bu}_2\text{Salen})(\text{OTf})_2]$ .



0.5 mmol (0.34 g) of  $[\text{Sn}(^4\text{Bu}_2\text{Salen})\text{Cl}_2]$  was used together with 0.5 mmol (0.13 g)  $\text{AgOTf}$  and 40 mL of DCM. The reaction was stirred for 5 days. The reaction mixture was filtered via cannula and the precipitated waste was washed three times with 2 mL of DCM. After evaporation of the solvent, the product was obtained



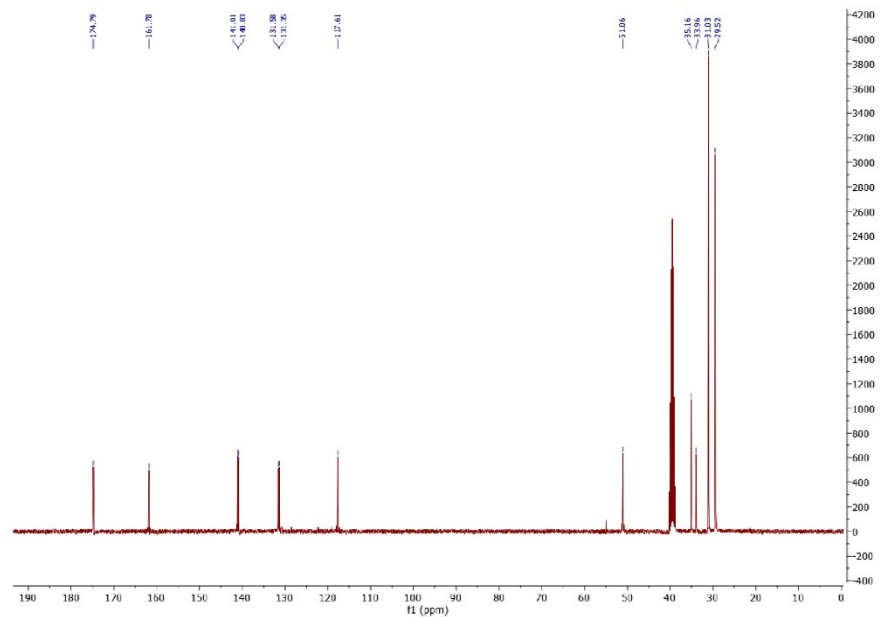


Figure 32:  $^{13}\text{C}$  NMR of  $[\text{Sn}(\text{Bu}_2\text{Salen})\text{Cl}(\text{OTf})]$  in  $\text{CDCl}_3$

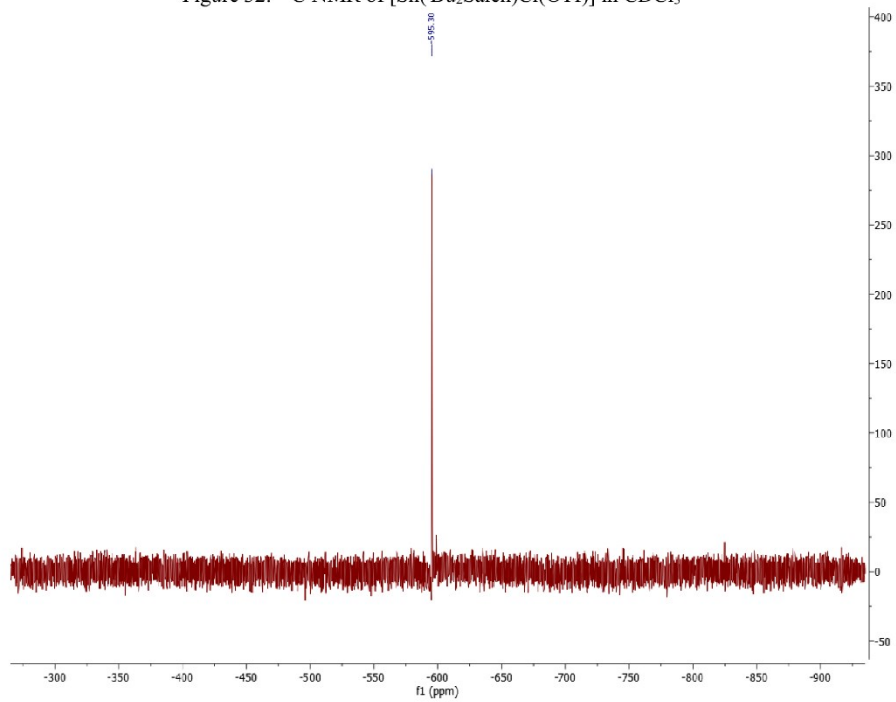


Figure 33:  $^{119}\text{Sn}$  NMR of  $[\text{Sn}(\text{Bu}_2\text{Salen})\text{Cl}(\text{OTf})]$  in  $\text{CDCl}_3$

in the form of yellow powder in 99 % (0.39 g) yield.  $^1\text{H}$  NMR (400 MHz,  $\text{CDCl}_3$ )  $\delta$  8.41 (s, 2H,  $J(\text{H-Sn}) = 95.4$ ), 7.71 – 7.61 (m, 2H), 7.10 (d,  $J = 2.5$  Hz, 2H), 4.47 – 4.25 (m, 2H), 4.24 – 4.00 (m, 2H), 1.48 (s, 18H), 1.31 (s, 20H).  $^{13}\text{C}$  NMR (101 MHz,  $\text{DMSO-d}_6$ )  $\delta$  175, 162, 141, 141, 132, 131, 118, 51, 35, 34, 31, 30.  $^{119}\text{Sn}$  NMR (149 MHz,  $\text{DMSO-d}_6$ )  $\delta$  -595.  $^{19}\text{F}$  NMR (376 MHz,  $\text{DMSO-d}_6$ )  $\delta$  -77.76. ESI + ( $m/z$ ) for  $\text{C}_{32}\text{H}_{46}\text{ClN}_2\text{O}_2\text{Sn}^+$  and  $\text{C}_{33}\text{H}_{49}\text{N}_2\text{O}_3\text{Sn}^+$  641.3, calculated 641.3 for  $\text{C}_{33}\text{H}_{49}\text{N}_2\text{O}_3\text{Sn}^+$  after loss of the triflate and chloride ligands and attachment of methoxide from the measurement. IR  $1610\text{ cm}^{-1}$   $\nu(\text{C}=\text{N})$ ,  $1540$ ,  $1461$ ,  $1440$ ,  $\nu(\text{C}=\text{C})_{\text{arom}}$ ,  $1240\text{ cm}^{-1}$   $\nu(\text{C-O})$ ,  $626\text{ cm}^{-1}$   $\nu(\text{Sn-O})$ ,  $547\text{ cm}^{-1}$   $\nu(\text{Sn-N})$ .

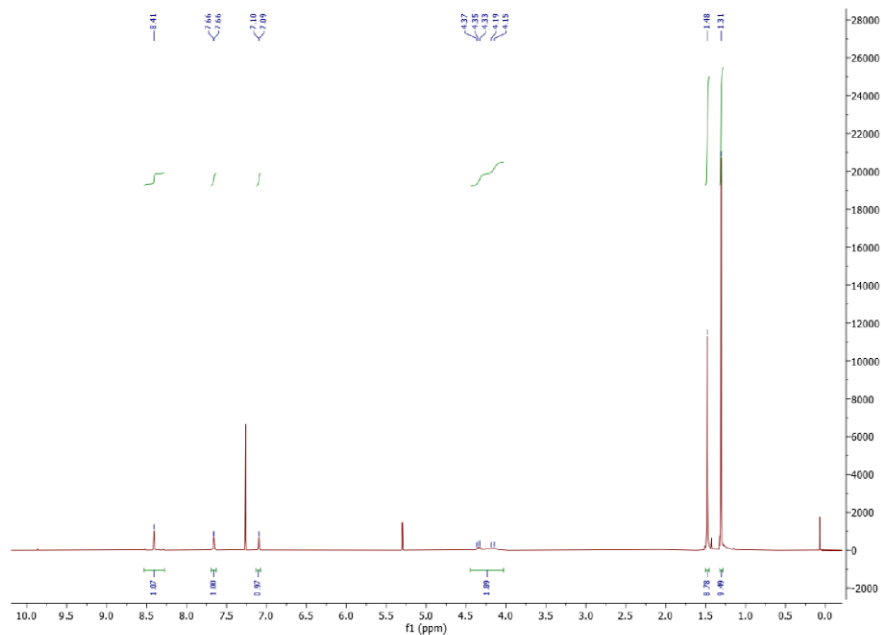


Figure 31:  $^1\text{H}$  NMR of  $[\text{Sn}(\text{tBu}_2\text{Salen})\text{Cl}(\text{OTf})]$  in  $\text{CDCl}_3$

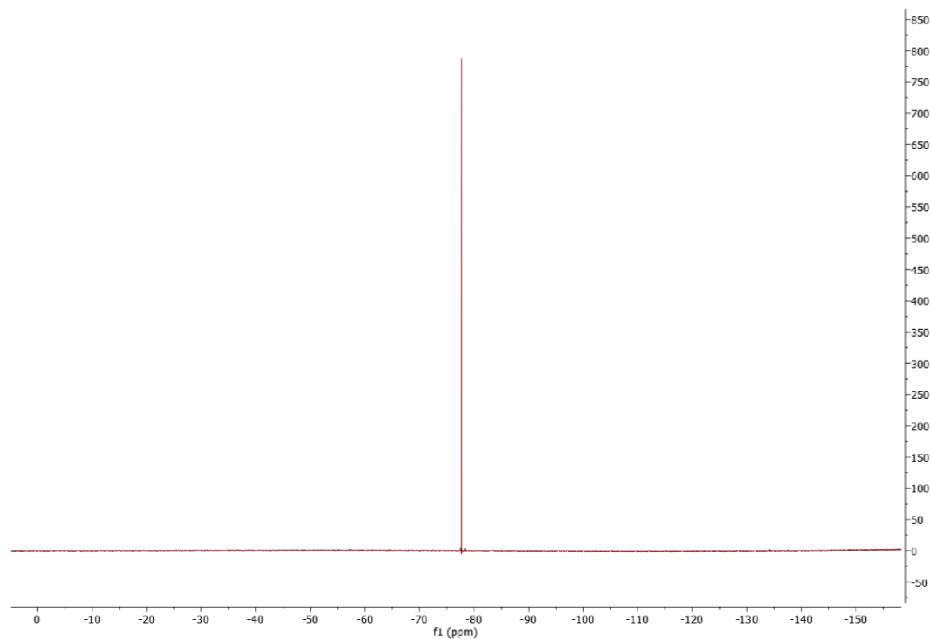


Figure 34:  $^{19}\text{F}$  NMR of  $[\text{Sn}(\text{tBu}_2\text{Salen})\text{Cl}(\text{OTf})]$  in  $\text{CDCl}_3$

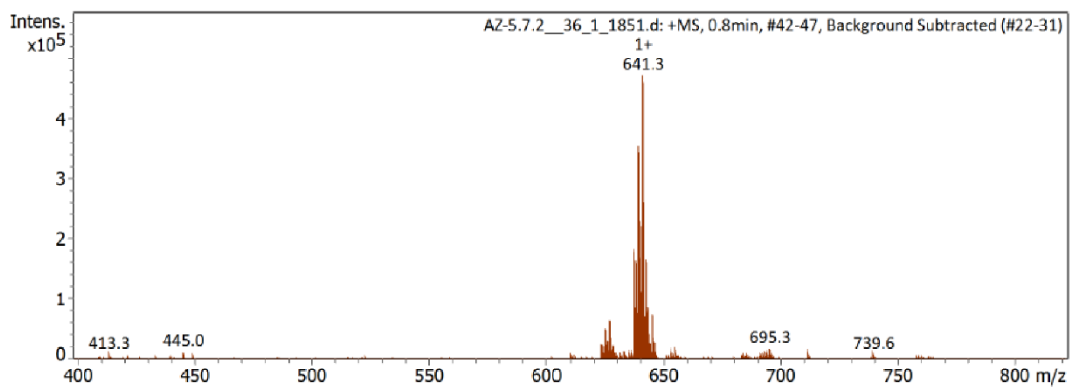


Figure 35: ESI-MS of  $[\text{Sn}(\text{tBu}_2\text{Salen})\text{Cl}(\text{OTf})]$

## Gutmann-Beckett acidity measurements

The  $^{31}\text{P}$  NMR experiments were performed under inert atmosphere in dry  $\text{CDCl}_3$ . A stock solution of  $\text{Et}_3\text{PO}$  ( $c = 0.13 \text{ M}$ ,  $0.1 \text{ mL}$ ) was added to a solution of complex with each measurement. The measurements were repeated with increasing quantity of the measured complex until the ppm of  $^{31}\text{P}$  signal of  $\text{Et}_3\text{PO}$  stopped shifting. The acceptance numbers (ANs) were calculated according to Equation 1. Experimental data and calculated values are displayed in **Error! Reference source not found.**

$$AN = 2.21 \cdot (\delta_{\text{sample}} - 41) \quad (1)$$

Table 1: NMR shifts and calculated values for Gutmann-Beckett acidity measurements.

Complex	$\delta$ [ppm]	AN
$[\text{Sn}(\text{}^t\text{Bu}_2\text{Salen})(\text{OTf})_2]$	78.8	83.6
$[\text{Sn}(\text{}^t\text{Bu}_2\text{Salen})\text{Cl}(\text{OTf})]$	73.5	71.8

## Activation of HD gas

Activation of HD gas was performed in high pressure sapphire NMR tubes. The desired complex  $[\text{Sn}(\text{Bu}_2\text{Salen})(\text{OTf})_2]$ ,  $[\text{Sn}(\text{Bu}_2\text{Salen})\text{Cl}(\text{OTf})]$  or  $[\text{Sn}(\text{Bu}_2\text{Salen})\text{Cl}_2]$  (0.01mmol) was dissolved in THF-d8 or  $\text{CDCl}_3$  (0.4 mL) and the NMR tube was pressurized with HD gas (10 bar).  $^1\text{H}$  NMR and  $^2\text{D}$  NMR were measured immediately then again after 4 hours and 17 hours. Activation of HD was observed with  $[\text{Sn}(\text{Bu}_2\text{Salen})(\text{OTf})_2]$  and  $[\text{Sn}(\text{Bu}_2\text{Salen})\text{Cl}(\text{OTf})]$  in THF-d<sub>8</sub> but not in  $\text{CDCl}_3$  confirming the necessity of the basic solvent, which acts as the FLP partner of the complex.

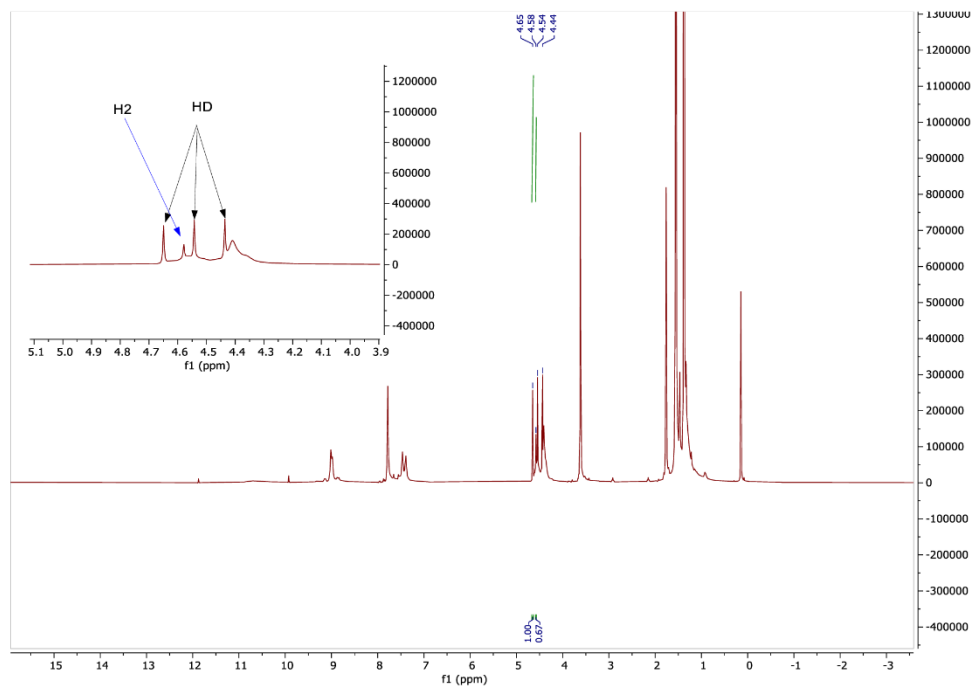


Figure 36:  $^1\text{H}$  NMR of  $[\text{Sn}(\text{Bu}_2\text{Salen})(\text{OTf})_2]$  in THF-d8 with HD gas at time 0 hrs

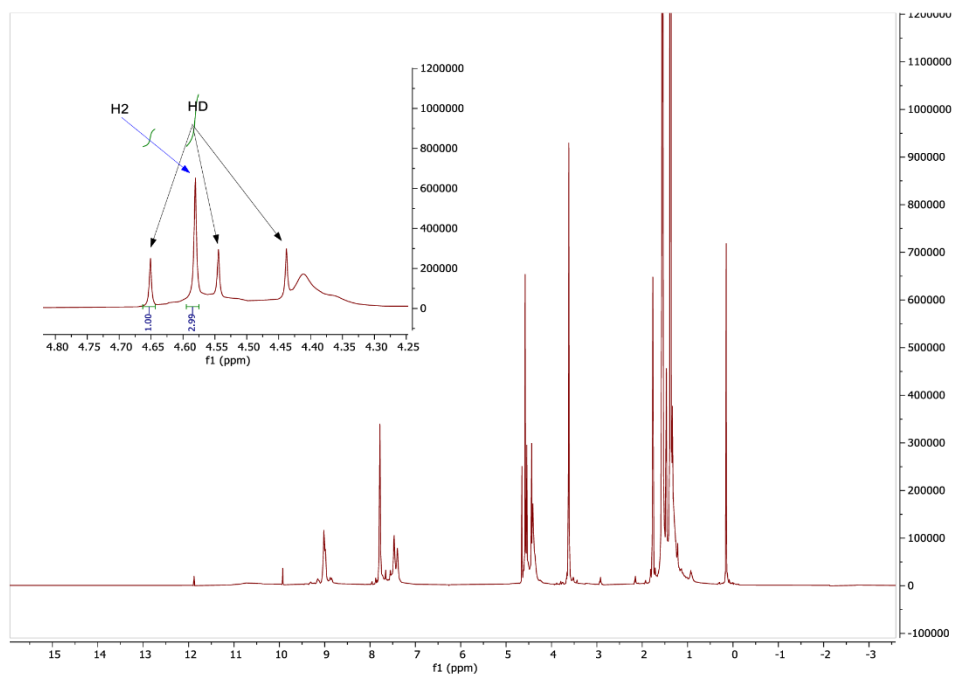


Figure 37:  $^1\text{H}$  NMR of  $[\text{Sn}(\text{'Bu}_2\text{Salen})(\text{OTf})_2]$  in  $\text{THF-d}_8$  with HD gas after 17 hrs at  $25^\circ\text{C}$

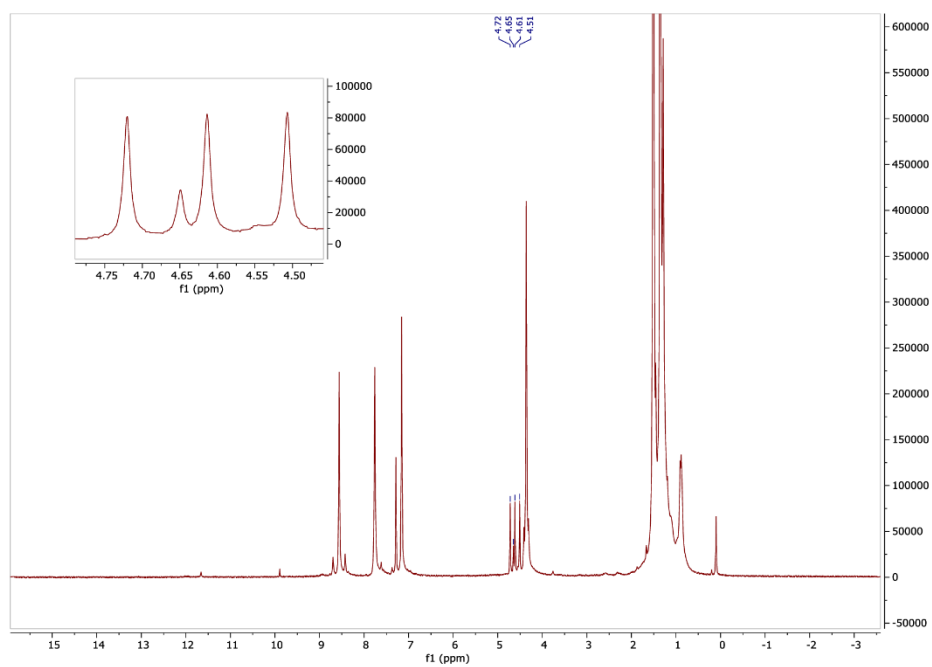


Figure 38:  $^1\text{H}$  NMR of  $[\text{Sn}(\text{'Bu}_2\text{Salen})(\text{OTf})_2]$  in  $\text{CDCl}_3$  with HD gas at time 0 hrs

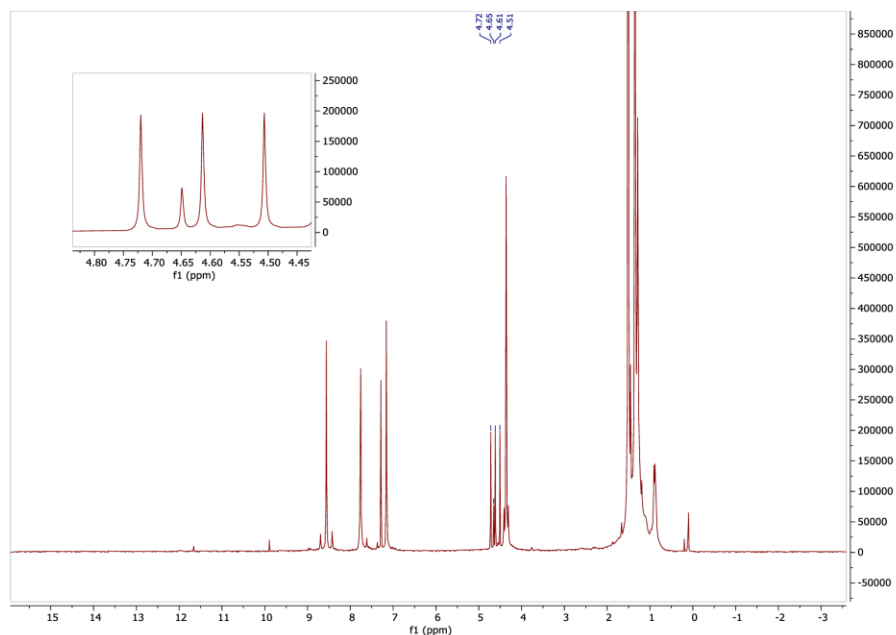


Figure 39:  $^1\text{H}$  NMR of  $[\text{Sn}(\text{'Bu}_2\text{Salen})(\text{OTf})_2]$  in  $\text{CDCl}_3$  with HD gas after 17 hrs at  $25^\circ\text{C}$

## Catalyst screening

In glove box, Salen-Sn compounds (0.5 mmol) and imine (1 mmol) were dissolved in sulfolane (4 mL) in a steel autoclave. The autoclave was then sealed and purged 3 times with the 50 bar  $\text{H}_2$ . The temperature and stirring rate were set using the Spec view program on Parr 5000 series multi reactor system.  $T = 0$  was defined as the time the heating starts. The heating was turned off 2 hours before the end of the stated reaction time and allowed to cool down under pressure over the course of the remaining 2 hours of the test i.e., for a reaction time of 17 hours the heating was turned off after 16 hours and the reaction was depressurized after the 17-hour mark. Dibromomethane (1 mmol) or in earlier tests dichloromethane was added to the reactor, stirred and an aliquot was taken for  $^1\text{H}$  NMR analysis in  $\text{CDCl}_3$ . The conversion of imine and the yield of product were quantified by  $^1\text{H}$  NMR analysis with the added Dibromo methane as the internal standard. Other reaction products were quantified by their respective  $\text{CH}_2$  signal in  $^1\text{H}$  NMR and structures confirmed by ESI spectra.

Table 2: Catalytic- test reproducibility

ENTRY	CATALYST	SOLVENT	TEMPERATURE	YIELD (cycle 1, 2, 3)
1	<b>[Sn(Salen)Cl<sub>2</sub>] (2-Cl<sub>2</sub>)</b>	sulfolane	180	50, 54, 56
2	<b>[Sn(<sup>t</sup>Bu<sub>2</sub>Salen) Cl<sub>2</sub>] (1-Cl<sub>2</sub>)</b>	sulfolane	180	25, 30, 31
3	<b>[Sn(<sup>t</sup>Bu<sub>2</sub>Salen)Cl(OTf)] (1-Cl(OTf))</b>	sulfolane	180	47, 50, 50
4	<b>[Sn(<sup>t</sup>Bu<sub>2</sub>Salen)(OTf)<sub>2</sub>] ([1-(OTf)<sub>2</sub>])</b>	sulfolane	180	9, 10, 11
5	<b>[Sn(<sup>t</sup>Bu<sub>2</sub>Salophen)Cl<sub>2</sub>] (4-Cl<sub>2</sub>)</b>	sulfolane	180	30, 24, 31
6	<b>[Sn(Salophen)Cl<sub>2</sub>] (3-Cl<sub>2</sub>)</b>	sulfolane	180	41, 45, 41

Example of Reproducibility results using [Sn(Salen)Cl<sub>2</sub>]

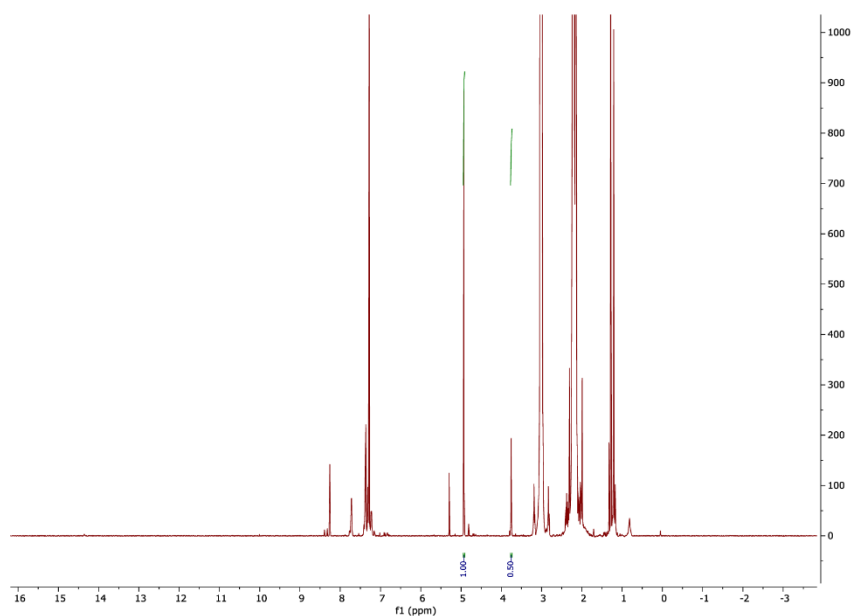


Figure 40: <sup>1</sup>H NMR of catalytic test 1 with [Sn(Salen)Cl<sub>2</sub>] with CH<sub>2</sub>Br<sub>2</sub> as internal standard



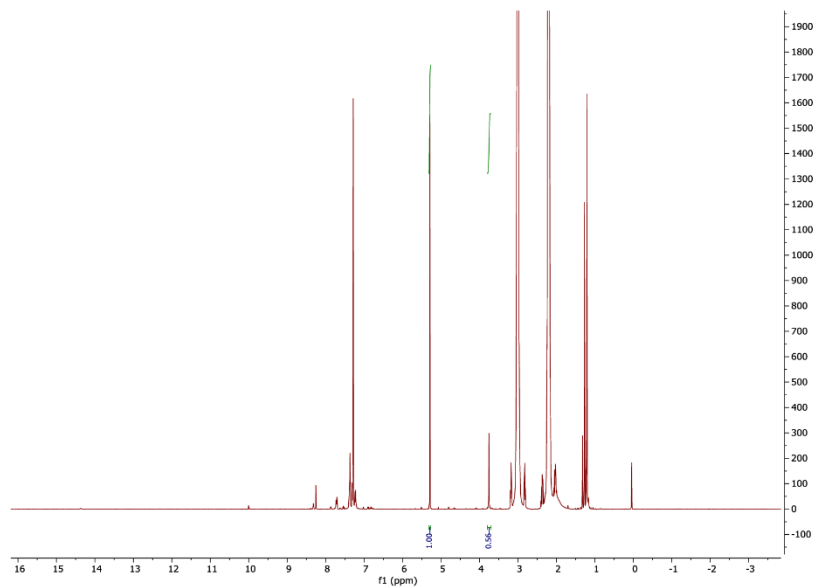


Figure 41:  $^1\text{H}$  NMR of catalytic test 2 with  $[\text{Sn}(\text{Salen})\text{Cl}_2]$  with DCM as internal standard

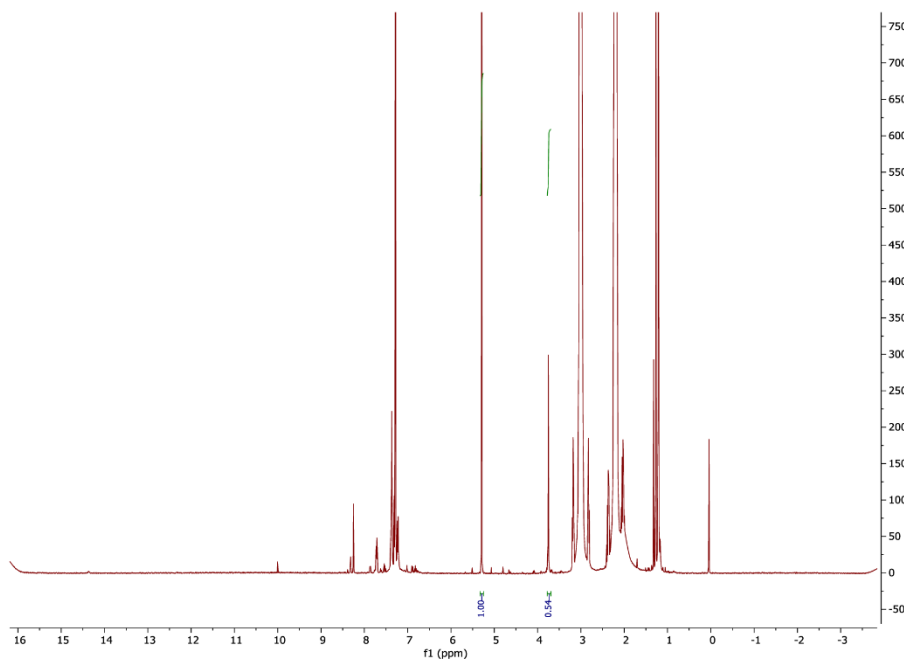


Figure 42:  $^1\text{H}$  NMR of catalytic test 3 with  $[\text{Sn}(\text{Salen})\text{Cl}_2]$  with DCM as internal standard

## Solvent screening

To determine the effect of different solvents, catalytic reduction of imine was carried out at 50 bar H<sub>2</sub> with toluene and 2,4,6-trimethylpyridine and the corresponding reproducible values are reported here.

Table 3: Solvent screening

CATALYST	SOLVENT	TEMPERATURE	YIELD
<b>[Sn(Salen)Cl<sub>2</sub>] (2-Cl<sub>2</sub>)</b>	sulfolane	180	50,54,56
<b>[Sn(Salen)Cl<sub>2</sub>] (2-Cl<sub>2</sub>)</b>	toluene	180	98,98,99
<b>[Sn(Salen)Cl<sub>2</sub>] (2-Cl<sub>2</sub>)</b>	2,4,6-trimethylpyridine	180	83,85,87
<b>[Sn(<sup>t</sup>Bu<sub>2</sub>Salen)Cl<sub>2</sub>] (1-Cl<sub>2</sub>)</b>	toluene	180	80,85,86
<b>[Sn(<sup>t</sup>Bu<sub>2</sub>Salen)Cl(OTf)] (1-Cl(OTf))</b>	toluene	180	85,86,87
<b>[Sn(<sup>t</sup>Bu<sub>2</sub>Salen)(OTf)<sub>2</sub>] (1-(OTf)<sub>2</sub>)</b>	toluene	180	27,30,32

Reproducibility test of [Sn(Salen)Cl<sub>2</sub>] in toluene

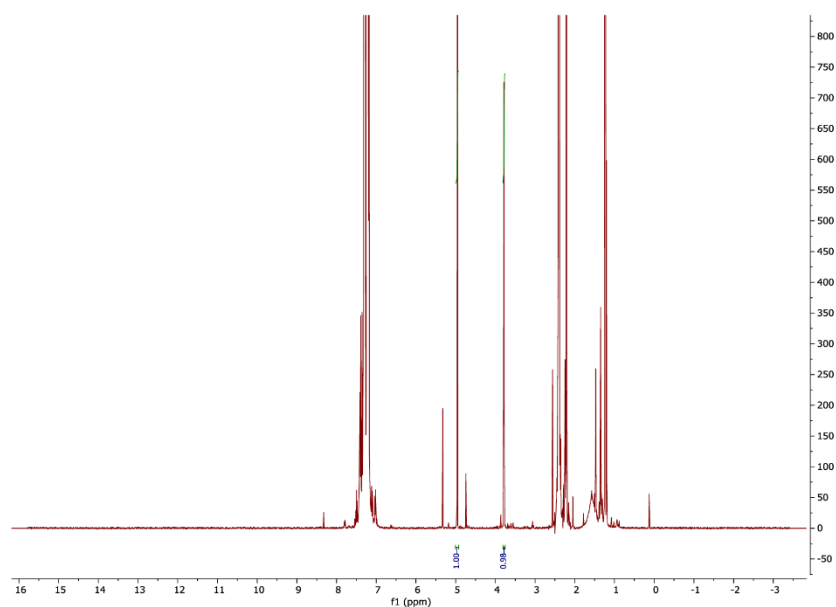


Figure 43: <sup>1</sup>H NMR of catalytic test-1 of [Sn(Salen)Cl<sub>2</sub>] in toluene, measured in CDCl<sub>3</sub>

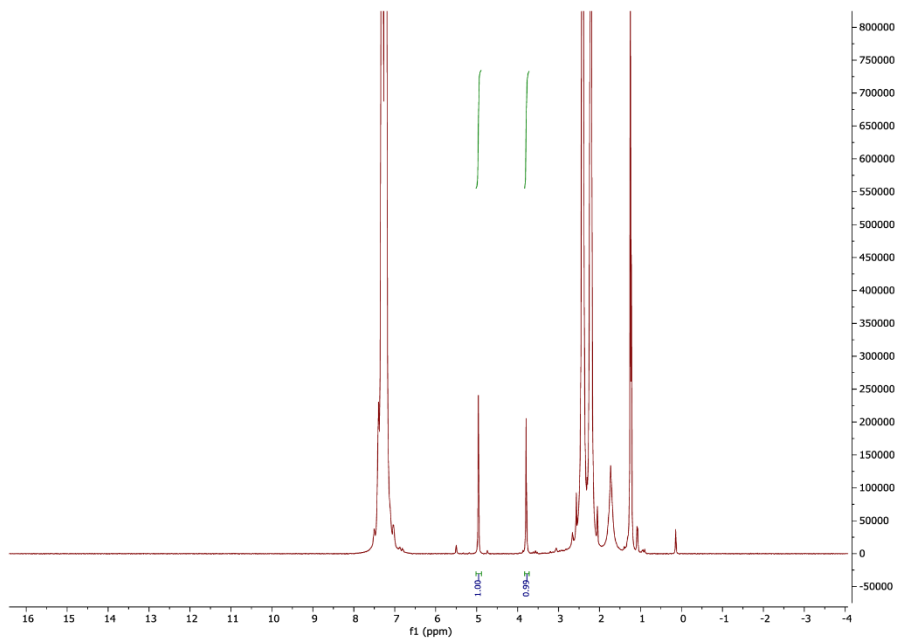


Figure 44: <sup>1</sup>H NMR of catalytic test-2 of [Sn(Salen)Cl<sub>2</sub>] in toluene, measured in CDCl<sub>3</sub>

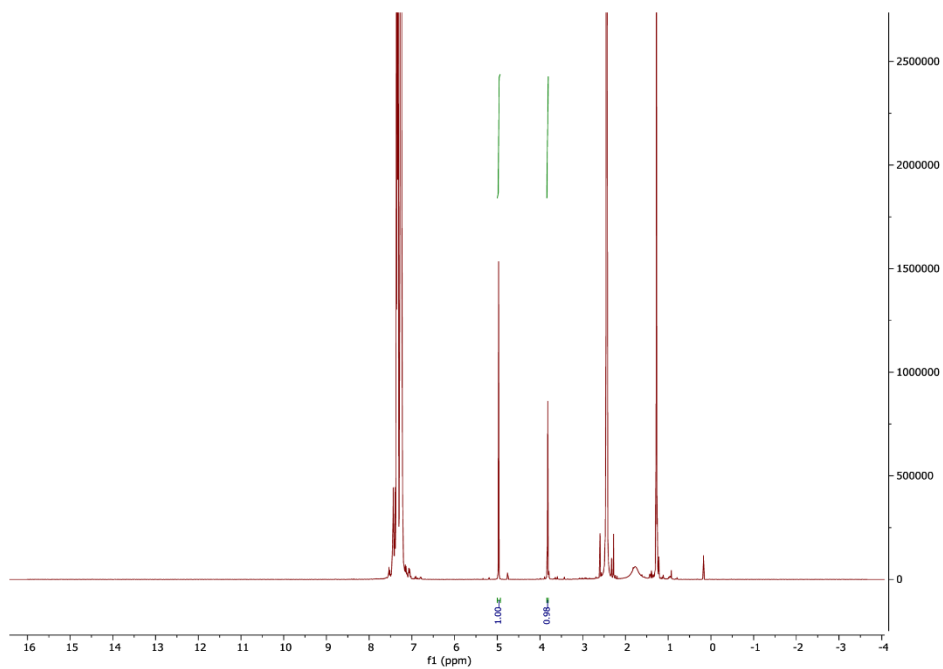


Figure 45: <sup>1</sup>H NMR of catalytic test-3 of [Sn(Salen)Cl<sub>2</sub>] in toluene, measured in CDCl<sub>3</sub>

## Temperature screening

Table 4: Temperature screening

CATALYST	SOLVENT	TEMPERATURE	YIELD
[Sn(Salen)Cl <sub>2</sub> ] (2-Cl <sub>2</sub> )	Toluene	180	98,98,99
[Sn(Salen)Cl <sub>2</sub> ] (2-Cl <sub>2</sub> )	Toluene	150	25,26,30
[Sn(Salen)Cl <sub>2</sub> ] (2-Cl <sub>2</sub> )	2,4,6-trimethylpyridine	180	83,85,87
[Sn(Salen)Cl <sub>2</sub> ] (2-Cl <sub>2</sub> )	2,4,6-trimethylpyridine	150	25,25,28
[Sn( <sup>t</sup> Bu <sub>2</sub> Salen)Cl <sub>2</sub> ] (1-Cl <sub>2</sub> )	toluene	180	80,85,86
[Sn( <sup>t</sup> Bu <sub>2</sub> Salen)Cl <sub>2</sub> ] (1-Cl <sub>2</sub> )	toluene	150	NR
[Sn( <sup>t</sup> Bu <sub>2</sub> Salen)Cl(OTf)] (1-Cl(OTf))	toluene	150	NR

# Screening of the catalyst $2\text{-Cl}_2$ with /without the added product (N-benzyl-2-methylpropan-2-amine)

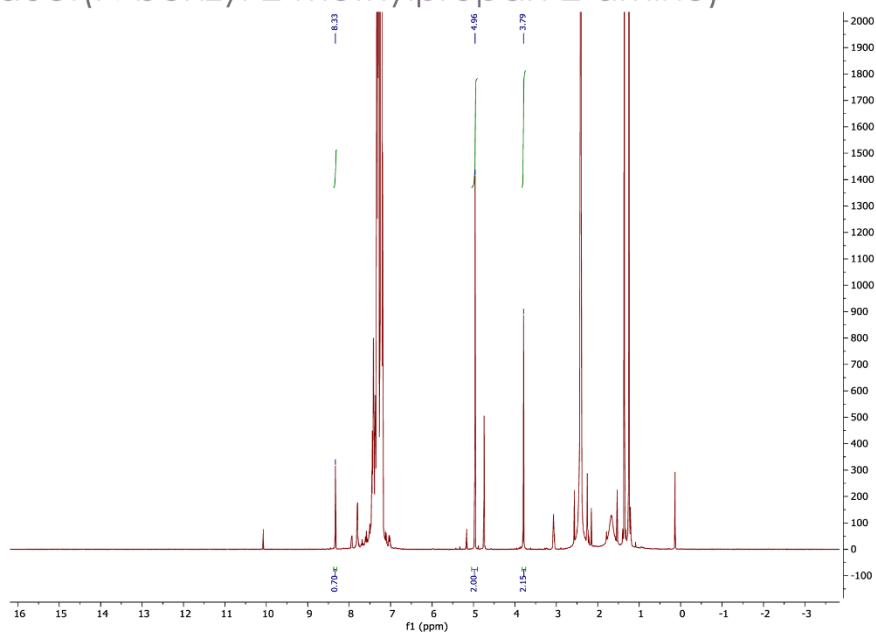


Figure 46: Test with 1mmole of added product using dibromo methane as internal standard

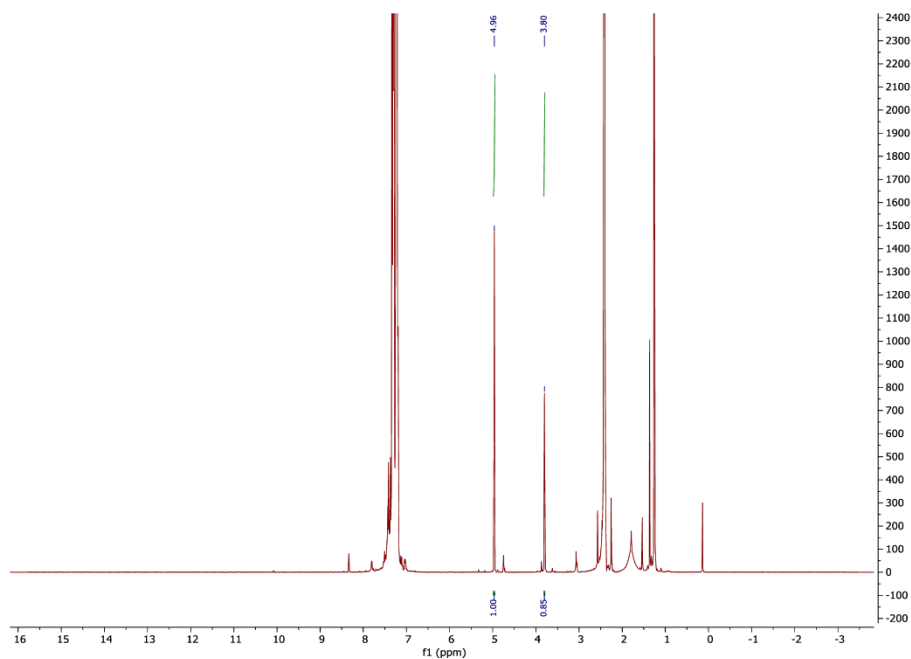


Figure 47: Test without the added product using dibromo methane as internal standard

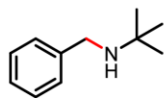
## Substrate scope

### General procedure for imine synthesis<sup>4-8</sup>

Different substituted Benzaldehydes were added to a Schlenk flask. 2eq of the respective amine was added dropwise under N<sub>2</sub> atmosphere in the presence of molecular sieves. the reaction was kept stirring overnight at room temperature. Next day the excess amine was evaporated under reduced pressure. It was then kept under vacuum overnight to obtain analytically pure imine.

### N-benzyl-2-methylpropan-2-amine

The corresponding imine was synthesized according to the reported procedures from literature.<sup>4</sup> Imine characterization: <sup>1</sup>H NMR (400 MHz, Chloroform-*d*) δ 8.34 (s, 1H), 7.91 – 7.77 (m, 2H), 7.57 – 7.40 (m, 3H), 1.37 (s, 9H).



<sup>1</sup>H NMR (400MHz, CDCl<sub>3</sub>): Product peak at 3.78 ppm All other product peaks were obscured by reaction solvent. ESI(+H): expected 163.3 (M+H), found 162.0

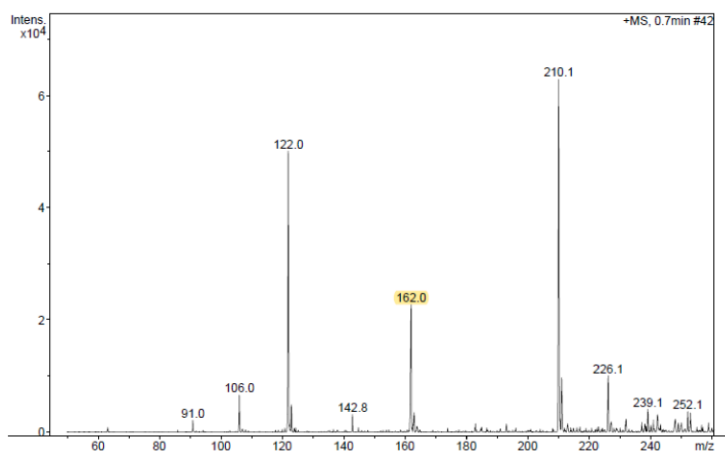


Figure 48:ESI-MS of N-benzyl-2-methylpropan-2-amine

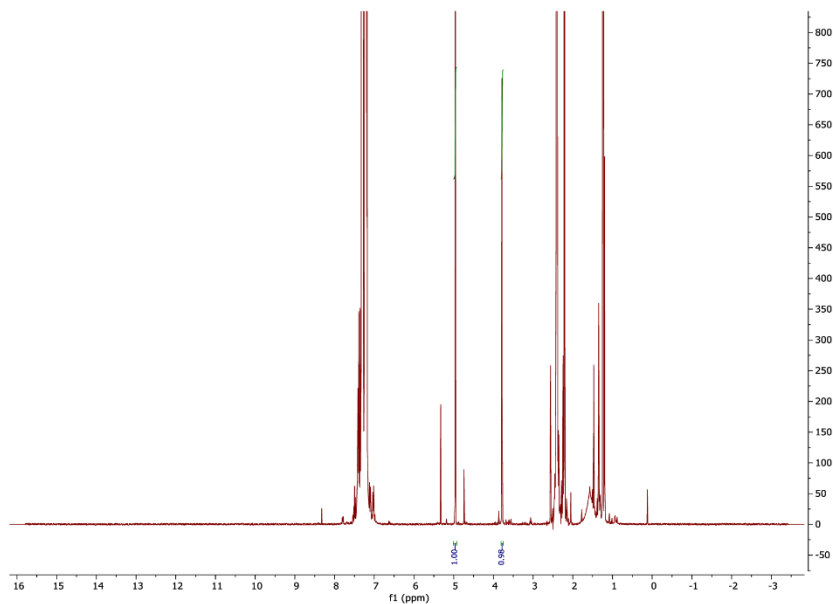
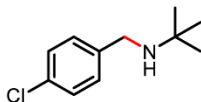


Figure 49:  $^1\text{H}$  NMR IN  $\text{CDCl}_3$  FOR N-benzyl-2-methylpropan-2-amine using  $\text{CH}_2\text{Br}_2$  as internal standard

## 2. N-(4-chlorobenzyl)-2-methylpropan-2-amine

The corresponding imine was synthesized according to the reported procedure.<sup>4</sup> Imine characterization:  $^1\text{H}$  NMR (400 MHz, Chloroform-d)  $\delta$  8.25 (s, 1H), 7.73 – 7.67 (m, 2H), 7.41 – 7.36 (m, 2H), 1.31 (s, 9H)



$^1\text{H}$  NMR (400MHz,  $\text{CDCl}_3$ ): product peak 3.75ppm (-CH<sub>2</sub> peak). All other product peaks were obscured by reaction solvent. ESI(+H): expected 198.09, found 198.1(M+H)

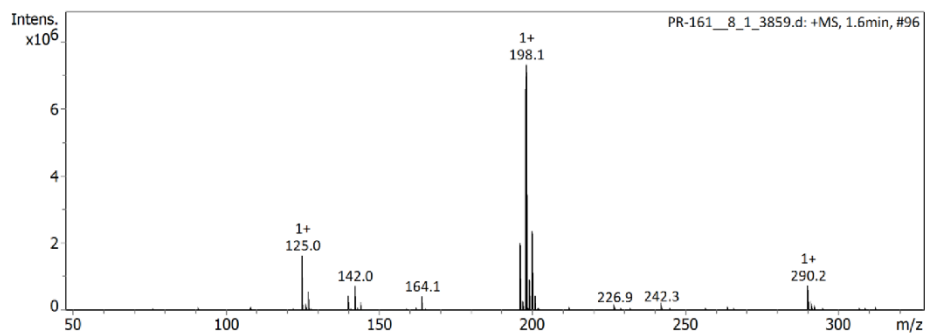


Figure 50: ESI-MS of N-(4-chlorobenzyl)-2-methylpropan-2-amine

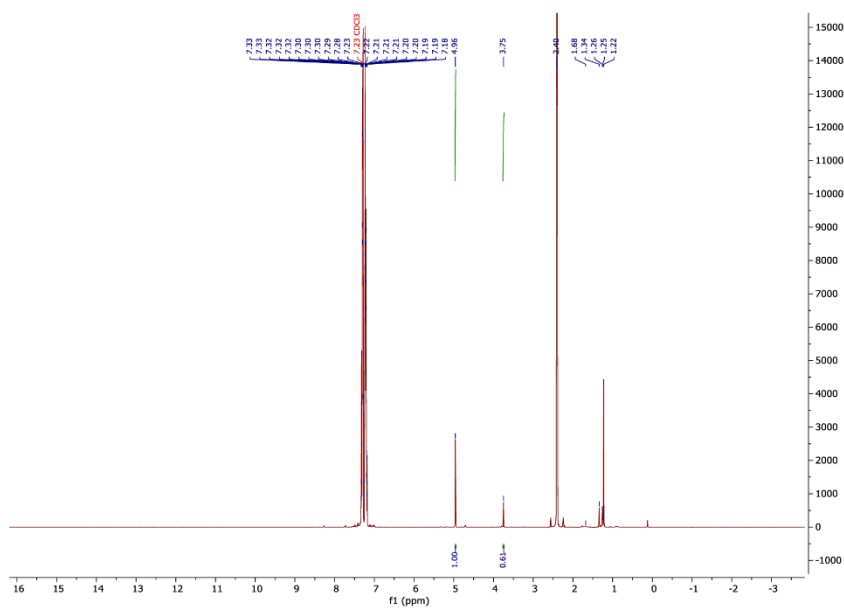
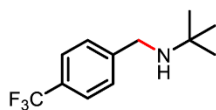


Figure 51: NMR of N-(4-chlorobenzyl)-2-methylpropan-2-amine with CH<sub>2</sub>Br<sub>2</sub> as internal standard

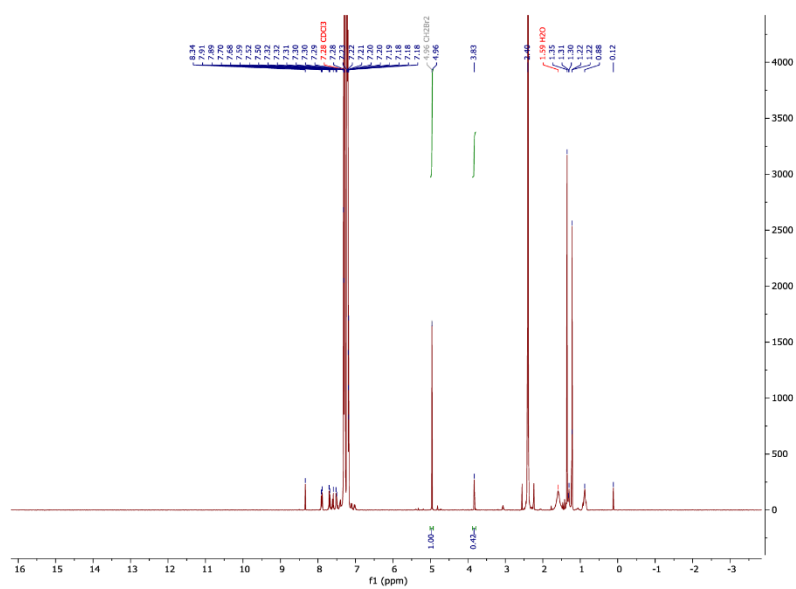
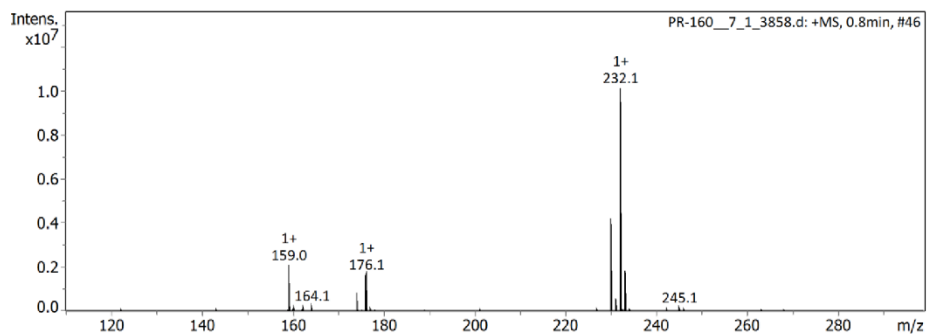
### 3. 2-methyl-N-(4-(trifluoromethyl)benzyl)propan-2-amine

The corresponding imine was synthesized according to the reported procedure.<sup>4</sup> Imine characterization: <sup>1</sup>H NMR (400 MHz, Chloroform-*d*) δ 8.31 (s, 1H), 7.87 (d, *J* = 8.1 Hz, 2H), 7.65 (d, *J* = 8.1 Hz, 2H), 1.32 (s, 9H).





$^1\text{H}$  NMR (400MHz,  $\text{CDCl}_3$ ) Product peak at 3.83 ppm. All other product peaks were obscured by reaction solvent. ESI(+H): Expected 232.12, found 232.1(M+H)



Catalytic test at increased H<sub>2</sub>-pressure(75bar)

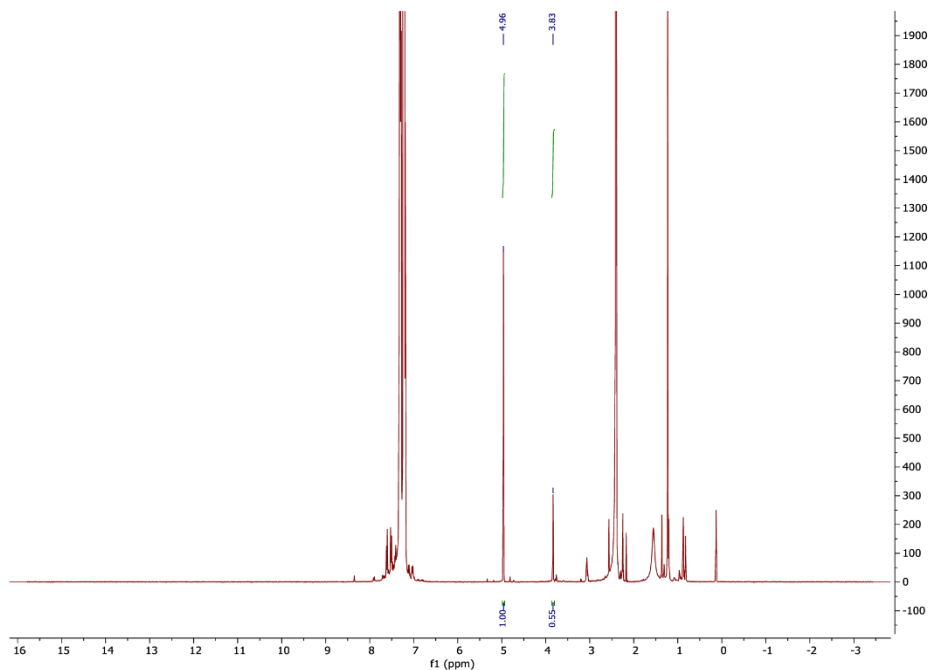


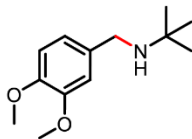
Figure 54: NMR of 2-methyl-N-(4-(trifluoromethyl)benzyl)propan-2-amine with CH<sub>2</sub>Br<sub>2</sub> as internal standard at 75 bar H<sub>2</sub> pressure

#### 4. 2-methyl-N-(4-nitrobenzyl)propan-2-amine

The corresponding imine was synthesized according to the reported procedure.<sup>5</sup> Imine characterization: <sup>1</sup>H NMR (400 MHz, Chloroform-*d*) δ 8.35 (s, 1H), 8.30 – 8.25 (m, 2H), 7.97 – 7.89 (m, 2H), 1.34 (s, 9H). Reduction of the imine was not observed.

#### 5. N-(3,4-dimethoxybenzyl)-2-methylpropan-2-amine

The corresponding imine was synthesized according to the reported procedure.<sup>4</sup> Imine characterization: <sup>1</sup>H NMR (400 MHz, Chloroform-*d*) δ 8.17 (d, *J* = 1.7 Hz, 1H), 7.49 – 7.39 (m, 1H), 7.15 (dt, *J* = 8.2, 1.8 Hz, 1H), 6.85 (dd, *J* = 8.2, 1.6 Hz, 1H), 3.95 – 3.91 (m, 4H), 3.88 (d, *J* = 2.0 Hz, 3H), 1.27 (d, *J* = 1.9 Hz, 9H).



$^1\text{H}$  NMR(400MHz,  $\text{CDCl}_3$ ): product peak at 3.72ppm. All other product peaks were obscured by reaction solvent. ESI(+H): expected 224.15 found 224.2 (M+H)

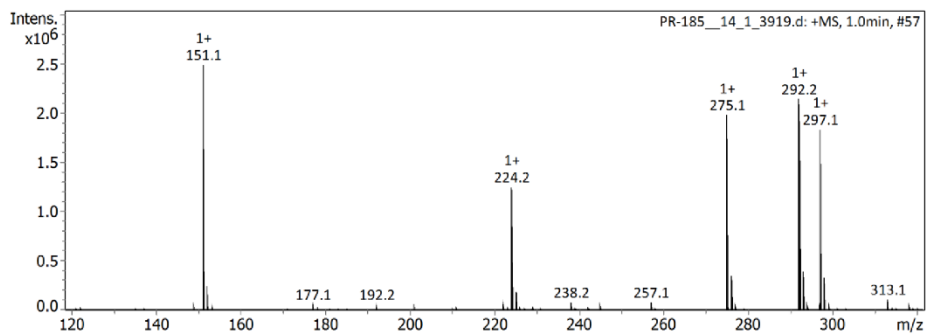


Figure 55: ESI-MS of N-(3,4-dimethoxybenzyl)-2-methylpropan-2-amine

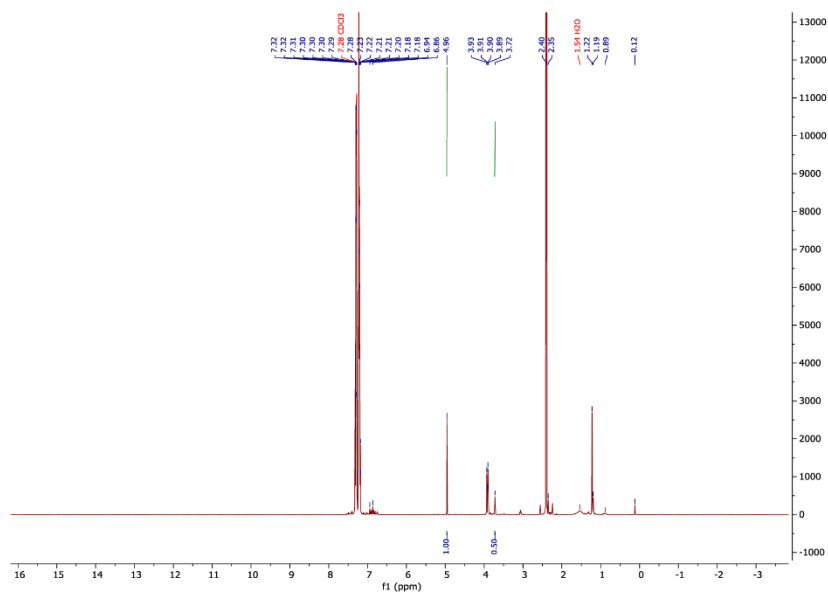
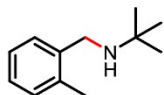


Figure 56:  $^1\text{H}$  NMR of N-(3,4-dimethoxybenzyl)-2-methylpropan-2-amine with  $\text{CH}_2\text{Br}_2$  as internal standard

## 6. 2-methyl-N-(2-methylbenzyl)propan-2-amine

The corresponding imine was synthesized according to the reported procedure.<sup>4</sup> Imine characterization:

<sup>1</sup>H NMR (400 MHz, Chloroform-*d*)  $\delta$  8.59 (s, 1H), 7.85 (dd,  $J = 7.4, 1.7$  Hz, 1H), 7.33 – 7.23 (m, 2H), 7.17 (ddt,  $J = 7.6, 1.6, 0.7$  Hz, 1H), 2.50 (s, 3H), 1.32 (s, 9H).



<sup>1</sup>H NMR (400MHz, CDCl<sub>3</sub>): Product peak at 3.77ppm. All other product peaks were obscured by reaction solvent. ESI(+H): Expected 177.15, found 177.

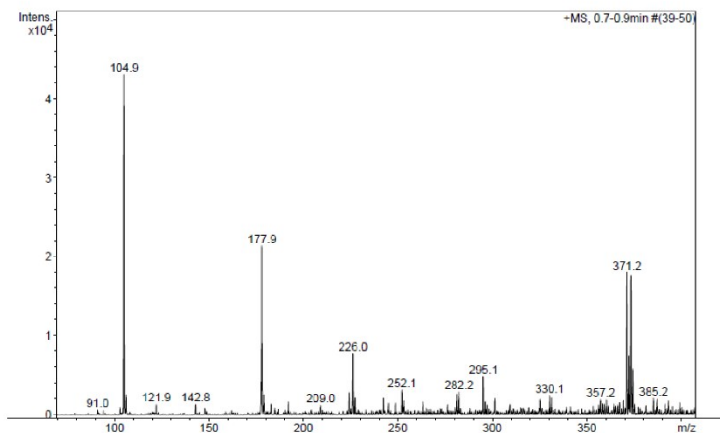


Figure 57: ESI-MS of 2-methyl-N-(2-methylbenzyl)propan-2-amine

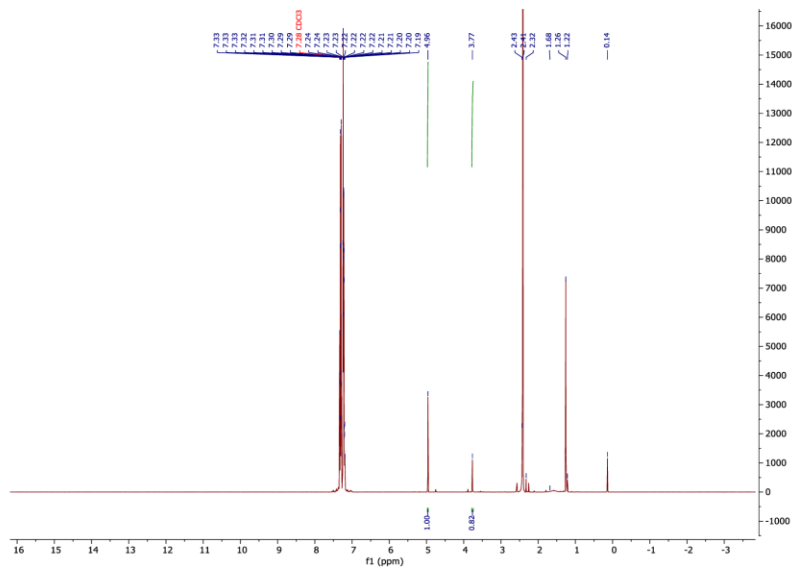
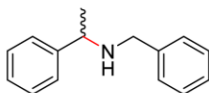


Figure 58: NMR of 2-methyl-N-(2-methylbenzyl)propan-2-amine with  $\text{CH}_2\text{Br}_2$  as internal standard

## 7. N-benzyl-1-phenylethan-1-amine

The corresponding imine was synthesized according to the modified reported procedure.<sup>9</sup> Reaction was performed in an inert atmosphere of  $\text{N}_2$  using Schlenk line apparatus and techniques. Solvents and glassware were dried according to the general procedure mentioned above. Molecular sieves (3A) were activated in vacuo by heating up to  $300\text{ }^\circ\text{C}$  for 5 minutes with a heat gun and leaving to cool down, the cycle was repeated three times.

To the activated molecular sieves was added toluene (10 mL) followed by 1 eq of acetophenone (20 mmol, 2.33 mL) and 1.2 eq of benzylamine (24 mmol, 2.62 mL). The reaction was stirred at RT and followed by NMR. After 44 h only approx. 33 % conversion was observed. The reaction mixture was heated up to  $70\text{ }^\circ\text{C}$  and stirred for 4 days. The molecular sieves were filtered off and washed with toluene (3 x 2 mL). The solvent was evaporated in vacuo. Resulting pale yellow liquid was mixed with pentane, overlaid with diethylether and placed in a freezer to crystallise. Crystals were filtered off, washed with diethylether, redissolved in chloroform and dried in vacuo. The filtrate was mixed with water and placed in a fridge to provide a second fraction of crystals. These crystals were filtered off, washed with water and dried in vacuo. The fractions were combined to provide product as yellow solid in 56 % (2.34 g) yield.  $^1\text{H}$  NMR (400 MHz,  $\text{CDCl}_3$ )  $\delta$  7.90 – 7.83 (m, 2H), 7.46 – 7.15 (m, 10H), 4.75 (s, 2H), 2.34 (s, 3H). ESI + ( $m/z$ ) for  $\text{C}_{15}\text{H}_{15}\text{N}^+$  210.1.



$^1\text{H}$  NMR(400MHz, $\text{CDCl}_3$ ): product peak at 1.38ppm. All other product peaks were obscured by reaction solvent. GC-MS retention time was 16.9 -17.0 minutes; EI ( $m/z$ ) 211.

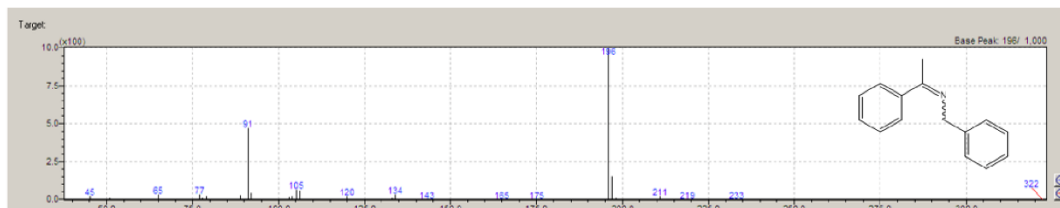


Figure 59 :GC-MS spectra of N-benzyl-1-phenylethan-1-amine

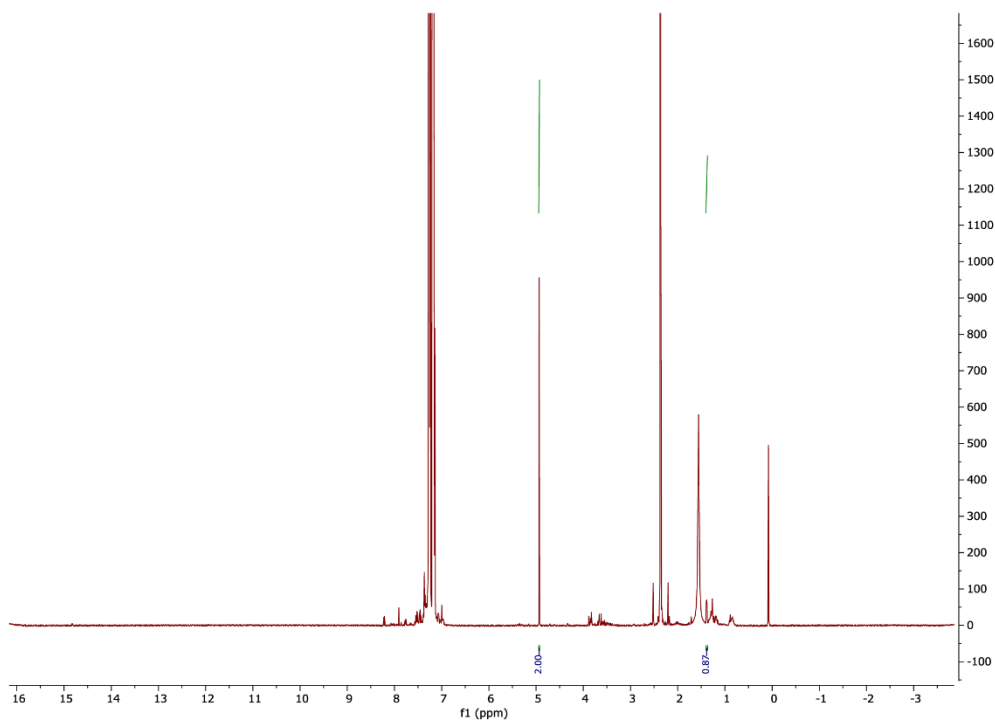
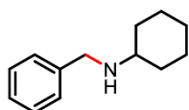


Figure 60:  $^1\text{H}$  NMR of N-benzyl-1-phenylethan-1-amine using  $\text{CH}_2\text{Br}_2$  as internal standard

## 8. N-benzylcyclohexanamine

The corresponding imine was synthesized according to the reported procedure.<sup>6</sup> Imine characterization:

$^1\text{H}$  NMR (400 MHz, Chloroform-*d*)  $\delta$  8.32 (s, 1H), 7.79 – 7.70 (m, 2H), 7.40 (ddt,  $J = 5.7, 3.9, 2.0$  Hz, 3H), 3.20 (tt,  $J = 10.5, 4.1$  Hz, 1H), 1.87-1.81(m,2H), 1.77 – 1.67 (m, 3H), 1.59 (dd,  $J = 7.0, 5.1$  Hz, 2H), 1.41 – 1.31 (m, 2H), 1.30 – 1.22 (m, 1H).



$^1\text{H}$  NMR(400MHz, $\text{CDCl}_3$ ): product peak at 3.86 ppm. All other product peaks were obscured by reaction solvent.

ESI(+H): expected 190.15, found 190(M+H)

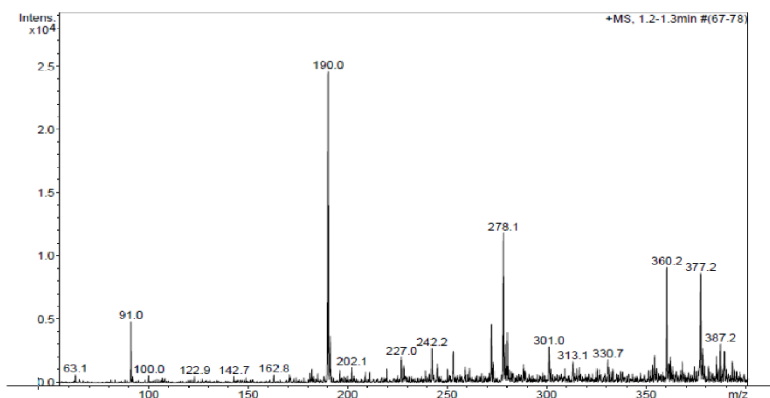


Figure 61: ESI-MS of - N-benzylcyclohexanamine

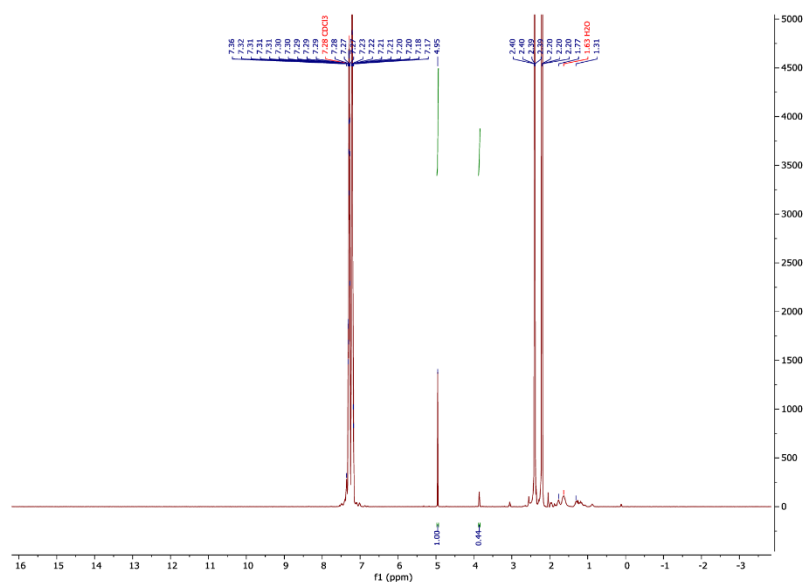


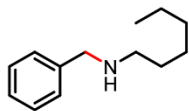
Figure 62: NMR of- N-benzylcyclohexanamine with  $\text{CH}_2\text{Br}_2$  as internal standard

## 9. N-benzylhexan-1-amine

The corresponding imine was synthesized according to the reported procedure.<sup>6</sup>

Imine characterization:  $^1\text{H}$  NMR (400 MHz, Chloroform-*d*)  $\delta$  8.28 – 8.14 (m, 1H), 7.65 (dp,  $J = 9.6, 3.6, 2.9$  Hz, 2H), 7.35 (ddt,  $J = 6.7, 4.1, 2.1$  Hz, 3H), 3.53 (tt,  $J = 7.0, 3.6$  Hz, 2H), 1.63 (ddd,  $J = 9.9, 6.9, 3.5$  Hz, 2H), 1.30 – 1.21 (m, 6H), 0.82 (dt,  $J = 7.9, 4.4$  Hz, 3H).





$^1\text{H}$  NMR(400MHz, $\text{CDCl}_3$ ): product peak at 3.86 ppm. All other product peaks were obscured by reaction solvent. ESI(+H): expected 192.16, found 192 (M+H)

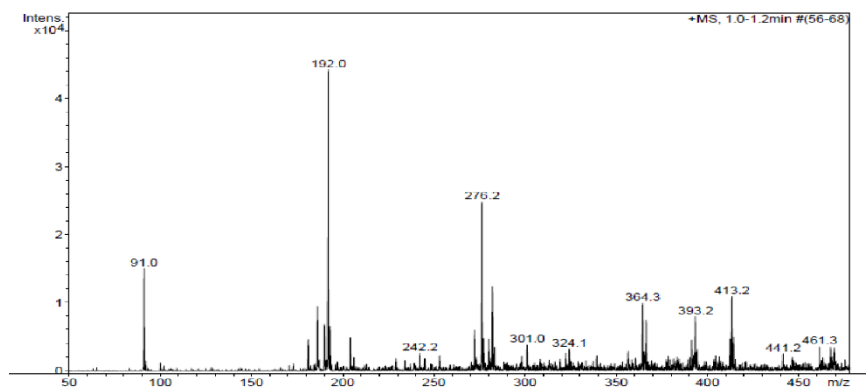


Figure 63: ESI-MS of N-benzylhexan-1-amine

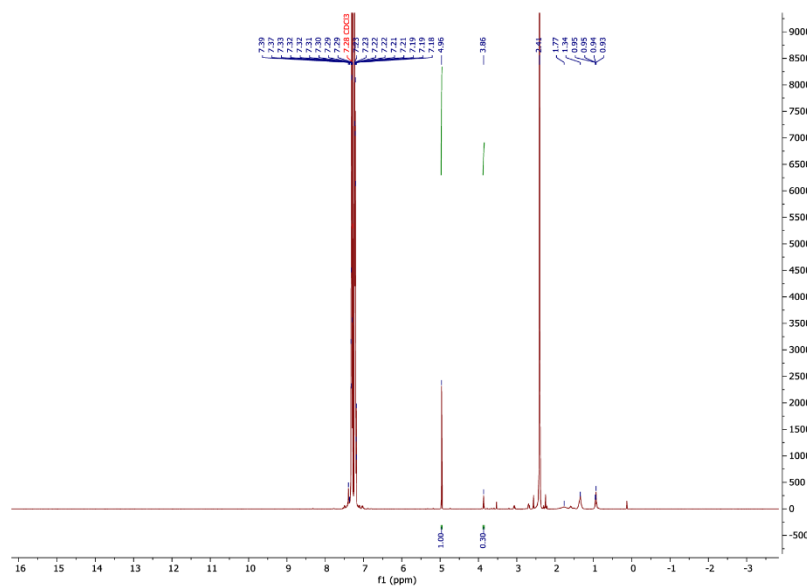


Figure 64: NMR of N-benzylhexan-1-amine with  $\text{CH}_2\text{Br}_2$  as internal standard

#### 48h catalytic test

$^1\text{H}$  NMR(400MHz,CDCl<sub>3</sub>): product peak at 3.86 ppm. All other product peaks were obscured by reaction solvent. GC-MS retention time was 13.5-13.6 minutes; EI ( $m/z$ ) 191.

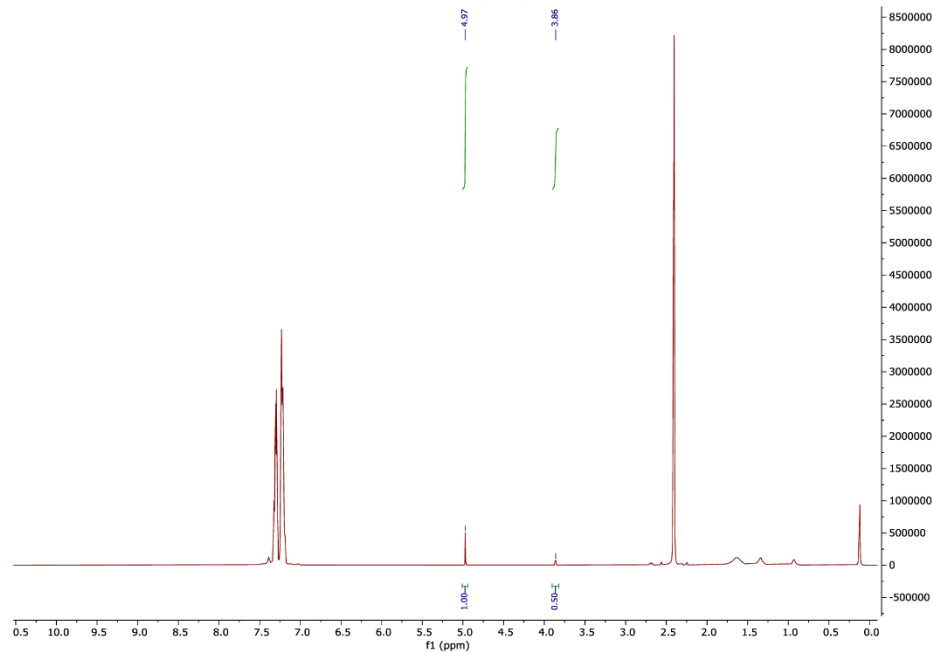


Figure 65: NMR of *N*-benzylhexan-1-amine with CH<sub>2</sub>Br<sub>2</sub> as internal standard, 48h test

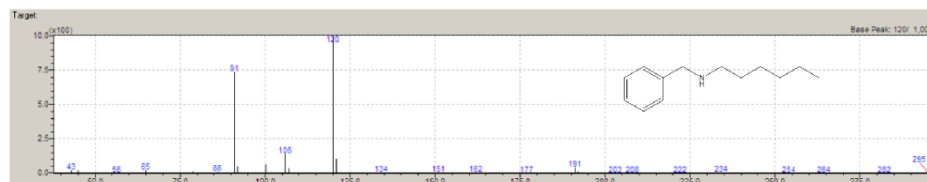


Figure 66: GC-MS spectra of *N*-benzylhexan-1-amine, 48 h test

#### 10% mol of catalyst test

$^1\text{H}$  NMR(400MHz,CDCl<sub>3</sub>): product peak at 3.83 ppm. All other product peaks were obscured by reaction solvent. ESI(+H) expected: 192.2; found 192.1 (M+H).

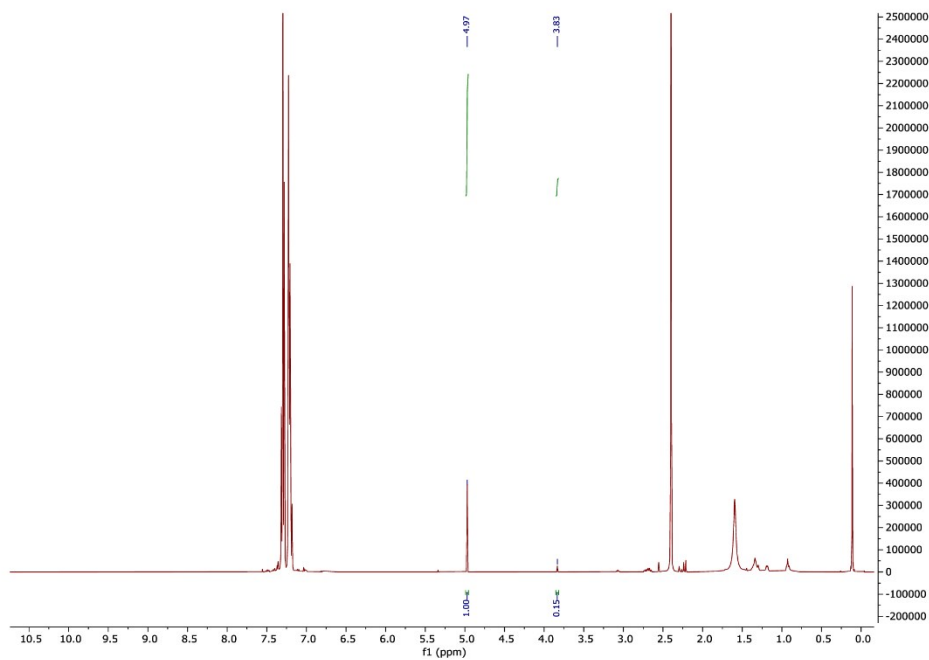


Figure 67: NMR of N-benzylhexan-1-amine with  $\text{CH}_2\text{Br}_2$  as internal standard, 10% mmol of catalyst

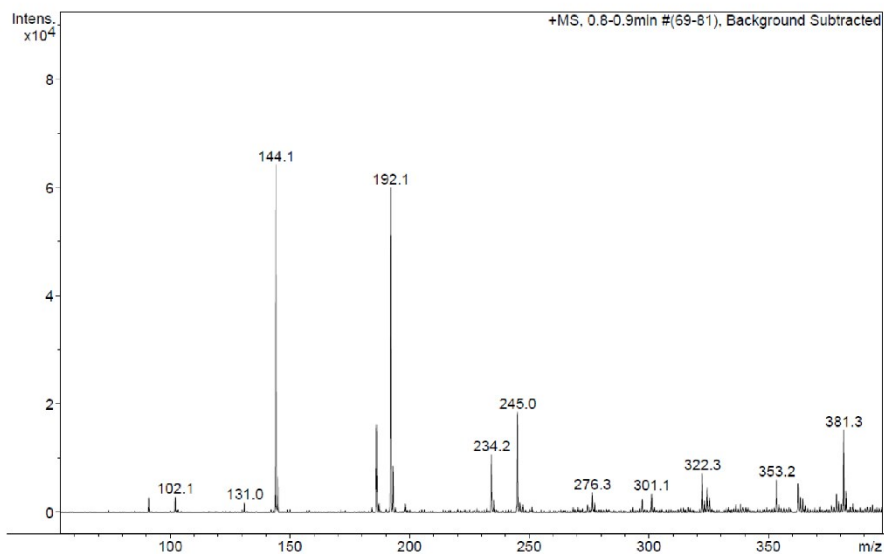


Figure 68: ESI-MS spectra of N-benzylhexan-1-amine, 10 % mmol of catalyst

#### 2,5% mol of catalyst test

$^1\text{H}$  NMR(400MHz, $\text{CDCl}_3$ ): product peak at 3.84 ppm. All other product peaks were obscured by reaction solvent.  
ESI(+H) expected: 192.2; found 192.0 (M+H).

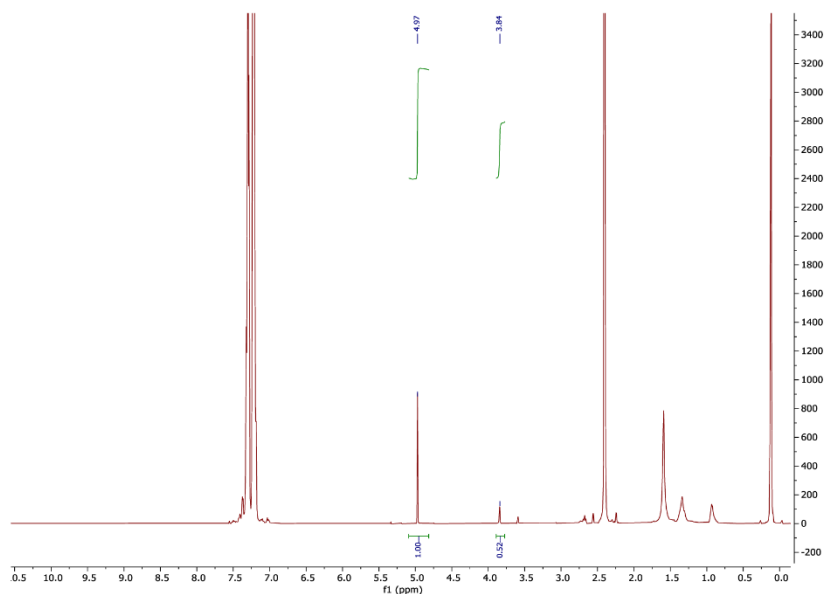


Figure 69: NMR of *N*-benzylhexan-1-amine with  $\text{CH}_2\text{Br}_2$  as internal standard, 2.5 % mmol of catalyst

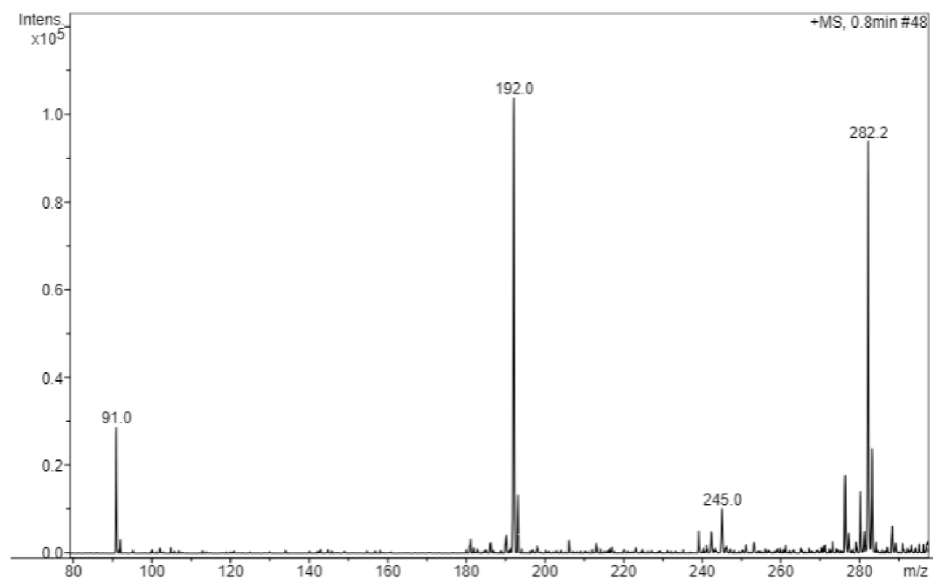
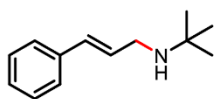


Figure 70 :ESI-MS spectra of *N*-benzylhexan-1-amine, 2.5 % mmol of catalyst.

#### 10.(*E*)-*N*-(*tert*-butyl)-3-phenylprop-2-en-1-amine

The corresponding imine was synthesized according to the reported procedure.<sup>8</sup> Imine characterization:  $^1\text{H}$  NMR (400 MHz, Chloroform-*d*)  $\delta$  8.01 (t,  $J = 4.1$  Hz, 1H), 7.50 – 7.40 (m, 2H), 7.40 – 7.22 (m, 3H), 6.92 (d,  $J = 4.1$  Hz, 2H), 2.47 – 2.24 (m, 2H), 1.24 (s, 9H).



$^1\text{H}$  NMR(400MHz, $\text{CDCl}_3$ ): Product peak at 3.77ppm. All other product peaks were obscured by reaction solvent. ESI(+H): expected 190.15, found 190(M+H)

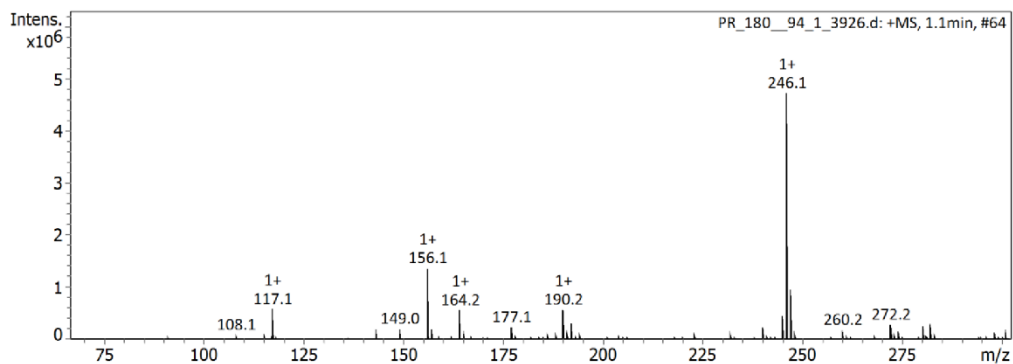


Figure 71: ESI-MS of -(E)-N-(tert-butyl)-3-phenylprop-2-en-1-amine

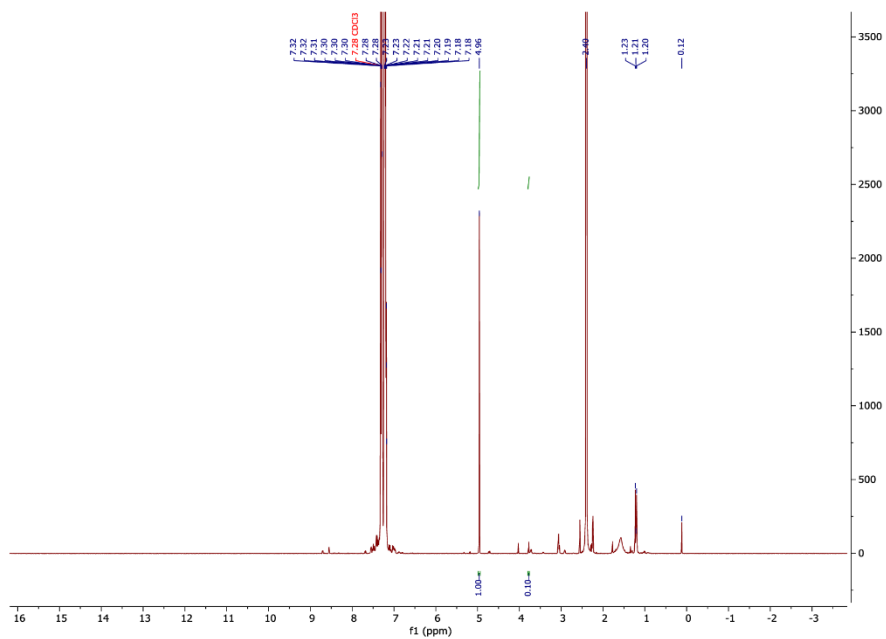
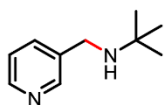


Figure 72: NMR of-(E)-N-(tert-butyl)-3-phenylprop-2-en-1-aminewith  $\text{CH}_2\text{Br}_2$  as internal standard

### 1.2-methyl-N-(pyridin-3-ylmethyl)propan-2-amine

The corresponding imine was synthesized according to the reported procedure.<sup>7</sup> Imine characterization: <sup>1</sup>H NMR (400 MHz, Chloroform-*d*) δ 8.75 (t, *J* = 2.2 Hz, 1H), 8.50 (ddd, *J* = 4.7, 3.0, 1.4 Hz, 1H), 8.26 – 8.16 (m, 1H), 8.04 (dp, *J* = 7.9, 2.0 Hz, 1H), 1.33 – 1.16 (m, 9H).



<sup>1</sup>H NMR(400MHz,CDCl<sub>3</sub>): product peak at 3.79ppm. All other product peaks were obscured by reaction solvent. ESI(+H): expected 165. Found 165 (M+H)

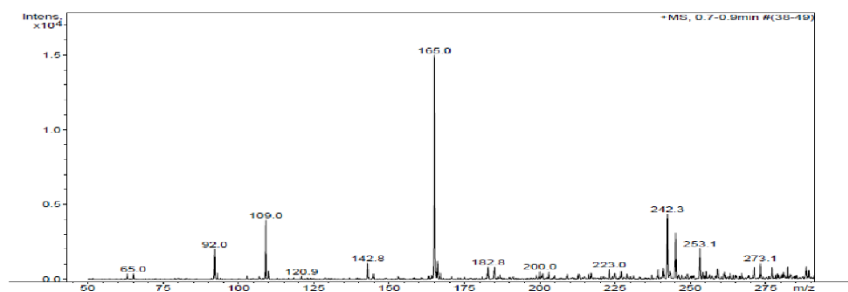


Figure 73: ESI-MS of 2-methyl-N-(pyridin-3-ylmethyl)propan-2-amine

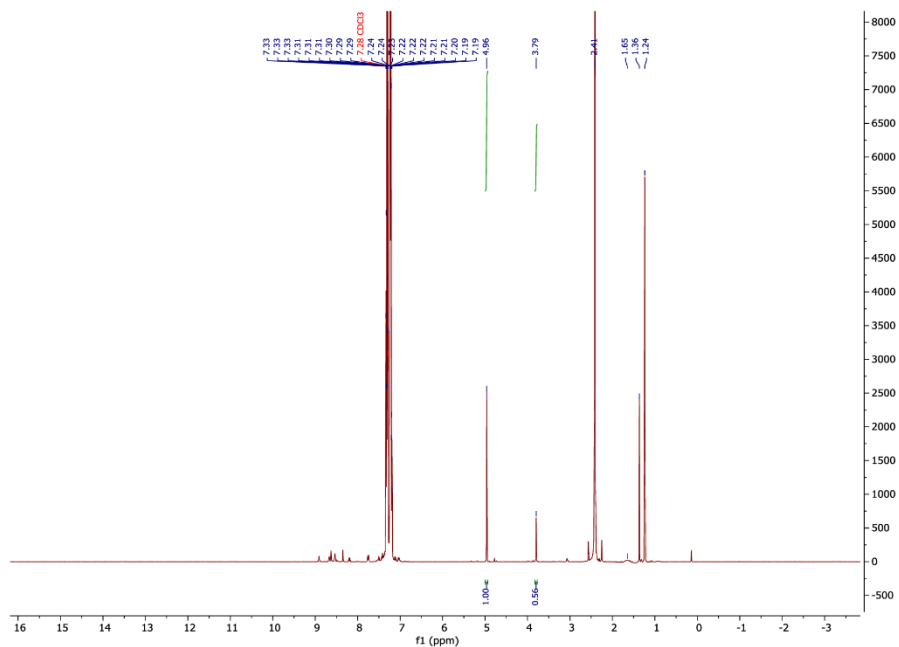
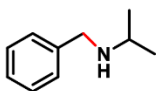


Figure 74: NMR of 2-methyl-N-(pyridin-3-ylmethyl)propan-2-amine with  $\text{CH}_2\text{Br}_2$  as internal standard

## 12. N-benzylpropan-2-amine

The corresponding imine was synthesized according to the reported procedure.<sup>10</sup> Imine characterization:  $^1\text{H}$  NMR (400 MHz, Chloroform-*d*)  $\delta$  8.32 (s, 1H), 7.72 – 7.75 (m, 2H), 7.39-7.41 (m, 3H), 3.51-3.59 (m, 1H), 1.24-1.31 (d, 6H).



$^1\text{H}$  NMR(400MHz,  $\text{CDCl}_3$ ): product peak at 3.84ppm. All other product peaks were obscured by reaction solvent. GC-MS(+H): 149

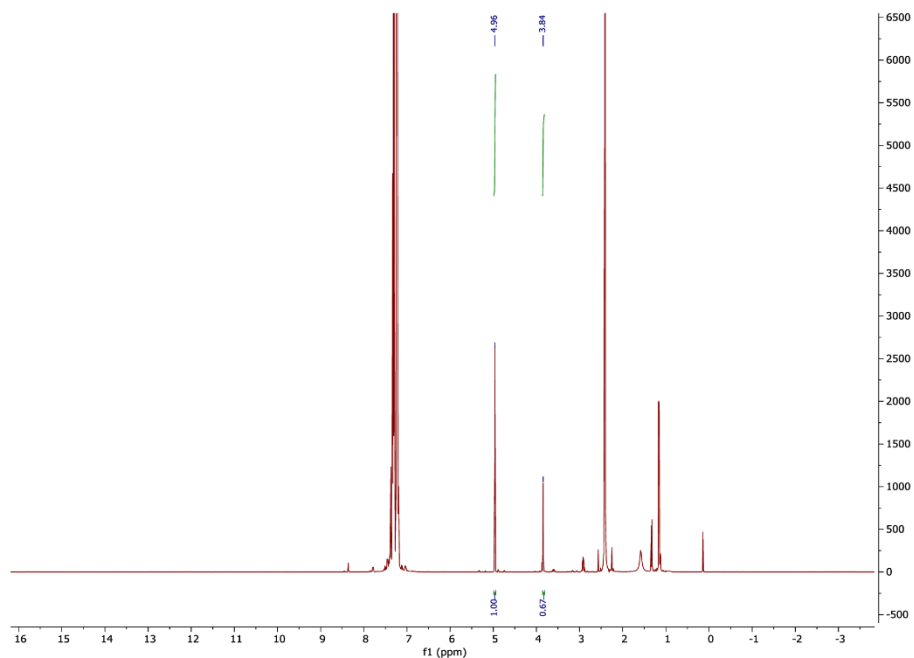


Figure 75: NMR of N-benzylpropan-2-amine with  $\text{CH}_2\text{Br}_2$  as internal standard

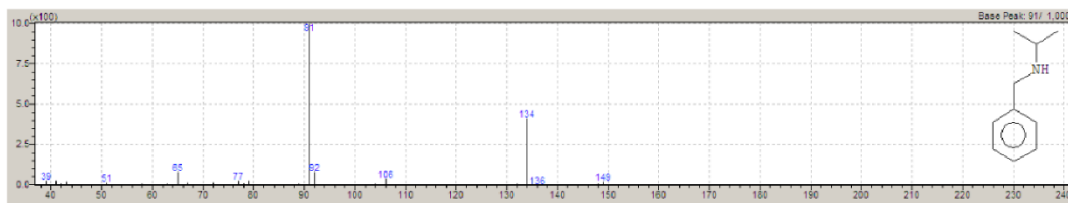
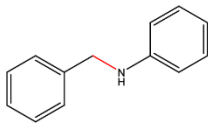


Figure 76: GC-MS of N-benzylpropan-2-amine

### 13 N-benzylaniline

The corresponding imine was synthesized according to the following synthesis. 10 mmol (1.02 mL) of benzaldehyde was dissolved in 50 mL of toluene. To the stirring solution was added 12 mmol (1.09 mL) of aniline. The mixture was refluxed in Dean-Stark apparatus overnight. After evaporation of the solvent, the crude mixture was heated to 80 °C in vacuum for 30 minutes. The product was obtained as a brown solid (94 % yield) NMR corresponds with literature.<sup>11</sup>  $^1\text{H}$  NMR (400 MHz,  $\text{CDCl}_3$ )  $\delta$  8.47 (s, 1H), 7.99 – 7.85 (m, 2H), 7.53 – 7.44 (m, 3H), 7.44 – 7.35 (m, 2H), 7.25 – 7.20 (m, 3H). GC-MS retention time was 17.8-18 minutes; EI ( $m/z$ ) 181.





$^1\text{H NMR}$ (400MHz,  $\text{CDCl}_3$ ): product peak at 4.40 ppm, 6.70-6.78 ppm, 6.80-6.85 ppm. All other product peaks were obscured by reaction solvent. GC-MS retention time was 19.5 -19.7 minutes; EI ( $m/z$ ) 183.

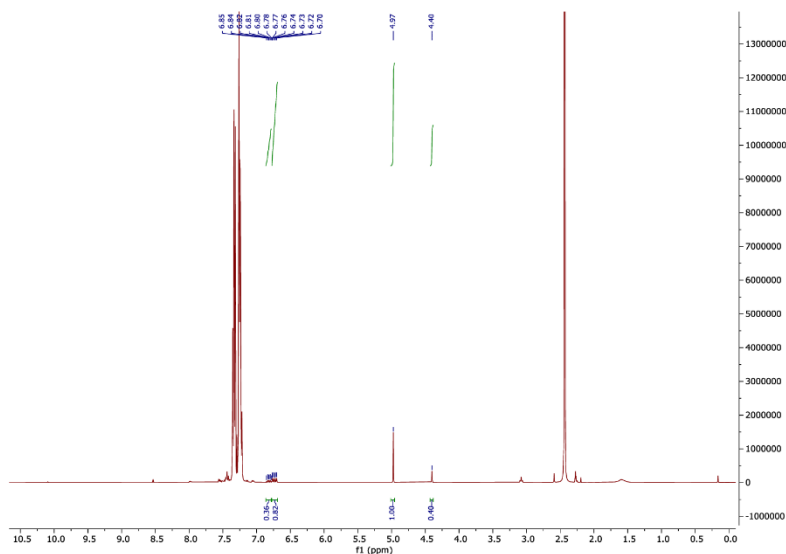


Figure 77: NMR of N-benzylaniline with  $\text{CH}_2\text{Br}_2$  as internal standard

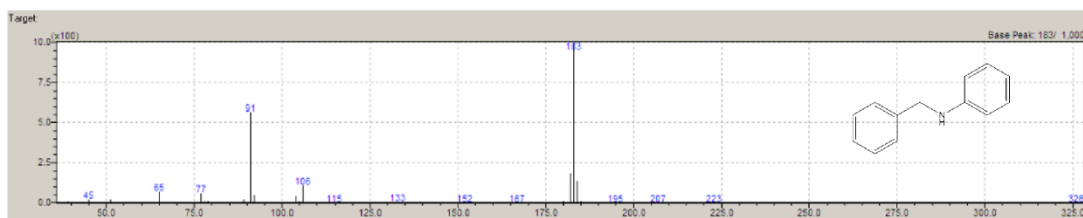


Figure 78: GC-MS spectra of N-benzylaniline

#### 48h catalytic test

$^1\text{H NMR}$ (400MHz,  $\text{CDCl}_3$ ): product peak at 4.38 ppm, 6.68-6.74 ppm, 6.76-6.82 ppm. All other product peaks were obscured by reaction solvent. GC-MS retention time was 19.6 -19.7 minutes; EI ( $m/z$ ) 183.

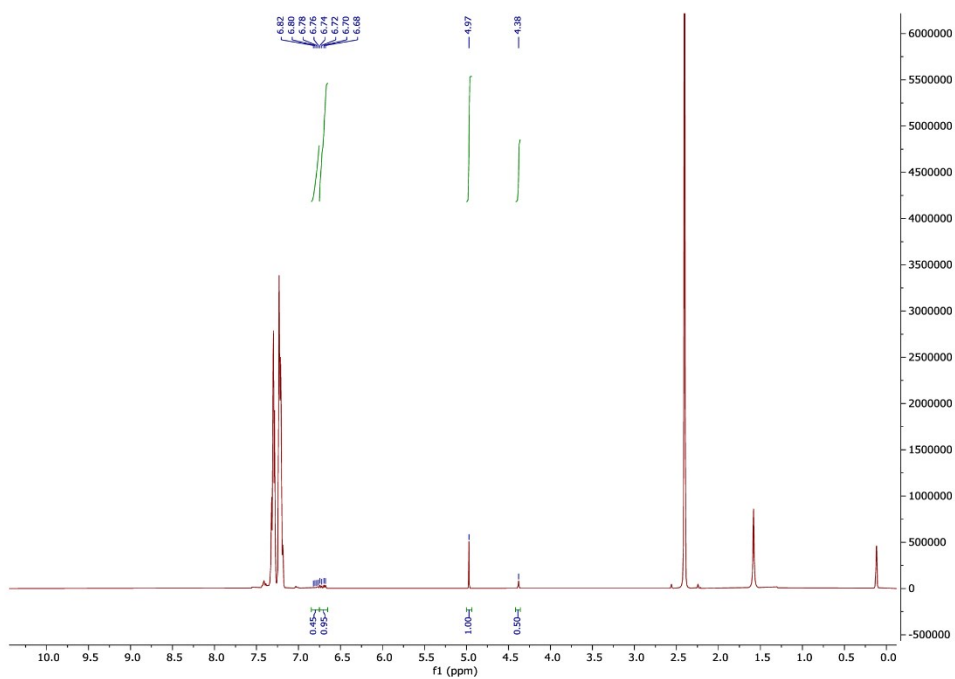


Figure 79: NMR of N-benzylaniline with CH<sub>2</sub>Br<sub>2</sub> as internal standard, 48h test



Figure 80: GC-MS spectra of N-benzylaniline, 48 h test

### 10 % mol of catalyst test

<sup>1</sup>H NMR(400MHz,CDCl<sub>3</sub>): product peak at 4.39 ppm, 6.60-6.75 ppm, 6.78-6.83 ppm. All other product peaks were obscured by reaction solvent. GC-MS retention time was 19.6 -19.8 minutes; EI (*m/z*) 183.

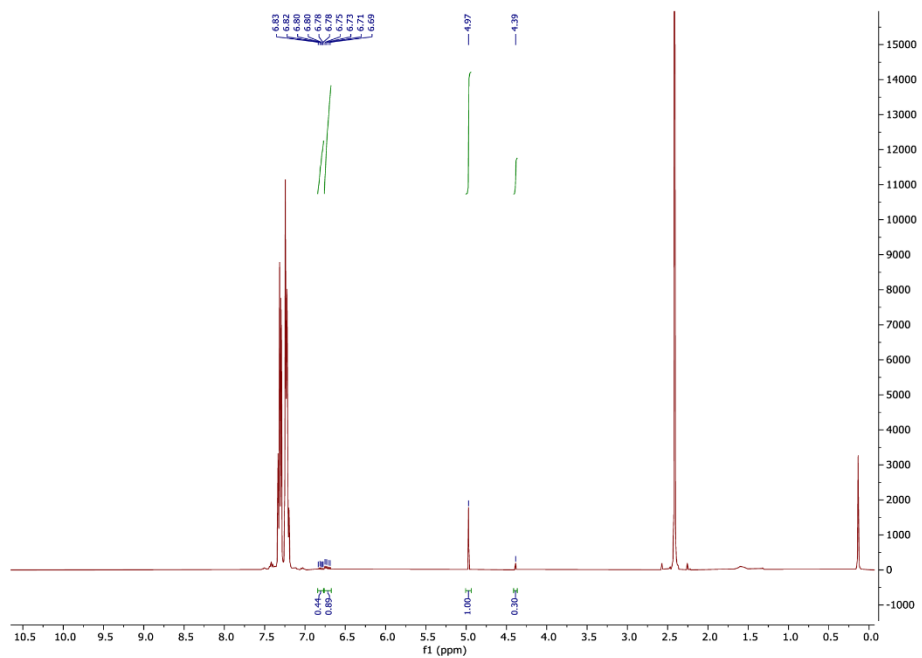


Figure 81: NMR of-N-benzylaniline with  $\text{CH}_2\text{Br}_2$  as internal standard, 10 % mmol catalyst test

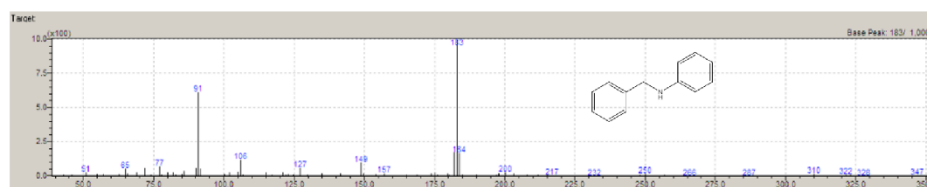


Figure 82: GC-MS spectra of N-benzylaniline, 10% mmol catalyst test

### 2,5 % mol of catalyst test

$^1\text{H}$  NMR(400MHz, $\text{CDCl}_3$ ): product peak at 4.38 ppm, 6.68-6.74 ppm, 6.76-6.82 ppm. All other product peaks were obscured by reaction solvent. GC-MS retention time was 19.7 -19.8 minutes; EI ( $m/z$ ) 183.

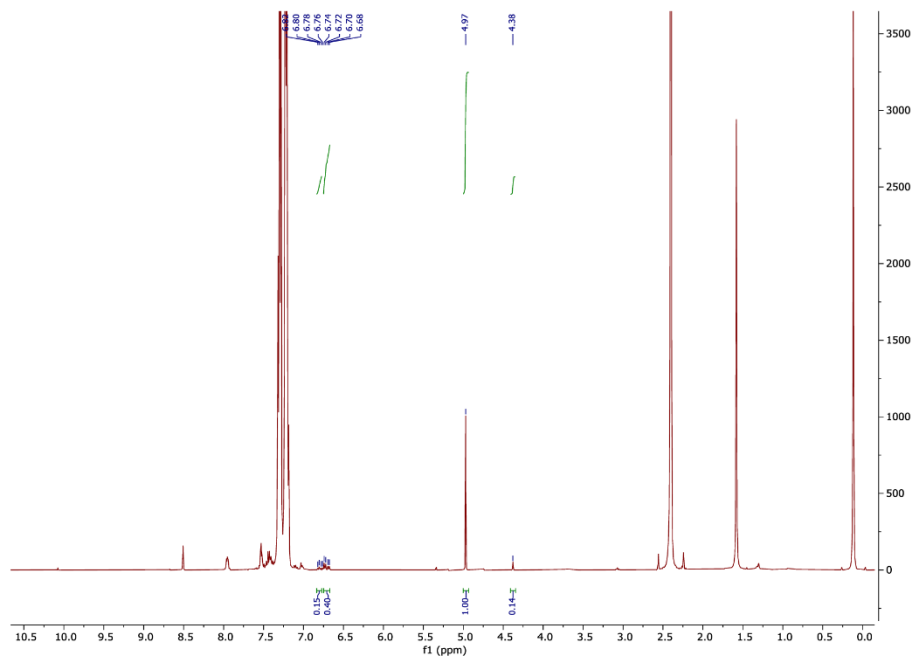


Figure 83: NMR of N-benzylaniline with  $\text{CH}_2\text{Br}_2$  as internal standard, 2.5 % mmol catalyst test.

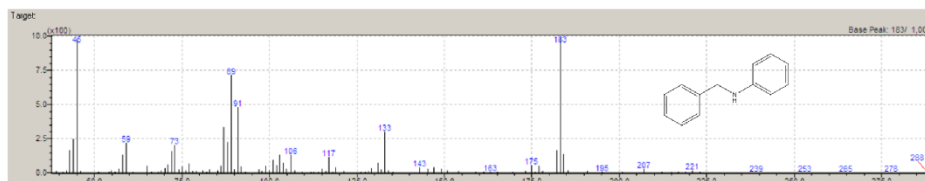
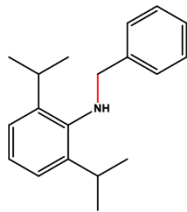


Figure 84: GC-MS spectra of N-benzylaniline, 2.5 % mmol catalyst test

## 14 2 N-benzyl-2,6-diisopropylaniline

The corresponding imine was synthesized according to the following synthesis. 12 mmol of 2,4-diisopropylaniline (2.26 mL) was added to the stirring solution of 10 mmol of benzaldehyde (1.02 mL). The mixture was refluxed in a Dean-Stark apparatus for 4 days. After evaporation of the solvent, the crude product was purified by distilling out the remaining starting material from reaction mixture. Product was obtained as brown oil, 2.42 g, 91 % yield. NMR corresponds with literature.<sup>12</sup>  $^1\text{H}$  NMR (400 MHz, Chloroform- $d$ )  $\delta$  8.20 (s, 1H), 7.96 – 7.87 (m, 2H), 7.57 – 7.45 (m, 3H), 7.19 – 7.09 (m, 3H), 2.98 (hept,  $J = 6.9$  Hz, 2H), 1.17 (d,  $J = 6.9$  Hz, 12H). GC-MS retention time was 17.8-17.9 minutes; EI (m/z) 265.



$^1\text{H}$  NMR(400MHz, $\text{CDCl}_3$ ): product peak at 4.10 ppm, 1.30 (d,  $J = 8$  Hz). All other product peaks were obscured by reaction solvent. GC-MS retention time was 17.4-17.5 minutes; EI ( $m/z$ ) 267.

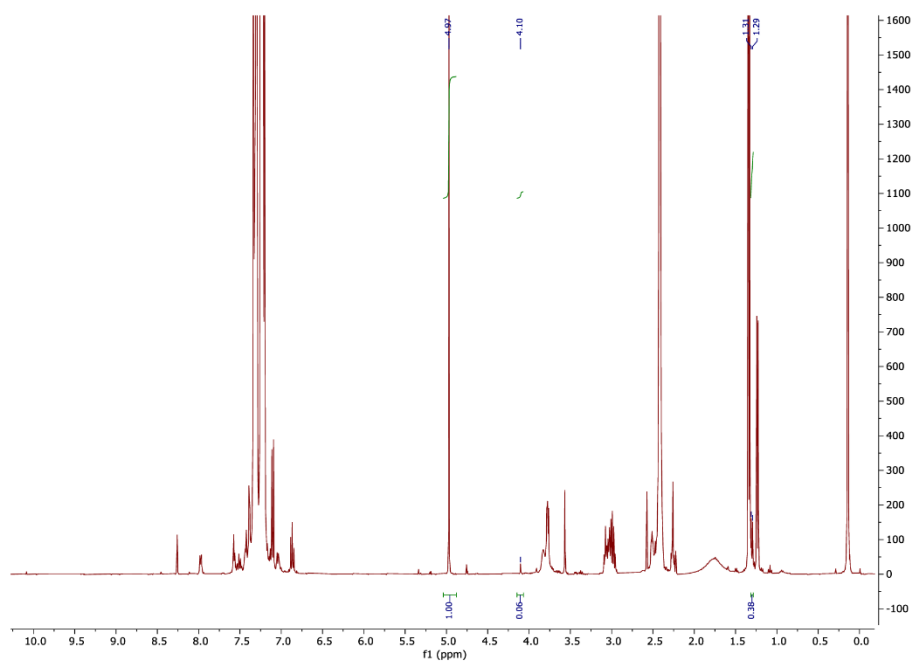


Figure 85: NMR of N-benzyl-2,6-diisopropylaniline with  $\text{CH}_2\text{Br}_2$  as internal standard

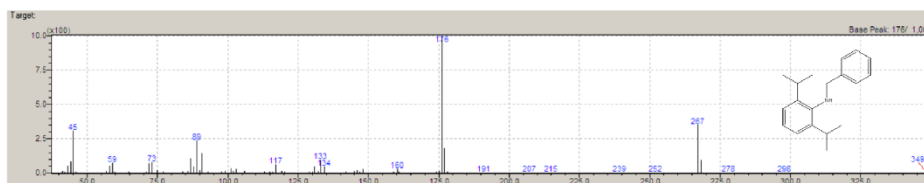
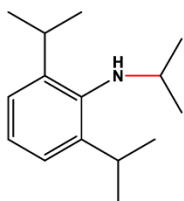


Figure 86: GC-MS spectra of N-benzyl-2,6-diisopropylaniline

## 15 N,2,6-triisopropylaniline

The corresponding imine was synthesized according to the modified reported procedure.<sup>13</sup> 10 mmol of 2,4-diisopropylaniline (1.89 mL) was refluxed in 50 mL of acetone over 5 g of 3A molecular sieves for six days. Crude product was purified by distillation (120 °C, 100 mbar) to obtain colorless oil, 0.27 g, 12 % yield. <sup>1</sup>H NMR (300 MHz, CDCl<sub>3</sub>) δ 7.11-7.02 (m, 3H), 2.93 (hept, *J* = 6.8 Hz, 23H), 1.29 (s, 6H), 1.26 (d, *J* = 2.1 Hz, 12H). GC-MS retention time was 11.5-11.6 minutes; EI (*m/z*) 217.



<sup>1</sup>H NMR(400MHz,CDCl<sub>3</sub>): product peak at 1.29 ppm (d, *J* = 8 Hz). All other product peaks were obscured by reaction solvent. GC-MS retention time was 11.0-11.1 minutes; EI (*m/z*) 219.

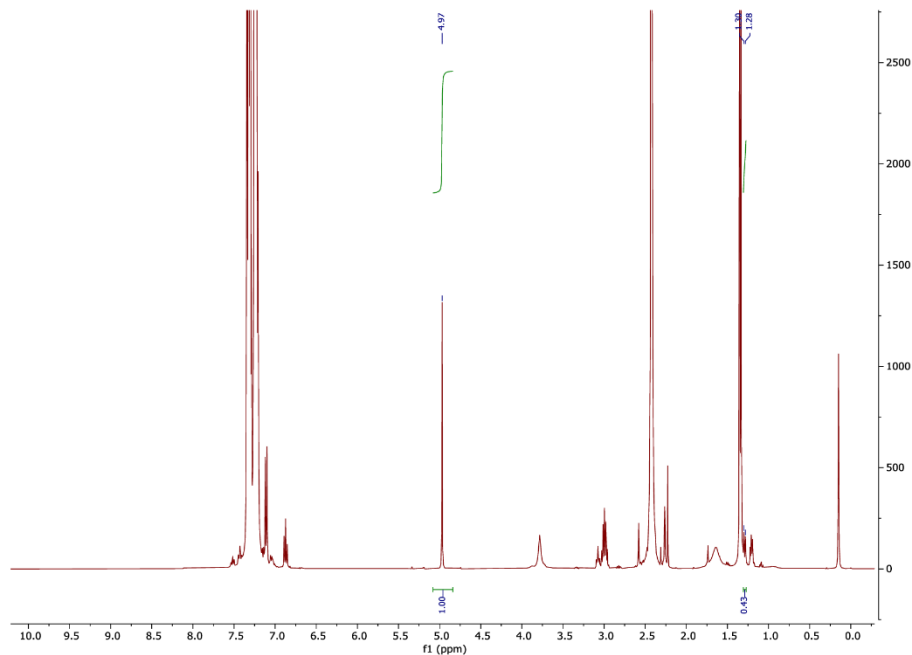


Figure 87: NMR of N,2,6-triisopropylaniline with CH<sub>2</sub>Br<sub>2</sub> as internal standard

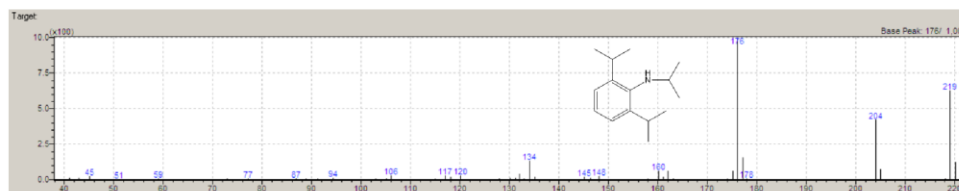


Figure 88: GC-MS spectra of N,2,6-triisopropylaniline

## Crystal structure of $[\text{Sn}(\text{Salen})\text{Cl}_2]$ and $[\text{Sn}(\text{}^t\text{Bu}_2\text{Salophen})\text{Cl}_2]$ complexes

The crystals of  $[\text{Sn}(\text{Salen})\text{Cl}_2]$  were obtained by evaporation of its dichloromethane solution under reduced pressure and the crystals of partially solvated  $[\text{Sn}(\text{}^t\text{Bu}_2\text{Salophen})\text{Cl}_2]$  were prepared by diffusion of hexane vapors into its dichloromethane solution. The selected crystals were mounted onto goniometer heads of a Bruker D8 VENTURE Kappa Duo diffractometer with a PHOTON100 detector and an  $I\mu\text{S}$  microfocus sealed tube source, equipped with Cryostream Cooler (Oxford Cryostreams). Full-set diffraction data ( $\pm h, \pm k, \pm l, 2\theta \leq 55^\circ$ ) were collected at 120(2) K using monochromated  $\text{MoK}\alpha$  radiation ( $\lambda = 0.71073 \text{ \AA}$ ) and reduced using the software of the diffractometer (SAINT<sup>[14]</sup>). The data were corrected for absorption using methods incorporated in the diffractometer software (SADABS<sup>[15]</sup>).

The structures were solved by direct methods with SHEXT-2018<sup>[16]</sup> and refined by weighted full-matrix least-squares against  $F^2$  using SHELXL-2019.<sup>[17]</sup> All non-hydrogen atoms were refined with anisotropic displacement parameters. All hydrogen atoms were located on the difference electron density maps and refined as riding atoms with their  $U_{\text{iso}}(\text{H})$  fixed to a 1.2 multiple of  $U_{\text{eq}}$  of their bond partners with the exception of the hydrogen atoms of the tert-butyl groups in the structure of partially solvated  $[\text{Sn}(\text{}^t\text{Bu}_2\text{Salophen})\text{Cl}_2]$  which were placed in the theoretical positions and refined as riding atoms with their  $U_{\text{iso}}(\text{H})$  fixed to a 1.5 multiple of  $U_{\text{eq}}$  of their bond partners. Two of the four tert-butyl groups (carbon atoms C21 – C24 and C25 – C28) in the structure of partially solvated  $[\text{Sn}(\text{}^t\text{Bu}_2\text{Salophen})\text{Cl}_2]$  were refined disordered over two positions mutually rotated around the pivotal bond to their quaternary carbon atoms (C21 and C25, respectively). The positions were restrained to be equivalent with relative occupancy ratios refined as 3:1 and 1:1, respectively. Additionally, rigid-bond restraints had to be applied to the anisotropic displacement parameters of the carbon atoms of the disordered tert-butyl groups to prevent them from becoming negative.

In the structure of partially solvated  $[\text{Sn}(\text{}^t\text{Bu}_2\text{Salophen})\text{Cl}_2]$ , a disordered dichloromethane molecule could not be satisfactorily modeled with full occupancy and was removed from the refinement using the PLATON SQUEEZE<sup>[18]</sup> routine which removed electron density amounting to a total of 21 electrons from a solvent accessible void of the potential volume of  $262 \text{ \AA}^3$  per unit cell. After the final cycle of refinement of the structure of  $[\text{Sn}(\text{}^t\text{Bu}_2\text{Salophen})\text{Cl}_2]$ , the residual difference electron density map maximum of  $1.84 \text{ e}\cdot\text{\AA}^{-3}$  was located in the vicinity of the tin atom and the residual difference electron density map minimum of  $-1.30 \text{ e}\cdot\text{\AA}^{-3}$  was located in the vicinity of one of the disordered tert-butyl groups.

Selected structure solution parameters are listed in Table 5. All geometric calculations and graphics were calculated and plotted using PLATON<sup>[19]</sup> software. Displacement ellipsoid ORTEP<sup>[20]</sup> plots are contained in the Figure 89. The complex  $[\text{Sn}(\text{Salen})\text{Cl}_2]$  crystallized in monoclinic system with space group  $Cc$  and 4 formula units in the unit cell (Figure 90). The partially solvated complex  $[\text{Sn}(\text{}^t\text{Bu}_2\text{Salophen})\text{Cl}_2]$  crystallized in triclinic system with space group  $P-1$  and 2 formula units in the unit cell (Figure 91). The respective selected valence parameters in the structures of  $[\text{Sn}(\text{Salen})\text{Cl}_2]$  and

[Sn(<sup>t</sup>Bu<sub>2</sub>Salophen)Cl<sub>2</sub>] are listed in Table 6 and Table 7. The values related to the atoms in refined positions are rounded with respect to their estimated standard deviations that are provided with one decimal place. The corresponding crystallographic information files for [Sn(Salen)Cl<sub>2</sub>] and [Sn(<sup>t</sup>Bu<sub>2</sub>Salophen)Cl<sub>2</sub>] can be accessed in Cambridge Crystallographic Data Centre at <https://www.ccdc.cam.ac.uk/structures/> under submission codes CCDC-2330171 and CCDC-2333521, respectively.



**Table 5:** Basic crystallographic data and structure refinement details for the crystals of [Sn(Salen)Cl<sub>2</sub>] and [Sn(<sup>t</sup>Bu<sub>2</sub>Salophen)Cl<sub>2</sub>].

Structure code	[Sn(Salen)Cl <sub>2</sub> ]	[Sn( <sup>t</sup> Bu <sub>2</sub> Salophen)Cl <sub>2</sub> ] (solvated)
Empirical formula	C <sub>16</sub> H <sub>14</sub> Cl <sub>2</sub> N <sub>2</sub> O <sub>2</sub> Sn	C <sub>36</sub> H <sub>46</sub> Cl <sub>2</sub> N <sub>2</sub> O <sub>2</sub> Sn
Formula weight [g·mol <sup>-1</sup> ]	455.90	728.34
Crystal system	monoclinic	triclinic
Space group	<i>Cc</i>	<i>P</i> -1
<i>a</i> [Å]	10.7059(4)	11.2684(8)
<i>b</i> [Å]	14.2716(4)	13.0888(9)
<i>c</i> [Å]	10.8582(3)	13.536(1)
$\alpha$ [°]		75.089(3)
$\beta$ [°]	101.977(1)	75.968(3)
$\gamma$ [°]		88.152(3)
<i>V</i> [Å <sup>3</sup> ]	1622.91(9)	1870.6(2)
<i>Z</i>	4	2
<i>F</i> (000)	896	752
Calculated density [g·cm <sup>3</sup> ]	1.866	1.293
$\mu$ (Mo K $\alpha$ ) [mm <sup>-1</sup> ]	1.913	0.857
crystal size [mm]	0.032 x 0.032 x 0.134	0.054 x 0.078 x 0.162
$\theta$ range [°]	2.412–27.481	1.864–28.426
Collected diffractions	17662	124490
Independent diffractions	3720	9370
Observed <sup>a</sup> diffractions	3687	8716
<i>R</i> <sub>int</sub> <sup>b</sup> [%]	3.11	5.26
Number of parameters	208	462
<i>R</i> , <i>wR</i> <sup>c</sup> (observed) [%]	1.47, 3.09	4.53, 10.46
<i>R</i> , <i>wR</i> <sup>c</sup> (all data) [%]	1.48, 3.09	4.93, 10.66
Goodness of fit <sup>d</sup>	1.071	1.149
$\Delta\rho_{\max}$ and $\Delta\rho_{\min}$ (e·Å <sup>-3</sup> )	-0.379, 0.288	-1.296, 1.841
Flack parameter	-0.013(9)	
Weighting scheme	$w = 1/[\sigma^2(F_o^2) + (aP)^2 + bP]$ ; where $P = (F_o^2 + 2F_c^2)/3$ .	
	a = 0.0089	a = 0.0296
	b = 0.3295	b = 5.4616

<sup>a</sup>  $I > 2\sigma(I)$

<sup>b</sup>  $R_{int} = \sum |F_o^2 - F_{o,mean}^2| / \sum F_o^2$

<sup>c</sup>  $R(F) = \sum ||F_o| - |F_c|| / \sum |F_o|$ ;  $wR(F^2) = [\sum(w(F_o^2 - F_c^2)^2) / \sum w(F_o^2)^2]^{1/2}$

<sup>d</sup>  $S = [\sum(w(F_o^2 - F_c^2)^2) / (N_{diffns} - N_{par})]^{1/2}$

**Table 6:** List of selected bond lengths and angles in [Sn(Salen)Cl<sub>2</sub>].

bond	value [Å]	angle	value [°]	torsion	value [°]
Sn1-O1	2.012(2)	O1-Sn1-O2	102.17(8)	C3-N1-C1-C2	144.6(3)
Sn1-O2	2.013(2)	O1-Sn1-N1	91.15(8)	Sn1-N1-C1-C2	-31.7(3)
Sn1-N1	2.142(2)	O2-Sn1-N1	166.34(8)	C4-N2-C2-C1	144.9(3)
Sn1-N2	2.145(2)	O1-Sn1-N2	169.11(9)	Sn1-N2-C2-C1	-34.1(3)
Sn1-Cl2	2.4190(8)	O2-Sn1-N2	88.69(9)	N1-C1-C2-N2	42.2(3)
Sn1-Cl1	2.4237(8)	N1-Sn1-N2	78.05(9)	C1-N1-C3-C6	177.1(3)
O1-C5	1.345(3)	O1-Sn1-Cl2	89.33(7)	Sn1-N1-C3-C6	-6.9(5)
O2-C11	1.345(3)	O2-Sn1-Cl2	92.54(7)	C2-N2-C4-C12	177.7(3)
N1-C3	1.277(4)	N1-Sn1-Cl2	90.60(7)	Sn1-N2-C4-C12	-3.5(4)
N1-C1	1.466(4)	N2-Sn1-Cl2	89.35(7)	Sn1-O1-C5-C10	-167.5(2)
N2-C4	1.285(4)	O1-Sn1-Cl1	89.43(6)	Sn1-O1-C5-C6	14.7(4)
N2-C2	1.464(4)	O2-Sn1-Cl1	90.68(7)	O1-C5-C6-C7	179.2(3)
C1-C2	1.529(4)	N1-Sn1-Cl1	86.39(7)	O1-C5-C6-C3	1.5(5)
C3-C6	1.446(4)	N2-Sn1-Cl1	91.29(7)	N1-C3-C6-C7	176.8(3)
C4-C12	1.440(4)	Cl2-Sn1-Cl1	176.72(3)	N1-C3-C6-C5	-5.4(5)
C5-C10	1.398(4)	C5-O1-Sn1	124.5(2)	Sn1-O2-C11-C16	-156.0(2)
C5-C6	1.418(4)	C11-O2-Sn1	124.7(2)	Sn1-O2-C11-C12	26.9(4)
C6-C7	1.412(4)	C3-N1-C1	122.8(3)	O2-C11-C12-C4	-2.8(5)
C7-C8	1.371(4)	C3-N1-Sn1	122.8(2)	N2-C4-C12-C13	171.5(3)
C8-C9	1.394(4)	C1-N1-Sn1	114.3(2)	N2-C4-C12-C11	-9.4(5)
C9-C10	1.379(4)	C4-N2-C2	122.0(2)		
C11-C16	1.395(4)	C4-N2-Sn1	124.1(2)		
C11-C12	1.419(4)	C2-N2-Sn1	113.9(2)		
C12-C13	1.408(4)	N1-C1-C2	109.7(2)		
C13-C14	1.377(5)	N2-C2-C1	109.5(2)		
C14-C15	1.391(5)	N1-C3-C6	126.5(3)		
C15-C16	1.377(4)	N2-C4-C12	125.9(3)		

**Table 7:** List of selected bond lengths and angles in [Sn(<sup>t</sup>Bu<sub>2</sub>Salophen)Cl<sub>2</sub>].

bond	value [Å]	angle	value [°]	torsion	value [°]
Sn1-O1	1.996(2)	O1-Sn1-O2	104.20(9)	C3-N1-C1-C20	-14.1(5)
Sn1-O2	1.999(2)	O1-Sn1-N2	166.13(9)	Sn1-N1-C1-C20	178.7(3)
Sn1-N2	2.146(3)	O2-Sn1-N2	89.19(9)	C3-N1-C1-C2	166.8(3)
Sn1-N1	2.150(3)	O1-Sn1-N1	89.4(1)	Sn1-N1-C1-C2	-0.4(4)
Sn1-C11	2.4136(9)	O2-Sn1-N1	166.1(1)	N1-C1-C2-C17	-178.4(3)
Sn1-C12	2.4287(9)	N2-Sn1-N1	77.4(1)	C20-C1-C2-N2	-177.9(3)
O1-C5	1.338(4)	O1-Sn1-C11	91.08(8)	N1-C1-C2-N2	1.2(4)
O2-C11	1.337(4)	O2-Sn1-C11	89.54(7)	C4-N2-C2-C17	-14.9(5)
N1-C3	1.305(4)	N2-Sn1-C11	92.65(7)	Sn1-N2-C2-C1	178.1(3)
N1-C1	1.416(4)	N1-Sn1-C11	87.21(8)	C4-N2-C2-C	165.5(3)
N2-C4	1.301(4)	O1-Sn1-C12	89.24(8)	Sn1-N2-C2-C1	-1.4(4)
N2-C2	1.420(4)	O2-Sn1-C12	90.25(7)	C1-N1-C3-C6	-174.1(3)
C1-C20	1.399(5)	N2-Sn1-C12	87.06(7)	Sn1-N1-C3-C6	-7.8(5)
C1-C2	1.411(4)	N1-Sn1-C12	92.93(8)	C2-N2-C4-C12	-172.6(3)
C2-C17	1.390(5)	C11-Sn1-C12	179.65(3)	Sn1-N2-C4-C12	-6.6(4)
C3-C6	1.421(5)	C5-O1-Sn1	127.5(2)	Sn1-O1-C5-C10	-157.8(2)
C4-C12	1.432(4)	C11-O2-Sn1	126.0(2)	Sn1-O1-C5-C6	24.8(4)
C5-C10	1.406(5)	C3-N1-C1	122.8(3)	N1-C3-C6-C7	176.8(3)
C5-C6	1.422(5)	C3-N1-Sn1	121.4(2)	N1-C3-C6-C5	-1.5(6)
C6-C7	1.421(4)	C1-N1-Sn1	114.5(2)	O1-C5-C6-C7	175.2(3)
C7-C8	1.361(6)	C4-N2-C2	122.1(3)	O1-C5-C6-C3	-6.5(5)
C8-C9	1.399(5)	C4-N2-Sn1	122.0(2)	O1-C5-C10-C9	-175.3(3)
C8-C21	1.548(5)	C2-N2-Sn1	114.6(2)	O1-C5-C10-C29	5.5(5)
C9-C10	1.396(5)	C20-C1-N1	124.1(3)	Sn1-O2-C11-C12	30.0(4)
C10-C29	1.547(5)	C2-C1-N1	116.8(3)	Sn1-O2-C11-C16	-153.8(2)
C11-C12	1.415(5)	C17-C2-N2	124.0(3)	O2-C11-C12-C13	172.6(3)
C11-C16	1.416(4)	C1-C2-N2	116.7(3)	O2-C11-C12-C4	-9.0(5)
C12-C13	1.416(4)	N1-C3-C6	127.9(3)	N2-C4-C12-C11	-2.7(5)
C13-C14	1.373(5)	N2-C4-C12	127.1(3)	N2-C4-C12-C13	175.9(3)
C14-C15	1.400(5)	O1-C5-C10	118.4(3)	O2-C11-C16-C15	-173.6(3)
C14-C25	1.538(5)	O1-C5-C6	122.1(3)	O2-C11-C16-C33	6.2(4)
C15-C16	1.393(5)	O2-C11-C12	122.4(3)	N2-C2-C17-C18	178.7(3)
C16-C33	1.546(5)	O2-C11-C16	118.3(3)	N1-C1-C20-C19	179.5(3)
C17-C18	1.375(5)				
C18-C19	1.389(6)				
C19-C20	1.369(6)				

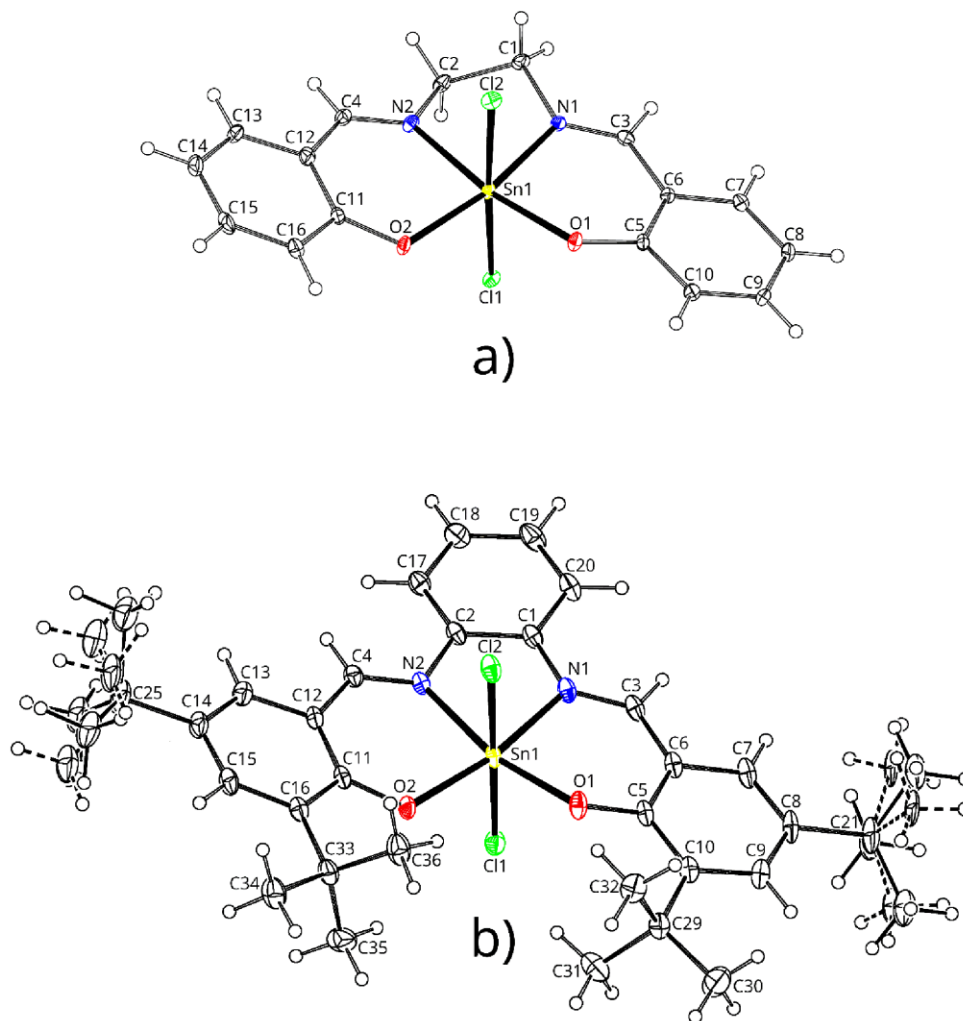


**Figure 89:** a) View of the molecular structure of [Sn(Salen)Cl<sub>2</sub>]. b) View of the molecular structure of [Sn(<sup>t</sup>Bu<sub>2</sub>Salophen)Cl<sub>2</sub>]. Thermal displacement ellipsoids are plotted at the 30 % probability level. Applied colors: C – black, H – black contour, Cl – green, N – blue, O – red, Sn – yellow.

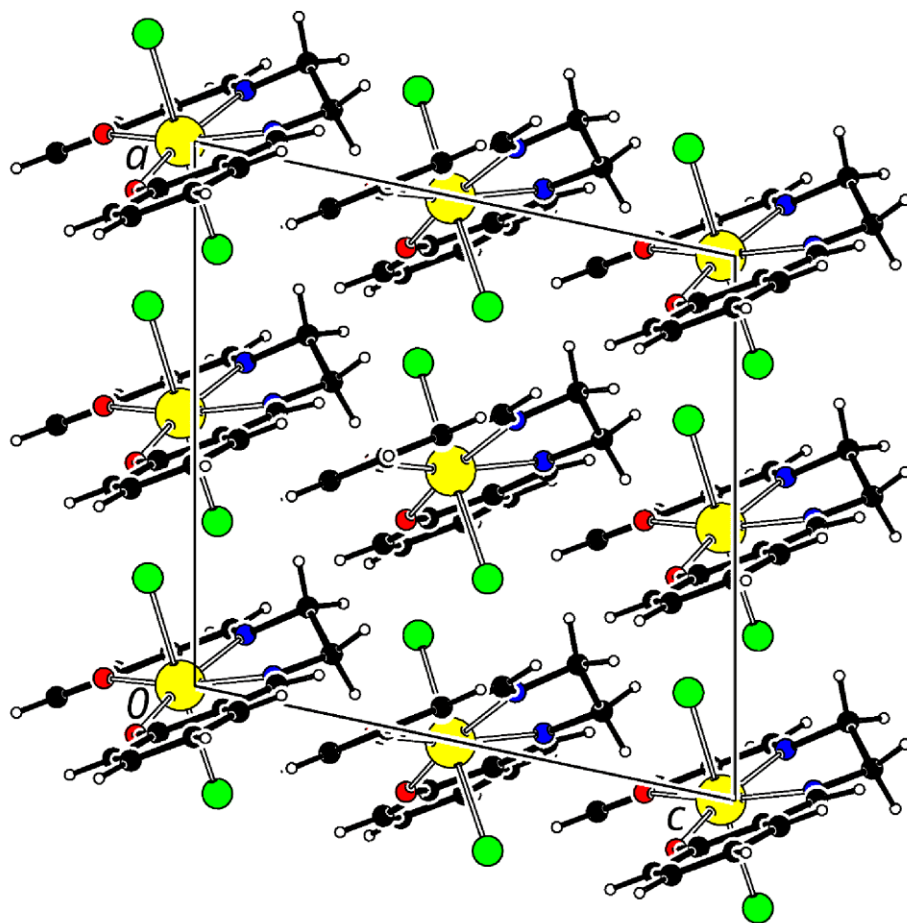


**Figure 90:** Crystal packing of  $[\text{Sn}(\text{Salen})\text{Cl}_2]$  viewed along the axis  $b$ . The unit cell is outlined by the solid line. Applied colors: C – black, H – black contour, Cl – green, N – blue, O – red, Sn – yellow.

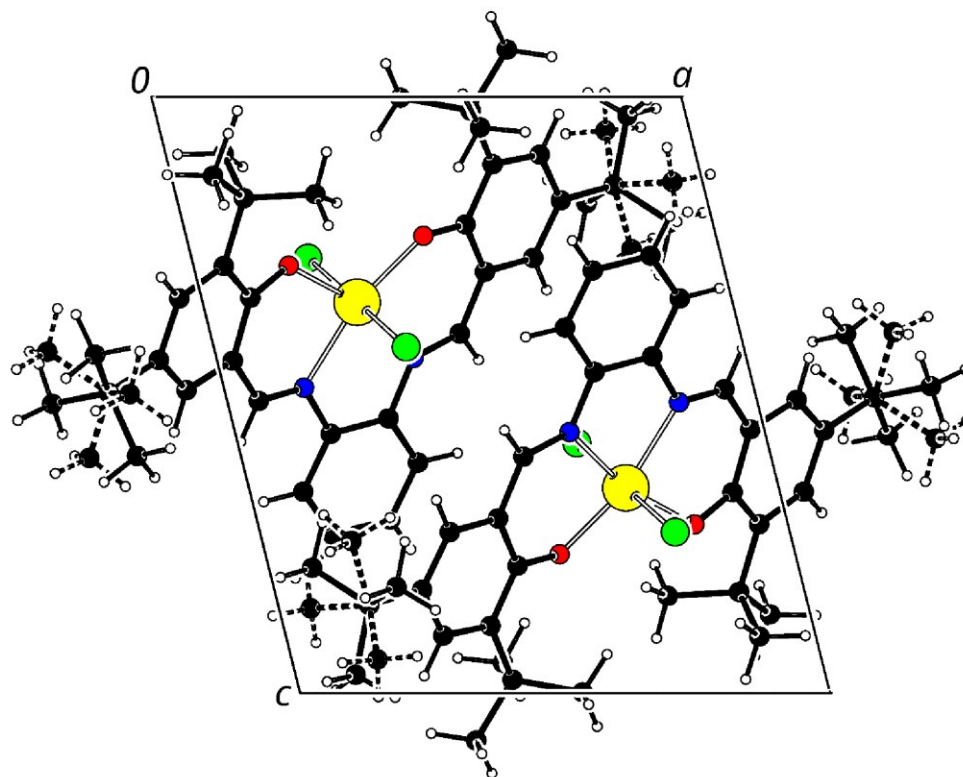


**Figure 91:** Crystal packing of [Sn(tBu<sub>2</sub>Salophen)Cl<sub>2</sub>] viewed along the axis *b*. The unit cell is outlined by the solid line.  
Applied colors: C – black, H – black contour, Cl – green, N – blue, O – red, Sn – yellow.

## Computational Details

The HIA values were calculated following a protocol validated by Greb et al<sup>20</sup> as follows.

Structure optimization of all involved LAs and the corresponding [LA-H] counterpart (see Figure 91) was performed at the threefold-corrected PBEh-3c/def2-mSVP level of theory as implemented in ORCA 5.0 software. Considering that the sixth ligand should be released to have a vacant active site, the calculations were carried out using the corresponding cations of the LAs. In the case of the LA with the two triflate ligands (1-OTf<sub>2</sub>), those ligands were not considered since the interaction with the Tin center is weak. In all cases, the structures were confirmed as local minima through normal analysis using frequency calculations. Zero-point energies and thermal corrections at 298 K were obtained at the same level of theory and subsequently used.

Previously optimized geometries were utilized for single-point calculations at the DSD-PBEP86-D3BJ / def2-QZVP level of theory which has been demonstrated to be suitable for HIA<sup>20</sup>. In all DFT calculations, the “resolution-of identity” and “chain of spheres” approximation in the form of RIJCOSX was used in combination with auxiliary basis sets (autoaux). In particular, the def2/C auxiliary basis set was applied. These electronic energies were combined with ZPE/Thermal corrections from the previous step, to obtain the total enthalpies of the Lewis acids and their hydride adducts.

The HIA values were calculated with isodesmic anchoring to the CCSD(T)/CBS values of the trimethylsilylium (TMS) system (924 kJ/mol). The isodesmic reaction corresponds to the calculation of the reaction enthalpy  $LA(+) + TMS-H \rightarrow LA-H + TMS(+)$  and subtracting the CCSD(T)/CBS value of  $TMS-H \rightarrow TMS(+) + H-$ . By doing so, a final absolute HIA is obtained.

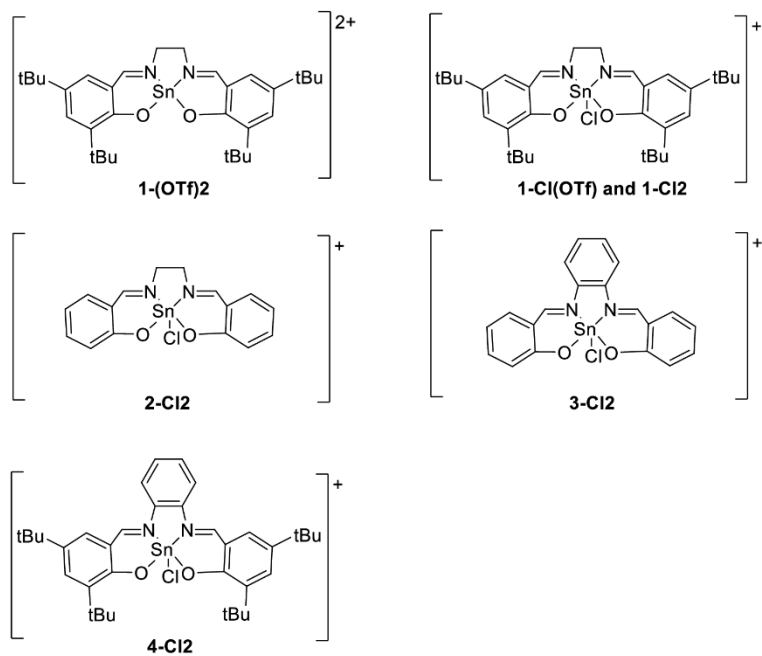
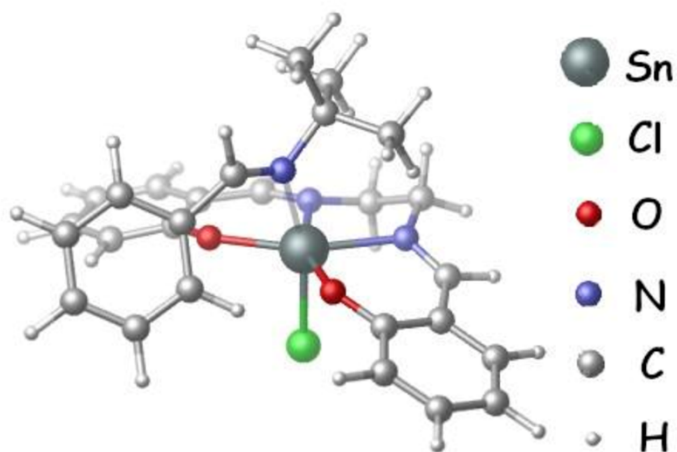


Figure 92: Chemical structure of LAs considered in the HIA analysis. 1-Cl(OTf) and 1-Cl<sub>2</sub> were considered as the same structure since both of them result in the same LA (cation).

To analyze the preorientation of the catalyst for the most active LA (2-Cl<sub>2</sub>), the frustrated Lewis Pair arising from the interaction between the model Imine and 2-Cl<sub>2</sub> was optimized.

Different structures were considered as initial guesses, and only the lowest energy structure was selected for the final Lewis pair shown in Figure 93. As can be noted, in the absence of t-Bu group Tin center can interact with the imine nitrogen ( $R_{\text{Sn-N}} = 2.33 \text{ \AA}$ )





**R Sn(LA)-N(LB)= 2.31 A**

Figure 93: Optimized structure corresponding to imine 2-Cl<sub>2</sub> FLP.

Cartesian Coordinates for optimized structures corresponding to LAs and LAHs

**1-OTf2**

83

FINAL HEAT OF FORMATION = -1716.682832

C	-0.020962	0.541833	0.072488
C	0.032333	0.368341	1.459036
C	1.261519	0.012721	2.098304
C	2.431302	-0.151135	1.318881
C	2.416270	0.009432	-0.046311
C	1.178664	0.347048	-0.618060
O	-1.094349	0.548688	2.164175
Sn	-1.461707	0.246645	4.033208
C	1.437090	-0.170659	3.484664
N	0.526184	-0.117997	4.430298
C	0.804897	-0.230782	5.856914
C	-0.137300	0.707083	6.624762
N	-1.477479	0.599223	6.061123
C	-2.587773	0.613696	6.764144
C	-3.908946	0.424917	6.310440
C	-4.289800	0.120867	4.965442
C	-5.636045	-0.064503	4.634455
C	-6.549882	0.065096	5.683891
C	-6.236928	0.355697	7.021903
C	-4.904534	0.527423	7.311210
O	-3.376299	0.014170	3.989189
H	1.846354	0.039367	6.071573
H	0.660395	-1.271663	6.183481
H	-0.138849	0.437487	7.688309
H	0.212453	1.747457	6.549501
H	2.462935	-0.371852	3.817038
H	-2.469819	0.781934	7.841682

72

H	3.356683	-0.413440	1.831892
C	3.691956	-0.163009	-0.869208
H	1.150006	0.470831	-1.695469
C	-1.310712	0.915116	-0.676243
H	-4.586586	0.749216	8.329867
C	-7.296723	0.445629	8.117348
H	-7.598585	-0.071104	5.441194
C	-6.114168	-0.371441	3.205943
C	-7.639676	-0.513059	3.157023
C	-5.739272	0.784123	2.262930
C	-5.520791	-1.700865	2.711546
H	-6.160175	0.598102	1.267564
H	-6.156368	1.735547	2.614815
H	-4.661130	0.912751	2.129855
H	-7.949313	-0.727689	2.128751
H	-8.011275	-1.339560	3.775029
H	-8.159385	0.405329	3.455790
H	-5.943326	-1.946265	1.730285
H	-4.433881	-1.678335	2.591246
H	-5.773397	-2.527013	3.386973
C	-8.713060	0.425507	7.541527
C	-7.118842	-0.761882	9.049411
C	-7.110227	1.748328	8.906352
H	-7.878757	1.832943	9.683126
H	-6.143274	1.800521	9.421365
H	-7.197268	2.630782	8.261004
H	-7.870111	-0.744532	9.847897
H	-7.233271	-1.709465	8.509304
H	-6.134646	-0.771551	9.534403
H	-9.442956	0.539369	8.349995
H	-8.888453	1.247477	6.836047
H	-8.952725	-0.519161	7.037658
C	-1.057145	1.032126	-2.183606
C	-2.375822	-0.177171	-0.481889
C	-1.830303	2.281216	-0.199168
H	-2.707136	2.569252	-0.791224
H	-2.141161	2.290471	0.849320
H	-1.076388	3.065286	-0.339262
H	-1.990765	1.307693	-2.685424
H	-0.326026	1.810991	-2.431308
H	-0.726398	0.088464	-2.634859
H	-3.255272	0.057677	-1.092617
H	-2.006755	-1.156514	-0.809879
H	-2.725568	-0.270883	0.550407
C	3.433220	0.019757	-2.364688
C	4.713638	0.889393	-0.414663
C	4.253360	-1.572546	-0.633878
H	5.638174	0.798011	-0.996601
H	4.335153	1.908704	-0.557224
H	4.991427	0.779970	0.641066
H	4.369551	-0.104004	-2.919233
H	2.729409	-0.720759	-2.765258
H	3.057259	1.021555	-2.606648
H	5.157407	-1.725796	-1.234159
H	4.537277	-1.745479	0.411620
H	3.533182	-2.348757	-0.918862

C	3.299726	-0.558700	-2.299509
C	4.715304	0.320977	-0.459906
C	3.853736	-2.033184	-0.373819
H	4.729856	-2.402861	-0.921006
H	4.081379	-2.114466	0.696286
H	3.018618	-2.712097	-0.585595
H	4.209855	-0.880957	-2.817987
H	2.497659	-1.235202	-2.618817
H	3.061810	0.448355	-2.664874
H	5.605362	0.006615	-1.018605
H	4.507269	1.364244	-0.726714
H	4.984944	0.297262	0.603025
C	-8.662509	1.369812	7.320696
C	-7.108197	0.170950	8.850240
C	-7.111404	2.679801	8.750482
H	-9.416285	1.447335	8.112279
H	-8.829326	2.209591	6.634711
H	-8.869082	0.439798	6.776613
H	-7.891445	2.743711	9.519135
H	-6.148332	2.735348	9.272006
H	-7.196276	3.570503	8.116074
H	-7.882783	0.166651	9.627381
H	-7.196266	-0.765996	8.286961
H	-6.137942	0.156807	9.361914
H	-1.212404	3.536632	3.656810

#### 1-C12

84

FINAL HEAT OF FORMATION = -2176.834085

C	-0.091713	0.555175	0.016238
C	-0.025777	0.691010	1.419305
C	1.200759	0.417199	2.089187
C	2.328720	-0.016414	1.357236
C	2.288655	-0.165234	-0.006443
C	1.065077	0.136362	-0.629988
O	-1.106274	1.030370	2.085594
Sn	-1.341444	1.801187	3.893754
N	0.538852	0.939842	4.388650
C	1.374657	0.501807	3.494321
O	-3.214530	1.189949	3.923166
C	-4.149472	1.260374	4.853727
C	-3.824916	1.452936	6.224936
C	-4.842258	1.471120	7.200582
C	-6.167371	1.328987	6.864491
C	-6.445560	1.146479	5.500970
C	-5.500054	1.098265	4.481664
C	-2.496352	1.597005	6.715963
N	-1.410623	1.703138	6.022219
C	-0.083995	1.797598	6.584908
C	0.829434	0.846656	5.811002
Cl	-1.082427	4.074155	3.608428
H	-0.072989	1.545841	7.653687
H	0.276089	2.833886	6.488643
H	1.881247	1.086310	6.017383
H	0.652700	-0.185683	6.149383
H	-2.393353	1.618965	7.809516
H	2.344702	0.145267	3.866437
H	-4.547580	1.605989	8.241905
C	-7.253951	1.340609	7.939198
H	-7.485622	1.029583	5.217137
C	-5.922508	0.863992	3.023739

75

**1H-OTf2**

84

FINAL HEAT OF FORMATION = -1717.675836

C	-0.103585	0.540632	0.012609
C	-0.040447	0.689204	1.417478
C	1.190825	0.425524	2.083193
C	2.325804	0.009493	1.351821
C	2.292624	-0.126782	-0.012927
C	1.061786	0.150744	-0.634748
O	-1.113258	1.031734	2.086633
Sn	-1.348982	1.874648	3.887537
N	0.517462	0.930169	4.384415
C	1.349258	0.483628	3.491668
O	-3.197630	1.149348	3.944901
C	-4.138511	1.228154	4.865373
C	-3.822491	1.412031	6.239389
C	-4.843570	1.445941	7.208646
C	-6.169792	1.339041	6.863360
C	-6.442890	1.157691	5.498672
C	-5.491009	1.085363	4.486972
C	-2.490972	1.526794	6.735018
N	-1.412307	1.674104	6.042200
C	-0.087509	1.712843	6.610144
C	0.797814	0.767548	5.802085
H	-0.082335	1.425156	7.670321
H	0.306224	2.740687	6.554217
H	1.856929	0.959625	6.022838
H	0.584163	-0.270880	6.098042
H	-2.385719	1.489316	7.828556
H	2.304206	0.090704	3.867581
H	-4.551817	1.570161	8.252327
C	-7.261342	1.390886	7.931777
H	-7.483257	1.062948	5.207707
C	-5.906476	0.852992	3.026708
H	3.240767	-0.203193	1.906200
C	3.526023	-0.591562	-0.787525
H	1.016244	0.045755	-1.713210
C	-1.396153	0.801140	-0.774147
C	-1.185067	0.582567	-2.276161
C	-2.499171	-0.170118	-0.325346
C	-1.852798	2.257503	-0.590904
H	-2.125040	0.771233	-2.806475
H	-0.437257	1.262218	-2.703880
H	-0.888619	-0.446271	-2.514228
H	-3.401192	-0.014999	-0.930809
H	-2.187622	-1.212385	-0.466535
H	-2.785828	-0.041679	0.721258
H	-2.719336	2.461500	-1.232134
H	-2.155621	2.485524	0.434300
H	-1.062259	2.961815	-0.878629
C	-7.431591	0.786962	2.887947
C	-5.427224	2.003834	2.126360
C	-5.346387	-0.489069	2.530554
H	-5.671319	-0.669471	1.498083
H	-4.253907	-0.526247	2.540185
H	-5.719384	-1.321091	3.140507
H	-5.838393	1.880280	1.116719
H	-5.775392	2.974288	2.501778
H	-4.340462	2.045486	2.019544
H	-7.694839	0.613982	1.838407
H	-7.873268	-0.035426	3.463700
H	-7.922929	1.720078	3.190869

H	3.243029	-0.235006	1.909983
C	3.510749	-0.662525	-0.777899
H	1.017326	0.029700	-1.708190
C	-1.373452	0.862631	-0.771214
C	-1.165765	0.644554	-2.273834
C	-2.514765	-0.069599	-0.333718
C	-1.772341	2.334996	-0.579801
H	-2.095933	0.874788	-2.804761
H	-0.390677	1.297251	-2.694503
H	-0.910011	-0.393878	-2.517940
H	-3.401035	0.115077	-0.953599
H	-2.238279	-1.122881	-0.466525
H	-2.815040	0.073731	0.706945
H	-2.647160	2.568520	-1.199376
H	-2.037359	2.580952	0.451597
H	-0.964020	3.008426	-0.890371
C	-7.447710	0.777401	2.895854
C	-5.464939	2.024754	2.125049
C	-5.349804	-0.470388	2.520400
H	-5.682423	-0.652342	1.490783
H	-4.256932	-0.495275	2.518077
H	-5.707003	-1.308209	3.131929
H	-5.867410	1.889340	1.113473
H	-5.839468	2.986209	2.497667
H	-4.379170	2.096881	2.026644
H	-7.715562	0.608353	1.846918
H	-7.874085	-0.055413	3.468206
H	-7.949453	1.701685	3.208379
C	3.281731	-0.639601	-2.289603
C	4.718619	0.228913	-0.460001
C	3.807836	-2.106721	-0.350136
H	4.675389	-2.499711	-0.894418
H	4.034784	-2.183058	0.720499
H	2.958227	-2.769481	-0.555282
H	4.183307	-0.986837	-2.806733
H	2.464119	-1.301447	-2.600090
H	3.065417	0.368874	-2.664147
H	5.600482	-0.107045	-1.018872
H	4.530196	1.274039	-0.733658
H	4.990778	0.207297	0.602320
C	-8.658145	1.305158	7.334719
C	-7.072796	0.104097	8.830290
C	-7.124484	2.614262	8.784430
H	-9.408280	1.353545	8.131935
H	-8.844573	2.154401	6.665670
H	-8.851259	0.381562	6.775065
H	-7.903862	2.647072	9.555528
H	-6.161952	2.676047	9.306114
H	-7.226879	3.516417	8.169301
H	-7.843254	0.069006	9.610799
H	-7.147034	-0.822416	8.247961
H	-6.099692	0.097158	9.336734

**1H-C12**

85

FINAL HEAT OF FORMATION = -2177.630033

C	0.018980	-0.178883	0.032139
C	0.012002	-0.143782	1.458404
C	1.218280	0.006966	2.179130
C	2.428114	0.144683	1.553483
C	2.409961	0.100063	0.142475

76

C	1.282180	-0.067611	-0.633304
C	-1.156834	-0.347879	2.260863
N	-2.383313	-0.388709	1.885471
C	-3.460420	-0.712100	2.784789
C	-4.670072	0.157474	2.449389
N	-4.905927	0.112037	1.028269
Sn	-3.046426	0.039877	-0.183274
O	-1.049144	-0.337539	-0.668125
C	3.751298	0.327360	2.291667
C	4.352979	1.689139	1.918819
C	1.366117	-0.142002	-2.163163
C	2.814988	-0.021117	-2.646915
C	-6.079137	-0.048702	0.534300
C	-6.465409	-0.141730	-0.842085
C	-7.837580	-0.375938	-1.056569
C	-8.376527	-0.492416	-2.314305
C	-7.469493	-0.400828	-3.384044
C	-6.109017	-0.175137	-3.258101
C	-5.573427	0.000463	-1.948374
C	-9.877972	-0.713411	-2.506155
C	-10.270600	-0.730958	-3.984195
O	-4.329436	0.320754	-1.797241
C	-5.201414	-0.120368	-4.493456
C	-5.992451	-0.368312	-5.782791
Cl	-3.396853	-2.309783	-0.478565
C	-10.283002	-2.055896	-1.882816
C	-10.652662	0.423064	-1.823920
C	-4.129483	-1.219153	-4.408551
C	-4.546912	1.264041	-4.629179
C	4.723098	-0.790957	1.890775
C	0.836388	-1.497385	-2.660576
C	0.580536	1.011177	-2.809030
H	-2.726722	1.713924	-0.126877
H	3.363820	0.200627	-0.370104
H	-0.956162	-0.492927	3.334235
H	-3.170966	-0.575068	3.838263
H	-3.728578	-1.771267	2.647924
H	-5.549120	-0.177819	3.021066
H	-4.464832	1.197669	2.750003
H	-6.914066	-0.140764	1.246525
H	-8.477693	-0.458684	-0.176158
H	-7.865598	-0.515627	-4.387263
H	1.151896	0.011705	3.266448
C	3.566603	0.277727	3.808013
H	-11.735025	0.291241	-1.953857
H	-10.460727	0.468915	-0.745112
H	-10.380576	1.397878	-2.246844
H	-10.008588	0.206223	-4.490450
H	-9.796161	-1.553970	-4.532684
H	-11.354976	-0.861742	-4.083166
H	-9.742914	-2.888735	-2.349213
H	-10.072427	-2.092057	-0.806916
H	-11.358341	-2.238379	-2.010370
H	-5.308149	2.050851	-4.708557
H	-3.895265	1.508613	-3.787754
H	-3.939739	1.302307	-5.543492
H	-6.480313	-1.351116	-5.794760
H	-6.761091	0.395047	-5.958000
H	-5.310815	-0.339244	-6.641069
H	-3.466779	-1.108557	-3.547644
H	-4.591928	-2.211743	-4.340596
H	-3.506106	-1.204336	-5.312179

H	-0.491497	0.960358	-2.606235
H	0.947649	1.983570	-2.456618
H	0.708325	0.986393	-3.899381
H	3.270687	0.938909	-2.373056
H	3.452980	-0.824846	-2.258465
H	2.844077	-0.089582	-3.740723
H	1.414804	-2.324148	-2.228828
H	-0.215018	-1.660214	-2.413115
H	0.937556	-1.561213	-3.752225
H	3.678540	2.508391	2.196283
H	5.309885	1.852204	2.432183
H	4.544377	1.773708	0.842268
H	4.316081	-1.778586	2.140188
H	4.940447	-0.787774	0.816254
H	5.681783	-0.681242	2.414473
H	4.534226	0.390119	4.311956
H	2.919330	1.084531	4.174459
H	3.138397	-0.676776	4.138543

## 2-Cl2

36

FINAL HEAT OF FORMATION = -1549.534518

C	-0.072075	0.258713	0.007665
C	-0.035349	0.317858	1.406166
C	1.194582	0.034441	2.064210
C	2.333494	-0.302944	1.292807
C	2.278835	-0.341747	-0.074708
C	1.061703	-0.057406	-0.710441
O	-1.147079	0.597455	2.045406
Sn	-1.361693	1.357222	3.868084
N	0.477614	0.381010	4.367275
C	1.343523	0.009120	3.475228
O	-3.295999	0.951114	3.864365
C	-4.191012	1.117565	4.817016
C	-3.865592	1.249179	6.195174
C	-4.906264	1.380773	7.144069
C	-6.221436	1.405651	6.759570
C	-6.528078	1.281960	5.398654
C	-5.539949	1.134718	4.446861
C	-2.535476	1.231843	6.699706
N	-1.446200	1.216168	6.004771
C	-0.122703	1.180209	6.585089
C	0.720186	0.189312	5.787264
Cl	-0.942799	3.606529	3.634386
H	-0.151081	0.886556	7.642677
H	0.322894	2.186054	6.535143
H	1.783633	0.318223	6.030006
H	0.441153	-0.838631	6.064424
H	-2.433982	1.235638	7.793761
H	2.303565	-0.375363	3.846499
H	-4.646185	1.471816	8.199031
H	-7.013126	1.518053	7.496451
H	-7.569135	1.302086	5.078563
H	-5.789735	1.035413	3.392206
H	3.267225	-0.531144	1.807364
H	3.160406	-0.594696	-0.658651
H	1.005363	-0.086645	-1.797995
H	-1.012845	0.473416	-0.495775

**2H-C12**

37

FINAL HEAT OF FORMATION = -1550.335286

C	0.126272	-0.025364	-0.066292
C	0.065344	-0.109025	1.343592
C	1.286194	0.086067	2.060488
C	2.477657	0.341306	1.348287
C	2.504442	0.420160	-0.020570
C	1.305767	0.231126	-0.723018
O	-1.064028	-0.399273	1.896478
Sn	-1.701660	0.025816	3.827792
N	0.462690	-0.128395	4.341420
C	1.407256	0.010699	3.486661
O	-3.737390	0.455526	3.952341
C	-4.434174	0.978339	4.898151
C	-3.935044	1.306406	6.198114
C	-4.814718	1.849631	7.162360
C	-6.141492	2.069829	6.900413
C	-6.628110	1.754716	5.622521
C	-5.805884	1.234415	4.653933
C	-2.567648	1.184417	6.606656
N	-1.576655	0.697005	5.953202
C	-0.224129	0.838964	6.444516
C	0.688460	-0.175211	5.761083
Cl	-1.321212	2.342902	3.324245
H	-0.172961	0.716313	7.537229
H	0.133259	1.853044	6.206571
H	1.738423	0.030839	6.020154
H	0.455669	-1.187543	6.128333
H	-2.358968	1.588491	7.609814
H	2.437226	0.085314	3.870112
H	-4.411738	2.100595	8.144810
H	-6.798938	2.485928	7.660130
H	-7.678355	1.928250	5.388585
H	-6.190874	0.996566	3.663771
H	3.399663	0.480537	1.914966
H	3.432975	0.622421	-0.549396
H	1.304595	0.288189	-1.811405
H	-0.800343	-0.171060	-0.618800
H	-2.011660	-1.616341	4.145359

**3-C12**

40

FINAL HEAT OF FORMATION = -1701.525111

C	-0.001057	-0.019616	0.006302
C	-0.000926	-0.036486	1.397815
C	1.220542	-0.026903	2.095633
C	2.418867	0.002112	1.388572
C	2.404741	0.050987	0.004871
C	1.197318	0.039525	-0.684711
N	-1.159513	-0.099724	2.187662
C	-2.334250	0.290495	1.784702
C	-3.548173	0.269472	2.513188
C	-3.652536	-0.123141	3.877001
C	-4.909180	-0.068359	4.493738
C	-6.016961	0.356010	3.791509
C	-5.928715	0.750680	2.448378

79



C	-4.709422	0.709266	1.828548
O	-2.629162	-0.506200	4.600830
Sn	-0.748925	-0.917805	4.130747
Cl	-0.509928	-3.172960	3.800776
N	1.128060	-0.086261	3.494904
C	2.070414	0.298979	4.305736
C	2.056083	0.272081	5.721950
C	0.931770	-0.116923	6.503198
C	1.037121	-0.068676	7.899050
C	2.207460	0.342839	8.499457
C	3.323086	0.731665	7.743223
C	3.238103	0.699939	6.377796
O	-0.213452	-0.493548	5.988767
H	-2.401578	0.703028	0.771281
H	2.981315	0.707581	3.852682
H	-4.618278	1.015522	0.786257
H	-6.981503	0.387096	4.296960
H	4.091884	1.004933	5.772513
H	2.261368	0.367799	9.587167
H	3.373001	-0.034945	1.910850
H	3.345320	0.072998	-0.541538
H	1.189564	0.052017	-1.772688
H	-0.934382	-0.074857	-0.551017
H	4.236269	1.057073	8.235323
H	0.174257	-0.362335	8.493676
H	-4.988084	-0.365231	5.537831
H	-6.813350	1.086508	1.912848

### 3H-Cl2

41

FINAL HEAT OF FORMATION = -1702.329125

C	-0.037692	-0.365327	-0.018766
C	0.035127	-0.334351	1.393082
C	1.180083	0.294818	1.976350
C	2.174093	0.846777	1.135701
C	2.071987	0.806011	-0.229596
C	0.947794	0.187235	-0.799713
O	-0.894047	-0.900337	2.081388
Sn	-1.559805	-0.355415	3.991127
N	0.616236	0.057432	4.337422
C	1.416507	0.389862	3.378597
O	-3.609223	-0.249375	4.409844
C	-4.222058	0.690494	5.042748
C	-3.631561	1.437234	6.110650
C	-4.400547	2.410934	6.788481
C	-5.700241	2.673834	6.444931
C	-6.276210	1.943873	5.392976
C	-5.565442	0.983898	4.714202
C	-2.293516	1.261928	6.569072
N	-1.369431	0.527192	6.043924
C	-0.093400	0.401497	6.589604
C	0.959524	0.153463	5.684624
Cl	-1.743335	1.876006	3.142713
C	2.254129	-0.018066	6.170877
H	-2.030744	1.851028	7.459001
H	2.389430	0.820222	3.654718
H	-3.933946	2.967965	7.602427
H	-7.308799	2.141041	5.105117
H	3.040866	1.319632	1.599647
H	0.850699	0.144675	-1.884437
C	2.514001	0.082847	7.528748

H	3.063808	-0.257609	5.483363
H	3.529277	-0.057123	7.895016
C	1.476727	0.327175	8.420223
C	0.179174	0.470649	7.954507
H	1.673797	0.380100	9.489274
H	-0.634945	0.614134	8.663354
H	2.844617	1.240945	-0.859410
H	-0.908327	-0.839572	-0.468280
H	-6.019229	0.423868	3.898500
H	-6.274603	3.431104	6.973523
H	-1.544933	-1.980156	4.465761

4-C12

88

FINAL HEAT OF FORMATION = -2328.824669

C	-0.100197	0.270705	0.047094
C	0.024969	0.476810	1.436235
C	1.299835	0.322201	2.050791
C	2.419805	-0.058682	1.279199
C	2.326686	-0.263050	-0.074558
C	1.054708	-0.081540	-0.644035
O	-1.046120	0.757954	2.150196
Sn	-1.236772	1.661202	3.896346
N	0.726411	0.929590	4.348548
C	1.543945	0.487831	3.436263
O	-3.176757	1.278192	3.858170
C	-4.096694	1.293401	4.797206
C	-3.748022	1.161019	6.171280
C	-4.757879	1.074377	7.155916
C	-6.088657	1.148471	6.831548
C	-6.387682	1.322362	5.468534
C	-5.457278	1.400135	4.438679
C	-2.420531	1.109806	6.657484
N	-1.308586	1.267210	5.994667
C	-0.034672	1.247644	6.583045
C	1.051266	1.064475	5.706208
Cl	-0.949972	3.930281	3.654037
C	2.348920	1.057025	6.212041
H	-2.330200	0.919674	7.732541
H	2.548890	0.200816	3.764812
H	-4.446830	0.959158	8.194837
C	-7.162804	1.069780	7.915616
H	-7.434417	1.402253	5.196053
C	-5.902288	1.602775	2.983772
H	3.374664	-0.180170	1.791767
C	3.556048	-0.659284	-0.891786
H	0.963428	-0.236105	-1.713517
C	-1.447017	0.399588	-0.678472
C	-1.282221	0.202876	-2.189338
C	-2.410546	-0.688014	-0.177843
C	-2.058119	1.796141	-0.471260
H	-2.258173	0.300419	-2.677333
H	-0.622271	0.953067	-2.642921
H	-0.900256	-0.792125	-2.447563
H	-3.369335	-0.612358	-0.705948
H	-2.009132	-1.690311	-0.371471
H	-2.621518	-0.609906	0.891896
H	-2.934201	1.913902	-1.120291
H	-2.396208	1.973195	0.552551
H	-1.347468	2.588014	-0.737974
C	-7.427049	1.717115	2.881272

81

C	-5.317170	2.911477	2.428200
C	-5.477779	0.406304	2.118887
H	-5.850544	0.537169	1.095171
H	-4.394128	0.285155	2.056330
H	-5.903298	-0.529072	2.503139
H	-5.684302	3.078362	1.408057
H	-5.630439	3.772081	3.032067
H	-4.225420	2.915843	2.378852
H	-7.710438	1.873601	1.834461
H	-7.941996	0.808198	3.216275
H	-7.825785	2.567382	3.448276
C	3.208696	-0.922036	-2.357265
C	4.585040	0.477924	-0.827900
C	4.165743	-1.939497	-0.304531
H	5.043793	-2.247839	-0.885218
H	4.501348	-1.809384	0.731650
H	3.449595	-2.770051	-0.318981
H	4.108668	-1.225549	-2.903930
H	2.476643	-1.731109	-2.473073
H	2.816397	-0.031053	-2.863059
H	5.480308	0.219851	-1.406554
H	4.179423	1.410477	-1.238429
H	4.912198	0.683707	0.198696
C	-8.573317	1.075695	7.326165
C	-6.979487	-0.225286	8.717651
C	-7.014578	2.282504	8.844607
H	-9.313047	0.979936	8.128850
H	-8.802199	2.007674	6.794455
H	-8.739300	0.239475	6.635716
H	-7.780798	2.268056	9.629654
H	-6.039437	2.303304	9.346556
H	-7.120699	3.224156	8.292519
H	-7.746031	-0.307924	9.497877
H	-7.062077	-1.110692	8.075671
H	-6.007334	-0.272171	9.223075
C	2.568265	1.208508	7.569950
H	3.204995	0.948953	5.549459
H	3.586038	1.200448	7.954437
C	1.495820	1.397835	8.434763
C	0.202795	1.431413	7.943155
H	1.669916	1.541421	9.499128
H	-0.618236	1.622404	8.631264

4H-C12

41

FINAL HEAT OF FORMATION = -1702.329125

C	-0.037692	-0.365327	-0.018766
C	0.035127	-0.334351	1.393082
C	1.180083	0.294818	1.976350
C	2.174093	0.846777	1.135701
C	2.071987	0.806011	-0.229596
C	0.947794	0.187235	-0.799713
O	-0.894047	-0.900337	2.081388
Sn	-1.559805	-0.355415	3.991127
N	0.616236	0.057432	4.337422
C	1.416507	0.389862	3.378597
O	-3.609223	-0.249375	4.409844
C	-4.222058	0.690494	5.042748
C	-3.631561	1.437234	6.110650
C	-4.400547	2.410934	6.788481
C	-5.700241	2.673834	6.444931

82

C	-6.276210	1.943873	5.392976
C	-5.565442	0.983898	4.714202
C	-2.293516	1.261928	6.569072
N	-1.369431	0.527192	6.043924
C	-0.093400	0.401497	6.589604
C	0.959524	0.153463	5.684624
Cl	-1.743335	1.876006	3.142713
C	2.254129	-0.018066	6.170877
H	-2.030744	1.851028	7.459001
H	2.389430	0.820222	3.654718
H	-3.933946	2.967965	7.602427
H	-7.308799	2.141041	5.105117
H	3.040866	1.319632	1.599647
H	0.850699	0.144675	-1.884437
C	2.514001	0.082847	7.528748
H	3.063808	-0.257609	5.483363
H	3.529277	-0.057123	7.895016
C	1.476727	0.327175	8.420223
C	0.179174	0.470649	7.954507
H	1.673797	0.380100	9.489274
H	-0.634945	0.614134	8.663354
H	2.844617	1.240945	-0.859410
H	-0.908327	-0.839572	-0.468280
H	-6.019229	0.423868	3.898500
H	-6.274603	3.431104	6.973523
H	-1.544933	-1.980156	4.465761

**TMS+**

13

FINAL HEAT OF FORMATION = -408.284834

Si	-0.043591	-0.486428	-0.183527
C	-1.867947	-0.464270	-0.158945
H	-2.290777	0.542850	-0.088465
H	-2.256511	-0.951068	-1.066748
H	-2.238794	-1.068051	0.683213
C	0.846011	-2.076967	-0.275218
H	1.555417	-2.162100	0.561776
H	0.183281	-2.948101	-0.272137
H	1.460472	-2.102913	-1.188729
C	0.889853	1.080013	-0.106053
H	0.569800	1.751328	-0.917001
H	0.645534	1.607152	0.829458
H	1.974591	0.944492	-0.160410

**TMSH**

14

FINAL HEAT OF FORMATION = -409.174447

C	0.009921	-0.016622	-0.011280
Si	0.020436	-0.036781	1.868811
C	1.789078	-0.016980	2.506879
H	-0.682460	1.181946	2.366578
C	-0.880030	-1.559142	2.507054
H	-1.013341	-0.010644	-0.406111
H	0.521838	0.869889	-0.405207
H	0.517491	-0.900681	-0.417770
H	-0.391663	-2.479822	2.163163
H	-0.897200	-1.583243	3.603592
H	-1.920121	-1.585902	2.159664
H	2.330842	0.871004	2.158803
H	1.821290	-0.014435	3.603309

H 2.342861 -0.899299 2.161362

**Imine--2-Cl2 FLP**

63

FINAL HEAT OF FORMATION = 0.000000

C	-0.439373	0.072860	0.095662
C	-0.282034	0.162974	1.486164
C	1.029878	0.084542	2.028097
C	2.136252	-0.007987	1.149935
C	1.963691	-0.042398	-0.212065
C	0.661746	-0.022110	-0.725994
O	-1.344732	0.291735	2.224744
Sn	-1.687932	-0.022239	4.197527
Cl	-1.643163	-2.383395	3.936168
C	1.314714	-0.067461	3.415571
N	0.497548	-0.037507	4.415914
C	0.959991	-0.504808	5.712170
C	0.009880	-0.047779	6.806251
N	-1.347462	-0.257870	6.376994
C	-2.188764	-0.899182	7.113006
C	-3.546389	-1.206042	6.815790
C	-4.211305	-0.774305	5.637675
C	-5.540190	-1.171270	5.448316
C	-6.192795	-1.933015	6.398465
C	-5.553214	-2.341468	7.571195
C	-4.242690	-1.981478	7.766428
O	-3.648482	0.019932	4.754556
H	1.974216	-0.138809	5.926005
H	1.002587	-1.604090	5.697382
H	0.229338	-0.587858	7.737821
H	0.162306	1.020891	7.020784
H	2.367702	-0.284034	3.644155
H	-1.829529	-1.256366	8.088903
H	3.140105	-0.071003	1.569579
H	2.823945	-0.111144	-0.872609
H	0.511259	-0.093570	-1.801877
H	-1.454126	0.088462	-0.290857
H	-3.722069	-2.299199	8.669524
H	-6.080029	-2.939119	8.310531
H	-7.228161	-2.221571	6.223658
H	-6.056743	-0.872468	4.538879
N	-2.143561	2.252778	3.991154
C	-2.775655	2.684194	2.973213
H	-2.875933	3.769948	2.880813
C	-3.396845	1.994678	1.827996
C	-2.987936	2.415793	0.558948
C	-4.448259	1.097572	1.955408
C	-3.575177	1.881382	-0.568952
H	-2.187788	3.148960	0.450912
C	-5.057547	0.589339	0.809907
H	-4.818393	0.815804	2.933191
C	-4.618439	0.964551	-0.447151
H	-3.234901	2.173640	-1.560819
H	-5.891537	-0.102515	0.911308
H	-5.092603	0.560837	-1.339318
C	-1.684884	3.256712	5.008976
C	-2.040642	4.706057	4.666864
H	-3.121809	4.869686	4.588830
H	-1.684430	5.346356	5.479138

H	-1.557106	5.062247	3.749943
C	-0.162384	3.171318	5.091947
H	0.219583	3.925067	5.788422
H	0.209944	2.205402	5.433493
H	0.294602	3.360257	4.113013
C	-2.365616	2.919491	6.334705
H	-2.220780	1.888434	6.656999
H	-1.971045	3.571213	7.122423
H	-3.446637	3.086004	6.273961

**Imine--2-Cl2 FLP**

63			
C	-0.369007	0.127899	0.068805
C	-0.203901	0.160762	1.463641
C	1.105756	0.008335	1.994483
C	2.202969	-0.128001	1.110922
C	2.024014	-0.131793	-0.248085
C	0.723704	-0.017060	-0.757649
O	-1.252921	0.321694	2.213612
Sn	-1.611698	-0.057345	4.176538
Cl	-1.587186	-2.404508	3.863846
C	1.385068	-0.146822	3.379656
N	0.573222	-0.085836	4.384019
C	1.036299	-0.564568	5.675882
C	0.086128	-0.123326	6.776002
N	-1.276420	-0.302544	6.339389
C	-2.140338	-0.885608	7.102050
C	-3.517255	-1.130243	6.845290
C	-4.183801	-0.725720	5.657728
C	-5.552722	-1.011661	5.538721
C	-6.229715	-1.653239	6.554487
C	-5.582420	-2.048633	7.731025
C	-4.242977	-1.788947	7.863359
O	-3.590500	-0.069147	4.697437
H	2.048044	-0.195187	5.894954
H	1.084210	-1.663371	5.650528
H	0.293087	-0.694432	7.691330
H	0.254737	0.935397	7.023914
H	2.431394	-0.394373	3.607821
H	-1.782887	-1.228717	8.083101
H	3.203355	-0.247981	1.526515
H	2.874244	-0.241068	-0.916095
H	0.573558	-0.055028	-1.835138
H	-1.378928	0.221090	-0.323491
H	-3.718531	-2.092154	8.769392
H	-6.131039	-2.553801	8.521663
H	-7.292378	-1.857994	6.433057
H	-6.073928	-0.714573	4.630634
N	-2.181914	2.177110	3.991731
C	-2.869149	2.599336	3.000424
H	-3.050525	3.676758	2.968844
C	-3.445759	1.956196	1.814063
C	-3.275922	2.680337	0.628990
C	-4.206839	0.787634	1.799078
C	-3.792362	2.208222	-0.564406
H	-2.734468	3.627009	0.638716
C	-4.753529	0.340303	0.605376
H	-4.407414	0.245077	2.715537
C	-4.538860	1.035627	-0.576732

H	-3.639078	2.762041	-1.488803
H	-5.363175	-0.561259	0.603480
H	-4.971595	0.677082	-1.508772
C	-1.781401	3.179977	5.034594
C	-2.132419	4.627197	4.676717
H	-3.212019	4.802147	4.603841
H	-1.764280	5.274977	5.477877
H	-1.652323	4.965264	3.751300
C	-0.264483	3.111524	5.185006
H	0.075632	3.820547	5.946864
H	0.102951	2.127577	5.476836
H	0.232295	3.366993	4.241514
C	-2.515093	2.836119	6.330796
H	-2.340759	1.818678	6.681500
H	-2.191445	3.516248	7.126649
H	-3.597107	2.956842	6.209412

## References

1. H. Schmitt, R. Lomoth, A. Magnuson, J. Park, J. Fryxelius, M. Kritikos, J. Mårtensson, L. Hammarström, L. Sun and B. Åkermark, *Chemistry - A European Journal*, 2002, **8**, 3757-3768
2. R. Gericke and J. Wagler, *Main Group Metal Chemistry*, 2014, **37**, DOI:10.1515/mgmc-2014-0004.
3. H. Jing, S. K. Edulji, J. M. Gibbs, C. L. Stern, H. Zhou and S. B. T. Nguyen, *Inorg Chem*, 2004, **43**, 14, 4315-4327.
4. R. Bisht and B. Chattopadhyay, *J Am Chem Soc*, 2016, **138**, 1, 84-87.
5. N. Guimond and K. Fagnou, *J Am Chem Soc*, 2009, **131**, 34, 12050-12051
6. F. Schaufelberger and O. Ramström, *Chemistry - A European Journal*, 2015, **21**, 12735-12740
7. J. Mlochowski, E. Kubicz, K. Kloc, M. Mordarski, W. Peczyńska and L. Syper, *Liebigs Ann Chem*, 1988, 455-464.
8. S. B. Said, J. Młochowski and J. Skarżewski, *Liebigs Ann Chem*, 1990, 461-464
9. D. Enders, A. Rembiak and M. Seppelt, *Tetrahedron Lett*, 2013 **54**, 470-473
10. C. Talotta, G. Concilio, M. De Rosa, A. Soriente, C. Gaeta, A. Rescifina, P. Ballester and P. Neri, *Org. Lett.*, 2021, **23**, 1804-1808.
11. D. Reimer, W. Schilling, A. Goetz., et al., *ASC catalysis*, 2018, **8**, 12, 11679-11687
12. N. Chrysochos, S. Patsch, B. Elvers, et al., *Chem. Commun.*, 2023,**59**, 12350-12353
13. J. Masuda, P. Wei, D. Stephan, *Dalton Trans.*, 2003, 3500-3505
14. I.E. Alamanova, N. Shyytyeva, Z. Berdalieva, N. Abdylidaeva, A. Duishonbaeva and Z. Abdullaeva, *Journal of Crystallization Process and Technology*, 2021, **10**, 1-9.
15. Sivakumar, S. G. Raj, G. R. Kumar and R. Mohan, *Journal of Crystallization Process and Technology*, 2012, **02**, 130-136.
16. I.G. Sheldrick, *Acta Crystallographica Section A Foundations and Advances*, 2018, **74**.
17. I.G. M. Sheldrick, *Acta Crystallographica Section C Structural Chemistry*, 2015, **71**, 3-8.
18. I.A. L. Spek, *Acta Crystallographica Section E Crystallographic Communications*, 2020, **76**, 1-11.
19. I.L. J. Farrugia, *Journal of Applied Crystallography*, 2012, **45**, 849-854.
20. P. Erdmann and L. Greb, *ChemPhysChem*, 2021, **22**, 935-943.



## Appendix 4 Unpublished results

### 1. General procedures

All reagents and solvents were purchased from commercial suppliers (Sigma-Aldrich, Merck, Alpha-Aesar, TCI, Across, abcr, Thermo scientific, Linde gas a.s. and Lach:ner). Specifically, Indium triflate was purchased from sigma aldrich. Synthetic reagents were used as received and without further purification including hydrogen gas (99.90%) and carbon dioxide for food industry (99.90%) purchased from Linde gas a.s. All solvents were used as received. Unless otherwise specified  $^1\text{H}$  NMRs were taken on a Bruker AVANCE-III (400 MHz) at 298 K spectrometer and reported in ppm ( $\delta$ ). Deuterated solvents were purchased from abcr and used as received. NMR spectroscopy abbreviations: s, singlet; d, doublet; t, triplet; m, multiplet. All the products of catalytic tests were identified by  $^1\text{H}$  NMR data in comparison with literature, by GC coupled to mass spectrometry on a Shimadzu QP-2010 GC-MS with a Supelcowax 10 column and where necessary by comparison with genuine samples of the targeted compounds.

### 2. Catalytic tests

#### 2.1 General Procedure:

In air  $\text{In}(\text{OTf})_3$  (0.05 mmol) and morpholine (1 mmol) were dissolved in the solvent mixture (4 mL) in a stainless-steel autoclave. The autoclave was then sealed and purged 5 times with the desired pressure of  $\text{CO}_2$ . The temperature and stirring rate were set using the Specview program on Parr 5000 series multi reactor system.  $T = 0$  was defined as the time the heating starts. The heating was turned off at  $T = \text{end of the stated reaction time}$  and immediately cooled down i.e., for a reaction time of 24 hours the heating was turned off after 24 hours, removed from the heating mantel and cooled immediately. After which, Dibromomethane (1 mmol) was added to the reactor, stirred and an aliquot was taken for  $^1\text{H}$  NMR analysis in  $\text{CDCl}_3$  or  $\text{DMSO}-d_6$ . The conversion of morpholine and the yield of N-formylmorpholine were quantified by  $^1\text{H}$  NMR analysis with the added Dibromomethane as the internal standard. Other reaction products were quantified by their respective C1 hydrogen signal in  $^1\text{H}$  NMR and structures confirmed by GC-MS on a Shimadzu QP-2010 GC-MS with a Supelcowax 10 column.

## 2.2 Typical result(s) of synthesis of:

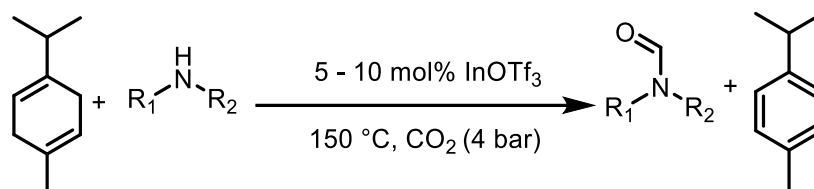
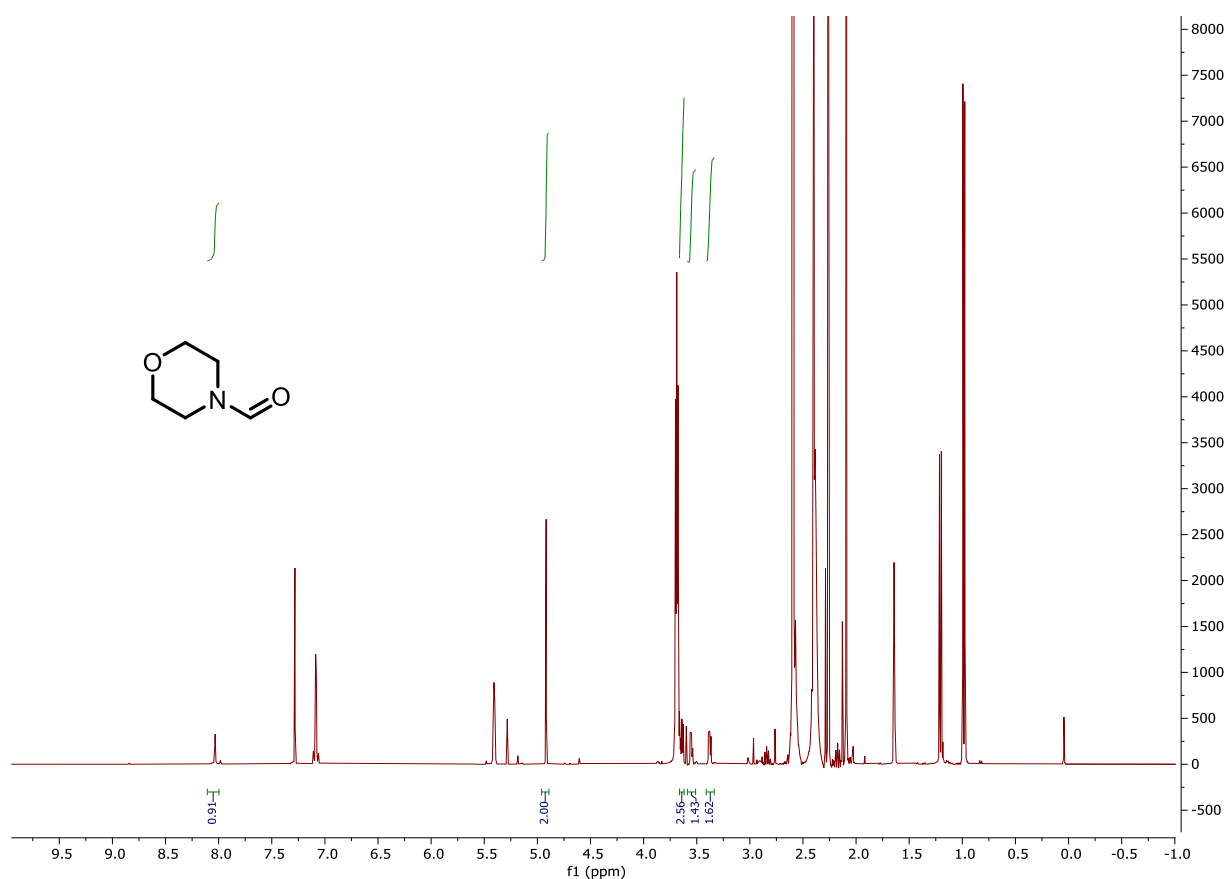


**Figure S4:**  $^1H$  NMR of a reaction mixture at the end of a catalytic test.



### N-formylmorpholine:

$^1H$  NMR (400 MHz,  $CDCl_3$ )  $\delta$ : 8.02 (s, 1H), 3.66 – 3.62 (m, 4H), 3.56 – 3.53 (m, 2H), 3.39 – 3.36 (m, 2H) GC retention time 13.1 minutes to 13.2 minutes; EI-MS (m/z) calculated: 115.1, found 115

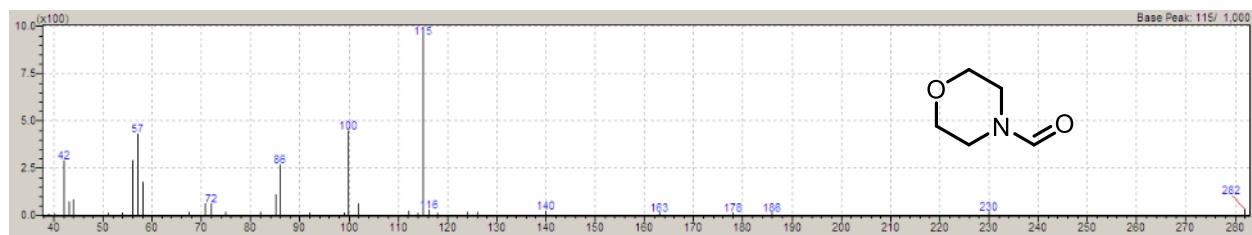


**Figure S5:** GC-MS analysis of a reaction mixture at the end of a catalytic test of synthesis of N-formylmorpholine.

## 2.4 Example of reproducibility between runs:

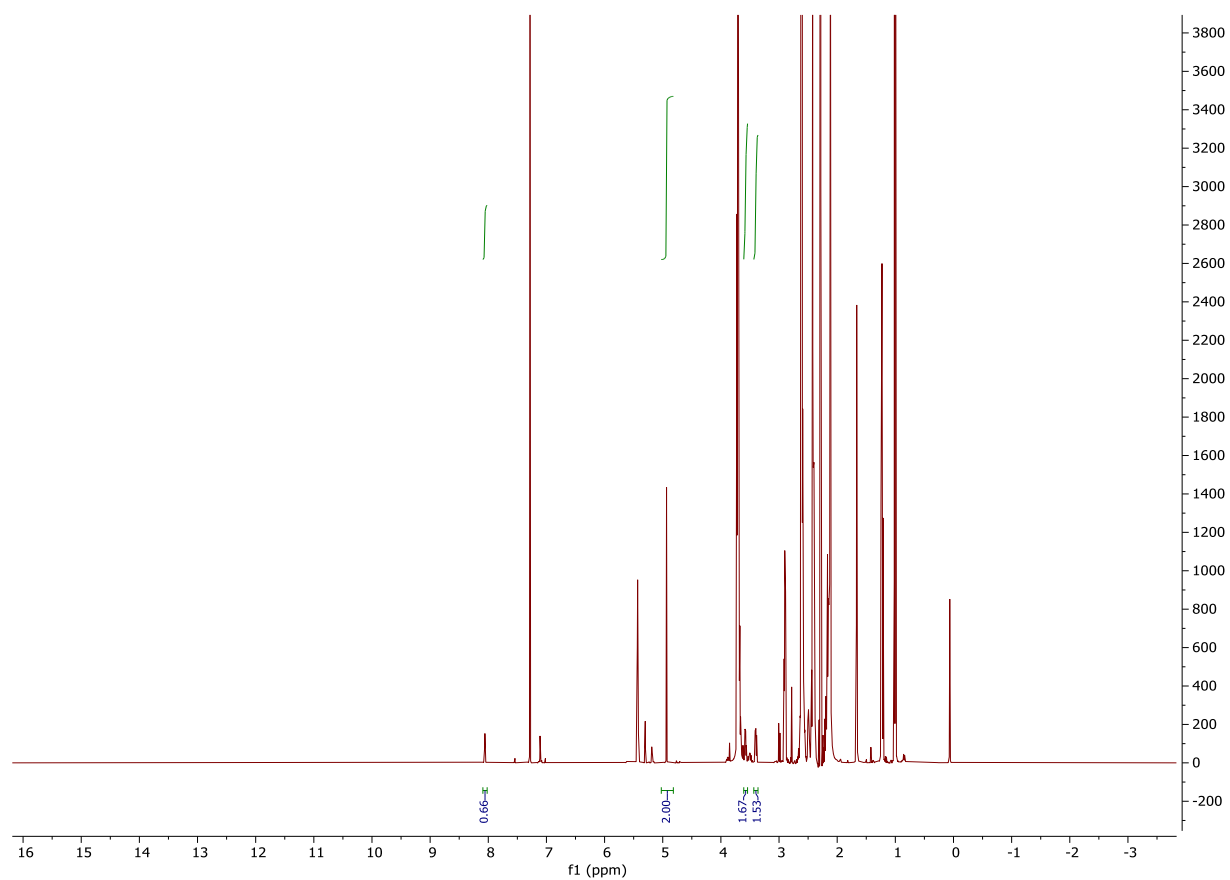


**Figure S3a:** <sup>1</sup>H NMR analysis of a reaction mixture at the end of a first run catalytic test of the transfer hydrogenation of CO<sub>2</sub> reductive coupling to morpholine at 130°C for 48hrs (table 1 entry 9).

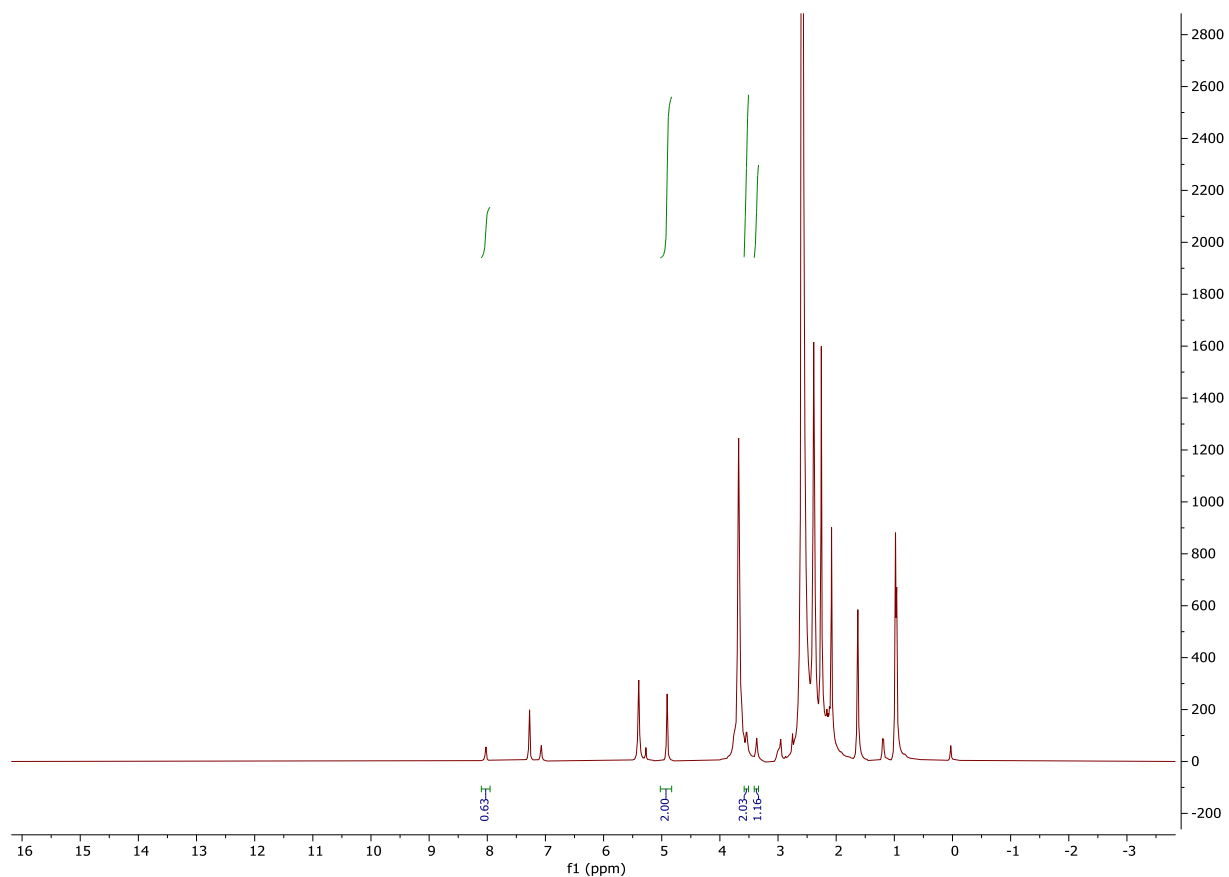


**Figure S3b:**  $^1\text{H}$  NMR analysis of a reaction mixture at the end of a second run of a catalytic test of  $\text{CO}_2$  reductive coupling to morpholine at  $130^\circ\text{C}$  for 48hrs (table 1 entry 9).

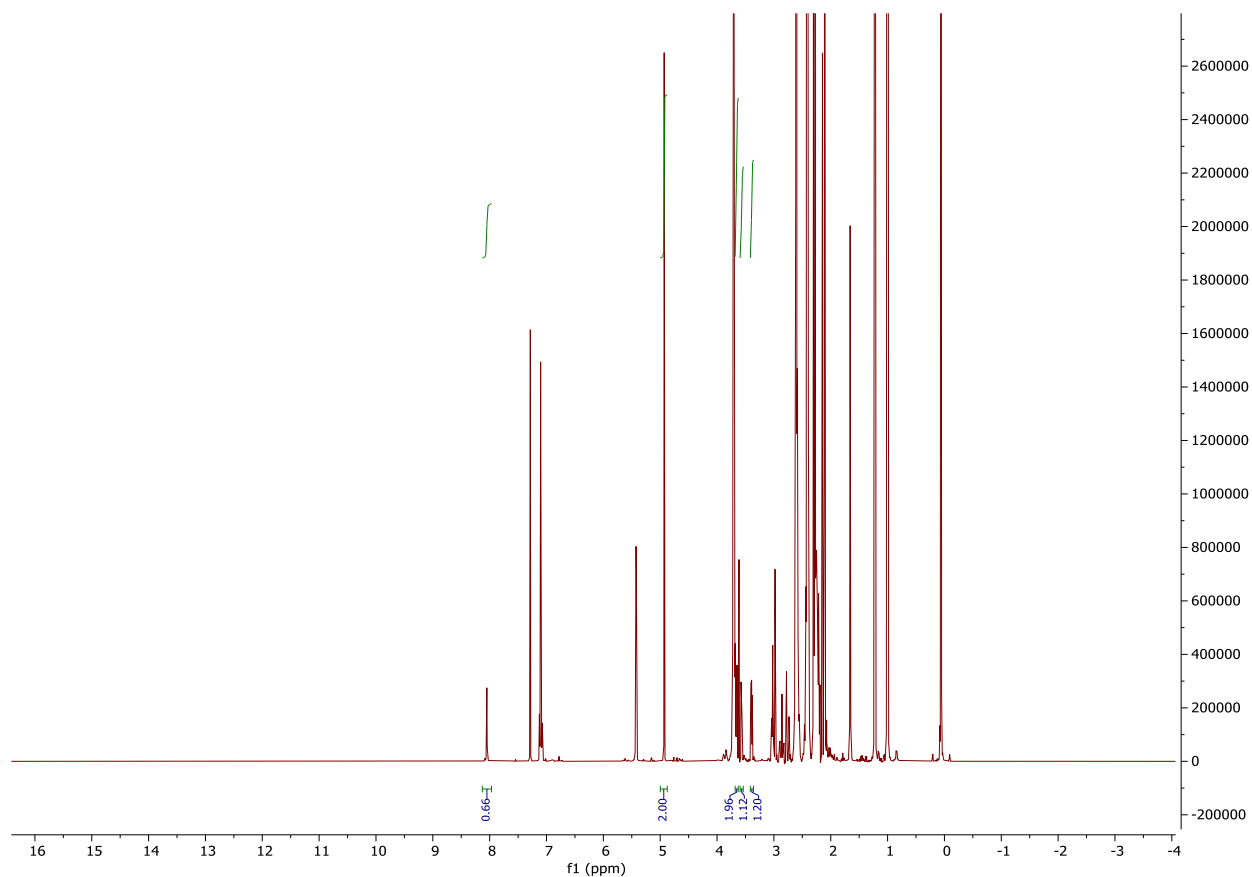


**Figure S3c:** <sup>1</sup>H NMR analysis of a reaction mixture at the end of a third run of a catalytic test of CO<sub>2</sub> reductive coupling to morpholine at 130°C for 48hrs (table 1 entry 9).

### 3. Catalyst optimization

Entry	LA	LB	Temp (°C)	CO <sub>2</sub> Pressure (bar)	Time (hours)	Yield (%)
1	GaOTf <sub>3</sub>	NMM	130	4	48	56
2	InOTf <sub>3</sub>	NMM	130	4	48	65
3	YbOTf <sub>3</sub>	NMM	130	4	48	30
4	AlOTf <sub>3</sub>	NMM	130	4	48	32
5	InCl <sub>3</sub>	NMM	130	4	48	31
6	InOTf <sub>3</sub>	DBU	130	4	48	26*
7	InOTf <sub>3</sub>	2,4,6 -col	130	4	48	31
8	InOTf <sub>3</sub>	NMM	130	4	48	26**

- \*Formation of 0.6 mmol formic acid (equivalent to 13 turnovers)
- \*\* Run with 0.5mol% of InOTf<sub>3</sub> which achieved 52 turnovers

## 4. Substrate scope

### 4.1 Dimethyl formamide

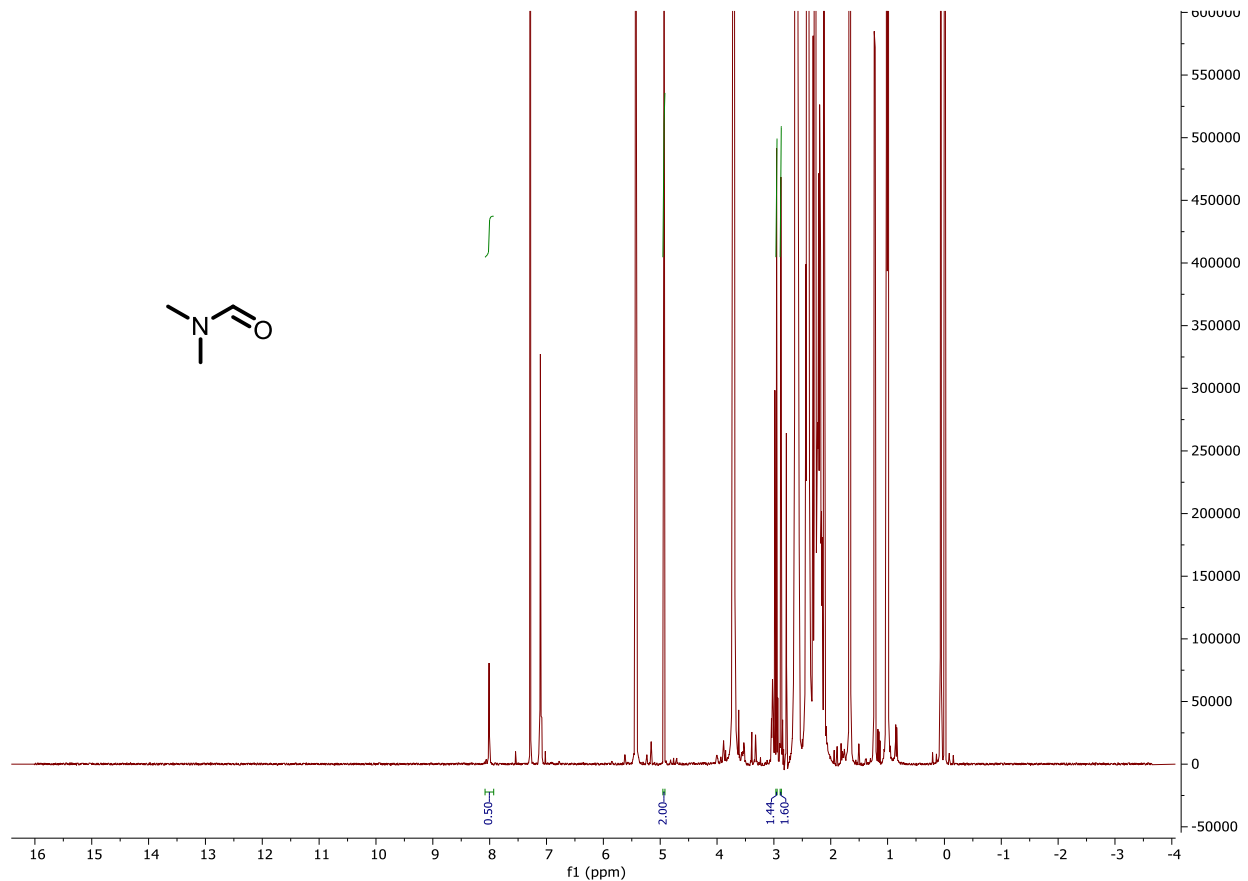


**Figure S4:** <sup>1</sup>H NMR analysis of the reaction product of dimethylammonium dimethyl carbamate.

<sup>1</sup>H NMR (400 MHz, CDCl<sub>3</sub>) δ: 8.00 (s, 1H), 2.95 (s, 3H), 2.87 (s, 3H) GC retention time 7.9 minutes to 8.1 minutes; EI-MS (m/z) calculated:73.1, found 73

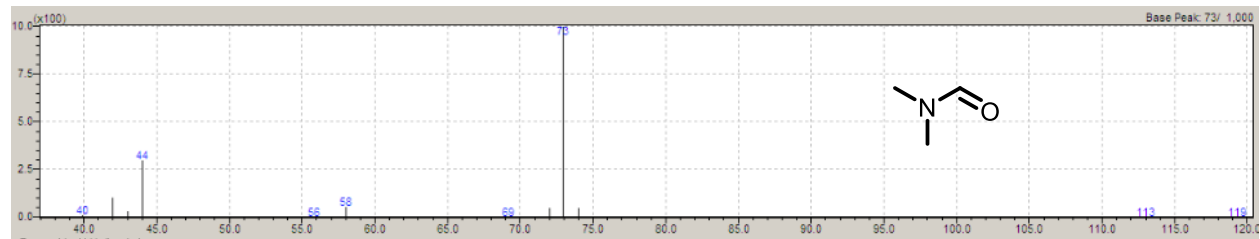


**Figure S4b:** EI-MS analysis of the reaction product of dimethylammonium dimethyl carbamate.



## 4.2 4-methylpiperazine-1-carbaldehyde

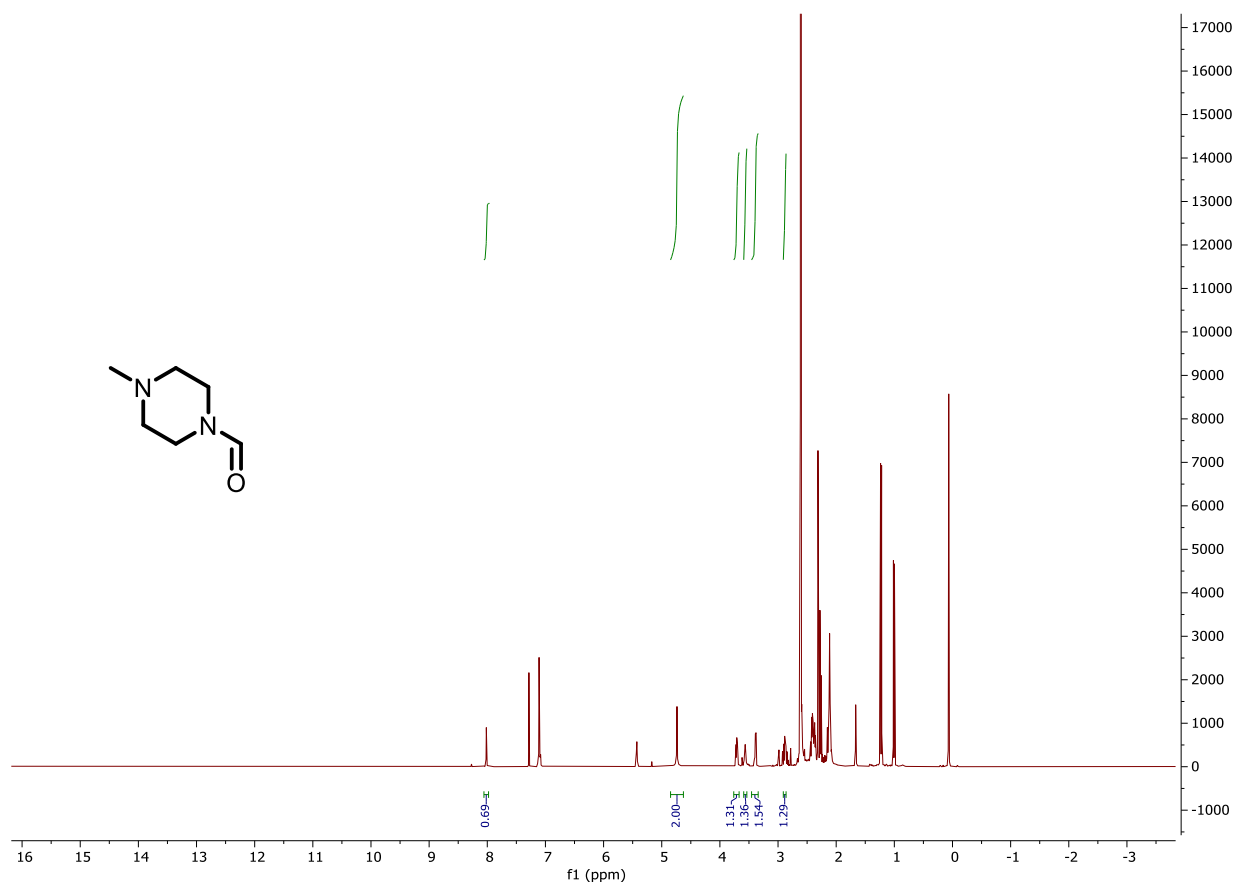


**Figure S5:** <sup>1</sup>H NMR analysis of the reaction product of N-methylpiperazine

<sup>1</sup>H NMR (400 MHz, CDCl<sub>3</sub>) δ: 8.01 (s, 1H), 3.73 – 3.68 (m, 2H), 3.59 – 3.54 (m, 2H), 3.41 – 3.37 (m, 2H), 2.90 – 2.86 (m, 2H). all other peaks were obscured by the reaction solvent. GC retention time 8.00 minutes to 8.2 minutes; EI-MS (m/z) calculated: 128.1, found 128

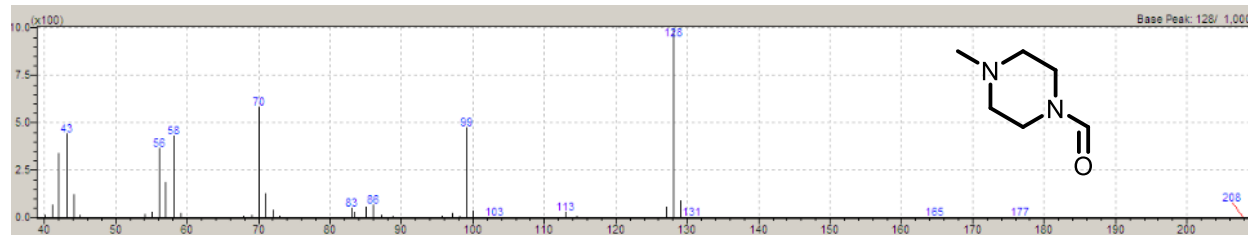


**Figure S5b:** EI-MS analysis of the reaction product of N-methylpiperazine

### 4.3 Pyrrolidine-1-carbaldehyde

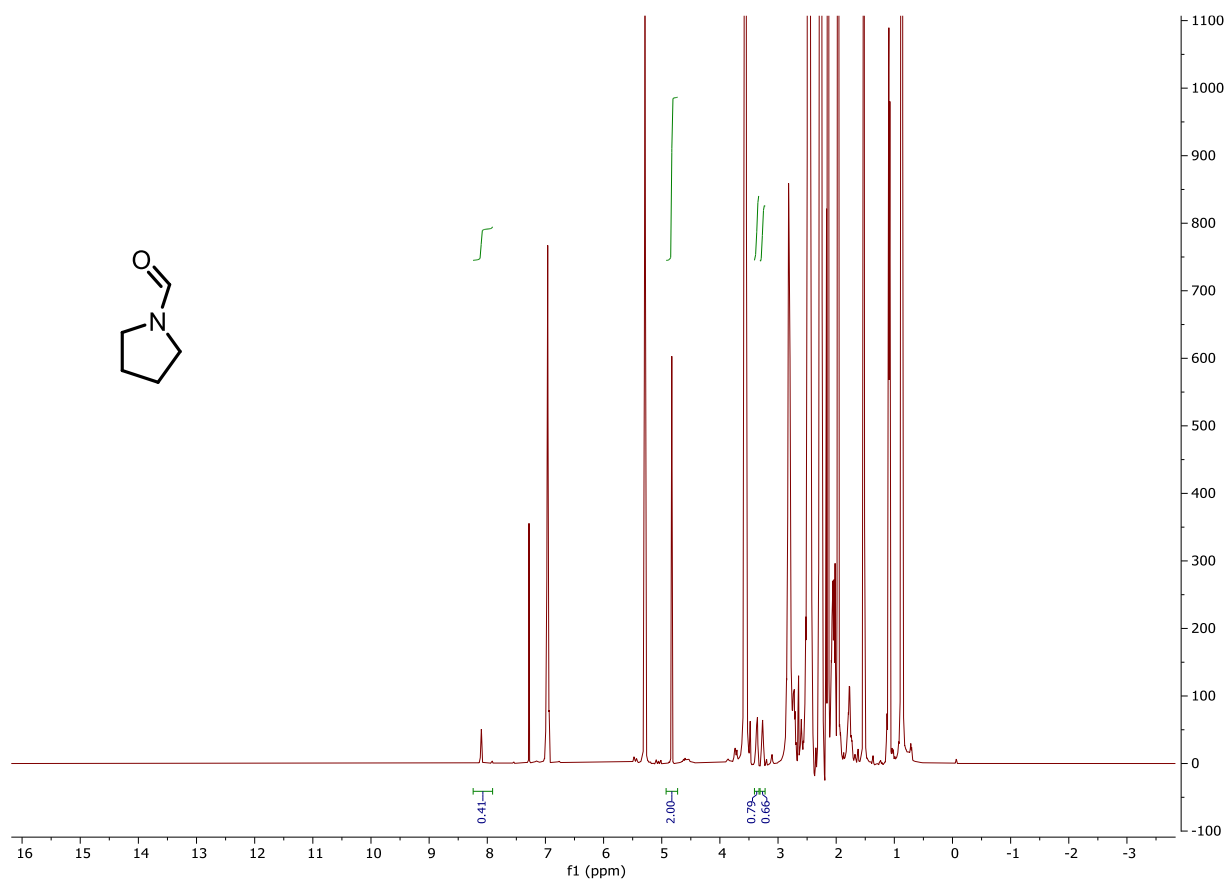


**Figure S6:**  $^1\text{H}$  NMR analysis of the reaction product of pyrrolidine

$^1\text{H}$  NMR (400 MHz,  $\text{CDCl}_3$ )  $\delta$ : 8.10 (s, 1H), 3.40 – 3.34 (m, 2H), 3.29 – 3.24 (m, 2H). All other peaks were obscured by the reaction solvent. GC retention time 11.9 minutes to 12.1 minutes; EIMS ( $m/z$ ) calculated: 99.1, found 99

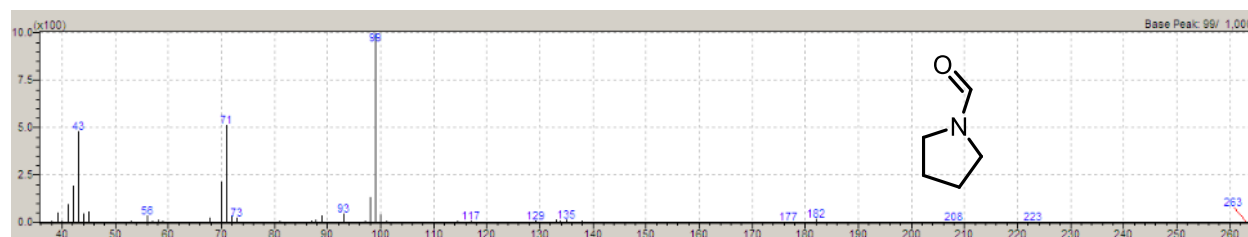


**Figure S6b:** ESI-MS analysis of the reaction product of pyrrolidine

#### 4.4 4-(hydroxymethyl)piperidine-1-carbaldehyde

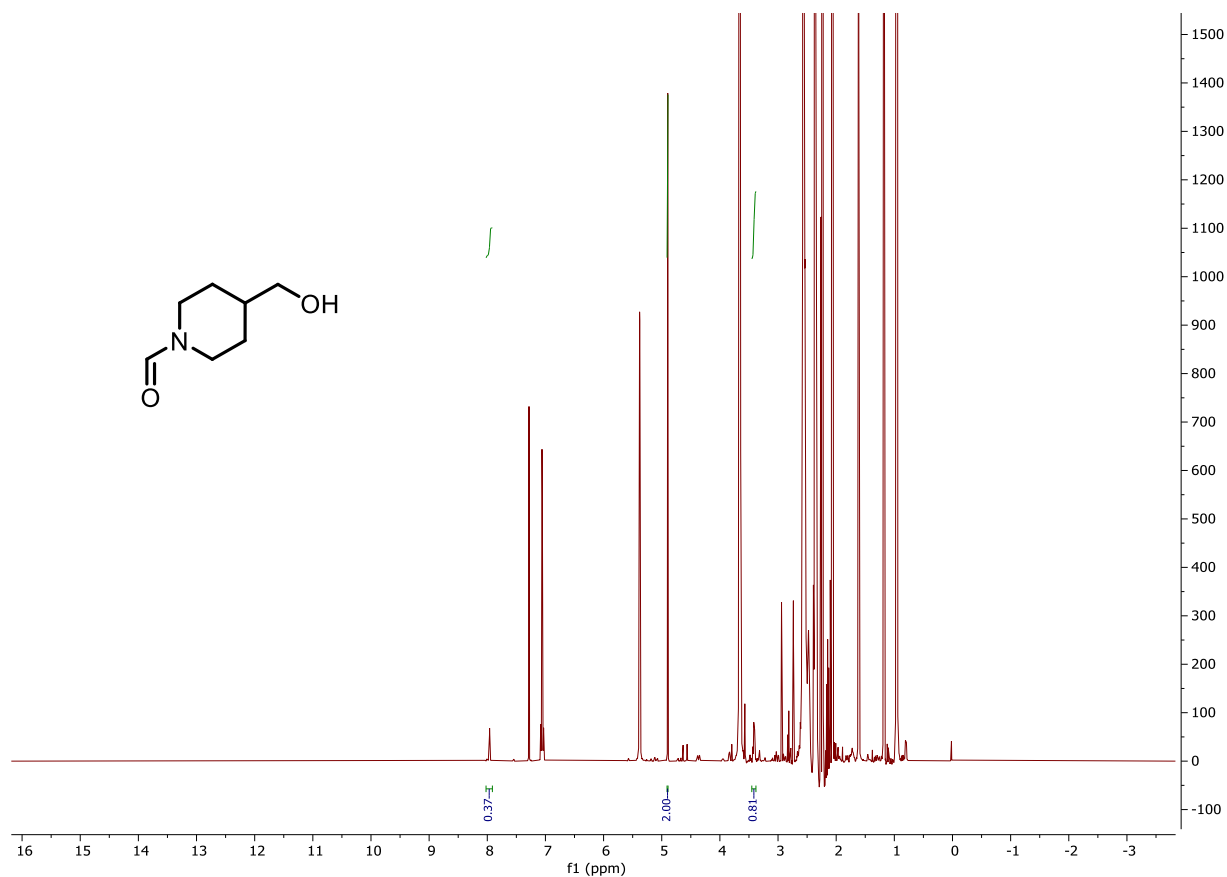


**Figure S7:** <sup>1</sup>H NMR analysis of the reaction product of piperidin-4-ylmethanol.

<sup>1</sup>H NMR (400 MHz, CDCl<sub>3</sub>) δ: 7.96 (s, 1H), 3.43 – 3.39 (m, 2H). All other peaks were obscured by the reaction solvent. GC retention time 21.1 minutes to 21.4 minutes; EI-MS (m/z) calculated: 143.2, found 143

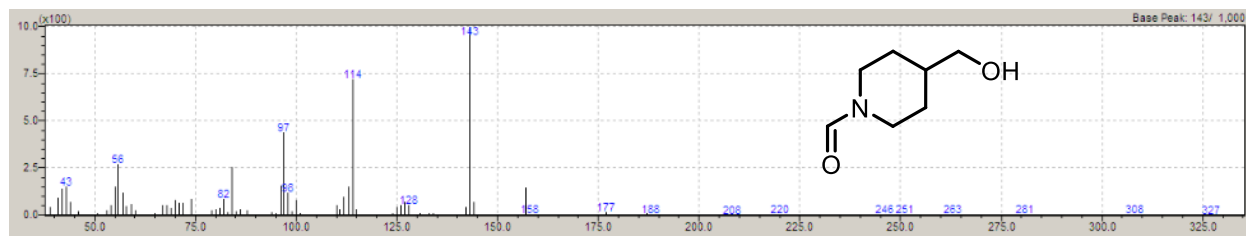


**Figure S7b:** EI-MS analysis of the reaction product of Piperidin-4-ylmethanol.

## 4.5 N-allyl-N-methylformamide

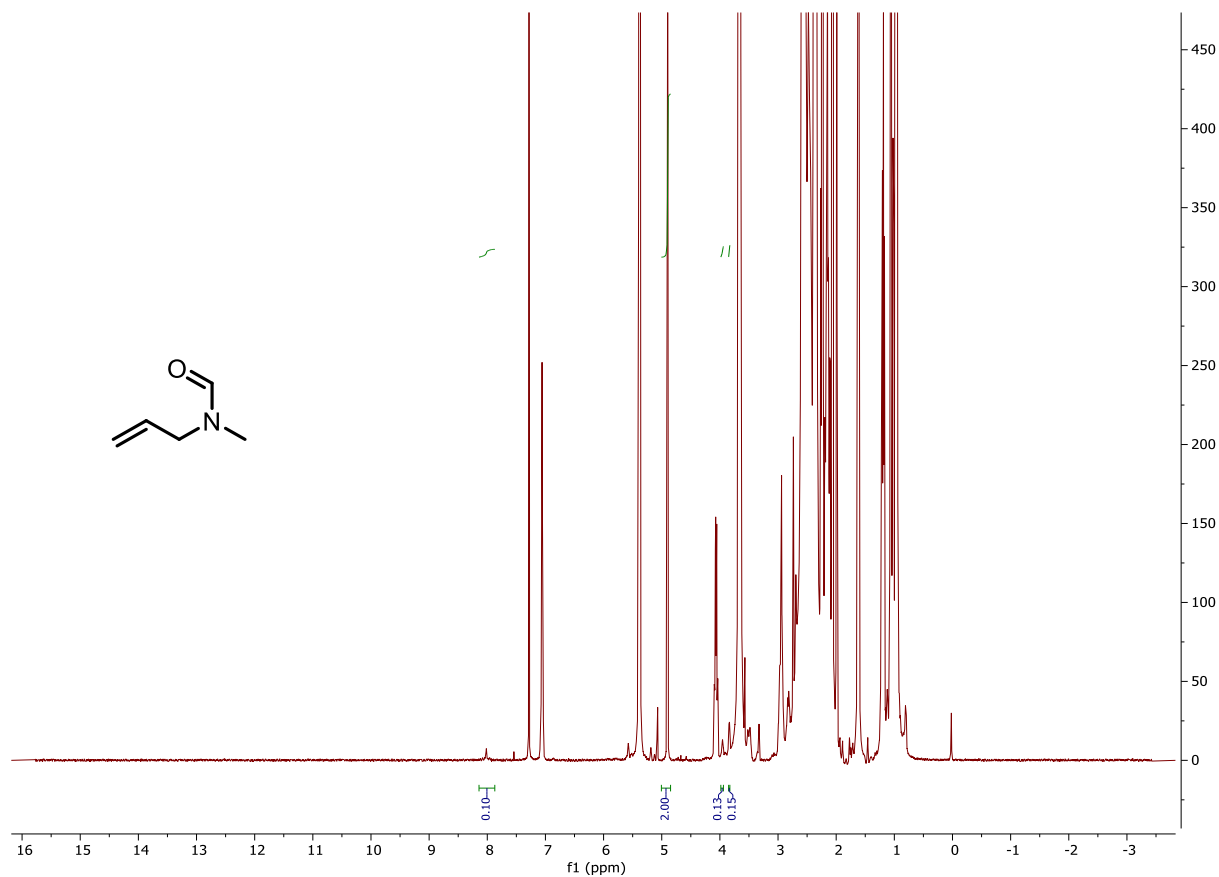


**Figure S8:** <sup>1</sup>H NMR analysis of the reaction product of N-allylmethylamine.

<sup>1</sup>H NMR (400 MHz, CDCl<sub>3</sub>) δ: 8.02 (s, 1H), 3.97 -3.93 (m, 1H), 3.86 – 3.82 (m, 1H). All other peaks were obscured by the reaction solvent. GC retention time minutes 9.5 to 9.7minutes; EI-MS (m/z) calculated: 99.1, found 99

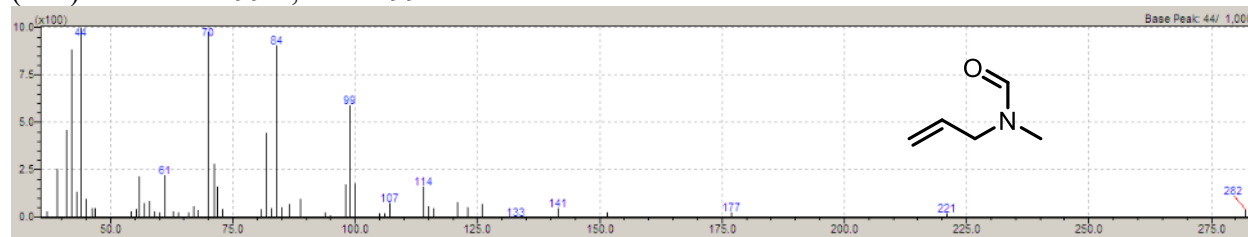


**Figure S8b:** EI-MS analysis of the reaction product of N-allylmethylamine.

## 4.6 N-cyclohexylformamide

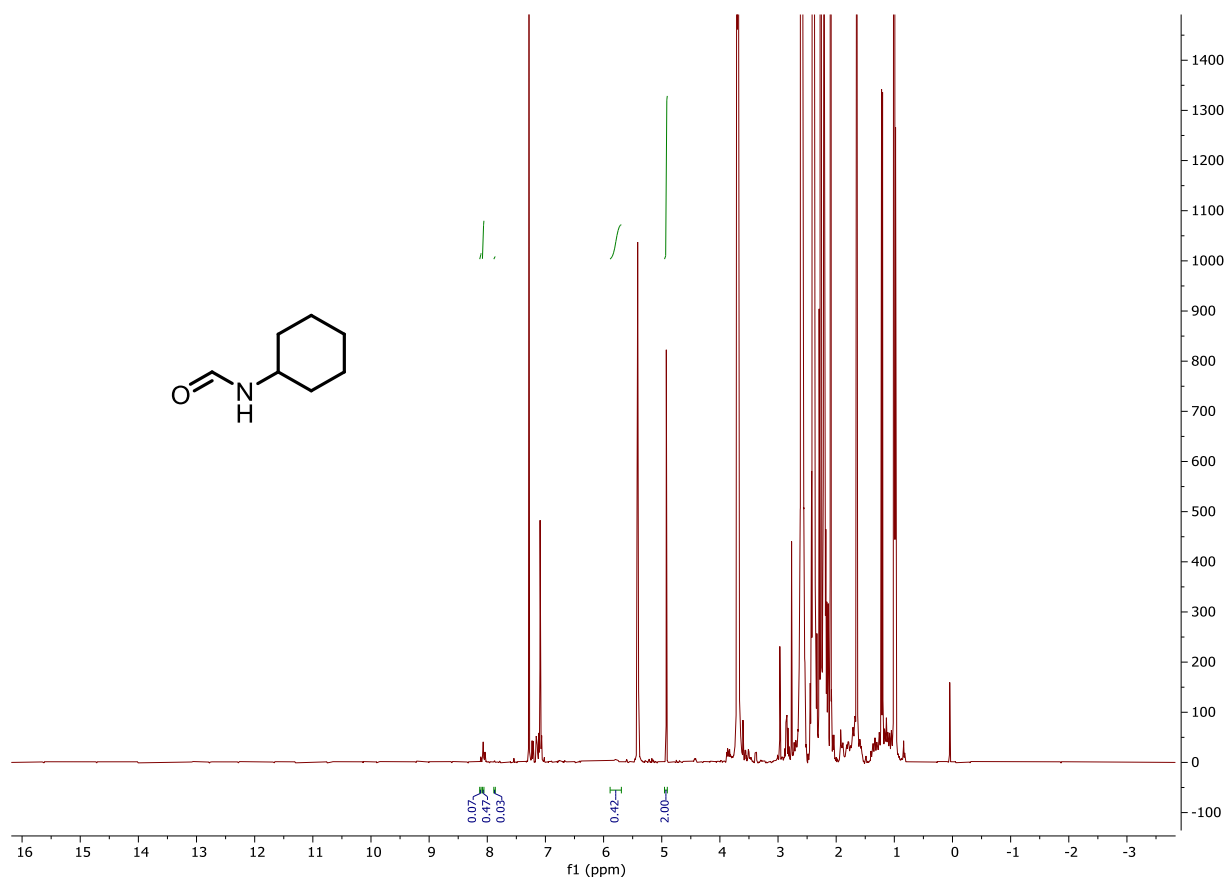


**Figure S9:** <sup>1</sup>H NMR analysis of the reaction product of cyclohexylamine

<sup>1</sup>H NMR (400 MHz, CDCl<sub>3</sub>) δ: 8.07 (s, 1H), 5.80 (br s, 1H). All other peaks were obscured by the reaction solvent. GC retention time 14.8 minutes to 15.1 minutes; EI-MS (m/z) calculated: 127.2, found 127

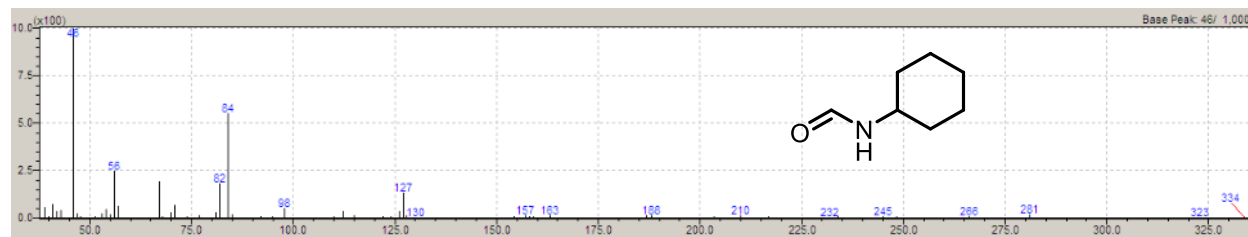


**Figure S9b:** EI-MS analysis of the reaction product of cyclohexylamine.

## 4.7 4-acetylpiperazine-1-carbaldehyde

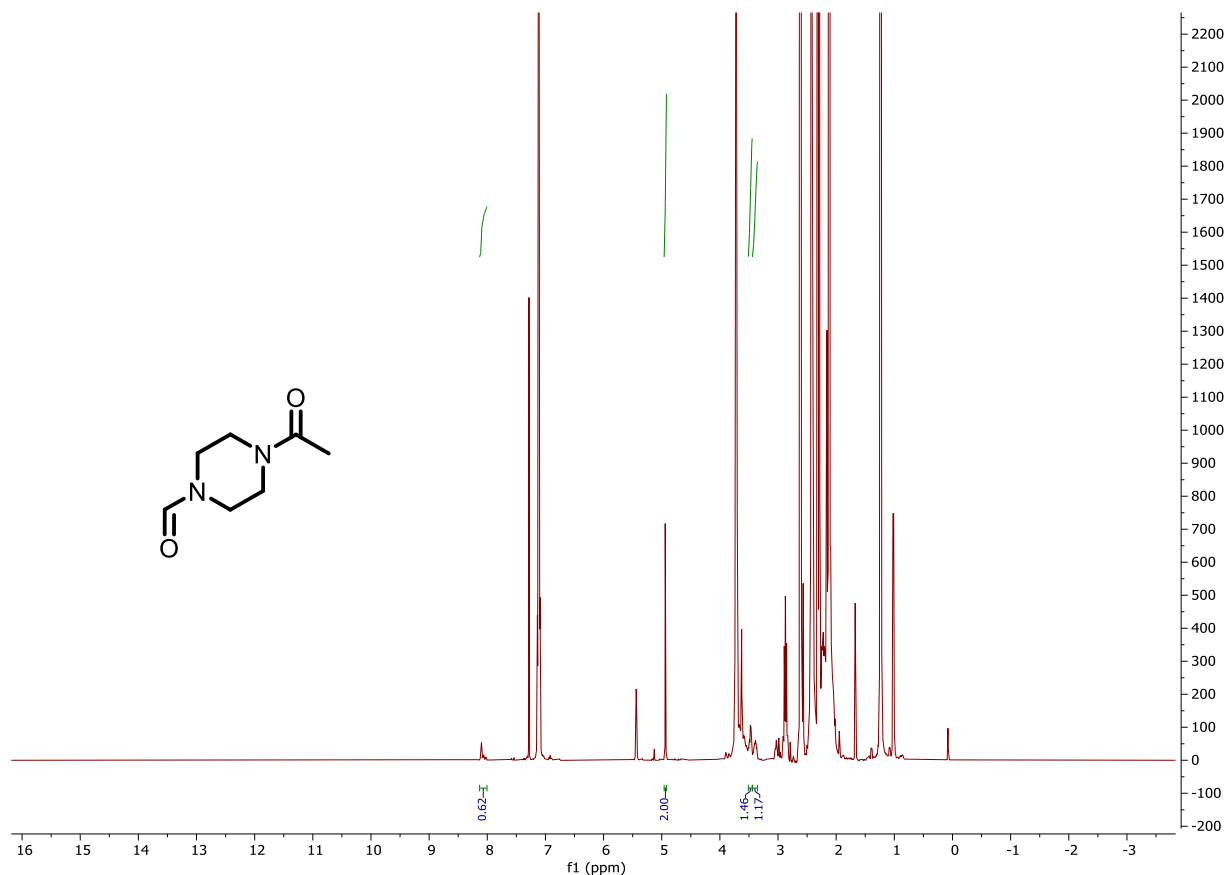


**Figure S10:**  $^1\text{H}$  NMR analysis of the reaction product of 4-acetylpiperazine

$^1\text{H}$  NMR (400 MHz,  $\text{CDCl}_3$ )  $\delta$ : 8.09 (s, 1H), 3.50 – 3.44 (m, 2H), 3.42 – 3.36 (m, 2H). All other peaks were obscured by the reaction solvent. GC retention time 25.2 minutes to 25.5 minutes; EI-MS (m/z) calculated: 156.1, found 156

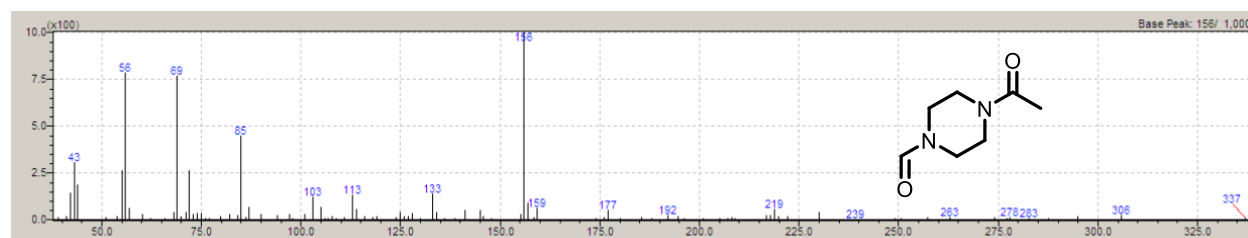


**Figure S10b:** EI-MS analysis of the reaction product of 4-acetylpiperazine.

## 4.8 n-hexylformamide

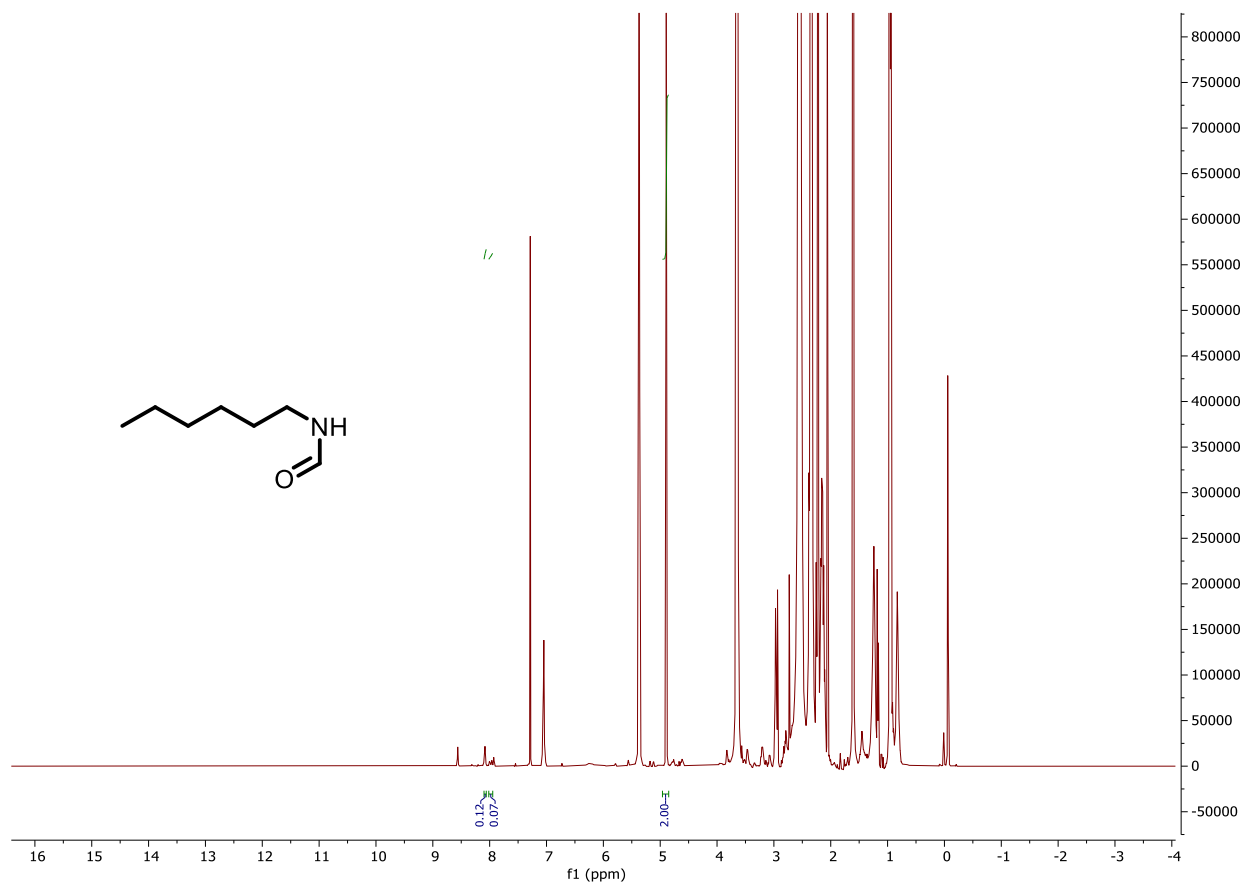


**Figure S11:** <sup>1</sup>H NMR analysis of the reaction product of n-hexylamine.

<sup>1</sup>H NMR (400 MHz, CDCl<sub>3</sub>) δ: 8.09 (s, 0.8H), 7.98 (d, 0.2H) All other peaks were obscured by the reaction solvent. GC retention time 14.0 minutes to 14.3 minutes; EI-MS (m/z) calculated: 129.1 found 129

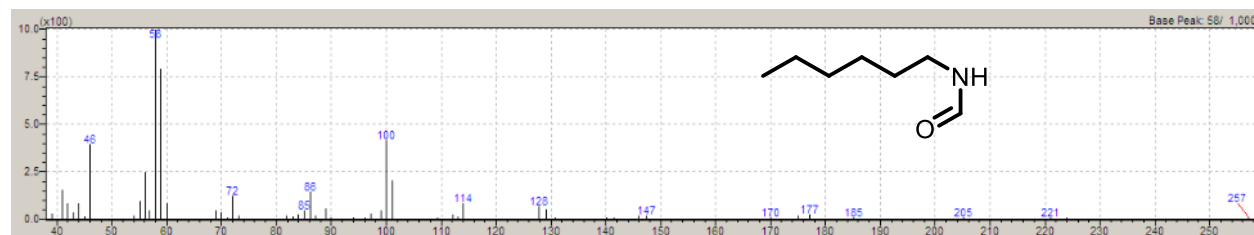


**Figure S11b:** EI-MS analysis of the reaction product of n-hexylamine.

## 4.9 N-benzylformamide

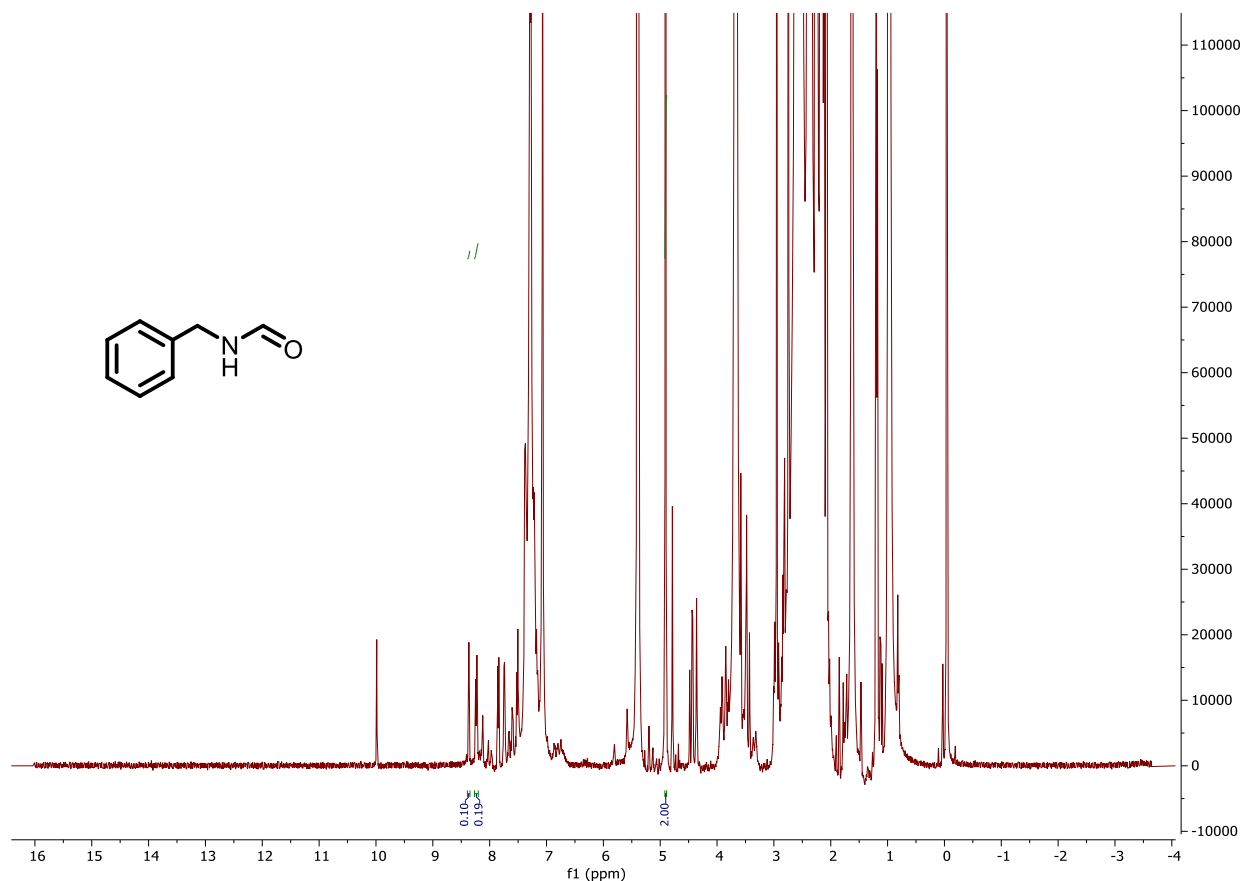


**Figure S12b:** <sup>1</sup>H NMR analysis of the reaction product of benzylamine.

<sup>1</sup>H NMR (400 MHz, CDCl<sub>3</sub>) δ: 8.36 (s, 0.8H), 8.24 (d, 0.2H). All other peaks were obscured by the reaction solvent. GC retention time minutes 7.8 to 8.0 minutes; EI-MS (m/z) calculated:135.1, found 135

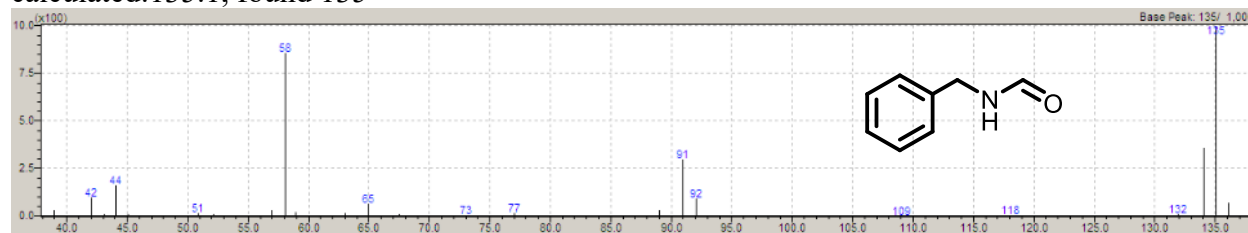


**Figure S12:** EI-MS analysis of the reaction product of Benzylamine.



## 4.10 Benzimidazole

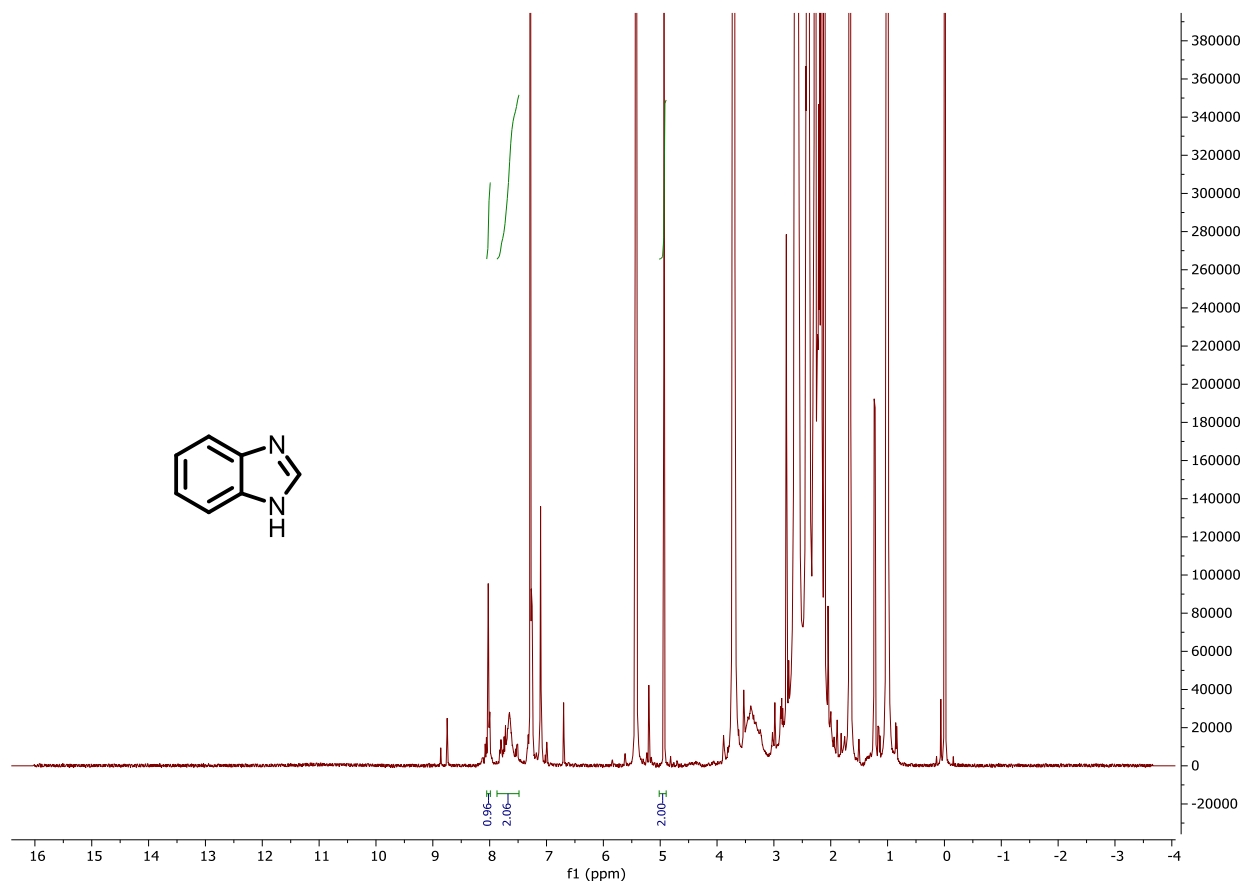


**Figure S13:**  $^1\text{H}$  NMR analysis of the reaction product of *o*-phenylenediamine.

$^1\text{H}$  NMR (400 MHz,  $\text{CDCl}_3$ )  $\delta$ : 8.07 (s, 1H) 7.82 – 7.48 (m, 4H). GC retention time 28.2 minutes to 28.7 minutes; EI-MS ( $m/z$ ) calculated: 118, found 118 all other peaks were obscured due to NMR solvent

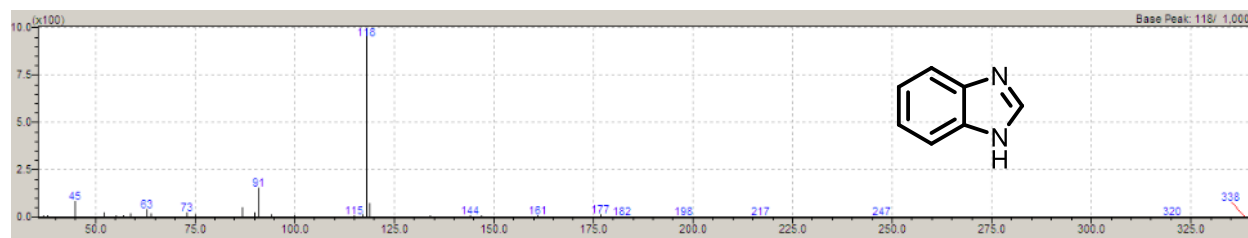


**Figure S13b:** EI-MS analysis of the reaction product of *o*-phenylenediamine.

## 4.11 Benzothiazole

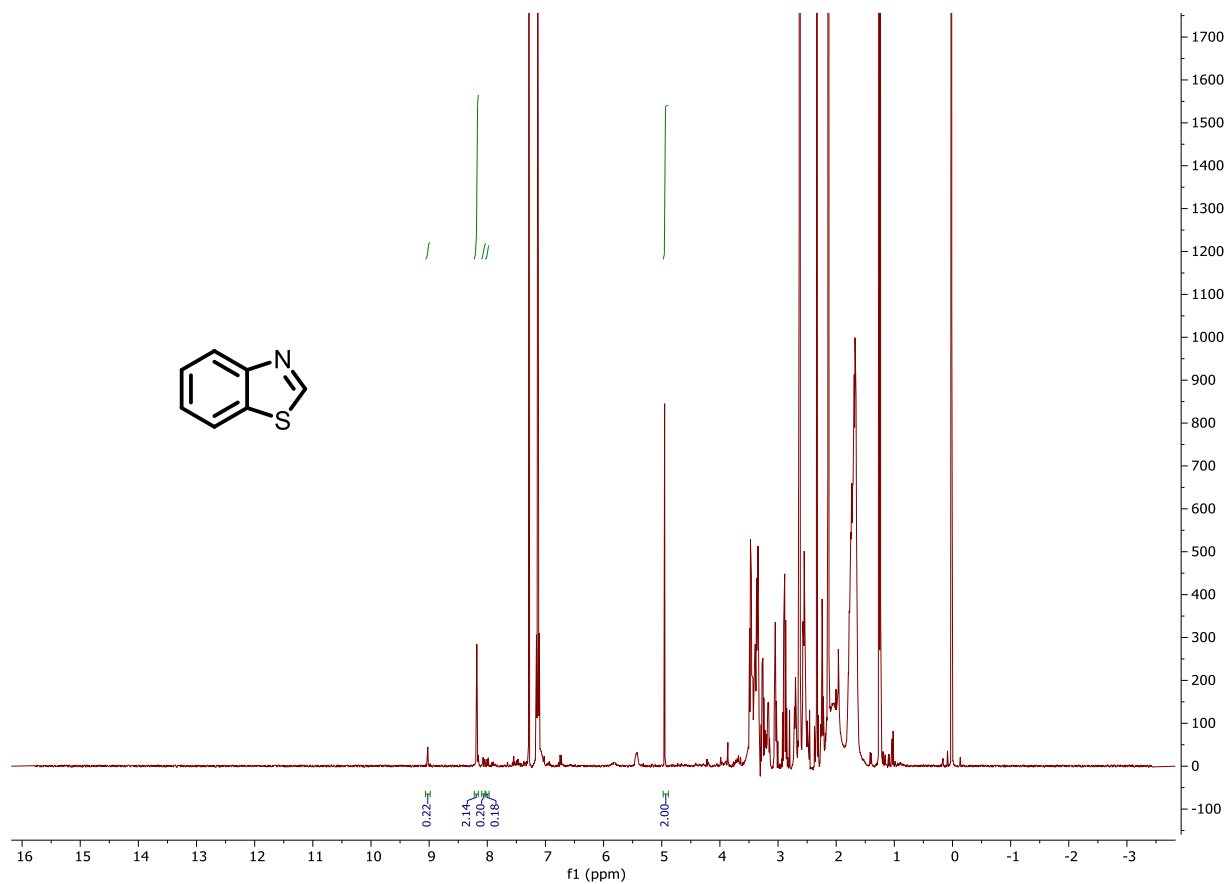


**Figure S14:**  $^1\text{H}$  NMR analysis of the reaction product of 2-aminobenzenethiol.

$^1\text{H}$  NMR (400 MHz,  $\text{CDCl}_3$ )  $\delta$ : 9.01 (s, 1H), 8.21 – 8.15 (m, 2H), 8.06 – 7.99 (m, 2H).

GC retention time 13.4 minutes to 13.7 minutes; EI-MS ( $m/z$ ) calculated: 135, found 135 all other peaks were obscured due to NMR solvent

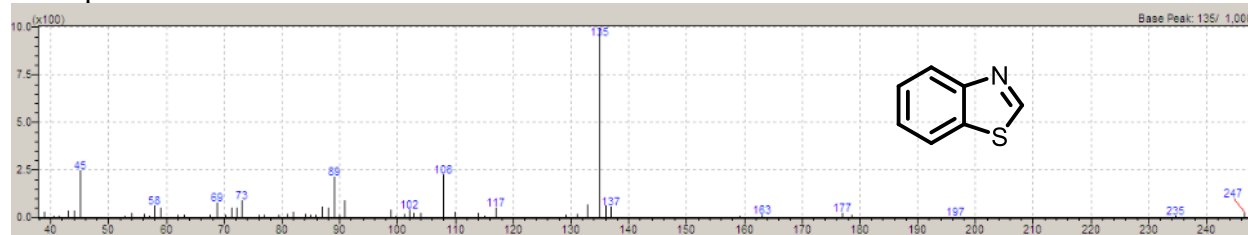


**Figure S14b:** EI-MS analysis of the reaction product of 2-aminobenzenethiol.

## 4.12 4-methylbenzimidazole

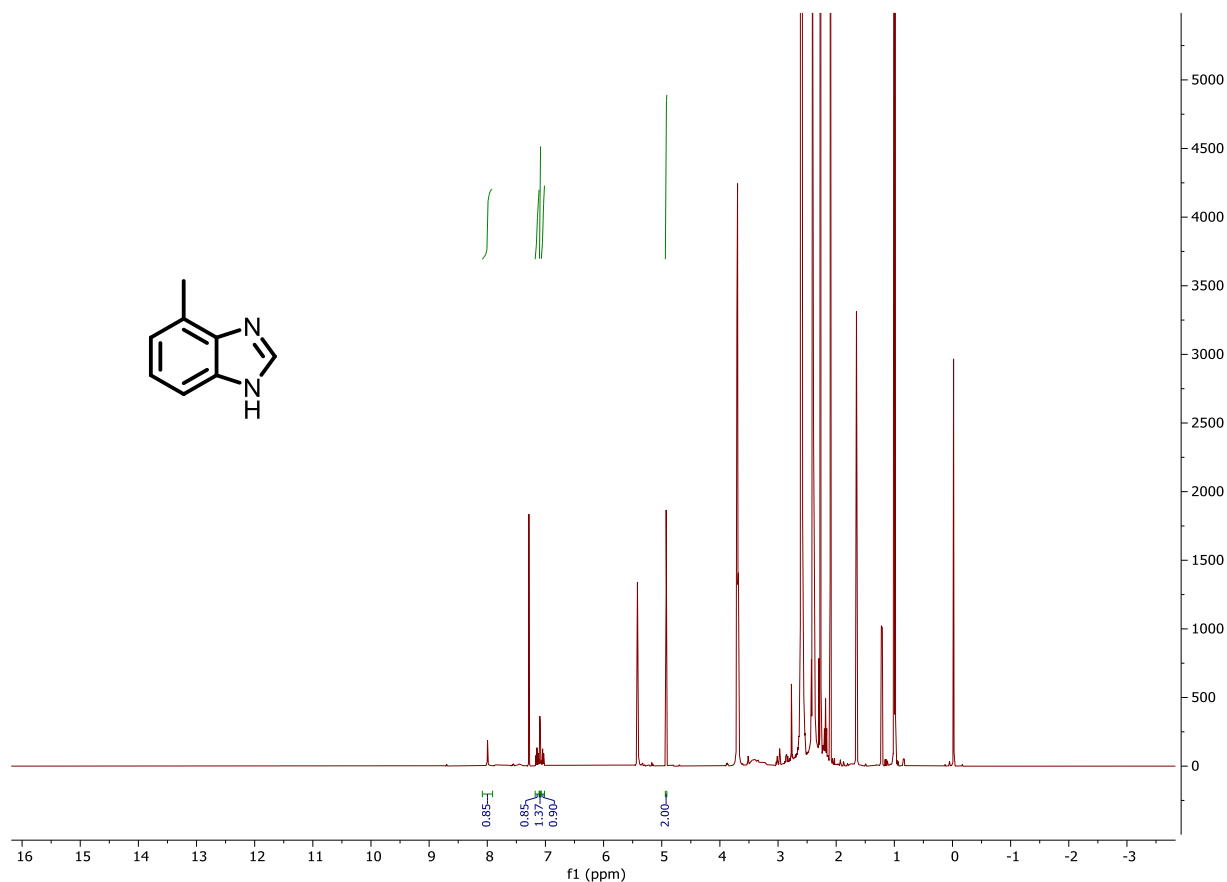


**Figure S15:** <sup>1</sup>H NMR analysis of the reaction product of 3-methyl-1,2-benzenediamine.

<sup>1</sup>H NMR (400 MHz, CDCl<sub>3</sub>) δ: 8.00 (s, 1H), 7.17 -7.12 (m, 1H), 7.10 – 7.08 (m, 1H), 7.07 – 7.02 (m, 1H) All other peaks were obscured by the reaction solvent. GC retention time 28.4 minutes to 28.8 minutes; EI-MS (m/z) calculated: 132.2, found 132

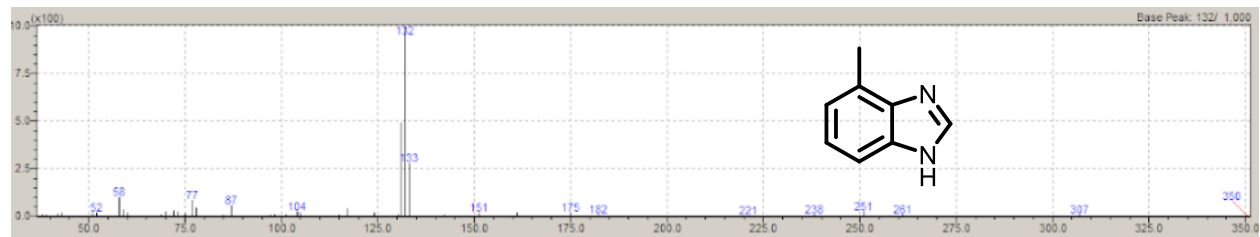


**Figure S15b:** EI-MS analysis of the reaction product of 3-methyl-1,2-benzenediamine.

### 4.13 N-phenylbenzimidazole

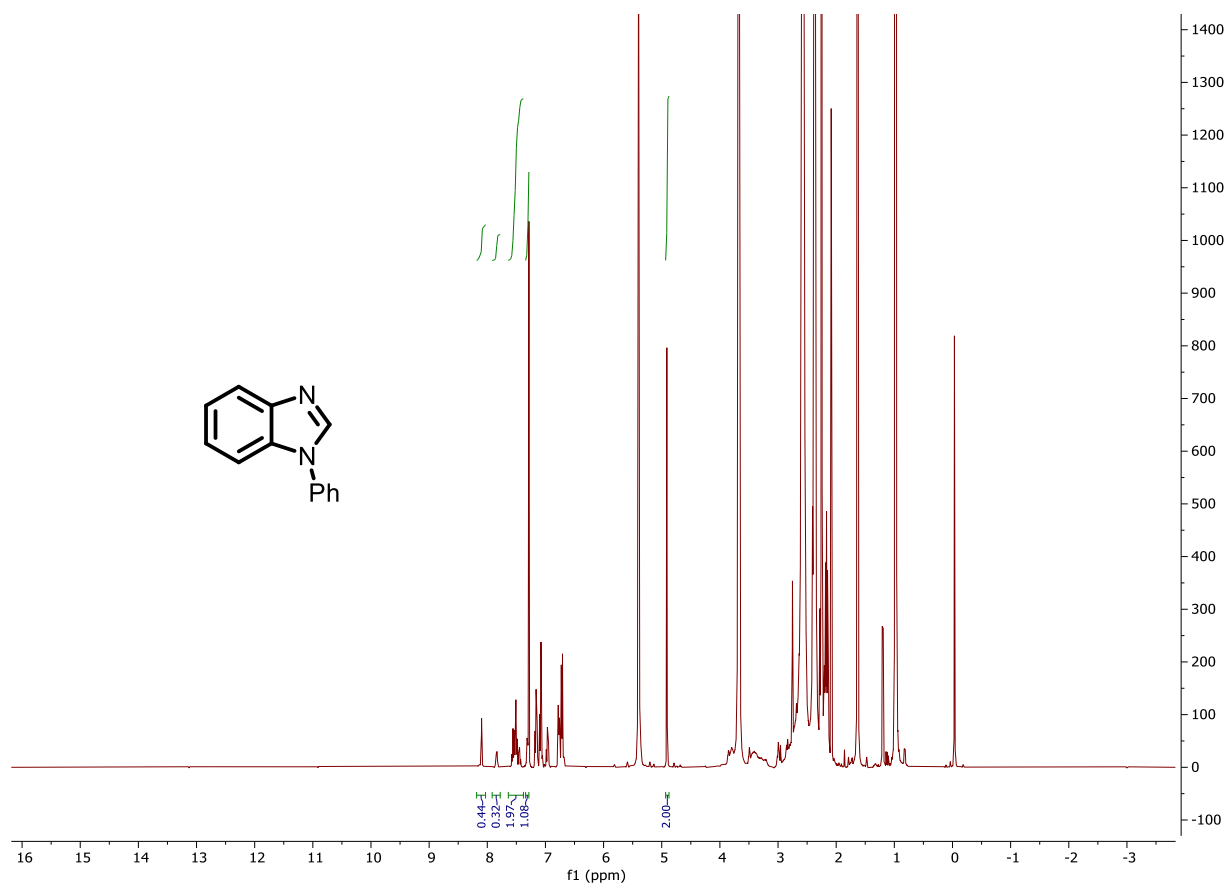


**Figure S16:** <sup>1</sup>H NMR analysis of the reaction product of 2-aminodiphenylamine.

<sup>1</sup>H NMR (400 MHz, CDCl<sub>3</sub>) δ: 8.10 (s, 1H), 7.87 – 7.81 (m, 1H), 7.56 – 7.40 (m, 6H), 7.36 – 7.27 (m, 2H) GC retention time 27.8 minutes to 28.1 minutes; EI-MS (m/z) calculated: 194, found 194 all other peaks were obscured due to NMR solvent

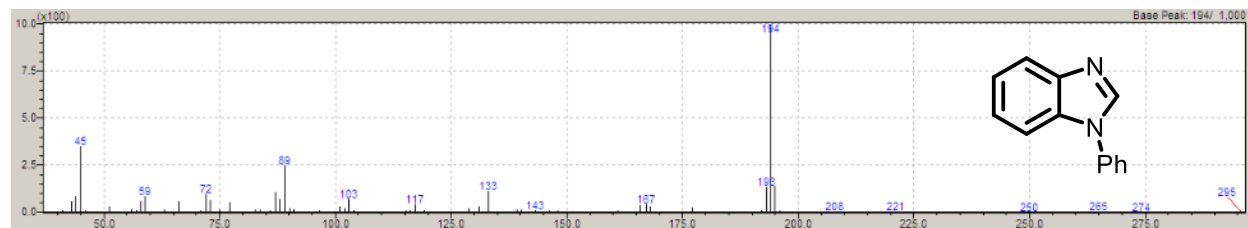


**Figure S16b:** EI-MS analysis of the reaction product of 2-aminodiphenylamine.

## 5. Direct formylation of morpholine using DBU formate and N-methylmorpholinium formate.

### 5.1 General Procedure:

In an NMR tube Lewis base (1 mmol of either N-methylmorpholine or DBU) and formic acid (1mmol) were dissolved in 1 mL of DMSO. The NMR tube was shaken vigorously and allowed to sit for 10 minutes. After which morpholine (1 mmol) was added and the NMR tube was heated to 130 °C for 24 hrs after which the sample was measured by NMR.

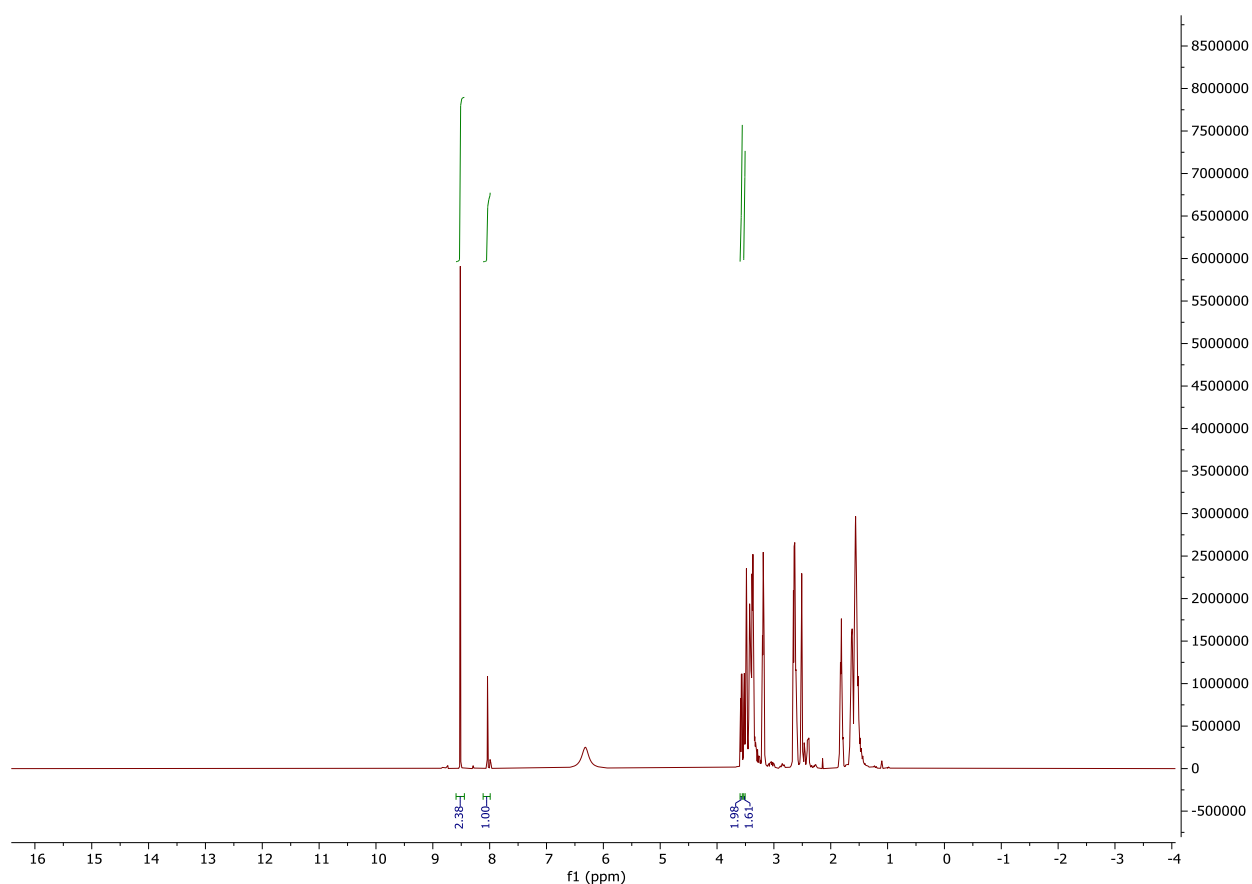


**Figure S17:** Result of the direct reaction between DBU formate and morpholine.

<sup>1</sup>H NMR (400 MHz, CDCl<sub>3</sub>) δ: 8.53 (s, 1H (dbu formate)), 8.02 (s, 1H (N-formylmorpholine)), 3.57 (m, 2H), 3.52 (m, 2H) all other peaks of N-formylmorpholine are covered by DBU formate

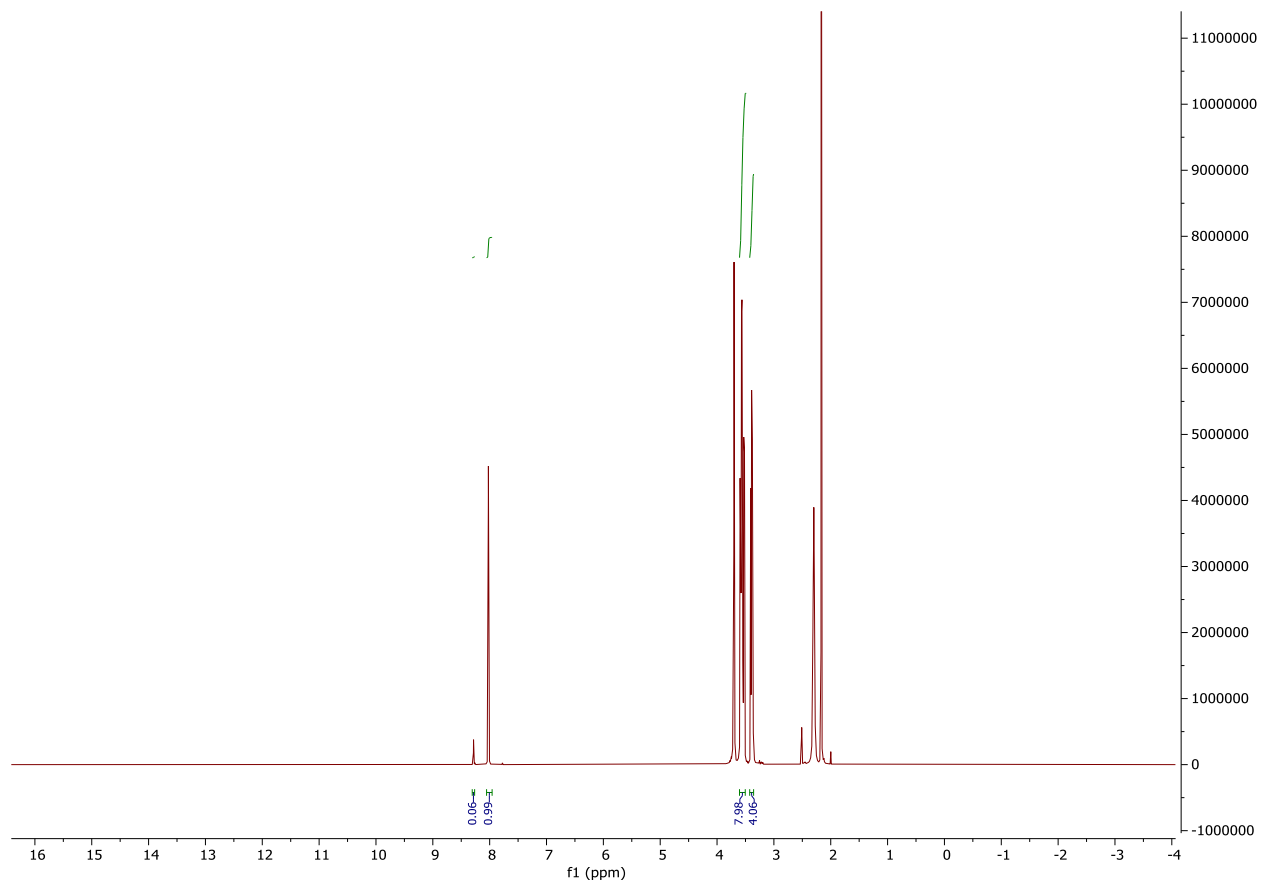


**Figure S18:** Result of the direct reaction between NMM formate and morpholine.

<sup>1</sup>H NMR (400 MHz, CDCl<sub>3</sub>) δ: 8.27 (s, 1H (NMM formate)), 8.02 (s, 1H (N-formylmorpholine)), 3.59- 3.54(m, 4H), 3.54- 3.51 (m, 2H) all other peaks of N-formylmorpholine are covered by NMM formate

## 6. Synthesis of DBU formate.

### 6.1 General Procedure:

In air  $\text{In}(\text{OTf})_3$  (0.05 mmol) was dissolved in the solvent mixture (4 mL (1 mL DBU, 1 mL  $\gamma$ -terpinene and 2 mL DMSO) in a stainless-steel autoclave. The autoclave was then sealed and purged 5 times with 4 bars of  $\text{CO}_2$ . The temperature and stirring rate were set using the Specview program on Parr 5000 series multi reactor system.  $T = 0$  was defined as the time the heating starts. The heating was turned off at  $T = \text{end}$  of the stated reaction time and immediately cooled down i.e., for a reaction time of 22 hours the heating was turned off after 22 hours, removed from the heating mantel and cooled immediately. After which, Dibromomethane (1 mmol) was added to the reactor, stirred and an aliquot was taken for  $^1\text{H}$  NMR analysis in  $\text{CDCl}_3$  or  $\text{DMSO}-d_6$ . The conversion of morpholine and the yield of N-formylmorpholine were quantified by  $^1\text{H}$  NMR analysis with the added Dibromomethane as the internal standard. Other reaction products were quantified by their respective C1 hydrogen signal in  $^1\text{H}$  NMR.

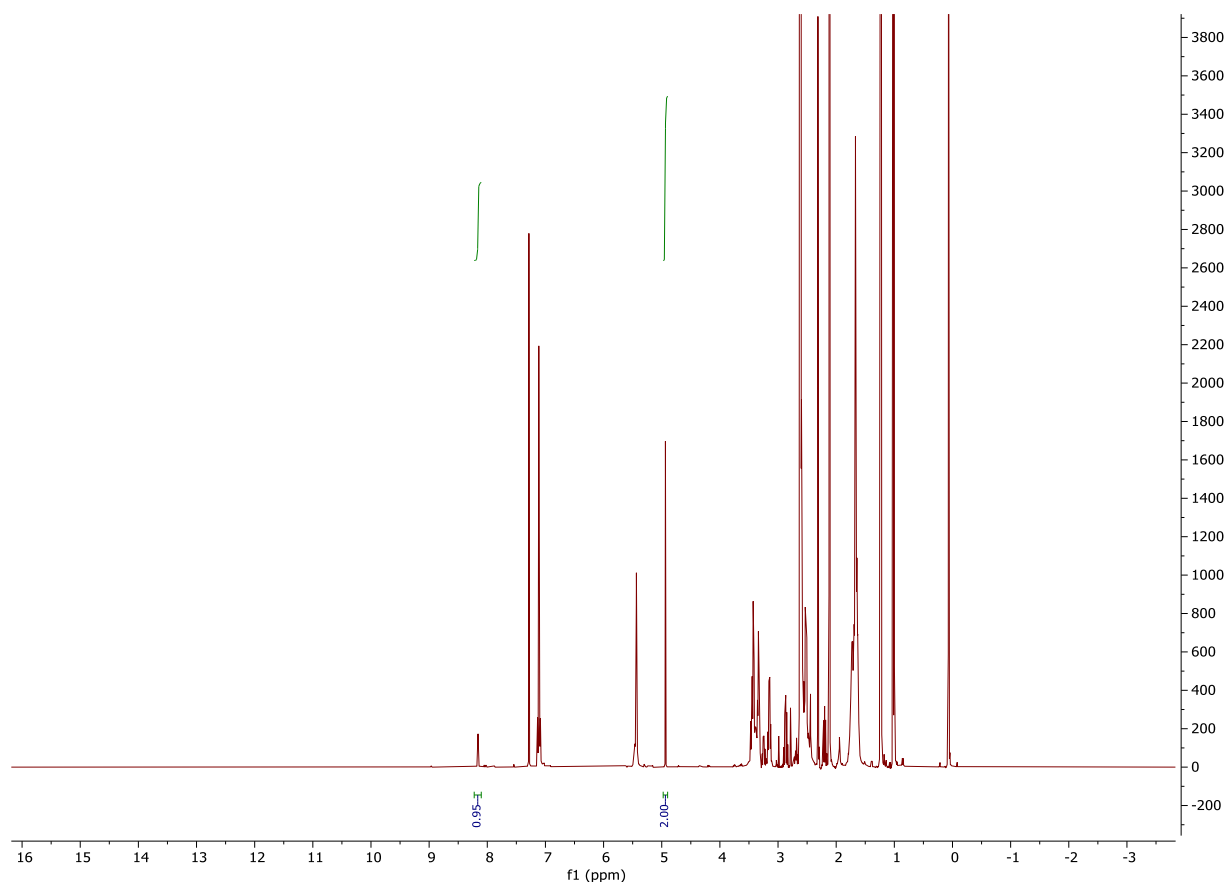


**Figure S19:** Result of the formation of DBU formate from  $\text{CO}_2$ .

$^1\text{H}$  NMR (400 MHz,  $\text{CDCl}_3$ )  $\delta$ : 8.16 (s, 1H). Peaks corresponding to the formate salt are covered by free DBU.

### 6.1: Effect of $\text{CO}_2$ pressure on synthesis of DBU formate

Entry	LA	LB	Temp ( $^\circ\text{C}$ )	$\text{CO}_2$ Pressure (bar)	Time (hours)	Mmol of formate produced
1	$\text{InOTf}_3$	DBU	130	4	48	0.95
2	$\text{InOTf}_3$	DBU	130	6	48	1.94
3	$\text{InOTf}_3$	DBU	130	10	24	0.88
4	$\text{InOTf}_3$	DBU	130	4	72	1.45



## 7. Formic acid decomposition.

### 7.1 General Procedure:

In an NMR tube  $\text{In}(\text{OTf})_3$  (0.05mmol), NMM (200  $\mu\text{L}$ ) and formic acid (1mmol) were dissolved in 1 mL of DMSO. The NMR tube was heated to 130  $^\circ\text{C}$  for 24 hrs after which the sample was measured by NMR. The yield of  $\text{H}_2$  gas was 50 % and was calculated by the ratio between the peak of  $\text{H}_2$  and the formate peak of formic acid.

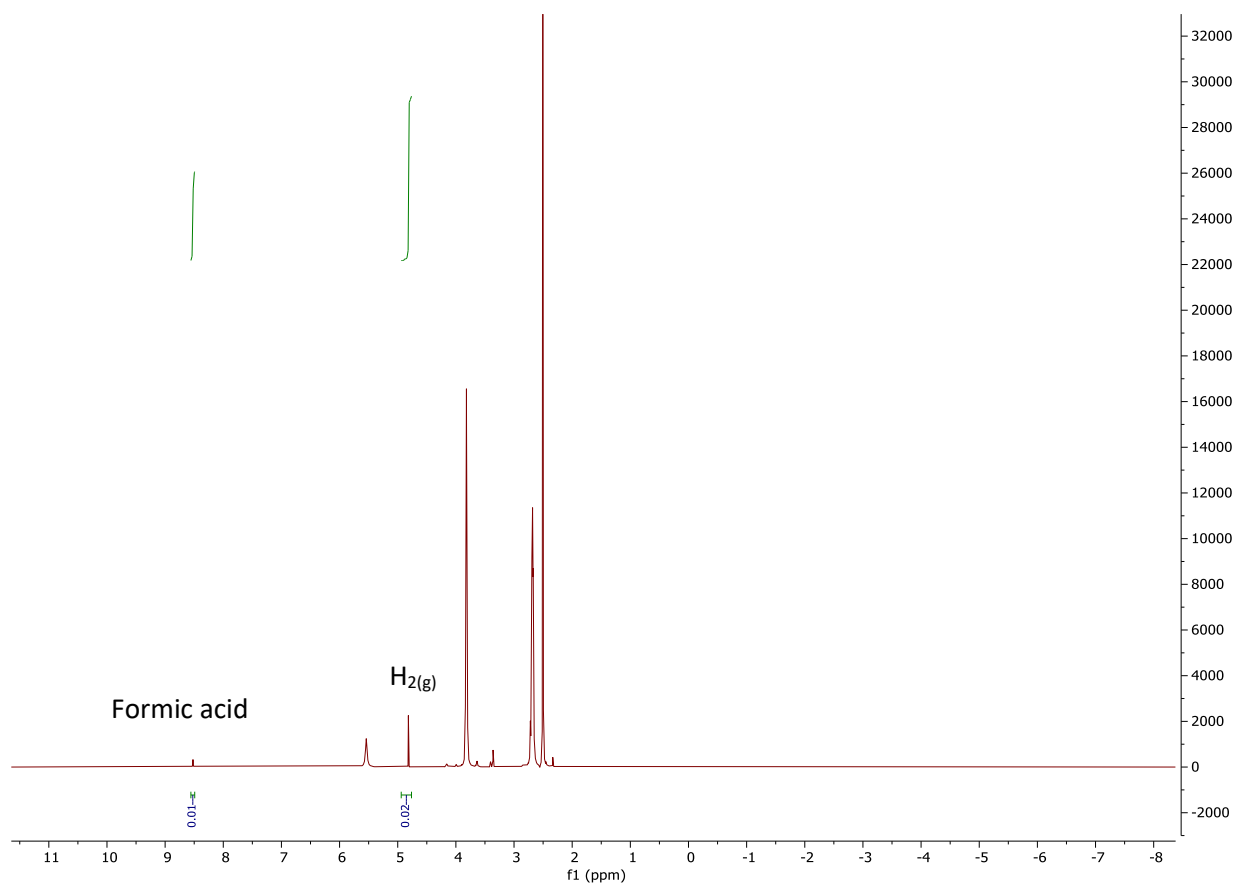


**Figure S20:** Result of the decomposition of formic acid by  $\text{In}(\text{OTf})_3$ .

$^1\text{H}$  NMR (400 MHz,  $\text{CDCl}_3$ )  $\delta$ : 8.01 (s, 1H, formic acid), 4.81 (s, 2H,  $\text{H}_2$ ).

## 8. Formation of partially deuterated amines.

### 8.1 General Procedure:

In air  $\text{In}(\text{OTf})_3$  (0.05 mmol) and morpholine (1 mmol) were dissolved in the solvent mixture (4 mL, including  $\text{DMSO-d}_6$ ) in a stainless-steel autoclave. The autoclave was then sealed and purged 5 times with the desired pressure of  $\text{CO}_2$ . The temperature and stirring rate were set using the Specview program on Parr 5000 series multi reactor system.  $T = 0$  was defined as the time the heating starts. The heating was turned off at  $T = \text{end}$  of the stated reaction time and immediately cooled down i.e., for a reaction time of 24 hours the heating was turned off after 24 hours, removed from the heating mantel and cooled immediately. After which, Dibromomethane (1 mmol) was added to the reactor, stirred and an aliquot was taken for  $^1\text{H}$  NMR analysis in  $\text{CDCl}_3$  or  $\text{DMSO-d}_6$ . The conversion of morpholine and the yield of *N*-formylmorpholine were quantified by  $^1\text{H}$  NMR analysis with the added Dibromomethane as the internal standard. Other reaction products were quantified by their respective C1 hydrogen signal in  $^1\text{H}$  NMR and structures confirmed by GC-MS on a Shimadzu QP-2010 GC-MS with a Supelcowax 10 column.

### 8.2 Results:

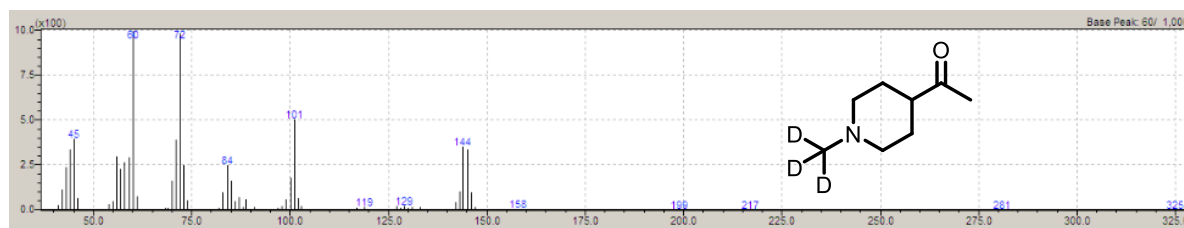


**Figure S21:** EI-MS analysis of the reaction product of 4-acetylpiperazine and  $\text{DMSO-d}_6$